Vol. 20, No. 5 (Supplent Issue), December, 2021
ISSN (Print): 0972-6268; ISSN (Online) : 2395-3454

# Nature Environment & Pollution Technology

A Multidisciplinary, International Journal on Diverse Aspects of Environment

Technoscience Publications
website: www.neptjournal.com

Technoscience Publications
A-504, Bliss Avenue, Balewadi,
Opp. SKP Campus, Pune-411 045
Maharashtra, India

www.neptjournal.com

# Nature Environment and Pollution Technology

**(An International Quarterly Scientific Research Journal)**



**Published by** : Mrs. T. P. Goel, Technoscience Publications, A-504, Bliss Avenue, Balewadi, Pune-411 045, Maharashtra, India

**Managing Office** : Technoscience Publications, A-504, Bliss Avenue, Balewadi, Pune-411 045, Maharashtra, India

**E-mail** : contact@neptjournal.com; journalnept@gmail.com

## INSTRUCTIONS TO AUTHORS

### Scope of the Journal

The Journal publishes original research/review papers covering almost all aspects of environment like monitoring, control and management of air, water, soil and noise pollution; solid waste management; industrial hygiene and occupational health hazards; biomedical aspects of pollution; conservation and management of resources; environmental laws and legal aspects of pollution; toxicology; radiation and recycling etc. Reports of important events, environmental news, environmental highlights and book reviews are also published in the journal.

### Format of Manuscript

- The manuscript (*mss*) should be typed in double space leaving wide margins on both the sides.
- First page of mss should contain only the title of the paper, name(s) of author(s) and name and address of Organization(s) where the work has been carried out along with the affiliation of the authors.

*Continued on back inner cover...*

# Nature Environment and Pollution Technology

**Vol. 20, No. 5 (Supplement Issue), December 2021**

## CONTENTS

1. **A. Benarabi, M. S. Nili and A. Douadi,** Study of Some Indicators of Environmental Pollution of Surface Soil for the City of Touggourt (Southeast Algeria) 1863-1871
2. **M. Bala, A. Sharma and G. Sharma,** Spatial Variation of Trace Metals between Industrial and Rural Dwelling Birds of India 1873-1879
3. **S. A. Abbasi, Tabassum-Abbasi and Pratiksha Patnaik,** Biomimetically Generated Nanoparticles in Boosting the Performance of Microbial Fuel Cells 1881-1886
4. **H.T. Hoang and T. Kato,** Biogas Production and Greenhouse Gas (GHG) Emissions Reduction due to Use of Biogas Digesters in Small Farms in Quang Tri Province, Vietnam 1887-1894
5. **Dinesh Kumar, Sukesh Trikha and Ranju Anthony,** Healthcare Waste, Pandemic Covid-19: A Case of India 1895-1902
6. **C.O. Ataguba and I. C. Brink,** Characterization and Assessment of Stormwater Runoff Quality from Automobile Workshops in Nigeria Using Multivariate Linear Regression 1903-1913
7. **D. P. Dave and K. V. Chauhan,** Current Approach to Develop $TiO_2$ Thin Film as Photocatalysts for Low-Density Plastic Degradation 1915-1921
8. **M. Ouzzane, M. T. Naqash and O. Harireche,** Assessment of the Potential Use of Shallow Geothermal Energy Source for Air Heating and Cooling in the Kingdom of Saudi Arabia 1923-1934
9. **Kshitij Upadhyay and Samir Bajpai,** Microplastics in Landfills: A Comprehensive Review on Occurrence, Characteristics and Pathways to the Aquatic Environment 1935-1945
10. **Sushil M. Chaudhari and Rohit B. Meshram,** A Comparative Life Cycle Assessment (LCA) of Gasoline Blending with Different Oxygenates in India 1947-1958
11. **Tareq W. M. Amen, Meng Sun, Mitsuharu Terashima and Hidenari Yasui,** Effect of Sludge Residence Time over Anaerobic Biodegradation of High Saline Biomass 1959-1965
12. **Jasvinder Kaur, Rajdeep Malik and Dushyant Gangwar,** A Reliable Cyclic Voltammetry Technique for the Degradation of Salicylaldehyde: Electrode Kinetics 1967-1972
13. **U.S.P.R. Arachchige, K.A. Viraj Miyuranga, D. Thilakarathne, R. A. Jayasinghe and N. A. Weerasekara,** Biodiesel-Alkaline Transesterification Process for Methyl Ester Production 1973-1980
14. **K. Nagamani, Prabhu Dass Batvari, S. Packialakshmi, C. Sai Kumar Reddy and B. Anuradha,** Groundwater Recharge Planning Using Field Survey for Talupula Mandal in Anantapur District, Andhra Pradesh, India 1981-1987
15. **Yajuan Li, Toru Matsumoto and Atsushi Fujiyama,** Consideration and Application of Evaluation Indicators of Regional Circular and Ecological Sphere (CES) for the Utilization of Woody Biomass 1989-1995
16. **Ramandeep Kaur and Joginder Singh,** Toxicity, Monitoring, and Biodegradation of Cypermethrin Insecticide: A Review 1997-2005
17. **Frances Roi Seston Tampubolon, Arief Sabdo Yuwono, Armansyah Halomoan Tambunan and Noer Azam Achsani,** Coal Mining Energy Utilization and Environmental Impact Management Strategy Using the LCA Method 2007-2015
18. **Bhumi Rajyaguru, Ajit Varma, Amit Kharkwal and Jasvir Singh,** Biosynthesis of Xanthan Gum by *Xanthomonas campestris* Using Cane Molasses as a Carbon Source 2017-2021
19. **A. Amuthini Sambhavi, K. Nagamani and B. Gowtham,** Evaluation of Fluoride Contamination Using GIS in Thirukkazhukundram Block, Tamil Nadu, India 2023-2030
20. **Ipsita Saha, Tatiana S. Smirnova and Vladimir A. Maryev,** Implementation of Eco-Industrial Park for Effectual Establishment of Circular Economy in Russia 2031-2040
21. **Priyanka Sharma and Kushal Qanungo,** Development of Eco-friendly Adsorbent Pellets from Low Fire Clay and Potato Starch for Potential Use in Methylene Blue Removal in Aquaculture 2041-2050
22. **Amgalan Magsar, Toru Matsumoto, Altanbold Enkhbold and Nandintsetseg Nyam-Osor,** Application of Remote Sensing and GIS Techniques for the Analysis of Lake Water Fluctuations: A Case Study of Ugii Lake, Mongolia 2051-2059
23. **R. Deepa, G. Madhu, Roy M Thomas and V. Sivanandan Achari,** Removal of Mefenamic Acid from Aqueous Solution by Fenton Process: Optimization Using Response Surface Methodology with Central Composite Design 2061-2067
24. **Maradi Sangrama Nayaka, T. Suresh, S. Manjappa and B. Suresh,** Hydrochemistry and Application of GIS in Groundwater Quality in Nagalapura Taluk, Bellary District, Karnataka, India 2069-2078

25. **S. Padmanabhan, C. Joel, Linda Joel, Obulareddy Yuvatejeswar Reddy, K.G.D. Sri Harsha and S. Ganesan,** Evaluation of Waste Plastic Pyrolysis Oil Performance with Diethyl Ether Additive on Insulated Piston Diesel Engine 2079-2086
26. **Korra Simhadri, Syam Kumar Bariki and A.V.V.S. Swamy,** Estimating the Potential of Carbon Sequestration in Tree Species of Chintapalle Forest Range, Narsipatnam Division, Visakhapatnam, Andhra Pradesh, India 2087-2097
27. **Jiawen Zhang and Toru Matsumoto,** Comparative Life Cycle Assessment Analysis of Sewage Sludge Recycling Systems in China 2099-2110
28. **R. Kanimozhi, D. Arvind Prasath, R. Dhandapani and Santhosh Sigamani,** Optimization of *Chlorella* Culture Conditions with Response Surface Methodology to Increase Biomass 2111-2116
29. **B. Prabhu Dass Batvari and K. Nagamani,** GIS-Based Surface Runoff Modeling Using Empirical Technique For A River Basin In South India 2117-2123
30. **Sudhir Kumar Chaturvedi,** Disaster Management: Tsunami and Remote Sensing Technology 2125-2136
31. **Sakshi Takkar, Anuj Kakran, Veerpal Kaur, Manik Rakhra, Manish Sharma, Pargin Bangotra and Neha Verma,** Recognition of Image-Based Plant Leaf Diseases Using Deep Learning Classification Models 2137-2147
32. **Kalivel Parameswari, M. Vijila and P. Jegathambal,** Statistical Modelling of a Comparative Phytotoxicity Study of Treated Yellow 10Gw Dye Solution With Copper and Aluminum in Electrocoagulation Process 2149-2156

# The Journal is Currently Abstracted and Indexed in:

CNKI Scholar (China National Knowledge Infrastructure)

NAAS Rating of the Journal (2019) = 3.85

Scopus®, SJR (0.154) 2020

Index Copernicus (2020) = 119.70

EI Compendex of Elsevier

Indian Science Abstracts, New Delhi, India

Chemical Abstracts, U.S.A.

Pollution Abstracts, U.S.A.

Elsevier Bibliographic Databases

Paryavaran Abstract, New Delhi, India

Zoological Records

Indian Citation Index (ICI)

Scopus CiteScore (2020) = 0.6

Electronic Social and Science Citation Index (ESSCI)

EBSCO: Environment Index™

Ulrich's (Refereed) database

CrossRef (DOI)

DOAJ

Zetoc

Google Scholar

ProQuest, U.K.

J-Gate

Environment Abstract, U.S.A.

British Library

Centre for Research Libraries

WorldCat (OCLC)

JournalSeek

Connect Journals (India)

CSA: Environmental Sciences and Pollution Management

Research Bible (Japan)

Indian Science

Geobase

Elektronische Zeitschriftenbibliothek (EZB)

SHERPA/RoMEO

Directory of Science

CNKI Scholar (China National Knowledge Infrastructure)

Access to Global Online Research in Agriculture (AGORA)

AGRIS (UN-FAO)

Present in UGC-CARE List (Group II)

UDL-EDGE (Malaysia) Products like *i*-Journals, *i*-Focus and *i*-Future

**www.neptjournal.com**

# Nature Environment and Pollution Technology

Nature Environment and Pollution Technology
An International Quarterly Scientific Journal

p-ISSN: 0972-6268
(Print copies up to 2016)
e-ISSN: 2395-3454

Vol. 20 | No. 5 (Suppl) | pp. 1863-1871 | 2021

Original Research Paper

https://doi.org/10.46488/NEPT.2021.v20i05.001

Open Access Journal

# Study of Some Indicators of Environmental Pollution of Surface Soil for the City of Touggourt (Southeast Algeria)

**A. Benarabi*†, M. S. Nili** and A. Douadi*****

*VPRS Laboratory, Faculty of Mathematics and Material Science, Kasdi Merbah University, Ouargla 30000, Algeria

**Laboratory of Biodiversity and Biotechnology Applications in the Agricultural Field, Faculty of Natural and Life Sciences, Echahid Hamma Lakhdar University, El-Oued 39000, Algeria

***Pollution & Waste Treatment Laboratory, Faculty of Mathematics and Material Science, Kasdi Merbah University, Ouargla 30000, Algeria

†Corresponding author. A. Benarabi; abdelkrim.benarabi@gmail.com

**Nat. Env. & Poll. Tech.**
**Website: www.neptjournal.com**

*Received:* 03-12-2020
*Revised:* 02-04-2021
*Accepted:* 11-04-2021

**Key Words:**
Potentially toxic metals
Contaminated soil
Pollution indicators
Touggourt city

## ABSTRACT

Soil is contaminated with various potentially harmful metals (PTMs). Therefore, the adequate protection of soil from contamination is imperative, as the soil is regarded as the primary cradle for living and environmental balance. Accordingly, the purpose of this study was to assess the contamination level by PTMs in Touggourt city, where soil samples have been collected randomly from 18 sites. These sites included manufacturing companies and institutions belonging to the industrial region of Touggourt city. The concentrations of six PTMs - zinc (Zn), iron (Fe), cobalt (Co), copper (Cu), lead (Pb) and manganese (Mn) were assessed using the atomic absorption spectrophotometer (AAS) instrument as well as the application of the modern pollution indices such as CF (Contamination Factor), PLI (Pollution Load Index) and EF (Enrichment Factor). The highest values of contamination factor (CF) for Zn, Fe, Co, Cu, and Pb were 0.605, 1.605, 0.277, 0.05, 0.438, and 0.01, respectively, and the highest value of pollution load index (PLI) was 0.139, while the results of enrichment factor (EF) for the Zn, Mn, Co, Cu and Pb metals were 2.608, 0.060, 0.740, 0.122, and 2.358, respectively. According to these pollution indices, the results of this study have indicated that human effects or industrial wastes and traffic, in particular, were the sources of heavy metal contaminating the studied region.

## INTRODUCTION

The massive increase in the volume of pollutants as a result of human activities on the one hand, and the increased level of potentially toxic metals (PTMs) in soil, water, and air, on the other hand, has sparked a worldwide interest in studying these toxic metals (Fang & Lin 2002, Woitke et al. 2003, Santos et al. 2002, Adamo et al. 2005). PTMs pollution has become a worldwide problem because these metals are considered non-organic pollutants with non-degradable nature, so they persist for long times and mostly accumulate in high levels in the environment, which leads to harmful effects (Ayangbenro & Babalola 2017).

PTMs are considered one of the most dangerous soil pollutants, which lead to the change in some of the soil physicochemical properties, However, some of these metals are essentially important for life but in low concentrations, which makes it one of the most serious ecological problems at all (Zheljazkov & Nielsen 1996, Adamo et al. 2018). Therefore, we consider the soil polluted when it contains high concentrations of the PTMs, regardless of the different sources of such metals, as it becomes toxic for humans, plants, and animals (Wuana & Okieimen 2011, Dehghani et al. 2017).

Soil is considered clean when the concentration of the PTMs is below the environmental level with a value similar to or lower the value naturally present. The background value is the total metal concentration obtained from soil, which is not affected by human activities (Silva et al. 2019).

Accordingly, many researchers and those interested in the environmental pollution field emphasized the necessity of assessing the pollution level of the non-agricultural area's soil with PTMs (Kelly et al. 1996, Chen et al. 1997, Manta et al. 2002).

Based on the fact that PTMs pollution originating mainly from industrial activities is considered one of the most serious problems that the world suffering from in the last few decades, the purpose of this study was, therefore, to investigate the source of topsoil contamination with some PTMs in Touggourt city by measuring some of the pollution indices, such as Contamination Factor (CF) (Victoria et al. 2014), Pollution Load Index (PLI) (Gong et al. 2008) and

Enrichment Factor (EF). The latter is considered a potent indicator for distinguishing and detecting whether the source of heavy metal pollution is anthropogenic or natural (Ozkan et al. 2012).

Touggourt city is located in the north Algerian Sahara. It is also a part Valley and known as the Upper Oued Righ. Touggourt city is characterized by having a central location, in which it lies at the junction between two national roads; N3 and N16 that connect many cities (Boulghobra et al. 2016). Accordingly, Touggourt city witnessed massive human movements throughout history and rapid expansion of urbanization and industrialization over the last decades. The Touggourt area is about 404 km², equivalent to 0.25 % of the state area. According to the 2019/2020 census, Touggourt district has a population of 200,007.

## MATERIALS AND METHODS

### Study Area

Touggourt, the capital of Oued Righ that literally means "gateway" as the historians called it because of the importance of its geographical location, which makes it a transit point and commercial center. Far away about 650 km from the capital Algiers between longitudes 5°59'20 " and 6 ° 48' 49" east of the Greenwich meridian and between two latitudes 33°12'89" and 33°85'67" north of the equator. It is 65-80 m above sea level (Daniel 1978).

In addition, the topography of the region and its suburbs is characterized by its diversity in terms of soil and vegetation as well as numerous sand dunes that surround it from east to west. It is interspersed with salt plains and some barren mud hills (Abdelhamid 1999).

Besides the agricultural land use in Touggourt, there are a lot of economic activities going on, such as oil and natural gas industries and others (Fig. 1). Hence, there are many anthropogenic sites and activities, such as fuel filling stations, factories, waste dumpsites, cars, markets, etc.

### Samples Collection, Preparation, and Analysis

Surface soil samples were collected from 18 sites after removing leaves, grasses, and other strange items at a depth of 0-10 cm using a soil auger. Table 1 provides the geographic

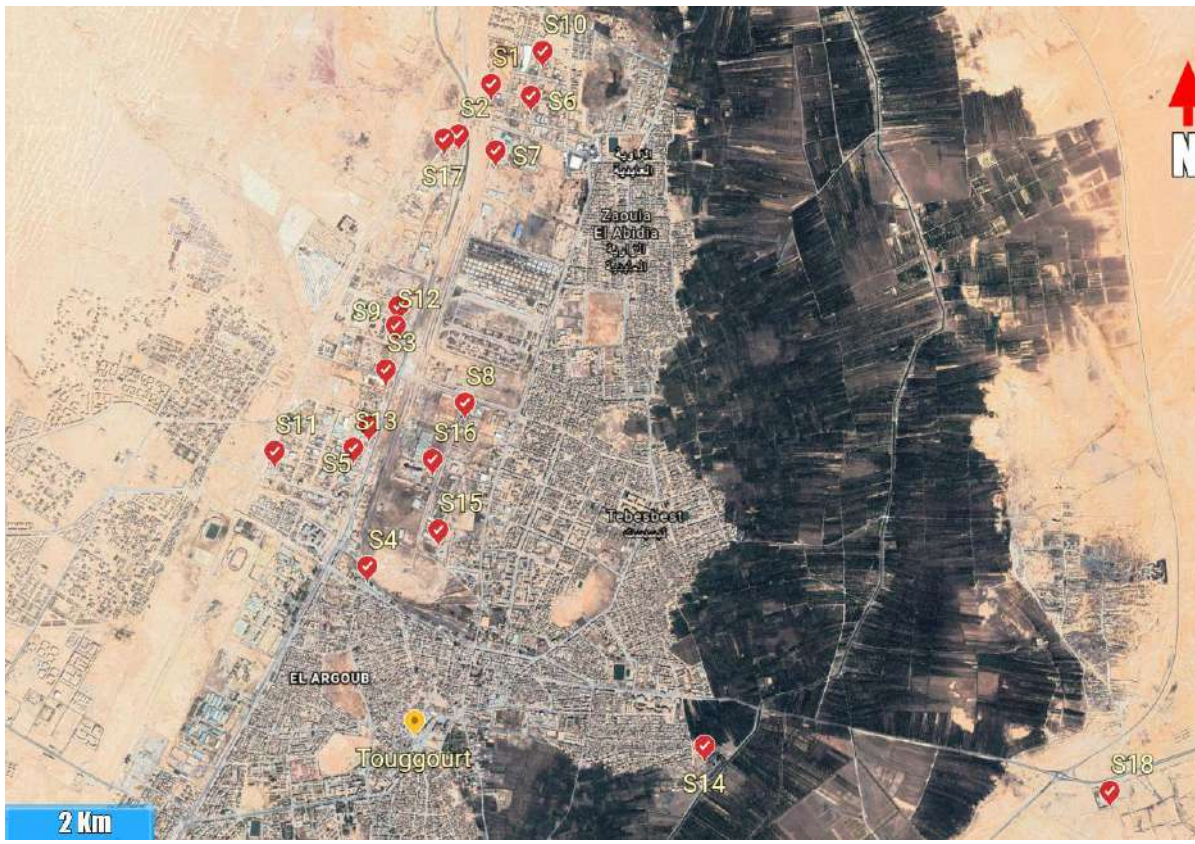


Fig. 1: Map of Touggourt city showing the locations of the sampling sites.

coordinates of sampling sites, while Fig. 1 represents the map of the study area with sampling sites on it. At each site, the samples were collected at random from 5 different points and then bulked together to ensure the representativeness and adequacy of samples. Bulked soil samples were placed on clean polyethylene plastic bags and sent to the lab for analysis. Standards were used for analysis according to the method used by Gee and Bauder (Galindo et al. 2011). First, the samples were air-dried, ground, kept in an electronic oven at 120°C for 24 h until the weight stabilized and sieved through a 0.2 µ sieve. Second, the samples were digested with acidic aqua regia solution (prepared from HCl and $HNO_3$ in ratio 1:3), where 2 g of the soil were weighted into a clean bottle. 15 mL of aqua regia were measured and added to the bottle, then the mixture was heated at a temperature of 120°C for 2 h, and then cooled at room temperature. Third, the mixture was filtered through 42 µ filter paper and kept in sealed plastic bottles (NOMA 2019). The concentrations of PTMs in these samples were detected using a flame atomic absorption spectrophotometer working with acetylene gas (Perkin Elmer, AA 900T). All tests for measuring the concentration of the following PTMS: Zn, Co, Fe, Cu, Pb and Mn were done in the Center for Scientific and Technical Research on Arid Regions (CRSTRA), Biskra (Algeria).

Table 1: Sampling sites names and geographic coordinates.

| Sampling site (s) | Longitude | Latitude |
|---|---|---|
| S1 | E 6° 43' 89'' | N 33° 85' 67'' |
| S2 | E 6° 36' 61'' | N 33° 82' 77'' |
| S3 | E 5° 60' 86'' | N 33° 13' 45'' |
| S4 | E 6° 35' 37'' | N 33° 65' 55'' |
| S5 | E 6° 36' 49'' | N 33° 81' 57'' |
| S6 | E 6° 35' 89'' | N 33° 74' 23'' |
| S7 | E 6° 48' 49'' | N 33° 82' 35'' |
| S8 | E 5° 59' 23'' | N 33° 16' 87'' |
| S9 | E 6° 35' 45'' | N 33° 75' 67'' |
| S10 | E 6° 35' 95'' | N 33° 10' 47'' |
| S11 | E 6° 32' 60'' | N 33° 72' 59'' |
| S12 | E 6° 55' 81'' | N 33° 75' 52'' |
| S13 | E 6° 35' 38'' | N 33° 73' 91'' |
| S14 | E 6° 36' 57'' | N 33° 55' 64'' |
| S15 | E 6° 40' 50'' | N 33° 76' 18'' |
| S16 | E 6° 43' 77'' | N 33° 85' 39'' |
| S17 | E 6° 34' 19'' | N 33° 76' 46'' |
| S18 | E 5° 59' 20'' | N 33° 12' 89'' |

## Pollution Indices

Assessment of the metal contamination in the soil is generally carried out by comparing the measured concentrations of PTMs in the tested soil with the geochemical background values (Pobi et al. 2020). The reference value used in the present study is based on the average continental crust of worldwide soils (Kabata-Pendias et al. 2007). Some pollution indices were used in this study, such as Contamination factor (CF), Enrichment factor (EF), and Pollution Load Index (PLI), which can determine the degree of PTMs contamination in Touggourt industrial soils and whether the source of pollution is anthropogenic or natural (Keshav & Rama 2016).

## Contamination Factor (CF)

The contamination factor is used the categorize the metals pollution degree in the study area. This factor can be computed using Equation (1):

$$CF = (Cm1)sample/Cm)background \quad \ldots(1)$$

In the above equation, the "(cm) sample" refers to the concentration of specific metal in the soil, while "(cm) Background" refers to the geochemical background reference value of the same metal (Chandrasekaran et al. 2015, Liu et al. 2005). As shown in the table below, the contamination factor was divided into four categories (Table 2).

## Enrichment Factor (EF)

The enrichment factor is considered one of the geochemical indices used for the assessment of anthropogenic pollution (Gałuszka & Migaszewski 2011). It can be computed from Equation (2):

$$CF = (Cm1)sample/Cm)background \quad \ldots(2)$$

Where (Cm/Cref Sample) is the ratio of heavy metal to the reference metal concentration in the same sample and (Cm/Cref) background is the ratio of the heavy metal to the reference metal concentration in a suitable geometrical background value (Zakir et al. 2008). Many metals have been proposed to be the potential conservative reference metal and used in literature for the measurement of the enrichment factor, such as Fe, Mn, Aluminum (Al), Scandium (Sc) Manganese (Mn), and others (Schiff & Weisberg 1999, Chen et al. 2020). Among these metals, Fe and Al are the most frequently used ones. The enrichment factor is classified into 5 categories as shown in Table 3.

## Pollution Load Index (PLI)

Pollution load index (PLI) indicator measures the cumulative metal pollution load in the study area and gives a clear picture

about the extent of PTMs toxicity in the tested soil sample through assessment of the contamination status of the soil so that the appropriate procedures for environmental protection could be taken (Hossain et al. 2015). PLI can be computed by using the CF value of every metal (Usero et al. 2000). This index is expressed by Equation (3):

$$PLI = (CF1*CF2*CF3*.....CFn) \quad ...(3)$$

Where n represents the number of metals. Parker et al. (2008) classified the Pollution Load Index (PLI) into 7 categories as shown in Table 4.

### Statistical Analysis

Results obtained from all samples were subjected to descriptive (mean, standard deviation, and ranges) statistics.

## RESULTS AND DISCUSSION

### Assessment of Level of Soil Contamination

The concentrations of PTMs in the surface soil samples taken from the study area are shown in Table 5. The spatial distribution of PTMs (Zn, Mn, Pb, Cu, Co, and Cu) from the industrial region in Touggourt were compared with their geochemical background reference level. These results indicate the variation in the average concentration of the tested PTMs, where the highest average concentration for Zn was 17.61 $mg.ml^{-1}$, 9.48 $mg.ml^{-1}$ for Fe, 5.6 $mg.ml^{-1}$ for Mn, 2.36 $mg.ml^{-1}$ for Pb, 0.7 $mg.ml^{-1}$ for Cu and 0.64 $mg.ml^{-1}$ for Co. Except for copper and cobalt, the average concentrations of the tested PTMs in the study area exceed their threshold limit values (TLV) in Algeria (OJPDRA 2006).

This contamination is a result of the solid, liquid, and gaseous wastes from the various industrial facilities within the study area that are derived from natural and anthropogenic inputs. For a better assessment of the anthropogenic inputs, computing of some pollution indices represented by the Contamination factor (CF), Pollution Load Index (PLI), and Enrichment factor (EF) is required.

### Contamination Factor (CF)

The contamination factor expresses the level of soil contamination with any heavy metal and also indicates the level of anthropogenic pollution of specific soil (Adamu et al. 2014). The CF values of metals in various sampling sites are presented in Table 6. From the results shown in Table 7, it can be noticed that the average CF values follow the ascending order of Mn < Cu < Co < Pb < Fe < Zn as shown in Table 7. All of these values belong to the low contamination factor category, CF < 1. This result indicates that the Earth's crust rocks are the main source of these metals (Szefer et al. 2008). The relatively higher CF value in the study area was for ZInc (Zn), which could be a result of the petroleum compounds emissions. In addition, the lowest CF value was for Manganese (Mn), being stable metal in the Earth's crust.

Table 2: Categories of contamination factor (CF).

| Class | CF value | Category |
|---|---|---|
| Class 1 | CF<1 | Low contamination factor |
| Class 2 | 1<CF<3 | Moderate contamination factor |
| Class 3 | 3<CF<6 | Considerable contamination factor |
| Class 4 | CF>6 | Very high contamination factor |

### Pollution Load Index (PLI)

PLI represents the number by which the heavy metal concentration in the soil exceeds its background value and it gives a clear picture of the extent of the heavy metal toxicity in the soil. It also represents the soil contamination in a certain location and it has many definitions, where it has been defined by Hakanson (1980) as the sum of contamination factor values and it has also been defined as the arithmetic mean or the geometric mean of the analyzed pollutants (Mmolawa et al. 2010).

According to the results of PLI shown in Table 8, the PLI values of all soil samples were 0 < PLI < 1 and belong to the low contamination category (PLI < 1.5). Since the pollution load index value is less than 1.5 (the error correction factor used in classification, Table 4), It does not necessarily mean that there is no intervention of anthropogenic activities in pollution induction. According to Muller (1969), PLI values less than 1.5 indicate that the source of the heavy metal is entirely from natural processes, while values greater than 1.5 suggest that the source is more likely to be anthropogenic. However, these low PLI values will not reflect the non-contamination of the studied soil samples with industrial wastes. In addition, the pollution load index value did not reach higher values because the contamination factor (CF) values of PTMs in the study area are very close to their background values in the reference soil.

Table 3: Categories of enrichment factor (EF).

| Class | EF value | Category |
|---|---|---|
| Class 1 | EF < 2 | Deficiency to minimal enrichment |
| Class 2 | 2 ≤ EF < 5 | Moderate enrichment |
| Class 3 | 5 ≤ EF <20 | Significant enrichment |
| Class 4 | 20 ≤ EF < 40 | Very high enrichment |
| Class 5 | EF ≥ 40 | Extremely high enrichment |

**Enrichment Factor (EF)**

The enrichment factor is widely used to confirm the presence and assess the magnification of the anthropogenic contamination of soil with PTMs, i.e. its value determines the degree of contamination (Barkett & Akün 2018). The results of EF of surface soils are represented in Table 9, where Fe has been chosen as a reference element for calculation. Akoto et al. (2008) illustrated that the EF values range between 0.5-1.5 indicate that the PTMs originate from natural geological processes, while the EF values greater than 1.5 indicate that the sources of the PTMs are anthropogenic processes. The EF values of PTMs in the soil of the study area in the following order Mn < Cu < Co < Pb < Zn as shown in Table 10

As given in Table 9, a significant enrichment is observed for Zn (at S7, S12, and S18), a moderate enrichment is observed for Zn and Pb (at most of the tested sites), and a

Table 4: Categories of Pollution Load Index (PLI).

| Class | PLI value | Category |
|---|---|---|
| Class 1 | PLI < 1. 5 | Clean or very low pollution |
| Class 2 | 1.5 ≤ PLI < 2 | Low pollution |
| Class 3 | 2 ≤ PLI < 4 | Moderate pollution |
| Class 4 | 4 ≤ PLI < 8 | Significant pollution |
| Class 5 | 8 ≤ PLI < 16 | Very high pollution |
| Class 6 | 16 ≤ PLI < 32 | Extremely high pollution |
| Class 7 | PLI ≥ 32 | Excessive pollution |

Table 5: Average concentration of PTMs in Touggourt industrial soil.

| Sampling site | Metal concentration (ppm) | | | | | |
|---|---|---|---|---|---|---|
| | Mn | Pb | Cu | Co | Fe | Zn |
| S1 | 7.365 | 2.025 | 0.506 | 0.447 | 7.823 | 11.820 |
| S2 | 3.856 | 0.950 | 0.500 | 0.470 | 3.463 | 4.206 |
| S3 | 3.862 | 0.562 | 0.445 | 0.384 | 3.757 | 6.225 |
| S4 | 7.467 | 2.937 | 0.645 | 0.636 | 6.283 | 14.76 |
| S5 | 6.041 | 0.817 | 2.881 | 2.777 | 80.25 | 24.86 |
| S6 | 7.044 | 0.875 | 0.703 | 0.538 | 6.908 | 22.50 |
| S7 | 5.392 | 4.084 | 0.573 | 0.499 | 5.235 | 52.49 |
| S8 | 2.254 | 0.667 | 0.260 | 0.285 | 2.338 | 9.205 |
| S9 | 3.300 | 1.534 | 0.487 | 0.508 | 4.779 | 11.06 |
| S10 | 1.212 | 0.917 | 0.292 | 0.426 | 2.237 | 8.572 |
| S11 | 25.96 | 6.134 | 0.866 | 1.011 | 19.74 | 41.84 |
| S12 | 3.068 | 6.920 | 1.394 | 0.350 | 5.302 | 42.37 |
| S13 | 3.821 | 2.171 | 0.286 | 0.338 | 2.967 | 16.42 |
| S14 | 1.416 | 1.138 | 0.319 | 0.370 | 4.455 | 5.222 |
| S15 | 3.848 | 3.118 | 0.579 | 0.367 | 3.187 | 9.011 |
| S16 | 3.464 | 1.151 | 0.348 | 0.377 | 2.879 | 5.620 |
| S17 | 9.276 | 3.033 | 1.059 | 0.926 | 8.245 | 22.330 |
| S18 | 2.106 | 3.430 | 0.372 | 0.746 | 0.770 | 8.480 |
| Background reference level (mg/kg) | 900 | 14 | 55 | 10 | 50 | 70 |
| Threshold limit value (TLV) (mg/ml) | 1 | 0.5 | 1 | 2 | 1 | 2 |

moderate enrichment for Co (at S18). However, the obtained results of EF for remaining PTMs showed very low enrichment (EF<1) in all industrial soils. Soil samples with EF > 2 for a specific metal are considered contaminated with this metal (Zakir et al. 2008). Accordingly, as shown in Table 10, most of the surface soil samples taken from the studied sites are considered contaminated with Pb and Zn, where the highest EF value for Zn was 2.608 (Moderate enrichment), while the highest EF value for Pb was 2.358 (Moderate enrichment). On the other hand, the highest EF values for Cu and Mn were recorded as 0.122 and 0.060, respectively (Deficiency to minimal enrichment) and the highest EF value for Co was recorded as 0.740 (Significant enrichment). The abundance of Zn and Pb in the soil of the Touggourt industrial region is low, but their higher enrichment suggests that Zn and Pb contamination in the study area is derived from various anthropogenic activities, such as industrial zones, especially the petroleum ones as well as gaseous emissions from traffic (Wang et al. 2017). are more likely to be the source of PTMs in the study area.

Touggourt city is characterized by the presence of high traffic density (cars, trucks, buses, agricultural tractors, motorcycles, etc.), besides the excessive use of brakes due to the irregular dump sites. Zn and Pb are classified as traf-

Table 6: Contamination factor (CF) of PTMs in soil samples of Touggourt industrial area.

| Sampling Site | Metal | | | | | |
|---|---|---|---|---|---|---|
| | Zn | Fe | Co | Cu | Pb | Mn |
| S1 | 0.168 | 0.156 | 0.044 | 0.01 | 0.145 | 0.008 |
| S2 | 0.060 | 0.069 | 0.047 | 0.01 | 0.068 | 0.004 |
| S3 | 0.088 | 0.075 | 0.038 | 0.01 | 0.040 | 0.004 |
| S4 | 0.210 | 0.126 | 0.063 | 0.011 | 0.209 | 0.008 |
| S5 | 0.355 | 1.605 | 0.277 | 0.052 | 0.058 | 0.007 |
| S6 | 0.321 | 0.138 | 0.053 | 0.012 | 0.063 | 0.007 |
| S7 | 0.749 | 0.107 | 0.049 | 0.010 | 0.292 | 0.006 |
| S8 | 0.131 | 0.046 | 0.028 | 0.004 | 0.048 | 0.003 |
| S9 | 0.158 | 0.095 | 0.050 | 0.008 | 0.109 | 0.004 |
| S10 | 0.122 | 0.044 | 0.042 | 0.005 | 0.065 | 0.001 |
| S11 | 0.597 | 0.394 | 0.101 | 0.015 | 0.438 | 0.029 |
| S12 | 0.605 | 0.106 | 0.035 | 0.025 | 0.494 | 0.003 |
| S13 | 0.234 | 0.059 | 0.033 | 0.005 | 0.155 | 0.004 |
| S14 | 0.075 | 0.089 | 0.037 | 0.006 | 0.081 | 0.002 |
| S15 | 0.128 | 0.063 | 0.036 | 0.011 | 0.222 | 0.004 |
| S16 | 0.080 | 0.057 | 0.037 | 0.006 | 0.082 | 0.004 |
| S17 | 0.319 | 0.165 | 0.092 | 0.019 | 0.216 | 0.010 |
| S18 | 0.121 | 0.015 | 0.074 | 0.007 | 0.245 | 0.002 |

Table 7: The average and range of contamination factor (CF) values of PTMs in soil samples of Touggourt industrial area.

| Metal | Contamination factor (CF) value | | Category |
|---|---|---|---|
| | Range | Average | |
| Zn | 0.06-0.749 | 0.244 | Low contamination factor |
| Fe | 0.015-1.6015 | 0.189 | // |
| Co | 0.028-0.277 | 0.059 | // |
| Cu | 0.004-0.052 | 0.012 | // |
| Pb | 0.040-0.494 | 0.155 | // |
| Mn | 0.001-0.029 | 0.006 | // |

Table 8: Pollution load index (PLI) of PTMs in soil samples of Touggourt industrial area.

| Sampling site | CF Zn | CF Fe | CF Co | CF Cu | CF Pb | CF Mn | PLI value |
|---|---|---|---|---|---|---|---|
| S1 | 0.168 | 0.156 | 0.044 | 0.010 | 0.145 | 0.008 | 0.055 |
| S2 | 0.060 | 0.069 | 0.047 | 0.010 | 0.068 | 0.004 | 0.033 |
| S3 | 0.088 | 0.075 | 0.038 | 0.010 | 0.040 | 0.004 | 0.031 |
| S4 | 0.210 | 0.123 | 0.063 | 0.011 | 0.209 | 0.008 | 0.063 |
| S5 | 0.355 | 1.605 | 0.277 | 0.052 | 0.058 | 0.007 | 0.133 |
| S6 | 0.321 | 0.138 | 0.053 | 0.012 | 0.063 | 0.007 | 0.054 |
| S7 | 0.749 | 0.107 | 0.049 | 0.010 | 0.292 | 0.006 | 0.071 |
| S8 | 0.131 | 0.046 | 0.028 | 0.004 | 0.048 | 0.003 | 0.025 |
| S9 | 0.158 | 0.095 | 0.050 | 0.008 | 0.109 | 0.004 | 0.042 |
| S10 | 0.122 | 0.044 | 0.042 | 0.005 | 0.065 | 0.001 | 0.024 |
| S11 | 0.597 | 0.394 | 0.101 | 0.015 | 0.438 | 0.029 | 0.139 |
| S12 | 0.605 | 0.106 | 0.035 | 0.025 | 0.494 | 0.003 | 0.074 |
| S13 | 0.234 | 0.059 | 0.033 | 0.005 | 0.155 | 0.004 | 0.038 |
| S14 | 0.075 | 0.089 | 0.037 | 0.006 | 0.081 | 0.002 | 0.029 |
| S15 | 0.128 | 0.063 | 0.036 | 0.011 | 0.222 | 0.004 | 0.043 |
| S16 | 0.080 | 0.057 | 0.037 | 0.006 | 0.082 | 0.004 | 0.030 |
| S17 | 0.319 | 0.165 | 0.092 | 0.019 | 0.216 | 0.010 | 0.085 |
| S18 | 0.121 | 0.015 | 0.074 | 0.007 | 0.245 | 0.002 | 0.032 |

Table 9: Enrichment factor (EF) of PTMs in soil samples of Touggourt industrial area.

| Sampling site | Metal | | | | |
|---|---|---|---|---|---|
| | Zn | Mn | Co | Cu | Pb |
| S1 | 1.079 | 0.052 | 0.286 | 0.059 | 0.924 |
| S2 | 0.868 | 0.062 | 0.679 | 0.131 | 0.980 |
| S3 | 1.184 | 0.057 | 0.511 | 0.108 | 0.534 |
| S4 | 1.678 | 0.066 | 0.506 | 0.093 | 1.669 |
| S5 | 0.221 | 0.004 | 0.173 | 0.033 | 0.036 |
| S6 | 2.326 | 0.057 | 0.389 | 0.093 | 0.452 |
| S7 | 7.162 | 0.057 | 0.477 | 0.100 | 2.786 |
| S8 | 2.812 | 0.054 | 0.609 | 0.101 | 1.019 |
| S9 | 1.653 | 0.038 | 0.531 | 0.093 | 1.146 |
| S10 | 2.737 | 0.030 | 0.952 | 0.119 | 1.464 |
| S11 | 1.514 | 0.073 | 0.256 | 0.040 | 1.110 |
| S12 | 5.708 | 0.032 | 0.330 | 0.239 | 4.661 |
| S13 | 3.953 | 0.072 | 0.570 | 0.088 | 2.613 |
| S14 | 0.837 | 0.018 | 0.415 | 0.065 | 0.912 |
| S15 | 2.020 | 0.067 | 0.576 | 0.165 | 3.494 |
| S16 | 1.394 | 0.067 | 0.655 | 0.110 | 1.428 |
| S17 | 1.935 | 0.063 | 0.562 | 0.117 | 1.314 |
| S18 | 7.866 | 0.152 | 4.844 | 0.439 | 15.909 |

fic-related metals that are the products of vehicle emission and/or mechanical wear of parts of cars (e.g. brake discs and tires). The EF value of Pb and Zn is found >1 in most of the sampling sites, suggesting that heavy traffic contributes to higher enrichment of Zn and Pb in the study area (Dytłow & Górka-Kostrubiec 2020).

## CONCLUSION

The study area is characterized by a significant number of productive facilities. It is well known that any industrial activity must leave a mark on the environmental resources surrounding it and the topsoil is surely one of the most affected resources by such industrial activities. Therefore, this current study has concluded that the study's soils content of PTMs exceeds the permissible limit, although the contamination factor results fall into the low contamination category, besides the pollution load index results, which need more detailed study. The fact that the pollution index values are in the low range does not imply that there is no contamination; rather, it reflects the high PTMs content in the reference soil, which is extremely near to the PTMs level in the study's soil samples. Hence, the most important conclusion from this study is that the anthropogenic activities are the major sources of the PTMs concentrations in the soil of the study area as shown in the computed pollution indices and this is

Table 10: The average and range of enrichment factor (EF) values of PTMs in soil samples of Touggourt industrial area.

| Metal | Enrichment factor (CF) value | | Category |
|---|---|---|---|
| | Range | Average | |
| Zn | 0.221-7.866 | 2.608 | Moderate enrichment |
| Co | 0.173-4.844 | 0.740 | Deficiency to minimal enrichment |
| Cu | 0.040-0.439 | 0.122 | Deficiency to minimal enrichment |
| Pb | 0.036-15.909 | 2.358 | Moderate enrichment |
| Mn | 0.004-0.152 | 0.060 | Deficiency to minimal enrichment |

reflected by the results of the Enrichment Factor, the main factor among the environmental pollution indices, which showed the deterioration in the soil of the study area. Detailed in-depth investigation regarding physicochemical properties of Touggourt industrial soil, bioavailable metal fractions in it, and associated health risks are still required.

## ACKNOWLEDGEMENT

The authors would like to thank the Algerian Ministry of Higher Education and Scientific Research and General Directorate of Scientific Research and Technological Development (DGRSDT) for their support and providing the necessary facilities to carry out this research.

## REFERENCES

Abdelhamid, I.Q. 1999. Definition of Oued Righ, In the Publication of Elwaffa llshahid Organization, Touugourt, Elamal for Printing, Oued Souf.

Abrahim, G. and Parker, R. 2008. Assessment of heavy metal enrichment factors and the degree of contamination in marine sediments from Tamaki estuary, Auckland, New Zealand. Environ. Monit. Assess., 136: 227-38.

Adamo, P., Agrelli, D. and Zampella, M. 2018. Chapter 9 - Chemical Speciation to Assess Bioavailability, Bioaccessibility, and Geochemical Forms of Potentially Toxic Metals (PTMs) in Polluted Soils. In De Vivo, B., Belkin, H.E. and Lima, A. (eds), Environmental Geochemistry (Second Edition). Elsevier, The Netherlands, pp. 153-94.

Adamo, P., Arienzo, M., Imperato, M. Naimo, D. and Nardi, M. 2005. Distribution and partition of heavy metals in surface and sub-surface sediments of Naples city port. Chemosphere, 61: 800-9. https://doi.org/10.1016/j.chemosphere.2005.04.001.

Adamu, S., Mangs, A., Murtala, A. and Lar, U. 2014. Assessment of potentially toxic metals in soil and sediments of the Keana Brinefield in the Middle Benue Trough, Northcentral Nigeria. Am. J. Environ. Prot., 3: 6-12.

Akoto, O., Bruce, T. and Darko, G. 2008. Heavy metals pollution profiles in streams serving the Owabi reservoir. Afr. J. Environ. Sci. Technol., 2: 354-359.

Ayangbenro, A.S. and Babalola, O.O. 2017. A new strategy for heavy metal polluted environments: A review of microbial biosorbents. Int. J. Environ. Res. Public Health, 14: 94.

Barkett, M.O. and Akün, E. 2018. Heavy metal contents of contaminated soils and ecological risk assessment in abandoned copper mine harbor in Yedidalga, Northern Cyprus. Environ. Earth Sci., 77: 378.

Boulghobra, N., N. Koull, and T. Benzaoui 2016. Four decades period of climatic data for assessing the aeolian hazard in the region of Touggourt (Low Algerian Sahara). Geographia Technica 11: 13-22. 10.21163/GT_2016.111.03.

Chandrasekaran, A., Ravisankar, R., Harikrishnan, N., Satapathy, K.K. and Prasad, M.V.R. 2015. Multivariate statistical analysis of heavy metal concentration in soils of Yelagiri Hills, Tamilnadu, India: Spectroscopical approach. Spectrochim. Acta. A, 137: 589-600.

Chen, S., Wu, C., Hong, S. and Chen, Q. 2020. Assessment, distribution and regional geochemical baseline of heavy metals in soils of densely populated area: A case study. Int. J. Environ. Res. Public Health, 17: 22-69.

Chen, T.B., Wong, J.W.C., Zhou, H.Y. and Wong, M.H. 1997. Assessment of trace metal distribution and contamination in surface soils of Hong Kong. Environ. Pollut., 96: 61-8.

Daniel, P. 1978. Systems of nomadic relations: Touggourt region, Algeria. PhD Thesis, High School of Social Sciences, France.

Dehghani, S., Moore, F., Keshavarzi, B. and Hale, B.A. 2017. Health risk implications of potentially toxic metals in street dust and surface soil of Tehran, Iran. Ecotoxicol. Environ. Safety, 136: 92-103.

Dytłow, S. and Górka-Kostrubiec, B. 2020. The concentration of heavy metals in street dust: an implication of using different geochemical background data in estimating the level of heavy metal pollution. Environ. Geochem. Health, 26: 726-735.

E, A. The Tomllinson Pollution Load Index Applied to Heavy Metals "Mussel-Watch" Data: A Useful Index to Assess Coastal Pollution. Sci. Total. Environ. 1996;187: 19-56.

Fang, T.H. and Lin, C.L. 2002. Dissolved and particulate trace metals and their partitioning in a hypoxic estuary: The Tanshui Estuary in Northern Taiwan. Estuaries, 25: 598-607.

Galindo, N., M. Varea, J. Gil-Moltó, E. Yubero, and J. Nicolás 2011. The Influence of Meteorology on Particulate Matter Concentrations at an Urban Mediterranean Location. Water, Air, & Soil Pollution 215: 365-72. 10.1007/s11270-010-0484-z.

Gałuszka, A. and Migaszewski, Z. 2011. Geochemical background: An environmental perspective. Mineralogia, 42: 7-17.

Gong, Q., Deng, J., Yunchuan, X., Qingfei, W. and Yang, L. 2008 Calculating pollution indices by heavy metals in ecological geochemistry assessment: A case study in Parks of Beijing. J. China Univ. Geosci., 19: 230-241.

Hakanson, L. 1980. An ecological risk index for aquatic pollution control: A sedimentological approach. Water Res., 14: 975-1001.

Hossain, M.A., Ali, N.M., Islam, M.S. and Hossain, H.M.Z. 2015. Spatial distribution and source apportionment of heavy metals in soils of Gebeng industrial city, Malaysia. Environ. Earth Sci., 73: 115-126.

Kabata-Pendias, A., Mukherjee,C. and Arun, B. 2007. Trace Elements from Soil to Human. Springer-Verlag, Berlin Heidelberg.

Kelly, J., Thornton, I. and Simpson, P.R. 1996. Urban geochemistry: A study of the influence of anthropogenic activity on the heavy metal content of soils in traditionally industrial and non-industrial areas of Britain. Appl. Geochem., 11: 363-70.

Keshav, K. A. and Rama, K.M. 2016. Distribution, correlation, ecological and health risk assessment of heavy metal contamination in surface

soils around an industrial area, Hyderabad, India. Environ. Earth Sci., 75: 411.

Likuku, S., Mmolawa, K. and Gaboutloeloe, G. 2013. Assessment of heavy metal enrichment and degree of contamination around the copper-nickel mine in the Selebi Phikwe region, Eastern Botswana. Environ. Ecol. Res., 1: 32-40.

Liu, W.H., Zhao, J.Z., Ouyang, Z.Y., Söderlund, L. and Liu, G.H. 2005. Impacts of sewage irrigation on heavy metal distribution and contamination in Beijing, China. Environ. Int. 31: 805-12. https://doi.org/10.1016/j.envint.2005.05.042.

Manta, D.S., Angelone, M., Bellanca, R. Neri, and M. Sprovieri, M. 2002. Heavy metals in urban soils: a case study from the city of Palermo (Sicily), Italy. Science of The Total Environment 300: 229-43. https://doi.org/10.1016/S0048-9697(02)00273-5.

Mmolawa, K., Likuku, S. and Gaboutloeloe, G. 2010. Assessment of heavy metal pollution in soils along major roadside areas in Botswana. Afr. J. Environ. Sci. Technol., 5: 221-239

Muller, G. 1969. Index of geo accumulation in sediments of the Rhine River. Geol. J., 2: 109-118.

National Office of Meteorology Algeria (NOMA). 2019. Meteorological Data. Regional Department of Touggourt, Algeria.

OJPDRA 2006. Official Journal of the People's Democratic Republic of Algeria N° 24 (Executive decree of April 15, 2006)

Ozkan, E., Bir, E., İzmir, K., Körfez, İ. and Metal, A. 2012. A new assessment of heavy metal contaminations in a eutrophicated bay (Inner Izmir Bay, Turkey). Turk. J. Fish. Aquat. Sci., 12: 135-147.

Pobi, K.K., Nayek, S., Gope, M., Rai, A.K. and Saha, R. 2020. Sources evaluation, ecological and health risk assessment of potentially toxic metals (PTMs) in surface soils of an industrial area, India. Environ. Geochem. Health, 10: 517-522.

Santos, A., Alonso, E., Callejón, M. and Jiménez, J.C. 2002. Heavy metal content and speciation in groundwater of the Guadiamar river basin. Chemosphere, 48: 279-85.

Schiff, K.C. and Weisberg, S.B. 1999. Iron as a reference element for determining trace metal enrichment in Southern California coastal shelf sediments. Marine Environ. Res., 48: 161-76.

Silva, Y.J.A.B.D., Cantalice, J.R.B., Singh, V.P., Nascimento, C.W.A.D. and Wilcox, B.P. 2019. Heavy metal concentrations and ecological risk assessment of the suspended sediments of a multi-contaminated Brazilian watershed. Acta Sci. Agron., 41: 132-143

Szefer, P., Szefer, K., Glasby, G.P., Pempkowiak, J. and Kaliszan, R. 2008. Heavy-metal pollution in surficial sediments from the Southern Baltic Sea off Poland. J. Environ. Sci. Health, 31: 2723-2754.

Usero, U., Garcia, A. and Fraidias, J. 2000. Quality of the waters and sediments of the Andalusian Coast. In: Sevilla, M. (ed.), Junta de Andalicia, 17: 164.

Victoria, A., S. Cobbina, S. Dampare, and A. Duwiejuah 2014. Heavy Metals Concentration in Road Dust in the Bolgatanga Municipality, Ghana. Int J Environ Res Public Health.

Wang, G., Zhang, S., Xiao, L., Zhong, Q. and Li, L. 2017. Heavy metals in soils from a typical industrial area in Sichuan, China: Spatial distribution, source identification, and ecological risk assessment. Environ. Sci. Pollut. Res. Int., 24: 16618-30.

Woitke, P., Wellmitz, J., Helm, D., Kube, P. and Lepom, P. 2003. Analysis and assessment of heavy metal pollution in suspended solids and sediments of the river Danube. Chemosphere, 51: 633-42.

Wuana, R.A. and Okieimen, F.E. 2011. Heavy metals in contaminated soils: A review of sources, chemistry, risks and best available strategies for remediation. ISRN Ecol., 2011: 20.

Zakir, H., Naotatsu, S. and Kazuo, O. 2008. Geochemical distribution of trace metals and assessment of anthropogenic pollution in sediments of Old Nakagawa River, Tokyo, Japan. Am. J. Environ. Sci., 4: 654-665.

Zheljazkov, V.D. and Nielsen, N.E. 1996. Effect of heavy metals on peppermint and corn mint. Plant Soil, 178: 59-66.

Nature Environment and Pollution Technology
An International Quarterly Scientific Journal

p-ISSN: 0972-6268
(Print copies up to 2016)
e-ISSN: 2395-3454

Vol. 20 | No. 5 (Suppl) | pp. 1873-1879 | 2021

Original Research Paper

https://doi.org/10.46488/NEPT.2021.v20i05.002

Open Access Journal

# Spatial Variation of Trace Metals Between Industrial and Rural Dwelling Birds of India

**M. Bala*, A. Sharma** and G. Sharma*†**
*School of Applied Sciences, Suresh Gyan Vihar University, Jaipur, Rajasthan, India
**Department of Zoology, Swargiya PNKS Government P.G. College, Dausa, Rajasthan, India
†Corresponding author: G. Sharma; gaurav.sharma@mygyanvihar.com

**Nat. Env. & Poll. Tech.**
**Website: www.neptjournal.com**

*Received:* 08-02-2021
*Revised:* 25-03-2021
*Accepted:* 30-04-2021

**Key Words:**
Trace metals
Blue rock pigeon
Anthropogenic activity
Bais Godam industrial region
Metal pollution

## ABSTRACT

A large quantity of trace metals has been continuously polluting the environment as a result of increasing urbanization and industrial processes. In 2016-2017, the metal (Cd, Cu, Cr, Ni, Pb, and Zn) levels were determined in fecal pellets of Blue Rock Pigeon (*Columba livia*) at Bais Godam (industrial location) in Jaipur and Chittora (rural location) in Rajasthan, India. Fecal pellets in industrial regions which are under higher anthropogenic influence exhibited higher metal concentrations when compared with the fecal pellets of the same species in rural area which have minimal anthropogenic input, with statistically significant industrial-rural differences in the metal concentrations except for Ni. Results obtained in this study, as well as the comparison with literature data, indicated that concentrations of Cr and Cu were high in fecal pellets of Blue Rock Pigeon in the industrial region of the present study. Furthermore, many significant correlations were also observed between metal levels in the industrial region which could be attributed to a similar source. Moreover, contamination levels of pigeon excrement serve as one of the most compelling indicators in terrestrial systems for the monitoring of metal pollution levels.

## INTRODUCTION

Heavy metal contamination is a continual global problem, especially evident in industrial regions where mobile and stationary sources discharge large quantities of pollutants comprising trace metals like nickel, zinc, iron, copper, manganese, cadmium, lead, cobalt, chromium and mercury in soil, vegetation and atmosphere exceeding the natural emission levels (Bilos et al. 2001, Chen & Chen 2001). However, a consolidation of environmental legislation, regulations, and the development of technology has resulted in diminished industrial emissions during the past decades (Kozlov et al. 2009). These metals are non-biodegradable, but they can be bio-amplified in the tropic web at low levels, making them increasingly dangerous. The level of heavy metals in birds can be analyzed in an array of samples, though records of metal content in blood, eggs, excrements, feathers, tissues, and organs dominate the literature (Markowski et al. 2013). Trace elements exposure and their lethal effects have been broadly studied among the class of aves (Berglund et al. 2014, Janssens et al. 2003, Rainio et al. 2013, Sanchez-Virosta et al. 2015). Even at concentrations that do not induce absolute mortality or other severe effects in aves, heavy metals can, nevertheless, have deep-rooted consequences in the form of increased susceptibility to infection, compromised reproductive potential, suppressed growth, developmental deformities, and changes in normal behavior (Eeva et al. 2012, Snoeijs et al. 2004, Swaileh & Sansur 2006). Previous studies have sparked interest in using avian birds as monitors for trace metal contamination at local, ancient, and global levels in the ecosystem because of their wide range of trophic occupancy in the food chain. Regular monitoring of toxic metal pollution is necessary to ensure that that there is no health threat to the biota and it is not feasible if birds were to be killed. Therefore, excrement could be a preferable alternative, as sampling is of a non-invasive type. Excreta samples have been employed seldomly than feathers; though it has been recommended by several researchers as a powerful tool for analysis of heavy metal residues (Berglund et al. 2011, Bravo et al. 2005, Costa et al. 2013, Gaba & Vashishat 2018, Sharma & Vashishat 2017). However, as far as we know, a number of articles, from different parts of the globe, have reported heavy metal contamination in pigeon excreta (Kaur & Dhanju 2013, Kler et al. 2014).

There were three specific objectives in the present study. First objective deals with measurement and evaluation of concentration of Cd, Cr, Cu, Ni, Pb, and Zn in excreta of Blue Rock Pigeon. Therefore, the present study aims at establishing baseline data about levels of metals from the Bais Godam industrial region and Chittora village. The second objective of this study was to evaluate the hypothesis that

individuals within a species have higher metal concentrations in an industrialized environment than those who live in rural areas, and finally, this study investigated whether pigeon's excrement serves as one of the most compelling indicators for the monitoring of metal pollution levels. The present research will also be useful to control pollution in relation to the health risk of biota.

## MATERIALS AND METHODS

### Study Area

The district Jaipur (26.9124° N, 75.7873° E) contains a cluster of industrial estates, some of which are part of the city and the rest of which are on the outskirts of the city. The present study picked up samples from two areas i.e. Bais Godam industrial region and Chittora as shown in Fig. 1. Bais Godam Industrial region (26.9125° N and 75.7873° E) has approximately 139 units under production which includes mechanical and electronic industries, wire and cables, dies, paint, printing and textile industries, zinc or aluminum die-casting, agricultural implements and equipments, which are thought to be the main source of metal contamination in this region. Moreover, metal loads from the industrial region are not solely due to extensive industrial operations but also comes from traffic and roads, as well as, many anthropogenic activities in high-density zones and urban activities. Furthermore, Chittora (26.6376° N, 75.7042° E) village is located approximately 38 km away in the South of Jaipur. It comes under Phagi Tehsil in Jaipur district, Rajasthan. Rural region have direct contact with nature and is under minimal anthropogenic input. These two sites i.e. industrial and rural vary markedly in terms of magnitude of human population, urban and industrial load, but they are similar in terms of the species preferred for this work that dwells at both locations. Pigeons have limited movements within their local environment and experience local pollution levels (Frantz et al. 2012). Therefore, we supposed that the phenomenon of metal contamination during bird migration is minimal, although it could never be ruled out completely. This gives a unique opportunity to make a comparison between industrial and rural areas and to determine the possible contamination, arising from different anthropogenic activities.

### Sample Preparation and Analysis

Sampling was done in six months' intervals, dry fecal pellets were collected in January and February, and in July and August in 2016 and 2017 i.e. sampling has been done four times during these 2 years. Samples were picked up from windows, rocky shelves, or accessible ledges on buildings or the roof void of a building in the industrial environment as well as from rural area in grip seal plastic bags with the help of a laboratory spatula. After that, the samples were marked with source, date, and time of collection. The excreta samples were dried at 60℃ for 24 h to attain a constant weight


Source: Base map from Google Earth

Fig. 1: Study area with sampling locations: Bais Godam; industrial region (red dot) and Chittora; rural area (blue dot).

(Janssens et al. 2003). 0.5 g of sample was weighed and their digestion was performed by keeping excreta samples on a water bath with concentrated nitric acid (Merck) and perchloric acid (Merck) in a 4:l ratio. After complete digestion, the solution was filtered using Whatman filter paper 1 and the volume was made 25 mL with distilled water. For analysis of six trace metals i.e. Cd, Cr, Cu, Pb, Ni and Zn, samples were subjected to a flame atomic absorption spectrophotometer (ZEEnit 700 P). The same is calibrated with standard solutions for the respective metals. Each analysis was performed three times and a single blank was run for 5 samples to ensure quality control. The obtained data ($mg.L^{-1}$) was converted into $\mu g.g^{-1}$. The data recorded, on a dry weight basis, is illustrated as mean ± standard deviation.

### Statistical Analysis

All statistical analysis was carried out using the Statistical Packages of Social Science (SPSS, trial version). Elemental concentration in excreta of blue rock pigeon was compared between areas (Industrial vs. Rural) using independent samples *t*-test. To check the relationship between the recorded concentrations of metals, a Pearson correlation analysis was performed. The level of significance was set at $p<0.05$.

## RESULTS AND DISCUSSION

The concentration of six trace metals was detected from the fecal pellets of the blue rock pigeon (Table 1). The fecal pellets were taken from selected industrial and rural areas for two consecutive years and examined for exposure in the environment to different trace metals at different levels. Furthermore, when compared to other metals, Cd and Zn metal appeared to have the lowest and highest concentrations respectively as average concentration levels of trace metals in industrial and rural areas were ordered (high to low) - Zn>Cu>Pb>Cr>Ni>Cd and Zn>Cu>Pb>Ni>Cr>Cd respectively.

Cadmium was the least abundant of trace metals examined in the present study. However, when compared with industrial metal concentration, Cd level was significantly low in rural area. Cd enters the industrial surroundings through its various uses like in plastics, coatings, pigments, alloys production, iron and steel fabrication, and metallurgy and metal plating. Cadmium is a highly toxic element that induces carcinogenicity in biota and also acts as a possible mutagen and teratogen (Khushwaha 2016). Our study found high concentrations of Cd in comparison to those reported by Kaur and Dhanju (2013) and Kler et al. (2014) for pigeon excrement. In general, concentrations of Cd in fecal pellets from the industrial environment of the current study were lower than those found by other authors in various avian species from around the world, such as American dipper (Morrissey et al. 2005), Black vulture (Bravo et al. 2005) and Great tit (Costa et al. 2013, Dauwe et al. 2000, 2004, Janssens et al. 2003). However, the results can also be compared to findings reported in the fecal matter of other bird species such as house crow (Sharma & Vashishat 2017), house sparrow (Pannu & Kler 2018) and spotted owlet (Gaba & Vashishat 2018) from agrifields, orchards, residential and rural areas of India. Furthermore, recommended normal range and toxic range of Cd in avian species is 0.02-1.5 $\mu g.g^{-1}$ and 70-140 $\mu g.g^{-1}$ respectively (Gaba & Vashishat 2018).

Table 1: Concentration of heavy metals in fecal pellets of pigeon from industrial and rural areas.

| Sampling sites | Sampling Year | Concentration of heavy metals ($\mu g.g^{-1}$ dw) | | | | | |
|---|---|---|---|---|---|---|---|
| | | Cd | Cr | Cu | Pb | Ni | Zn |
| Industrial | | | | | | | |
| | 2016 | 0.12 | 5.18 | 42.25 | 11.35 | 6.17 | 150.5 |
| | 2017 | 1.35 | 17.44 | 159.5 | 19.83 | 6.97 | 164.58 |
| | Mean | 0.73±0.71 | 11.31±7.35 | 100.88±68.1 | 15.57±4.95 | 6.57±1.07 | 157.54±16.3 |
| Rural | | | | | | | |
| | 2016 | ND | 5.48 | 9.18 | 5.19 | 5.23 | 49.74 |
| | 2017 | 0.47 | 6.38 | 15.38 | 8.40 | 7.82 | 112.12 |
| | Mean | 0.235±0.43 | 5.93±0.48 | 12.28±7.1 | 6.80±3.63 | 6.52±2.99 | 80.93±45.64 |
| Spatial Variation | | | | | | | |
| | *t*-value | 2.90 | 3.61 | 6.46 | 6.71 | 0.07 | 7.14 |
| | *p*-value | < 0.05 | < 0.05 | < 0.05 | < 0.05 | .948 | < 0.05 |

The data is represented as mean ± standard deviation of 20 samples (10 samples for each year) collected from both urban and rural areas. For independent samples, the *t*-value and *p*-value are used. the *t*-test is performed to compare study sites; $p<0.05$ is considered significant; ND = concentration below the instrument detection limit.

Chromium is an essential element that is required by the body to execute many specific functions. But, it becomes toxic whenever it exists above the threshold level and severely affects the early embryonic development, hatching, and even viability of a bird (Kertesz & Fancsi 2003). Worldwide, there are few reports on the occurrence of Cr in the fecal pellets of wild avian species. Furthermore, excrement from the studied industrial region is contaminated with significantly high Cr concentrations as compared to the rural area. Anthropogenic activities such as cement manufacturing, steel and iron fabrication, metal plating, dyes and pigments, tanning, wood preserving, and textile industries might have resulted in Cr contamination in the studied environment. The concentration of Cr found in our industrial area was higher than those reported in previous studies in fecal pellets of pigeon (Kaur & Dhanju 2013, Kler et al. 2014) but was comparable with those documented for other avian species from agricultural and rural areas of India (Gaba & Vashishat 2018, Pannu & Kler 2018, Sharma & Vashishat 2017). Moreover, Cr concentrations found in the present study were also higher than the findings of Janssens et al. (2003) conducted on excreta of great tit inhabiting near a pollution source. Furthermore, recommended normal concentration range of Cr for avian species is 0.05-0.4 $\mu g.g^{-1}$ and the toxic concentration range is 19-170 $\mu g.g^{-1}$ (Gaba & Vashishat 2018). However, a comparison of our results with documented research clearly signalled a severe Cr contamination in our industrial region.

The essential element, copper is the second most abundant of heavy metals examined in the present study. However, the measured Cu value in excrement samples in the rural area was significantly lower than that obtained from the industrial region. Cu pollution in our industrial area could be caused by its widespread use in electrical wiring and equipment, alloys production, electroplating, leather processing, wood perseverates and paints, agricultural chemicals, textiles and automobile industries. Cu is needed in low concentration to meet many physiological requirements but high dose and chronic exposure may pose serious hazardous effects including damage to endocrine, gastrointestinal, hematologd ical, hepatic, reproductive and respiratory systems as well as causing carcinoma (Abdullah et al. 2015, ATSDR 2004). Conversely, recorded Cu concentration from our industrial area was higher than those reported for same or similar birds, not only from agricultural and rural areas of India (Kaur & Dhanju 2013, Pannu & Kler 2018, Sharma & Vashishat 2017) but also from most polluted areas worldwide (Dauwe et al. 2000, 2004, Costa et al. 2013). Indeed, Cu concentrations found in the present study were also higher than the findings of Bravo et al. (2005) and Morrissey et al. (2005) conducted on excreta of black vulture and American dipper respectively. Furthermore, the normal recommended range of Cu for avian species is 3-15 $\mu g.g^{-1}$ (Gaba & Vashishat 2018). As a result, a comparison to the literature reveals that this bird species is highly exposed to Cu in the examined industrial zone.

According to Hashmi et al. (2013), the avian community is exposed to lead is reported to have a reduction in body weight and reproductive impairment. Furthermore, rural area is associated with the significantly lower value of Pb than industrial region under study. Pb in the industrial environment of the present study may be contributed by several sources including lead paints and acid batteries, rubber products, steel fabrication, glass, and electronic industries. However, the Pb concentration in our samples from the industrial region was higher than those reported by other studies in pigeon excrement from orchids, agricultural and residential areas from India (Kaur & Dhanju 2013, Kler et al. 2014). Further, the Pb concentration found in the industrial region is also higher than those previously documented for other avian species (Costa et al. 2013, Morrissey et al. 2005). Moreover, previous studies on polluted environments (Dauwe et al. 2000, 2004, Janssens et al. 2003) detected considerably higher concentrations of this toxic metal in the excrement of Great tit as compared to present work. Gaba and Vashishat (2018) and Pannu and Kler (2018) also recorded high Pb concentration in fecal pellets of spotted owlet and house sparrow respectively than our present study. The recommended normal range of Pb in avian species is 0.01-1 $\mu g.g^{-1}$. The toxic range that has been defined for Pb in avian species is 8-1600 $\mu g.g^{-1}$ (Gaba & Vashishat 2018).

Ni is extensively distributed in the environment due to its various agricultural and industrial uses. In the current study, the level of Ni recorded from the industrial region was comparable to the rural area. This ubiquitous metal is widely used in the metallurgical and electroplating operations, production of nickel, steel and iron alloys, manufacturing of electrical appliances such as Ni-Cd batteries, automobile, chemical industries, especially as pigments and catalysts which contribute towards the Ni burdens in the studied industrial environment. In views of Samal & Mishra (2011) and Van Wyk et al. (2001), Ni concentration above the required level can cause DNA damage, vomiting, asthma, birth abnormalities, and disrupts functions of vital organs thereby affecting the health of organisms. The Ni concentration observed in the industrial environment of the present study was relatively in accordance or lower compared to the levels reported by other studies in the Indian subcontinent (Kaur & Dhanju 2013, Kler et al. 2014, Gaba & Vashishat 2018, Pannu & Kler 2018, Sharma & Vashishat 2017). Furthermore, the value found in the industrial area of our study was far lower than previously reported for nickel levels in excrements of great tit inhabiting near to a contamination source (Dauwe et al.

2000, 2004; Janssens et al. 2003). The normal recommended range of Ni for avian species is 0.04-0.13 $\mu g.g^{-1}$. The toxic range of Ni in birds varies between 10-12 $\mu g.g^{-1}$ (Gaba & Vashishat 2018).

Zinc is an essential element of the body as it is involved in body formation and protection against renal Cr toxicosis (Malik & Zeb 2009) though toxicities of Zn and Cu develop at doses that are much higher than environmental levels (Wright & Welbourn 2002). According to Carpenter et al. (2004), Zn can induce toxic effects on the kidneys and also impairs reproduction. In our study, the avian excrements exhibited the highest concentrations of Zn among all the studied metals and differed significantly between the studied areas. The reason for such concentration in our study may be related to numerous Zn sources in the studied industrial area such as electroplating, metal casting in the automobile industry, iron and steel fabrication, plastics, motor oil hydraulic fluid, tire dust, zinc, or aluminum die-casting, pigments, paint and Zn alloys. Zn concentration in excreta of blue rock pigeon in orchids, agrifields, and residential areas of Ludhiana, India (Kaur & Dhanju 2013) was higher than observed in the present study. Furthermore, the level of Zn reported in the industrial area was also lower than the levels reported by Bravo et al. (2005), Costa et al. (2013), Dauwe et al. (2000, 2004), Janssens et al. (2003), and Morrissey et al. (2005). Moreover, the normal and toxic range of Zn for birds is 22-40 $\mu g.g^{-1}$ and 300-800 $\mu g.g^{-1}$respectively (Gaba & Vashishat 2018).

On the other hand, metal concentrations were however also recorded from the rural area. The possible source of metals for later include vehicle emission, residential burning (burning of firewood) and nearby agriculture practices. Overall, results for concentrations of metals in fecal pellets from the rural area of the current study were lower than the data obtained by other authors in the same or similar birds in different parts of the world (Bravo et al. 2005, Dauwe et al. 2000, Gaba & Vashishat 2018, Kaur & Dhanju 2013, Pannu & Kler 2018, Sharma & Vashishat 2017). The significant rural-industrial differences are probably due to different exposure at these locations due to nearby industries, traffic, urban areas, and agricultural land. Furthermore, because of elemental interaction, and the concentration and composition of certain metals may influence their impact on aves, the source of pollution and environmental state of the study site plays an essential role (Turzanska-Pietras et al. 2018). In addition to the site, sex, age, morphological and physiological aspects are relevant factors to consider in biomonitoring studies (Zarrintab et al. 2016) that can account for variation in the pattern of bio-accumulation and ultimately excretion in wild populations with recent exposure to high concentrations of these metals. Furthermore, comparison of the repercussions of toxic metals in the fecal matter of avian species is very challenging, due to interspecies variation in bionomics, particularly diet, including their potential to stand against and eliminate metal load (Koivula & Eeva 2010). There are studies that spotlighted considerable differences in metals accumulation and excretion in even closely-related species (Burger & Gochfeld 2009, Eeva et al. 2009, Hofer et al. 2010) such as pigeon and ringdove i.e. trace metals content in pigeon feces were lower than ring dove inhabiting the same area (Kler et al. 2014). This may be associated with variations in their detoxification capacity or antioxidant defense.

### Correlation Between Heavy Metal Concentrations

The assessment of the correlation between heavy metal levels is eye-catching since the metals may display synergism or antagonism effects from one to another. This can cause effects on their concentration levels. Furthermore, correlation coefficients indicate that accumulated correlating metals in birds are of the same origin because the coefficient among metal concentrations increases with the pollution levels (Silva et al. 2018)**.** In the present study, the results of Pearson correlation analysis between the metals from the industrial site are presented in Table 2. These results indicate that metal combinations showing strong positive correlations like Cd-Cr, Cd-Cu, Cd-Pb, Cr-Cu, Cr-Cu, Cu-Pb and Ni-Zn may have a similar source of origin. However, such associations between metals are obscure and remain to be investigated further.

## CONCLUSION

The study offers a new insight to educate about levels of contamination in the industrial region and rural area. It was shown that the highest metal values in fecal pellets of Blue Rock Pigeons are found in the investigated industrial region rather than the rural area. These site-specific differences could be due to different emission sources of heavy metals in different sites. Further, the results obtained in this study, as well as the comparison with literature data indicated that concentrations of Cr and Cu were high in fecal pellets of Blue Rock Pigeon in the industrial region of the present study. This may indicate the influence of anthropogenic activities on the deposition of heavy metals in the ambient environment. Therefore, efforts should be made to minimize hazardous metals' access to the environment to counteract their bioaccumulation and, as a result, their poisonous effect on bird species. The analysis of toxic metals at different sites of Rajasthan may help to assess the status of metal exposure in the excrement of aves giving, in turn, a clue to the toxicity of metal emissions globally. In addition, contamination levels of pigeon's excrement serve as one of the most compelling

Table 2: Pearson correlation coefficients between metal concentrations in the excrement of pigeon from the industrial environment.

| | Cd | Cr | Cu | Pb | Ni | Zn |
|---|---|---|---|---|---|---|
| Cd | 1 | | | | | |
| Cr | 0.95[a] | 1 | | | | |
| Cu | 0.98[a] | 0.96[a] | 1 | | | |
| Pb | 0.94[a] | 0.91[a] | 0.92[a] | 1 | | |
| Ni | 0.35 | 0.48[a] | 0.41 | 0.43 | 1 | |
| Zn | 0.50[a] | 0.66[a] | 0.57[a] | 0.55[a] | 0.70[a] | 1 |

[a]Correlation is significant at the 0.05 level.

indicators in terrestrial systems for the monitoring of metal pollution levels.

## ACKNOWLEDGEMENTS

Immeasurable appreciation and deepest gratitude to Dr. Asha Sharma, Associate Professor in Zoology and Dr. Gaurav Sharma, Professor in Microbiology for their guidance, worthy support, and cooperation through all the phases of the present study and authors are also very grateful to the Suresh Gyan Vihar University, Jaipur and Rajasthan state pollution control board, Jaipur for catering mandatory facilities to execute this research work.

## REFERENCES

Abdullah, M., Fasola, M., Muhammad, A., Malik, S.A., Bostan, N., Bokhari, H., Kamran, M.A., Shafqat, M.N., Alamdar, A., Khan, M., Ali, N. and Eqani, S.A.M.A.S. 2015. Avian feathers as a non-destructive biomonitoring tool of trace metals signatures: A case study from severely contaminated areas. Chemosphere, 119: 553-561.

ATSDR (Agency for Toxic Substances and Disease Registry). 2004. Toxicological Profile for Copper. U.S. Department of Health and Human Services, Atlanta, GA.

Berglund, A.M.M., Koivula, M.J. and Eeva, T. 2011. Species- and age-related variation in metal exposure and accumulation of two passerine bird species Environ. Pollut., 159: 2368-2374.

Berglund, A.M.M., Rainio, M.J., Kanerva, M., Nikinmaa, M. and Eeva, T. 2014. Antioxidant status in relation to age, condition, reproductive performance, and pollution in three passerine species. J. Avian Biol., 45(3): 235-246.

Bilos, C., Colombo, J.C., Skorupka, C.N. and Presa, M.J.P. 2001. Source, distribution, and variability of airborne trace metals in La Plata City area, Argentina. Environ. Pollut., 111: 149-158.

Bravo, A., Marinela, C., Azuero, S. and Salas, R. 2005. Heavy metal levels in plasma and fecal material samples of the black vulture (*Coragyps atratus*). Rev. Cient., 15(4): 319-325.

Burger, J. and Gochfeld, M. 2009. Comparison of arsenic, cadmium, chromium, lead, manganese, mercury, and selenium in feathers in a bald eagle (*Haliaeetus leucocephalus*), and comparison with common eider (*Somateria mollissima*), glaucous-winged gull (*Larus glaucescens*), pigeon guillemot (*Cepphus columba*), and tufted puffin (*Fratercula cirrhata*) from the Aleutian Chain of Alaska. Environ. Monit. Assess., 152: 357-367.

Carpenter, J.W., Andrews, G.A. and Beyer, W.N. 2004. Zinc toxicosis in a free-flying trumpeter swan (*Cygnus buccinator*). J. Wildl. Dis., 40(4): 769-774.

Chen, Y. and Chen, M. 2001. Heavy metal concentrations in nine species of fishes caught in coastal waters of Ann-ping SW Taiwan. J. Food Drug Anal., 9: 107-114.

Costa, R.A., Eeva, T., Eira, C., Vaqueiro, J. and Vingada, J.V. 2013. Assessing heavy metal pollution using Great Tits (*Parus major*): feathers and excrements from nestlings and adults. Environ. Monit. Assess., 185(6): 5339-5344.

Dauwe, T., Bervoets, L., Blust, R., Pinxten, R. and Eens, M. 2000. Can the excrement and feathers of nestling songbirds be used as biomonitors for heavy metal pollution? Arch. Environ. Contam., 39: 227-234.

Dauwe, T., Bervoets, L., Blust, R., Pinxten, R. and Eens, M. 2004. Relationships between metal concentrations in great tit nestlings and their environment and food. Environ. Pollut., 131(3): 373-380.

Eeva, T., Ahola, M. and Lehikoinen, E. 2009. Breeding performance of blue tits (*Cyanistes caeruleus*) and great tits (*Parus major*) in a heavy metal polluted area. Environ. Pollut., 157: 3126-3131.

Eeva, T., Belskii, E., Gilyazov, A.S. and Kozlov, M.V. 2012. Pollution impacts bird population density and species diversity at four non-ferrous smelter sites. Biol. Conserv., 150(1): 33-41.

Frantz, A., Pottier, M.A., Karimi, B., Corbel, H., Aubry, E., Haussy, C., Gasparini, J. and Castrec-Rouelle, M. 2012. Contrasting levels of heavy metals in the feathers of urban pigeons from close habitats suggest limited movements at a restricted scale. Environ. Pollut., 168: 23-28.

, Y. and Vashishat, N. 2018. Estimation of heavy metal residues in excreta of spotted owlet (*Athene brama*) and barn owl (*Tyto alba*) from agroecosystems of Punjab. J. Entomol. Zool., 6(3): 525-529.

Hashmi, M.Z., Malik, R.N. and Shahbaz, M. 2013. Heavy metals in eggshells of cattle egret (*Bubulcus ibis*) and little egret (*Egretta garzetta*) from the Punjab province, Pakistan. Ecotoxicol. Environ. Saf., 89: 158-165.

Hofer, C., Gallagher, F.J. and Holzapfel, C. 2010. Metal accumulation and performance of nestlings of passerine bird species at an urban brownfield site. Environ. Pollut., 158: 1207-1213.

Janssens, E., Dauwe, T., Pinxten, R., Bervoets, L., Blust, R. and Eens, M. 2003. Effects of heavy metal exposure on the condition and health of nestlings of the great tit (*Parus major*), a small songbird species. Environ. Pollut., 126(2): 267-274.

Kaur, N. and Dhanju, C. K. 2013. Heavy metals concentration in excreta of free-living wild birds as an indicator of environmental contamination. The Bioscan, 8(3): 1089-1093.

Kertesz, V. and Fancsi, T. 2003. Adverse effects of (surface water pollutants) Cd, Cr, and Pb on the embryogenesis of the mallard. Aquat. Toxicol., 65(4): 425-433.

Kler, T.K., Vashishat, N. and Kumar, M. 2014. Heavy metal contamination in excreta of avian species from Ludhiana district of Punjab. Int. J. Adv. Res., 2(7): 873-879.

Khushwaha, S. 2016. Heavy Metal concentrations in feathers of critically-endangered long-billed vultures (*Gyps Indicus*) in Bundelkhand Region, India. Int. J. Life Sci. Sci.Res., 2(4): 365-375.

Koivula, M.J. and Eeva, T. 2010. Metal-related oxidative stress in birds. Environ. Pollut., 158(7): 2359-2370.

Kozlov, M., Zvereva, E. and Zverev, V. 2009. Impacts of Point Polluters on Terrestrial Biota: Comparative Analysis of 18 Contaminated Areas. Springer, Dordrecht, The Netherlands.

Malik, R.N. and Zeb, N. 2009. Assessment of environmental contamination using feathers of Bubulcus ibis L., as a bio-monitor of heavy metal pollution, Pakistan. Ecotoxicology, 18(5): 522–536.

Markowski, M., Kalinski, A., Skwarska, J., Wawrzyniak, J., Banbura, M., Markowski, J., Zielinski, P. and Banbura, J. 2013. Avian feathers as bioindicators of the exposure to heavy metal contamination of food. Bull. Environ. Contam. Toxicol., 91(3): 302-305.

Morrissey, C.A., Bendell-Young, L.I. and Elliott, J.E. 2005. Assessing trace-metal exposure to American dippers in mountain streams of southwestern British Columbia, Canada. Environ. Toxicol. Chem., 24: 836-845.

Pannu, K.K. and Kler, T.K. 2018. Heavy metal contamination in excreta of house sparrow (*Passer domesticus*) from rural areas of Ludhiana. J. Entomol. Zool., 6(1): 77-81.

Rainio, M.J., Kanerva, M., Salminen, J.P., Nikinmaa, M. and Eeva, T. 2013. Oxidative status in nestlings of three small passerine species exposed to metal pollution. Sci. Total Environ., 454: 466-473.

Samal, L. and Mishra, C. 2011. Significance of nickel in livestock health and production. Int. J. Agro Vet. Med. Sci., 5(3): 349-361.

Sanchez-Virosta, P., Espin, S., Garcia-Fernandez, A.J. and Eeva, T. 2015. A review on exposure and effects of arsenic in passerine birds. Sci. Total Environ., 512: 506-525.

Sharma, C. and Vashishat, N. 2017. Assessment of heavy metals in excreta of house crow (*Corvus splendens*) from different Agroecosystems of Ludhiana. J. Entomol. Zool., 5(4): 1891-1895.

Silva, R.C., Saiki, M., Moreira, E.G. and Oliveira P.T. 2018. The great egret (*Ardea alba*) as a bioindicator of trace element contamination in the Sao Paulo metropolitan region, Brazil. J. Radioanal. Nucl., 315(3): 447-458.

Snoeijs, T., Dauwe, T., Pinxten, R., Vandesande, F. and Eens, M. 2004. Heavy metal exposure affects the humoral immune response in a free-living small songbird, the great tit (*Parus major*). Arch. Environ. Contam., 46: 399-404.

Swaileh, K.M. and Sansur, R. 2006. Monitoring urban heavy metal pollution using the house sparrow (*Passer domesticus*). Environ. Monit. Assess, 8(1): 209-213.

Turzanska-Pietras, K., Chachulska, J., Polechonska, L. and Borowiec, M. 2018. Does heavy metal exposure affect the condition of Whitethroat (*Sylvia communis*) nestlings? Environ. Sci. Pollut., 25(8): 7758-7766.

Wright, D.A. and Welbourn, P. 2002 Metals and other inorganic chemicals. In: Wright, D.A. and Welbourn, P. (Eds.), Environmental Toxicology. Cambridge University Press, Cambridge, pp. 249-348.

Van Wyk, E., Van der Bank, F.H., Verdoorn, G. H. and Hofmann, D. 2001. Selected mineral and heavy metal concentrations in blood and tissues of vultures in different regions of South Africa. J. Anim. Sci., 31(2): 57-63.

Zarrintab, M., Mirzaei, R., Mostafaei, G., Dehghani, R. and Akbari, H. 2016. Concentrations of metals in feathers of magpie (*Pica pica*) from Aran-O-Bidgol City in Central Iran. Bull. Environ. Contam. Toxicol., 96(4): 465-471.

Nature Environment and Pollution Technology
An International Quarterly Scientific Journal

p-ISSN: 0972-6268
(Print copies up to 2016)
e-ISSN: 2395-3454

Vol. 20 | No. 5 (Suppl) | pp.1881-1886 | 2021

Original Research Paper

https://doi.org/10.46488/NEPT.2021.v20i05.003

Open Access Journal

# Biomimetically Generated Nanoparticles in Boosting the Performance of Microbial Fuel Cells

**S. A. Abbasi*†, Tabassum-Abbasi** and Pratiksha Patnaik***

*Centre for Pollution Control & Environmental Engineering, Pondicherry University, Chinakalapet, Puducherry-605 014, India

**School of Engineering, University of Petroleum and Energy Studies, Bidholi, Dehradun-248007, India

†Corresponding author: S. A. Abbasi; abbasi.cpee@gmail.com

**Nat. Env. & Poll. Tech.**
**Website: www.neptjournal.com**

*Received:* 26-02-2021
*Revised:* 20-04-2021
*Accepted:* 29-04-2021

**Key Words:**
Microbial fuel cells
Catalysts
Gold nanoparticle
Silver nanoparticle
Waste treatment

## ABSTRACT

Studies are presented in the context of the past attempts at finding nanocatalysts that can boost the performance of microbial fuel cells (MFCs) — in terms of waste treatment and energy generation. Given the great potential of biomimetically synthesized nanoparticles (BMNPs) in providing less expensive and more environmentally friendly alternatives to NPs synthesized by physical and chemical methods, as well as a near-total lack of previous work in this area, the current research was undertaken. Effect of gold and silver nanoparticles (NPs), synthesized biomimetically using five freely available weeds, was assessed as catalysts in the MFCs. In all cases, the nanoparticles were seen to enhance the coulombic efficiency (reflective of the reduction in the waste's organic carbon load), maximum attainable power density, and overall energy yield of the MFCs by >200% relative to the uncatalyzed MFCs. Gold nanoparticles were more effective than silver nanoparticles by ≥ 20%. The results reveal that biomimetically synthesized NPs can be highly effective in reducing the operational costs as well as ecological footprints of MFCs and further work should be focused on NPs of non-precious metals.

## INTRODUCTION

### The Economic Unviability of Microbial Fuel Cells (MFCs) and the Need to Remedy it

As reviewed by us recently (Tabassum-Abbasi et al. 2019), microbial fuel cells (MFCs) have been explored extensively in recent years for the dual objective of generating energy while treating organic waste. Despite having aroused expectations that they may provide an avenue for waste cleaning as well as energy production (Moqsud et al. 2013, Rahimnejad et al. 2015, Kumar et al. 2018), MFCs have not become economically viable due to their high cost, added to their significant ecological footprint. Life cycle analyses have shown time and again that from their birth to decommissioning, MFCs consume much more energy than they generate (Tabassum-Abbasi et al. 2019). For this reason, most contemporary research on MFCs is devoted to improving their economic viability by reducing their fabrication and operational costs along with improving their efficiency (Kodali et al. 2018, Palanisamy et al. 2019).

### Factors that Have Led to the Exploration of Nanoparticles

The ability of an MFC to treat wastewater and generate energy is directly influenced by the rate at which redox reactions take place in its substrate (Rodrigo et al. 2007, Rittman et al. 2008). During the initial phase of MFC research, compounds called 'mediators'– which could induce electrons to come out from the cells of growing microorganisms and supply them to the anode – were tried to boost the redox reactions. But the mediators turned out to be either toxic to the microorganisms or were too expensive to be viable, or both (Mustakeem 2015, Santoro et al. 2017).

The next emphasis was on the use of catalysts, abiotic as well as biotic. Abiotic catalysts, based either on platinum group metals (PGMs), or other metals (OMs), have since been explored extensively (Noori et al. 2020). However, PGM catalysts are not only expensive but they may also be poisoned, which is a problem in MFCs that use wastewater as a source of energy. The OM catalysts, especially carbon-based ones, have shown greater resistance towards deactivation (Firdous et al.2018, Palanisamy et al. 2019), but their catalytic efficiency has not been adequate (Pan et al. 2016, Santoro et al.2017).

This background has prompted efforts on the use of nanoparticles in speeding up the redox reactions occurring in the MFCs. Nano catalysts derived from platinum group metals (PGMs), other metals (OMs), and non-metals (NMs), have been explored. The reports published so far on these catalysts have been reviewed by Rajalakshmi (2019) and Noori et al.

(2020). The reviews reveal that the use of NPs in MFCs is an emerging area, with less than 100 reports published so far. And nearly all of the reports have been on the use of NPs synthesized by chemical or physical methods. But it is well-known that both these routes entail large ecological footprints, consuming significant quantities of energy and/or materials (Ganaie et al. 2019). The chemical routes also lead to pollutant emissions (Rajalakshmi 2019). In contrast, biomimetic methods of NP synthesis, especially the ones involving extracts of plants (botanical species), are benign and non-toxic, involving only a little use of energy and causing no emissions because the spent plants can be vermicomposted (Ganaie et al. 2019, Rajalakshmi 2019). These authors and others have further enhanced the eco-friendliness of biomimetic NP synthesis methods by utilizing aquatic and terrestrial weeds such as water hyacinth, lantana, ipomoea, mimosa, pistia parthenium, and coral vine (Ganaie et al. 2014, 2015, 2016a, 2017, Pirathiba et al. 2018). Such weeds are widely and freely available and have no acknowledged utility. They, rather, harm the environment by monopolizing the natural resources of the areas they colonize and inflict great damage to biodiversity (Ganaie et al. 2016b, 2016c). Hence harvesting them for the purpose of NP synthesis reduces the harm to the environment they would otherwise cause.

From the foregoing, it emerges that the use of biomimetically synthesized NPs (BMNPs) in MFCs has the potential of reducing the latter's ecological footprint. But this avenue is almost totally unexplored so far with only a solitary report by Harshiny et al. (2017). These authors synthesized iron oxide NPs using the leaf extract of amaranthus (*Amaranthus dubius*) and then coated carbon paper with it for use as electrodes in MFCs. They found that coating of the NPs led to a 31% enhancement in the accruable power density, attaining 145.5 $mW.m^{-2}$. The NP coating also led to 68.5% COD removal efficiency as compared to 63.1% achieved in the bare electrode, even as anodic charge transfer resistance decreased by the NPs.

Available reports on the use of NPs synthesized with chemical or physical methods (Rajalakshmi 2019, Noori et al. 2020) show that NPs help in increasing MFC performance by reducing the biofouling caused by fungi such as *Cladosporinm* spp and *Aspergillus* spp, thereby reducing ohmic over potential and proportionately enhancing the MFC's energy output. They also enhance the oxygen release rate (ORR), a major step in MFC functioning (Li et al. 2016, Anusha et al. 2018); thus serving as efficient electrochemical catalysts.

Besides single-element NPs like AgNPs, the NPs of silver, gold, manganese oxide, titanium oxide, vanadium pentoxide, etc, either coated upon or in general modified with carbon paper or nanotubes, have been explored in enhancing the waste reduction and energy generation capabilities of MFCs (Naruse et al. 2011, Alatraktchi et al. 2012, Kalathil et al. 2013, Noori et al. 2016, Sui et al. 2017, Zakaria et al. 2018). All the studies have indicated a beneficial effect which makes a strong case for exploring the use of BMNPs so that similar or better benefits can be achieved but at much lesser costs and much greater eco-friendliness. This report is a step in that direction.

### The Present Work

In the present work, we have explored the use of AgNPs and AuNPs, in boosting MFC performance. The NPs were biomimetically synthesized using aqueous extracts of obnoxious and freely available weeds lantana (*Lantana camara*), water hyacinth (*Eichhornia crassipes*), mimosa (*Mimosa pudica),* parthenium (*Parthenium hysterophorus*), and coral vine (*Antigono nleptopus*). No past report of this kind is available. Another highlight of this study is that the MFC chambers were linked through a salt bridge rather than a membrane, as most other authors have done. We have done this switch because membranes are not only costlier than salt bridges by several orders of magnitude but also cause a much greater burden on the environment than the salt bridge during their manufacture and decommissioning. Even otherwise, whereas membranes have some advantages in comparison to salt brides, they are also besieged with serious drawbacks (Rajalakshmi 2019).

## MATERIALS AND METHODS

Duel-chambered MFCs of 1500 mL capacity were fabricated with 3 mm thick plastic (Fig. 1). The chambers were linked via a salt bridge, containing agar (3%, w/v) and NaCl (10%, w/v). Twenty-two such units were deployed.

The energy source was an aqueous solution of glucose (1 $g.L^{-1}$), inoculated with 0.1 $g.L^{-1}$ fresh cow dung as the microorganism source. Phosphate buffer (100 mm) was used as the catholyte. The electrodes comprised copper rods with a surface area of 8.5 $mm^2$.

### The MFCs

The anodic chambers were sealed with an epoxy resin to maintain anaerobic conditions. It was possible to do it because the MFCs were operated in batch mode. Otherwise, for continuously operated MFCs, it is necessary to provide feed inlet and $CO_2$ outlet in the anode chamber. On the other hand, the aerobic atmosphere was ensured at the cathode chamber by providing a hole at its top for the passage of air.

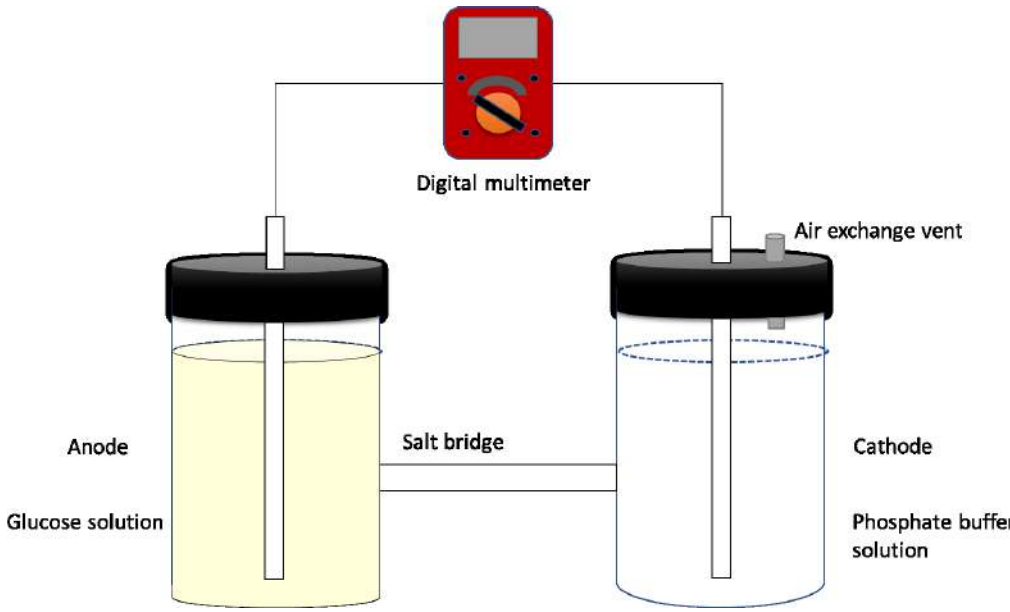


Fig. 1: The schematic of the MFCs.

All the units were housed in a common room so as to be at identical temperature (30 ± 4ºC). Two of the MFCs were used as controls. The MFC voltage was recorded using a Haoyue (DT 830D) digital multimeter. The other 20 MFCs contained duplicate sets spiked with AuNPs or AgNPs synthesized from the corresponding weeds, as shown in Table 1. Adequate quantities of the NPs were added to the catholyte to attain a concentration of 0.02 mg.$L^{-1}$ in the catholyte solution.

### Quantifying MFC Performance Indicators

Besides peak voltage (PV), the other MFC performance indicators were computed as follows.

Maximum power density (MPD)

$$= \frac{Power}{Electorde\ surface\ area}, \frac{mW}{m^2}$$

$$\text{Coulombic efficiency (CE)} = \frac{Ci - Cf}{Ci} \times 100, \text{ as \%}$$

Where Ci and Cf represent Ci-initial COD (mg.$L^{-1}$) and Cf-final COD (mg.$L^{-1}$).

$$\text{Total energy output}(\text{TEO}), \text{ in watts} = \int_{t_1}^{t_2} Pt.dt$$

Where P is power and was obtained by measuring areas under the wattage-time curves of which a typical one is shown in Fig. 2.

## RESULTS AND DISCUSSION

The results are summarized in Table 1. The information has been presented in terms of a) the peak voltage (PV) which reflects the maximum deliverable power by an MFC; b) the coulombic efficiency (CE) which is a measure of the ability of the MFC to treat the given organic waste, and c) the total energy generated by the MFC. Since the electrodes of all the MFCs had identical surface areas, the maximum power density (MPD) values are directly proportional to the PV values in the present investigation.

The control MFC could deliver a PV and a total energy output (TEO) of only 131 ± 2 mV and 20mW, respectively. But the use of either of the NPs boosted the PV by 5-7 times. The TEO was spiked to similar extents.

The AuNPs of all the weeds were seen to enhance the MFC performance to a greater extent than their AgNPs; the difference being statistically significant at > 99% confidence level. The order in which the nature of the weed influenced the PVs attained by the corresponding AuNPs was *L. camara* > *A. leptopus* > *E. crassipes* > *M. pudica* > *P. hysterophorus.*

The order for the PVs attained with AgNPs was similar except that the AgNP of *M. pudica* led to slightly better PV than the AgNPs of *E. crassipes*. The CE values, the MPD values, and the TEO essentially followed the order of the PV values.

Compared to the MPD of 145.5 mV.$m^{-2}$ attained in the lone previous report on the use of BMNPs in MFCs — by

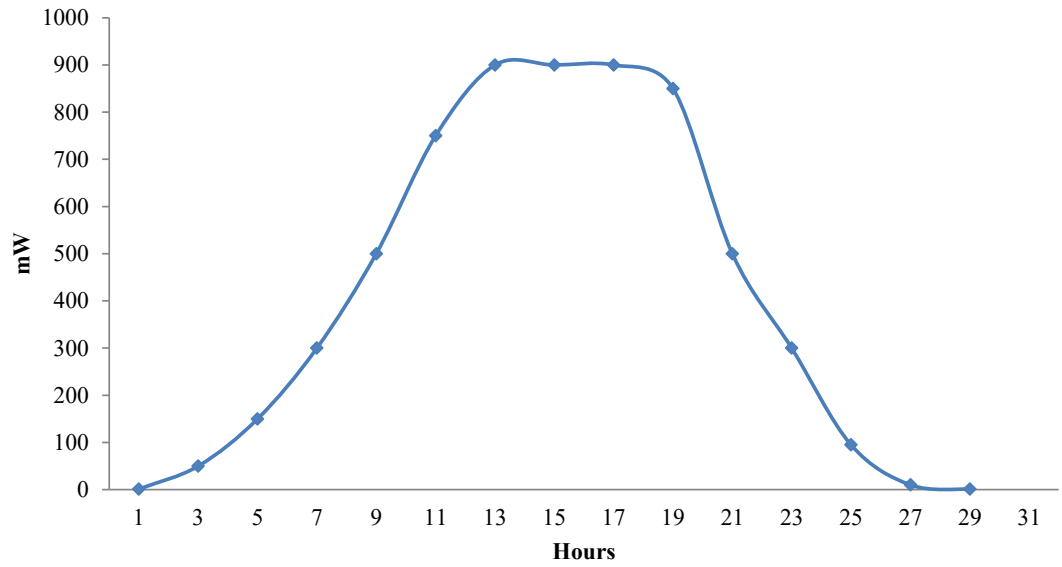


Fig. 2: A typical watt-time curve of the power generated by the MFCs used in the present study. This curve pertains to AuNP synthesized with the SLE of *A. leptopus.*

Table 1**:** Effect of gold and silver nanoparticles synthesized from 5 pernicious weeds on the efficacy of the MFCs. All the MFCs had anodes of 1500 mL capacity, and in each, MFC glucose solution (1 $g.L^{-1}$) and phosphate buffer solution (100 mm) were used as an anolyte and catholyte, respectively. Their copper electrodes were connected with a salt bridge.

| The plant utilized | NP Used | Peak voltage, (mV)* | Coulombic Efficiency, % | Maximum power density attained, ($mW.m^{-2}$) | Total energy output, (mW) |
|---|---|---|---|---|---|
| None | - | 131 ± 2 | 21 | 23 | 20 |
| *Lantana camara* | Au | 948± 3 | 80 | 133 | 121 |
| *Eichhornia crassipes* | Au | 916± 2 | 77 | 129 | 114 |
| *Mimosa pudica* | Au | 907 ± 3 | 78 | 125 | 133 |
| *Parthenium hysterophorus* | Au | 841 ± 1 | 68 | 106 | 108 |
| *Antigonon leptopus* | Au | 921± 2 | 66 | 89 | 119 |
| *L. camera* | Ag | 771 ± 3 | 59 | 78 | 89 |
| *E. crassipes* | Ag | 735 ± 1 | 59 | 77 | 86 |
| *M. pudica* | Ag | 741 ± 2 | 55 | 74 | 87 |
| *P. hysterophorus* | Ag | 677± 2 | 51 | 61 | 86 |
| *A. leptopus* | Ag | 739 ± 1 | 53 | 72 | 96 |

* Average of duplicates

Harshiny et al. (2017), the maximum MPD attained by the MFCs in the present report is 133 $mV.m^{-2}$. But these authors have used a salt bridge instead of a membrane. Its advantage in terms of lower cost and ecological footprint more than compensates for marginally lower MPD.

As for the comparison with past work on the use of NPs synthesized by chemical or physical methods in catalyzing MFCs, it is seen that the MPDs/PVs generated by our MFCs have been superior to the MFDs/PVs attained with those NPs in several cases. For instance, Kalathil et al. (2013), using a plain carbon paper modified with a composite of carbon nanotube (NT) and $MnO_2$ NPs, attained an MPD of 120 ± 1.7 $mW.m^2$. Asghary et al. (2019), employing a carbon paste electrode (GPE), combined with CNT and AuNPs, achieved an MPD of 80 $mW.m^{-2}$. Khajeh et al. (2020) electrochemically deposited CuO/ZnO NPs on a graphite cathode used in MFC to obtain an MPD of 51.9 $mW.m^{-2}$. By using NPs of $Cu_2O$ in conjunction with reduced grapheme oxide cathode in their MFC, a PV of 223 mV was realized (Xin et al. 2020) in comparison to the PVs of 677-948 achieved by the authors in the current work.

Fan et al. (2007) had obtained an MPD of 74.4 $mW.m^{-2}$ from MFCs spiked with AuNPs while in all the MFCs reported in this paper, the MPD values have been significantly higher at 89-133 $mW.m^{-2}$.

As for coulombic efficiency, only nine of the past authors, as reviewed by Rajalakshmi (2019), have reported it. In six of those studies, the efficiencies obtained have been lesser than the maximum of 80% obtained achieved by the present MFCs. Given that all the past authors have achieved enhancement in the performance of their MFCs using the highly expensive Nafion membrane, or a cation exchange membrane, we have attained the same using only the inexpensive salt bridge.

The work described in this paper is based on the BMNPs of Ag and Au because these two metals have been most extensively studied of all BMNPs. But further work should aim at the use of less expensive metals and metal oxides to bring down the MFC cost.

## CONCLUSION

This paper has presented studies on the performance of biomimetically synthesized gold and silver nanoparticles (BMNPs), using the weeds lantana (*Lantana camara),* water hyacinth (*Eichhornia crassipes*), mimosa *(mimosa pudica),* coral vine *(Antigonon leptopus)*, and parthenium (*Parthenium hysterophorus)* in boosting energy output from microbial fuel cells (MFCs). Dual compartment, batch fed, MFCs of 1500 mL capacity in which salt bridge was used as the electrode interface, were employed for the purpose. The study is the first of its kind because only one previous report exists on the use of BMNPs in enhancing MFC performance and none deal with the use of weeds, or salt bridge, or report overall energy yield.

It was seen that the NPs of both the metals with all the five weeds enhanced the MFC performance several times as compared to the control MFCs.

All the NP-spiked MFCs had peak voltage, coulombic efficiency, and energy output that were favorably comparable to the ones achieved by previous authors using NPs generated by chemical or physical means.

## ACKNOWLEDGEMENT

SAA thanks Indian National Science Academy (INSA), New Delhi, for support.

## REFERENCES

Alatraktchi, F.A., Zhang, Y., Noori, J.S. and Angelidaki, I. 2012. Surface area expansion of electrodes with grass-like nanostructures and gold nanoparticles to enhance electricity generation in microbial fuel cells. Bioresour. Technol., 123: 177-183.

Anusha, G., Noori, M.T. and Ghangrekar, M.M. 2018. Application of silver-tin dioxide composite cathode catalyst for enhancing the performance of microbial desalination cell. Mater. Sci. Energy Technol., 11: 78-99.

Asghary, M., Raoof, J.B., Rahimnejad, M. and Ojani, R. 2019. Usage of gold nanoparticles/multi-walled carbon nanotubes-modified CPE as a nano-bioanode for enhanced power and current generation in a microbial fuel cell. J. Iran. Chem. Soc., 16(8): 1677-1685.

Fan, Y.Z., Hu H.Q. and Liu, H. 2007. Enhanced Coulombic efficiency and power density of air-cathode microbial fuel cells with an improved cell configuration. Power Sources, 171: 383-354.

Firdous, S., Jin, W., Shahid, N., Bhatti, Z.A., Iqbal, A., Abbasi, U., Mahmood, Q. and Ali, A. 2018. The performance of microbial fuel cells treating vegetable oil industrial wastewater. Environ. Technol. Innov., 10: 143-151.

Ganaie, S.U, Rajalakshmi, R., Abbasi, T. and Abbasi, S.A. 2017. Clean green synthesis of silver nanoparticles with shape/size control using aquatic weed Pistia stratiotes and their antioxidant, antibacterial, and catalytic activity. J. Indian Chem. Soc., 94: 1203-1212.

Ganaie, S.U., Abbasi, T. and Abbasi, S.A. 2016a. Low-cost, environment-friendly synthesis of palladium nanoparticles by utilizing a terrestrial weed Antigononleptopus. Part. Sci. Technol., 34(2): 201-208.

Ganaie, S.U., Abbasi, T. and Abbasi, S.A. 2016b. Green synthesis of silver nanoparticles using an otherwise worthless weed mimosa (Mimosa pudica): Feasibility and process development towards shape/size control. Part. Sci. Technol., 33: 638-644.

Ganaie, S.U., Abbasi, T. and Abbasi, S.A. 2016c. Utilization of the terrestrial weed Antigononleptopusin the rapid and green synthesis of stable gold nanoparticles with shape/size control. Environ. Prog. Sustain. Energy, 1(3): 1-7.

Ganaie, S.U., Abbasi, T., Anuradha, J. and Abbasi, S.A. 2014. Biomimetic synthesis of silver nanoparticles using the amphibious weed ipomoea and their application in pollution control. J. King Saud. Univ. Sci., 26: 222-229.

Ganaie, S.U., Rajalakshmi, R., Abbasi, T. and Abbasi S.A. 2019. Green synthesis of silver nanoparticles by coral vine and assessment of their properties. Bioinspired Biomim. Nanobiomater., 15: 45-69

Ganaie, S.U., Ravindran, S., Abbasi, T. and Abbasi, S.A. 2015. Rapid and clean biomimetic synthesis of bimetallic Au-Ag nanoparticles using an otherwise worthless and noxious weed ipomoea (Ipomoea carnea). J. Nano Res., 31: 1-14.

Harshiny, M., Samsudeen, N., Kameswara, R.J. and Matheswaran, M. 2017. Biosynthesized FeO nanoparticles coated carbon anode for improving the performance of microbial fuel cells. Int. J. Hydrog. Energy, 42: 26488-26495.

Kalathil, S., Nguyen, V.H., Shim, J.J., Khan, M.M., Lee, J. and Cho, M.H. 2013. Enhanced performance of a microbial fuel cell using CNT/MnO2 nanocomposite as a bioanode material. J. Nanosci. Nanotechnol., 13(11): 7712-7716.

Khajeh, R.T., Aber, S. and Nofouzi, K. 2020. Efficient improvement of microbial fuel cell performance by the modification of graphite cathode via electrophoretic deposition of CuO/ZnO. Mater. Chem. Phys., 240: 122208.

Kodali, M., Herrera, S., Kabir, S., Serov, A., Santoro, C., Ieropoulos, I. and Atanassov, P. 2018. Enhancement of microbial fuel cell performance by introducing a nano-composite cathode catalyst. Electrochimicaacta, 265: 56-64.

Kumar, R., Singh, L.A., Wahid, Z., Mahapatra, D.M. and Liu, H. 2018. Novel mesoporous MnCo2O4 nanorods as oxygen reduction catalyst at neutral pH in microbial fuel cells. Bioresour. Technol., 254: 1-6.

Li, D., Liu, J., Qu, Y., Wang, H. and Feng, Y. 2016a. Analysis of the effect of biofouling distribution on electricity output in microbial fuel cells. RSC Adv., 10: 039

Moqsud, M.A., Omine, K., Yasufuku, N., Hyodo, M. and Nakata, Y. 2013.

Microbial fuel cell (MFC) for bioelectricity generation from organic wastes. Waste Manage., 33(11): 2465-2469.

Mustakeem, M. 2015. Electrode materials for microbial fuel cells: Nanomaterial approach. Mater. Renew. Sustain. Energy, 4: 22

Naruse, J., Sugano, Y., Ikeuchi, T., Yoshikawa, H., Saito, M. andTamiya, E. 2011. Development of biofuel cells based on gold nanoparticle decorated multi-walled carbon nanotubes. Biosens. Bioelectron., 30(1): 204-210.

Noori, M.T., Ghangrekar, M.M. and Mukherjee, C.K. 2016. V2O5 micro flower decorated cathode for enhancing power generation in air-cathode microbial fuel cell treating fish market wastewater. Int J. Hydrog. Energy, 41(5): 3638-3645.

Noori, M.T., Ghangrekar, M.M., Mukherjee, C.K. and Min, B. 2020. Biofouling effects on the performance of microbial fuel cells and recent advances in biotechnological and chemical strategies for mitigation. Biotechnol. Adv., 65: 107420.

Palanisamy, G., Jung, H.Y., Sadhasivam, T., Kurkuri, M.D., Kim, S.C. and Roh, S.H. 2019. A comprehensive review on microbial fuel cell technologies: Processes, utilization, and advanced developments in electrodes and membranes. J. Cleaner Prod., 221: 598-621.

Pan, Y., Mo, X., Li, K., Pu, L., Liu, D. and Yang, T. 2016. Iron–nitrogen–activated carbon as cathode catalyst to improve the power generation of single-chamber air-cathode microbial fuel cells. Bioresour. Technol., 206: 285-289.

Pirathiba, S., Ganaie, S.U., Rajalakshmi, R., Abbasi, T. and Abbasi, S.A. 2018. Synthesis of AuNPs with catalytic and antioxidant properties using the dreaded weed mimosa. Bioinspired Biomim. Nanobiomater., 7: 1-11

Rahimnejad, M., Adhami, A., Darvari, S., Zirepour, A. and Oh, S.E. 2015. The microbial fuel cell as new technology for bioelectricity generation: A review. Alex. Eng. J., 54(3): 745-756.

Rajalakshmi, R. 2019. An approach towards energy conservation and process simplification in the biomimetic synthesis of nanoparticles. Thesis, Pondicherry University, Pondicherry, pp. 1-310.

Rittman, B.E., Krajmalnik-Brown, R. and Halden, R.U. 2008. Pre-genomic, genomic, and post-genomic study of microbial communities involved in bioenergy. Nat. Rev. Microbiol., 6(8): 604-612.

Rodrigo, M.A., Canizares, P., Lobato, J., Paz, R., Sáez, C. and Linares, J.J. 2007. Production of electricity from the treatment of urban wastewater using a microbial fuel cell. J. Power Sources, 169(1): 198-204.

Santoro, C., Arbizzani, C., Erable, B. and Ieropoulos, I. 2017. Microbial fuel cells from fundamentals to applications. A review. J. Power Sources, 356: 225-244.

Sui, M., Dong, Y., Wang, Z., Wang, F. and You, H. 2017. A biocathode-driven photocatalytic fuel cell using an Ag-doped TiO<inf>2</inf>/Ti mesh photoanode for electricity generation and pollutant degradation. J. Photochem. Photobiol. A Chem., 348: 238-245.

Tabassum-Abbasi, T., Abbasi, T. and Abbasi, S.A. 2019. Microbial fuel cells as the source of clean energy potential and pitfalls. Nat. Environ. Pollut. Technol., 18(3): 789-797.

Xin, S., Shen, J., Liu, G., Chen, Q., Xiao, Z., Zhang, G. and Xin, Y. 2020. Electricity generation and microbial community of single-chamber microbial fuel cells in response to Cu2O nanoparticles/reduced graphene oxide as a cathode catalyst. Chem. Eng. J., 380: 122446.

Zakaria, B.S., Barua, S., Sharaf, A., Liu, Y. and Dhar, B.R. 2018. Impact of antimicrobial silver nanoparticles on anode respiring bacteria in a microbial electrolysis cell. Chemosphere, 213: 259-267.

Nature Environment and Pollution Technology
An International Quarterly Scientific Journal

p-ISSN: 0972-6268
(Print copies up to 2016)
e-ISSN: 2395-3454

Vol. 20 | No. 5 (Suppl) | pp. 1887-1894 | 2021

Original Research Paper

https://doi.org/10.46488/NEPT.2021.v20i05.004

Open Access Journal

# Biogas Production and Greenhouse Gas (GHG) Emissions Reduction due to Use of Biogas Digesters in Small Farms in Quang Tri Province, Vietnam

**H.T. Hoang* and T. Kato**†**

*Graduate School of Environmental Engineering, The University of Kitakyushu, Kitakyushu, Fukuoka 808-0135, Japan
**Faculty of Environmental Engineering, The University of Kitakyushu, Kitakyushu, Fukuoka 808-0135, Japan
†Corresponding author: T. Kato; tkato@kitakyu-u.ac.jp

**Nat. Env. & Poll. Tech.**
**Website: www.neptjournal.com**

*Received:* 14-06-2021
*Revised:* 28-06-2021
*Accepted:* 03-09-2021

**Key Words:**
Biogas digester
Livestock waste treatment
Greenhouse gas reduction
Environmental impacts
Biogas production

## ABSTRACT

This research aims to assess the greenhouse gas (GHG) emissions reductions due to the use of biogas technology in Quang Tri Province. With a total of over 354,000 cattle in Quang Tri Province, Vietnam, waste from livestock becomes large. The GHG emitted from the livestock industry is not small, affecting the environment. Currently, there is little concern or documentation about the reduction of GHG emissions in small farms using biogas digesters in central Vietnam. This province has applied technological solutions, typically biogas digesters, but the amount of biogas production is not calculated accurately. Our survey was conducted in Vinh Linh District and Cam Lo District in March 2019 and involved 50 farms equipped with biogas digesters and 20 farms without it. The respondents were selected based on the information provided by local authorities, satisfying two conditions: livestock households and biogas users. The former group was asked 25 questions and the latter was asked 10 questions needed to calculate GHG emissions such as the number of animals and petroleum gas/firewood consumption. This study uses formulas described in the 2006 guideline issued by IPCC to estimate reduced GHG emissions. The results showed that the average biogas production is 5.52 $m^3$.household$^{-1}$.day$^{-1}$. Only 2% of the farms made the best use of the biogas digester. The surveyed households have not really used the most optimal amount of biogas production. In this scenario, this study recommends some solutions for solving the problem. In addition, the average annual emissions before having a biogas digester are estimated to be 20.53 tons $CO_2$e/household/year. After using the biogas, the GHG emissions are reduced to 4.52 t$CO_2$e.household$^{-1}$.day$^{-1}$. Thus, the replacement of daily cooking energies with biogas helps reduce 16.01 t$CO_2$e of greenhouse gas for each farm per year.

## INTRODUCTION

With the current growth of the livestock industry in Vietnam, based on calculations based on animal physiological science and statistics, it can be seen that the solid waste emissions of livestock raising rate increases according to the scale growth, with the average emission estimated at 1.5 kg of pig manure.head$^{-1}$.day$^{-1}$, 15 kg of buffalo, cow manure.head$^{-1}$.day$^{-1}$, and 0.2 kg of poultry manure.head$^{-1}$.day$^{-1}$ (Quang Tri Department of Agriculture and Rural Development 2016). The average annual emission from the entire country's livestock population is much more than 85 million tonnes, with tens of billions of cubic meters of liquid waste and hundreds of millions of tonnes of gas waste. However, the management and treatment of animal waste have not been given due attention. The main reason is due to the low awareness and responsibility of farm owners. Most farmers do not have proper waste treatment measures, thus environmental pollution in livestock has not been completely overcome and tends to increase.

In this circumstance, low-cost biogas digesters are a good selection for reducing environmental impacts and improving the standard of living of rural families. Low-cost digesters are considered to be a clean and environmentally friendly technology that can help small-scale farmers to treat livestock waste in a sustainable way while producing biofertilizer (digestate) and meeting their energy needs (i.e., by providing biogas) (Kinyua et al. 2016). Biogas refers to the collection of gases from the decomposition and fermentation of animal, human, and plant waste resulting from the lack of oxygen and the activities of anaerobic bacteria in anaerobic digestion. This is an effective way of minimizing the negative impacts of animal waste on the environment and human health. Since the installation of the biogas digester, pollution has been reduced, households can now use the gas produced, and also families have a clean environment, which helps people get out of the air pollution caused by animal waste. Realizing the potential benefits from biogas, the Vietnamese government, local authorities, as well as farmers, have decided to invest in this renewable technology. The number of household biogas digesters has considerably increased in Vietnam during the past two decades (Nguyen 2011, Nguyen et al. 2012). According to Teune (2007), there

were over 200,000 small-scale biogas digesters in use in Vietnam in 2007. This figure continued to rise, with around 500,000 biogas digesters installed in livestock farms across the country (Mayhew 2015, Ho et al. 2015).

Nowadays, global warming and climate change are issues of great concern. Even though environmental advantages are more significant when biogas production fully satisfies a family's cooking needs or in large-scale projects, household biogas digesters offer a viable approach for reducing GHG emissions. Biogas digesters are currently used for cooking and lighting in many developing countries and can provide an alternative energy source from traditional fuels such as firewood and liquefied petroleum gas (Hessen 2014, Mengistu et al. 2015, Roopnarain & Adeleke 2017). Zhang et al. (2013) showed that the long-term, stable running of a household biogas technology is potential in quantifying carbon emission reduction in rural China. The use of biogas technology has led to a dramatic reduction in the consumption of fossil fuels, and a reduction in fueling problems, especially in rural areas of the developing country.

This study aims to make an assessment of biogas production in Quang Tri Province located in the central of Vietnam. In addition, a study was conducted to determine the potential for household-scale biogas digesters to reduce GHG emissions from livestock production, thereby analyzing the development potential of biogas digesters in Vietnam.

## MATERIALS AND METHODS

### Research Materials

Our data compilation comprised both primary and secondary data. The primary data of the study was gathered via the questionnaire-based survey. An in-person interview was conducted in Vinh Linh District and Cam Lo District in Quang Tri Province as shown in Fig. 1 from February 26$^{th}$ to March 7$^{th}$, 2019 by the first author of this article. The survey involved 70 households including 50 farms equipped with a biogas digester and 20 farms without it. The 25-item questionnaire was used to conduct in-person interviews of the 50 households with a biogas digester. The remaining 20 households without a biogas digester were interviewed with a questionnaire consisting of 10 questions. The questionnaire was created to collect detailed information about household biogas use in terms of economic, environmental, and social factors such as the number of pigs that households are raising, and the consumption of fuel (i.e., gas, firewood, coal, etc.) before and after the installation of the digester. This interview method was combined with site visits to biogas digesters to collect reliable information. The secondary techno-economic data was gathered from the Department of Agriculture and Rural Development in Quang Tri Province.

### Research Methods

The statistical methods used in this study to obtain the key results are explained below.

### Method of Calculating the Amount of Biogas Produced

This research uses the feedstock use method from International Renewable Energy Agency (IRENA) to calculate the amount of biogas production and consumption. According to IRENA, there are five methodologies for estimating biogas production. Estimates can be based on digester capacity, appliance use, or feedstock use, or by comparing the fuel use in households with and without a biogas digester. Biogas production may also be measured directly.

Here, the feedstock use method is used to calculate the amount of biogas produced. This method calculates the biogas production based on feedstock use rather than assumptions about the capacity utilization of biogas digesters. To apply this method, it is necessary to collect data on digester sizes, digester technology, and feedstock use. Biogas production is calculated for a wide range of temperatures and retention times, as follows (IRENA 2016 p.16):

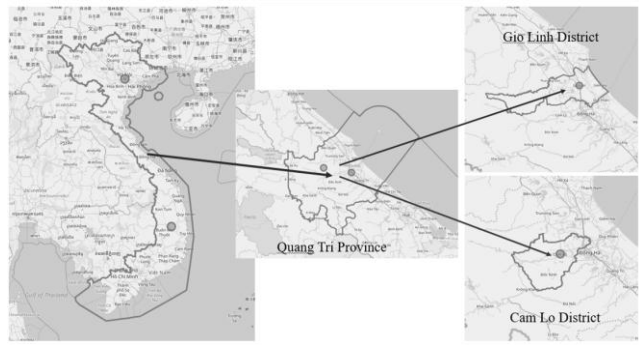


Fig. 1: The map of the survey area.
(OpenStreetMap is used for these maps)

$$G = \frac{Y \times V_d \times S}{1000}$$

Where:
$G$ = the biogas production, $m^3.day^{-1}$
$Y$ = a yield factor based on temperature and the feedstock retention time
$V_d$ = the biogas digester volume, $m^3$
$S$ = the initial concentration of volatile solids in the slurry, $kg.m^{-3}$

The digester volume ($V_d$) was obtained by asking the farmers in our survey. The initial concentration of volatile solids ($S$) was calculated as follows. First, the total feedstock volume was estimated. In the two districts in Quang Tri Province selected for this research, the main input source of biogas digesters is pig manure. The surveyed households did not have a large population of cows, buffaloes, or poultry, and the amount of manure from these animals was small. Thus, we considered only pig manure. According to Table 5 in IRENA (2016), the total animal waste feedstock per day for each pig is 5 kg, of which the volatile solids account for 1 kg. These numbers were multiplied by the number of pigs reported in our survey to estimate the total daily weight of animal waste and volatile solids. Assuming that 1 kg of animal waste is approximately equal to a volume of 1 L, we obtained the volume of the pig waste. This waste volume was multiplied by 3 to obtain the daily feedstock volume, because we learned that the local government recommended that farmers add a volume of water equal to as much as twice the volume of waste to operate the digesters. The initial concentration of volatile solids ($S$) was calculated by dividing the daily weight of volatile solids by this daily feedstock volume. To determine the yield factor ($Y$) from Table 7 in IRENA (2016), the temperature in the digester and the feedstock retention time ($R$) are necessary. The average temperature in Quang Tri Province is 25°C (Doan et al. 2014), and the digester temperature is 2°C higher when the digester is located underground; thus, the temperature range is 25-27°C. The feedstock retention time was estimated by dividing the digester volume by the daily feedstock volume.

## Method of Calculating Greenhouse Gas Emissions Reduction

The effect of reducing greenhouse gas emissions when using biogas is realized by calculating the difference between the amount of greenhouse gas emissions before and after the use of biogas digesters by households. Following the guidance of the Intergovernmental Panel on Climate Change (IPCC 2006), a number of key greenhouse gases have been selected to calculate emissions from manure pits, fuel combustion, and biogas leakage. In addition, the parameters used for calculating greenhouse gas emissions are also referenced by IPCC (2006). Fig. 2 shows the system boundary of greenhouse gas emissions calculation before and after using the biogas digesters that were used for calculating in this study.

The process of calculating the amount of greenhouse gas emissions before using the biogas digesters is made according to the following formulas:

## Calculating the Average GHG Emissions Before the Households Use the Biogas Digesters (IPCC 2006)

***Step 1:*** Determining $CH_4$ emission factor from pig manure

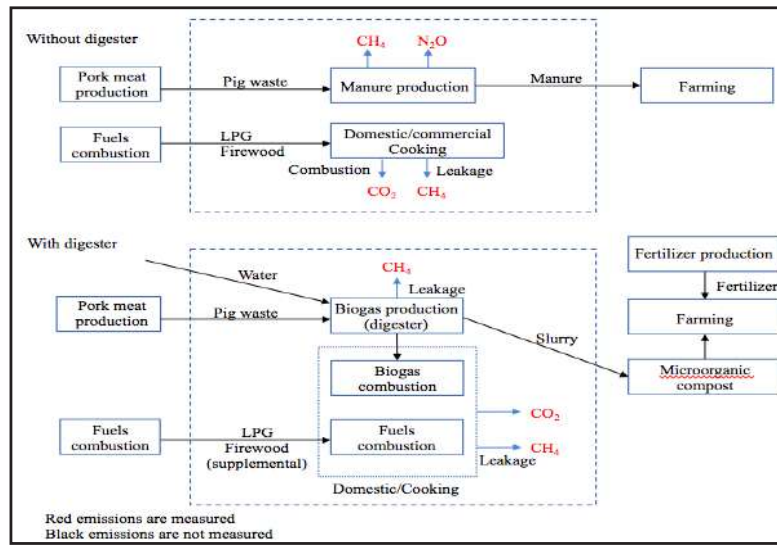


Fig. 2: System boundary of greenhouse gas emissions calculation before and after using the biogas digesters.

corresponding to climatic conditions of Quang Tri Province

$$EF_{(T)} = \left(VS_{(T)} \times 365\right) \times \left[B_{o(T)} \times 0.67 kg/m^3 \times \sum_{S,k} \frac{MCF_{S,k}}{100} \times MS_{(T,S,k)}\right] \quad \ldots(1)$$

Where:

$EF_{(T)}$ = annual $CH_4$ emission factor for livestock category $T$, kg.$CH_4$.animal$^{-1}$.year$^{-1}$

$VS_{(T)}$ = daily volatile solid excreted for livestock category $T$, kg.dry matter$^{-1}$.animal. $^{-1}$.day$^{-1}$

*365* = basis for calculating annual VS production, days/year

$B_{o(T)}$ = maximum methane producing capacity for manure produced by livestock category $T$, m$^3$.$CH_4^{-1}$.kg$^{-1}$ of VS excreted

*0.67* = conversion factor of m$^3$.$CH_4^{-1}$ to kg.$CH_4^{-1}$

$MCF_{(S,k)}$ = methane conversion factors for each manure management system $S$ by climate region $k$, %

$MS_{(T, S,k)}$ = fraction of livestock category $T$'s manure handled using manure management system $S$ in climate region $k$, dimensionless

According to IPCC (2006), the calculation coefficients are as follows: the annual average temperature of Quang Tri Province is 25ºC, the daily volatile solid (*VS*) excreted from pigs is 0.30 kg per head, maximum methane producing capacity by pig $B_o$ is 0.29 m$^3$.kg$^{-1}$ of *VS* excreted, methane correction factor *MCF* for the manure treatment system is 65%, the handled fraction of manure management *MS* equals to 100%.

***Step 2:*** *Calculating $CH_4$ emission factor from manure management:*

$$CH_{4(manure)} = GWP_{CH_4} \times N_{(T)} \times EF_{(T)} \times 10^{-3} \quad \ldots(2)$$

Where:

$CH_{4(manure)}$ = $CH_4$ emissions from manure management, for a defined population, t$CO_2$e.year$^{-1}$

$GWP_{CH4}$ = 28: the possibility of causing $CH_4$ greenhouse effect compared to $CO_2$

$EF_{(T)}$ = emission factor for the defined livestock population, kg $CH_4$.head$^{-1}$.year$^{-1}$

$N_{(T)}$ = the number of head of livestock species/category $T$ in the country

$T$ = species/category of livestock

***Step 3:*** *Calculating direct $N_2O$ emissions from manure management*

$$N_2O_{(manure)} = GWP_{N_2O} \times \left[\sum_S \left[\sum_T (N_{(T)} \times N_{ex(T)} \times MS_{(T,S)}\right] \times EF_{3(S)}\right] \times \frac{44}{28} \times 10^{-3} \quad \ldots(3)$$

Where:

$N_2O$ = direct $N_2O$ emissions from manure management in the country, t$CO_2$e.year$^{-1}$

$GWP_{N2O}$ = 265: the possibility of causing greenhouse effect of $N_2O$ compared to $CO_2$

$N_{(T)}$ = number of head of livestock species/category $T$ in the country

$N_{ex(T)}$ = annual average N excretion per head of species/category $T$ in the country, kg.N$^{-1}$.animal$^{-1}$.year$^{-1}$

$MS_{(T, S)}$ = fraction of total annual nitrogen excretion for each livestock species/category $T$ that is managed in manure management system $S$ in the country, dimensionless

$EF_{3(S)}$ = emission factor for direct $N_2O$ emissions from manure management system S in the country, kg.$N_2O$-N.kg.N$^{-1}$ in manure management system $S$

$S$ = manure management system

$T$ = species/category of livestock

*44/28* = conversion of ($N_2O$-N) $_{(mm)}$ emissions to $N_2O_{(mm)}$ emissions

Table 1: Thermal parameters and emission factors of some fuels following IPCC (2006).

| Type of fuel | Heat [MJ.kg$^{-1}$] | Emission factor [t$CO_2$e. TJ$^{-1}$] | |
|---|---|---|---|
| | | $CO_2$ | $CH_4$ |
| Firewood | 30.5 | 112 | 0.03 |
| LPG | 47.3 | 63.1 | 0.001 |

Table 2: The average amount of biogas production corresponds to the retention time periods.

| Retention time [days] | 6-10 | 11-20 | 21-35 | 36-50 | >50 |
|---|---|---|---|---|---|
| Biogas production [m$^3$.day$^{-1}$] | 10.87 | 9.18 | 5.30 | 4.14 | 3.38 |

***Step 4:*** *Calculate the amount of $CO_2$ and $CH_4$ emissions from household fuels*

$$CO_{2(fuels)} = \sum(BG_j \times NCV_j \times EF_{CO_{2j}}) \times 10^{-6} \quad \ldots(4)$$

$$CH_{4(fuels)} = \sum(BG_j \times NCV_j \times EF_{CH_{4j}}) \times 10^{-6} \quad \ldots(5)$$

Where:

$CO_{2(fuels)}$, $CH_{4(fuels)}$ = $CO_2$ and $CH_4$ are emissions from fuel burning, $tCO_2e.year^{-1}$

$BG_j$ = amount of fuel *j* consumed annually by the household before the biogas digester is available, $kg.year^{-1}$

$NCV_j$ = Heat of fuel *j*, $MJ.kg^{-1}$

$EF_{CO2j}$ = $CO_2$ emission factor of fuel *j*, $tCO_2e.TJ^{-1}$

$EF_{CH4j}$ = $CH_4$ emission factor of fuel *j*, $tCO_2e.TJ^{-1}$

Based on the IPCC guidelines (IPCC 2006), the value of parameters of firewood and gas are shown in Table 1.

***Step 5:*** *Calculating total GHG emissions before using the biogas digester*

$$Emissions_{BEFORE} = CH_{4(manure)} + N_2O_{(manure)} + CO_{2(fuels)} + CH_{4(fuels)} \quad (6)$$

**Calculating the Amount of GHG Emissions after using the Biogas Digester (IPCC 2006)**

***Step 1:*** *Calculating the amount of $CH_4$ released due to leakage from the biogas digester*

$$CH_{4(biogasleakage)} = LF_{CH_4} \times \left(GWP_{CH_4} \times B_o \times D_{CH_4} \times VS \times 365 \times LN_2\right) \times 10^{-3} \quad \ldots(7)$$

Where:

$CH_{4(biogasleakage)}$ = the amount of $CH_4$ emissions due to leakage from the biogas digester, $tCO_2e.year^{-1}$

$LF_{CH4}$ = leakage coefficient $CH_4$ from anaerobic digester, $LF_{CH4} = 0.1$

$D_{CH4}$ = specific gravity of $CH_4$, $D_{CH4} = 0.67\ kg.m^{-3}$ under normal conditions

$VS$ = volatile solid waste in pig waste, $kg.dry\ matter^{-1}.head^{-1}.day^{-1}$

$LN_2$ = average number of pigs in a household with biogas digester, heads/year

**Step 2:** *Calculate the amount of $CO_2$ and $CH_4$ emissions from household fuels*

$CO_2$ and $CH_4$ emissions from fuels are calculated similarly to the case when there was no biogas digester.

For biogas fuel, the amount of GHG emissions is calculated by the formula:

$$CO_{2(biogas)} = H \times B_0 \times D_{CO_2} \times VS \times 365 \times LN_2 \times 10^{-3} \quad (8)$$

Where:

$CO_{2(biogas)}$ = amount of $CO_2$ due to biogas burning, $tCO_2e.year^{-1}$

$B_o$ = the maximum $CH_4$ volume generated from pig manure treated in biogas, $m^3.kg^{-1}$

$D_{CO2}$ = specific gravity of $CO_2$, $D_{CO2} = 1.798\ kg.m^{-3}$ under normal conditions

$H$ = gas producing efficiency $CH_4$, H = 0.9

***Step 3:*** *Calculating the total amount of greenhouse gas emitted after using the biogas digester*

$$Emissions_{AFTER} = CH_{4(biogasleakage)} + CO_{2(biogas)} + CO_{2(fuels)} + CH_{4(fuels)} \quad (9)$$

## RESULTS AND DISCUSSION

### Biogas Production

After constructing the biogas digesters, the households changed to using biogas to cook or produce products as an alternative fuel instead of liquefied petroleum gas (LPG) or firewood. The amount of biogas production was calculated by the formula referenced from IRENA explained in section Method of Calculating the Amount of Biogas Produced. The relevant factors were calculated including average feedstock volume which is $0.39\ m^3$, average retention time is 37.95 days, initial concentration of volatile solids is $66.67\ kg.m^{-3}$, and the average yield factor is 6.98. The results showed that the average amount of biogas production was $5.52\ m^3$ per household per day. A higher rate of gas production was recorded at the shorter retention periods (Table 2) than at longer retention periods.

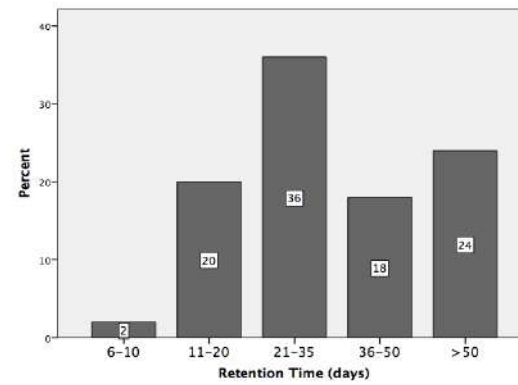


Fig. 3: The retention time on biogas production.

According to Table 7 in IRENA (2016), when the temperature is between 25 and 27°C, the yield factor reaches a maximum value of 13.59 when retention time is 6-10 days. When the yield factor has the maximum value, the amount of biogas produced from the digester reaches optimum efficiency. Fig. 3 showed that the number of households using biogas digesters with retention time being 6-10 days only accounts for 2% of the 50 surveyed households with biogas digesters. With 80 heads of pigs, this household chose to build a biogas digester with a volume of 12 $m^3$ and collected 10.87 $m^3$ of biogas production for serving family activities each day. It is evident that the amount of biogas production they obtained was approximate to the biogas digester volume. The remaining households had a longer retention time, with one family having up to 133 days. Obviously, the surveyed households have not really used the most optimal amount of biogas production.

Decreasing the retention time will reduce the size–and thereby the costs of construction–of the biogas digesters. This study suggests an economic design of biogas digesters by reducing the size suitable for the number of livestock raised. The second solution we recommend is that farmers mix the collected pig manure with other feedstocks consisting of volatile solids such as cereals/grains, rice straw, wheat straw, grass, corn stalks, fruit waste, vegetable waste, fat, mixed food waste, or mixed organic waste.

## Reduction of Greenhouse Gas Emissions

According to our surveyed data from the 50 households with the biogas digesters, 14% used firewood for cooking, 24% used LPG, and the remaining 62% used both before installing a biogas digester. After constructing the biogas digesters, residents could use biogas instead of other fuels such as firewood or gas. There are 41 homes that have stopped using firewood for cooking, accounting for 58.6% of all households interviewed, and 33 houses that have stopped using LPG, accounting for 47.1 percent of all households interviewed.

The GHG emission from manure composting was calculated following formulas (2) and (3) shown in Section Method of Calculating Greenhouse Gas Emissions Reduction with the parameters corresponding to climatic conditions of Quang Tri Province. Additionally, the number of pigs was obtained from question Q3 in the questionnaire that asks the respondents to provide information about the type and number of pigs they were raising. Based on the information on the number of pigs provided by the households, we calculated the amount of $CH_4$ and $N_2O$ emissions from the manure management. From these parameters, we obtained the results that the total GHG emissions from manure composting is 12.51 $tCO_2e.year^{-1}$. $household^{-1}$ before using the biogas digesters, including 11.52 $tCO_2e$ of $CH_4$ and 0.99 $tCO_2e$ of $N_2O$. Totally, GHG emissions from 50 surveyed households is 625.37 $tCO_2e.year^{-1}$. In particular, $CH_4$ accounts for 92.08% of total GHG from composting.

To calculate the amount of greenhouse gases emitted by household fuels including $CO_2$ and $CH_4$, we gathered information on the annual amount of gas and firewood used by each household through questionnaires. Question Q12 was provided to the respondents for the purpose of calculating the amount of fuels used by the households and the cost they paid before constructing the biogas digesters. In the study area, citizens use 12kg gas bottles sold by petrol retailers. To obtain information on how much LPG each household used, the question was adjusted to: "How long does it take for your farm to use one 12 kg bottle of LPG?" The annual amount of gas and firewood used by each household was calculated based on the collected data, from which we computed the

Table 3: Total GHG emissions per year before using the biogas digesters.

| | From manure pits | | From using LPG | | From using firewood | | Total |
|---|---|---|---|---|---|---|---|
| | $CH_4$ emission [$tCO_2e.year^{-1}$] | $N_2O$ emission [$tCO_2e.\ year^{-1}$] | $CO_2$ emission [$tCO_2e.\ year^{-1}$] | $CH_4$ emission [$tCO_2e.\ year^{-1}$] | $CO_2$ emission [$tCO_2e.\ year^{-1}$] | $CH_4$ emission [$tCO_2e.\ year^{-1}$] | |
| Household average | 11.52 | 0.99 | 0.19 | 0.00000304 | 7.83 | 0.002098 | 20.53 |
| 50 households | 575.83 | 49.54 | 9.60 | 0.000152 | 391.63 | 0.1049 | 1026.70 |

Table 4: Total GHG emissions per year after using the biogas digesters.

| | From using biogas | From biogas digester | From using LPG | | From using firewood | | Total |
|---|---|---|---|---|---|---|---|
| | $CO_2$ emission [$tCO_2e.\ year^{-1}$] | $CH_4$ emission [$tCO_2e.\ year^{-1}$] | $CO_2$ emission [$tCO_2e.\ year^{-1}$] | $CH_4$ emission [$tCO_2e.\ year^{-1}$] | $CO_2$ emission [$tCO_2e.\ year^{-1}$] | $CH_4$ emission [$tCO_2e.\ year^{-1}$] | |
| Household average | 1.77 | 1.53 | 0.0486 | 0 | 1.17 | 0.000314 | 4.52 |
| 50 households | 88.58 | 76.41 | 2.43 | 0 | 58.60 | 0.0157 | 226.04 |

amount of GHG emissions from the fuels using formulas (4) and (5) in Section Method of Calculating Greenhouse Gas Emissions Reduction. On average, each household use 52.58 kg of LPG per year for cooking needs. The GHG emissions amount from firewood and LPG of 50 households are 401,34 $tCO_2e.year^{-1}$ (8,03 $tCO_2e.household^{-1}.year^{-1}$), in which the main contributor is $CO_2$ (401,23 $tCO_2e.household^{-1}.year^{-1}$), accounting for 99,97%. The total amount of GHG emissions before using the biogas digesters is equal to the total GHG emissions from manure pits and household fuels. Table 3 showed that with 50 surveyed households before using the biogas digesters, the total amount of GHG emissions into the environment is 1026.70 $tCO_2e$ per year. This is a fairly large number and seriously affects the environment. If the number of households expanded further, GHG emissions amount would increase more. It can be seen that the amount of greenhouse gas emissions from composting and burning fuels is huge. Therefore, without green development solutions, the livestock sector will be a major contributor to climate changes causes.

The emissions from the biogas digesters were calculated based on the number of pigs per household raised in combination with the parameters provided by the IPCC guidelines. Equations (7) and (8) are applied to estimate the amount of $CH_4$ and $CO_2$. The previous fuels have been almost replaced by biogas for cooking or making products. However, biogas generated from the biogas digesters was not enough to completely replace cooking fuels in some households, so they combined biogas for cooking with firewood and gas. The amount of $CO_2$ and $CH_4$ from firewood and gas was calculated similarly as before using the biogas digesters. Table 4 showed that the emission due to leakage from the biogas digesters of the surveyed households is 164.99 $tCO_2e$ per year (3.30 $tCO_2e.household^{-1}.year^{-1}$) consisting of 88.58 $tCO_2e$ of $CO_2$ and 76.41 $tCO_2e$ of $CH_4$. The amount of greenhouse gas emitted from firewood and LPG is 61.05 $tCO_2e.year^{-1}$, which is composed mainly of $CO_2$. The reduction of using firewood and gas has contributed to making a significant reduction in GHG emissions. The amount of $CO_2$ emitted from LPG decreased to a quarter compared to before and the emissions from firewood also decreased from 391.73 $tCO_2e.year^{-1}$ to 58.62 $tCO_2e.year^{-1}$. After using the biogas digesters, the total greenhouse gas emissions had reduced to 226.04 $tCO_2e.year^{-1}$, less than one-quarter of the GHG emissions from the surveyed households before using the biogas digesters.

The difference between the amount of greenhouse gas emissions before and after using the biogas digesters was 16.01 $tCO_2e$ for each household every year. Straightforwardly, the replacement of daily cooking energies with biogas helps reduce a large amount of greenhouse gases. This is a potential approach chosen to mitigate climate change. In addition, the improvement of this technology also contributes to depreciating firewood consumption and deforestation.

## CONCLUSION AND RECOMMENDATIONS

This study provides an overview of the importance of biogas production using livestock waste in central Vietnam. The daily average amount of biogas production was 5.52 $m^3$ per household, however, this is not the maximum amount of biogas the households can obtain. Despite the good potential for biogas production in central Vietnam, it has not been much developed in the country. In consequence, the economic policies we propose in this article need to be considered for implementation.

A small-scale biogas digester is a very useful manure management tool for reducing global warming impacts. The traditional use of firewood and gas for cooking in central Vietnam was replaced by biogas. The findings of this study showed that the amount of GHG emissions before using the biogas digesters is less than one-quarter of them when biogas was used as an alternative fuel instead of firewood and gas. The annual difference in the amount of GHG emitted before and after the farmers used biogas is 16.01 $tCO_2e.household^{-1}$.

Although using biogas as alternative energy helps to reduce the greenhouse gas effect, it cannot be denied that there is still a small amount of greenhouse gases emitted from the biogas digesters. When they are used inappropriately, the amount of biogas will be released into the environment. More in-depth research is needed to come up with the right policies for biogas use. We also suggested that detailed training for biogas users is needed so that users can maximize the benefits they obtain from the digesters. Experimental studies that check and monitor the use of biogas digesters are also essential.

## REFERENCES

Doan, D.T., Nguyen, V.H. and Nguyen, V.L. 2014. Study of climatic drought status in Quang Tri Province. J. Sci. Earth, 36: 160-168.

Hessen, J.V. 2014. An Assessment of Small-Scale Biodigester Programmes in the Developing World: The SNV and Hivos Approach. Institute for Environmental Studies, University of Amsterdam, The Netherlands.

Ho, T.B., Roberts, T.K. and Lucas, S. 2015. Small-scale household biogas digesters as a viable option for energy recovery and global warming mitigation: Vietnam case study. J. Agric. Sci. Technol., A(5): 387-395.

IPCC. 2006. Chapter 10: Emissions from livestock and manure management. Forestry, p.4.

IRENA. 2016. Measuring Small-Scale Biogas Capacity and Production. International Renewable Energy Agency (IRENA), Abu Dhabi, p. 16.

Kinyua M., Zhang J., Fabricio, C.C. and Andres E.T.M. 2016. Use of physical and biological process models to understand the performance of tubular anaerobic digesters. Biochem. Eng., 107, 35-44

Mayhew, J. 2015. Biogas Rising: The Biogas Industry in Indochina. ASEAN Briefing. https://www.aseanbriefing.com/news/biogas-rising-biogas-industry-indochina/

Mengistu, M.G., Simane, B., Eshete, G. and Workneh, T.S. 2015. A review on biogas technology and its contributions to sustainable rural livelihood in Ethiopia. Renew. Sustain. Energy Rev., 48: 306-316.

Nguyen, V.C.N. 2011. Small-scale anaerobic digesters in Vietnam: Development and challenges. J. Viet. Env., 1(1): 12-18.

Nguyen, V.C.N., Phan, T.H. and Vo, H.N. 2021. Review on the most popular anaerobic digester models in Mekong Delta. J. Viet. Env., 2(1): 8-19.

Quang Tri Department of Agriculture and Rural Development. 2016. Project of Constructing Biogas Digesters, Treating Livestock Waste, Taking Biofuel, Contributing to Environmental Treatment in Household Breeding. Quang Tri Department of Agriculture and Rural Development, Vietnam.

Roopnarain, A. and Adeleke, R. 2017. Current status, hurdles, and future prospects of biogas digestion technology in Africa. Renew. Sustain. Energy Rev., 67: 1162-1179.

Teune, B. 2007. The biogas program in Vietnam: Amazing results in poverty reduction and economic development. Boiling Point, 53: 11-13.

Zhang, L.X., Wang, C.B. and Song, B., Carbon emission reduction potential of a typical household biogas system in rural China. J. Cleaner Prod., 47: 415-421.

Nature Environment and Pollution Technology
An International Quarterly Scientific Journal

p-ISSN: 0972-6268
(Print copies up to 2016)
e-ISSN: 2395-3454

Vol. 20 | No. 5 (Suppl) | pp. 1895-1902 | 2021

Original Research Paper

https://doi.org/10.46488/NEPT.2021.v20i05.005

Open Access Journal

# Healthcare Waste, Pandemic Covid-19: A Case of India

**Dinesh Kumar†, Sukesh Trikha and Ranju Anthony**
Center of Social Medicine & Community Health, Jawaharlal Nehru University, New Delhi-110067, India
Corresponding author: Dinesh Kumar; dr.dinesh999@yahoo.com

**Nat. Env. & Poll. Tech.**
**Website: www.neptjournal.com**

*Received:* 12-02-2021
*Revised:* 20-04-2021
*Accepted:* 30-04-2021

**Key Words:**
Healthcare waste
Covid-19 pandemic
Biomedical waste management
PPE

## ABSTRACT

The present pandemic, while causing economic slowdown and global panic, also generated healthcare waste in unprecedented amounts across the globe, due to mass screenings/diagnosing/treatment. This paper aims to explore the prospects of the current and future challenges with respect to the risk to human health due to environmental contamination with the healthcare waste generated as a result of and caused by the Covid-19 pandemic in the Indian context. Peer-reviewed literature with respect to healthcare waste generation during the pandemic, its burden, challenges, and policies promulgated during the pandemic and their implications for the future was searched on various databases like PubMed, Google Scholar, and Science Direct and reviewed. Many research studies and international reports have demonstrated that the quantity of biomedical waste has increased in the times of the Covid-19 pandemic across the globe. Additionally, the danger of general waste getting contaminated has also multiplied, in part due to increased quarantine facilities and home quarantines, along with hospitals managing Covid-19 patients and also due to inadequate segregation at the point of generation of such waste, which is a major concern in itself. The occupational exposure of this increased waste to hospital and municipal waste collection workers has also increased, though World Health Organization (WHO) declines having any evidence of transmission of coronavirus while handling healthcare waste. Enough policies existed before the pandemic and few newer guidelines are also issued to address various additional aspects, which are to be implemented to manage the healthcare waste, minimize threats to the environment and human health. Cleaner, greener waste management facilities, the inclusion of bio-disaster in disaster management, the social impact of waste management policies, and waste reduction are to be prioritized.

## INTRODUCTION

Around late December, China, in one of its provinces, reported a cluster of pneumonia-like cases, which were later confirmed and diagnosed as 'Covid-19' cases on 7th January 2020 (Holshue et al. 2020). Thereafter, the newly diagnosed disease 'Covid-19' was declared a global health emergency by WHO on 31st January 2020 (Yu et al. 2020), which has put healthcare delivery systems under severe strain globally. Barely, in the past three decades, many pathogens like HIV/ novel-influenza have caused pandemics and novel-coronavirus is the latest in this series (Tandon 2020), but may not be the last. Subsequent to the Severe Acute Respiratory Syndrome (SARS-CoV-1) and Middle East Respiratory Syndrome (MERS-CoV-2), epidemics in the recent past have caused not only economic predicament in the affected countries but have also led to a global trepidation (Holshue et al. 2020). Similarly, and uniquely, the current pandemic of Covid-19 has posed perilous challenges and raised questions afresh with respect to biomedical waste management to different stakeholders all around the globe and specifically in India, namely, the authorities (policymakers), hospital managements, urban local bodies, common biomedical waste treatment facilities, Panchayati Raj Institutions, and last but not the least, to the society at large.

The healthcare waste generation is an obvious outcome in the process of mass screening, diagnosing and treatment of diseases, especially in the epidemic/pandemic, albeit in huge amounts. The improper /unscientific disposal of healthcare waste generated from healthcare facilities poses a serious threat to the environment and human health. Keeping these in view, the healthcare waste is defined as "any waste which is generated during the diagnosis, treatment or immunization of human beings or animals or research activities pertaining thereto or in the production or testing of biological or in health camps, including the categories mentioned in Schedule 1 of Biomedical Waste Management (BMWM) rules, 2016" (CPCB 2016). Furthermore, the Ministry of Environment, Forest and Climate Change (MoEFCC) revised the BMWM rules 1998 in 2016, "to improve the collection, segregation, processing, treatment and disposal of biomedical waste, in an environmentally appropriate manner, to reduce the generation of biomedical waste and its impact on environment thereof" (CPCB 2014, 2016). Over and above that National

Green Tribunal adjudicated that "Unscientific disposal of bio-medical waste had the potential of serious diseases such as Gastrointestinal infection, Respiratory infection, Eye infection, Genital infection, Skin infection, Anthrax, Meningitis, AIDS, Hemorrhagic fevers, Septicemias, Viral Hepatitis type A, Viral Hepatitis type B and C, etc. Such unscientific disposal also causes environmental pollution leading to the unpleasant smell, growth and multiplication of vectors like insects, rodents, and worms, and may lead to the transmission of diseases like typhoid, cholera, hepatitis, and AIDS through injuries from syringes and needles contaminated with various communicable diseases" (CPCB 2014, 2016).

This paper aims to explore the impact, burden and prospects of the current & future challenges with respect to the risk to human health due to environmental contamination with the healthcare waste generated as a result of and caused by the Covid-19 pandemic. Peer-reviewed literature with respect to healthcare waste generation during the pandemic, its burden, challenges, and management was searched on various databases like PubMed, Google Scholar, and Science Direct and reviewed for exploration.

## IMPACT AND BURDEN

As per WHO (2020a), out of the total healthcare waste generated globally, 85% is general non-hazardous waste, whereas the remaining 15% is considered hazardous which could be infectious, toxic, and radioactive (WHO 2020b). Though, in the present pandemic, some studies depict that the major chunk of the healthcare waste (75%) is general waste while the remaining 25% of the healthcare waste is hazardous infectious waste (Wang et al. 2020), which amounts to an increase in the hazardous category and is a serious concern in itself. Moreover, inadequate segregation of infectious and non-infectious healthcare waste, at the point of generation, could lead to a further increase in the quantum of infectious waste as a result of mixing of infectious healthcare waste with non-infectious waste. Therefore, in the wake of this ensuing pandemic, WHO emphasized ensuring good waste management practices, which will further help to prevent human to human transmission of Covid-19 (WHO 2020c).

Additionally, and obviously, due to the lockdown effect in view of the epidemic, recycling processes were also hampered (Zambrano-Monserrate et al. 2020). Studies are suggesting that discarded personal protective equipment (PPE) is problematic, as there is a considerable increase in healthcare waste with the use of these products. The PPE includes gloves, medical masks, goggles, or a face shield and gowns/coveralls for specific procedures. In addition, it includes respirators (N95 or FFP2 standard or equivalent) and aprons (WHO 2020d). But WHO cautioned that PPE is only one of the effective measures 'within a package of administrative and engineering control'. Further WHO stipulates that PPE should be used based on the risk of exposure and transmission dynamics of pathogen and the overuse of PPE may globally impact its supply chain. Another study forewarns that when millions of people using single-use masks or gloves, the amount of trash or biomedical waste generated would be substantial and the consequences thereof, would be far-reaching. The environmental impact of it will not only affect human health but also, will invariably affect the natural habitat and health of other species in the environment (WHO 2020e).

In the current times of pandemic, hazardous medical waste, which is mostly constituted of plastic is posing a great threat to the earth's ecosystem. Furthermore, the PPE which is mostly plastic and water-resistant material is often used for a single shift/day and gets discarded. This waste might often get disposed-off in landfills or oceans. The environmental impact of such waste would affect not only the health of the communities but also affect the natural habitat of other organisms & species. A large amount of single-use discarded masks were found floating at 100-meter at a beach stretch (Sadat et al. 2020). Over and above that, general waste such as linen used tissues, and paper waste may also get contaminated. As one of the studies has suggested that these viruses could be found active on the surfaces even up to 72 hours (Ranjan et al. 2020). Irrevocably, the contaminated waste generated from laboratory facilities that are conducting diagnostic tests for Covid-19 patients, should be efficiently treated and stored within the laboratory till it is transported for final disposal (Maurya 2020). As a consequence, the problem of healthcare waste is actually compounding with an ever-increasing number of hospitals, nursing homes, and clinics (Hasaan et al. 2008), along with quarantine facilities/ laboratories in the present situation.

Presumably, the increase in the use of disposable materials has increased with the advancements in healthcare technology, which, has also led to enhancement of the problem (Sengodan 2014). But, in the present pandemic, the generation of biomedical waste has increased exponentially (Yu et al. 2020). The healthcare waste generation in Hubei province, increased by (+370%) with a high proportion of plastic during the pandemic Covid-19 (Klemes et al. 2020). Also, it was estimated that hospitals were producing six times more healthcare waste (Ranjan et al. 2020). Asian Development Bank reported that many of the big Asian cities are producing tons of extra healthcare waste during the current pandemic, e.g., Manila 280 tons.day$^{-1}$, Jakarta 212 tons.day$^{-1,}$ and Bangkok 210 tons.day$^{-1}$ (ADB 2020). Approximately, 550 tons of biomedical waste is generated in India on daily

basis (Ranjan et al. 2020). Around 28% of BMWs are left untreated and discarded improperly (Ramteke & Sahu 2020). 181 tons of Covid-19 related waste was generated on the daily basis in October 2020 according to Central Pollution Control Board (CPCB) (CPCB 2020a). It was estimated that there was 3.41 kg per day of biomedical waste generation by each Covid-19 patient which is double the biomedical waste generated in pre-covid times. Additionally, the proportion of yellow category biomedical waste was 50.4 percent out of total biomedical waste (Thind et al. 2021). According to CPCB (2020a), Delhi alone generated 11 tons of Covid-19 related biomedical waste and 27 tons of non-covid related biomedical waste each day. "Quantity of household medical waste may reach up to 0.1% of the total mixed municipal solid waste stream" (Yordanova et al. 2014). The quantity of biomedical waste generated from households must have multiplied due to provisions like home quarantine, home isolation, and asymptomatic patients.

The healthcare waste generated finds its way to common biomedical waste treatment facilities or onsite treatment facilities for proper treatment and disposal. The patients suffering from Covid-19 are not restricted to hospitals only. A lot of people with mild symptoms around the globe are receiving home treatment, in addition to people in quarantine and isolation centers. Therefore, a lot of pathogen-contaminated waste is generated by the people quarantined in households. This pathogen-contaminated waste may probably contaminate the general waste and the waste collectors, if not segregated or handled appropriately. The WHO reports that till now there is no evidence of catching the coronavirus infection while handling the healthcare waste (WHO 2020). However, newer and newer studies are generating fresh evidence. Therefore, in the absence of evidence or till the evidence is generated, it is the stakeholder's responsibility to mitigate the risk of pandemic Covid-19, to the environment and human health.

Importantly, specified people are vulnerable to the risk posed by excessive healthcare waste, including waste collectors, cleaners, support staff, and health personnel (Sadat et al. 2020). The magnitude of occupational exposure to municipal and hospital waste collection workers has been the subject of many studies in the light of increased public concern about environmental and workers' health issues (Ferreira et al. 1999). The cleaning and maintenance services attendant may get contaminated via skin puncture, splash, infected surfaces, and additionally while cleaning and handling fecal material of the infected patient. Also, a person may get contaminated while handling the waste generated during patient care (CPCB 2020b). The WHO, in its interim guidelines on Water Sanitation and Hygiene (WASH) (WHO 2020), has categorically mentioned that the volume of infectious waste during the Covid-19 pandemic is expected to increase, especially through the use of PPE. Therefore, WHO emphasized the importance of enhancing the capacity of appropriate disposal of such infectious waste (WHO 2020).

Universal masking is becoming a norm in different parts of the world. Universal masking in health facilities is defined as "the requirement to wear a mask by all health workers and anyone entering the facility, no matter what activities are undertaken" (WHO 2020). However, wearing face masks in some Asian countries like Hong Kong, Japan, Taiwan, and South Korea is very common, partly because of air pollution and partly because of response to past outbreaks such as SARS and MERS outbreaks (Greenhalgh et al.2020). In East Asian countries face masks are even mandated by the governments (Javid et al. 2020). After social distancing (though physical distancing is apt), which is considered to be the most effective means of controlling the spread of the virus, the use of face masks is a popular non-pharmaceutical choice in the communities (Aggarwal et al. 2020). In addition to the discussion of whether masks should be used or not, WHO also stipulates that "for any type of mask, appropriate use and disposal are essential to ensure that they are as effective as possible and to avoid any increase in transmission" (WHO 2020). Additionally, the veterinary health facilities generate a considerable amount of biomedical waste which is similar in nature and quantum to biomedical waste generated by health facilities for humans. Therefore, the establishment of a joint surveillance system with a "one health approach" can have far-reaching benefits in current times.

Furthermore, the demand and supply cycles along with logistics/supply chain are severely impacted during the period of lockdown. According to WHO, the demand for the plastic product (PPE, Gloves, Masks, and Syringes, etc.), used as prevention, to protect the general public, health workers and patients, have arisen sharply. Additionally, due to the restricted movements driven scenario, the online delivery services demand increased, which has led to the increase in the use of plastic as a packaging material (Klemes et al. 2020). Even earlier, the management of plastic waste was a grave environmental issue. While now with the present pandemic, the possibility of pathogen-contaminated plastic has increased manifold, which ought to be treated as infectious hazardous waste and therefore, the quantum of waste generation in this pandemic has reached never before proportions, presumably.

**Wastewater**

It is of great significance to reduce the risk to the environment and public health through proper management of healthcare wastewater in times of the current pandemic. While dissem-

inating guidelines for managing the Covid-19 biomedical waste generated from healthcare facilities/home care/isolation wards, CPCB has not done any significant revision in the guidelines for the treatment of wastewater discharged from such facilities. A large quantum of patients are asymptomatic and receiving care in the form of home care or home quarantine. While citing information provided by the Center for Disease Control (CDC) of USA, CPCB mentioned that 'the risk of coronavirus causing Covid-19 through sewage wastewater appears to be low' and therefore did not make any significant change in the guidelines for managing Covid-19 infected wastewater. But, the contact of hospital effluents with the aquatic ecosystem poses serious long-term threats to aquatic life (Syed et al. 2012).

There are studies that indicate that SARS-CoV-2 may infect the drainage systems as it is found active in hospital wastewater. Coronavirus has been found in the sewage sludge of an infected area (Ranjan et al. 2020). Also, SARS-CoV-2 has been cultured in a single stool sample (Wang et al. 2020). In quarantine or isolation centers including the home where suspected or confirmed cases are kept, fecal material should be considered as a biohazard and treated accordingly (WHO 2020). Presence of coronaviruses in the sewage system and stool samples may indicate the possibility of fecal-oral transmission of the virus. Therefore, such frameworks (fecal-oral transmission) are also being proposed for further research (Heller et al. 2012). If such a hypothesis is confirmed, other far-reaching dynamics will unfold which will impact pandemic and control strategies (Heller et al 2020). Therefore, it necessitates the careful disinfection, treatment, and disposal of healthcare wastewater.

Apart from the safe treatment and disposal, wastewater from healthcare facilities and communities could be analyzed for the presence of coronavirus in the wastewater or sewage sludge. Due to resource constraints, it is nearly impossible to do clinical testing of all the individuals. Also, stool samples for coronavirus may test positive even after the nasopharyngeal swab sample test negative. Additionally, studies have suggested that coronavirus may show more waves of the epidemic (Sundararaman 2020). In such scenarios of emergence and re-emergence of coronavirus, wastewater monitoring could be a viable option to assess the state of infection in a community (Kumar 2020).

## TREATMENT

A study conducted by Singh and Prakash (2007) in India, revealed that the proportion of bio-medical waste in total general waste generated was comparatively high ranging from 12.5% to 69.3%, which indicates inappropriate waste handling processes followed at the point of generation (Syed et al. 2012). Strangely, out of 2.7 lac identified health facilities, only 1.1 lac health facilities are authorized under BMW management rules 2016 so far. Therefore, State Pollution Control Boards/ Pollution Control Committees will have to make serious efforts to identify and appropriately manage this lacuna (CPCB 2020c). According to CPCB, a total of 198 Common Biomedical Waste Treatment Facilities (CBWTF) are operating in the country. Few states like Goa and Sikkim are devoid of any CBWTF. According to CPCB's annual report of 2018 (CPCB 2018), a total of 2,60,889 healthcare facilities are estimated to generate 608 MT biomedical waste per day, out of which only 528 MT is treated and disposed of through common biomedical waste treatment facilities. According to the National Green Tribunal, available capacity of incineration is 840 MT per day and only 55 percent of cumulative incinerator capacity is being utilized.

The present available biomedical waste treatment facilities were designed and made operational for the quanta of waste generated in pre-Covid-19 conditions and are not geared up for conditions like the present pandemic, where there is a sudden and rapid increase in the quantities of healthcare waste. The healthcare waste generation in Wuhan, increased from 40 tons.day$^{-1}$ to 240 tons.day$^{-1}$, during the peak of the pandemic. However, the available maximum incineration capacity for biomedical waste in Wuhan was 49 tons.day$^{-1}$. Therefore, healthcare waste generation exceeded far more than the handling capacity of treatment facilities. In such conditions, the life cycle approach could provide guidance for the identification and use of the most suitable alternative for the environment (Klemes et al. 2020). The concepts like plastic footprints and plastic waste footprints are introduced as a measure of the burden of plastic on the environment (Klemes et al. 2020). It is becoming very crucial for the governments to find a solution soon enough for the disposal of this increased healthcare waste as treatment facilities are limited with further limited capacities (Sadat et al. 2020).

## POLICIES

The management of healthcare waste received little attention in South East Asian countries until the last millennium. With the outbreak of SARS in 2002, many countries reviewed their healthcare waste management system, which was further catalyzed by the Avian flu (H5N1) outbreak (Kuhling & Pieper 2012). International agencies like WHO, CDC of USA, and Public Health of England have come up with additional guidelines for biomedical waste management generated during the current pandemic. Preventively, enough guidelines around the globe have advocated for the use of PPE/ single-use masks, and scientific management and disposal of

these used items, which can minimize the unforeseen impacts on human health and the environment (Klemes et al. 2020).

The Bio-medical waste management & handling rules 2016, under Environment Protection Act 1986 stipulates that "it is the responsibility of every hospital, clinic, nursing home, dispensary, veterinary institutions, animal house, and pathological laboratories & blood banks to ensure that such waste is handled without any adverse effect to human health and environment" (CPCB 2017). Further, BMW rules also stipulate that it is the responsibility of the occupier to ensure that generated biomedical waste is treated and disposed of within 48 hours (CPCB 2020d). CPCB is the implementing agency for the implementation of BMWM rules in India. CPCB in India has issued guidelines for handling, treatment, and disposal of waste generated during treatment/diagnosis/quarantine of Covid-19 patients, in addition to the existing Biomedical Waste Management guidelines (BMWM & Handling Rules 2016) keeping in mind the current challenges posed by the pandemic. It has prescribed responsibilities of different stakeholders such as Health facilities, Common Biomedical waste treatment facilities, Urban Local Bodies, State Pollution Control Boards/Pollution Control Committees, Quarantine Camps/homes, and isolation facilities for proper handling & management of healthcare waste generated from healthcare activities (CPCB 2020e).

Some of the notable additions to existing BMW management rules 2016 concerning Covid-19 are;

a. Healthcare facilities having isolation wards need to keep color-coded bins labeled as "Covid-19 Waste" with a foot-operated lid and a double layer bag (2 bags) that should be used for the collection of waste.
b. Bins having Covid-19 waste could be directly lifted from isolation wards to Common Biomedical Waste Treatment Facilities (CBWTF).
c. A separate record of Covid-19 waste is to be maintained on daily basis.
d. Dedicated trolleys and collection bins should be used in isolation wards and these vehicles should be sanitized with 1 percent Sodium Hypochlorite solution after each trip.
e. Opening of any Covid care facility or sample collection laboratories must be reported to SPCB/PCC and CBMTF. Also, these facilities need to get registered on the mobile application "COVID19BMW" and update the daily generation of BMW.
f. Feces from Covid-19 confirmed cases must be treated as biomedical waste and must be handled accordingly.
g. Used PPE such as goggles, face shield, splash-proof apron, plastic coverall, hazmat suit, nitrile gloves should be collected into red bags. Used masks, semi-plastic coveralls, shoe-cover, and disposable gowns should be collected into yellow bags. Also, used disposable items, leftover food, plate, glass, masks, and tissues of Covid-19 patients must be collected in yellow bins.
h. Urban local bodies need to provide yellow-colored bags to collect infected waste from isolation wards/homes/quarantine camps.
i. The person taking care of home care/isolation wards/quarantine camps must hand over biomedical waste collected in yellow bags to CBMWTF or ULBs.
j. Used masks of persons not infected by Covid-19 must be kept for 72 hours in a paper bag and are advisable to cut the mask before final disposal. Used masks or PPEs by infected or asymptomatic patients along with other infected waste generated during home care or home quarantine should be collected in different yellow bags and bins.
k. To minimize the waste, non-disposable items must be used and dry & wet solid waste bags must be handed over to ULB's collector on daily basis.
l. BMWM in remote and rural areas devoid of any CBMWTF must be done through deep burial pits. In case of an increase in the quantity of biomedical waste beyond the capacity of existing treatment facilities, industrial incinerators may be used to dispose of the Covid-19 related biomedical waste safely.

Further, the person dealing with soiled clothes, beddings, and towels of Covid-19 patients should wear appropriate PPE before touching it which includes gloves, goggles, or face shield for eye protection, long-sleeved fluid-resistant gown, or an apron with boots or closed shoes. Hand hygiene must be maintained after the removal of these items. MoEFCC in Biomedical waste management rules stipulates that biomedical waste generated from households shall be segregated as per these rules in separate bags and shall be handed over to waste collectors. Urban Local Bodies shall have a tie-up with CBMWTF for the safe disposal of such waste in a prescribed manner. However, with the fast spread of coronavirus disease, challenges are getting intense with the safe disposal of biomedical waste management (CPCB 2020f).

## CHALLENGES

### Challenges in Urban Areas

Most of the secondary and tertiary level healthcare facilities in India are located in urban areas which include Community Health Centers (CHCs), District Hospitals, Medical Colleges,

and Private health facilities. These facilities contribute to the generation of a major chunk of biomedical waste. In addition, a large chunk of the healthcare services is provided by informal healthcare workers both in urban and rural areas. These providers are not a direct part of the health services system in India. However, they are present in huge numbers and generate a large amount of biomedical waste in various forms. These health providers or facilities are not authorized or recognized by the health service system or with pollution control authorities. Therefore, biomedical waste generated by them is not treated or disposed of in a scientific manner. The facility for biomedical waste disposal and treatment through CBMWTF is located in urban areas or near the urban areas and is invariably shared between two or three districts. But notably, these facilities are designed for limited capacities and operations in a steady-state manner. With the addition of newer and temporary health facilities, quarantine camps, and isolation centers, these disposal facilities would definitely be under pressure. Enormous human, material, and infrastructural resources would be required for the safe and scientific disposal of biomedical waste as per the guidelines mentioned above for its disposal.

### Challenges in Rural Areas

The majority of the Indian population still lives in rural areas. The requisite infrastructure of waste management viz. segregation, storage, collection, treatment, and disposal is lacking in rural areas. Informal health providers in rural areas also generate some quantity of biomedical waste in the form of needles, syringes, pathological and pharmaceutical waste. While, the quantity of biomedical waste from primary level facilities is low, but explicit guidelines are required for environmentally appropriate waste disposal. In rural areas, home isolation, or home care scenarios, persons dealing with Covid-19 suspected, asymptomatic, or confirmed patients are at risk of contracting coronavirus infection. A lot of infected generals and biomedical waste will be generated during such care. This waste would be treated as domestic hazardous waste and must be treated according to BMWM rules (CPCB 2017).

Recent guidelines or revisions to BMWM rules have established provisions for urban areas by defining the responsibilities of ULBs, while rural areas have been left out. The majority of the Indian population resides in villages; a lot of hazardous biomedical waste would be generated in rural areas in such situations. Who will be responsible for the dissemination of the information regarding yellow bin category waste? Who will provide yellow bags and who will guide villagers about standards of deep burial pit? Inadequate and improper biomedical waste and infected general waste management may catalyze the spread of infection.

## FUTURE OUTLOOK

The WHO in its interim guidelines on WASH recommended that additional waste treatment capacity may need to be created, keeping in mind the increased use of disposal items like PPE during the Covid-19 pandemic. Preferable methods should include alternative treatment technologies such as autoclaving or high-temperature burn incinerators. Also, their sustained operation needs to be ensured (WHO 2020). The need is to develop waste management systems that incorporate a clean, green way of disposal.

Current disaster management systems are focused narrowly on natural calamities like earthquakes, tsunamis and flood, etc. Explicit decision-making tools are needed to be focused on waste management planning for special conditions like pandemic Covid-19 (Klemes et al. 2020). A detailed planning for bio-disaster response needs to be included in disaster management policy, though a chapter is added in draft National Disaster plan.

The experiences of Wuhan in management of excessive healthcare waste with application of reverse logistical models could be a potential solution. These models are focused on reverse flow in a supply chain. The ultimate aim is to maximize the value recovery from end of use & end of life products through reuse, remanufacturing, recycling and energy recovery. Such models could provide quantitative and managerial support for effective management of biomedical waste (Yu et al. 2020). Furthermore, establishment of temporary waste transit centers and temporary waste treatment centers for treatment of excessive biomedical waste from temporary health facilities could be a viable option. Treated waste then could be sent to final waste disposal centers. However, selection of appropriate location in such scenarios would be the most important step of the whole process (Yu et al. 2020). The focus of such measures is to balance the trade-off between environmental risk related to management of medical waste and economic performance.

Under solid waste management rules 2016, it is necessary to have a district environment plan to be operated by district committee (as a part of part of District Planning Committee under Article 243 ZD). In the current times of pandemic such plan may be extended to block and village levels to effectively monitor and guide biomedical waste disposal practices at these echelons. NGT (2020) has flagged the issues pertaining to household generation and management of biomedical waste. It highlighted that there is a need for further revisions in these guidelines to cover all the aspects and incorporate not merely institutions, but also households and dealing with the situations where facilities like incinerators are not available. Any unmindful deep burial without adequate safeguard can adversely affect the ground water and pose danger to health

and safety of people (CPCB 2016). In techno-economic assessments of disaster responses, social factors need to find their space. The impacts on societies must be the concern and disaster responses should be designed accordingly. For the society at large, waste prevention/reduction should be at highest priority in all the policies, especially in healthcare waste management policies.

## KEY MESSAGE

The current outbreak of the Covid-19 pandemic has led to a substantial increase in Biomedical waste (BMW) generation. Context-specific policy guided BMW management is critical for effective control of Covid-19 pandemic in urban & rural areas of India.

## REFERENCES


Aggarwal, N., Dwarakanathan, V., Gautam, N. and Ray, A. 2020. Facemasks for prevention of viral respiratory infections in community settings: a systematic review and meta-analysis. Indian J. Pub. Health, 64(6): 192.

Asian Development Bank (ADB). 2020. Managing Infectious Medical Waste During the COVID-19 Pandemic, 2020. Available from: https://www.adb.org/sites/default/files/publication/578771/managing-medical-waste-covid19.pdf. Accessed 21 June 2020.

Central Pollution Control Board (CPCB). 2014. Biomedical Waste Management; An Overview, 2014. Available from: http://www.cpcbenvis.nic.in/envis_newsletter/BMW%20Newsletter.pdf. Accessed 23 June 2020.

Central Pollution Control Board (CPCB). 2016. Biomedical Waste Management Rules; 2016. New Delhi.

Central Pollution Control Board (CPCB). 2017. Biomedical Waste Management Rules; 2016 (amended). Available from: http://www.cpcbenvis.nic.in/pdf/BMW_Amended_10.05.2019.pdf. Accessed 15 June 2020.

Central Pollution Control Board (CPCB). 2018. Annual Report 2017-18. Ministry of Environment & Forests, GOI.

Central Pollution Control Board (CPCB). 2020b. Guidelines for Handling, Treatment, and Disposal of Waste Generated during Treatment/Diagnosis/ Quarantine of COVID-19 Patients – Revision 1, 2020. Available from: https://hspcb.gov.in/content/BMW/covid19/BMW-GUIDELINES-COVID2.pdf. Accessed 16 June 2020.

Central Pollution Control Board (CPCB). 2020c. Scientific Disposal of Bio-Medical Waste Arising Out of COVID-19 Treatment- Compliance of BMW Rules, 2016. Available from: https://hspcb.gov.in/content/BMW/covid19/NGT_Order_covid_28.04.2020.pdf. Accessed 16 June 2020.

Central Pollution Control Board (CPCB). 2020d. Guidelines for Handling, Treatment, and Disposal of Waste Generated during Treatment/Diagnosis/ Quarantine of COVID-19 Patients – Reg, 2020. Available from: https://hspcb.gov.in/content/BMW/covid19/BMW-GUIDELINES-COVID1.pdf. Accessed 16 June 2020.

Central Pollution Control Board (CPCB). 2020e. Guidelines for Handling, Treatment, and Disposal of Waste Generated during Treatment/Diagnosis/ Quarantine of COVID-19 Patients– Revision 3, 2020. Available from: https://cpcb.nic.in/openpdffile.php?id=TGF0ZXN-0RmlsZS8yOTdfMTU5MjE0NzcwMF9tZWRpYXBob3RvMzA3NDgucGRm. Accessed 15 June 2020.

Central Pollution Control Board (CPCB). 2020f. Guidelines for Handling, Treatment, and Disposal of Waste Generated During Treatment/Diagnosis/ Quarantine of COVID-19 Patients – Revision 2, 2020. Available from: http://www.cpcbenvis.nic.in/pdf/BMW-GUIDELINES-COVID_1.pdf. Accessed 15 June 2020.

Central Pollution Control Board 2020a. Public Notice to HCFs and CBWTFs Regarding Handling, Collection, Transportation, and Disposal of Bio-Medical Waste Generated from Covid-19 affected Persons, 2020. Available from: https://hspcb.gov.in/content/BMW/covid19/HSPCB_Adv_Corona_Guidelines.pdf. Accessed 2020 June 22.

Ferreira, J.A., Tambellini, A.T., da Silva, C.L.P. and Guimarães, M.A.A. 1999. Hepatitis B morbidity in municipal and hospital waste collection workers in the city of Rio de Janeiro. Infect. Control Hosp. Epidemiol., 20(9): 591-592.

Greenhalgh, T., Schmid, M.B., Czypionka, T., Bassler, D. and Gruer, L. 2020. Face masks for the public during the covid-19 crisis. Br. Med. J., 369: m1435.

Hasaan, M.M., Ahmed, S.A., Rahman, K.A. and Biswas, T.K. 2008. The pattern of medical waste management: an existing scenario in Dhaka city, Bangladesh. BMC Pub. Health, 8(1): 1-10.

Heller, L., Mota, C.R. and Greco, D.B. 2020. COVID-19 faecal-oral transmission: are we asking the right questions? Sci. Tot. Environ., 729: 138919.

Holshue, M.L., DeBolt, C., Lindquist, S., Lofy, K.H., Wiesman, J., Bruce, H., Spitters, C., Ericson, K., Wilkerson, S., Tural, A. and Diaz, G. 2020. The first case of the 2019 novel coronavirus in the United States. N. Engl. J. Med., 382: 929-936.

Javid, B., Weekes, M.P. and Matheson, N.J. 2020. Covid-19: Should the public wear face masks? Br. Med. J., 369: m144

Joint COVID-19 Taskforce. Second joint statement of the IPHA, IAPSM, and IAE- Public health approach for COVID-19 pandemic control in India. Indian Journal of Public Health 2020, 64: S84-6.

Klemes, J.J., Van Fan, Y., Tan, R.R. and Jiang, P. 2020. Minimizing the present and future plastic waste, energy, and environmental footprints related to COVID-19. Renew. Sustain. Energy Rev., 127: 109883.

Kuhling, J.G. and Pieper, U. 2012. Management of healthcare waste: developments in Southeast Asia in the twenty-first century. Waste Manage. Res., 30(9_suppl): 100-104.

Kumar, M. 2020. Wastewater monitoring and public health surveillance of SARS-CoV-2. Indian J. Pub. Health, 64(6): 247-8.

Maurya, D.T., Sapkal, G., Yadav, P.D., Belani, S.K.M., Shete, A. and Gupta, N. 2020. Biorisk assessment for infrastructure & biosafety requirements for the laboratories providing coronavirus SARS-CoV-2/(COVID-19) diagnosis. Indian J. Med. Res., 151(2-3): 172.

NGT. 2020. Before The National Green Tribunal Principal Bench, New Delhi. In reply to Scientific Disposal of Bio-Medical Waste arising out of Covid-19 treatment- Compliance of BMW Rules 2016. Available from: https://greentribunal.gov.in/gen_pdf_test.php?filepath. Accessed on 20 April 2021.

Ramteke, S., & Sahu, B. L. 2020. Novel coronavirus disease 2019 (COVID-19) pandemic: considerations for the biomedical waste sector in India. Case Stud. Chem. Environ. Eng., 2: 100029.

Ranjan, M.R., Tripathi, A. and Sharma, G. 2020. Medical waste generation during COVID-19 (SARS-CoV-2) pandemic and its management: an Indian perspective. Asian J. Environ. Sci., pp.10-15.

Sadat, S., Rawtani, D. and Hussain, C.M. 2020. The environmental perspective of COVID-19. Sci. Tota. Environ., 128: 138870.

Sengodan, V.C. 2014. Segregation of biomedical waste in the South Indian tertiary care hospital. J Nat. Sci. Biol. Med., 5(2): 378.

Singh, S. and Prakash, V. 2007. Toxic environmental releases from medical waste incineration: a review. Environmental Monitoring and Assessment,132(1): 67-81.

Sundararaman, T. 2020. Health systems preparedness for COVID-19 pandemic. Indian J. Pub. Health, 64(6): 91.

Syed, E.H., Mutahara, M. and Rahman, M. 2012. Medical waste management (MWM) in Dhaka, Bangladesh: It's a review. Home Health Care Manag. Pract., 24(3): 140-145.

Tandon, P.N. 2020. COVID-19: Impact on health of people & wealth of nations. Indian J. Med. Res., 151(2-3): 121.

Thind, S.P., Sareen, A., Singh, D.D., Singh, S. and John, S. 2021. The compromising situation of India's bio-medical waste incineration units during the pandemic outbreak of COVID-19: Associated environmental-health impacts and mitigation measures. Environ. Pollut., 1; 276: 116621.

Wang, J., Shen, J., Ye, D., Yan, X., Zhang, Y., Yang, W., Li, X., Wang, J., Zhang, L. and Pan, L. 2020. Disinfection technology of hospital wastes and wastewater: suggestions for disinfection strategy during coronavirus Disease 2019 (COVID-19) pandemic in China. Environmental Pollution, 128: 114665.

Wang, J., Shen, J., Ye, D., Yan, X., Zhang, Y., Yang, W., Li, X., Wang, J., Zhang, L. and Pan, L. 2020. Disinfection technology of hospital wastes and wastewater: Suggestions for disinfection strategy during coronavirus Disease 2019 (COVID-19) pandemic in China. Environ. Pollut., 128: 114665.

World Health Organization (WHO) 2020b. Advice on the Use of Masks in The Context of COVID-19: Interim Guidance, 2020.

World Health Organization (WHO). 2020a. Available from: https://www.who.int/emergencies/diseases/novel-coronavirus-2019?gclid=Cj0KCQjw6PD3BRDPARIsAN8pHuG27VS4NA4r-K2nRRqvntrcY3CvZYpkPmv2HSBNovUAXZ0F8jiXjGYaAqihEALw_wcB. Accessed 1 July 2020.

World Health Organization (WHO). 2020c. Rational Use of Personal Protective Equipment (PPE) for Coronavirus Disease (COVID-19): Interim Guidance, 19 March 2020.

World Health Organization (WHO). 2020d. Water, Sanitation, Hygiene and Waste Management for COVID-19: Technical Brief, 03 March 2020.

World Health Organization (WHO). 2020e. Situation Report-11 Novel Coronavirus (2019-ncov), 31 January 2020. Available from: https://www.who.int/docs/default-source/coronaviruse/situation-reports/20200131-sitrep-11-ncov.pdf?sfvrsn=de7c0f7_4. Accessed 23 June 2020.

World Health Organization (WHO). 2020f. Health Care Waste. Available from: https://www.who.int/news-room/fact-sheets/detail/health-care-waste. Accessed 23 June 2020.

Yordanova, D., Angelova, S., Kyoseva, V. and Dombalov, I. 2014. Household medical waste-threat to the environment and human health. Journal of Chemical Technology & Metallurgy, 49(2).

Yu, H., Sun, X., Solvang, W.D. and Zhao, X. 2020. Reverse logistics network design for effective management of medical waste in epidemic outbreaks: insights from the coronavirus disease 2019 (COVID-19) outbreak in Wuhan (China). Int. J. Environ. Res. Public Health, 17(5): 1770.

Zambrano-Monserrate, M.A., Ruano, M.A. and Sanchez-Alcalde, L. 2020. Indirect effects of COVID-19 on the environment. Sci. Tot. Environ., 728: 138813.

Nature Environment and Pollution Technology
An International Quarterly Scientific Journal

p-ISSN: 0972-6268
(Print copies up to 2016)
e-ISSN: 2395-3454

Vol. 20 | No. 5 (Suppl) | pp. 1903-1913 | 2021

Original Research Paper

https://doi.org/10.46488/NEPT.2021.v20i05.006

Open Access Journal

# Characterization and Assessment of Stormwater Runoff Quality from Automobile Workshops in Nigeria Using Multivariate Linear Regression

**C.O. Ataguba† and I. C. Brink**
Department of Civil Engineering, Stellenbosch University, Stellenbosch, South Africa
†Corresponding author. C.O. Ataguba; clematrix2008@gmail.com

**Nat. Env. & Poll. Tech.**
**Website: www.neptjournal.com**

*Received:* 18-02-2021
*Revised:* 25-04-2021
*Accepted:* 03-05-2021

**Key Words:**
Automobile workshop
Electrical conductivity
Heavy metals
Multivariate regression
Stormwater runoff

## ABSTRACT

An investigation into the pollution of stormwater runoff from automobile workshops in Nigeria was performed. Also, multivariate regression was used to predict the pH, oil, and grease (O&G) as well as the electrical conductivity (EC) in relation to the characteristics of the solids and metals pollutants of the untreated automobile workshop stormwater. The results indicated that automobile workshops contributed notable amounts of pollutants to stormwater runoff. Results were compared with Nigerian and USEPA standards. It was found that most of the parameters had mean value ranges far greater than standard limits. The multivariate regression showed variations in the results obtained from different automobile workshops. These variations could be due to the influence of factors such as the volume of automobile servicing activities and the waste generated from these activities that flow in the stormwater runoff. However, the bulk of the EC and pH of the stormwater were associated with the concentrations of the total dissolved solids and copper while the bulk of the O&G concentration was associated with the concentrations of lead and cadmium. It is recommended to treat automobile workshop stormwater to prevent detrimental effects in aquatic systems. Future research is aimed at modeling such treatment using multivariate regression techniques is warranted.

## INTRODUCTION

Economic activities in Nigerian urbanized areas have been identified as non-point sources of pollution in natural water bodies (Ohwo & Abotutu 2015). Automobile workshops are included in such activities and generate, *inter alia*, debris, waste, oils, and greases that are conveyed, untreated, via stormwater drainage systems to natural water bodies. This contributes to the high degree of surface water pollution (Chukwu 2017). This stormwater runoff pollution source has received little attention to date.

Because the types and magnitudes of pollutants produced by automobile workshops are unpredictable, it is difficult to predict the quality of runoff water from these workshops. Automobile workshops and the pollution they generate are distinct from typical diffuse urban pollutant sources due to the activities of the host, requiring a case-specific approach. Additionally, automobile workshops are typically spatially dispersed in the study towns making a centralized treatment system impractical; and funding opportunities for stormwater quality improvement applications in these cases are limited.

Dealing with polluted stormwater runoff and implementing adequate treatment measures, necessitates novel approaches influenced by the nature of the pollutants, their sources (automotive workshops), and the lack of funds for water quality improvement in developing countries. Due to difficulties in dealing with the problem, stormwater runoff is a major source of pollutant mass flows to rivers, which poses a risk to the health of human beings, plants, and animals (Gaffield et al. 2003).

In metropolitan regions, the mechanic village option is characterized by higher levels of pollution. (Nwachukwu et al. 2014). Adewoyin et al. (2013) studied the impacts of auto-mechanic workshops on soil and groundwater in Ibadan, Nigeria. The study revealed the presence of Cadmium, Lead, and Iron in high concentrations. Additionally, water quality analyses showed high values of oil and grease concentration. Demie (2015) studied the level of contamination by metals on soils in some selected auto-mechanical workshops in Shashemane, Ethiopia with the aim of comparing results with existing standards and to determine the effects on human beings and surroundings. The results showed that the overall contamination of soils within the selected study areas was very high for Lead, Nickel, Cadmium, and Cobalt. The need for remedial action to reclaim these areas was emphasized. Similarly, Abidemi (2011), collected soil samples from auto-repair workshops in Osun State, Nigeria to determine the levels of Cobalt, Iron, Lead, and Cadmium on the soil of the auto-repair workshop. The results revealed that the soils in the auto repair workshops were heavily polluted with Iron and

Lead. The study recommended the use of Phytoremediation to remove these metals from the soil. It is therefore apparent that automobile workshops and maintenance centers in developing countries, besides being haphazardly placed, lack waste management and stormwater treatment facilities culminating in environmental pollution (Udebuani et al. 2011).

Documented studies, therefore, show automobile workshops to be a significant source of pollutants metals, oil, and grease. These pollutants are washed off via surface water runoff during rain events and discharged into natural water bodies. This can cause significant harm to the natural environment and pollute human water sources. However, limited literature is available on the profile of pollutants from stormwater runoff from automobile workshops in Nigeria.

Multivariate linear regression is a statistical technique that attempts to predict the relationship/association between two or more explanatory (predictor) variables and response (criterion) variables by fitting a linear equation to observed data (Alexopoulos 2010). Literature has reported the wide application of multivariate statistical techniques in water quality assessment, treatment, and modeling ranging from surface water to groundwater (Arora & Reddy 2013, Charulatha et al. 2017, Kazi et al. 2009, Saleem et al. 2012, Zhao & Cui 2009, Liu et al. 2018). Charulatha et al. (2017) reported the usefulness of multivariate statistical techniques for linear correlations where multiple variables of groundwater pH, TDS, nitrate, sodium, chloride, silicate, and fluoride were used as predictor variables to obtain the criterion variable nitrite ion in a linear regression model. Multivariate regression models predicted the electrical conductivity of surface water very well at a 5% significance level from a study carried out by Saleem et al. (2012).

The aims of this study were: (1) to characterize the untreated stormwater runoff from selected automobile workshops in Nigeria to identify the concentration/profile of selected pollutants and (2) to use the multivariate linear regression to predict the pH, oil, and grease as well as the electrical conductivity in relation to the characteristics of the solids and metals pollutants of the untreated automobile workshop stormwater samples.

## MATERIALS AND METHODS

Data were obtained from the towns of Idah and Lokoja, both in the Guinea Savanna of North Central Nigeria. Idah is located at 7°05'0" N, 6°45'0" E with a total land area of 36 $km^2$ while Lokoja is located at 7°48'32" N, 6°44'15" E with a total land area of 64 $km^2$. The average annual rainfall in the Guinea Savanna is between 1000 and 1200 mm (Salami et al. 2015, Adeoye 2012). Idah is located at the bank of River Niger and Lokoja is located at the confluence of Rivers Niger and Benue in Nigeria. Three (3) automobile workshops were selected for research from Idah and two (2) automobile workshops from Lokoja as given in Table 1. Fig. 1 shows the locations of the study towns from Google Map.

Site inspection revealed that the automobile workshops lacked formal stormwater conveyance systems. The characteristic stormwater runoff was sheet flow. Stormwater

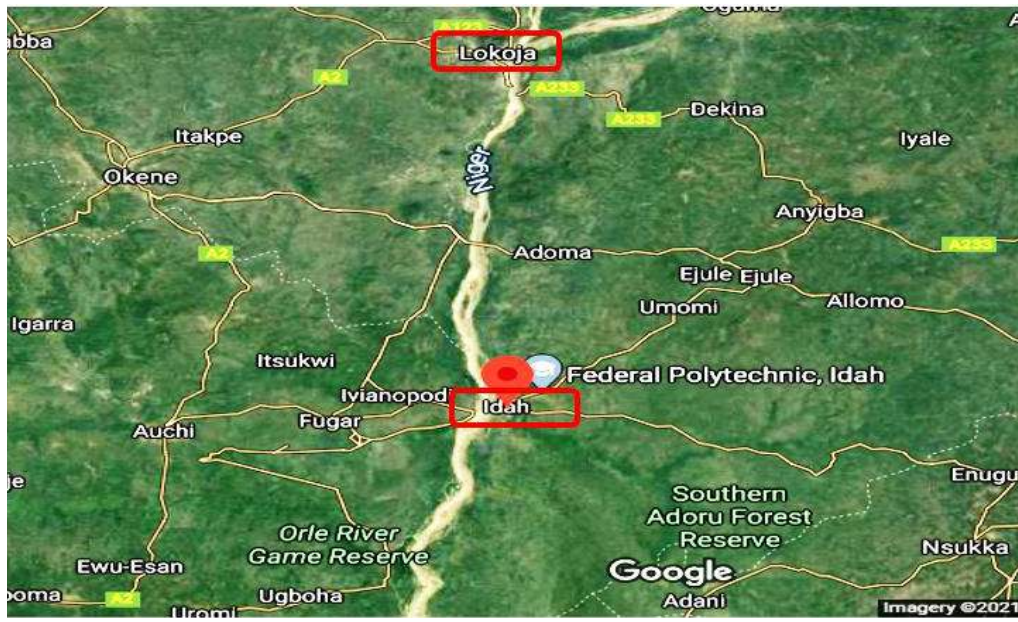


Fig. 1: Satellite imagery of the study areas (Source: Google Map 2021).

Table 1: Automobile Workshops.

| Label | Location | Approximate Area ($m^2$) |
|---|---|---|
| Workshop 01 | Idah | 1 600 |
| Workshop 02 | Idah | 1 800 |
| Workshop 03 | Idah | 1600 |
| Workshop 04 | Lokoja | 3 600 |
| Workshop 05 | Lokoja | 2 400 |

catch-pits were constructed at low points on the workshop premises for the collection of runoff samples. The methodology described in Lowe et al. (2018) was adopted for the collection of the stormwater runoff samples. Sampling involved the collection of stormwater runoff samples from each automobile workshop and water quality tests carried out on weekly basis for a period of nine weeks during the rainy season. Samples were collected in clean laboratory sampling bottles of one and half (1.5 L) Liters capacity for laboratory water quality testing. The following water quality parameters were tested for pH, Conductivity, Turbidity, Oil and Grease, Dissolved Oxygen, Total Dissolved Solids, Total Solids, Total Suspended Solids, Cadmium, Copper, Lead and Iron. Tests were carried out in accordance with APHA (2017) Method 1664B (USEPA 2010). Testing apparatus used: ICE 3000 Series AA spectrometer. All water quality analyses were performed by the Water Quality Control Laboratory at the National Geosciences Research Laboratories in Kaduna, Nigeria. The profile of the pollutants has been shown in Figs. 2-13. The results obtained from the characterization were used for the multivariate regression analyses.

In carrying out the multivariate regression analyses, three different pollutants concentrations namely: pH, electrical conductivity as well as oil & grease were selected as dependent variables while the solids and heavy metals (total dissolved solids, total suspended solids, cadmium, copper, lead, and iron) were used as the independent variables. The mathematical and statistical computations in this work were carried out using Microsoft Excel at 5% significance as described in Charulatha et al. (2017). The association between the dependent and independent variables was determined. The equation for the multivariate regression as adopted from Charulatha et al. 2017 is described in equation 1:

$$Y = \beta_0 + \beta_1 X_1 + \beta_2 X_2 + \cdots + \beta_m X_m + \varepsilon \quad \ldots(1)$$

Where,

Y represents the dependent variable,

$X_1 \ldots X_m$ = the several independent variables,

$\beta_o \ldots \beta_m$ = the regression coefficient

$\varepsilon$ = the standard error from the analyses.

The contributions of each pollutant to the total variation in the measured independent variable concentration $MR^2$ for each of the automobile workshop was computed using equation 2

$$T_x(\%) = \frac{R^2(i)}{\sum MR^2} * 100 \quad \ldots(2)$$

Where

Tx = Contribution of the pollutant in question to the total variation in the measured independent variable concentration

$R^2(i)$ = coefficient of determination of the pollutant concentration under consideration

$MR^2$ = Multivariate coefficient of determination for all the pollutants concentration considered for each (automobile) workshop

The estimated multivariate regression equations relating EC, pH, and O&G with the studied pollutants of the solids and metals were derived for all 5 workshops by the authors. The details of the equations could not be included in this article because of limited space. However, interested readers can contact the corresponding author for further details.

## RESULTS AND DISCUSSION

### Automobile Workshop Stormwater Characterization

Water quality analysis results are presented in Figs. 2 to 13. The Nigerian Standards (NESREA 2011) and USEPA Standard (USEPA 1986, 1988) are also indicated. In this research, the authors have used the upper limits of the standards which serve as the threshold for a disposal to surface water, to compare with the tested parameters as depicted by the red and black dotted lines in Figs. 2- 13. pH values in all cases were highly alkaline (Fig. 2). It ranged from 11.36 (Workshop 03) to 13.95 (Workshop 02). pH values were in all cases higher than the Nigerian and USEPA effluent discharge standards of 6.5 – 8.5 (NESREA 2011, USEPA 1986). A possible cause of high pH may be waste incineration in the workshops. These values indicate that runoff from automobile workshops could be harmful to aquatic ecosystems. For example, fish species typically do not survive in water with a pH above 10 (Cole et al. 1999).

Electrical Conductivity (EC) ranged from 1078.76 µS.cm-1 (Workshop 02) to 4380.5 µS.cm-1 (Workshop 04) (Fig. 3). Workshops 01-03 (Idah) had notably lower values than Workshops 04-05 (Lokoja). However, all values obtained were higher than both the Nigerian and USEPA approved standards range of 200-1000 µS.cm$^{-1}$ (NESREA 2011, USEPA 1986). Reasons for differences in the values for different locations could not be determined. Discharging water with very high conductivity into surface water has been reported as harmful to aquatic animals (et al. 2017).

Turbidity ranged from 302 NTU (Workshop 04 and 05) to 444 NTU (Workshop 02) as shown in Fig. 4. Workshops 01-03 (Idah) typically had higher turbidities than Workshops 04-05 (Lokoja). All values obtained were notably higher than the Nigerian approved standard of 70 NTU and USEPA approved standard of 50 NTU (NESREA 2011, USEPA 1986). It is posited that bare earth platforms used in Workshops 01 – 03 may have been the cause of differences in turbidity values between the different locations (Workshops 04 – 05 had concrete platforms). Stormwater discharge with high turbidity is detrimental to aquatic ecosystems such as reducing the amount of light available for photosynthesis of aquatic plants which some aquatic animals consume and increasing the temperature of water (Boyd 2015) among other effects.

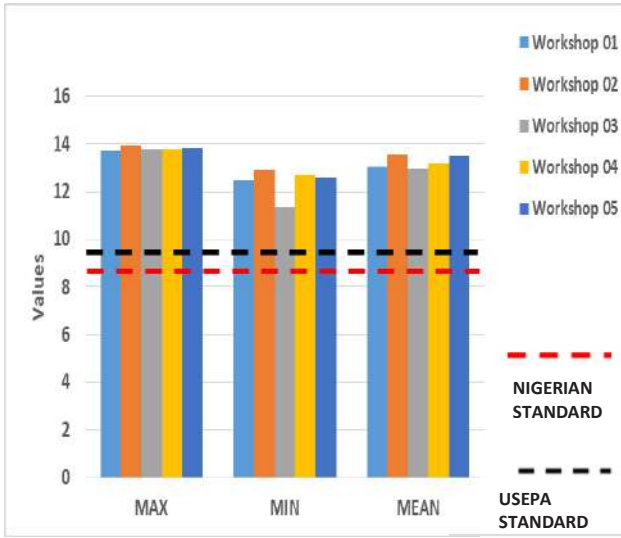


Fig. 2. pH values.

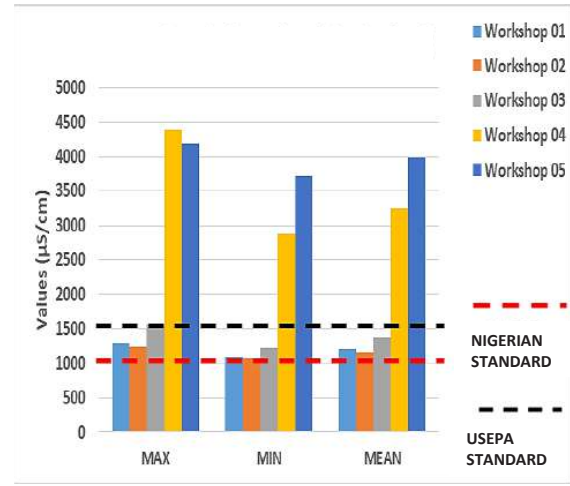


Fig. 3. Electrical conductivity values.

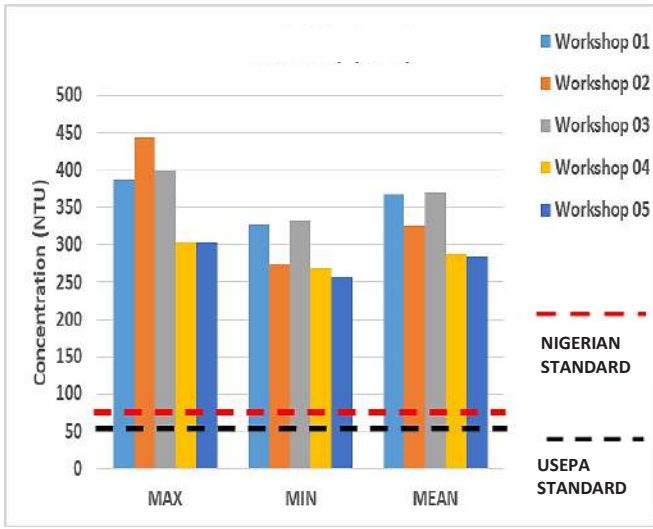


Fig. 4. Turbidity concentration.

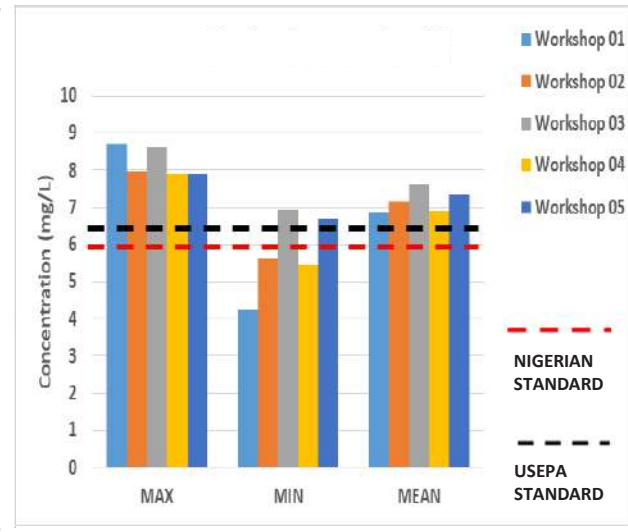


Fig. 5. Dissolved oxygen concentration.

Dissolved Oxygen (DO) ranged from 4.24 mg.L$^{-1}$ (Workshop 01) to 8.7 mg.L$^{-1}$ (also Workshop 01). The mean dissolved oxygen values obtained from Workshops 01-05 ranged between 6.8 and 7.62 mg.L$^{-1}$ (Fig. 5). The values were within acceptable Nigerian and USEPA approved standards of 6.0 mg.L$^{-1}$ and 6.5 mg.L$^{-1}$ minimum respectively (NESREA 2011, USEPA 1986) as values higher than the minimum standards are practically desired (USEPA 1988). Dissolved oxygen is important for respiration by aquatic species (Droste and Gehr 2019).

Total dissolved solids concentrations (TDS) ranged from 936 mg.L$^{-1}$ (Workshop 02) to 3041 mg.L$^{-1}$(Workshop 05) (Fig. 6). Mean values ranged between 832 and 2774 mg.L$^{-1}$. Results varied between locations with TDS from Workshops 01-03 (Idah) mostly close to or below the Nigerian limits of 1000-2000 mg/L (NESREA 2011) and USEPA limits of 1000 mg.L$^{-1}$, and TDS from Workshops 04-05 (Lokoja) above USEPA limits in all cases and Nigerian limits in some cases. Similar trends were observed in the EC results as can be expected due to the capacity of the water sample to conduct electricity being principally dependent on the concentration of dissolved ions (Taylor et al. 2018). Specific reasons for differences in results from the different locations could not be determined. Discharging stormwater with elevated TDS into surface waters inhibits the growth and development of aquatic animals/organisms (Weber-Scannel & Duffy 2007).

Total suspended solids concentrations (TSS) ranged between 465 mg.L$^{-1}$ (Workshop 04) and 2984 mg.L$^{-1}$(also Workshop 04) (Fig. 7). Mean TSS ranged between 1588 and 2504 mg.L$^{-1}$. All values in all cases were higher than Nigeria's discharge limit of 500 mg.L$^{-1}$ and USEPA discharge limit of 100 mg.L$^{-1}$ (NESREA 2011, USEPA 1986). This result is unsurprising and can be explained by the generation of particles through typical automobile workshop activities (grinding, welding, the addition of dirt brought on car tire surfaces, etc.). Discharging stormwater with a high concentration of TSS can affect water clarity with a host of subsequent detrimental effects on aquatic ecosystems (Boyd 2015).

Total solids result from different waste materials generated in the automobile workshops and carried in the runoff stream as solids, liquids, or particles. This study recorded the highest total solids value of 6668 mg/L from Workshop 02. The lowest total solids value of 1336 mg.L$^{-1}$ was obtained from Workshop 01. Mean TS ranged between 2577 and 5278 mg.L$^{-1}$(Fig. 8). The maximum TS concentrations were higher than the Nigerian maximum limit of 2500 mg.L$^{-1}$ and USEPA maximum limit of 1100 mg.L$^{-1}$ (NESREA 2011, USEPA 1986).

Oil and Grease ranged between 3.2 mg.L$^{-1}$ (Workshop 01) and 6.9 mg.L$^{-1}$ (Workshop 02). The mean values are between 5.1 and 6.2 mg.L$^{-1}$ (Fig. 9). The narrow range of mean concentrations is interesting and could indicate a typical concentration of this parameter to be expected from Automobile Workshops. This indicates that future research into this possibility is warranted. All concentrations were significantly higher than Nigeria and USEPA approved standard of 0.1 mg.L$^{-1}$ (NESREA 2011, USEPA 1986). Vehicle servicing activities are indicated as the main contributor of oil and grease in stormwater runoff. Spillage of oil from the change of engine oil in these workshops was observed to be minimal as onsite used oil management involved the collection of used oils from the vehicle engines directly into

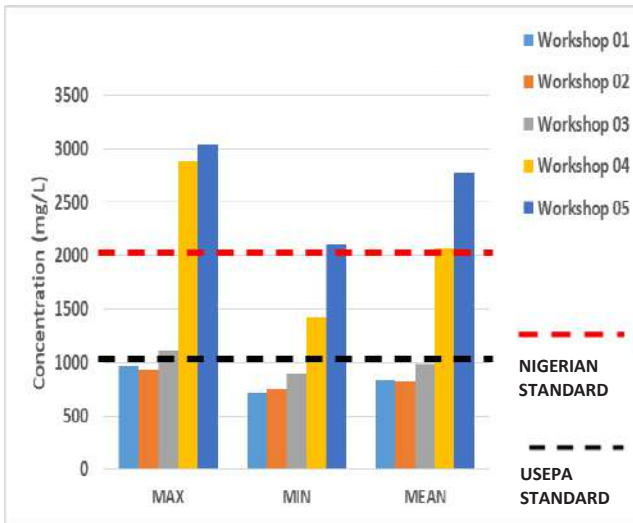


Fig. 6. Total Dissolved Solids concentration.

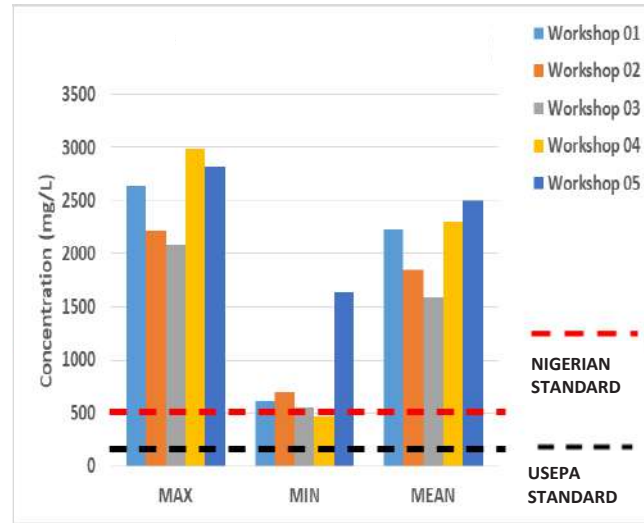


Fig. 7. Total Suspended Solids concentration.

plastic gallons, which are stored and sold for some other uses such as preservatives, for wood seasoning, etc. Much of the oil spillage resulted from the cleaning of oil/grease parts with premium motor spirit (PMS). High oil and grease concentration in surface waters can cause damage to plants and animals in the aquatic ecosystem (Khwakarami 2016).

A range of metal particles is generated in Automobile Workshops. Scraps of vehicle parts, mechanic tools, auto-electrical parts/activities, wear from vehicle tires, etc. are major sources of metals that can easily be transported in any stormwater runoff from an automobile workshop. A possible major source of Lead and Cadmium Automobile Workshops is car battery discharge. (Utang et al. 2013) Fuel in Nigeria (Premium Motor Spirit or PMS) is unleaded and is therefore not a probable source of Lead. Welding and bodywork activities as well as vehicle engine fixing are major sources of Iron Oxide particles (Abidemi 2011, Utang et al. 2013). Electrical activities, metal bushings, and metal-bearing wears are major sources of Copper and Iron (Mohammed & Naik 2011).

Metals concentrations as shown in Figs. 10-13 indicated a trend similar to the work of Prestes et al. (2006) in some cases. The mean concentrations of Lead, Copper, and Cadmium in the stormwater runoff were in the order *Pb>Cu>Cd* for Workshops 01, 03, and 04. Minimum concentrations were, Method Detection Limit (MDL) of 0.005 mg.$L^{-1}$ for Lead; 0.00044 mg.$L^{-1}$ for Cadmium (Workshop 03, Zhong et al. 2016, Golbedaghi et al. 2012) and 0.01 mg.$L^{-1}$ for Copper (Workshop 02). Maximum concentrations were 1.91 mg.$L^{-1}$ for Lead (Workshop 04), 0.062 mg.$L^{-1}$ for Cadmium (Workshop 05) and 0.06 mg.$L^{-1}$ for Copper (Workshops 03 and 05). The mean Copper and Cadmium concentrations from all Workshops ranged between 0.014-0.040 mg.$L^{-1}$. These were higher than Nigerian and USEPA limits of 0.01 mg.$L^{-1}$ and 0.02 mg.$L^{-1}$ for Copper and Cadmium respectively (NESREA 2011, USEPA 1986). The mean Lead concentrations ranged between 0.30-1.33 mg.$L^{-1}$. These were also higher than the Nigerian and USEPA limits of 0.1 mg.$L^{-1}$(NESREA 2011, USEPA 1986).

For Iron, concentrations ranged between 25.4 mg.$L^{-1}$ (Workshop 03) and 43.6 mg.$L^{-1}$ (Workshop 01). Mean values ranged between 32.7-38.0 mg.$L^{-1}$. The mean values obtained for the iron concentration were higher than Nigerian and USEPA limits of 0.5 mg.$L^{-1}$ and 1 mg.$L^{-1}$ respectively (NESREA 2011, USEPA 1986). It is notable that the Iron concentrations were at least 30 times higher than the acceptable discharge limits (Fig. 13). Additionally, the narrow ranges in results indicate that further research into a typical runoff Iron concentration for Workshops is indicated.

Metals concentrations from different workshops were variable, with the exception of Iron. Cadmium in runoff from Workshop 05 was notably high when compared to other workshops, possibly due to more auto-electrical and welding works activities. Copper concentrations in runoff from Workshop 03 were generally higher than that of other workshops, possibly due to auto-electrical works. Workshops 01, 04, and 05 had higher concentrations of Lead when compared with Workshops 02 and 03, possibly due to the high level of auto-electrical repair/servicing activities generating this pollutant there. As noted above, Iron concentrations were similar for all workshops, possibly due to the high level of activities generating this pollutant in all the

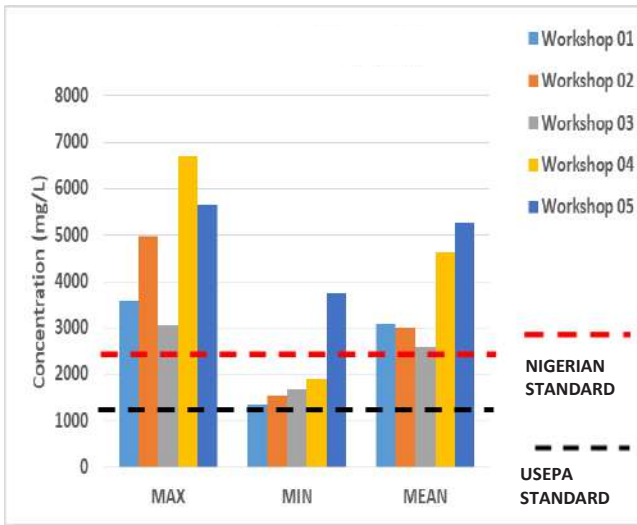


Fig. 8. Total Solids concentration.

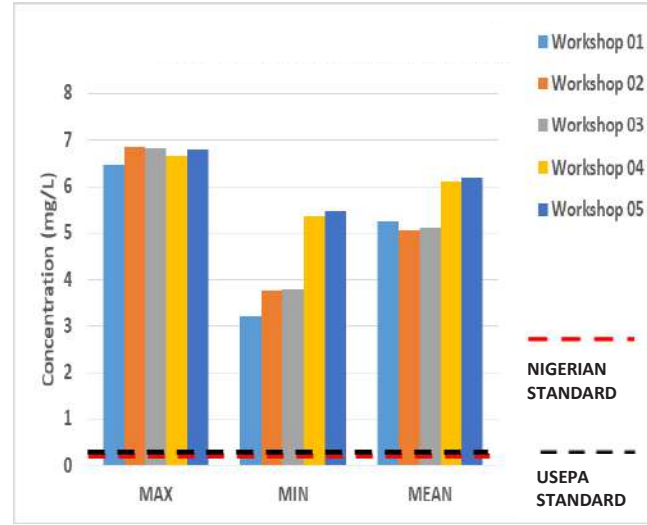


Fig. 9. Oil and Grease concentration.

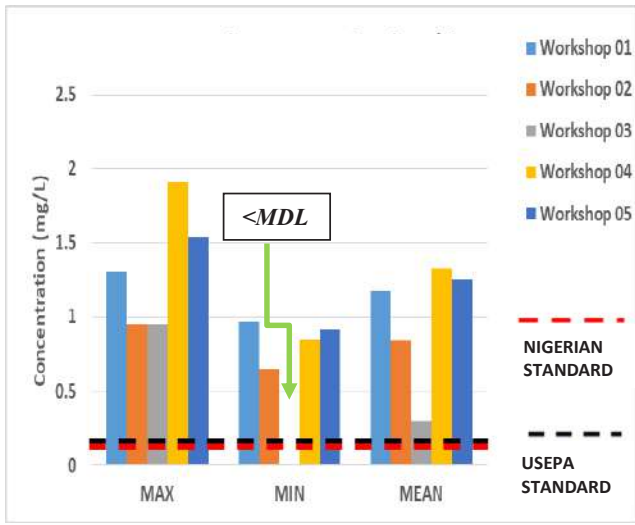


Fig. 10. Lead concentration.

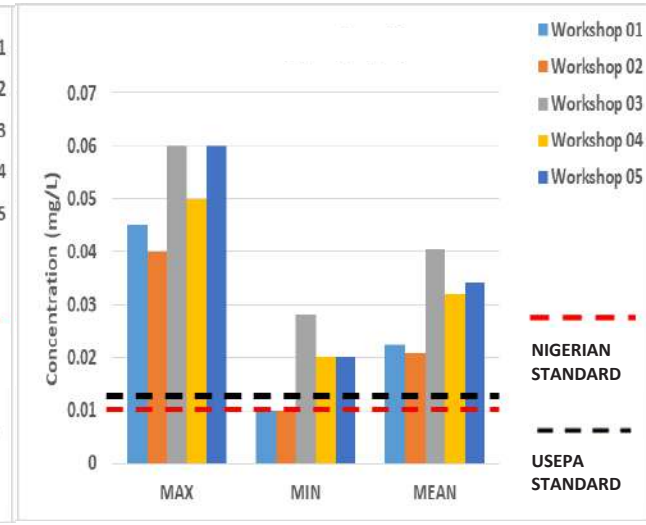


Fig. 11. Copper concentration.

workshops. Metals pollution in surface runoff causes poisoning of aquatic life, human organs, and the nervous system (Shah 2017).

### Multivariate Regression Analyses

The results of the multivariate regression analyses showing the multivariate coefficient of correlation (MR), multivariate coefficient of determination ($MR^2$), and statistical F- values from the ANOVA test have been presented in Tables 2-4. These analyses have investigated the associations/relationships of the EC, pH, and O&G concentrations with metals and solids concentrations in raw automobile workshop stormwater characteristics.

### Electrical Conductivity (EC) vs the Solids and the Metals

From Table 2, the untreated stormwater from workshops 1-4 exhibited very strong $R^2$ ranging from 0.949 to 0.992 for electrical conductivity vs total dissolved solids with an average overall multivariate $R^2$ = 0.998. Similarly, untreated stormwater from workshops 1-3 exhibited strong-very strong positive $R^2$ ranging from 0.686-0.917 for electrical conductivity vs copper concentration. It was observed that an increase in the concentration of copper and total dissolved solids was positively associated with an increase in the electrical conductivity of the untreated stormwater samples from workshops 01-05 as identified above.

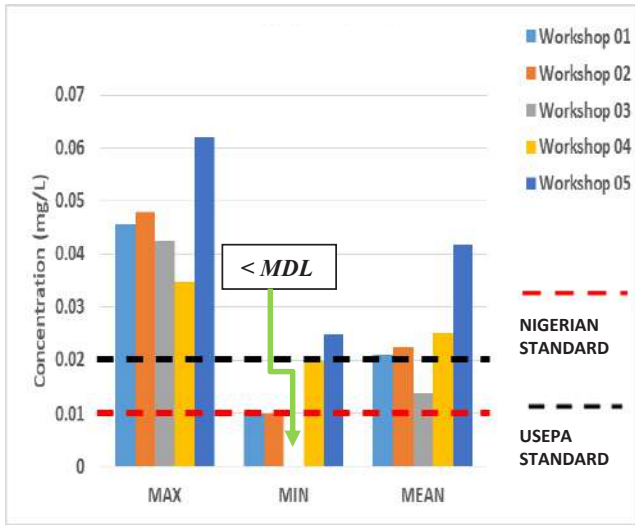


Fig. 12. Cadmium concentration.

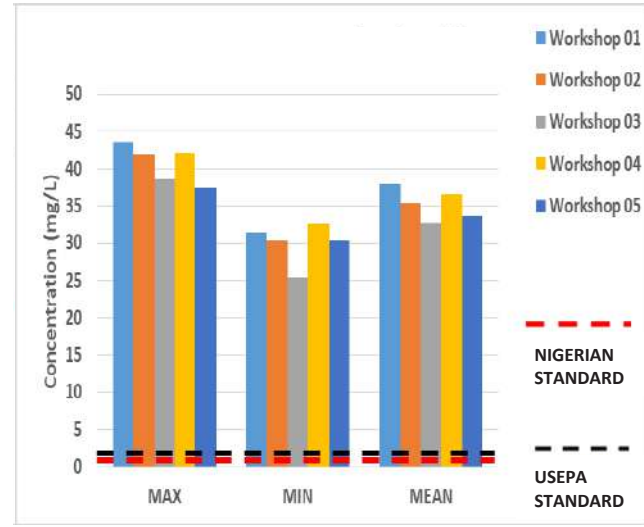


Fig. 13. Iron concentration.

Workshops 02 and 03 exhibited strong $R^2$ (0.670 and 0.766) for electrical conductivity vs lead concentration from untreated stormwater samples. Strong $R^2$ values of 0.686, 0.67, and 0.642 were obtained for EC vs Cu concentration, EC vs Pb concentration, and EC vs Fe concentration respectively from untreated stormwater from workshop 03 while EC vs Cd from untreated stormwater from Workshop 02 produced $R^2 = 0.606$.

The relationships between EC and the other parameters produced a fairly strong $R^2$ with $0.5 \leq R^2 \leq 0.599$: EC vs TSS from Workshops 03 and 04; EC vs Cd from Workshops 01 and 03; as well as EC vs Pb from Workshop 05. Similarly, the relationships between EC and the other parameters produced weak $R^2$ with $0.3 \leq R^2 \leq 0.499$: EC vs TSS from Workshop 02; EC vs Cd from Workshops 04 and 05; EC vs Pb from Workshop 01; as well as EC vs Fe from Workshops 01, 02 and 05. It was also observed that very week $R^2$ values were obtained from the relationships between EC and other parameters with $0.001 \leq R^2 \leq 0.299$: EC vs TDS from Workshop 05, EC vs TSS from Workshops 01 and 05, EC vs Fe from Workshop 04, EC vs Cu from Workshops 01 and 02 as well as EC vs Pb from workshop 04.

From the overall analyses for the electrical conductivity of the untreated stormwater from Workshops, EC concentrations from Workshops 01-05 exhibited a very strong association/relationship with TDS, TSS, Cd, Cu, Pb, and Fe ($R^2$ ranging from 0.991 to 0.999) with multiple correlation R = 0.995 to 0.999.

From Table 5, an EC prediction with a multivariate $R^2$ value of 0.999 in Workshop 01, which represented 99.9% variation in the measured EC, could be attributed to the combined effect of TDS, TSS, Cd, Cu, Pb, and Fe concentrations in the following proportion 37.74%, 0.71%, 20.68%, 10.69%, 16.0%, and 16.08% respectively as determined from equation 2. The same principle was applied to all the Workshops (Table 5) for the prediction of EC concentration in relation to the mentioned pollutants.

The association/relationship between EC and TDS with an average $R^2$ of 0.802 is similar when compared with the research carried out by Noori et al. (2010). These researchers used the canonical correlation analysis and reported that the association between EC and TDS was dominantly very strong with $R^2$ values of 0.993 and 0.822.

## pH vs the Solids and the Metals

Considering the overall analyses for the pH of the untreated stormwater from the automobile workshops, pH concentration from workshop 03 exhibited a very strong association/relationship with Fe ($R^2 = 0.909$) with multiple correlation R = 0.830. Similarly, the pH concentration from workshops

Table 2: $R^2$ from multivariate regression analyses of electrical conductivity with respect to solids and metals pollutants.

| Automobile Workshop | EC vs TDS | EC vs TSS | EC vs Cd | EC vs Cu | EC vs Pb | EC vs Fe | Remarks |
|---|---|---|---|---|---|---|---|
| 01 | 0.956 | 0.019 | 0.553 | 0.286 | 0.428 | 0.43 | MR = 0.999, $MR^2$ = 0.999, F = 7671 |
| 02 | 0.949 | 0.319 | 0.606 | 0.294 | 0.766 | 0.433 | MR = 0.999, $MR^2$= 0.999, F = 10728 |
| 03 | 0.992 | 0.589 | 0.598 | 0.686 | 0.67 | 0.642 | MR = 0.999, $MR^2$= 0.997, F = 116 |
| 04 | 0.957 | 0.536 | 0.309 | 0.899 | 0.253 | 0.02 | MR = 0.999, $MR^2$= 0.997, F = 123.73 |
| 05 | 0.158 | 0.001 | 0.406 | 0.917 | 0.52 | 0.487 | MR = 0.995, $MR^2$= 0.991, F = 35.686 |

Table 3: $R^2$ from multivariate regression analyses of pH with respect to solids and metals pollutants.

| Automobile Workshop | pH vs TDS | pH vs TSS | pH vs Cd | pH vs Cu | pH vs Pb | pH vs Fe | Remarks |
|---|---|---|---|---|---|---|---|
| 01 | 0.096 | 0.079 | 0.1 | 0.554 | 0.11 | 0.015 | MR = 0.843, $MR^2$= 0.711, F = 0.822 |
| 02 | 0.601 | 0.104 | 0.405 | 0.264 | 0.469 | 0.183 | MR = 0.722, $MR^2$= 0.522, F = 0.364 |
| 03 | 0.744 | 0.371 | 0.392 | 0.473 | 0.45 | 0.909 | MR = 0.830, $MR^2$= 0.689, F = 0.739 |
| 04 | 0.31 | 0.254 | 0.329 | 0.488 | 0.02 | 0.001 | MR = 0.899, $MR^2$= 0.808, F = 1.405 |
| 05 | 0.211 | 0.005 | 0.018 | 0.334 | 0.09 | 0.024 | MR = 0.903, $MR^2$= 0.815, F = 1.470 |

02 and 03 exhibited strong association/relationship with TDS ($R^2$ = 0.601 and 0.744 respectively). An increase in TDS and Fe concentrations resulted in an increase in the pH of the stormwater in the mentioned workshops. This implied that the alkalinity of the stormwater samples from workshops 02 and 03 increased with the concentration of the TDS and Fe concentrations. The relationship between the pH of the untreated stormwater and the other pollutants as shown in Table 3 revealed that fairly strong, weak, and very weak associations exist. From Table 6, a pH prediction with a multivariate $R^2$ value of 0.522 in automobile workshop 02, representing 52.2% variation in the measured pH, could also be attributed to the combined effect of TDS, TSS, Cd, Cu, Pb, and Fe concentrations in the following proportion 15.48%, 2.68%, 10.43%, 6.80%, 12.08%, and 4.72% respectively as computed from equation 2. The same principle was also applied to all the automobile workshops (Table 6) for the prediction of pH concentration in relation to the mentioned pollutants.

**O&G vs the solids and the metals**

The overall analyses for the O&G of the untreated stormwater from automobile workshops, (Table 4) have revealed that O&G concentration from automobile workshop 04 exhibited a very strong association/relationship with Pb ($R^2$= *0.912*) with multiple correlation R = 0.929. Table 4 also revealed that fairly strong, weak, and very weak relationships exist between the O&G concentration of untreated stormwater and the other pollutants. O&G prediction with a multivariate $R^2$ value of 0.695 in automobile workshop 05 shown in Table 7, represented 69.5% variation in the measured O&G concentration, could be attributed to the combined effect of TDS, TSS, Cd, Cu, Pb, and Fe concentrations in the following proportion: 0.20%, 7.60%, 18.55%, 12.44%, 9.03%, and 21.67% respectively as calculated from equation 2. The same procedure was also used for all the workshops (Table 7) for the prediction of O&G concentration in relation to the pollutants mentioned above.

The results have also revealed a dominantly weak association/relationship between O&G and TSS with an average $R^2$ of 0.113 from automobile workshops 1-5.

This study has shown that there is a strong association between the electrical conductivity of the automobile workshop stormwater and the total dissolved solids contained in the water sample. This trend was also reported in Saleem et al (2012) from a study where EC concentration exhibited a strong significant and positive relationship with $Cl^-$, $HCO3^-$, $Mg2^+$ and TS with an $R^2$ value of 0.804. This phenomenon could mean that bulk of the electrical conductivity of the stormwater is associated with the concentrations of the total dissolved solids and copper (mean values of 25% and 20.5% respectively) from Table 5. Similarly, from Table 6 the bulk of the pH of the stormwater is associated with the concentrations of copper and the total dissolved solids (mean values

Table 4: $R^2$ from multivariate regression analyses of O&G with respect to solids and metals pollutants.

| Automobile Workshop | O&G vs TDS | O&G vs TSS | O&G vs Cd | O&G vs Cu | O&G vs Pb | O&G vs Fe | Remarks |
|---|---|---|---|---|---|---|---|
| 01 | 0.096 | 0.185 | 0.469 | 0.028 | 0.438 | 0.501 | MR = 0.980, $MR^2$ = 0.960, F = 8.025 |
| 02 | 0.391 | 0.092 | 0.149 | 0.00009 | 0.481 | 0.215 | MR = 0.984, $MR^2$ = 0.967, F = 9.863 |
| 03 | 0.128 | 0.021 | 0.381 | 0.32 | 0.362 | 0.00004 | MR = 0.983, $MR^2$ = 0.966, F = 9.473 |
| 04 | 0.358 | 0.0004 | 0.041 | 0.216 | 0.912 | 0.046 | MR = 0.929, $MR^2$ = 0.863, F = 2.097 |
| 05 | 0.007 | 0.266 | 0.649 | 0.435 | 0.316 | 0.758 | MR = 0.934, $MR^2$ = 0.695, F = 0.759 |

Table 5: Proportion of $R^2$(%) for EC relationship with each pollutant making up the overall multivariate $R^2$ for each automobile workshop.

| Automobile Workshop | EC vs TDS (%) | EC vs TSS (%) | EC vs Cd (%) | EC vs Cu (%) | EC vs Pb (%) | EC vs Fe (%) | Multivariate $R^2$(%) |
|---|---|---|---|---|---|---|---|
| 01 | 35.74 | 0.71 | 20.68 | 10.69 | 16.00 | 16.08 | 99.9 |
| 02 | 28.16 | 9.46 | 17.98 | 8.72 | 22.73 | 12.85 | 99.9 |
| 03 | 23.68 | 14.06 | 14.27 | 16.37 | 15.99 | 15.32 | 99.7 |
| 04 | 32.08 | 17.97 | 10.36 | 30.14 | 8.48 | 0.67 | 99.7 |
| 05 | 6.29 | 0.04 | 16.16 | 36.51 | 20.70 | 19.39 | 99.1 |

Table 6: Proportion of $R^2$(%) for pH relationship with each pollutant making up the overall multivariate $R^2$ for each automobile workshop.

| Automobile Workshop | pH vs TDS (%) | pH vs TSS (%) | pH vs Cd (%) | pH vs Cu (%) | pH vs Pb (%) | pH vs Fe (%) | Multivariate $R^2$(%) |
|---|---|---|---|---|---|---|---|
| 01 | 7.15 | 5.89 | 7.45 | 41.29 | 8.20 | 1.12 | 71.1 |
| 02 | 15.48 | 2.68 | 10.43 | 6.80 | 12.08 | 4.72 | 52.2 |
| 03 | 15.35 | 7.66 | 8.09 | 9.76 | 9.29 | 18.76 | 68.9 |
| 04 | 17.87 | 14.64 | 18.96 | 28.12 | 1.15 | 0.06 | 80.8 |
| 05 | 25.21 | 0.60 | 2.15 | 39.91 | 10.76 | 2.87 | 81.5 |

Table 7: Proportion of $R^2$(%) for O&G relationship with each pollutant making up the overall multivariate $R^2$ for each automobile workshop.

| Automobile Workshop | O&G vs TDS (%) | O&G vs TSS (%) | O&G vs Cd (%) | O&G vs Cu (%) | O&G vs Pb (%) | O&G vs Fe (%) | Multivariate $R^2$(%) |
|---|---|---|---|---|---|---|---|
| 01 | 5.37 | 10.34 | 26.22 | 1.57 | 24.49 | 28.01 | 96.00 |
| 02 | 28.47 | 6.70 | 10.85 | 0.01 | 35.02 | 15.66 | 96.71 |
| 03 | 10.20 | 1.67 | 30.37 | 25.50 | 28.85 | 0.00 | 96.60 |
| 04 | 19.64 | 0.02 | 2.25 | 11.85 | 50.04 | 2.52 | 86.32 |
| 05 | 0.20 | 7.60 | 18.55 | 12.44 | 9.03 | 21.67 | 69.50 |

of 25.2% and 16.2% respectively). However, the bulk of the O&G concentration (Table 7) of the automobile workshop stormwater is associated with the concentrations of lead and cadmium (mean values of 29.5% and 17.7% respectively).

## CONCLUSION

Automobile workshop runoff was typically very alkaline (pH > 11) in all cases. EC was greater than 1000 µS/cm, Turbidity was greater than 300 NTU, TSS was greater than 465 $mg.L^{-1,}$ and Oil and Grease were higher than 3.2 $mg.L^{-1}$ in all cases. All these values were greater than both the Nigerian and USEPA discharge limits NESREA 2011; USEPA 1986). TDS concentrations were close to or below discharge limits for workshops located in Idah, and above limits for Workshops located in Lokoja. Reasons for these differences could not be determined. Cadmium, Lead, Copper, and Iron had mean values greater than discharge limits in all cases. Iron concentrations were notably more than 30 times higher than discharge limits.

Some parameters had narrow ranges despite being tested in different locations and even different towns. For example, the narrow range of mean Oil and Grease as well as Iron concentrations is interesting and could indicate a typical concentration of this parameter to be expected from Automobile Workshops.

The multivariate analyses of the concentration of the pollutants using regression analyses enabled the identification of contributions of these pollutants in the overall stormwater quality from the selected automobile workshops. The study has revealed that while the association/relationship between EC and TDS was dominantly the strongest, the association/relationship between O&G and TSS was dominantly the weakest from all the automobile workshops. It is possible that the influence of certain factors such as the volume of automobile servicing activities as well as the waste generated from these activities that are carried in the stormwater runoff have affected variations in results obtained.

Automobile workshop runoff, therefore, has a great potential of harm to receiving aquatic ecosystems and even humans. It is therefore recommended that designs for onsite treatment of stormwater runoff from automobile workshops be implemented to reduce the concentration of pollutants before discharge into the receiving water. The need for future research into establishing typical runoff parameters or ranges for certain pollutants, to be used in future design, is warranted.

## ACKNOWLEDGMENT

This research was funded by the Tertiary Education Trust Fund, Nigeria.

## REFERENCES


Abidemi, O.O. 2011. Levels of Pb, Fe, Cd, and Co in soils of automobile workshops in Osun State, Nigeria. J. Appl. Sci. Environ. Manage., 15(2): 279-282.

Adeoye, N.O. 2012. Spatio-Temporal analysis of land use/cover change of Lokoja: A confluence town. J. Geogr. Geol., 4(4): 40-51.

Adewoyin, O.A., Hassan, A.T. and Aladesida, A.A. 2013. The impacts of auto-mechanic workshops on soil and groundwater in Ibadan metropolis. Afr. J. Environ. Sci. Technol., 7(9): 891-898.

Alexopoulos, E.C. 2010. Introduction to multivariate regression analysis. Hippokratia, 14(Suppl 1): 23-28.

APHA. 2017. Standard Methods for the Examination of Water and Wastewater. 23rd Edition. American Public Health Association, U.S.A.

Arora, A.S. and Reddy, A.S. 2013. Multivariate analysis for assessing the quality of stormwater from different urban surfaces of the Patiala city, Punjab (India). Urban Water J., 10 (6): 422-433.

Boyd, C.E. 2015. Water Quality: An Introduction. Second Edition. Springer International Publishing Switzerland. 357pp.

Charulatha, G., Srinivasalu S., Uma Maheswari, O., Venugopal, T. and Giridharan, L. 2017. Evaluation of groundwater quality contaminants using linear regression and artificial neural network models. Arab. J. Geosci., 10: 128.

Chukwu, K.E. 2017. Pollution of surface water resources in Nigeria. Int. J. Academic Res. Environ. Geogr., 4(1): 78-92.

Cole, S., Codling, I., Parr, W. and Zabel, T. 1999. Guidelines for Managing Water Quality Impacts within UK European Marine Sites. Water Research Council (WRC), Swindon, 441pp

Demie, G. 2015. Analyzing soil contamination status in garage and auto mechanical workshops of Shashemane City: implication for hazardous waste management. Environ. Systems Res., 4(15): 46-71.

Droste, R. and Gehr, R. 2019. Theory and Practice of Water and Wastewater Treatment. Second Edition. John Wiley, USA. 816pp.

Gaffield, S.J., Goo, R.L., Richards, L.A. and Jackson, R.J. 2003. Public health effects of inadequately managed stormwater runoff. Am. J. Public Health, 93(9): 1527-1533.

Golbedaghi, R., Jafari, S., Yaftian, M.R., Salehzadeh, S. and Jaleh, B. 2012. Determination of cadmium(II) ion by atomic absorption spectrometry after cloud point extraction. J. Iran Chem. Soc., 9: 251-256.

Google Map. 2021. Locational Map of Idah and Lokoja Towns in Nigeria. https://www.google.com/maps/search/Idah+and+Lokoja/@7.4380131,6.5431331,8.12z. (Accessed on 13th February 2021).

Imo, C.I., Nwakuba, N.R., Asoegwu, S.N. and Okereke, N.A.A. 2017. Impact of brewery effluents on surface water quality in Nigeria: A review. Chem. Res. J., 2: 101-113.

Kazi, T.G., Arain, M.B., Jamali, M.K., Jalbani, N., Afridi, H.I., Sarfraz, R.A., Baig, J.A. and Shah, A.Q. 2009. Assessment of water quality of polluted lake using multivariate statistical techniques: A case study. Ecotoxicol Environ. Safety, 72(2): 301-309.

Khwakarami, A.I. 2016. Effects of fat, oil, and grease discharge pollutants on water quality of Qalyasan Stream, Tanjero River and impact of fat, oil, and grease on Darbandikhan Reservoir in Sulaimani City-Kurdistan region of Iraq-Iraq. Inter. J. Environ. Eco. Family Urb. Studies, 6: 1-12.

Liu, Z., Joo, J.C., Choi, S.H., Heo, N., Jang, J. and Hur, J.W. 2018. Assessment of surface water quality in Geum River Basin, Korea using multivariate statistical techniques. Int. J. Appl. Eng. Res., 13(9): 6723-6732.

Lowe, J., Deleon, D., Collins, J., Hoover, R. and Book, S. 2018. Standard Operating Procedure for Collecting Grab Samples from Stormwater Discharges v1.1. Washington State Department of Ecology, Olypia,WA. 15p.PublicationNo. 18-10-023. https://fortress wa.gov/ecy/publications/summarypages/1810023.html.

Mohammed, S.A.S. and Naik, M. 2011. Utilization of red soils and amended soils as a liner material for attenuation of copper from aqueous solution: Isotherm and kinetic studies. J. Environ. Sci. Technol., 4: 504-519.

NESREA 2011. National Environmental (Surface and Ground Water Quality Control) Regulations. National Environmental Standards and Regulations Enforcement Agency. Federal Ministry of Environment. Federal Republic of Nigeria Official Gazette, 98(49).

Noori, R., Sabahi, M.S., Karbassi, A.R., Baghvand, A. and Zadeh, H.T. 2010. Multivariate statistical analysis of surface water quality based on correlations and variations in the data set. Desalination, 260(1-3): 129-136.

Nwachukwu, M.A., Umunna, N.A., Ntesat, B. and Umunna, C.P. 2014. Concept and design of environmentally friendly automobile mechanic village. J. Civil Environ. Eng., 4, 136.

Ohwo, O. and Abotutu, A. 2015. Environmental impact of urbanization in Nigeria. Current Journal of Appl. Sci. Technol., 9(3): 212-221.

Prestes, E.C., dos Anjos, V.E., Sodré, F.F. and Grassi, M.T. 2006. Copper, lead and cadmium loads and behavior in urban stormwater runoff in Curitiba, Brazil. J. Braz. Chem. Soc., 17(1): 53-60.

Salami, A.W., Mohammed, A.A., Adeyemo, J.A. and Olanlokun, O.K. 2015. Assessment of the impact of climate change on runoff in the Kainji lake basin using statistical methods. Int. J. Water Resour. Environ. Eng., 7(2): 7-16.

Saleem, A., Dandigi, M.N. and Vijaykumar K. 2012. Correlation-regression model for physico-chemical quality of groundwater in the South Indian city of Gulbarga. Afr. J. Environ. Sci. Technol., 6(9): 353-364.

Shah, A.I. 2017. Heavy metal impact on aquatic life and human health – An overview. In: Proceedings of the 37th Annual Conference of the International Association for Impact Assessment. 4-7 April 2017, Le Centre Sheraton, Montréal, Canada.

Taylor, M., Elliot, H.A. and Navitsky, L.O. 2018. Relationship between total dissolved solids and electrical conductivity in Marcellus hydraulic fracturing fluids. Water Sci. Technol., 77(8): 1998-2004.

Udebuani, A.C., Okoli, C.I., Nwaigwe, H. and Ozoh, P. 2011. Effect of spent engine oil pollution on arable soil of Nekede mechanic village Owerri, Imo State Nigeria. Int. J. Nat. Appl. Sci., 7: 257-260.

USEPA 2010. Method 1664, Revision B: n-Hexane Extractable Material (HEM; Oil and Grease) and Silica Gel Treated n-Hexane Extractable Material (SGT-HEM; Non-polar Material) by Extraction and Gravimetry. The United States Environmental Protection Agency, 35pp.

USEPA 1988. Dissolved Oxygen. Water Quality Standards Criteria Summaries: A compilation of State/Federal Criteria. The United States Environmental Protection Agency Office of Water Regulations and Standards, Washington DC 20460. Report No. 460/5-88-024.

USEPA 1986. Quality Criteria for Water. The United States Environmental Protection Agency Office of Water Regulations and Standards, Washington DC 20460. Report No. 440/5-86-001.

Utang, P., Eludoyin, O. and Ijekeye, C. 2013. Impacts of automobile workshops on heavy metals concentrations of urban soils in Obio/Akpor LGA, Rivers State, Nigeria. Afr. J. Agric. Res., 8: 3476 – 3482. http://dx.doi.org /10.5897/AJAR2013.6753.

Weber-Scannell, P.K. and Duffy, L.K. 2007. Effects of total dissolved solids on aquatic organisms: A review of literature and recommendations for Salmonid Species. Am. J. Environ. Sci., 3(1): 1-6.

Zhao, Z.W., and Cui, F.Y. 2009. Multivariate statistical analysis for the surface water quality of Luan River, China. J. Zhejiang Univ. Sci. A, 10: 142-148.

Zhong, W.S., Ren, T. and Zhao, L.J. 2016. Determination of Pb (Lead), Cd (Cadmium), Cr (Chromium), Cu (Copper), and Ni (Nickel) in Chinese tea with high-resolution continuum source graphite furnace atomic absorption spectrometry. J. Food Drug Anal., 24(1): 46-55,

Nature Environment and Pollution Technology
An International Quarterly Scientific Journal

p-ISSN: 0972-6268
(Print copies up to 2016)
e-ISSN: 2395-3454

Vol. 20 | No. 5 (Suppl) | pp. 1915-1921 | 2021

Original Research Paper

https://doi.org/10.46488/NEPT.2021.v20i05.007

Open Access Journal

# Current Approach to Develop $TiO_2$ Thin Film as Photocatalysts for Low-Density Plastic Degradation

**D. P. Dave† and K. V. Chauhan**

CHAMOS Matrusanstha Department of Mechanical Engineering, Chandubhai S. Patel Institute of Technology (CSPIT), CHARUSAT, Changa-388421, Gujarat, India

†Corresponding author: D. P. Dave; davedivyesh01@gmail.com

**Nat. Env. & Poll. Tech.**
**Website: www.neptjournal.com**

*Received:* 27-02-2021
*Revised:* 25-04-2021
*Accepted:* 02-05-2021

**Key Words:**
Titania thin film
Photocatalysis
Low-density plastic
Degradation

## ABSTRACT

Low-density plastic bags waste disposal is a big issue in the current scenario which gives rise to grave threats to human beings and environmental health also. Amid the various approaches applied for dealing with the problem, photocatalytic biodegradation in visible light irradiation is an advanced prospect that has received attention nowadays. The present review paper is to provide an outline of the current progress on the synthesis of titania ($TiO_2$) thin-film photocatalysts for solid waste removal. The Photocatalysis method contains the photoinduced redox reactions in the photocatalyst which facilitates the degrading of almost organic compounds like polyethylene into carbon dioxide ($CO_2$), water, and other substance. One of the most excellent photocatalysts which has grabbed attention in an application is titania because of its high photocatalytic activity and chemical stability. The synthesis of the photocatalyst as a thin film is a result of the unfeasible application of conventional powder photocatalyst which may cause a certain environmental hazard. The photocatalyst-coated thin film along with some environmental applications have also been reviewed. Likewise, various approaches for modifying thin-film property, film deposition techniques, and deposition on various substrates are used for the enhanced photocatalytic activity of the $TiO_2$ thin film.

## INTRODUCTION

Plastic waste is a worldwide issue; still, there is variability from region to region. Fumes released from plastic burning are one of the sources of environmental air pollution. Furthermore, dumping plastic into the ocean leads to releasing toxic chemicals contained in it because of which a large amount of water is polluted. Plastic waste accounts for approximately 10% of all household waste disposed of in landfills (Barnes et al. 2009, Hopewell et al. 2009). However, 60 to 80 percent of waste is generated along coastlines, with the amount varying depending on the ocean (Barnes 2002, Derraik 2002). According to Central Pollution Control Board (CPCB) estimation, 8 million tons per annum of plastic is used in India, and annually about 5.7 million tons of plastic is transformed into waste (Rathi 2007). The rise in plastic consumption and production has resulted in increases in plastic waste (UNEP 2009). As a result, in 2007, higher than 250 million tons of plastic waste was generated. Plastic materials are not biodegradable and have a low density, making them unsuitable for landfill disposal. Since 1950, this figure has risen at an average annual pace of roughly 9%, reaching 245 million tonnes in 2008. Plastic bags and other plastics have been a focus since they have been linked to several other problems in India, including animal deaths, contaminated soils, and clogged sewers (Gawande et al. 2012).

Large amounts of plastic will result in an increase in waste and have an adverse impact on the environment. Due to the lack of proper waste management practices, plastic waste will increase, adding to the already existing plastic waste. There is no evidence that specifies a definite time for plastic degradation, however, it could be thousands of years (Kershaw et al. 2011).

Waste disposal in landfills results in the irrevocable loss of major crude materials and energy. The incomplete ignition of Polyethylene (PE), Polystyrene (PS), and Polypropylene (PP) at the time of thermal usage can lead to a high amount of carbon monoxide (CO) and emanations, whereas PVC produces carbon black, dioxins, and aromatics compounds such as pyrene and chrysene. Bromide and different color pigments containing heavy metals such as copper, chromium, selenium, cobalt, cadmium, and lead, among others, can be detected in a noxious discharge. Plastic wastes are always accumulated at open grounds, drifts, railroad tracks, and drains (Islam et al. 2011). Despite many efforts to manage waste, over 91% of MSW gathered is still landfilled or unloaded on open grounds (Verma et al. 2016).

Every year, around 140 million tonnes of plastic are produced, with the excess amount ending up in the environment as an industrial waste dump (Shimao 2001). Cosmetics, food packaging, synthetic compounds, pharmaceuticals,

and cleansers account for about 30% of all plastics used worldwide. Furthermore, this is still increasing at a rapid rate of 12 percent every year (Sangale et al. 2012). Plastics have supplanted paper and other cellulose-based items for packing as plastics have good elasticity, delicacy, protection from water, and microbial resistance. Usually applied plastics have mostly been used in polyethylene (Low Density, medium density, high density, and linear low density), polystyrene (PS), polyvinyl chloride (PVC), and polypropylene (PP) (Khanam & AlMaadeed 2015). Because of its hydrophobic backbone chain, low-density polyethylene is classified as a thermoplastic (Pramila & Ramesh 2015). It is considered non-degradable in nature (Misra et al. 2015). As a result, several countries have been forced to devise measures to counteract the threat.

The environmental impact of main and secondary sources of microplastics must be addressed immediately (Arthur et al. 2009). More research is needed to determine how many degrees of exposure are caused by plastic waste, as well as the components of plastic that may impact humans and animals. Those at the high degree of the food chain would be exposed to synthetic substances in larger quantities.

## $TiO_2$ as a Photocatalysts

Since ancient times, $TiO_2$ powders have been widely used in paints to get white shades (Hashimoto et al. 2005). Later, its photocatalytic activity was explored and considered the most effective photocatalyst (Fujishima & Honda 1972). $TiO_2$ is known for its different properties, including strong photoactivity, high stability, low cost, and low toxicity (Pant et al. 2014a, Pant et al. 2020). Over the last few years, TiO2-based nanomaterial has received a lot of attention in academia and has been used in a variety of applications, including the removal of natural toxins, sensors, photovoltaics, antimicrobials, and energy conservation (Bai & Zhou 2014, Hsu et al. 2019, Nakata & Fujishima 2012, Pant et al. 2014a, 2019b, 2020, 2016).

$TiO_2$ nanostructures with a bandgap of 3.0–3.2 eV can be activated in the presence of UV light irradiation. Because of this, the use of $TiO_2$ is limited because only 5% of the sunlight falls inside the UV spectrum (Daghrir et al. 2013, Pant et al. 2014b, 2019a). $TiO_2$ is found in three types of crystal structures i.e. anatase, rutile, and brookite (Allen et al. 2018). Although brookite is known as the most unstable structure and is not favored for photocatalytic activity, rutile and anatase type crystal forms are examined for photocatalysis (Di Paola et al. 2013, Zhang et al. 2008). The bandgaps of mass anatase and rutile are 3.2 and 3.0 eV respectively, which relate to the absorbance at 388 nm and 414 nm, individually (Dette et al. 2014). In comparison to rutile, the anatase phase crystal structure is favored as the most photo catalytically active due to its ability to adsorb hydroxyl groups and water (Wang et al. 2018). Research has indicated that the synergistic impact among anatase and rutile is useful in upgrading the photocatalytic activity of the $TiO_2$ nano-structures (Zhang et al. 2008).

When a photon (with energy equal to or greater than the bandgap of $TiO_2$) stimulated the $TiO_2$ thin film or nanoparticles, the electrons moved from the valance bandwidth to the conduction bandwidth and generated electron-hole pairs. The created charge particles travel to the surface area and quickly react with the adsorbed organic compounds, resulting in the organic pollutant and solid waste being degraded. Fig. 1 depicts the technique for highly excited oxidant production and breakdown of organic waste.

## Correlation of Thin-film Structure and Photocatalytic Activity

Titania ($TiO_2$) has been documented as an efficient photocatalyst along with high chemical stability and potent photocatalytic activity. As the outcome of various research, it was found that Titania has better photocatalytic activity than Zirconium oxide ($ZrO_2$), Tungsten trioxide ($WO_3$), Tin (IV) oxide ($SnO_2$), and Cadmium sulfide CdS. For instance, for the decomposition of phenol organic compound, $TiO_2$ was exhibited higher photocatalytic activity compared to CdS (Thiruvenkatachari et al. 2008). Titania is present in three different types of crystal structure; rutile, brookite, and anatase. Titania is primarily used in the anatase-type crystal structure as the photocatalyst since it has greater bandgap energy than rutile. Because of this, the anatase crystal structure can reduce electron-hole recombination, resulting in a higher degree of surface hydroxylation and the ability to create more hydroxyl radicals as the surface is illuminated. Certainly, this can lead to the efficiency of photocatalytic activity. On the other side, the crystal structure with a rutile type can absorb the beams that are somewhat nearer to the visible light range. It is accepted that the rutile type is more desirable as a photocatalyst for photocatalysis applications. Nonetheless, the rutile type energy structure is unable to provide the preferred photocatalytic execution since its conduction band is close to the redox potential of hydrogen, resulting in its reduced ability.

The oxygen ions present on the surface of the anatase crystal structure are displayed in a triangle shape, allowing better absorption of organic substances such as polyethylene (Thiruvenkatachari et al. 2008). Furthermore, the location of Ti ions provides a more favorable environment for reaction, as does the absorbed organic compound, which is not accessible in the rutile crystal structure (Thiruvenkatachari et

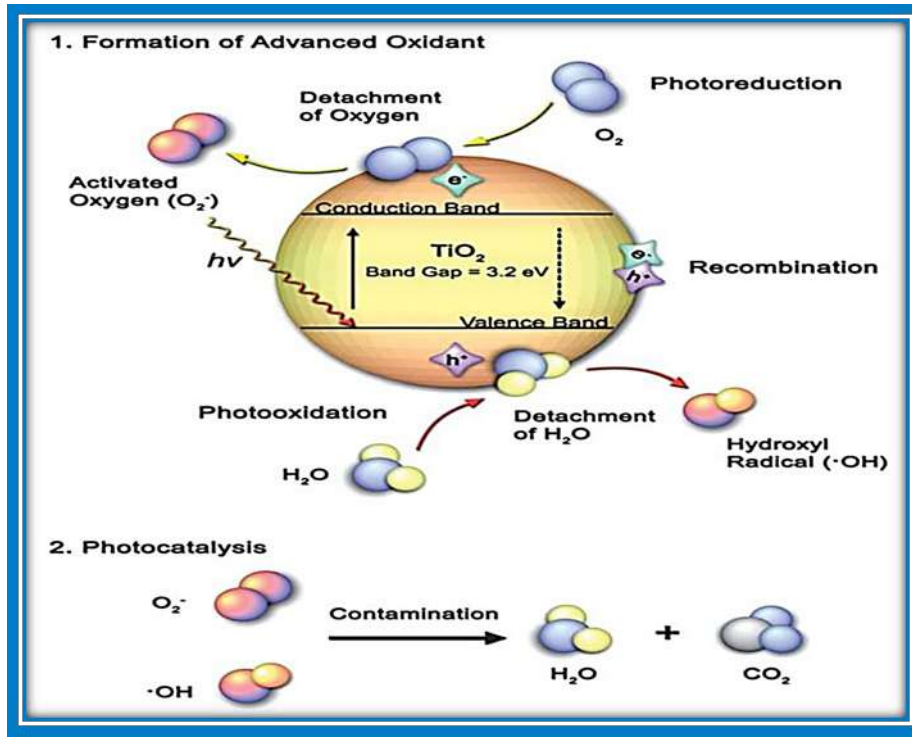


Fig. 1: A schematic diagram of photocatalysis by $TiO_2$ nanostructure (Tung & Daoud 2011).

al. 2008). This remarkable property of anatase would result in strong photocatalytic activity. Nonetheless, a few studies revealed that pure anatase titania would not result in significantly improved photocatalytic activity (Thiruvenkatachari et al. 2008). The presence of a mesoporosity type structure and more extensive pore dissemination in a small percentage of the rutile phase crystal structure could explain the increased photocatalytic action. One of the instants is the commercially accessible Degussa P25 $TiO_2$, which consists of 70% anatase and 30% rutile type crystal structure.

The three-sided layout of oxygen particles on the uncovered precious stone surface of anatase allows for strong organic retention (Thiruvenkatachari et al. 2008). Furthermore, the presence of titanium particles provides a positive response state with assimilated organics that are inaccessible to the rutile structure (Thiruvenkatachari et al. 2008). This special character of anatase would prompt high photocatalytic movement. In any case, a few specialists expressed that unadulterated anatase $TiO_2$ would not lead to much better photocatalytic execution (Thiruvenkatachari et al. 2008). The inclusion of a few percent of the rutile stage results in a mesoporosity structure and more widespread pore dissemination, which could explain the increased photocatalytic activity. One of the models is the financially accessible Degussa P25 $TiO_2$, which contains 70% anatase and 30% rutile.

The surface area of photocatalytic agents is also a key factor that influences photocatalytic activity. a small size particle has a larger surface area and thus increases the availability of active sites per square meter, which boosts pollutant absorption on the photocatalytic agent's surface. Photocatalytic activity is boosted as a result of this mechanism (Thiruvenkatachari et al. 2008).

Several investigations support that $TiO_2$ is a better photocatalytic agent for the degradation of organic compounds like polymer. Moreover, after degradation, no harmful by-products are released and this method has been confirmed as potent in eradicating trace concentrations of organic substance present in the liquid or gaseous phase. For instant; organic acid (Fallet et al. 2006, Sheng et al. 1999), alcohol (Choi et al. 2004, Xianyu et al. 2001), organic dyes (Bouras & Lianos 2005, Funakoshi & Nonami 2007, Ge et al. 2006, Gu et al. 2007, Jung & Imaishi 2001, Stoyanov et al. 2006, Yu et al. 2002b, Yuan et al. 2006, Zhou et al. 2006b), oxide gaseous (Takeuchi et al. 2000, Yu et al. 2006a, 2006b, Yusuf et al. 2002), and aldehyde gas (Chiba et al. 2005, Noguchi et al. 1998, Sopyan 2007, Sopyan et al. 1996, Watanabe et al. 2000) have been decomposed by $TiO_2$ photocatalytic activity. Various searches for biodegradation of organic

substances such as various plastics using microflora such as bacteria, fungi, and algae have also been documented (Ditta et al. 2008, Sunada et al. 1998, Sunada et al. 2003). To date, only fine powders type photocatalysts are applied for decomposing pollutants as it has more oxidation ability to make photo-generated holes on the outer surface photocatalysts. Nevertheless, the application of fine powder photocatalysts may cause some serious problems such as [a] Complications to separate suspension and the photocatalyst (Begum & Ahmed 2008, Cho et al. 2007, Ge & Xu 2007, Zhou et al. 2006a), [b] High amount of fine powder of photocatalysts may be aggregated with suspended particles (Cho et al. 2007), and [c] Photocatalyst powder can be easily separated from weak adhesion supports if it is covered with particular support (Cho et al. 2007). As a result, advanced approaches such as a thin coated layer on solid wafer material, which makes it a more potent photocatalyst, should be used for critical environmental applications. Numerous materials like polymer, cement, clay, silica and mild steel have been applied as the adherence of $TiO_2$ photocatalytic agents. In the current review, $TiO_2$ film as a photocatalyst and various methods for the improvement of photocatalytic characteristics, $TiO_2$ deposition methods, and its environmental application for degradation of polyethylene will be also discussed.

## Photocatalyst Thin Films

Nanocrystalline semiconductor thin films found a network in which electronic conduction can happen (Beydoun et al. 1999). A photocatalyst-coated thin film has unique efficiency properties that make it ideal for environmental purification. It is evidenced that titania thin films are extensively applied in various fields like adsorbent catalysts, as sensors (humidity and gas) functional materials, and mainly pollutant removal from wastewater and air (Machida et al. 1999, Mei et al. 2006). A photocatalyst-coated thin film can prevent inhaling particle problems caused by nano-photocatalyst powder, which can be hazardous to human health (Yu et al. 2006a). Furthermore, it is more dependable than the immobilization method, and as a result, photocatalyst-coated thin films may be applied to a number of substrates, such as thin film-coated stainless steel for a building, which has greater chemical corrosion resistance and mechanical strength. Besides this, the building material could be converted into an air-purifying and self-cleaning substance after being coated with a thin film of photocatalyst (Yu et al. 2006a). The penetration of UV or visible light is a key drawback for the photocatalysis process using slurry or powder of nanoparticles. However, these problems can be overcome by photocatalyst-coating on a solid substrate. Contrasting the nanoparticle, the photocatalyst-coated thin film has the ability to avoid light scattering and improve the light transmittance and ultimately increase the efficiency of photoreaction (Ge et al. 2006, Kitano et al. 2007, Otsuka et al. 2008, Sheng et al. 1999, Yu et al. 2002a, 2002b). Furthermore, the advantage of the photocatalyst-coated thin film is connected with an external layer only.

## Deposition Method for the Development of Photocatalyst Thin Film

Various techniques have been applied for coating the photocatalyst thin film on different substrates such as reactive magnetron sputtering (Choi et al. 2004, Sheng et al. 1999), RF reactive ion plating (Chiba et al. 2005), solgel (Hu et al. 2008), liquid phase deposition (LPD) (Gu et al. 2007, Yu et al. 2006b, Zhou 2006b), vapor phase deposition (Chemical vapor deposition and metal-organic Chemical vapor deposition (Jung & Imaishi 2001), physical vapor deposition (PVD) (Aziz & Sopyan 2009), reactive evaporation (Kitano et al. 2007), atomic layer deposition (ALD) (Clouser et al. 2008), ionized cluster beam (ICB) (Zhou et al. 2006a), electrophoretic deposition (Chan et al. 2002), and pulsed laser deposition (PLD) (Kitano et al. 2007). Each technique has its specific pros and cons. For example, the solgel method required high-temperature calculations after treatment to achieve the required stabilities and mechanical strengths of thin coated films. (Zhou et al. 2006a). It could occur as a result of damage to porous substrates. The properties of TiO2 thin films are largely dependent on the deposition process as well as the deposition parameter, according to several research findings (Hasan et al. 2008). All the above methods have been modified by researchers to obtain and develop nano-sized thin film along with required specific physical characteristics such as size, porosity, shape, crystalline structure, and surface area as per their application.

## Magnetron Sputtering Method

Some deposition methods have limitations for developing photocatalytic active thin films, such as spray coating, which requires a high temperature to decompose metallorganics during the heating process and is limited to non-refractory substrates (Fig. 2). Sheng et al. (1999) made an effort to develop photocatalytically active Pt-titania thin films along with the anatase crystalline structure at 200°C temperature on a flexible substrate i.e. polyamide to broaden the application of film as a photocatalyst. Fleetingly, they used the tripole magnetron sputtering system to develop thin films by applying two different methods of deposition. In the first method, interchangeably, sputtering co-axially placed titanium and platinum targets, and for platinum, the deposition time was 2 s, while for titanium it varied from 20 s to 140 s throughout each cycle to prepared different compositions. In the second method, the Pt-titania film was developed with

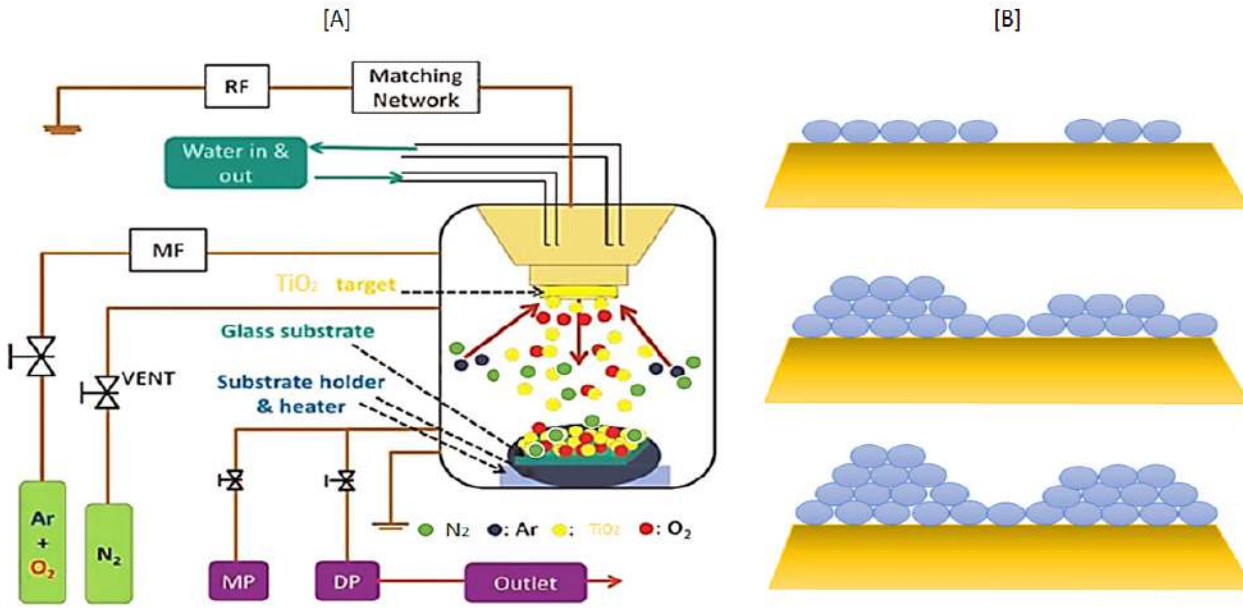


Fig.2: [A] A schematic diagram of RF magnetron sputtering machine [B] A diagram of thin-film growth mode.

pure titania film depositing first on a polyamide substrate, afterward coating a thin layer of platinum on the surface then again coated with titania thin film. They revealed that coating using the second method is to provide bonding strength between film and polyamide along with anatase crystalline structure at 200°C deposition temperature. Tomaszewski et al. (2007) used DC magnetron sputtering on ceramic targets to create transparent nanostructured $TiO_2$ thin films. Mei et al. (2012) used DC reactive magnetron sputtering to create transparent titania thin films on silica substrates at varied deposition temperatures (300-600°C). They discovered that at 500°C, $TiO_2$ thin films had the maximum photocatalytic activity, owing to the crystalline structure of $TiO_2$ thin films (Mei et al. 2012). Kavaliunas et al. (2020) studied the effect of dopants Mg, Cu, and Ni on photocatalytic activity of amorphous titania thin film which was developed by reactive magnetron sputtering. The results showed that dopant concentrations in titania films between 0.1 and 0.9 percent gave the best photocatalytic activity. SantAna et al. (2020) investigated of optical transmittance of photocatalytic active titania films which were deposited using radiofrequency magnetron sputtering (SantAna et al. 2020). They revealed the optimum deposition parameter such as 0.2 electric currents (A), 437 voltage (V), 87 RF power (W), 3600 deposition time (s), $9.2 \times 10^{-3}$ background pressure (mbar). Moreover, the experimental results show that the TiO2 films deposited on glass were associated with the anatase phase with a [0 0 4] preferred orientation. Ultraviolet near-infrared spectroscopy revealed the high transmittance of the films in visible light and high absorption in the ultra-violet region under most deposition conditions.

## CONCLUSION

This review emphasized the necessity of the elimination of plastic waste contaminants from landfills. Various types of plastic waste pollutants have been listed and the constraint of initial titania photocatalysis on plastic degradation was discussed. Some deposition parameters which have significant impacts on the titania-based photocatalytic degradation, and depositing parameters like dopant, particle size, catalyst concentration, temperature, crystalline structure, and selection substrate that aids in the use of titania as a photocatalyst for further commercialization were reviewed. Hence, photocatalytic process design and technical deposition method optimization are critical to investigate using a key emphasis on low-density plastic deterioration.

## REFERENCES

Allen, N.S., Mahdjoub, N., Vishnyakov V., Kelly, P.J. and Kriek, R.J. 2018. The effect of crystalline phase (anatase, brookite, and rutile) and size on the photocatalytic activity of calcined polymorphic titanium dioxide ($TiO_2$). Polym. Degrad. Stab., 150: 31-36.

Arthur, C., Baker, J.E. and Bamford, H.A. 2009. Proceedings of the International Research Workshop on the Occurrence, Effects, and Fate of Microplastic Marine Debris, September 9-11, 2008, University of Washington Tacoma, Tacoma, WA, USA.

Aziz, R.A. and Sopyan, I. 2009. Recent progress on the development of $TiO_2$ thin film photocatalysts for pollutant removal. Recent Pat. Mater. Sci., 2(2): 88-111.

Bai, J. and Zhou, B. 2014. Titanium dioxide nanomaterials for sensor applications. Chem. Rev.., 114(19): 10131-10176.

Barnes, D.K. 2002. Invasions by marine life on plastic debris. Nature, 416(6883): 808-809.

Barnes, D.K, Galgani F, Thompson R.C. and Barlaz M. 2009. Accumulation and fragmentation of plastic debris in global environments. Philos. Trans. R. Soc. Lond., B, Biol. Sci., 364(1526): 1985-1998.

Begum, N.S. and Ahmed, H.F. 2008. Synthesis of nanocrystalline $TiO_2$thin films by liquid phase deposition technique and its application for photocatalytic degradation studies. Bull. Mater. Sci., 31(1): 43-48.

Beydoun, D., Amal, R., Low, G. and McEvoy. S. 1999. Role of nanoparticles in photocatalysis. J. Nanopart. Res., 1(4): 439-458.

Bouras. P. and Lianos, P. 2005. Photodegradation of dyes in aqueous solutions catalyzed by highly efficient nanocrystalline titania films. J. Appl. Electrochem., 35(7-8):831-836.

Chan, A.H., Porter, J.F., Barford, J.P. and Chan, C.K. 2002. Effect of thermal treatment on the photocatalytic activity of TiO2 coatings for photocatalytic oxidation of benzoic acid. J. Mater. Res., 17(7): 1758-1765.

Chiba, Y., Kokai, H. and Kashiwagi, K. 2005. Effect of the plasma surface treatment on an anatase TiO 2 film. J. Mater. Sci.: Mater., 16(10): 645-648.

Cho, D.L., Min, H., Kim, J.H., Cha, G.S., Kim G.S., Kim, B.H. and Ohk, S.H. 2007. Photocatalytic characteristics of $TiO_2$thin films deposited by PECVD. J. Indian Eng. Chem., 13(3): 434-437.

Choi, Y.L., Kim, S.H., Song, Y.S. and Lee, D.Y. 2004. Photodecomposition and bactericidal effects of $TiO_2$ thin films prepared by a magnetron sputtering. J. Mater. Res., 39(18): 5695-5699.

Clouser, S., Samia, A.C., Navok, E., Alred, J. and Burda C. 2008. Visible-light photodegradation of higher molecular weight organics on N-doped $TiO_2$ nanostructured thin films. Top Catal., 47(1-2): 42-48.

Daghrir, R., Drogui, P. and Robert, D. 2013. Modified $TiO_2$ for environmental photocatalytic applications: A review. Ind. Eng. Chem. Res., 52(10): 3581-3599.

Derraik, J.G. 2002. The pollution of the marine environment by plastic debris: A review. Mar. Pollut. Bull., 44(9): 842-852.

Dette, C., Pérez-Osorio, M.A., Kley, C.S., Punke, P., Patrick, C.E., Jacobson, P., Giustino, F., Jung, S.J. and Kern, K. 2014. $TiO_2$ anatase with a bandgap in the visible region. Nano Lett., 14(11): 6533-6538.

Di Paola, A., Bellardita, M. and Palmisano, L. 2013. Brookite, the least known $TiO_2$ photocatalyst. Catalysts, 3(1): 36-73.

Ditta, I.B., Steele, A., Liptrot, C., Tobin, J., Tyler, H., Yates, H.M., Sheel, D.W. and Foster, H.A. 2008. Photocatalytic antimicrobial activity of thin surface films of TiO 2, CuO, and TiO 2/CuO dual layers on Escherichia coli and bacteriophage T4. Appl. Microbiol. Biotechnol., 79(1): 127.

Fallet, M., Permpoon, S., Deschanvres, J.L. and Langlet, M. 2006. Influence of physico-structural properties on the photocatalytic activity of sol-gel derived TiO 2 thin films. J. Mater. Res., 41(10):2915-2927.

Fujishima, A. and Honda, K. 1972. Electrochemical photolysis of water at a semiconductor electrode. Nature, 238(5358): 37-38.

Funakoshi, K. and Nonami, T. 2007. Photocatalytic treatments on dental mirror surfaces using hydrolysis of titanium alkoxide. J. Coat. Technol. Res., 4(3): 327-333.

Gawande, A., Zamare, G., Renge, V., Tayde, S. and Bharsakale, G. 2012. An overview on waste plastic utilization in asphalting of roads. J. Eng. Res., 3(2): 1-5.

Ge, L. and Xu, M. 2007. Fabrication and characterization of TiO 2 photocatalytic thin film prepared from peroxo titanic acid sol. J. Solgel Sci. Technol., 43(1): 1-7.

Ge, L., Xu, M. and Fang, H. 2006. Preparation and characterization of silver and indium vanadate co-doped TiO 2 thin films as visible-light-activated photocatalyst. J. Solgel Sci. Technol., 40(1): 65-73.

Gu, D.E., Yang, B.C. and Hu, Y.D. 2007. A novel method for preparing V-doped titanium dioxide thin-film photocatalysts with high photocatalytic activity under visible light irradiation. Catal. Lett., 118(3-4): 254-259.

Hasan, M., Haseeb, A., Saidur, R. and Masjuki, H.H. 2008. Effects of annealing treatment on optical properties of anatase $TiO_2$ thin films. Int. J. Chem. Biol. Sci., 1(2): 92-96.

Hashimoto, K., Irie, H. and Fujishima, A. 2005. $TiO_2$ photocatalysis: a historical overview and future prospects. Jpn. J. Appl. Phys., 44(12R): 8269.

Hopewell, J., Dvorak, R. and Kosior, E. 2009. Plastics recycling: challenges and opportunities. Philos. Trans. R. Soc. Lond., B, Biol. Sci., 364(1526): 2115-2126.

Hsu, K.C., Fang, T.H., Hsiao, Y.J. and Wu, P.C. 2019. Response and characteristics of $TiO_2$/perovskite heterojunctions for CO gas sensors. J. Alloys Compd., 794: 576-584.

Hu, H., Xiao, W., Yuan, J., Shi, J., He, D. and Shangguan, W. 2008. High photocatalytic activity and stability for decomposition of gaseous acetaldehyde on TiO 2/Al 2 O 3 composite films coated on foam nickel substrates by sol-gel processes. J. Solgel Sci. Technol., 45(1): 1-8.

Islam, M.A., Mohsanin, S., Chowdhury, G.W., Chowdhury, S.U., Aziz, M.A., Uddin, M., Saif, S., Chakma, S., Akter, R. and Jahan, I. 2011. Current status of Asian elephants in Bangladesh. Gajah., 35: 21-24.

Jung, S.C. and Imaishi, N. 2001. Preparation, crystal structure, and photocatalytic activity of TiO 2 films by chemical vapor deposition. Korean J. Chem. Eng., 18(6): 867-872.

Kavaliunas, V., Krugly, E., Sriubas, M., Mimura, H., Laukaitis, G. and Hatanaka, Y. 2020. Influence of Mg, Cu, and Ni dopants on amorphous $TiO_2$ thin films photocatalytic activity. Materials, 13(4): 886.

Kershaw, P., Katsuhiko, S., Lee, S. and Woodring, D. 2011. Plastic Debris in the Ocean, United Nations Environment Programme, Nairobi, Kenya.

Khanam, P.N. and AlMaadeed, M.A.A. 2015. Processing and characterization of polyethylene-based composites. Adv. Manuf.: Polym. Compos. Sci., 1(2): 63-79.

Kim, J.S. and Lee, T.K. 2001. Effect of humidity on the photocatalytic degradation of trichloroethylene in the gas phase over TiO 2 thin films treated by different conditions. Korean J. Chem. Eng., 18(6): 935-940.

Kim, S.B., Kim, G.S. and Hong SC. 2006. Degradation of Gaseous Trichloroethylene Over a Thin-Film TiO~ 2 Photocatalyst. J. Ind. Eng. Chem., 12(5): 749.

Kitano, M., Mitsui, R., Eddy, D.R., El-Bahy, Z.M., Matsuoka, M., Ueshima, M. and Anpo, M. 2007. Synthesis of nanowire TiO 2 thin films by hydrothermal treatment and their photoelectrochemical properties. Catal. Lett., 119(3-4): 217-221.

Machida, M., Norimoto, K., Watanabe, Te., Hashimoto, K. and Fujishima, A. 1999. The effect of $SiO_2$ addition in super-hydrophilic property of $TiO_2$photocatalyst. J. Mater. Res., 34(11): 2569-2574.

Mei, F., Liu, C., Zhang, L., Ren, F., Zhou, L., Zhao, W. and Fang, Y. 2006. Microstructural study of binary $TiO_2$: $SiO_2$ nanocrystalline thin films. J. Cryst. Growth., 292(1): 87-91.

Mei, F., Yang, Z., Wu, L., Zhou, Y. and Zhang, D. 2012. Influence of annealing temperature on structure and photocatalytic activity of TiO 2 thin films prepared by DC reactive magnetron sputtering method. Wuhan Univ. J. Nat. Sci., 17(4): 309-314.

Misra, P.K., Dash, U. and Maharana, S. 2015. Investigation of bovine serum albumin-surfactant aggregation and its physicochemical characteristics. Colloids Surf. A Physicochem. Eng. Asp., 483: 36-44.

Nakata, K. and Fujishima, A. 2012. $TiO_2$ photocatalysis: Design and applications. J. Photochem. Photobiol. C., 13(3):169-189.

Noguchi, T., Fujishima, A., Sawunyama, P. and Hashimoto, K. 1998. Photocatalytic degradation of gaseous formaldehyde using $TiO_2$ film. Environ. Sci. Technol., 32(23): 3831-3833.

Otsuka, E., Kurumada, K., Suzuki, A., Matsuzawa, S. and Takeuchi, K. 2008. An application of transparent mesoporous bulk silica to a titanium dioxide photocatalyst with adsorption and decomposition functions. J. Solgel Sci. Technol., 46(1): 71-78.

Pant, B., Barakat, N.A., Pant, H.R., Park, M., Saud, P.S., Kim, J.W. and Kim, H.Y. 2014a. Synthesis and photocatalytic activities of CdS/$TiO_2$ nanoparticles supported on carbon nanofibers for high efficient

adsorption and simultaneous decomposition of organic dyes. J. Colloid Interface Sci., 434: 159-166.

Pant, B., Pant, HR., Park, M., Liu, Y., Choi, J.W., Barakat, N.A. and Kim, H.Y. 2014b. Electrospun CdS– $TiO_2$ doped carbon nanofibers for visible-light-induced photocatalytic hydrolysis of ammonia borane. Catal. Commun., 50: 63-68.

Pant, B., Park, M. and Park, S.J. 2019a. $MoS_2$/CdS/ $TiO_2$ ternary composite incorporated into carbon nanofibers for the removal of organic pollutants from water. Inorg. Chem. Commun., 102: 113-119.

Pant, B., Park, M. and Park, S.J. 2019b. $TiO_2$ NPs assembled into a carbon nanofiber composite electrode by a one-step electrospinning process for supercapacitor applications. Polymers, 11(5): 899.

Pant, B., Park, M. and Park, S. J. 2020. Hydrothermal synthesis of Ag2CO3-$TiO_2$ loaded reduced graphene oxide nanocomposites with highly efficient photocatalytic activity. Chem. Eng. Commun., 207(5):688-695.

Pant, B., Saud, P.S., Park, M., Park, S.J. and Kim, H.Y. 2016. General one-pot strategy to prepare Ag– $TiO_2$ decorated reduced graphene oxide nanocomposites for chemical and biological disinfectant. J. Alloys Compd., 671: 51-59.

Park, H. and Choi, W. 2004. Effects of $TiO_2$ surface fluorination on photocatalytic reactions and photoelectrochemical behaviors. J. Phys. Chem. B 108(13): 4086-4093.

Pramila, R. and Ramesh, K.V. 2015. Potential biodegradation of low-density polyethylene (LDPE) by Acinetobacter baumannii. J. Bacteriol. Res., 7(3): 24-28.

Rathi, S. 2007. The need for separation of plastics from municipal solid waste. Chem. Week. Bombay, 53(18): 177.

Sangale, M., Shahnawaz, M. and Ade, A. 2012. A review on biodegradation of polythene: the microbial approach. J. Bioremed. Biodegr., 3: 1-9.

SantAna, P.L., Bortoleto, J.R.R., da Cruz, N.C., Rangel, E.C., Durrant, S.F., Azevedo. S, Simões C.I.S. and Teixeira, V. 2020. Study of optical transmittance of photocatalytic titanium dioxide films deposited by radiofrequency magnetron sputtering. Braz. J. Vacuum Appl., 39(1): 24-32.

Sheng, J., Shivalingappa, L., Karasawa, J. and Fukami, T. 1999. Low-temperature formation of photocatalytic Pt-anatase film by magnetron sputtering. J. Mater. Res., 34(24): 6201-6206.

Shimao, M. 2001. Biodegradation of plastics. Curr. Opin. Biotechnol., 12(3): 242-247.

Sopyan, I. 2007. Kinetic analysis on photocatalytic degradation of gaseous acetaldehyde, ammonia, and hydrogen sulfide on nanosized porous $TiO_2$ films. Sci. Technol. Adv., 8(1-2): 33-39.

Sopyan, I., Watanabe, M., Murasawa, S., Hashimoto, K. and Fujishima, A. 1996. An efficient $TiO_2$ thin-film photocatalyst: photocatalytic properties in gas-phase acetaldehyde degradation. J. Photochem. Photobiol. A., 98(1-2): 79-86.

Stoyanov, S., Mladenova, D. and Dushkin, C. 2006. Photocatalytic properties of mixed TiO 2/V 2 O 5 films in water purification at varying ph. React. Kinet. Catal. Lett., 88(2): 277-283.

Sunada, K., Kikuchi, Y., Hashimoto, K. and Fujishima, A. 1998. Bactericidal and detoxification effects of $TiO_2$ thin film photocatalysts. Environ. Sci. Technol., 32(5):726-728.

Sunada, K., Watanabe, T. and Hashimoto, K. 2003. Bactericidal activity of copper-deposited $TiO_2$ thin film under weak UV light illumination. Environ. Sci. Technol., 37(20): 4785-4789.

Takeuchi, M., Yamashita, H., Matsuoka, M., Anpo, M., Hirao, T., Itoh, N. and Iwamoto, N. 2000. Photocatalytic decomposition of NO on titanium oxide thin film photocatalysts prepared by an ionized cluster beam technique. Catal Lett., 66(3): 185-187.

Thiruvenkatachari, R., Vigneswaran, S. and Moon, I.S. 2008. A review on UV/TiO 2 photocatalytic oxidation process (Journal Review). Korean J. Chem. Eng., 25(1): 64-72.

Tomaszewski, H., Eufinger, K., Poelman, H., Poelman, D., De Gryse, R., Smet, P.F. and Marin, G.B. 2007. Effect of substrate sodium content on crystallization and photocatalytic activity of $TiO_2$ films prepared by dc magnetron sputtering. Int. J. Photoenergy., 2007: 54-69.

Tung, W.S. and Daoud, W.A. 2011. Self-cleaning fibers via nanotechnology: A virtual reality. J. Mater. Chem., 21: 7858-7869.

UNEP 2009. Marine Litter: A Global Challenge. Nairobi: UNEP.

Verma, R., Vinoda, K., Papireddy, M. and Gowda, A. 2016. Toxic pollutants from plastic waste-a review. Procedia Environ. Sci., 35: 701-708.

Wang, H., Huang, X., Li, W., Gao, J., Xue, H., Li, R.K. and Mai, Y.W. 2018. $TiO_2$ nanoparticle decorated carbon nanofibers for removal of organic dyes. Colloids Surf. A Physicochem. Eng. Asp., 549: 205-211.

Watanabe, T., Fukayama, S., Miyauchi, M., Fujishima, A. and Hashimoto, K. 2000. Photocatalytic activity and photo-induced wettability conversion of $TiO_2$ thin film prepared by sol-gel process on soda-lime glass. J. Solgel Sci. Technol., 19(1-3): 71-76.

Xianyu, W.X., Park, M.K. and Lee, W.I. 2001. Thickness effect in the photocatalytic activity of TiO 2 thin films derived from solgel process. Korean J. Chem. Eng., 18(6): 903-907.

Yu, H., Lee, S., Yu, J. and Ao, C. 2006a. Photocatalytic activity of dispersed $TiO_2$ particles deposited on glass fibers. J. Mol. Catal. A Chem., 246(1-2): 206-211.

Yu, J., Jimmy, C.Y., Cheng, B. and Zhao, X. 2002a. Photocatalytic activity and characterization of the sol-gel derived Pb-doped TiO 2 thin films. J. Solgel Sci. Technol., 24(1): 39-48.

Yu, J., Jimmy, C.Y. and Zhao, X. 2002b. The effect of $SiO_2$ addition on the grain size and photocatalytic activity of TiO 2 thin films. J Solgel Sci Technol., 24(2): 95-103.

Yu, J., Yu, H., Ao, C., Lee, S., Jimmy, C.Y. and Ho, W. 2006b. Preparation, characterization, and photocatalytic activity of in situ Fe-doped $TiO_2$ thin films. Thin Solid Films, 496(2): 273-280.

Yuan, Z., Li, B., Zhang, J., Xu, C. and Ke, J. 2006. Synthesis of $TiO_2$ thin film by a modified sol-gel method and properties of the prepared films for photocatalyst. J. Solgel Sci. Technol., 39(3): 249-253.

Yusuf, M.M., Imai, H., Hirashima and H. 2002. Preparation of porous titania film by modified sol-gel method and its application to photocatalyst. J. Solgel Sci. Technol., 25(1): 65-74.

Zhang, J., Xu, Q., Feng, Z., Li, M. and Li, C. 2008. Importance of the relationship between surface phases and photocatalytic activity of $TiO_2$. Angew. Chem. Int., 120(9): 1790-1793.

Zhou, J., Takeuchi, M., Zhao, X., Ray, A.K. and Anpo, M. 2006a. Photocatalytic decomposition of formic acid under visible light irradiation over V-ion-implanted $TiO_2$ thin film photocatalysts prepared on quartz substrate by ionized cluster beam (ICB) deposition method. Catal. Letters., 106(1-2):67-70.

Zhou, L., Yan, S., Tian, B., Zhang, J. and Anpo, M. 2006b. Preparation of $TiO_2$ –$SiO_2$ film with high photocatalytic activity on PET substrate. Mater. Lett., 60(3): 396-399.

Nature Environment and Pollution Technology
An International Quarterly Scientific Journal

p-ISSN: 0972-6268
(Print copies up to 2016)
e-ISSN: 2395-3454

Vol. 20 | No. 5 (Suppl) | pp. 1923-1934 | 2021

Original Research Paper

https://doi.org/10.46488/NEPT.2021.v20i05.008

Open Access Journal

# Assessment of the Potential Use of Shallow Geothermal Energy Source for Air Heating and Cooling in the Kingdom of Saudi Arabia

**M. Ouzzane*, M. T. Naqash*† and O. Harireche***

*Faculty of Engineering, Islamic University in Madinah, Islamic University of Medina, Medina, P.O. Box: 170, Kingdom of Saudi Arabia

†Corresponding author: M. T. Naqash; tayyab@iu.edu.sa, engr.tayyabnaqash@gmail.com

**Nat. Env. & Poll. Tech.**
**Website: www.neptjournal.com**

*Received:* 18-04-2021
*Revised:* 27-06-2021
*Accepted:* 14-07-2021

**Key Words:**
Ground temperature profile
Geothermal energy
Canadian well
Earth-air heat exchanger

## ABSTRACT

A large part of the total energy consumption in buildings in the Kingdom of Saudi Arabia (K.S.A.), is devoted to air cooling. This leads to high electricity costs for residents and a high amount of equivalent $CO_2$ emissions. The work presented in this paper aims at evaluating and applying shallow geothermal energy for cooling and heating to reduce cost and environmental issues in the Kingdom. The system is based on the earth-air heat exchanger (EAHE) equipped with an air circulation fan. In this study, six cities have been selected; Madinah city, where our university is located, and five other cities representing five different climatic zones. A new parameter called "geothermal percentage" is proposed to calculate the ratio of geothermal energy to the cooling/heating total load. It has been shown that the proposed system covers part of the cooling load and the total heating needs for almost all the country's territory. However, both heating and cooling needs can be fulfilled by the EAHE for few cities such as Guriiat and Khamis, characterized by a moderate climate.

## INTRODUCTION

Due to the global warming phenomenon, environmental scientists and international researchers are becoming more worried about the environment. Actions must be taken quite urgently to find solutions to reduce the emission of Greenhouse Gases (GHG) that are causing this problem. Many sectors are concerned about this issue (transportation, industry, residential and institutional), and many efforts have been made by promoting renewable energy and increasing energy efficiency. In buildings, air heating and cooling present an essential part of the total energy consumption, especially in cold and hot climates. Among the potential solutions for using environmentally friendly energy sources in air conditioning, shallow geothermal energy constitutes an interesting option to replace or be used alongside conventional energy systems. The simplest way to exploit geothermal energy is to use an earth/air heat exchanger called "Canadian well". Many works in this field have been conducted during the last decade (Liang 2020, Kazemiani-Najafabadi & Amiri Rad, 2020, Dalla Longa 2020).

Al-Ajmi et al. (2006) conducted a theoretical work on building air cooling using Canadian well technology. It has been shown that, during the peak summer season, the proposed system can contribute to reducing the cooling load by 30% for a typical house. Thiers et al. (2012) developed a mathematical model for the simulation of earth/air heat exchangers considering all the parameters and phenomena of thermal exchanges except for water infiltration into the soil. The computing module used in this model is currently integrated with a software called "COMFIE". Bisoniya et al. (2013) and Yan & Xu (2018) had published a review of theoretical and experimental works on earth-air-heat exchangers. This system alone is not sufficient to satisfy the cooling and heating all the year. However, they can preheat/precool the air to increase the energy efficiency of the conventional air conditioning system. Benhammou & Draoui (2015) and Benhammou et al. ( 2017) applied their theoretical model to the Algerian Sahara climate (hot and arid) to predict the performance of cooling earth-to-air heat exchanger for different geometrical and operational parameters. They have shown that in transient conditions, the efficiency of the EAHE is more affected by the duration of operation, pipe diameter, and air velocity. Because of the high cooling loads, they have recommended insulating the building well and choosing a material with good thermal properties. Ghaith & Razzaq (2018) studied the performance and the environmental impact of a hybrid system conventional/EAHE. It was shown that this proposed system can reduce the annual energy and carbon emissions by 11% compared with the conventional system. Benrachi (2020) proposed a new spiral-shaped configuration of EAHE for air cooling in a hot and arid region in Algeria. By using a commercial C.F.D. Software "ANSYS", had conducted an EAHE parametric effect on the

system's performance (C.O.P.). It was shown that this new configuration permits the reduction of the land size of the geothermal system. Recently, Wei et al. (2021) performed an experimental study on two similar buildings. One of the two buildings was equipped with EAHE. The results showed that the EAHE system reduce the ambient air temperature by 9.12°C during summer and increases the ambient air by 5.53°C during winter (Yueer et al. 2013, Wang & He 2014).

The Kingdom of Saudi Arabia is characterized by a long cooling season, which leads to high energy consumption by air conditioning systems. This energy presents around 50% of the total energy consumption in the residential sector alone (Albogami & Boukhanouf 2019). However, most of the HVAC systems used are based on the mechanical compression principle. In this system, the heat energy released to the ambient outdoor air through the condenser is higher than the cooling capacity produced in indoor air. This means that this system is contributing more to heating the external environment. On the other side, the main electrical energy source in K.S.A. is generated from power plants based on natural gas combustion. Its efficiency is low (around 30% of the total consumed energy), which results in high greenhouse gas emissions and pollution. In addition to the environmental context, in K.S.A., the cost of electricity has tripled during the last few years. As a result, the cooling electricity bill becomes difficult for the population's middle class to afford.

The primary purpose of the present work is to reduce electricity consumption (electricity bill) and GHG emission by proposing a shallow geothermal energy source. Unfortunately, in K.S.A., the exploitation of this source of clean energy is almost non-existent. This study shows the potential of using the EAHE for air cooling/heating in many big cities in K.S.A., selected from different climatic zones.

## Climatic Zones and Selected Cities

Saudi Arabia has a vast desert characterized by a long summer season with a high daily temperature and a significant drop in temperature during the night. This arid climate has a deficient annual rainfall. However, the K.S.A. has a western and eastern coast on the Persian Gulf and red sea, respectively, with higher annual relative humidity. According to the Saudi Building Code (SBC-602E) (The Saudi Building Code National Committee 2007), three different climatic zones have been identified. However, this classification does not consider differences due to the presence of sea that results in high humidity. In 2015, Alrashed & Asif (2015) investigated more than 16 scientific models of climatic classification to propose the appropriate energy studies in a building. The authors developed and applied specific criteria to the mentioned methods to propose five climatic zones without considering the Empty Quarter region. The colored map in Fig. 1 presents the results. These zones are characterized by hot/cold dry desert subzone, hot-dry with a maritime/maritime desert subzone, and subtropical with a Mediterranean subzone and a mountainous subtype. Five cities from the above five climatic zones plus Madinah city have been selected in this study (see Table 1). The purposes of choosing Madinah city are:

- Location of University,
- Need for information and technical results for planned experimental work.

## Ground Temperature

Earth is a vast solar collector that absorbs about half of the incident solar radiation. Its surface exchanges heat with the air and sky. Depending on the air ambient temperature, the ground surface loses or gains heat by convection. However, since the sky temperature is always very low, the ground surface loses heat to the sky by longwave radiation. Applying the heat energy balance on the ground surface will result in a heat flux driven by conduction in the soil. The typical ground temperature profile is characterized by two different parts, as shown in Fig. 2,

a) from the ground surface to 4 m depth, a high-temperature gradient is observed, and

b) from 4 m to about 11 m depth, the temperature change is damped. The temperature remains constant throughout the year, providing a warm water source and a cold source in summer.

These depths depend on the local soil properties and climate. The constant temperature of 9°C is called "undisturbed ground temperature" (Fig. 2).

## Undisturbed Ground Temperature $T_g$

The undisturbed ground temperature (U.G.T.) represents the primary indicator of the potential of shallow geothermal sources based on which engineers perform the preliminary

Table 1. Selected cities and location coordinates.

| City | Madinah | Riyadh | Guriat | Khamis | Jeddah | Dahran |
|---|---|---|---|---|---|---|
| Latitude | 24.5°N | 24.7°N | 31.4°N | 18.3°N | 21.5°N | 26.2°N |
| Longitude | 39.5°E | 46.7°E | 37.3°E | 42.8°E | 39.2°E | 50.0°E |

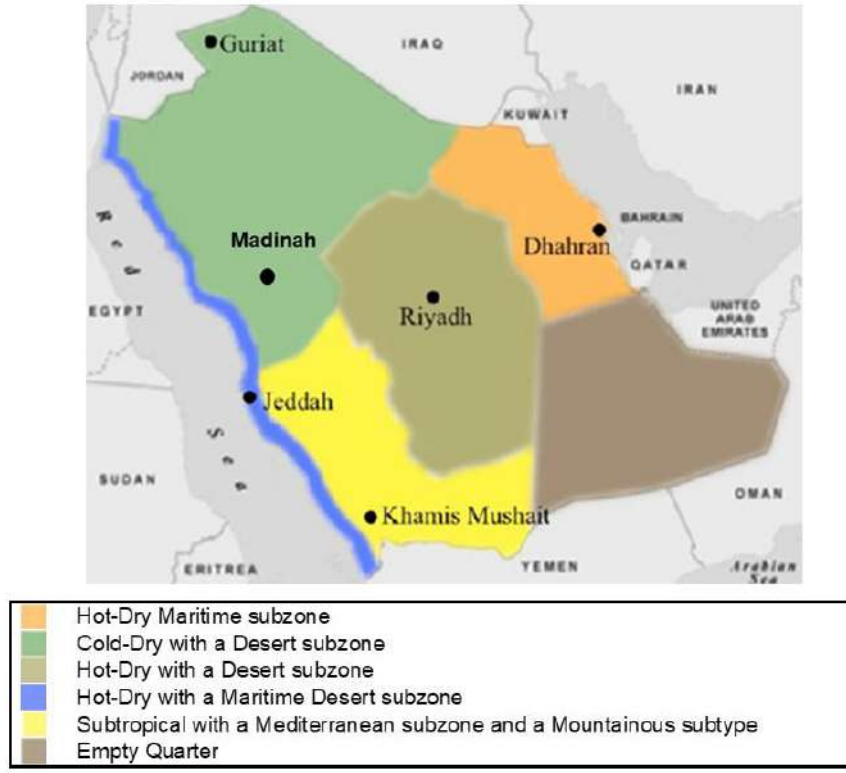


Fig. 1: Climatic zones in K.S.A.

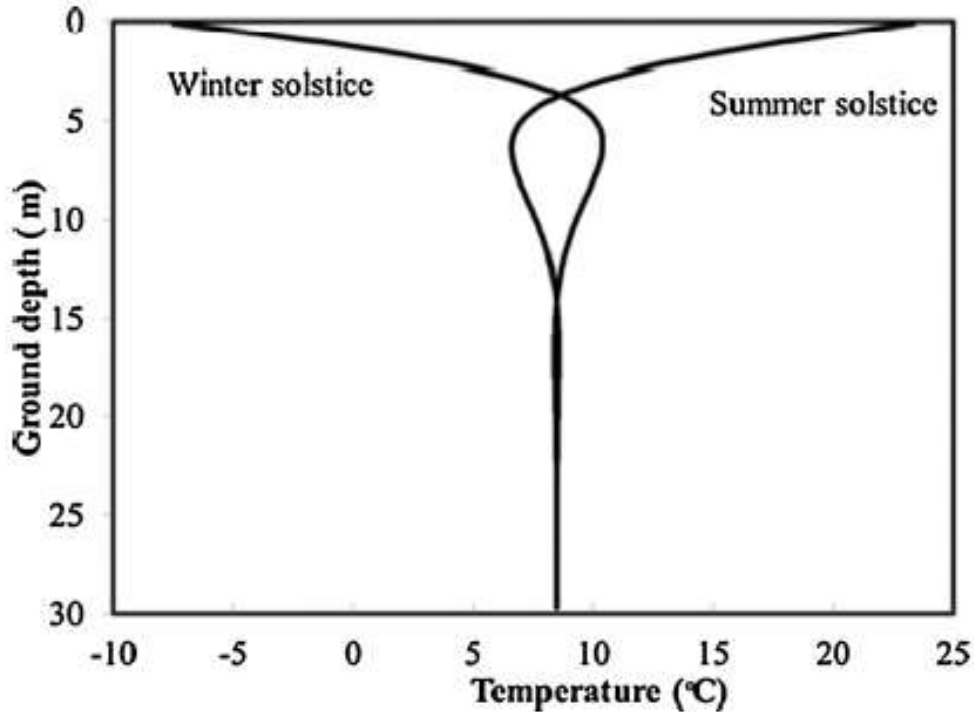


Fig. 2: Typical ground temperature.

design of their geothermal systems. For a large shared geothermal field used for heating and cooling with a ground source heat pump, one well is used to conduct a Thermal Response Test (TRT). This test provides the value of the undisturbed ground temperature, the diffusivity and thermal conductivity of the soil, and the geological structure of different layers of the soil. Based on TRT reports of seventeen sites covering a wide range of climates; from the cold climate in Alert (Nunavut, Canada, Latitude=82.5 $^0$N) to hot climate in Dahran (Saudi Arabia, Latitude=26.28 $^0$N), Ouzzane (2015) developed a simple correlation between the U.G.T. and the long-term yearly average ambient temperature given by Equation (1):

$$Tg = 0.9513 \times T_{amb} + 17.898 \quad ...(1)$$

$T_{amb}$ and $T_g$ are in Kelvin.

Equation (1) has been used to generate U.G.T. for different cities of the Kingdom (more than 70 cities), and isotherms have been plotted on the map of the country (Fig. 3). The U.G.T. ranges from 21°C to 32°C, which presents possibilities for air cooling and heating. This information helps engineers and researchers to perform a feasibility study to apply ground source heat pumps for cooling and heating.

## Ground Temperature Profile

The variation of the soil temperature with depth presents a profile as shown in Fig. 2. Due to the high thermal inertia of the soil, the diurnal and seasonal air temperatures are damped along the soil's depth. This profile is characterized by the cosine wave and exponential function described by Equation (2), proposed by Kasuda and Archenbach (Kusuda & Archenbach 1965). Several commercial software such as RETScreen (Natural Resources Canada 2013) and TRNSYS (Solar Energy Laboratory 2012) have implemented this Equation for their calculations related to the ground source heat pumps. However, for the boundary condition on the ground surface, the air ambient temperature profile is applied, which affects the accuracy of the results.

$$T(y,t) = \overline{T}_m - A_s exp^{-\frac{y}{\delta}} \cos\left(\omega t - \Phi_s - \frac{y}{\delta}\right) \quad ...(2)$$

Where:

$y$(m) is the depth of the soil from the surface of the ground ($y$=0).

T($y$,$t$) ( °C) is the soil temperature at time $t$ (days) and depth $y$ (m).

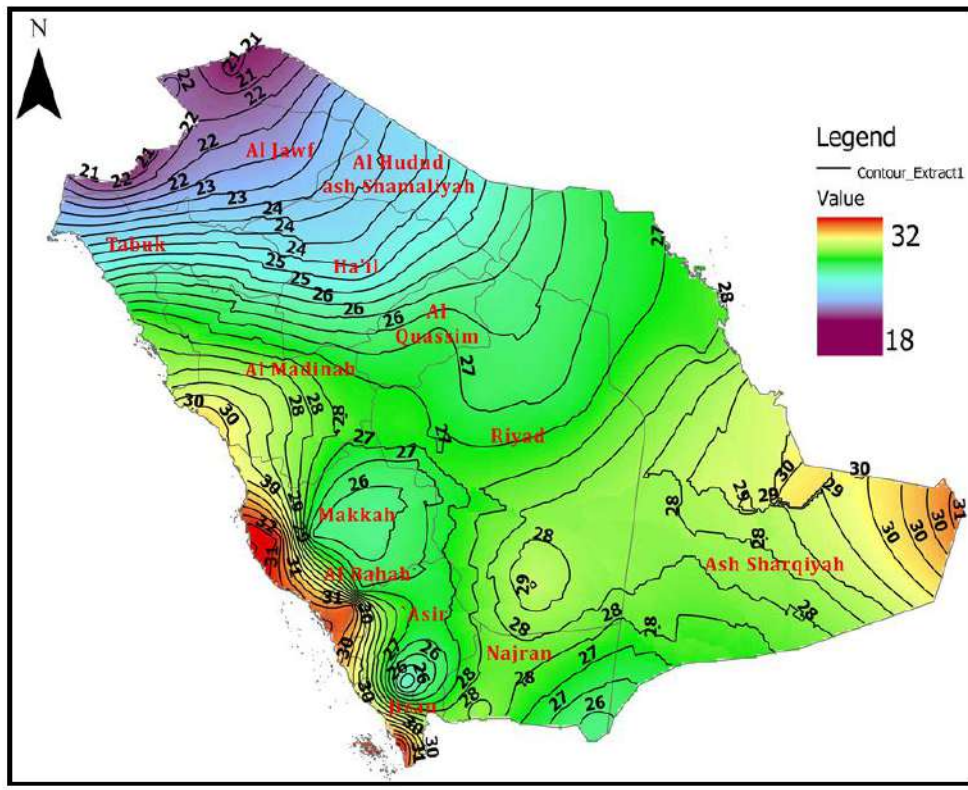


Fig. 3: Isotherms of the undisturbed ground temperature for K.S.A.

$\overline{T}_m$ (°C) is the annual average ground surface temperature.

$A_s$ (°C) is the annual amplitude of the soil surface temperature.

δ is the damping depth (m) of annual fluctuation of the ground temperature given by Equation (3):

$$\delta = \sqrt{\frac{2a}{\omega}} \quad ...(3)$$

ω is the angular frequency: ω = 2xα/365.

$\Phi_s$ is the phase angle (radian).

The ground temperature profile for Madinah city is shown in Fig. 4 and Fig. 5. The main parameters in Equation (2) are calculated using the model proposed by Badache (2016). This model consists of a new approach to improve the determination of the ground temperature profile and is based on a Fourier series approximation for sky temperature, ambient temperature, and global solar radiation on a horizontal surface. The annual amplitude $A_s$ and the phase angle $F_s$ are calculated using Equation (4) and Equation (5), respectively. The thermal properties of the soil chosen for Madinah are typical of arid soil.

$$A_s = \left\| \frac{h_r \bar{A}_a + \alpha_g \bar{A}_G e^{i(\varphi_G - \varphi_a)} + h_{rad} \bar{A}_{sky} e^{i(\varphi_{sky} - \varphi_a)}}{(h_e + k_s \delta')} \right\| \quad ...(4)$$

$$\varphi_s - \varphi_a = \mathrm{Arg}\left[ \frac{h_r \bar{A}_a + \alpha_G \bar{A}_G e^{i(\varphi_G - \varphi_a)} + h_{rad} \bar{A}_{sky} e^{i(\varphi_{sky} - \varphi_a)}}{(h_e + k_s \delta')} \right] \quad ...(5)$$

Where

$h_r = h_{conv}(1 + c.a.f.H_R)$ and $h_e = h_{conv}(1 + c.a.f) + h_{rad}$

$H_r$ is the ambient relative humidity.

a, c and f are constants; a = 103 (Pa/K), c=0.0168 (K/Pa)

f = 1 (saturated soil), f = 0.6 to 0.8 (moist soil)

f = 0.4 to 0.5 (dry soil) and f = 0.1 to 0.2 (arid soil)

$\alpha_g$ absorption coefficient of the ground surface.

$h_{rad}$ linearized radiation heat transfer coefficient (W/m$^2$.K).

δ' is the n$^{th}$ harmonic damping depth.

Meteorological data for one representative year obtained from a long-term duration (Natural Resources Canada 2013) and (*Medina, Saudi Arabia Weather Conditions | Weather Underground*, no date) have been used for this work.

The typical ground temperature for Madinah is well reflected in Fig. 4 and Fig. 5. In Fig. 4, the value of U.G.T. is around 31°C, located from 10 meters depth. On the other hand, the annual temperature amplitude at the ground surface (z=0 m) in Fig. 5 attenuates gradually as depth increases, reflecting the damping phenomenon due to the properties of the soil. It is presented by parameter δ and given by Equation (3).

**Canadian Well**

Several techniques with different configurations exploit the shallow geothermal energy source, such as ground source heat pumps (horizontal and vertical wells, direct expansion, and secondary loops) and Canadian well called earth to air heat exchanger (EAHE). The Canadian well is a technique that allows us to take advantage of the heating and cooling of the subsoil (Fig. 6). Therefore, due to its simplicity and low initial cost, especially for newly constructed buildings, it has been selected in this work. The principle is to circulate the outside air in pipes buried at a depth where the ground temperature is almost stable. Depending on the seasons, the supplied air temperature can reach 14°C lower/higher than the ambient temperature. The buried air pipes system and the ground constitute a heat exchanger. The effectiveness of the earth/air heat exchanger given by Equation (6) is defined as the ratio of the actual heat transfer rate for a heat exchanger to the maximum possible heat transfer rate. It depends on the air's velocity, the length and diameter of the buried pipe, the properties of the soil, air temperature at the inlet, and ground temperature.

Canadian well has been applied in many countries and investigated by many researchers and engineers. In general, this kind of system cannot fulfill alone the cooling and heating needs of comfort during the winter and the summer. It depends strongly on the climate of its location. For cold climate countries, the EAHE system can easily fulfill the cooling load during the hot season and only partly the heating load during the cold season and vice versa in hot climate countries. To remedy this insufficiency and to improve the energy efficiency, several solutions have been proposed such as:

- the combination with the conventional heat pump system (Bojić 2000),
- the combination with the heat recovery ventilation system (Lapertot 2021),
- the integration of the EAHE with the hollow core floor (Xu 2014),

Table 2: The yearly average ambient temperature and U.G.T. of the Selected cities.

| City | Madinah | Riyadh | Guriat | Khamis | Jeddah | Dahran |
|---|---|---|---|---|---|---|
| $T_{amb}$ (°C) | 28.4 | 25.1 | 19.8 | 18.9 | 27.9 | 25.8 |
| UGT (°C) | 31.6 | 28.5 | 23.4 | 22.6 | 31.1 | 29.1 |

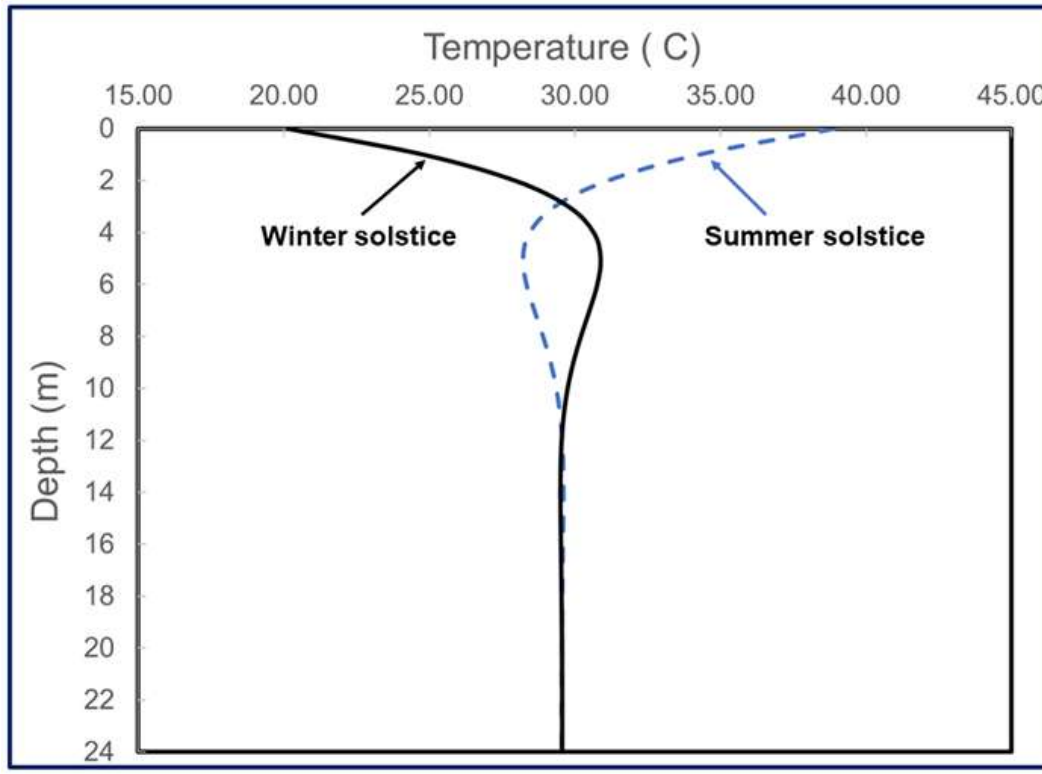


Fig. 4: Ground temperature profile for Madinah city.

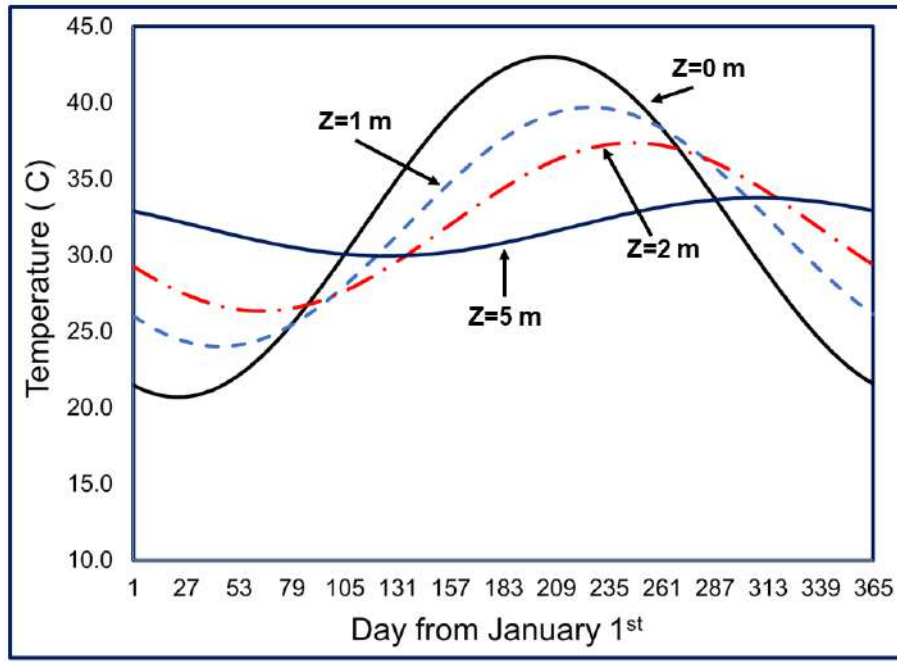


Fig. 5: Yearly variation of the soil temperature at different depths for Madinah city.

- the integration of the EAHE with the exterior building wall which has a ventilation passage embedded inside (Yan & Xu 2018).

The advantages of this technology are many. Some of them are summarized as a) A well-known system applied in several countries, b) Simplicity and low initial cost, especially for the new buildings, c) Use of clean energy helps to reduce pollution and the emission of greenhouse gases, d) Reduction of the energy consumption and the electricity bill as its operation practically does not require energy e) Passive system, preheating or cooling the air in a natural way.

**Geothermal Percentage and Analysis**

The Canadian well presented in Fig. 6 is used for cooling and heating analysis in six selected cities (Table 1) around K.S.A. The primary purpose is to know whether this system can fully or partially compensate for the heating/cooling load. To this end, a new parameter called "Geothermal Percentage" has been introduced. It is defined by the cooling/heating capacity ratio to the total cooling/heating load. The following Equation (7) provides an expression of this parameter:

In practice, the air supplied temperature must be few degrees lower/higher than the set point temperature for cooling/heating.

Fgeo-cool/heat's value ranges between 0 and 1, and the following different situations can occur.

- If $F_{geo\text{-}cool/heat} = 0$ (the geothermal system is not applicable) whereas,
- If $0 < F_{geo\text{-}cool/heat} < 1$ (the geothermal system can partly fulfill the cooling/heating needs or can precool/heat the ambient air. An auxiliary energy source is needed) and
- If $F_{geo\text{-}cool/heat} = 1$ (the geothermal system alone can satisfy the needed cooling/heating capacity)

$T_{set\text{-}cool/heat}$ is the cooling/heating indoor temperature settings for residential buildings. The Saudi building code (The Saudi Building Code National Committee 2007) recommends the following values:

- For heating mode, $T_{set\text{-}heat} = 20^{o}C$
- For cooling mode, $T_{set\text{-}cool} = 25.5^{o}C$

The temperature of the supplied air to the house $T_{ou}$ is calculated using Equation (6) by assuming the effectiveness of the earth/air heat exchanger value $\varepsilon = 0.9$. The calculations and analysis below are based on average monthly ambient temperature (Table 3) for the long term. The approach includes the different steps shown by the flowchart in Fig. 7. The following parameters $T_{amb}$, $T_{ou}$, $T_g$, $T_{set\text{-}cool}$, and $T_{set\text{-}heat}$, allow judging the need for cooling or heating. It also helps to assess if the geothermal system can overcome the heating or cooling load. With this, different situations are possible:

- **Case 1:** If $(T_{amb}-T_{set\text{-}heat}) < 0$ (needs heating)
- **Case 2:** If $0 < (T_{amb}-T_{set\text{-}heat}) < (T_{set\text{-}cool}-T_{set\text{-}heat}) =$

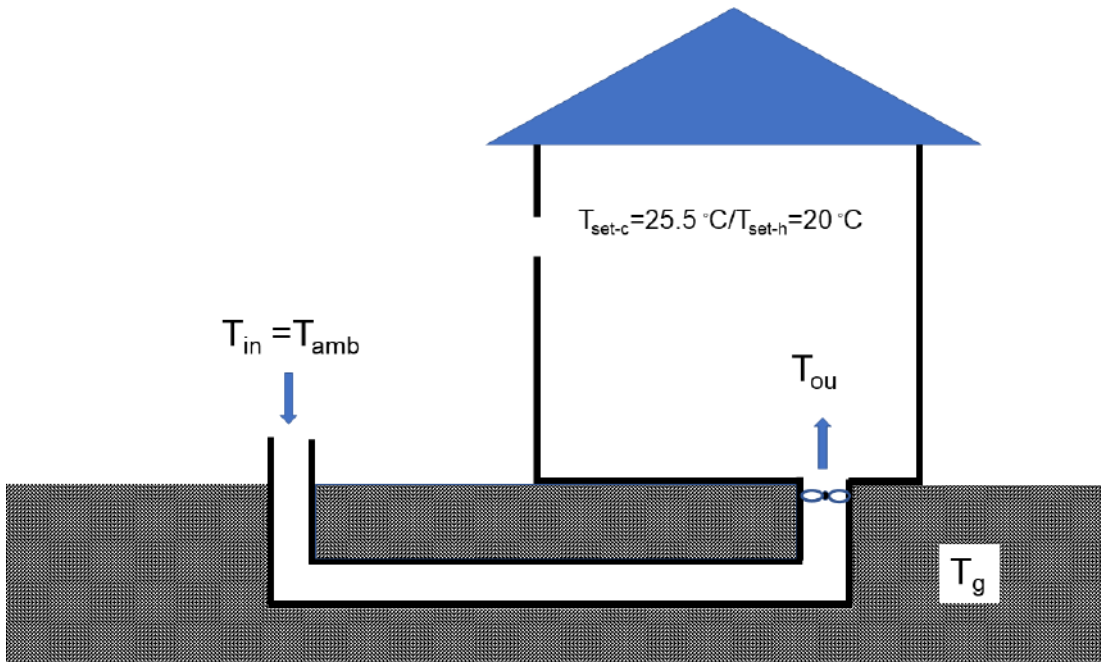


Fig. 6: Schematic representation of the Canadian well.

5.5 °C (no cooling, no heating needed)

- **Case 3:** If $(T_{amb}-T_{set\text{-}heat}) > (T_{set\text{-}cool}-T_{set\text{-}heat}) = 5.5^{o}C$ (needs cooling)

In this work, Madinah city is considered as a base case for the detailed analysis. Fig. 8 shows the monthly temperature difference between the ambient air and the supplied air to the house ($T_{in} - T_{ou}$). The positive values observed during the five months of the summer seasons, starting from May to September, confirmed that the ground is warmer than the ambient air. However, from October to April, the negative values mean that the ground is colder than the outside air

Table 3: Monthly average ambient temperature in (°C).

| Month | Madinah | Riyadh | Guriat | Khamis | Jeddah | Dahran |
|---|---|---|---|---|---|---|
| Jan | 18.3 | 15.1 | 7.5 | 13.5 | 23.9 | 15.0 |
| Feb | 20.2 | 16.5 | 10.0 | 16.0 | 24.8 | 16.5 |
| Mar | 24.4 | 22.7 | 12.0 | 17.0 | 26.4 | 20.0 |
| Apr | 28.2 | 26.6 | 18.0 | 20.0 | 28.8 | 24.9 |
| May | 34.1 | 32.5 | 23.0 | 23.0 | 31.8 | 30.5 |
| Jun | 37.8 | 36.0 | 27.0 | 26.0 | 32.8 | 34.8 |
| Jul | 37.9 | 37.4 | 30.0 | 26.0 | 33.9 | 35.9 |
| Aug | 37.3 | 36.5 | 30.0 | 25.0 | 33.9 | 36.2 |
| Sep | 37.0 | 33.9 | 27.0 | 23.0 | 32.7 | 33.9 |
| Oct | 31.0 | 27.5 | 23.0 | 22.0 | 31.0 | 29.1 |
| Nov | 24.9 | 20.4 | 15.0 | 17.0 | 28.5 | 23.9 |
| Dec | 20.5 | 16.1 | 8.0 | 15.0 | 26.1 | 16.8 |

N.N.: No cooling, no heating is needed.
N.W: No working.

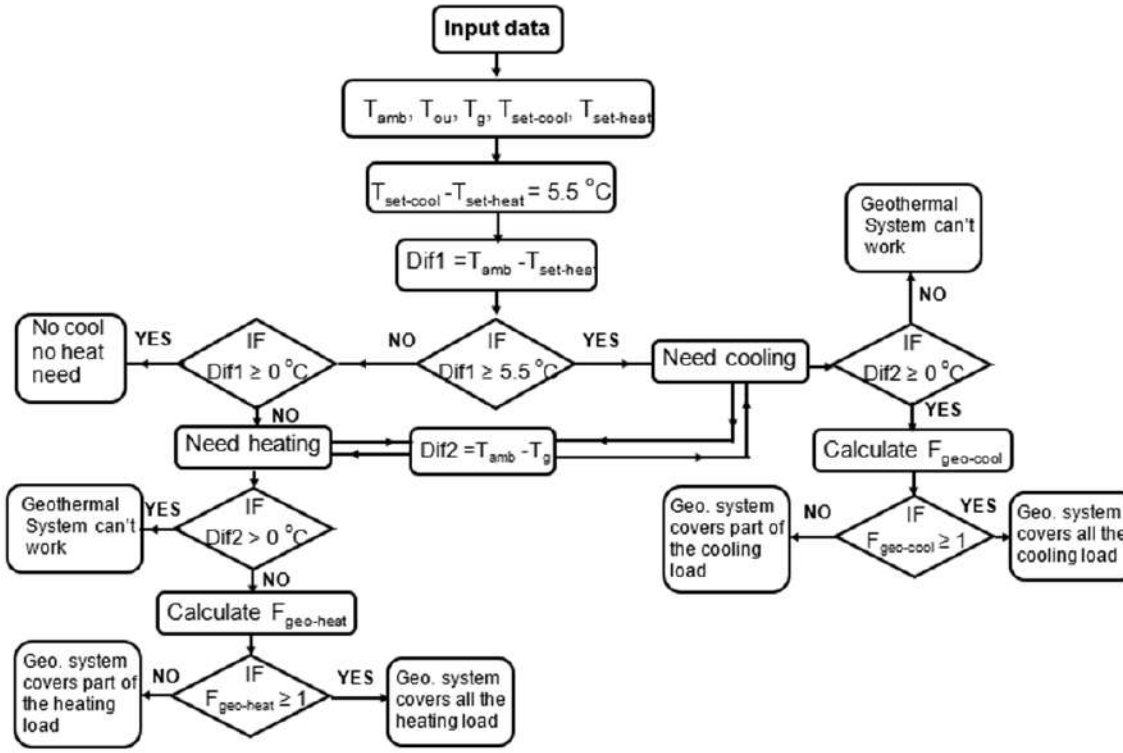


Fig. 7: Flowchart of different steps of the approach used.

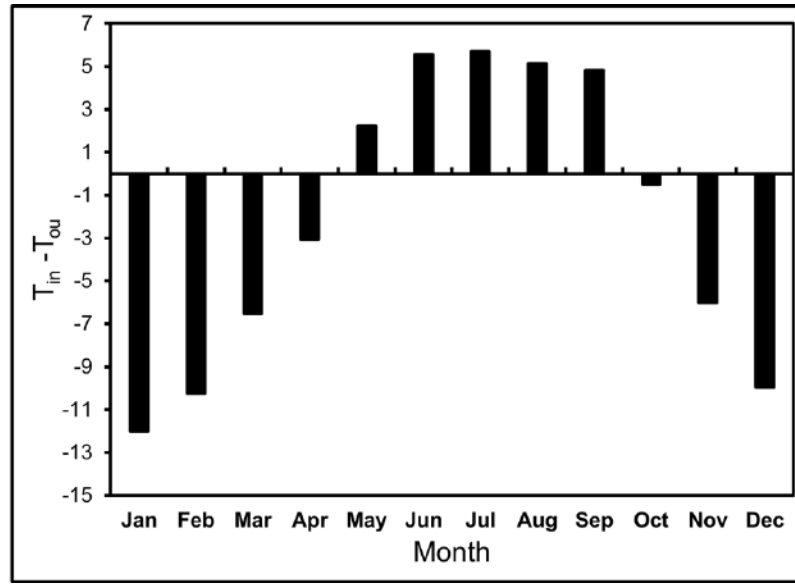


Fig. 8: The monthly temperature difference between ambient air and supplied air to the house for Madinah city.

during the remaining months. The highest absolute values in July and January reflect the highest existing potential for cooling and heating, respectively. Table 4 presents results regarding the above algorithm applied to analyze the Canadian well for heating and cooling. It illustrates that heating is only a concern in January (case 1), February, March, November, and December fall in case 2, where the climate is moderate. Hence, there is no need for cooling or heating. From April till October, the remaining months, the climate is hot, and there is a need for cooling (case 3). However, there is an exception for April and October. Therefore, the geothermal system cannot work because the ground is warmer than the ambient air. During cooling and heating periods, the geothermal percentage factor is calculated and presented in the two last columns of Table 4. For the cooling mode, the geothermal energy source can contribute 26% to 46%. The remaining part should be provided from an auxiliary energy source. However, the Canadian well can fulfill all the needs (100 %).

Fig. 9 permits us to know which city has the highest potential of geothermal contribution for air cooling and

Table 4: Geothermal contribution for cooling and heating in Madinah.

| Month | $T_{amb}$ | $T_g$ | $T_{ou}$ | $T_{amb}$-$T_{set\text{-}heat}$ | Need for Cool/Heat | $T_{amb}$-$T_{ou}$ | $F_{geo\text{-}cool}$ | $F_{geo\text{-}heat}$ |
|---|---|---|---|---|---|---|---|---|
| Jan | 18.3 | 31.6 | 30.3 | -1.7 | Need Heat | -12.0 | x | 100% |
| Feb | 20.2 | 31.6 | 30.5 | 0.2 | NN | x | x | NA |
| Mar | 24.4 | 31.6 | 30.9 | 4.4 | NN | x | x | NA |
| Apr | 28.2 | 31.6 | 31.3 | 8.2 | Need Cool but Geo N W | x | x | NA |
| May | 34.1 | 31.6 | 31.8 | 14.1 | Need Cool | 2.2 | 0.26 | NA |
| Jun | 37.8 | 31.6 | 32.2 | 17.8 | Need Cool | 5.5 | 0.45 | NA |
| Jul | 37.9 | 31.6 | 32.2 | 17.9 | Need Cool | 5.7 | 0.46 | NA |
| Aug | 37.3 | 31.6 | 32.2 | 17.3 | Need Cool | 5.1 | 0.44 | NA |
| Sep | 37.0 | 31.6 | 32.1 | 17.0 | Need Cool | 4.8 | 0.42 | NA |
| Oct | 31.0 | 31.6 | 31.5 | 11.0 | Need Cool but Geo N W | x | x | NA |
| Nov | 24.9 | 31.6 | 30.9 | 4.9 | NN | x | x | NA |
| Dec | 20.5 | 31.6 | 30.5 | 0.5 | NN | x | x | NA |

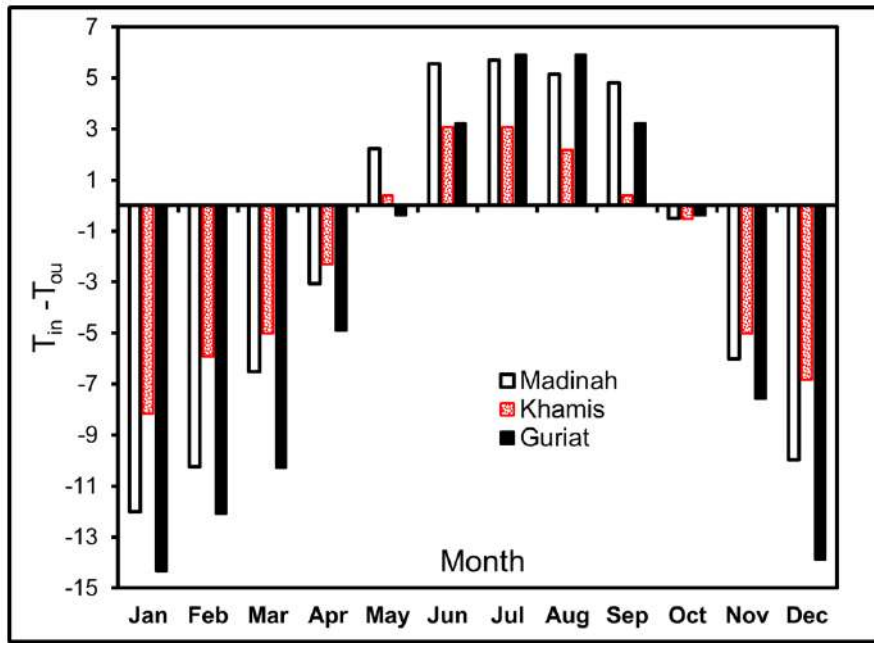


Fig. 9: The monthly temperature difference between ambient air and supplied air to the house for different cities.

heating. Here, only three cities have been chosen among the six previously selected.

Riyadh, Jeddah, and Daman cities have not been chosen; they do not show an essential difference with Madinah city. Madinah presents the highest temperature difference during the summer season and then the best geothermal potential for cooling. However, even in Madinah, with a Canadian well, heating can be provided easily. Guriat presents the highest potential for heating with a temperature difference near -15 $^{o}$C.

Table 5 and Fig. 10 show the monthly geothermal Percentage of cooling/heating for the different cities in a typical K.S.A climate dominated by hot weather results in high undisturbed ground temperature (U.G.T.) over most of the K.S.A. cities than the heating indoor temperature settings $T_{set\text{-}heat}$. Consequently, the Canadian well is an appropriate technology to fulfill easily ($F_{geo\text{-}heat} = 100\%$) the heating load as presented in Table 5. However, for the cooling mode, in most of the cities, the geothermal system can provide only part of the air conditioning needed ($F_{geo\text{-}cool} < 100\%$), except for Khamis and Guriat. These two cities have a moderate climate, and the Canadian well system alone can fulfill the heating and cooling loads. Riyadh has the highest geothermal percentage in July with $F_{geo\text{-}cool} = 67.5\%$, followed by Dahran $F_{geo\text{-}cool} = 59.4\%$ in August and then Madinah with $F_{geo\text{-}cool} = 45.9\ \%$ in July. Jeddah presents the low percentage with $F_{geo\text{-}cool} = 29.9\%$. Therefore, during the summer season and the Canadian well system, Madinah, Riyadh, Jeddah, and Dahran need an auxiliary energy source to satisfy the comfort in the building.

## CONCLUSION

A potential assessment of the Canadian and a shallow geothermal energy source for cooling and heating in Saudi Arabia has been conducted. The study is based on monthly average ambient temperature for a long-term period in six different cities selected according to the diverse climatic zones in K.S.A. The undisturbed ground temperature has been determined for more than 70 cities and applied to generate isotherms presented on the map of K.S.A. This information is beneficial for engineers who are interested in shallow geothermal applications. In addition, a new factor has been proposed to estimate the percentage of geothermal contribution. For all cities, the shallow geothermal energy sources can easily satisfy all the heating needs and partly the cooling needs for the hottest cities as; Madinah, Jeddah, Riyadh, and Dahran. However, an auxiliary energy source must be added.

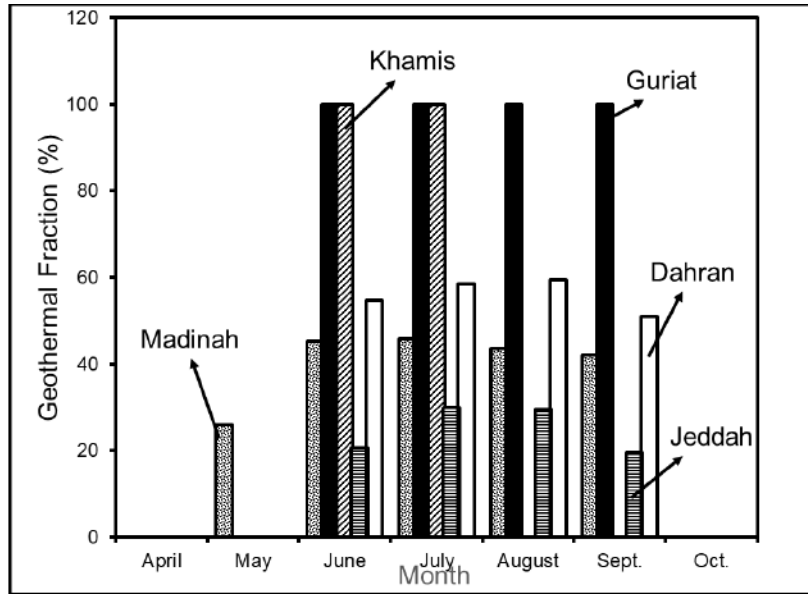


Fig. 10: Monthly geothermal percentage of cooling for different cities.

Table 5: Comparison of geothermal Percentage for different cities.

| Month | Madinah | | Riyadh | | Guriat | | Khamis | | Jeddah | | Dahran | |
|---|---|---|---|---|---|---|---|---|---|---|---|---|
| | Cool | Heat | Cool | Heat | Cool | Heat | Cool | Heat | Cool | Heat | Cool | Heat |
| Jan | | 100 | | 100 | | 100 | | 100 | | | | 100 |
| Feb | | | | 100 | | 100 | | 100 | | | | 100 |
| Mar | | | | | | 100 | | 100 | | | | |
| Apr | | | | | | 100 | | | | | | |
| May | 25.98 | | 51.58 | | | | | | | | | |
| Jun | 45.24 | | 64.51 | | 100 | | 100 | | 20.61 | | 54.78 | |
| Jul | 45.85 | | 67.48 | | 100 | | 100 | | 29.88 | | 58.51 | |
| Aug | 43.52 | | 65.75 | | 100 | | | | 29.54 | | 59.39 | |
| Sep | 42.07 | | 58.18 | | 100 | | | | 19.54 | | 51.01 | |
| Oct | | | | | | | | | | | | |
| Nov | | | | | | 100 | | 100 | | | | |
| Dec | | | | 100 | | 100 | | 100 | | | | |

## Nomenclature

| | |
|---|---|
| A | the amplitude of the temperature, (K) |
| F | geothermal percentage |
| h | thermal conductivity, (W/m.K) |
| t | time, (days) |
| T | temperature, (K) |
| y | depth in the ground, (m) |

## Greek symbols

| | |
|---|---|
| $\alpha$ | thermal diffusivity, ($m^2$/day) |
| $\alpha_s$ | absorption coefficient |
| E | effectiveness of EAHE |
| $\delta$ | damping depth, (m) |
| $\Phi$ | phase angle (radians) |
| $\omega$ | angular frequency, (radians/day) |

### Subscript

| | |
|---|---|
| a, amb | ambient |
| conv | convective heat transfer |
| G | Global solar radiation on a horizontal surface |
| g | ground |
| geo-cool | geothermal cooling |
| geo-heat | geothermal heating |
| in | inlet |
| ou | outlet |
| s | ground surface |
| sky | sky |
| conv | convection |

## ACKNOWLEDGMENTS

The authors would like to thank the Saudi Ministry of Education and the Research deanship of the Islamic University in Madinah for the funding support under Project No. 20/12.

## REFERENCES

Al-Ajmi, F., Loveday, D.L. and Hanby, V.I. 2006. The cooling potential of earth-air heat exchangers for domestic buildings in a desert climate. Build. Environ., 27(1): 67-79.

Albogami, S.M. and Boukhanouf, R. 2019. Residential building energy performance evaluation for different climate zones. IOP Conf. Series: Earth Environ. Sci., 32(9): 57-80.

Alrashed, F. and Asif, M. 2015. Climatic classifications of Saudi Arabia for building energy modeling. Energy Procedia, 7: 245.

Badache, M. 2016. A new modeling approach for improved ground temperature profile determination. Renew. Energy, 6: 20.

Benhammou, M. and Draoui, B. 2015. Parametric study on the thermal performance of earth-to-air heat exchanger used for cooling of buildings. Renew. Sustain. Energy Rev., 12: 14-30.

Benhammou, M., Draoui, B. and Hamouda, M. 2017. Improvement of the summer cooling induced by an earth-to-air heat exchanger integrated into a residential building under a hot and arid climate. Appl. Energy, 12: 212-239.

Benrachi, N. 2020. Numerical parametric study of a new earth-air heat exchanger configuration designed for hot and arid climates. Int. J. Green Energy, 17: 121-156.

Bisoniya, T.S., Kumar, A. and Baredar, P. 2013. Experimental and analytical studies of earth-air heat exchanger (EAHE) systems in India: A review. Renew. Sustain. Energy Rev., 11: 23.

Bojić, M. 2000. Optimization of heating and cooling of a building by employing refuse and renewable energy. Renew. Energy, 6: 117-122.

Dalla Longa, F. 2020. Scenarios for geothermal energy deployment in Europe. Energy, 16: 118-126.

Ghaith, F.A. and Ur Razzaq, H. 2018. Thermal performance of earth-air heat exchanger systems for cooling applications in residential buildings. ASME International Mechanical Engineering Congress and Exposition, Proceedings (IMECE), 9-15 November 2018, Pittsburgh, Pennsylvania, USA. ASME, New York, USA, pp. 1-12.

Kazemiani-Najafabadi, P. and Amiri Rad, E. 2020. Optimization of an improved power cycle for geothermal applications in Iran. Energy, 11: 83-97.

Kusuda, T. and Archenbach, P. 1965. Earth temperature and thermal diffusivity at selected stations in the United States, ASHRAE Transaction.

Lapertot, A. 2021. Optimization of an earth-air heat exchanger combined with heat recovery ventilation for residential building needs. Energy Build., 10: 702-713.

Liang, J.D. 2020. Experimental investigation of a liquid desiccant dehumidification system integrated with shallow geothermal energy. Energy, 11: 52-64

Medina, Saudi Arabia Weather Conditions. n.d. Weather Underground. Available at: https://www.wunderground.com/weather/sa/medina/24.45999908,39.61999893 (Accessed: 1 March 2021).

Natural Resources Canada. 2013. RETScreen ® International. RETScreen Clean Energy Project Analysis Software.

Ouzzane, M. 2015. 'New correlations for the prediction of the undisturbed ground temperature. Geothermics, 8: 11-21

Solar Energy Laboratory. 2012. Trnsys 17. University Wisconsin-Madison, USA.

The Saudi Building Code National Committee. 2007. '601: Energy conservation requirements. Saudi Building Code, SA.

Thiers, S. 2012. Thermal modeling of an air-ground heat exchanger for building cooling. Solar Energy, 82(9): 820-831.

Wang, Z. and He, T. 2014. Influence of urban heat island on office building energy consumption. Nature Environ. Pollut. Technol., 54: 11-21.

Wei, H. 2021. Field experiments on the effects of an earth-to-air heat exchanger on the indoor thermal environment in summer and winter for a typical hot-summer and cold-winter region', Renew. Energy, 6(3): 32-47.

Xu, X. 2014. Research and application of active hollow core slabs in building systems for utilizing low energy sources. Appl. Energy, 9: 64.

Yan, T. and Xu, X. 2018. Utilization of Ground Heat Exchangers: A Review. Current Sustainable/Renewable Energy Reports.

Yueer, H., Shini, P. and Meng, L. 2013. Impact analysis on the energy-saving and land-saving properties of green buildings with different per capita floor space of residential buildings. Nature Environ. Pollut. Technol., 5: 717

Nature Environment and Pollution Technology
An International Quarterly Scientific Journal

p-ISSN: 0972-6268
(Print copies up to 2016)
e-ISSN: 2395-3454

Vol. 20 | No. 5 (Suppl) | pp. 1935-1945 | 2021

Review Research Paper | https://doi.org/10.46488/NEPT.2021.v20i05.009 | Open Access Journal

# Microplastics in Landfills: A Comprehensive Review on Occurrence, Characteristics and Pathways to the Aquatic Environment

**Kshitij Upadhyay† and Samir Bajpai**
Department of Civil Engineering, National Institute of Technology, Raipur-492010, Chhattisgarh, India
†Corresponding author: Kshitij Upadhyay; kshitij.upadhyay111@gmail.com

**Nat. Env. & Poll. Tech.**
**Website: www.neptjournal.com**

*Received:* 12-03-2021
*Revised:* 28-04-2021
*Accepted:* 02-05-2021

**Key Words:**
Microplastics
Landfill
Leachate
Degradation
Transfer pathways

## ABSTRACT

Microplastics, a multi-dimensional environmental stressor group, capable of transboundary migration, are a threat to the global ecosystem. Transboundary migration of microplastics across all environmental matrices is known to originate from a multitude of sources and acts in conjugation with each other. This inter-dependence of sources calls for a detailed scientific analysis of all the sources that are in play. Waste management facilities have already been established as a significant contributor of microplastics to the aquatic and terrestrial environment. A systematic overview of the scientific literature reveals that the existing body of scientific knowledge is mainly focused on wastewater treatment facilities as a source/pathway of microplastics in the environment. Recently the focus shifted towards solid waste management facilities through landfills. Poor plastic waste management practices made discarded plastics the most dominant component of solid wastes. This review elucidates the occurrence and distribution of microplastics, characteristics of microplastics, including size, shapes, colors, and polymer types, in leachate and refuse of landfills. Furthermore, we discussed the transport mechanisms and pathways used by microplastic present in landfills to migrate to subsurface or groundwater and adjacent aquatic bodies. Last, based on the findings, we summarized the gaps in existing studies and suggested future perspectives to be focused on the future. The abundance of microplastics is attributed to the volume of plastic waste in landfills, management of leachate originating from landfills, application of leachate, and age of landfills. Microplastics abundance and characteristics vary in leachate and refuse. Smaller microplastics are predominant in leachate while larger microplastics are predominant in refuse. Landfills are capable of generating secondary microplastics from fragmentation and degradation. Further studies on microplastics in landfills are necessary to tackle this ever-growing menace.

## INTRODUCTION

Mass production and increased consumption of plastics resulted in plastic accumulation in terrestrial and aquatic habitats (Colton & Knapp 1974, Coe & Rogers 2012). The plastic material, after its usefulness, ends up in the environment as waste or garbage (Gregory 1996, Moore et al. 2002, Derraik 2002). Plastic waste in the environment exists in different sizes range and classified as macroplastics, mesoplastics, and microplastics (Gregory & Andrady 2003, Van Sebille et al. 2015). The term 'microplastic' was used by Thompson in 2004, to define smaller plastic pollutants present in the marine environment with emphasis been given to their size (Thompson et al. 2004). The size boundary used in defining microplastics was further refined by various authors (Andrady 2011, Arthur et al. 2008, Verschoor 2015).

The most popular and widely used definition of microplastics was proposed by United States National Oceanic and Atmospheric Administration (NOAA), defining 'microplastics' as any piece of plastic with upper size < 5 mm, covering all types of plastic in the environment, regardless of the difference in chemical composition. Recently, a group of experts from this field, fixed the lower size limit of microplastics to 1 μm, to make results of future studies comparable and introduced a definition for submicron plastics (Size < 1 μm) known as nano plastics (Hartman et al. 2019).

The ever-growing body of scientific understanding from the studies demonstrates that microplastics are ubiquitous in the terrestrial environment and the terrestrial environment act as a "source and sink" for microplastics. A study reports that annual plastics released to land are estimated to be 4–23 times higher than that released to oceans (Geyer et al. 2017).

The major portion of plastic garbage after material/resource recovery and subsequent reuse, eventually ends up in landfills. It has been roughly estimated that 95 % of MSW generated in the world ends up in landfills. The large portion of wastes in landfills is of plastic origin with a rough estimate to be 79 %, thereby suggesting landfills to be abundant with microplastics (Zhou et al. 2014). While waste management facilities such as wastewater treatment plants and landfills are presumed to be a potential source of microplastics, our

understanding of the role of landfills as a source or sink of microplastics is limited (Ngo et al. 2019, Kazour et al. 2019, Cowger et al. 2019).

Landfill leachate, whether treated or otherwise, has been known to pollute environmental matrices with heavy metals and other toxic compounds, primarily in the soil and groundwater. Such contamination of groundwater results in a substantial risk to local groundwater resource users and the ecosystem. The presence of toxic plasticizers in leachate has been reported in many studies, which establish that landfills are a significant source of plastic-associated pollutants (Jonsson et al. 2003, Asakura et al. 2004, Baderna et al. 2011, Kalanatarifard & Yang 2012, Wowkonowicz et al. 2013). Besides primary microplastics already present in the solid waste and landfills generates secondary microplastics due to the substantial amount of plastic waste buried in landfills and providing favorable environmental conditions for progressive and continuous degradation of macroplastics to microplastics (Ishigaki et al. 2004, Webb et al. 2013).

Thus, it is likely that landfills are also capable of storing, fragmenting, and releasing microplastics further in the environment, and may likely be the crucial link in better understanding the cyclic movement of microplastics in the environment. This paper aims to provide a review of the existing literature reporting microplastic pollution in landfills, focusing on their abundance and characteristics. Further, we examined whether landfills act as a sink, source of microplastics, or both and discussed transfer mechanisms of microplastics to the aquatic environment. Last, we discussed current gaps in knowledge regarding the understanding of microplastic pollution in landfills.

## RESULTS AND DISCUSSION

### Microplastic Occurrence and Abundance in Landfills

Results from 31 landfills that were examined in five studies portray that number of microplastics varies significantly with almost none to 25 particles per liter. The abundance of microplastics from each landfill site is mentioned in Table 1. The five studies considered under this review are geographically dispersed, spreading across Nordic countries of Europe to south Asian countries like China and Thailand, suggesting that microplastics are heterogeneously dispersed in landfills around the globe (Kilponen 2016, Praagh et al. 2018, He et al. 2019, Su et al. 2019, Puthcharoen & Suchat 2019). This trend is in line with microplastic distribution in the aquatic and terrestrial environment around the globe, though microplastic abundances in landfills remain lower than in the aquatic ecosystem. Microplastics are found to be abundant in mostly all leachate samples.

This section also includes studies in which the reported quantity of microplastics in freshwater, sediment, and wastewater treatment plants are on par with the abundance of microplastics in landfills. Microplastic abundance and distribution in Flemish rivers of Belgium, River Seine of France, Lake Hovsgol of Mongolia, Great Lakes of USA, and various lakes of Switzerland are reported to be 17 particles.$L^{-1}$, 0.03 particles.$L^{-1}$, 0.00012 particles.$L^{-1}$, 0.016 particles.$L^{-1}$, and 20 particles.$L^{-1}$ respectively (Slootmaekers et al. 2019, Dris et al. 2015, Eriksen et al. 2013, Van Wezel et al. 2016, Faure et al. 2015).

A significant difference in microplastic abundance was observed among the analyzed landfill sites, with the highest abundance of microplastics recorded at landfill No. 2 of Shanghai, China (24.58 particles.$L^{-1}$) and lowest around landfill site of Tali, Helniski (0.002 particles.$L^{-1}$). Furthermore, microplastic abundance varies from landfill to landfill within a country and other countries. Country-wise the maximum abundance was found at Álfsnes landfill (4.51 particles.$L^{-1}$) in Iceland, Böler landfill (1.3 particles.$L^{-1}$) in Norway, Hollola landfill (1.97 particles.$L^{-1}$) in Finland, and Shanghai landfill No. 2 (24.58 particles.$L^{-1}$) in China. This trend can be attributed to the difference in living standards, human activity, and type of industries, waste management practices, the quantity of plastic waste in MSW, and local laws and policies among countries. The nature and quantity of waste generated and handled by landfills are likely to be different, in turn influencing the abundance and characteristics of microplastics present in landfills. For example, the municipal solid waste of China has been reported to have less plastic content when compared with plastic content in municipal solid waste of Nordic countries (Yang et al. 2018). The other important aspect which affects the variation in microplastics abundance is the targeted microplastics size in the study. Variation in the mesh sizes or filter paper used during sampling and analysis influences the abundance of microplastic particles present in the samples.

Apart from leachate, refuse and dry waste from landfills was analyzed for the presence of microplastics in two studies. In the refuse sample obtained from Laogang landfill in Shanghai, China, the microplastic abundance was found to be in the range of 20-91 particle.$g^{-1}$. Similarly, in 12 landfills of Thailand, microplastic abundance in refuse was in the range of 0.6-2.2 particle.$g^{-1}$. Microplastic abundance in landfill refuse is reportedly higher when compared with microplastic abundance in aquatic sediments, agricultural soil, and sewage sludge, again solidifying landfills as one of the major land-based sources of microplastics (Hu et al. 2015, Li et al. 2018, Liu et al. 2018).

Variation in leachate composition and concentration

of pollutants when compared with refuse is attributed to the amount of water that infiltrates or percolates into the landfill and the environmental degradation and fragmentation processes occurring inside the landfill. Landfills are known to behave like an anaerobic reactor due to a favorable environment (sufficient moisture and lack of oxygen etc.), where a diverse range of microbial communities thrive. These microorganisms have the potential to bio-degrade plastic waste present in landfills depending on the environmental conditions of the landfill and the chemical nature of the polymer. Degradation of biodegradable plastics, through microbial activities in the landfill, results in the production of methane and biomass while degradation of other polymeric materials results in the production of microplastics. Hence the abundance of microplastics in landfills directly depends upon the volume of plastic waste present in the landfill, the volume of primary microplastics present in the landfill, and the degradation process occurring in the landfill (Ishigaki et al. 2004, Themelis & Ulloa 2007)

## Characteristics and Nature of Microplastics in Landfill

Characteristics of microplastics play a key role in the distribution and transference of microplastics in the environment. It is a common practice to characterize microplastics into different sizes; shapes, colors, and polymer types, etc. which aids in identifying the source, transfer pathway, fate, degradation status, potential to act as a vector for toxic chemicals and microbes, their interaction with organisms, and impact on the environment. The characteristics of microplastics from studies on landfills are summarized in Table 1.

### Size of Microplastics

The size of the microplastics plays a crucial role in their interaction with the biotic component and long-term threat to the ecosystem. The lowest boundary of mesh size used during the sampling and analysis portion will fix the size of microplastics reported in the study. Continuous environmental degradation of macroplastics and microplastics keeps

Table 1: Abundance and characteristics of microplastics found in landfills.

| Location | Abundance (Particle/L) | Size Classification | Shape | Microplastics polymer composition (%) | Reference |
|---|---|---|---|---|---|
| Álfsnes Iceland | 4.51 | 5,000-500 µm and 500-50 µm | NM | PE (41.46%), PP (4.27%), PVC (2.07%), PS (12.26 %), PET (13.91%), PUR (21.35.%), PA (0.55%), PMMA (4.13%). | A |
| Anonymous 1*Finland | 0.30 | | | | |
| Anonymous 2* Norway | 1.40 | | | | |
| Böler Norway | 1.3 | | | | |
| Fiflholt new cell Iceland | 0.20 | | | | |
| Fiflholt old cell Iceland | - | | | | |
| Gjerdrum Norway | 1 | | | | |
| Hollola Finland | 1.97 | | | | |
| Korvenmäki Finland | 1.10 | | | | |
| Kujala Finland | 0 | | | | |
| Topinoja Finland | 0.16 | | | | |
| LF1 Shangha | CW: 3.58 EB: 18.38 | 1,000-5000 µm and 1000-100 µm | lines (14.81%), flakes (22.87%) fragments (58.62%), pellets (0.64 %) and foams (3.06%) | PE (34.94%), PP (34.94%), PVC (0.32%), PS (4.99%), ABS (0.32%), PET (5.96%), PUR (1.45%), EVA (0.64%), PA (0.64%), PES (2.74%), EP (0.32%), PF (0.16%), PPC (0.16), PMMA (0.32%), ALK (4.35%), PMDS (2.25%), PTFE (5.48%). | B |
| LF2 Shanghai | CW: 0.79 EB: 24.58 | | | | |
| LF# Shanghai | CW: 1.38 EB: 1.17 | | | | |
| LF4 Wuxi | CW: 0.96 EB: 0.96 | | | | |
| LF5 Suzhou | CW: 0.42 EB: 2.96 | | | | |
| LF6 Changzhou | CW: 2.21 EB: 3.58 | | | | |
| Laogang, Shanghai, China | 4 to 13 | < 0.5 mm; 0.5-1 mm; 1-5 mm | Leachate: fiber (60%), granules (24.62%) , fragments (15.38%) ,Refuse: fragments (59.28 %) granules (18.57 %) , fibre (13.39 %) films (7.86 %) and rods (0.36%) | Leachate: Cellophane (45.12%), PE (9.76%), PP (8.54%) and PS (8.54%, refuse) Refuse: PE, PEUR, PS, EPM, and PP polymers (60 %) | C |

Table cont....

| Location | Abundance (Particle/L) | Size Classification | Shape | Microplastics polymer composition (%) | Reference |
|---|---|---|---|---|---|
| Tali, Helsinki | 0.002 and 0.017. | <300 µm;100 µm -300 µm and 100 µm to 20 µm. | Textile fibres : 0.080 to 0.261 fibres/L and synthetic particle : 0.002 and 0.017 particle/L | NM | D |
| 12 landfill of Thailand | 13.5- 27.5 Items/ kg.dry weight | 330 µm to 5000 µm | Grannules: 32% films 27%, irregulars 22% and spheres 1% leachates: granules 47% films (28%), fibers (17%), irregular (8%) and spheres (0%). | PS, PP, PET | E |

References: A - Praagh et al. (2018); B - He et al. (2019); C - Su et al. (2019); D - Kilponen (2016); E - Puthcharoen & Suchat (2019)

generating secondary microplastics, making exact estimation of microplastics based on size tough. Furthermore, smaller microplastics with a larger surface area are more prone to sorptive processes making a higher possibility of adsorption of toxic pollutants. Out of 5 studies, size distribution was mentioned in 3 studies, Detail of various size classifications used in the studies are summarized in Table 1.

Microplastics present in the leachate of 11 landfills of Nordic countries were classified in two size range- 5,000–500 µm and 500–50 µm. Results concluded that when compared with raw or treated sewage, landfill leachate is likely to be a relatively small source of microplastic particles between 5000 and 50 µm**.** Microplastics present in leachate samples from 6 landfills of China were reported in 3 size classification. The highest percentage (74.88%) of microplastics was found to be in the size range of 100-1000. Microplastics in leachate and refuse from Shanghai landfill were categorized into 3 classes, < 0.5 mm, 0.5-1 mm, and 1-5 mm. The size of microplastics ranged from 0.07 to 3.67 mm in leachate, and 0.23 to 4.97 mm for refuse samples. The average size of microplastics in refuse (1.03 mm) was larger than leachate (0.83 mm) suggesting large microplastic particle entraps in refuse while smaller microplastics particles migrate to the leachate. It can also be inferred that, due to continuous environmental degradation of the large microplastic particle, smaller secondary microplastics are being generated which migrates to the leachates. Microplastics in leachate sample collected near Talli, Helniski were classified into 3 size groups: <300 µm;100 µm -300 µm, and 100 µm to 20 µm.

Results of the five studies revealed that the abundance of microplastic varies with the size fraction of microplastics. The smaller microplastics remain abundant in leachate while larger microplastics are abundant in refuse. In the aquatic environment, smaller particles are reported to be dominant in the entire microplastics size range due to continuous degradation and fragmentation; results from the landfill studies also confirm this trend (Isobe et al. 2014, Zhang et al. 2017, Auta et al. 2017).

Problems associated with reporting size distribution and abundance of microplastics in microplastic research studies due to different sampling strategies and analytical methods being used by researchers, make comparative studies challenging. Standardization and harmonization of the microplastic analysis protocols and guidelines for reporting the size distribution of microplastics are much needed to use the size distribution data efficiently (Filella, 2015).

## Shape of Microplastics

Microplastics in the environment appear in a wide diversity of shapes. Visual identification of microplastics through naked eyes and microscopes reveals morphological characteristics such as shape and color. Microplastic morphologies commonly described in research literature include spheres, beads, pellets, foam, fibers, fragments, films, and flakes. The shape of environmental microplastics depends upon the type of microplastics. Primary microplastics are intentionally made in that form, as the specific shape of primary microplastics serves a specific purpose, for example, microbeads in facial cleansers and face scrubs. In nature, degradation and fragmentation of microplastics occur, where a wide range of mechanical forces act on the surface of plastic which results in rugged and irregular-shaped secondary microplastics. Secondary microplastics with sharp edges illustrate a recent introduction into the environment while smooth edges are associated with a large residence time (Hidalgo-Ruz et al. 2012, Free et al. 2017, Paco et al. 2014, Weinstein et al. 2016, Upadhyay & Bajpai 2021).

Out of 5 studies, only 3 studies report the shape of microplastics. Microplastics in 12 leachate samples from 6 landfills were categorized into 5 groups: lines, flakes, fragments,

pellets, and foams. Fragments and flakes were found in all samples. Pellets and foam were found only in the landfills of Shanghai. The majority of the microplastics found were irregular in shape and had rough edges suggesting that secondary microplastics are the major source of microplastics in landfill leachate. Morphologically, microplastics from Leogang, Shanghai, China was categorized as fibers, granules, films, rods, and fragments in leachate and fibers, granules, and films in refuse. In leachate samples, fibers (60%) were abundant while in soil samples, fragments (59.28 %) were abundant as mentioned in Table 1.

Microplastics in leachate from a landfill in Talli, Helsinki, were analyzed for the presence of textile fiber and synthetic particles. Fibers were prevalent in all the samples. Microplastics in 12 soil samples and 10 leachates from 12 landfills of Thailand were categorized as fibers, films, spheres, granules, and irregular. In soil and leachate samples, granules (32% & 47% respectively) were the dominant type of microplastics.

The shape is crucial in determining the sources and types of microplastics. The shape also reveals the residence time of microplastic, meaning when the microplastics entered into the environment. Resins and pellets are reported to be dominant in the aquatic environment near industrial activities, suggesting the use of primary microplastic in industries while fragments and foams remain dominant near heavy marine aquatic traffic, tourist spots, and marine environment, suggesting secondary microplastics due to degradation. In domestic wastewater and wastewater treatment plants, beads found in personal care products and textile fibers from textile washing forms the majority of microplastics while fibers form the major component of microplastics deposited from the atmosphere (Napper et al. 2015, Dris et al. 2016, Hernandez et al. 2017)

The abundance of irregular shapes and rough edges of microplastics resulting from fragmentation and degradation of microplastics, and the volume of plastic waste buried in landfills implies a long-term process of generation, accumulation, and release of microplastics in the landfills. Earlier studies concluded that the abundance of the fragment in the aquatic environment is the result of environmental weathering and fragmentation of larger plastic products, or input of effluents from the wastewater treatment plants and industrial activities or derived from vessel activities (cargo, fishing, etc.). Furthermore, microplastics of smaller size having an irregular shape and rough surface provides active sorption sites which increases the sorptive potential of microplastics. This coupled with a higher residence time of microplastics in the environment (more residence times, increases the likelihood to), enhances the environmental risk of leachate discharged to the environment (Koelmans et al. 2016, Machado et al, 2018).

## Color of Microplastics

Pigments and dyes are used by plastic manufacturing industries to produce colored macroplastics and microplastics. The consensus among microplastic pollution researchers remains in favor of reporting color classification of microplastics with the majority of microplastic studies reporting quantitative data on different colors of microplastic in the environment; still, none of the studies on landfill reports any information related to microplastic color. Microplastics have been reported in a range of colors, including red, orange, yellow, brown, tan, off-white, white, grey, blue, green, etc. Transparent microplastics originate from single-use plastic such as plastic bags and plastic plates or cups or from industries where transparent microplastics are used as feed material. Colored microplastics are mainly secondary microplastics

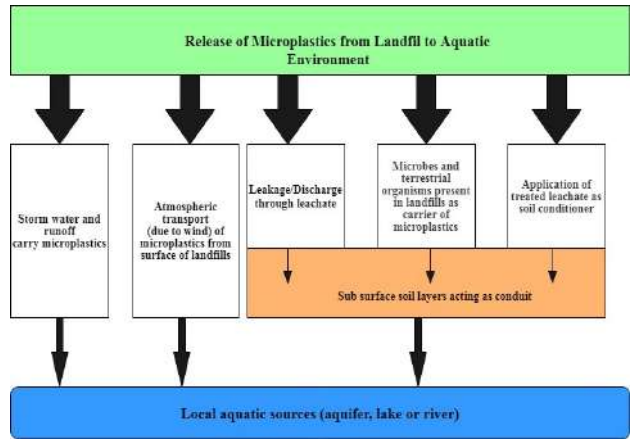


Fig.1: Potential pathways for microplastics migration and transference from landfills to aquatic environment.

resulting from the fragmentation of colored macroplastics. However, the color of the plastic particle cannot easily be used to deduce the type or origin. Importantly, color information can be biased as brighter colors are spotted more easily during visual inspection.

**Polymer Type of Microplastics**

Analysis of the microplastic composition mainly in form of polymer types reveals pertinent useful information on an individual particle. The polymeric information alone can point towards sources and origin in most cases, but when supplemented with morphological information, will reveal the completed information (Digka et al. 2018).

726 microplastics present in 16 leachate samples (treated and untreated) from 11 landfills of the Nordic nation were identified to confirm the presence of 8 polymer types. PE (301 particles) was found to be abundant. 17 types of polymers were found in 621 microplastics particles from 12 leachate samples of 6 landfills in China. PE (217 particles) and PP (217 particles) dominated the entire polymer group (92). Microplastics present in leachate and refuse from landfills near Laogang, Shanghai, China were analyzed for polymer identification. For refuse samples, the highest abundance was represented by PE. In leachate samples, the highest abundance was represented by cellophane.

Polyethylene is the most dominating polymer type found in landfills. Cellophane, a typical semi-synthetic material, classified as microplastics, was abundant in landfills near Laogang, Shanghai, China. PE is also observed to be the most frequent polymer type found in other environmental matrices. In the aquatic environment, PE, PP, and PS microplastics are dominant. Similarly, PS and PE are the most detected microplastic polymer in wastewater samples (Van Sebille et al. 2015, Galgani et al. 2015, Ballent et al. 2016, Talvitie et al. 2017).

Polythene dominates the most produced polymer type in the world and has a wide range of applications such as packaging material and in personal care products. PS is extensively used in packaging and for manufacturing disposable items (coffee cups and food containers, eating utensils), while PP is used to make rigid plastic tools and furnishings, such as textile floor coverings, carpets, and fishing nets. Cellophane is often used as packing material for food items, batteries, and cigars (Vianello et al. 2013, 2019, Su et al. 2016, Kershaw & Rochman 2016).

**Migration and Transport of Microplastics from Landfills to Aquatic Environment**

The fate of microplastics in landfills not only deals with microplastics buried in the landfill but also the secondary microplastics generated in landfills. Waste present in landfills, over time, gets decomposed and starts sweating, and generates a sufficient quantity of liquid waste known as 'leachate'. Landfill leachate can be defined as the liquid effluents generated from rainwater percolation or infiltration through a landfill, as well as, the moisture present in the waste and the degradation of waste (Mukherjee et al. 2015, Costa et al. 2018). The quantity of leachate generated depends upon the intensity and duration of rainfall, evapotranspiration, surface runoff, groundwater infiltration, and degree of compaction of waste in landfills.

Landfill facilities have a special arrangement for the collection of leachates which are eventually being disposed of in the environment, with or without treatment (Salem et al. 2018). Areas near landfills have a greater possibility of groundwater contamination because of the potential pollution source of leachate originating from the nearby site (Mor et al. 2006). The leachate pollutes large amounts of groundwater, rendering it unsuitable for use. Such contamination of groundwater resources poses a substantial risk to local resource users and the natural environment (Han et al. 2016). The plastic waste present in landfills is subjected to various environmental forces that facilitate their fragmentation or degradation and horizontal or vertical movement either due to groundwater underflow or infiltration. Overtime the leachate generated in the landfill starts accumulating at the bottom of the landfill and percolates through the soil and reaches the groundwater (El-Fadel et al. 1997, Islam & Singhal 2004, Themelis & Ulloa 2007, Bilgili et al. 2007).

Microplastic contamination of groundwater from landfill leachate is of paramount importance due to its association with chemicals and pathogens. Their eco-toxicological effect depends upon various factors such as volume and toxicity of microplastics present in leachate, permeability and nature of the geological strata which govern vertical and horizontal distribution, and direction of groundwater flow. Of these factors, groundwater flow is crucial as groundwater moves slowly and continuously through the pervious strata of soil. If a landfill contaminates groundwater with microplastics, a plume of contamination will occur and aquatic sources in that plume will be contaminated. The dry (long) and wet (intense) cycle leads to accelerated dispersion of leachate in the surrounding areas causing microplastic contamination of subsurface water.

The transport mechanism of microplastics from landfills is complex and remains unidentified, though few mechanisms have been conceptualized based on the transport and fate of microplastics in soil and terrestrial environment. Microplastics from landfills can transfer to groundwater and nearby water bodies using 5 distinct routes as shown in Fig. 1.

**I. Stormwater or surface runoff carries microplastics from landfills into aquatic systems:** Stormwater runoff is an important pathway for the transport of microplastics from landfills to groundwater and aquatic bodies. Macroplastics and microplastics present near roads, on the ground surface, in open solid waste dumping sites and landfills, gets carried away with surface runoff which eventually ends up being part of groundwater or aquatic system. The presence of microplastics in surface runoffs has already been reported and modeling studies confirm that surface runoffs carry microplastics (including tire wear and road wear/dust particle) from terrestrial to the aquatic environment (Nizzetto et al. 2016, Siegfried et al. 2017, Vogelsang et al. 2019, Kole et al. 2017).

**II. Atmospheric transport (due to wind) of microplastics from the surface of landfills to the aquatic environment:** Microplastics are light in weight and their atmospheric transport has been highlighted as an important pathway that carries microplastics in the environment. Microplastics having low buoyancy, get carried away from the surface of the landfill by the wind and may deposit into aquatic bodies. Researchers have discovered that wind pushes and mixes the lightweight plastic particle down into the water (Rezaei et al. 2019). The wind can carry microplastics from the ground surface, open solid waste dump sites, and landfills and deposits them in environments farther from their original site, including the aquatic environment (et al. 2021).

**III. Transference through leachate either by direct discharge or leakage from drainage:** Leakage of leachate due to defects in landfill liners have been a matter of concerns for so long, Sufficient evidence is available which suggests that leakage through landfill liners would be a pathway for microplastics to enter into the adjacent environmental matrix (from subsurface soil to groundwater which eventually ends up in aquatic sources) (Foose et al. 2001). The immediate surface below landfill and landfill themselves are composed of porous soil medium containing pores of different sizes. These pores provide an opportunity for contaminants like microplastics to escape from the landfill. Recent studies discussed the vertical and horizontal distribution of microplastics in soil. Smaller microplastics easily move through soil pores while larger microplastic gets trapped. Similarly, in landfills, smaller microplastics migrate through the pores while larger microplastics get trapped in the pore. Trapped microplastics are under constant environmental degradation forces and with time, they break down into smaller microplastics, which then escape through the pores and reach aquifers via soil (Foose et al. 2001, Blasing & Amelung 2018, Grayling et al. 2018, Yong et al. 1992, Brandon et al. 2016).

**IV. Microbes and terrestrial organisms present in landfills as the carrier of microplastics**: The most recent studies demonstrate that microbes and terrestrial organisms present in soil act as a carrier of microplastics. In laboratory conditions, two collembola species (i.e. *Folsomia candida* and *Proisotoma minuta*) carried and distributed microplastics. A study showed that mite (i.e. *Hypoaspis* aculeifermoved) can also move and disperse the commercial PVC microplastics. Similarly, earthworms were also observed to be the carrier of microplastics. Due to the abundance of microplastics in the terrestrial environment and terrestrial trophic transfer of microplastics, microplastics get ingested by terrestrial organisms and microbes. These organisms carry microplastics into the environment and release microplastics back to the environment through excretion. Microplastics can also get attached to the outer surface of organisms and migrate freely (Maaß et al. 2017, Zhu et al. 2018a, 2018b, Rillig et al. 2017, Huerta Lwanga et al. 2017a, 2017b)

**V. Application of treated leachate as soil conditioner:** Leachate, a toxic mix of chemicals, also contains minerals and nutrients (iron, nitrogen, phosphorus, and biomass from anaerobic digestion, etc.). Effluent from leachate treatment plants, after removal of toxic chemicals, contains a sufficient quantity of nutrients, which is used as a soil stabilizer and conditioner. Although technologies for the treatment of landfill leachate are mainly focused on the removal of toxic chemicals, they remain efficient in microplastic removal too. But the high volume of leachate effluent generated daily contains a huge amount of microplastics and when applied as a soil conditioner, will reintroduce microplastics back to the terrestrial environment from where they will migrate to aquatic sources (Nunes Júnior et al. 2017, Praagh et al. 2018).

Among transport mechanisms discussed above, leaking and disposal of leachate appear to be the dominant mechanism. Leachate being a highly concentrated chemical soup often undergoes treatment facilities to reduce its toxicity and volume. Despite the complex, efficient, and sophisticated treatment processes, just like wastewater effluent from wastewater treatment facilities, a substantial amount of microplastics remains present in treated leachate which eventually gets discharged either into the terrestrial environment or aquatic sources. Common leachate treatment processes include conditioning off leachate in equalization basins and subsequent physio-chemical and biological treatment units. The pathway for microplastic released from landfills to the environment will depend upon the discharge procedures adopted for treated leachate. Furthermore, the presence of microplastics from closed landfills of China highlights the importance of considering closed landfills as a source of microplastic pollution as degradation and fragmentation of microplastics is a continuous process.

The age of landfills is also an important fact to consider while addressing microplastic pollution in landfills. Landfill

age is considered to be a determinant factor controlling the leachate composition because physio-chemical and biological properties change as the landfill tends to stabilize. The abundance and characteristics of microplastics in refuse have been reported to vary with different landfill ages. Due to increased plastic consumption in the last 3 decades, young landfills are abundant with microplastics while older landfill shows the presence of secondary microplastics resulting from environmental degradation (Kjeldsen et al. 2002, Kulikowska & Klimiuk 2008, Su et al. 2019)

Apart from the aforementioned active traditional pathways, few passive transport pathways are available for microplastics to use. Landfill mining (excavation, screening, and separation of valuable materials in landfills) is an important form of resource recovery being used in many countries. The application of landfill materials (having high organic content and low toxic substances) as soil conditioner has been studied in various literature and are now being practiced (Hogland et al. 2004, Krook et al. 2012, Quaghebur et al. 2013, Jones et al. 2013, Canopoli et al. 2018). Sufficient evidence is now available which confirms that wastewater sludge used as soil conditioner contributes to soil contamination by microplastics (Corradini et al. 2019, Edo et al. 2020). The soil application of landfill refuse may introduce microplastics to the soil, from where they can either migrate to groundwater, accumulate in soils, or be transported and redistributed by wind or carried by surface run-off to the aquatic environment (Zubris & Richards 2005, Duis & Coors 2016, Da Costa 2018).

Compared with the aquatic environment, landfills are also a complex and heterogeneous medium where many factors (heterogeneous plastic waste, environmental condition, physio-chemical and biological properties of leachate and refuse) influence the transport of microplastics. The meteorological forces directly influence the abundance, distribution, and migration of microplastics. In the post-monsoon season, due to precipitation, the volume of leachate generated and volume of surface runoff increases, similarly, high wind may plausibly carry more microplastics from landfill surface (Van Breukelen et al. 2004, Wijesekara et al. 2014). How do these factors in association with external transport mechanisms affect the transport and retention of microplastics in landfills remains unsolved which affects our understanding of the transport of microplastics from landfills to soil and the aquatic environment. Future studies (laboratory studies, field studies, column experiments, transport modeling, and in-situ imaging) are required, considering all transport mechanisms individually and simultaneously to fill the knowledge gap highlighted in the next section.

## Knowledge Gap

In this section, we are highlighting several key gaps in understanding microplastic pollution in landfills based on the published literature.

All the studies considered engineered landfills for analysis except few landfills in Thailand. Open dumping of municipal solid waste is commonly practiced in developing countries. Due to a lack of infrastructure and resources, these dumpsites generate leachate which directly flows to the drains or migrates to the groundwater. A holistic approach encompassing engineered landfills and open dumps is required to increase our understanding.

- The physicochemical properties of leachate have not been reported in many studies which makes it difficult to assess the overall risk of leachate on the ecosystem.
- Several studies have theoretically conceptualized the transfer route of microplastics from landfills to aquatic bodies, yet scientific understanding of transport mechanisms remains unclear. It is of paramount importance to understand the transport processes of microplastics originating from landfills to the environment. The microplastic transport and distribution among various zones of landfills must be modeled to estimate the level of microplastic abundance and distribution that has happened and that is going to happen. Furthermore, these models will help propose preventive measures.
- The body of knowledge available on microplastics in landfills is based on studies conducted in developed countries. Developing countries rely mostly on landfills and open dumps to deal with solid wastes. Given the fact that microplastics are capable of long-term transportation and transboundary migration, it is therefore important to address the presence of microplastic in developing countries.
- Further studies should focus on the plastic biodegradation process and underlying mechanism in the landfill, such as the isolation of microorganisms capable of degrading polymer and rate of degradation in field condition and controlled laboratory stimulated condition to make the predictive estimation of microplastics likely to generate in near future.
- Future studies need to investigate the ecotoxicological impact of microplastics originating from landfills by studying their interaction with toxic chemicals and pathogens already present in the landfill.
- Toxicological studies on the interaction of chemicals in leachate with microplastics in a laboratory simulated landfill environment are required to understand the distribution characteristics of microplastic-associated chemicals and sorptive behavior in the environment.

## CONCLUSION

Despite profound efforts to limit the use of landfills, landfills remain the most popular method to handle solid wastes. A review of the available literature indicates that microplastics are abundant in both active and closed landfills. The abundance and characteristics of microplastics varied across different regions. Fibers and fragments are the most dominant microplastic shapes and polyethylene is the most dominant polymer type in landfill leachate. Comparison of results is not possible due to varying size classification used in the study to report the abundance of microplastics. None of the studies reports a color classification of microplastics. Degradation and fragmentation of microplastics seem to generate secondary microplastics in landfills. The migration of microplastics present in landfills to groundwater is a continuous process that does not stop even after the ceasing of landfill operations. Hence, it is very essential to keep assessing and monitoring the surroundings of decommissioned landfill sites.

Finally, only through collaborative efforts of legislation, public participation, multi-disciplinary research effort, and advancement in research and monitoring, the issue of microplastic pollution can be properly addressed.

## REFERENCES


Andrady, A.L. 2011. Microplastics in the marine environment. Mar. Pollut. Bull., 62: 1596-1605.

Arthur, C., Baker, J. and Bamford, H. 2008. The occurrence, effects, and fate of microplastic marine debris. Proceedings of the International Research Workshop on Microplastic Marine Debris, September 9-11, 2008, University of Washington Tacoma, Washington, USA, pp. 9-11.

Asakura, H., Matsuto, T. and Tanaka, N. 2004. The behavior of endocrine-disrupting chemicals in leachate from MSW landfill sites in Japan. Waste Manage., 24: 613-622.

Auta, H.S., Emenike, C.U. and Fauziah, S.H. 2017. Distribution and importance of microplastics in the marine environment: A review of the sources, fate, effects, and potential solutions. Environ. Int., 102: 165-176.

Baderna, D., Maggioni, S., Boriani, E., Gemma, S., Molteni, M., Lombardo, A. and Benfenati, E. 2011. A combined approach to investigate the toxicity of an industrial landfill's leachate: Chemical analyses, risk assessment, and in vitro assays. Environ. Res., 111: 603-613.

Ballent, A., Corcoran, P.L., Madden, O., Helm, P.A. and Longstaffe, F.J. 2016. Sources and sinks of microplastics in Canadian Lake Ontario nearshore, tributary, and beach sediments. Mar. Pollut. Bull., 110(1): 383-395.

Bilgili, M.S., Demir, A. and Özkaya, B. 2007. Influence of leachate recirculation on an aerobic and anaerobic decomposition of solid wastes. J. Hazard. Mater., 143(1-2): 177-183.

Blasing, M. and Amelung, W. 2018. Plastics in soil: Analytical methods and possible sources. Sci. Total Environ., 612: 422-435.

Brandon, J., Goldstein, M. and Ohman, M.D. 2016. Long-term aging and degradation of microplastic particles: Comparing in situ oceanic and experimental weathering patterns. Mar. Pollut. Bull., 110: 299-308.

Bullard, J.E., Ockelford, A., O'Brien, P. and Neuman, C.M. 2021. Preferential transport of microplastics by the wind. Atmos. Environ., 245:118038.

Canopoli, L., Fidalgo, B., Coulon, F. and Wagland, S.T. 2018. Physico-chemical properties of excavated plastic from landfill mining and current recycling routes. Waste Manage., 76: 55-67.

Coe, J.M. and Rogers, K.L. 2012. Marine debris: Sources, Impacts, and Solutions. Springer Science & Business Media, Berlin, Germany.

Colton, J.B., Knapp, F.D. and Burns, B.R. 1974. Plastic particles in surface waters of the North-Western Atlantic. Science, 185: 491-497.

Corradini, F., Meza, P., Eguiluz, R., Casado, F., Huerta-Lwanga, E. and Geissen, V. 2019. Evidence of microplastic accumulation in agricultural soils from sewage sludge disposal. Sci. Total Environ., 671: 411-420.

Costa, J., Paço, A., Santos, P.S.M., Duarte, A.C. and Rocha-Santos, T. 2018. Microplastics in soils: Assessment, analytics and risks. Environ. Chem 16, 18-30.

Cowger, W., Gray, A.B., Eriksen, M., Moore, C. and Thiel, M. 2019. Evaluating wastewater effluent as a source of microplastics in environmental samples. In Karapanagioti, H.K. and Kalavrouziotis, I.K. (eds.), Microplastics in Water and Wastewater, IWA Publishing, London, UK, pp. 109-131.

Da Costa, J.P. 2018. Micro-and nano plastics in the environment: research and policymaking. Curr. Opin. Environ. Sci. Health, 1: 12-16.

Derraik, J.G. 2002. The pollution of the marine environment by plastic debris: A review. Mar. Pollut. Bull., 44: 842-852.

Digka, N., Tsangaris, C., Kaberi, H., Adamopoulou, A., Zeri, C. 2018. Microplastic abundance and polymer types in a Mediterranean environment. Proceedings of the International Conference on Microplastic Pollution in the Mediterranean Sea, 15-18 September, Italy, Springer, Cham, pp. 17-24.

Dris, R., Gasperi, J., Rocher, V., Saad, M., Renault, N. and Tassin, B. 2015. Microplastic contamination in an urban area: A case study in Greater Paris. Environ. Chem., 12: 592-599.

Dris, R., Gasperi, J., Saad, M., Mirande, C. and Tassin, B. 2016. Synthetic fibers in atmospheric fallout: A source of microplastics in the environment? Mar. Pollut. Bull., 104: 290-293.

Duis, K. and Coors, A. 2016. Microplastics in the aquatic and terrestrial environment: Sources (with a specific focus on personal care products), fate and effects. Environ. Sci. Europe, 28: 2.

Edo, C., González-Pleiter, M., Leganés, F., Fernández-Piñas, F. and Rosal, R. 2020. The fate of microplastics in wastewater treatment plants and their environmental dispersion with effluent and sludge. Environ. Pollut., 259: 113837.

El-Fadel, M., Findikakis, A.N. and Leckie, J.O. 1997. Modeling leachate generation and transport in solid waste landfills. Environ. Technol., 18(7): 669-686.

Eriksen, M., Mason, S., Wilson, S., Box, C., Zellers, A., Edwards, W., Farley, H. and Amato, S. 2013. Microplastic pollution in the surface waters of the Laurentian Great Lakes. Mar. Pollut. Bull., 77: 177-182.

Faure, F., Demars, C., Wieser, O., Kunz, M. and De Alencastro, L.F. 2015. Plastic pollution in Swiss surface waters: Nature and concentrations, interaction with pollutants. Environ. Chem., 12: 582-591.

Filella, M. 2015. Questions of size and numbers in environmental research on microplastics: Methodological and conceptual aspects. Environ. Chem., 12: 527-538.

Foose, G.J., Benson, C.H. and Edil, T.B. 2001. Predicting leakage through composite landfill liners. Journal of Geotechnical and Geoenvironmental Engineering 127, 510-520.

Free, C.M., Jensen, O.P., Mason, S.A., Eriksen, M., Williamson, N.J. and Boldgiv, B. 2014. High levels of microplastic pollution in a large, remote, mountain lake. Marine Pollution Bulletin 85, 156-163.

Galgani, F., Hanke, G. and Maes, T. 2015. Global Distribution, Composition, and Abundance of Marine Litter. In Bergmann,M., Gutow, L. and Klages, M. (Eds.), Marine Anthropogenic Litter . Springer, Cham, pp. 29-56.

Geyer, R., Jambeck, J. and Law, K.L. 2017. Production, use, and, the fate of all plastics ever made. Sci. Adv., 3: 1207-1221.

Grayling, K.M., Young, S.D., Roberts, C.J., Heer, M.I., Shirley, I.M. and Sturrock, C.J. 2018. The application of X-ray micro Computed Tomog-

raphy imaging for tracing particle movement in the soil. Geoderma, 321: 8-14.

Gregory, M.R. 1996. Plastic 'scrubbers' in hand cleansers: A further (and minor) source for marine pollution identified. Mar. Pollut. Bull., 32: 867-871.

Gregory, M.R. and Andrady, A.L. 2003. Plastics in the marine environment. Plastics Environ., 379: 389-390.

Han, Z., Ma, H., Shi, G., He, L., Wei, L. and Shi, Q. 2016. A review of groundwater contamination near municipal solid waste landfill sites in China. Sci. Total Environ., 569: 1255-1264.

Hartman, N.B., Hüffer, T., Thompson, R.C., Hassellöv, M., Verschoor, A., Daugaard, A.E., Rist, S., Karlsson, T., Brennholt, N., Cole, M. and Herrling, M.P. 2019. Are we speaking the same language? Recommendations for a definition and categorization framework for plastic debris. Environ. Sci. Technol. 2019, 53, 3, 1039-1047,

He, P., Chen, L., Shao, L., Zhang, H. and Lü, F. 2019. Municipal solid waste (MSW) landfill: A source of microplastics?-Evidence of microplastics in landfill leachate. Water Res., 159: 38-45.

Hernandez, E., Nowack, B. and Mitrano, D.M. 2017. Polyester textiles as a source of microplastics from households: A mechanistic study to understand microfiber release during washing. Environ. Sci. Technol., 51: 7036 7046.

Hidalgo-Ruz, V., Gutow, L., Thompson, R.C. and Thiel, M. 2012. Microplastics in the marine environment: A review of the methods used for identification and quantification. Environmental Science & Technology 46, 3060-3075.

Hogland, W., Marques, M. and Nimmermark, S. 2004. Landfill mining and waste characterization: A strategy for remediation of contaminated areas. J. Mater. Cycles Waste Manag., 6: 119-124.

Hu, L., Chernick, M., Hinton, D.E. and Shi, H. 2018. Microplastics in small water bodies and tadpoles from Yangtze river delta, China. Environ. Sci. Technol 52, 8885 8893.

Huerta Lwanga, E., Gertsen, H., Gooren, H., Peters, P., Salanki, T. and Ploeg, M. 2017a. Incorporation of microplastics from litter into burrows of Lumbricus terrestris. Environ. Pollut., 220: 523-531.

Huerta Lwanga, E., Mendoza Vega, J., Ku Quej, V., Angeles Chi, J., Cid, L. and Chi, C. 2017b. Field evidence for transfer of plastic debris along a terrestrial food chain. Sci. Rep., 7: 1-7.

Ishigaki, T., Sugano, W., Nakanishi, A., Tateda, M., Ike, M. and Fujita, M. 2004. The degradability of biodegradable plastics in aerobic and anaerobic waste landfill model reactors. Chemosphere, 54: 225-233.

Islam, J. and Singhal, N. 2004. A laboratory study of landfill-leachate transport in soils. Water Res., 38(8): 2035-2042.

Isobe, A., Kubo, K., Tamura, Y., Kako, S., Nakashima, E. and Fujii, N. 2014. Selective transport of microplastics and mesoplastics by drifting in coastal waters. Mar. Pollut. Bull., 89, 324-330.

Jones, P.T., Geysen, D., Tielemans, Y., Van Passel, S., Pontikes, Y., Blanpain, B., Quaghebeur, M. and Hoekstra, N. 2013. Enhanced Landfill Mining in view of multiple resource recovery: A critical review. J. Cleaner Prod., 55: 45-55.

Jonsson, S., Ejlertsson, J., Ledin, A., Mersiowsky, I. and Svensson, B.H. 2003. Mono-and diesters from o-phthalic acid in leachates from different European landfills. Water Res., 37: 609-617.

Kalanatarifard, A. and Yang, G.S. 2012. Identification of the municipal solid waste characteristics and potential of plastic recovery at Bakri Landfill, Muar, Malaysia. J. Sustain. Dev., 5: 11.

Kazour, M., Terki, S., Rabhi, K., Jemaa, S., Khalaf, G. and Amara, R. 2019. Sources of microplastics pollution in the marine environment: Importance of wastewater treatment plant and coastal landfill. Mar. Pollut. Bull., 146: 608-618.

Kershaw, P.J. and Rochman, C.M. 2015. Sources, fate, and effects of microplastics in the marine environment: Part 2 of a global assessment, in: Reports and Studies-IMO/FAO/Unesco-IOC/WMO/IAEA/UN/UNEP Joint Group of Experts on the Scientific Aspects of Marine Environmental Protection (GESAMP.

Kjeldsen, P., Barlaz, M.A., Rooker, A.P., Baun, A., Ledin, A. and Christensen, T.H., 2002. Present and long-term composition of MSW landfill leachate: A review. Crit. Rev. Environ. Sci. Technol 32, 297-336.

Koelmans, A.A., Bakir, A., Burton, G.A. and Janssen, C.R. 2016. Microplastic as a vector for chemicals in the aquatic environment: Critical review and model-supported reinterpretation of empirical studies. Environ. Sci. Technol., 50: 3315 3326.

Kole, P.J., Löhr, A.J., Van Belleghem, F.G. and Ragas, A.M. 2017. Wear and tear of tires: A stealthy source of microplastics in the environment. Int. J. Environ. Res. Public Health, 14(10): 1265.

Krook, J., Svensson, N. and Eklund, M. 2012. Landfill mining: A critical review of two decades of research. Waste Manage., 32: 513-520.

Kulikowska, D. and Klimiuk, E. 2008. The effect of landfill age on municipal leachate composition. Bioresour. Technol., 99: 5981-5985.

Li, J., Zhang, H., Zhang, K., Yang, R., Li, R.and Li, Y. 2018. Characterization, source, and retention of microplastic in sandy beaches and mangrove wetlands of the Qinzhou Bay, China. Mar. Pollut. Bull., 136: 401-406.

Liu, M., Lu, S., Song, Y., Lei, L., Hu, J., Lv, W., Zhou, W., Cao, C., Shi, H., Yang, X. and He, D. 2018. Microplastic and mesoplastic pollution in farmland soils in suburbs of Shanghai, China. Environ. Pollut., 242: 855-862.

Maaß, S., Daphi, D., Lehmann, A. and Rillig, M.C. 2017. Transport of microplastics by two collembolan species. Environ. Pollut., 225: 456-459.

Machado, A.A.D.S., Kloas, W. and Zarf, C.S.H. 2018. Microplastics as an emerging threat to terrestrial ecosystems. Glob. Chang. Biol., 24: 1405-1416.

Moore, C.J., Moore, S.L., Weisberg, S.B., Lattin, G.L. and Zellers, A.F. 2002. A comparison of neustonic plastic and zooplankton abundance in southern California's coastal waters. Mar. Pollut. Bull., 44: 1035-1038.

Mor, S., Ravindra, K., Dahiya, R.P. and Chandra, A. 2006. Leachate characterization and assessment of groundwater pollution near a municipal solid waste landfill site. Environ. Monit. Assess., 118(1): 435-456.

Mukherjee, S., Mukhopadhyay, S., Hashim, M.A. and Sen Gupta, B. 2015. Contemporary environmental issues of landfill leachate: Assessment and remedies. Crit. Rev. Environ. Sci. Technol., 45: 472-590.

Napper, I.E., Bakir, A., Rowland, S.J. and Thompson, R.C. 2015. Characterization, quantity and sorptive properties of microplastics extracted from cosmetics. Mar. Pollut. Bull., 99: 178-185.

Ngo, P.L., Pramanik, B.K. and Shah, K. 2019. Pathway, classification, and removal efficiency of microplastics in wastewater treatment plants. Environ. Pollut., 255: 411-431.

Nizzetto, L., Bussi, G., Futter, M.N., Butterfield, D. and Whitehead, P.G. 2016. A theoretical assessment of microplastic transport in river catchments and their retention by soils and river sediments. Environ. Sci.: Process. Imp., 18(8):1050-1059.

Nunes Júnior, F.H., Gondim, F.A., Pereira, M.D.S., Braga, B.B., Pontes Filho, R.A. and Barbosa, F.E. 2016. Sanitary landfill leachate as a source of nutrients on the initial growth of sunflower plants. Rev. Bras. de Eng. Agricola e Ambient., 20: 746-750.

Paco, A., Duarte, K., Costa, J.P., Santos, P.S., Pereira, R., Pereira, M.E., Freitas, A.C., Duarte, A.C. and Rocha-Santos, T.A. 2017. Biodegradation of polyethylene microplastics by the marine fungus Zalerion maritimum. Sci. Total Environ., 586: 10-15.

Praagh, M.V., Hartman, C. and Brandmyr, E. 2018. Microplastics in Landfill Leachates in the Nordic Countries. Nordic Council of Ministers, Copenhagen, Denmark, pp. 1-53.

Puthcharoen, A. and Suchat, L. 2019. Determination of microplastics in soil and leachate from the Landfills. Thai Environ. Eng. J., 33: 39-46.

Quaghebeur, M., Laenen, B., Geysen, D., Nielsen, P., Pontikes, Y., Van Gerven, T. and Spooren, J. 2013. Characterization of landfilled materials: Screening of the enhanced landfill mining potential. J. Cleaner Prod., 55: 72-83.

Rezaei, M., Riksen, M.J., Sirjani, E., Sameni, A. and Geissen, V. 2019. Wind erosion as a driver for transport of light density microplastics. Sci. Total Environ., 669: 273-281.

Rillig, M.C., Ziersch, L. and Hempel, S. 2017. Microplastic transport in soil by earthworms. Sci. Rep., 7: 1362.

Salem, Z., Hamouri, K., Djemaa, R. and Allia, K., 2008. Evaluation of landfill leachate pollution and treatment. Desalination, 220(1-3):108-114.

Siegfried, M., Koelmans, A.A., Besseling, E. and Kroeze, C. 2017. Export of microplastics from land to sea. A modelling approach. Water Res., 127: 249-257.

Slootmaekers, B., Carteny, C.C., Belpaire, C., Saverwyns, S., Fremout, W., Blust, R. and Bervoets, L. 2019. Microplastic contamination in gudgeons (Gobio gobio) from Flemish rivers (Belgium). Environ. Pollut., 244: 675-684.

Su, L., Xue, Y., Li, L., Yang, D., Kolandhasamy, P., Li, D. and Shi, H. 2016. Microplastics in Taihu lake. China. Environ. Pollut., 216: 711-719.

Su, Y., Zhang, Z., Wu, D., Zhan, L., Shi, H. and Xie, B. 2019. Occurrence of microplastics in landfill systems and their fate with landfill age. Water Research 164, 114968.

Talvitie, J., Mikola, A., Koistinen, A. and Setälä, O. 2017. Solutions to microplastic pollution–Removal of microplastics from wastewater effluent with advanced wastewater treatment technologies. Water Res., 123: 401-407.

Themelis, N.J. and Ulloa, P.A. 2007. Methane generation in landfills. Renew. Energy 32: 1243-1257.

Themelis, N.J. and Ulloa, P.A. 2007. Methane generation in landfills. Renew. Energy., 32(7): 1243-1257.

Thompson, R.C., Olsen, Y., Mitchell, R.P., Davis, A., Rowland, S.J., John, A.W. and Russell, A.E. 2004. Lost at sea: Where is all the plastic? Science, 304: 838.

Upadhayay, K., Bajpai, S. 2021. Microplastics: Pollution of emerging concern- what do we know so far? - A review. Pollution Research, 140-2.

Van Breukelen, B.M., Griffioen, J., Röling, W.F. and Van Verseveld, H.W. 2004. Reactive transport modeling of biogeochemical processes and carbon isotope geochemistry inside a landfill leachate plume. J. Contam. Hydrol., 70(3-4): 249-269.

Van Sebille, E., Wilcox, C., Lebreton, L., Maximenko, N., Hardesty, B.D., Van Franeker, J.A. and Law, K.L. 2015. A global inventory of small floating plastic debris. Environmental Research Letters 10: 124006.

Van Wezel, A., Caris, I. and Kools, S.A. 2016. Release of primary microplastics from consumer products to wastewater in The Netherlands. Environ, Toxicol. Chem., 35(7): 1627-1631.

Verschoor, A.J. 2015. Towards a definition of microplastics: Considerations for the specification of physico-chemical properties. RIVM Letter Report 2015-0116, National Institute for Public Health and the Environment, Bilthoven, The Netherlands

Vianello, A., Boldrin, A., Guerriero, P., Moschino, V., Rella, R., Sturaro, A. and Da Ros, L. 2013. Microplastic particles in sediments of Lagoon of Venice, Italy: First observations on occurrence, spatial patterns and identification. Estuar. Coast Shelf Sci., 130: 54 61.

Vianello, A., Jensen, R.L., Liu, L. and Vollertsen, J. 2019. Simulating human exposure to indoor airborne microplastics using a Breathing Thermal Manikin. Sci. Rep., 9: 1-11.

Vogelsang, C., Lusher, A., Dadkhah, M.E., Sundvor, I., Umar, M., Ranneklev, S.B., Eidsvoll, D. and Meland, S. 2019. Microplastics in road dust–characteristics, pathways, and measures. NIVA-Report, Oslo, Norway

Webb, H.K., Arnott, J., Crawford, R.J. and Ivanova, E.P. 2013. Plastic degradation and its environmental implications with special reference to poly (ethylene terephthalate). Polymers, 5: 1-18.

Weinstein, J.E., Crocker, B.K. and Gray, A.D. 2016. From macroplastic to microplastic: Degradation of high-density polyethylene, polypropylene, and polystyrene in a salt marsh habitat. Environ. Toxicol. Chem., 35: 1632-1640.

Wijesekara, S.S.R.M.D.H.R., Mayakaduwa, S.S., Siriwardana, A.R., de Silva, N., Basnayake, B.F.A., Kawamoto, K. and Vithanage, M. 2014. Fate and transport of pollutants through a municipal solid waste landfill leachate in Sri Lanka. Environ. Earth Sci., 72(5): 1707-1719.

Wowkonowicz, P. and Baranski, A. 2013. Release of di (2-ethylhexyl) and dibutyl phthalates from municipal landfills in Poland. Przem. Chem., 92: 2345-2350.

Yang, N., Damgaard, A., Scheutz, C., Shao, L.M. and He, P.J. 2018. A comparison of chemical MSW compositional data between China and Denmark. J. Environ. Sci., 74, 1 10.

Yong, R.N., Mohamed, A.M.O. and Warkentin, B.P. 1992. Principles of contaminant transport in soils. Stud. Environ. Sci., 70: 57-74.

Zhou, C., Fang, W., Xu, W., Cao, A. and Wang, R. 2014. Characteristics and the recovery potential of plastic wastes obtained from landfill mining. J. Cleaner Prod., 80: 80-86.

Zhu, D., Bi, Q.F., Xiang, Q., Chen, Q.L., Christie, P. and Ke, X. 2018a. Trophic predator-prey relationships promote the transport of microplastics compared with the single Hypoaspis aculeifer and Folsomia candida. Environ. Pollut., 235: 150-154.

Zhu, D., Chen, Q.L., An, X.L., Yang, X.R., Christie, P. and Ke, X. 2018b. Exposure of soil collembolans to microplastics perturbs their gut microbiota and alters their isotopic composition. Soil Biol. Biochem., 116: 302-310.

Zubris, K.A.V. and Richards, B.K. 2005. Synthetic fibers as an indicator of land application of sludge. Environ. Pollut., 138: 201-211.

Nature Environment and Pollution Technology
An International Quarterly Scientific Journal

p-ISSN: 0972-6268
(Print copies up to 2016)
e-ISSN: 2395-3454

Vol. 20 | No. 5 (Suppl) | pp. 1947-1958 | 2021

Original Research Paper

https://doi.org/10.46488/NEPT.2021.v20i05.010

Open Access Journal

# A Comparative Life Cycle Assessment (LCA) of Gasoline Blending with Different Oxygenates in India

**Sushil M. Chaudhari* and Rohit B. Meshram**†**
*Institute of Chemical Technology, Matunga, Mumbai-400019, India
**CSIR National Metallurgical Laboratory, Jamshedpur-831007, India
†Corresponding author: Rohit B. Meshram; rohitmeshramiit@gmail.com

**Nat. Env. & Poll. Tech.**
**Website: www.neptjournal.com**

*Received:* 16-02-2021
*Revised:* 20-04-2021
*Accepted:* 25-05-2021

**Key Words:**
Gasoline
Methanol
Ethanol
n-butanol
Life cycle assessment

## ABSTRACT

This paper includes a cradle-to-gate life cycle impact evaluation of gasoline blends in India. The potential environmental impacts of gasoline blends with three major components, i.e., methanol, ethanol, and n-butanol are assessed. The production of methanol from the natural gas reforming process, ethanol from hydrogenation with nitric acid, and n-butanol from the oxo process are considered in the current study. The results show that the gasoline blending with methanol has the lowest impact (11 categories) and is nearly constant from 5 to 15%. For gasoline with ethanol as an additive, the global warming potential, ozone depletion potential, and abiotic depletion potential rise with increasing ethanol addition. Meanwhile, increasing ethanol addition reduces the acidification potential and terrestric ecotoxicity potential impact of gasoline blends. Similarly, gasoline with n-butanol as an additive has higher acidification potential, eutrophication potential, human toxicity potential, terrestric ecotoxicity potential, marine aquatic ecotoxicity potential, and photochemical ozone creation potential compared to methanol and ethanol.

## INTRODUCTION

India's energy security has become a critical issue with major concerns about oil and other fossil fuel depletion, environmental issues (in particular climate change), reliance on foreign sources, etc. Pollution is a major contributor to climate change. Many national and international policymakers are making reforms continuously to curtail pollution. Alcohol usage as an oxygenate fuel has the potential to reduce current emissions pollution occurring due to the properties of gasoline and its content (Yusri et al. 2017, Surisetty et al. 2011). Mainly, methanol ($CH_3OH$), ethanol ($C_2H_5OH$), n-butanol ($C_4H_9OH$), and dimethyl ether ($C_2H_6O$) were commonly used as potential fuels (Yusri et al. 2017).

However, alcohol is a clean-burning fuel that has been blended into gasoline since 1980 (Chen et al. 2018). Because of its higher octane rating and high intramolecular oxygen concentration, it can be used as a fuel in machines that have a greater compression ratio and higher thermal efficiency. However, due to the hydrophilic property of alcohol, it leads to phase separation, which is a major difficulty in alcohol blended fuels, causing operational problems and engine damage. Different blending agents have been reported by researchers to avoid methanol-gasoline phase separation (Karaosmanoglu et al. 2000). It has proven scientific records for methanol to blends of M5 to M100 (Sheehy et al. 2010, Yuen et al. 2010) and ethanol to blends of E5, E10, and E85 (Shirvani et al. 2020) where M and E represent the percentage of methanol and ethanol in the blend and remaining is gasoline.

Multiple researchers have reported that the blending of alcohol with gasoline can minimize air pollution. Alcohol emits lesser pollutants such as nitrogen oxides (NOx), SOx, and particulate matter compared to gasoline (Canakci et al. 2013, Yanju et al. 2008).

The environmental impact of any fuel was observed in two conditions, one is during production and the second during vehicular emission or combustion. In India, similar to China, the majority of coal to methanol process is feasible due to the abundance of coal (Saraswat & Bansal 2017). Hence, the scientific community and government authorities considered oxidative additives as oxygen for the energy sector, with the goal of reducing foreign dependency in the future. Out of multiple oxygenates, methanol and ethanol prove low-cost sustainable options for gasoline blending (Shirvani et al. 2020, Saraswat & Bansal 2017).

There are mainly two sources reported for the production of methanol, i.e., natural gas, and coal. Natural gas (NG) to methanol emits much carbon dioxide per unit of energy used as gasoline. Whereas, methanol produced from coal produces double carbon dioxide, even if emission remains

the same. Butanol has better fuel properties as compared to ethanol such as higher heating value, lower vapor pressure, lower heat of vaporization, etc. That is why butanol can be used 100% as fuel in a spark-ignition (SI) engine. The only major issue is that biological and chemical pathways to butanol synthesis are both expensive (Ndaba et al. 2015, Popuri & Bata 1993). Henceforth, it is necessary to understand how to oxygenate blended gasoline and its production route may impact the transportation network, storage, and environmental impacts, among other things (Chen et al. 2018, Karaosmanoglu et al. 2000).

In India, according to Economics Times, the Government transport ministry is looking to push legislation to increase the ethanol and methanol blending in gasoline to reduce the import of fossil-based gasoline. As per Indian Government policy, the Indian Oil Corporation produces a 10% ethanol and 15% methanol (depends on availability) blend. Methanol production costs are less than half of what ethanol costs to produce, which is meant to be blended at 10%, but producers are struggling to supply sufficient ethanol to meet the mandate.

Life cycle assessment (LCA) of gasoline and diesel blending options is a well-defined track for crude oil (Mata et al. 2003). Many researchers studied the life cycle assessment of methanol, ethanol, and butanol blended with gasoline and compared environmental impacts and leak emissions only during transportation. However, depending on the type of engine, the research octane number and Reid vapor pressure after blending with gasoline have limitations. Most of the emissions comparison has been shown with different methanol blends. The research on gasoline blending, different additives, and its development technology has high growth in India. However, very few authors have studied the gasoline blending production impacts. It has been noticed that no literature is accessible on the comprehensive LCA of gasoline blending in India. The objective of the present investigation is to examine cradle-to-gate ecological implications of gasoline blending with different oxygenates, namely, (a) methanol, (b) ethanol, and (c) n-butanol in India during the year 2020-2021.

## MATERIALS AND METHODS

### Alcohol Production

### Methanol production

Despite the growing demand for methanol as a transportation fuel component and an alternative fuel in India, conventional processes are still dominant. The most common route for the production of methanol is via syngas, although there are numerous available sources of feedstock for syngas production. The traditional route for methanol production could be summarized as:

Carbon Source + oxygen (or air) → Syngas (CO + hydrogen) → methanol

Syngas production can be prepared using several methods such as steam reforming of natural gas or naphtha (Heo et al. 2020), partial oxidation of natural gas and other hydrocarbons (Ma et al. 2019), auto thermal reforming (Hu et al. 2020), gasification technologies (Ramalingam et al. 2020), etc. India's present focus is on producing methanol via syngas from low-grade coal and solid waste (fossil or biomass) that would otherwise be burned or incinerated, as well as by-products of other sectors such as steel factories, cement plants, and refineries.

$$CH_4 + H_2O \leftrightarrow CO + 3H_2 \quad ...(1)$$

$$CO + 2H_2 \rightarrow CH_3OH \quad ...(2)$$

The chemical reactions carried out in the production of methanol are mentioned in Eq. 1 and Eq. 2. Whereas, Eq. (1) and Eq. (2) the overall reaction is endothermal at reactor pressure 5- 30 MPa, and temperature around 300-350°C. The detailed process unit operations used for the production of methanol from NG are shown in Fig. 1. The highest efficiency reported in the manufacturing of methanol from NG is 66% (Kajaste et al. 2018). The coal to methanol production route contributes to higher $CO_2$ emissions with low energy efficiency (Xiang et al. 2015).

### Ethanol production (96 % concentrated)

Before 1947, ethanol was produced by indirect hydration of ethene. However, after industrialization, production was routed via direct hydration of ethene as shown in equation 3 (Weissermel & Arpe 2008, Liu et al. 2019). Ethanol (96%) production from the hydrogenation of the nitric acid process is shown in Fig. 2.

$$H_2C = CH_2 + H_2O \leftrightarrow C_2H_5OH \quad ...(3)$$

The reaction occurs in a gas phase reactor with acid catalysis. The catalyst is nitric acid. The conversion rate is quite low (only 5.6%), so unreacted ethylene and ether from side reactions are recycled. The raw product is purified by distillation and the addition of sodium hydroxide to remove aldehydes (Falano et al. 2014, Li et al. 2018).

Currently, India produces ethanol from B-heavy molasses and damaged food grains to fulfill the demand for blending. Ethanol production through molasses is a fermentation biological process, in which molasses are converted into cellular energy, ethanol, and carbon dioxide (Soam et al. 2015).

Production data for molasses to ethanol mainly for en-

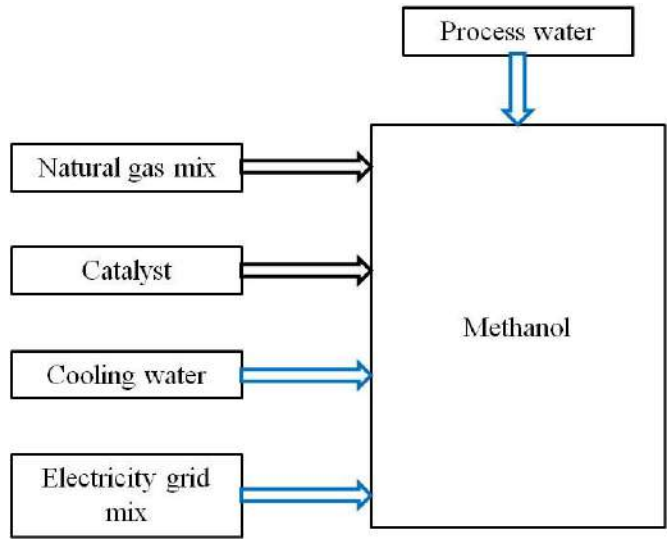


Fig. 1: Methanol production from natural gas.

zyme and yeast were found fluctuating in literature, so we have considered only hydration process production data for further analysis.

**n-Butanol Production**

Production of n-butanol can be done by two processes, i.e., petrochemical and biobased. The organic manufacture of butanol was one of the greatest commercial fermentation techniques in the early twentieth century, but it lost popularity in 1960 when researchers developed more cost-effective substrates and more efficient petrochemical processes, such as the oxo-synthesis (Patil et al. 2019). Hydroformylation of propene is also known as an Oxo-synthesis process. Oxo-synthesis process is propene and syngas ($CO + H_2$) in the presence of a catalyst with several reaction conditions (pressure, temperature) used as a feed stream for the production of n-butanol. The detailed reaction is shown in equation 4. Uyttebroek et al. (2015) demonstrated a hydroformylation process using Rh base catalyst at low pressure, producing 95% of n-butanol and 5% 2-methyl-1-propanol (Uyttebroek et al. 2015). A detailed overview of n-butanol production from the Oxo process is shown in Fig. 3.

Production is modeled using the Oxo synthesis process or propylene hydroformylation. This low-pressure liquid-phase

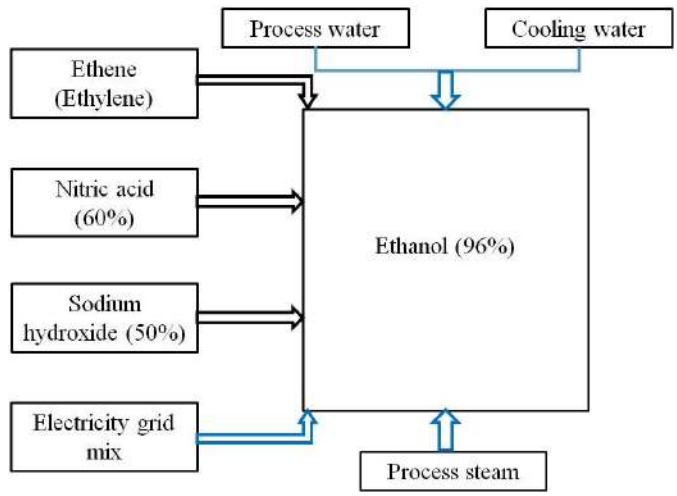


Fig. 2: Ethanol (96%) production from the hydrogenation of nitric acid.

process combines liquid-phase propylene and synthesis gas (a 1:1 mixture of hydrogen and carbon monoxide) in the presence of modified Rhodium catalysts to produce aldehydes, which are further hydrogenated to produce butanol isomers. This process is typically optimized for the production of n-butanol, with yields of up to 98% n-butanol.

$$R-CH=CH_2+CO+H_2 \rightarrow R-CH_2-CH_2CHO \quad ...(4)$$

The properties of gasoline and alcohol considered in the present study are mentioned in Table 1.

## Life Cycle Assessment (LCA)

LCA is a tool for systematic analysis of ecological features of products, and unit processes. Its importance has been grown in recent years as it helps to make environmental-based decisions. Detailed LCA framework for gasoline blending production study is shown in Fig. 4.

As per ISO a 14040 norm, LCA is performed in four phases:

1. Goal and scope
2. Inventory analysis
3. Impact assessment
4. Interpretation

## Goal and scope

The goal and scope generally depend on the application, the geographical locations, and the time frame. The goal of the current study is to provide an outline of the cradle-to-gate LCA of different gasoline blending in an Indian context. The LCA included all raw materials and utilities. It excludes the construction, distribution, fugitive emissions, and use phases. In the present study, 1.0 t production of gasoline with different ratios (5-100 wt.%) of methanol, ethanol, and n-butanol as an additive is considered as a functional unit.

## Inventory Analysis

The inventory describes the product system and its sub-processes by gathering data and calculating allocation. For inventory analysis of the gasoline blend, the mass balance is estimated on a according to per ton basis.. The primary data on the production of the additives is collected from the GaBi Indian database. For methanol and ethanol, data was directly collected from GaBi. The inventory was created for n-butanol as this was not available in the database.

## Impact Assessment

In impact assessment, the information collected is analyzed for the probable environmental emissions. These impacts are expressed in equivalent units. In this paper, the CML 2001 method is used for emissions category representation.

## Interpretation

In the interpretation phase, the results are analyzed including

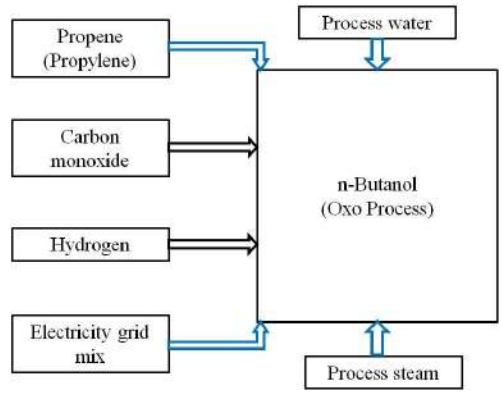


Fig. 3: n-butanol production from oxo process.

Table 1: Properties of gasoline and alcohol. →

| Properties | Gross calorific value (MJ/kg) | Net calorific value (MJ/kg) | Density (kg/L) |
|---|---|---|---|
| Gasoline | 47.1 | 43.9 | 0.732 |
| Methanol | 22.7 | 19.9 | 0.794 |
| Ethanol | 29.7 | 26.8 | 0.809 |
| n-butanol | 36 | 33.1 | 0.813 |

the relative contribution of individual process steps to the total with the above three phases. The conclusions are drawn depending on the findings of overall and component-based environmental impact.

## RESULTS AND DISCUSSION

In order to convey the information included in the inventory and its significance to the environment, an impact assessment is carried out. The process flow scheme for the gasoline blend with different oxygenates is developed in GaBi. GaBi Professional software version 8.7 with the Indian Extension Database is used to analyze the environmental impacts.

### Global Warming Potential (GWP)

Global warming is the increase in the warming of the troposphere due to the increase in anthropogenic greenhouse gases (GHG) in the atmosphere. The potential greenhouse effects of these gases are converted in reference to carbon dioxide ($CO_2$).

GWP of gasoline blending production with methanol (M), ethanol (E), and n-butanol (B) is shown in Fig. 5. From Fig. 5, it is clearly indicated that with increasing % of blending from 5% to 100%, GWP of methanol blended gasoline remains nearly constant. Whereas, GWP of ethanol and n-butanol blended gasoline gradually increases with increasing % blending. Gasoline blending with ethanol showed the highest GWP followed by n-butanol and methanol. The reason could be that during ethanol production there are major two contributors to GWP, i.e., process steam from natural gas and ethene production. Whereas, in the case of n-butanol gasoline blend, n-butanol itself, propene (Pereira et al. 2015) and hydrogen production are major contributors to GWP as compared to gasoline. In the case of methanol gasoline blending, the primary pollution is because of natural gas production only (Lemonidou et al. 2003).

Most of the researchers reported GWP for methanol blended gasoline: 0.462 kg $CO_2$ eq.$kg^{-1}$ $CH_3OH$ and which is lower than the present study i.e. 0.832 kg $CO_2$ eq.$kg^{-1}$ $CH_3OH$ (Yadav et al. 2020). Whereas, for ethanol-blended gasoline, GWP was found to be 2.22 kg $CO_2$ eq.$kg^{-1}$ g $C_2H_5OH$, which is quite higher as compared to cradle-to-gate in Western Europe i.e. 1.3 kg $CO_2$ eq.$kg^{-1}$ (Muñoz et al. 2014). The higher values of GWP found in the present study for ethanol-blended gasoline may be due to the electricity generation from coal, transportation, and also the reporting method used (ReciPe). Individually, gasoline production has the lowest GWP (13.52 g $CO_2$ eq.$MJ^{-1}$) among methanol, ethanol, and n-butanol which is in the range of most results (10 and 15 g $CO_2$ eq.$MJ^{-1}$ fuel) (Eriksson & Ahlgren 2013). Alcohol production from biomass particularly minimizes GHGs creation and result in global warming (Dalena et al. 2018).

### Acidification Potential (AP)

Acidification potential is an increase in the acidity of the earth, a waterbody, or atmosphere due to human activities.

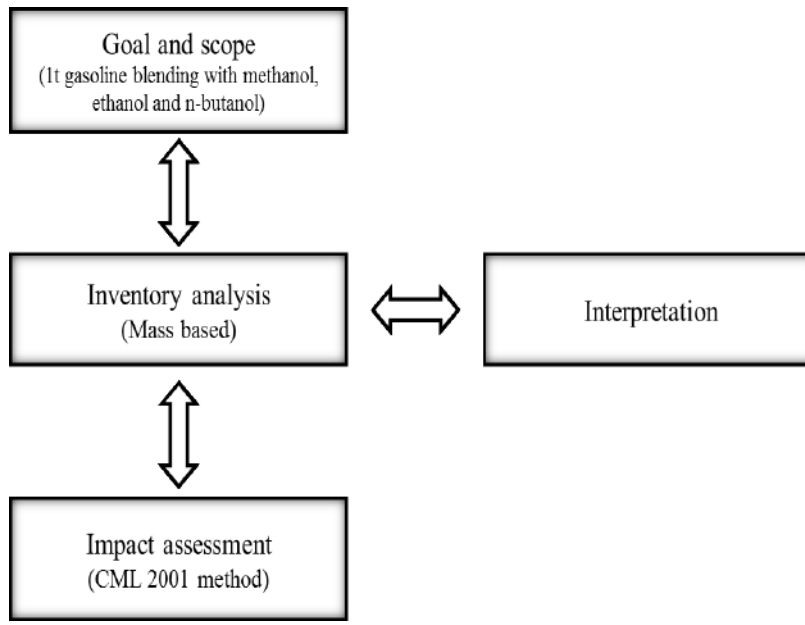


Fig. 4: LCA framework for gasoline blending production study.

The increase in the acidity of the air leads to an increase in the pH value.

The detailed AP from the production of gasoline blending with methanol, ethanol, and n-butanol is shown in Fig. 6. AP of methanol and ethanol-blended gasoline increases with increasing blending % from 5% to 15% whereas, decreases from 50% and onwards. The reason could be, independently gasoline production has the second most AP (6.3E-03 kg $SO_2$ eq.$kg^{-1}$). In the case of n-butanol blended gasoline, the authors found an almost constant AP irrespective of % blending. The higher values of AP in the case of n-butanol (7.88E-03 kg $SO_2$ eq.$kg^{-1}$) are on account of electricity and process steam generation. However, it was reported that n-butanol production from the petrochemical route had lower AP than bio-butanol due to the use of fertilizer during the agricultural stage (Pereira et al. 2015).

**Eutrophication Potential (EP)**

The EP is the excessive addition of nutrients such as nitrogen and phosphorus liberated into water and land. Phosphorus and nitrogen from agriculture, combustion processes, and industry effluents mainly cause eutrophication. Emissions of pollutants are converted into kg $PO_4$- eq. EP of methanol, ethanol, and n-butanol blended gasoline comparative results are shown in Fig. 7. As the percentage of methanol blending increases from 5% to 15%, EP showed higher values whereas, with an increase in methanol blending from 50% to 100%, EP decreases. However, for ethanol blending with gasoline, it is nearly constant. Discrete production comparison shows gasoline has the second most EP (0.418E-3 kg Phosphate eq.$kg^{-1}$). EP of gasoline blended with n-butanol contributes 28 times higher followed by gasoline. The EP of alcohol blended gasoline from discrete production potential is lowest compared with methanol (0.16E-3 kg $PO_4$- eq.$kg^{-1}$) ethanol, and n-butanol. The highest EP (0.53 kg $PO_4$- eq.$kg^{-1}$) in the case of n-butanol may be contributed because of the electricity, process, steam generation, propene, and carbon monoxide. Pereira et al. (2015) reported that petrochemical n-butanol has lower EP compared to biobutanol. However, in the case of ethanol blending, it is due to process steam production only. Falano et al. (2014) also calculated EP for ethanol ($PO_4$- eq.) as 1.17 gm.$L^{-1}$ which is nearly equal to 0.91 gm.$L^{-1}$ calculated in the present study.

**Ozone Depletion Potential (ODP)**

This impact highlights the deterioration of the ozone layer of the stratosphere which protects living beings from ultraviolet rays. Halocarbons like chloro-fluoro-carbons or synthetic halogenated compounds prevent stratospheric ozone creation and thus limit the regeneration of the ozone layer.

ODP with respect to methanol, ethanol, and n-butanol blended gasoline is shown in Fig. 8. It was observed that with an increase in alcohol blending % in gasoline, the ODP also increases in the case of ethanol and n-butanol except for methanol. Methanol blended gasoline production does not show much effect even though it increases from 5% to 100%. ODP is maximum for the gasoline blending with ethanol followed by n-butanol mostly in case of higher blending from 50%, 85%, and 100%. Principally, ethene ($CH_2$= $CH_2$), water ($H_2O$) and sodium hydroxide (NaOH) production are the

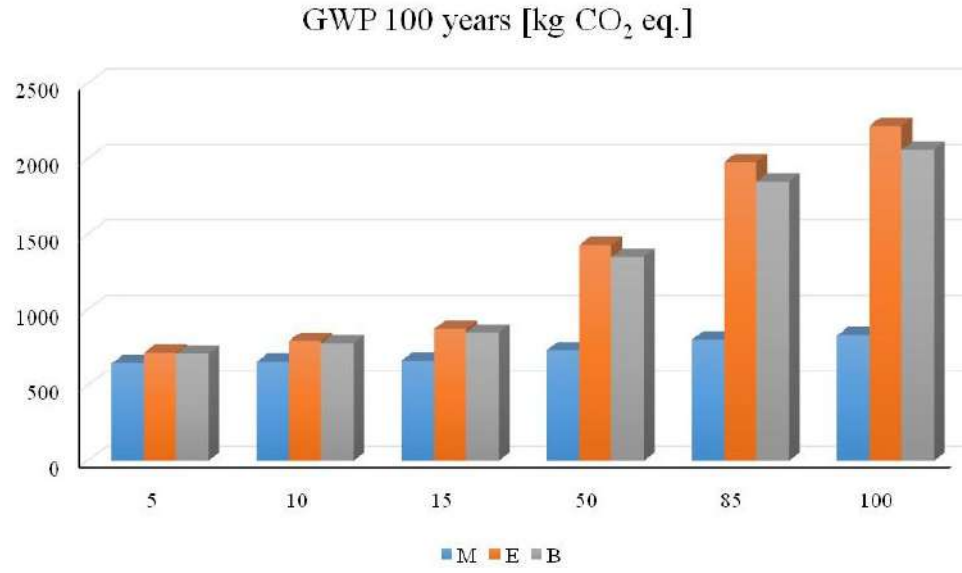


Fig. 5: GWP of gasoline blending production with methanol (M), ethanol (E) and n-butanol (B).

primary contributors that damage ozone. ODP for gasoline blending with n-butanol is mainly contributed by propene and electricity generation of n-butanol. Similar results were disclosed by Pereira et al. (2015), in the case of petrochemical route n-butanol production. The authors mentioned that the use of propylene and heat from natural resources during the production stage were major contributors. Independent production observed the lowest ODP for gasoline (8.19E-15 kg R11 eq.kg$^{-1}$).

**Abiotic Depletion Potential (ADP) for Elements and Fossil**

The impact category was subdivided into two categories, using two sets of ADPs: the ADP for elements and the ADP for fossil fuels. Fig. 9 (a) and (b) shows ADP (element) and ADP (fossils), respectively, for gasoline blending with methanol, ethanol, and n-butanol. ADP element for gasoline blending with n-butanol is mainly due to propene production. It is also seen that gasoline production has the lowest

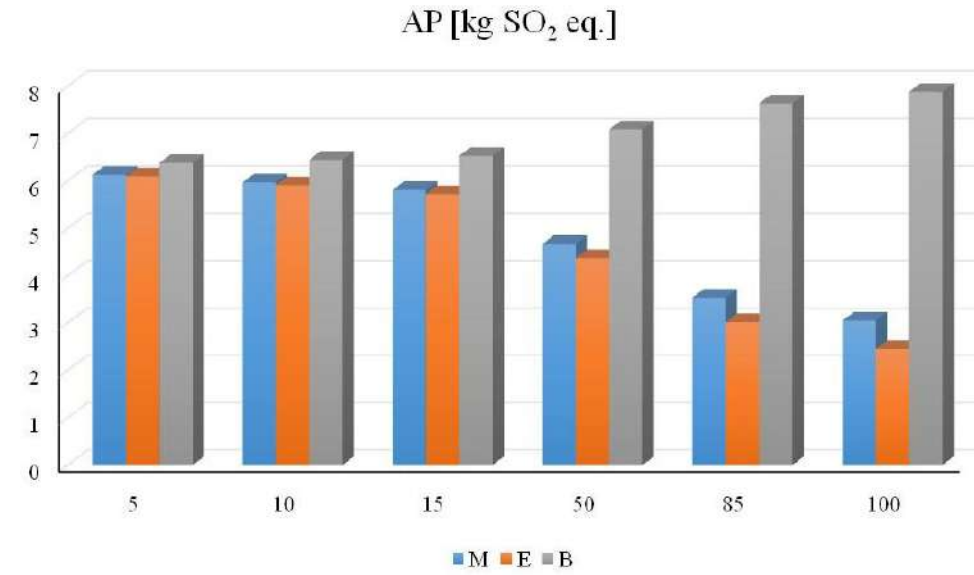


Fig. 6: AP of gasoline blending production with methanol (M), ethanol (E), and n-butanol (B).

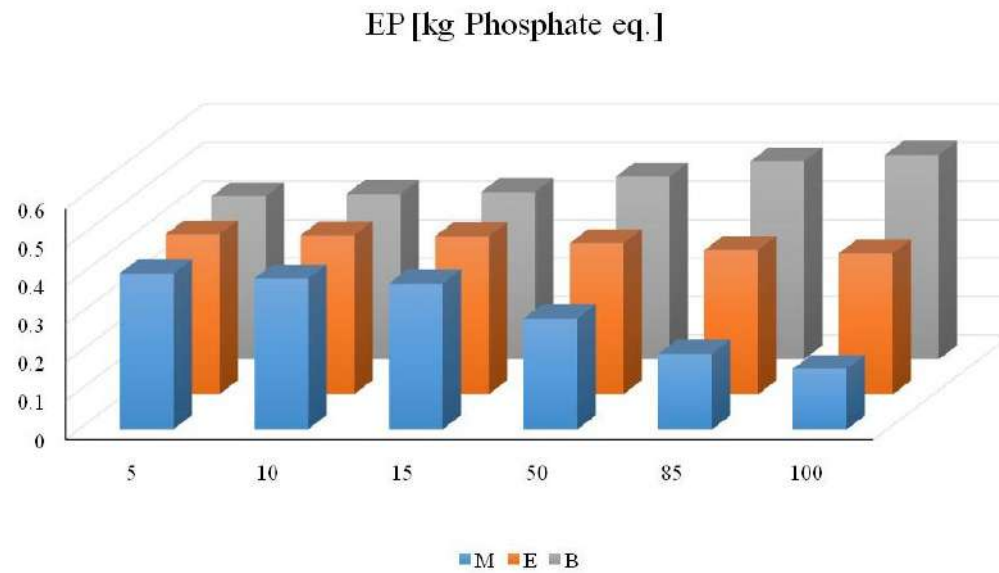


Fig. 7: EP of gasoline blending production with methanol (M), ethanol (E) and n-butanol (B).

ADP elements. ADP (element) is the highest for gasoline blending with ethanol followed by methanol. As % blending of alcohol increases, ADP also increases. Initial 5% to 15% alcohol blended gasoline showed the lowest ADP and increased afterward with increasing alcohol blending %. This is mainly on account of ethane and sodium hydroxide production (Li et al. 2018).

ADP fossil impact for alcohol gasoline blending is nearly constant up to 15%. Ethene and process steam from natural gas are major contributors to ethanol ADP (fossil) impact. ADP (fossil) for gasoline blending with n-butanol is mainly contributed by propene and hydrogen production of n-butanol and the equal contribution by gasoline. It is also observed that individually, gasoline production has the third most (49.1 $MJ.kg^{-1}$) ADP fossils. In the present study (India), ADP (fossil) is calculated around 36.4 $GJ.t^{-1}$ methanol which is coherent with the 33.4 $GJ.t^{-1}$ methanol reported by Li et al. 2018.

**Human Toxicity Potential (HTP)**

HTP is a continuous toxicological impact on humans. The effect of percentage gasoline blending with methanol, ethanol, and n-butanol is shown in Fig. 10. For gasoline blending with n-butanol, n-butanol contributes 73% higher than gasoline. Process steam generation mainly contributes to n-butanol followed by propene and electricity generation. However, Pereira et al. (2015) reported that petrochemical n-butanol production had similar HTP compared with biobutanol. Individually, gasoline production has the second most HTP. It is interesting to observe that the methanol addition helps to reduce the HTP impact. Khoo et al. (2016) also found (HTP) 0.4 kg DCB eq..$kg^{-1}$ $CH_3OH$ which is higher than 0.075 kg DCB eq..$kg^{-1}$ $CH_3OH$ calculated in the current study. Falano et al. (2014) calculated HTP (DCB eq.) for ethanol as 142 $gm.L^{-1}$ and in the present study, it is around 192 $gm.L^{-1}$. The difference in the impact values may be due to the different sources of electricity generation, fuel composition, and also the reporting method used.

**Terrrestric (TETP), Marine Aquatic Ecotoxicity Potential (MAETP), and Photochemical Ozone Creation Potential (POCP)**

TETP, MAETP, and POCP are the highest for gasoline blending with n-butanol as shown in Fig. 11, 12, and 13, respectively. TETP for gasoline blending with n-butanol, gasoline, and n-butanol contribute nearly in equal proportions, i.e., 1.6E-3 and 1.8E-3 kg DCB $eq.kg^{-1}$ respectively. Process steam and electricity generation contribute to n-butanol TETP impact. Similarly, electricity generation is also the main contributor to methanol production.

MAETP for gasoline blending with n-butanol, n-butanol contributes 5.6 times higher than gasoline. Process steam and electricity generation mainly add to this impact.

POCP impact is related to ozone creation and it is expressed in the amount of ethene equivalent emitted. Khoo et al. (2016) reported POCP 1.25E-4 kg ethene $eq.kg^{-1}$ $CH_3OH$,

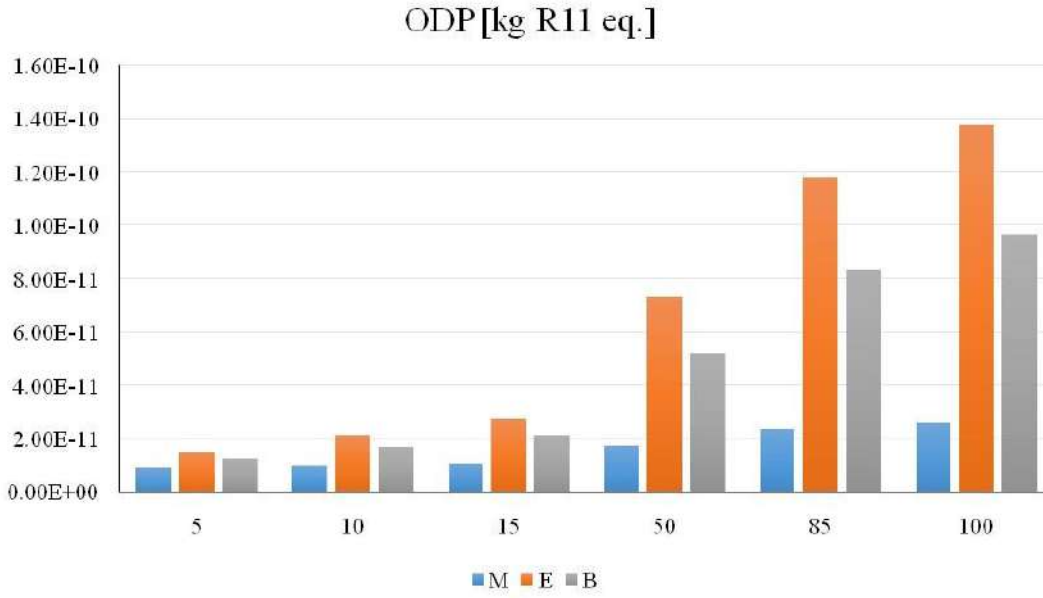


Fig. 8: ODP of gasoline blending production with methanol (M), ethanol (E), and n-butanol (B).

which is lower than 3.1E-4 kg ethene eq.kg$^{-1}$ $CH_3OH$ calculated in the current study. POCP for gasoline blending with n-butanol is mainly contributed by gasoline (6.48E-4 kg ethene eq.kg$^{-1}$) followed by n-butanol (5.57E-4 kg ethene eq.kg$^{-1}$). POCP of gasoline is added due to volatile organic compound emissions in transport and distribution (Furuholt 1995). In n-butanol, propene and hydrogen production contribute to the impacts compared to biobutanol (Pereira et al. 2015).

## CONCLUSION

A detailed investigation of the environmental impact and implications of blending gasoline with (varying percents) methanol, ethanol, and n-butanol for the first time in India is presented in this paper on LCA methodology. The alcohol production through the chemical route, i.e., methanol from natural gas reforming process, ethanol from hydrogenation with nitric acid, and n-butanol from oxo process are considered.

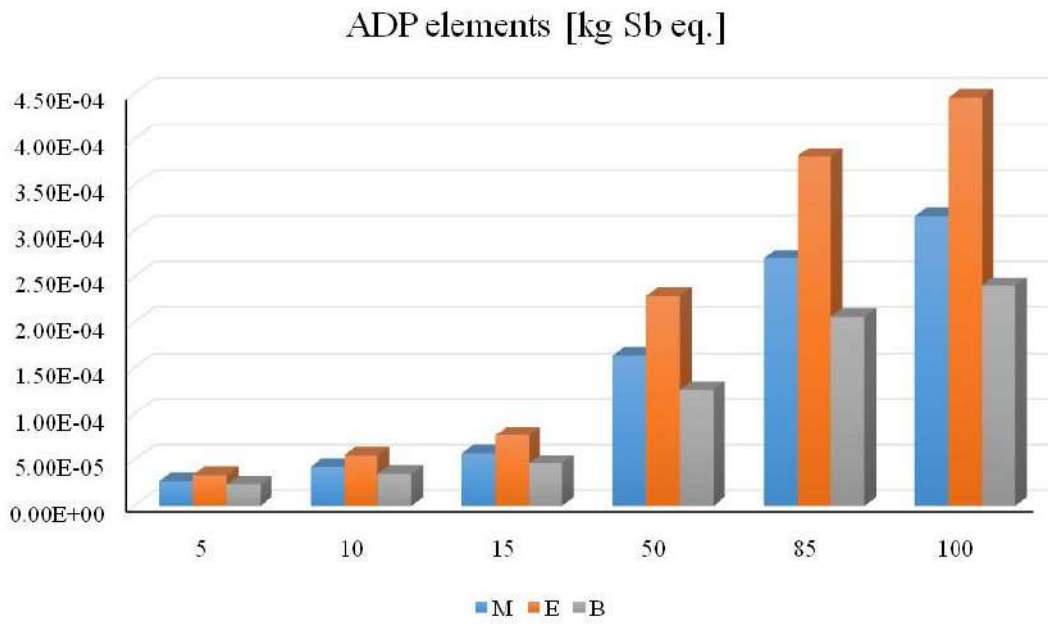


Fig. 9 (a): ADP (elements) of gasoline blending production with methanol (M), ethanol (E), and n-butanol (B).

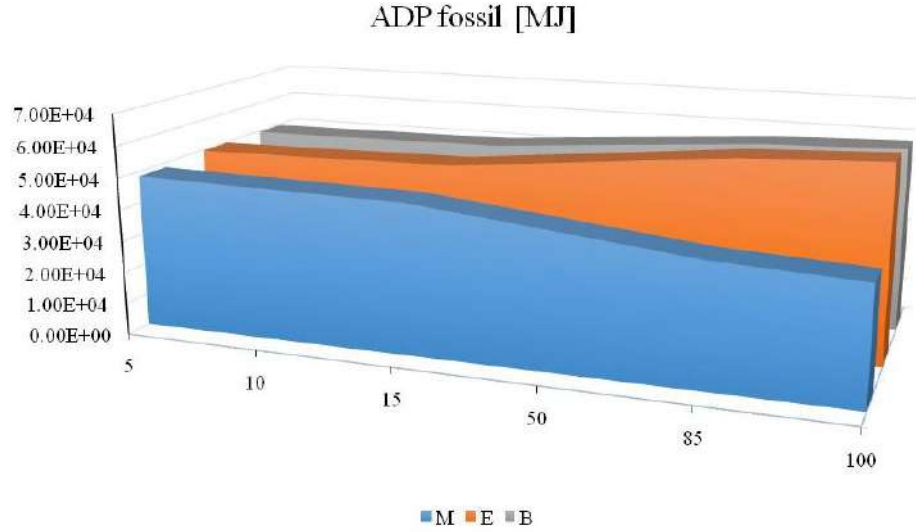


Fig. 9 (b): ADP (fossil) of gasoline blending production with methanol (M), ethanol (E), and n-butanol (B).

The results show that the gasoline blending with methanol has the lowest impact and is nearly constant from 5 to 15%. For gasoline with ethanol as an additive, the GWP, ODP, and ADP rise with increasing ethanol addition. Meanwhile, increasing ethanol addition reduces the AP and TETP impact of gasoline. Similarly, n-butanol has higher environmental impacts such as AP, EP, HTP, TETP, MAETP, and POCP compared to methanol and ethanol. Gasoline production has the second-most AP, EP, HTP, and TETP impact. Thus, out of 11, 6 of the environmental impact categories of n-butanol as an additive were consistently higher than that of methanol and ethanol.

It is not possible to state which alcohol or which route (petrochemical or biomass) is environmentally friendly overall. Blending during the production, use, and end-of-life cycle in India must be examined economically, environmentally, and sustainably. Gasoline blending appears to be more sustainable only when the additives are produced through the biological route for cleaner energy. However, the overall efficiency, energy use, and economic evaluation can play a deciding role.

## DISCLAIMER

The results are based on information and data from the GaBi Indian database.

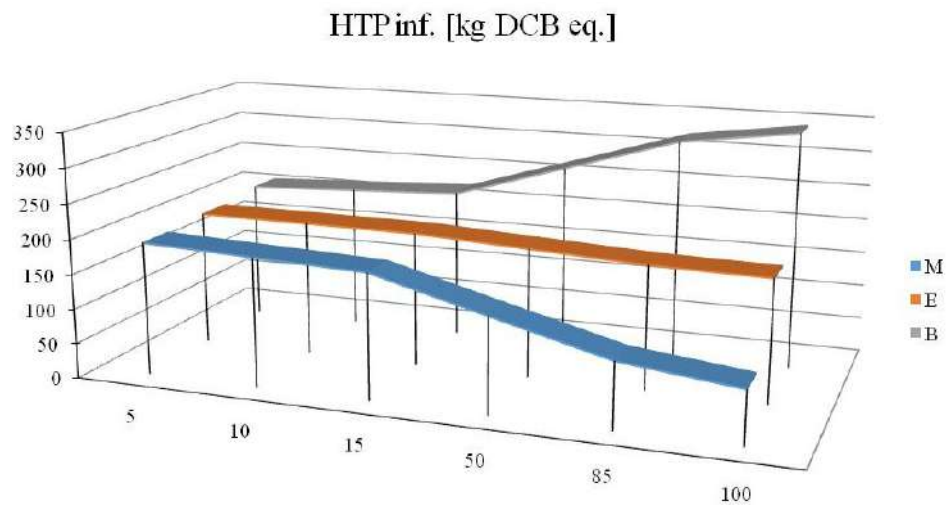


Fig. 10: HTP of gasoline blending production with methanol (M), ethanol (E), and n-butanol (B).

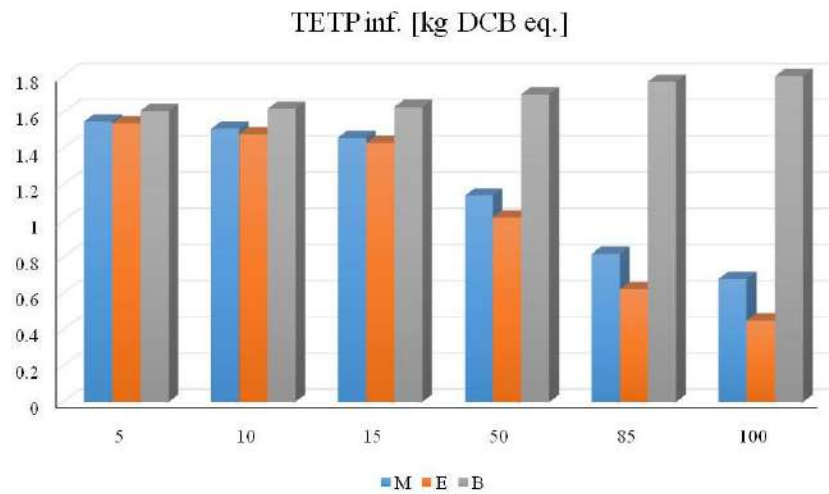


Fig. 11: TETP of gasoline blending production with methanol (M), ethanol (E), and n-butanol (B).

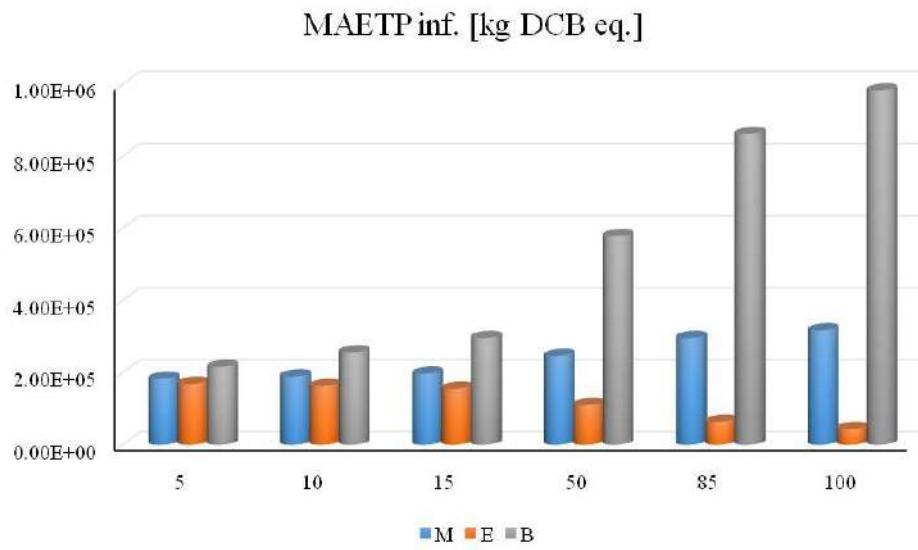


Fig. 12: MAETP of gasoline blending production with methanol (M), ethanol (E), and n-butanol (B).

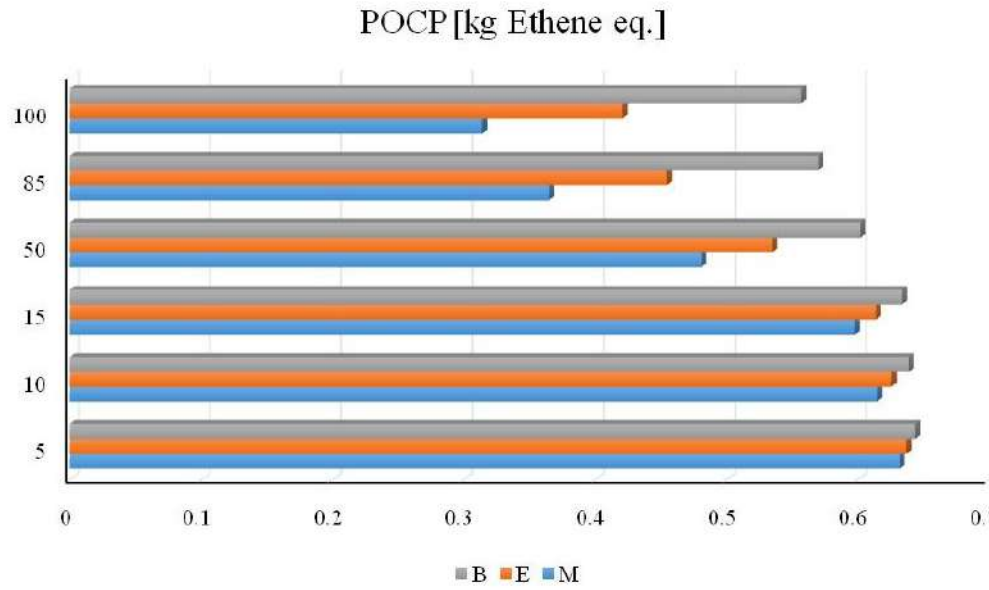


Fig. 13: POCP of gasoline blending production with methanol (M), ethanol (E), and n-butanol (B).

## ABBREVIATIONS

ADP - Abiotic depletion potential
AP - Acidification potential
DCB - Di-chloro Benzene
EP - Eutrophication potential
GHG - Greenhouse gas
GWP - Global warming potential
HTP - Human toxicity potential
LCA - Life cycle assessment
MAETP - Marine aquatic ecotoxicity potential
NG - Natural gas
ODP - Ozone depletion potential
POCP - Photochemical ozone creation potential
TETP - Terrestric ecotoxicity potential

## REFERENCES


Canakci, M., Ozsezen, A.N., Alptekin, E. and Eyidogan, M. 2013. Impact of methanol-gasoline fuel blends on the exhaust emission of an SI engine. Renew. Energy, 52: 111-117.

Chen, Y., Ma, J., Han, B., Zhang, P., Hua, H., Chen, H. and Su, X. 2018. Emissions of automobiles fueled with alternative fuels based on engine technology: A review. J. Traffic Transp. Eng. Engl. Ed., 5(4): 318-334.

Dalena, F., Senatore, A., Basile, M., Knani, S., Basile, A. and Iulianelli, A. 2018. Advances in methanol production and utilization, with a particular emphasis toward hydrogen generation via membrane reactor technology. Membranes, 8(4): 98.

Eriksson, M. and Ahlgren, S. 2013. LCAs of petrol and diesel: A literature review. Report, 2013: 058.

Falano, T., Jeswani, H.K. and Azapagic, A. 2014. Assessing the environmental sustainability of ethanol from integrated biorefineries. Biotechnol. J., 9(6): 753-765.

Furuholt, E. 1995. Life cycle assessment of gasoline and diesel. Resour. Conserv. Recy., 14(3-4): 251-263.

Heo, J.N., Son, N., Shin, J., Do, J.Y. and Kang, M. 2020. Efficient hydrogen production by low-temperature steam reforming of propane using catalysts with very small amounts of Pt loaded on $NiMn_2O_4$ particles. Int. J. Hydrog. Energy, 45(41) : 20904-20921.

Hu, X., Yang, J., Sun, W., Wang, N., An, S., Wang, Q., Zhang, Y., Xie, X. and Huang, L. 2020. The Y-Zr-O solid solution supported Ni-based catalysts for hydrogen production via auto-thermal reforming of acetic acid. Appl. Catal. B-Environ., 278: 119264.

Kajaste, R., Hurme, M. and Oinas, P. 2018. Methanol-managing greenhouse gas emissions in the production chain by optimizing the resource base. AIMS Energy, 6(6): 1074-1102.

Karaosmanoglu, F., Isigigur-Ergudenler, A. and Aksoy, H.A. 2000. A new blending agent and its effects on methanol-gasoline fuels. Energy Sources, 22(3): 235-245.

Khoo, H.H., Ee, W.L. and Isoni, V. 2016. Bio-chemicals from lignocellulose feedstock: sustainability, LCA and the green conundrum. Green Chem., 18 (7): 1912-1922.

Lemonidou, A.A., Valla, J. and Vasalos, I.A. 2003. Methanol Production from Natural Gas. In: Aresta M. (eds), Carbon Dioxide Recovery and Utilization. Springer, Dordrecht, pp. 379-394.

Li, J., Ma, X., Liu, H. and Zhang, X. 2018. Life cycle assessment and economic analysis of methanol production from coke gas compared with coal and natural gas routes. J. Clean. Prod., 185: 299-308.

Liu, C., Li, K., Wen, Y., Geng, B., Liu, Q. and Lin, Y. 2019. Bioethanol: New opportunities for an ancient product. Adv. Bioenergy, 4: 1-34.

Ma, R., Xu, B. and Zhang, X. 2019. Catalytic partial oxidation (CPOX) of natural gas and renewable hydrocarbons/oxygenated hydrocarbons- A review. Catal. Today, 338: 18-30.

Mata, T.M., Smith, R.L., Young, D.M. and Costa, C.A.V. 2003. Life cycle assessment of gasoline blending options. Environ. Sci. Technol., 37(16): 3724-3732.

Muñoz, I., Flury, K., Jungbluth, N., Rigarlsford, G., Canals, L. and King, H. 2014. Life cycle assessment of bio-based ethanol produced from different agricultural feedstocks. Int. J. Life Cycle Assess., 19: 109-119.

Ndaba, B., Chiyanzu, I. and Marx, S. 2015. n-Butanol derived from biochemical and chemical routes: A review. Biotechnol. Rep., 8: 1-9.

Patil, R.C., Suryawanshi, P.G., Kataki, R. and Goud, V.V. 2019. Chapter 8 - Current Challenges and Advances in Butanol Production. Sustainable Bioenergy- Advances and Impact, 225-256.

Pereira, L.G., Chagas, M.F., Dias, M., Cavalett, O. and Bonomi, A. 2015. Life cycle assessment of butanol production in sugarcane biorefineries in Brazil. J. Clean. Prod., 96: 557-568.

Popuri, S.S. and Bata, R.M. 1993. A performance study of iso-butanol-, methanol-, and ethanol-gasoline blends using a single-cylinder engine. SAE Tech. Paper, 932953: 1-22.

Ramalingam, S., Rajendiran, B. and Subramiyan, S. 2020. Recent advances in the performance of co-current gasification technology: A review. Int. J. Hydrog. Energy, 45(1): 230-262.

Saraswat, V.K. and Bansal, R. 2017. India's Leapfrog to Methanol Economy. NITI Aayog, Government of India. Delhi, India, pp. 1-11.

Sheehy, P., Law, K. and Jackson, M.D. 2010. Methanol Fuel Blending and Materials Compatibility Report: Overview of TIAX Report on U.S. Marketplace. The Methanol Institute, Rev A, TIAX Case No. D5607, Arlington, VA, pp. 1-40.

Shirvani, S., Shirvani, S., Shamekhi, A.H. and Reitz, R.D. 2020. A study of using E10 and E85 under direct dual fuel stratification (DDFS) strategy: Exploring the effects of the reactivity-stratification and diffusion-limited injection on emissions and performance in an E10/diesel DDFS engine. Fuel, 275: 117870.

Soam, S., Kumar, R., Gupta, R.P., Sharma, P.K., Tuli, D.K. and Das, B. 2015. Life cycle assessment of fuel ethanol from sugarcane molasses in northern and western India and its impact on Indian biofuel program. Energy, 83: 307-315.

Surisetty, V.R., Dalai, A.K. and Kozinski, J. 2011. Alcohols as alternative fuels: An overview. Appl. Catal. A-Gen., 404(1-2): 1-11.

Uyttebroek, M., Hecke, W.V. and Vanbroekhoven, K. 2015. Sustainability metrics of 1-butanol. Catal. Today, 239: 7-10.

Weissermel, K. and Arpe, H.J. 2008. Industrial Organic Chemistry (Google eBook). John Wiley & Sons, New York.

Xiang, D., Yang, S., Mai, Z. and Qian, Y. 2015. Comparative study of coal, natural gas, and coke oven gas blend methanol to olefins processes in China. Comput. Chem. Eng., 83: 176-185.

Yadav, P., Athanassiadis, D., Yacout, D., Tysklind, M. and Upadhyayula, V. 2020. Environmental impact and environmental cost assessment of methanol production from wood biomass. Environ. Pollut. Part-A, 265: 114990.

Yanju, W., Shenghua, L., Hongsong, L., Rui, Y., Jie, L. and Ying, W. 2008. Effects of methanol/gasoline blends on spark-ignition engine performance and emissions. Energy Fuels, 22(2): 1254-1259.

Yuen, P.K., Beckett, J., Villaire and W. 2010. Automotive materials engineering challenges and solutions for the use of ethanol and methanol blended fuels. SAE Tech. Paper, 2010: 729.

Yusri, I.M. , Mamat, R., Najafi, G., Razman, A., Awad, O.I., Azmi, W.H., Ishak, W.F.W. and Shaiful, A.I.M. 2017. Alcohol-based automotive fuels from first four alcohol family in compression and spark ignition engine: A review on engine performance and exhaust emissions. Renew. Sustain. Energ. Rev., 77: 169-181.

Nature Environment and Pollution Technology
An International Quarterly Scientific Journal

p-ISSN: 0972-6268
(Print copies up to 2016)
e-ISSN: 2395-3454

Vol. 20 | No. 5 (Suppl) | pp. 1959-1965 | 2021

Original Research Paper

https://doi.org/10.46488/NEPT.2021.v20i05.011

Open Access Journal

# Effect of Sludge Residence Time over Anaerobic Biodegradation of High Saline Biomass

**Tareq W. M. Amen*†, Meng Sun*, Mitsuharu Terashima* and Hidenari Yasui***

Faculty of Environmental Engineering, The University of Kitakyushu, Hibikino 1-1, Wakamatsu-ku, Kitakyushu-shi, Fukuoka 808-0135, Japan

†Corresponding author: Tareq W. M. Amen; t-amen@kitakyu-u.ac.jp; eng.twa@gmail.com

**Nat. Env. & Poll. Tech.**
**Website: www.neptjournal.com**

*Received:* 30-07-2021
*Revised:* 02-09-2021
*Accepted:* 11-09-2021

**Key Words:**
Halophytes
Anaerobic digestion
Methane generation
Salt-tolerant biomass

## ABSTRACT

Halophytes are unique in that they can thrive in a wide range of soil conditions, from normal to extremely saline. This has recently prompted researchers to consider using halophytes as a phytoremediation end-product as a source for biogas generation. Therefore, applying the anaerobic digestion process for halophytes may have the potential advantage in terms of efficient land utilization, soil remediation, and biogas production. Based on this, the anaerobic digestion efficiency of high saline biomass was investigated in continuous laboratory-scale anaerobic reactors at two different sludge residence times (SRT) of 40 and 80 days. Under mesophilic atmosphere, two reactors were operated, one reactor used organic substrate with 30 g-$Na^{+}$.$L^{-1}$ originating from sodium chloride whereas the other was operated with the presence of sodium bicarbonate and sodium sulfate. The salt-tolerant microorganism was gradually developed and the salt concentrations were selected based on the elemental analyses results of 30 species of wild halophyte plants taken from the saline-affected area of the Aral Sea in Uzbekistan during the early phase of the operation. For 40 and 80 days of SRT, respectively, 65.56 percent and 60.42 percent of the feed COD were converted into methane gas by the chloride system. However, only about 60% of the feed COD was converted into methane for bicarbonate, and the remaining fraction of gas was assigned to sulfide as a final product of increased sulfate reduction bacteria activity. These findings showed that the salt-tolerant microorganism could be incubated and the anaerobic digestion process could be adapted for a high-saline substrate, implying that the biodegradability of phytoremediation end-products may be used for methane production.

## INTRODUCTION

Because of urbanization and the increasing worldwide population, arable land is decreasing. Soil salinity is one of the most serious environmental factors limiting agricultural crop productivity and the quality of crops. Because most ordinary crops are salt sensitive, salinity affects a large percentage of agricultural fields, making conventional agriculture ineffective. Several practical measures, including soil washing and irrigation control, are now being used to restore the affected lands (Toderich et al. 2009). Moreover, a biological engineering solution called phytoremediation using halophyte plants is a promising approach to reform the salinized lands.

Halophytes are distinguished as they can flourish well in soils ranging from normal to severely saline conditions and it can offer an interesting alternative feedstock for the process of biogas production. Consequently, anaerobic digestion of residual phytoremediated biomass provides the ability to produce methane which can be used as electrical and thermal energy.

It is anticipated that the integration of anaerobic digestion of phytoremediated biomass in biogas production will become an environmentally sustainable and economically feasible solution in terms of renewable energy and saving resources. Applying anaerobic digestion under saline conditions is an appropriate process for integration into halophytes biogas production and/or salts recovery, and is of utmost importance for increasing the feasibility of the phytoremediation technologies.

The use of halophytes as a substrate for anaerobic digestion presents at least two distinct challenges. The first is the physico-chemical characteristics of the halophytes biomass as a substrate feedstock for anaerobic digestion, which will determine the biodegradable portion of the biomass, and the second is the high salinity associated with halophytic culture conditions, which will determine the biodegradable portion of the biomass. Lefebvre et al. (2007) and Margesin & Schinner (2001) both concluded the potentials of adaptation of salt-tolerant microorganisms in anaerobic treatment processes under saline conditions because a high diversity

could be maintained in an anaerobic reactor despite the increase in NaCl concentration.

However, according to Wood (2015), excessive saline concentrations cause dehydration and plasmolysis because of the osmotic pressure across the microbial cell membrane. Clearly, the ability of microbial communities to live in a wide range of salinities expands the possibilities for anaerobic digestion applications for phytoremediated biomass, allowing the process to gradually recover its efficiency (Luo et al. 2016). Sierra et al. (2018) found that the proliferation of salt-tolerant microorganisms resulted in an enduring microbial community, which increased the process performance robustness over a wide range of sodium concentrations.

Therefore, further research is required to build up the understanding of the successful application of anaerobic digestion under high saline conditions. Based on that, this study aims to evaluate the bioconversion performance and material balance fractionations in the continuous operation of anaerobic bioreactors that are carried out with the addition of different salt sources at different sludge ages. Two reactors were operated and the sludge retention time (SRT) was changed through the course of operation, one reactor used organic substrate with high sodium chloride concentration whereas the other was operated with the presence of sodium bicarbonate and sodium sulfate.

## MATERIALS AND METHODS

### Bioreactor Set-Up and Operation

At the initial phase, two lab-scale anaerobic tank reactors with a 4–L working volume namely chloride system and bicarbonate system were continuously operated with daily feeding. The reactors were constantly mixed by regular stirring, which was controlled by an electrical motor attached to the reactor. Over the course of the experiment, both reactors were started, filling the working volume with a fresh inoculum in a chemostat mode at 35°C and neutral pH. Fresh inoculum sludge was taken from a full-scale experiment anaerobic digester treating municipal sewage at Kitakyushu's Hiagari sewage treatment plant (STP) and was sieved through a 2.3 mm screen before use.

No additional alkalinity, or buffer, was introduced into the inoculum. Whereas the artificial halophytes were formed using fodder plant of *Panicum coloratum* which was used as the substrate from the beginning of the experiment. To facilitate injection of the substrate into the systems, the fodder plants were ground into fine particles using a blender and then mixed with targeted salt concentrations as listed in Table 1. The substrate was manually fed once a day using a 100 mL plastic syringe. The experiments were started with an acclimation period were started with a low organic loading rate (OLR), then the OLR was carefully and gradually increased until 2.0 g-COD/L/day. The two reactors then were subjected to two different SRTs of 40 and 80 days.

At a predetermined time, samples were taken from each reactor and directly were separated using a centrifugal solid/liquid separation unit. Then, the supernatant was used to measure the soluble organic content and the settled pellets were used to measure the particulate organic fraction besides retaining the reactors to ensure the operated SRT. Methane gas production was continuously logged using a gas counter (MGC-1, Litre Meter Limited, UK) after passing it through caustic pellets to remove $CO_2$ in the biogas. The produced methane volume was corrected to standard pressure and temperature.

### Process and Physicochemical Analyses

The obtained supernatant was filtered using a glass filter (Whatman GF/F) then the soluble COD concentrations were calculated based on the soluble TOC measurements and

Table 1: Influent composition of 1 kg for the chloride and bicarbonate substrates.

| | | Chloride System | Bicarbonate System | Unit |
|---|---|---|---|---|
| NaCl | | 76.27 | - | $g.kg^{-1}$ |
| $Na_2SO_4$ | | - | 29.57 | $g.kg^{-1}$ |
| $NaHCO_3$ | | - | 74.645 | $g.kg^{-1}$ |
| $FeCl_2 \times 4H_2O$ | | | 17.49 | $g.kg^{-1}$ |
| $H_2O$ | | 873.73 | 721.45 | $g.kg^{-1}$ |
| Organic - *Panicum coloratum* - | | 44 | 44 | $g\text{-}VSS.L^{-1}$ |
| Crude fiber | Hemicellulose | 212.77 | $g.kg\text{-}DM^{-1}$ | $g.kg\text{-}DM^{-1}$ |
| | Cellulose | 328.42 | $g.kg\text{-}DM^{-1}$ | $g.kg\text{-}DM^{-1}$ |
| | Lignin | 64.42 | $g.kg\text{-}DM^{-1}$ | $g.kg\text{-}DM^{-1}$ |

the soluble COD/TOC factor whereas the particulate COD concentrations were calculated based on the ratio of COD/VSS and measurements of VSS based on #2540 in Standard Methods (APHA, 2005) and. Volatile fatty acids (VFA) concentrations were measured using an ion chromatography system (Dionex ICS 1000) with Pac AS11-HC column, Thermo Fisher Scientific Inc., USA.

The feedstock plant was characterized for both volatile solids and ash content based on calculating the differences between the suspended solids content and the ash content. The suspended solid was determined by drying the samples at 105°C for 24 h to ensure a constant weight, where the ash content was determined after using the oven-dried samples and placed in pre-weighted ceramic crucibles and then ignited for 2 h at 550 °C in a muffle furnace.

The structural composition and the fiber components of fodder plant powders were determined based on AOAC (Chemists & Horwitz 1975). The cellulose, hemi-cellulose, and lignin fraction were calculated based on the measurements of neutral detergent fiber (NDF), acid detergent fiber (ADF), and acid detergent lignin (ADL) as detailed by Segura-Campos et al. (2014). Prior to analysis, all data was validated for homogeneity of variance.

The evaluation of the ultimate amount of methane produced under anaerobic conditions (mL $CH_4.g^{-1}$ COD) is crucial to predict the performance of the anaerobic digestion process (Kianmehr et al. 2014). Therefore, the efficiency of the anaerobic digestion process was mainly calculated in terms of biodegradability percentage (1) (Mottet et al. 2009).

$$\% \text{ Biodegradation} = \frac{\text{Produced Methane}}{\text{Potential Methane}} . 100\% \quad \ldots(1)$$

where the potential methane is theoretically calculated under the reactor's operation conditions as 0.35 L of methane gas can be generated for each 1 g of COD under normal conditions, and the produced methane is the generated methane from each reactor that is directly related to the degradation of the substrate. (273.15 K and 101.325 kPa).

Biochemical methane potential (BMP) experiments based on anaerobic respirometric batch tests employing respirometric apparatus (Challenging Systems Inc., USA (AER-8)) were used as COD fractionation assays to determine the proportion of soluble COD retained in reactor conversion. 500 mL glass bottles were used as reactors and then each reactor was filled with 400 mL of inoculum. To ensure only methane gas will be recorded and the $CO_2$ will be absorbed, caustic material was placed between the sensing device and the temperature-controlled incubator.

The soluble substrate of the two reactors was used as a substrate. The tests were anaerobically incubated at 35℃ after tightly being closed. The net generated methane volumes were calculated based on the Gay-Lussac law and then normalized to the volume of gas under normal conditions. Additionally, the theoretical methane production potential of biomass residues used in this study was calculated based on the ratio between the VS and COD, considering the operation conditions of the respirometer as temperature and pressure.

The fraction of COD converted into methane can be measured by monitoring the methane production rate, and the inert fraction of COD was calculated by equation (2).

$$COD_I = COD_T - \text{Produced } CH_4 \quad \ldots(2)$$

where, $COD_I$ is the inert COD, $COD_T$ is the total COD initially introduced substrate.

## RESULTS AND DISCUSSION

### Inoculum and Substrate Basic Composition

Table 2 presents the average basic proximate and structural characteristics of the inoculum and substrate composition. The particulate composition of fodder plant which is used as the organic substrate mainly consists of cellulose and hemi-

Table 2: Inoculum and the influent feed basic proximate and structural characteristics.

| | Seeding Sludge [Inoculum] | Fodder Plant [Substrate] | Unit |
|---|---|---|---|
| Origin | Hiagari STP | *Panicum coloratum* | - |
| VSS | 16.87 | 47.27 | g-VSS.$L^{-1}$ |
| Ash | 26.33 | 5.47 | wt.% |
| Cellulose | 71.12 | 328.42 | g.kg-$DM^{-1}$ |
| Hemi cellulose | 241.28 | 212.77 | g.kg-$DM^{-1}$ |
| Lignin | 367.19 | 64.42 | g.kg-$DM^{-1}$ |
| Lipid | N.A. | 12.86 | g.kg-$DM^{-1}$ |
| Protein | N.A. | 73.06 | g.kg-$DM^{-1}$ |

cellulose which reflects the substrate potential for anaerobic digestion process since it would release a high amount of intermediates which eventually will be consumed by different strains of methanogens.

The dried mass (DM) of the fodder plant residues was found to include 328.42, 212.77, and 64.42 (g.kg-$DM^{-1}$) of cellulose, hemicellulose, and lignin, respectively. The presence of lignin in the substrate will prevent cellulose from being degraded by enzymes since it can act as a coating material to protect cellulose

**Effect of Sludge Retention Time**

Initially, the methane production rate was gradually increased in accordance with the expected methane production rate by increasing the OLR. Experimentally, at the initial phase of incubation, the VFAs were detected and as the process progressed, the VFAs decreased and were maintained under the inhibition level as a consequence of methanogens adaptation and its subsequent methane generation (Fig. 1). Consequently, the methane generation rate increased until achieving a steady state.

Both reactors were run on a 40-day SRT before being switched to an 80-day SRT to promote the low-activity-rate microorganisms involved in salt-tolerant biomass degradation. As these salt-tolerant microorganisms grew bigger, more substrate hydrolysis activities occurred, and the rate of methane conversion increased.

Once the systems have reached a steady state, the increasing trend of particulate COD, particularly for the chloride system, is not readily visible, indicating that the biodegradability has improved as the SRT increased. In contrast, the particulate concentration in the bicarbonate system still has an increasing trend.

The soluble COD concertation for chloride and bicarbonate systems was in the range of 1.35 g-$COD.L^{-1}$ to 3.15 g-$COD.L^{-1}$ and 1.36 g-$COD.L^{-1}$ to 2.10 g-$COD.L^{-1}$, respectively (Fig. 2). Soluble COD signals the hydrolysis conversion of plant biomass lignocellulosic components into fermentable intermediates that will eventually contribute to methane generation (Gallipoli et al. 2014).

Likewise, the variation in soluble and particulate COD for anaerobic digestion process for both chloride and bicarbonate systems, the produced methane for two systems, are presented in Fig. 3

The time course evaluation for the two reactors was observed based on comparing the mass balance outcomes in terms of produced methane percentage that was lost to the atmosphere, soluble COD lost with effluent, and the particulate COD in the reactor as shown in Fig. 4. The anaerobic digestion shows a stable production rate of methane for both SRT at 40 and 80 days. When we compare Fig. 4(a), (b) with Fig. 4(c), (d), we can see that this is the case for both the particulate and soluble fractions of COD.

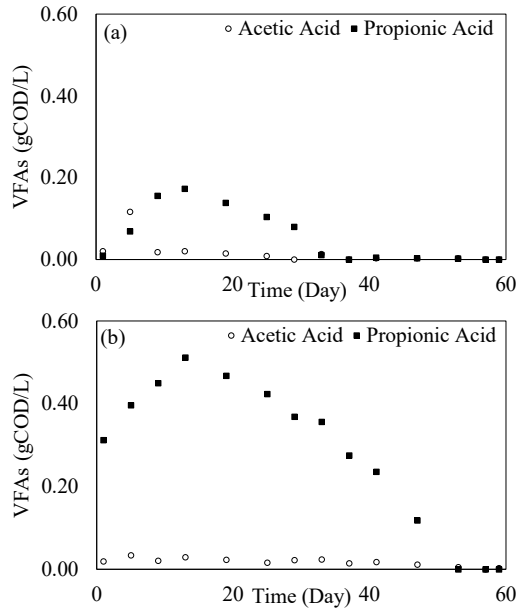


Fig. 1: The VFAs concentrations at the accumulation phase for (a) chloride reactor and (b) bicarbonate reactor.

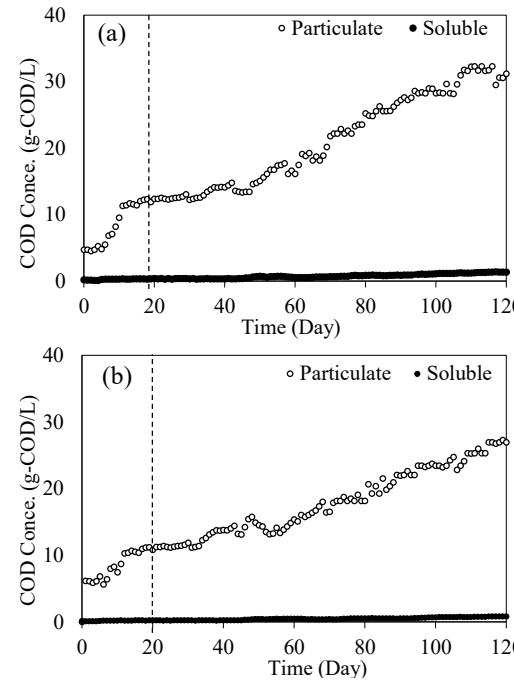


Fig. 2: Measured soluble, and particulate COD for (a) chloride system and (b) bicarbonate system.

In terms of the efficiency of anaerobic digestion processes, more than 60% of the feed substrate was converted to a gas phase which means it is possible to get high methane production from artificial halophytes and this outcome is in the agreement with Ras et al. (2011) who achieved 51% of COD conversion to methane under SRT of 28 days. This result is also in line with Sierra et al. (2018) who showed that a short-term continuous fluctuation between 18 and 20 g-$Na^{+}.L^{-1}$ eventually has no impact on the bioconversion anymore after a long-term operation, suggesting a successful gradual adaptation to higher sodium concentrations.

### Conversion Rate at Steady State

The steady-state outcomes for the chloride system for both 40 and 80 days of SRT showed 65.56 percent and 60.42 percent of the feed COD was converted in methane

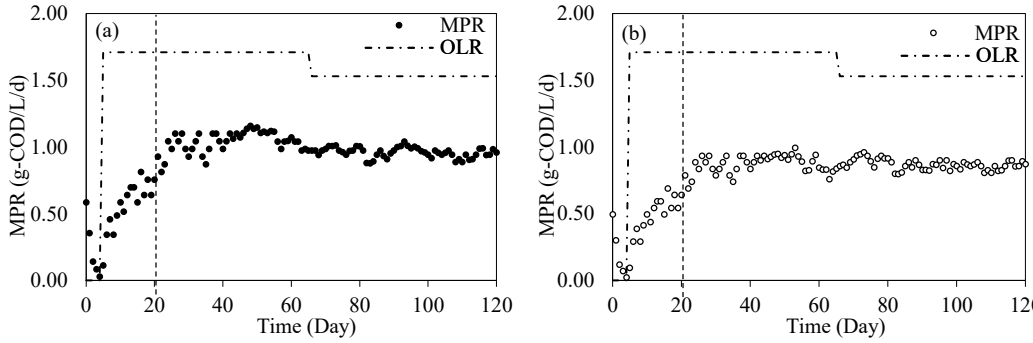


Fig. 3: Methane produced rate for (a) chloride system and (b) bicarbonate system.

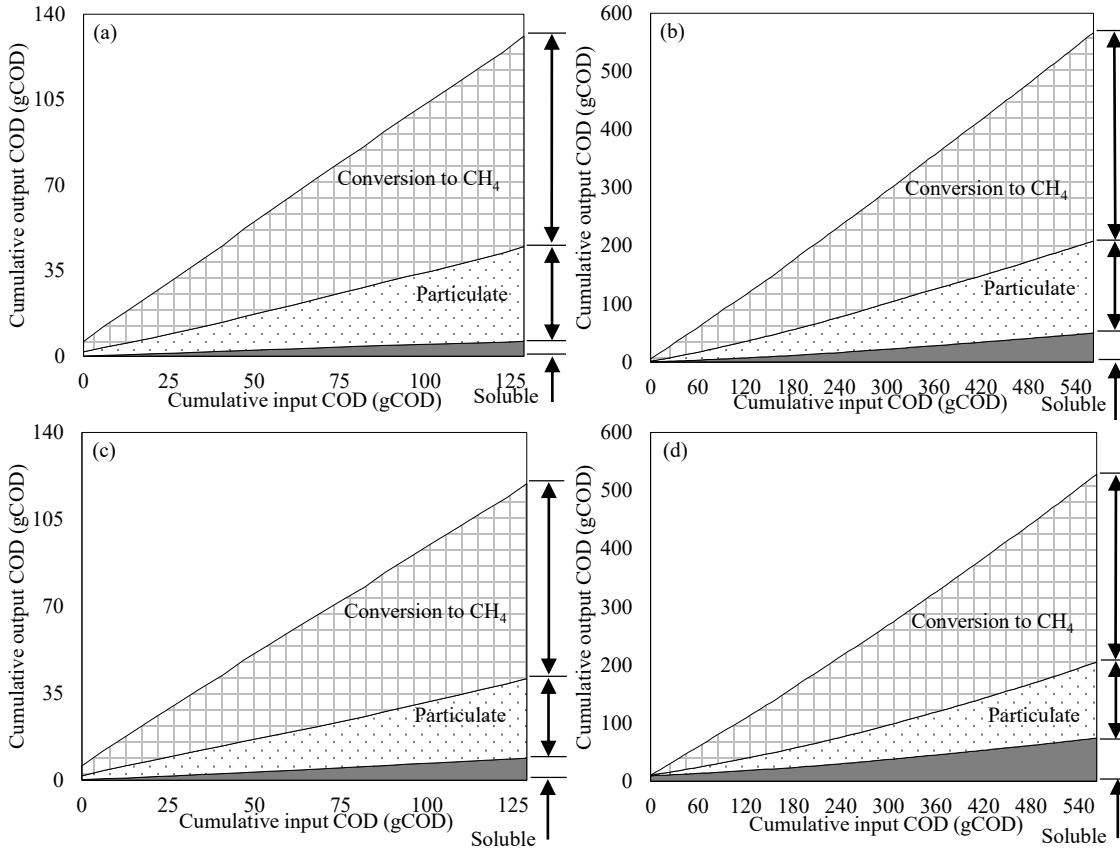


Fig. 4: The COD mass balance breakdown components for (a) chloride reactor at SRT 40 days, (b) chloride reactor at SRT 80 days, (c) bicarbonate reactor at SRT 40 days, and (d) bicarbonate reactor at SRT 80 days.

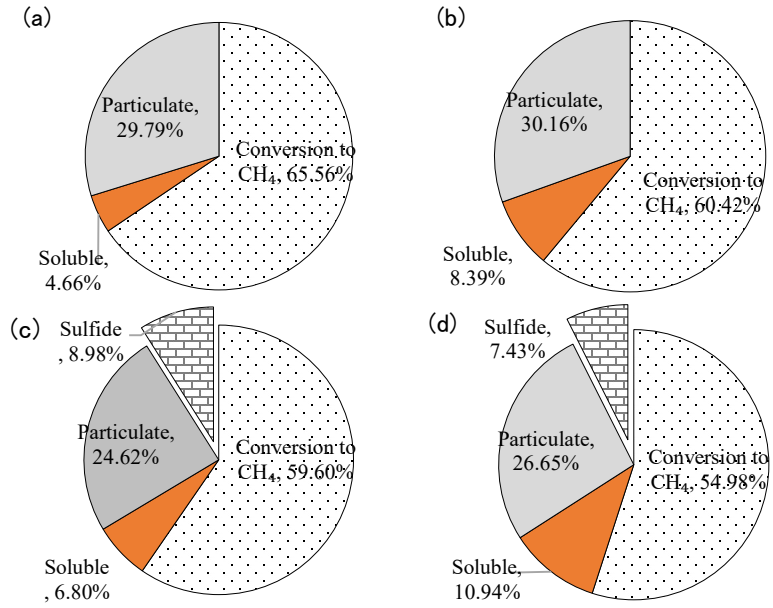


Fig. 5: Conversion rate at steady state for (a) chloride reactor at SRT 40 days, (b) chloride reactor at SRT 80 days, (c) bicarbonate reactor at SRT 40 days, and (d) bicarbonate reactor at SRT 80 days.

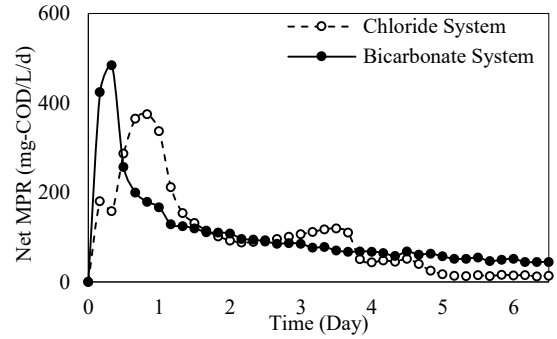


Fig. 6: Methane production rate of undecomposed substrate for chloride and bicarbonate systems.

gas, respectively, as shown in Fig. 5. In contrast, Aslan & Ekerda (2016) discovered that when saline was fed with 20 g-$Na^{+}$.$L^{-1}$ in a UASB reactor, COD bioconversion was significantly reduced. Despite the SRT, less than 60% of input COD was converted to the bicarbonate system, and the remaining fraction of gas was assigned to sulfide as an end product of increased sulfate-reducing bacteria activity. The other components of the particulate fraction were nearly the same as for the chloride system, as well as for a soluble fraction as a small proportion of substrate remained in the digesters.

Therefore, salt-tolerant plant residues harvested from saline-contaminated soil could be disposed of by anaerobic digestion and could be considered as a substrate for methane production. These outcomes offer a promising outlook for future work and may play an important role in future biofuel operations.

## Identify the Remaining Amount of Biodegradable Soluble Fractions

Anaerobic respirometric tests may be able to predict the BMP of substrates because they can detect both easily biodegradable and slowly biodegradable substrates (Argiz et al. 2020). Approx. 80 % soluble fractions were biodegraded as calculated from the BMP experiments results as shown in Fig. 6. Furthermore, the generated methane started immediately and kept increasing until it reached its peak on the first day of the test. Furthermore, methane production was drastically reduced, and after 5 days of digestion, about 90% of the experimental methane output was obtained. The degradation

of readily degradable materials in the salt-tolerant biomass caused the MPR curves to the peak.

## CONCLUSION

This study focused on the anaerobic digestion performance under high saline conditions. The results obtained in this study suggested that:

1. Salt-tolerant microorganisms can be incubated and survived under conventional and relatively high SRT because the microorganism was promoted in the system and therefore, improve the phytoremediation plant biodegradation.
2. When compared to the bicarbonate system, the results show that the chloride system produced more methane because the activation of sulfate reduced the microbes in the bicarbonate system.
3. Halophyte biomass would be deemed an effective source of renewable energy generation, notwithstanding the fact that its biodegradability increases at high saline conditions.

## ACKNOWLEDGMENT

The authors are very grateful to the japan society for the promotion of science (JSPS) for the supported the research by grants-in-aid for scientific research, japan #19h02278 and grant-in-aid for JSPS fellows, japan #19f19370.

## REFERENCES

APHA. 2005. Standard methods for the examination of water and wastewater. 21st Edition, American Public Health Association/American Water Works Association/Water Environment Federation, Washington DC.

Argiz, L., Reyes, C., Belmonte, M., Franchi, O., Campo, R., Fra-Vázquez, A. and Campos, J.J.J. 2020. Assessment of a fast method to predict the biochemical methane potential based on biodegradable COD obtained by fractionation respirometric tests. J. Environ. Manag., 269: 110695.

Aslan, S., Şekerdağ, N.J.D. and Treatment, W. 2016. Salt inhibition on anaerobic treatment of high salinity wastewater by upflow anaerobic sludge blanket (UASB) reactor. Desalin.Water Treat., 57(28): 12998-13004.

Chemists, A.O. and Horwitz, W. 1975. Official Methods of Analysis (Vol. 222). Association of Official Analytical Chemists, Washington, DC.

Gallipoli, A., Gianico, A., Gagliano, M. and Braguglia, C.J. 2014. Potential of high-frequency ultrasounds to improve sludge anaerobic conversion and surfactants removal at different food/inoculum ratios. Bioresour. Technol., 159: 207-214.

Kianmehr, P., Mansoor, W. and Kfoury, F.A. 2014. Prediction of biogas generation profiles in wastewater treatment plants using neural networks. J. Clean Energy Technol., 2(3), 201-205.

Lefebvre, O., Quentin, S., Torrijos, M., Godon, J.J., Delgenes, J.P. and Moletta, R.J.A. 2007. Impact of increasing NaCl concentrations on the performance and community composition of two anaerobic reactors. Appl. Microbiol. Biotechnol., 75(1): 61-69.

Luo, W., Phan, H.V., Hai, F.I., Price, W.E., Guo, W., Ngo, H. H. and Nghiem, L.D.J. 2016. Effects of salinity build-up on the performance and bacterial community structure of a membrane bioreactor. Bioresour. Technol., 200: 305-310.

Margesin, R. and Schinner, F.J.E. 2001. Potential of halotolerant and halophilic microorganisms for biotechnology. Extremophiles, 5(2): 73-83.

Mottet, A., Steyer, J.P., Déléris, S., Vedrenne, F., Chauzy, J. and Carrère, H.J.B. 2009. Kinetics of thermophilic batch anaerobic digestion of thermal hydrolyzed waste activated sludge. Biochem. Eng. J., 46(2): 169-175.

Ras, M., Lardon, L., Bruno, S., Bernet, N. and Steyer, J.P.J. 2011. Experimental study on a coupled process of production and anaerobic digestion of Chlorella vulgaris. Bioresour Technol., 102(1): 200-206.

Segura-Campos, M., Barbosa-Martín, E., Matus-Basto, Á., Cabrera-Amaro, D., Murguía-Olmedo, M., Moguel-Ordo, Y. and Betancur-Ancona, D.J.A. 2014. Comparison of chemical and functional properties of Stevia rebaudiana (Bertoni) varieties cultivated in Mexican Southeast. Amr. J. Plant Sci., 5(3): 286-293.

Sierra, J.D.M., Oosterkamp, M.J., Wang, W., Spanjers, H. and Van Lier, J.B.J. 2018. Impact of long-term salinity exposure in anaerobic membrane bioreactors treating phenolic wastewater: performance robustness and endured microbial community. Front. Bioeng. Biotechnol., 141: 172-184.

Toderich, K., Shuyskaya, E., Ismail, S., Gismatullina, L., Radjabov, T. and Bekchanov, B. 2009. Phytogenic resources of halophytes of Central Asia and their role for rehabilitation of sandy desert degraded rangelands. Land Degrad. Develop., 20(4): 386-396.

Wood, J.M.P. 2015. Bacterial responses to osmotic challenges. J. Gen. Physiol., 145(5): 381-388.

Nature Environment and Pollution Technology
An International Quarterly Scientific Journal

p-ISSN: 0972-6268
(Print copies up to 2016)
e-ISSN: 2395-3454

Vol. 20 | No. 5 (Suppl) | pp. 1967-1972 | 2021

Original Research Paper

https://doi.org/10.46488/NEPT.2021.v20i05.012

Open Access Journal

# A Reliable Cyclic Voltammetry Technique for the Degradation of Salicylaldehyde: Electrode Kinetics

**Jasvinder Kaur†, Rajdeep Malik and Dushyant Gangwar**
Department of Chemistry, Gurukula Kangri (Deemed to be University), Haridwar-249404, Uttarakhand, India
†Corresponding author: Jasvinder Kaur; jasvinderkaur2911@gmail.com

**Nat. Env. & Poll. Tech.**
**Website: www.neptjournal.com**

*Received:* 16-04-2021
*Revised:* 13-05-2021
*Accepted:* 25-05-2021

**Key Words:**
Salicylaldehyde
Cyclic voltammetry
Water treatment
Platinum electrode
Electro-oxidation

## ABSTRACT

Salicylaldehyde (SA) is used in numerous biological, pharmaceutical and industrial applications. Releasing effluents from these industries contaminates water. So the degradation of salicylaldehyde is necessitated. The electrochemical degradation of salicylaldehyde in buffered media was studied using the eco-friendly cyclic voltammetry (CV) technique on a platinum electrode at different scan rates. Kinetic and electrochemical parameters were evaluated for the reaction such as standard heterogeneous rate constant ($k^0$, $2.468\times10^3$ $s^{-1}$), anodic electron transfer rate constant ($k_{ox}$, $2.507\times10^3$ $s^{-1}$), electron transfer coefficient of reaction (α, 0.673), and formal potential ($E^0$, 1.0937) under the influence of scan rate. The nature of the reaction is found to be diffusion controlled. The concentration study in the range of 1 mM to 4 mM was calibrated. The limit of detection and the limit of quantification were calculated to be 0.0031 mM and 0.0103 mM respectively.

## INTRODUCTION

Salicylaldehyde (SA) is used in numerous industrial, chemical and pharmaceutical fields such as dyes, fragrances, essential oils, drugs and biological applications (Alasmi & Merza 2017). It is mainly used for the production of coumarin. In addition salicylaldehyde is used as a precursor for aspirin. The Saligenin process is the main process for the production of salicylaldehyde (Pouramini & Moradi 2012). Also, it is naturally found in tomatoes, cinnamon, grapes, coffee, tea, and dairy products. Due to the extensive uses of salicylaldehyde, it becomes an organic pollutant and finds its path into the aqueous system through pharmaceutical and industrial fields (Wang et al. 2014). Several methods previously used for the degradation of salicylaldehyde such as colorimetric (Nonoyama et al.1987), differential pulse polarographic (López et al.1996), uv/spectroscopy (Matyasovszky et al. 2009), spectroelectrochemistry (Wang et al. 2014), cyclic and normal pulse voltammetry (Kiss et al. 2019), electrochemical (Kiss & Kunsági-Máté 2019) and also salicylaldehyde is determined in natural and treated water by applying GC-MS (Crompton 1999). In recent years, the increase of contaminants in water bodies has necessitated the need to develop cost-effective methods for their removal or degradation (Rasalingam et al. 2014). The electroanalytical technique is used for monitoring and trace level detection of pollutants in water (Martinez-Huitle & Ferro 2006). It is a powerful analytical technique with high sensitivity, accuracy, precision, rapid response and low operating cost, which is used in the pharmaceutical industry, metal industry and environmental applications (Farghaly et al. 2014, Chatterjee 2017). Currently, voltammetry is well renowned and eco-friendly technique to investigate pollutants and other compounds (Nicholson & Shain 1964). It is widely employed for the determination and kinetic mechanism of the reaction (Allen & Larry 2001, Compton & Banks 2018). In the voltammetric technique, a platinum electrode (solid electrode) is usually a working electrode. Platinum is the most suitable choice of inert electrode for electroanalysis (Monk 2001) because it gives appropriate electron-transfer kinetics and a large anodic potential window range (Wang 2000).

In this work, we reported electro-oxidation of salicylaldehyde in aqueous media using the cyclic voltammetry technique. However, to the best of our knowledge salicylaldehyde has not yet been investigated in an aqueous solvent using these parameters.

## MATERIALS AND METHODS

### Materials

Salicylaldehyde was obtained from Sigma- Aldrich and used without further purification. A stock solution of SA was prepared in 30 % ethanol. Britton-Robinson (BR) buffer was

prepared with 0.04 M boric, phosphoric and acetic acids and 0.1 M KCl as the supporting electrolyte. All other chemicals used were of analytical grade. All solutions were prepared with doubled distilled water.

### Instrumentation

An Autolab model PGSTAT 101 potentiostat/galvanostat 663 VA Stand (Metrohm AG, Netherlands) was used to perform the cyclic voltammetry (CV) technique. Electrochemical cell along with three-electrode setup is used in this technique. Pt disc electrode (PE) (0.031 $cm^2$) acted as working electrode (WE), Ag/AgCl/3M KCl electrode act as the reference electrode, and Pt wire acted as the counter electrode. The solution pH calculation was done using Elico LI 120 pH meter (Elico Ltd., India). In preparation for investigation, the working electrode was polished with alumina powder (particle size 0.05 mm) on a cloth polishing pad and washed with doubled distilled water. All the experiments have been performed at an ambient temperature of 25 ± 1°C.

## RESULTS AND DISCUSSION

### Effect of pH

The electro-oxidation of 10 mM was studied over the pH range of 2.2-11.0 in Britton- Robinson (BR) buffer solution by cyclic voltammetry (Fig.1). However, the finest peak was observed on pH 2.2 (Acidic medium). Hence further experiment was performed in this range.

### Cyclic Voltammetry Experiment of Salicylaldehyde (SA)

The electrochemical behavior of SA was recorded on the platinum electrode, using a cyclic voltammetry technique. The cyclic voltammogram was obtained for 10 mM SA at a scan rate of 20 $mVs^{-1}$, which shows a well-defined anodic peak at Pt electrode from potential window range +0.7 to +1.3 V Fig. 2(b). This peak indicates that the irreversible reaction occurred on the platinum electrode surface. On scanning the reverse direction there was no cathodic peak shown.

### Influence of Scan Rate

The influence of scan rate on SA is examined at Pt electrode by using cyclic voltammetry method with different scan rates ranging from 20 $mVs^{-1}$ - 90 $mVs^{-1}$ (Fig. 3). As the scan rate was increased, the peak current (Ipa) for oxidation of SA was also increased.

The reversibility of electrochemical reaction rate is controlled by adsorption and diffusion, and it is dependent on two factors: Ip on $V^{1/2}$ and log Ip on log v (Nicholson 1965) (Fig. 3(a) and Fig. 3(b)). If the origin of the coordinates is not intercepted by the linear fit (Fig. 3(a)), the electrode process is diffusion-controlled and proceeded by chemical reaction (Wudarska et al.2013). At various scan rates (v) ranging from 0.02 to 0.09 $Vs^{-1}$, peak current(Ip) depends linearly on the square root of v (equation below):

$$Ip(\mu A)= 147.32v^{1/2} (V^{1/2}s^{-1/2}) – 5.8517 (r=0.988)$$

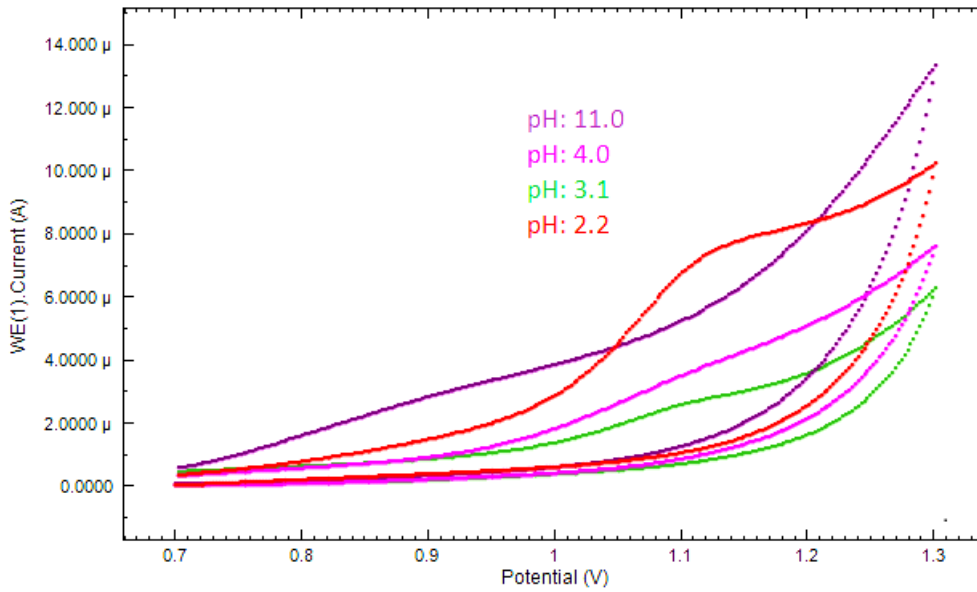


Fig. 1: Cyclic voltammograms of 10 mM SA at different pH values (a) 11.0, (b) 2.2, (c) 4.0, (d) 3.1

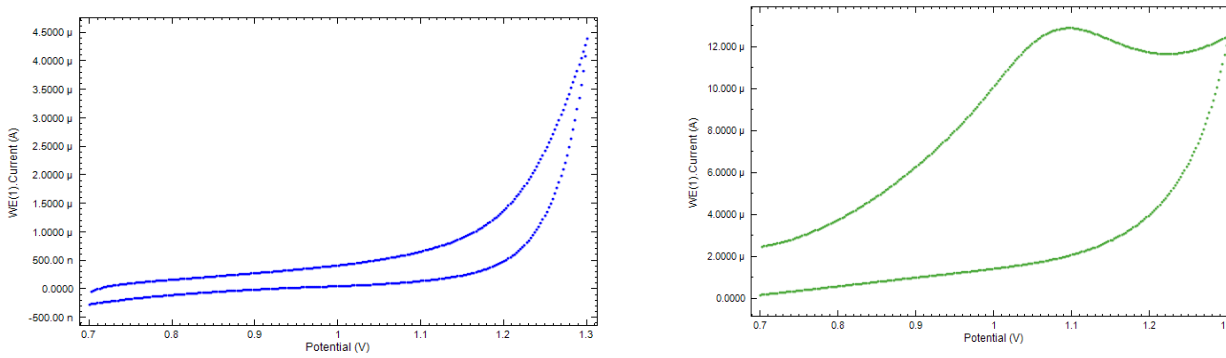


Fig. 2: Cyclic voltammogram for 10 mM SA on Pt electrode in 0.04 m BR buffer. (a) Blank (b) SA at scan rate (ν) = 20 $mVs^{-1}$

Alternatively, a linear relationship was observed between log Ip and log v (Fig. 3(b)) corresponding to the equation.

log Ip (μA)=0.63 log v($Vs^{-1}$)+2.2593 (r=0.986)

The slope value of this linear fit (Fig. 3(b)) is 0.63. Therefore, according to Bard and Faulkner, and others (Allen & Ferry 2001), this process is only controlled by diffusion, which confirms that the electro-oxidation of SA was a diffusion-controlled reaction. With an increase in scan rate, the peak potential was observed in the range 0.02-0.09 $Vs^{-1}$ as shown in Fig. 3(c). The relationship can be expressed as:

Ep(V)=0.0468 log v($Vs^{-1}$)+ 1.1768 (r=0.970)

For irreversible electrode process, Laviron (1979) equation is given below to define Ep:

$E_p = E^0 + (2.303RT/\alpha nF) \log(RTk^0/\alpha nF) + (2.303RT/\alpha nF) \log v$

Where $E^0$ is the formal standard redox potential, α is the transfer coefficient, n is the number of electrons transferred, $k^0$ is the standard heterogeneous rate constant of the reaction, and v is the scan rate. Thus, from the slope of the plot Ep vs log v, the value of $\alpha n$ can be easily calculated as

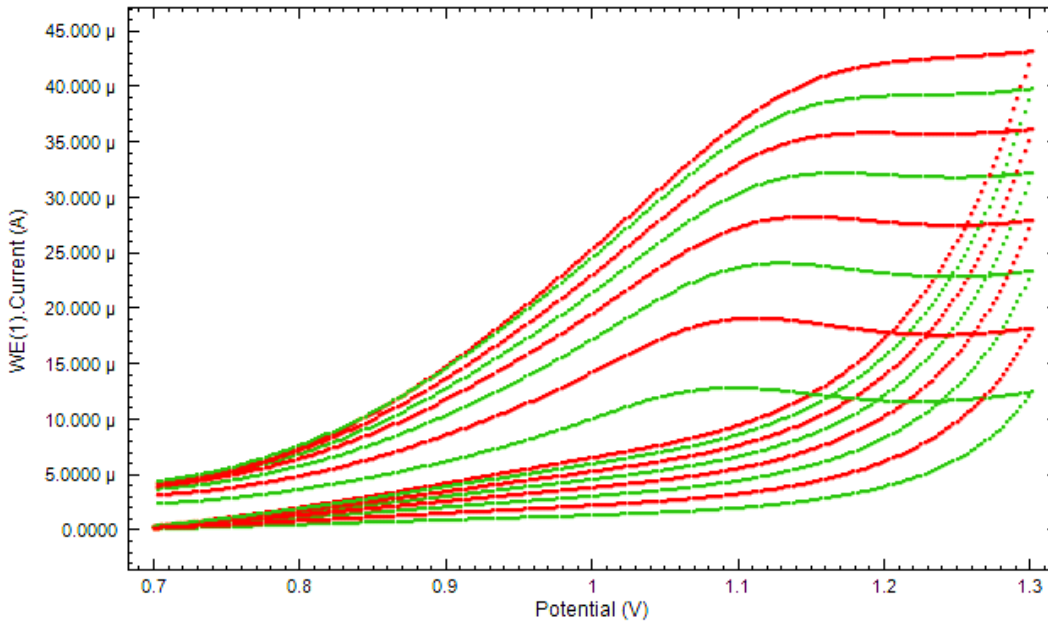


Fig. 3: Cyclic voltammograms of 10 mM SA at different scan rates 20, 30, 40, 50, 60, 70, 80, and 90 $mVs^{-1}$.

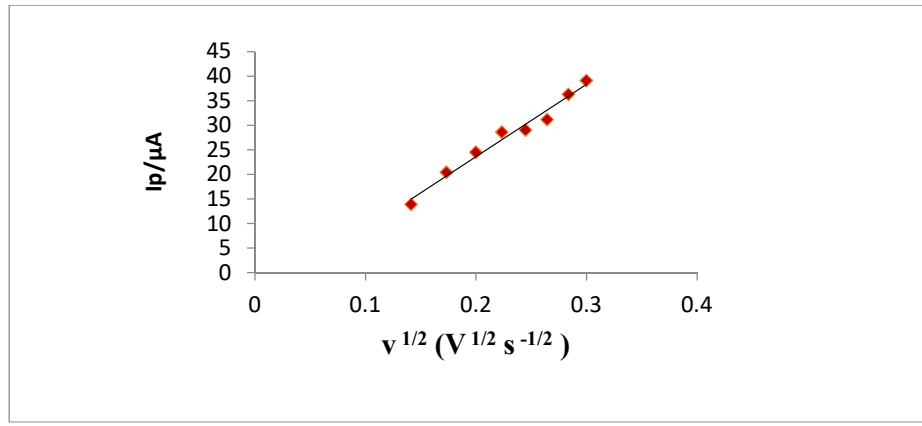


Fig. 3(a): $I_{pa}$ vs $v^{1/2}$

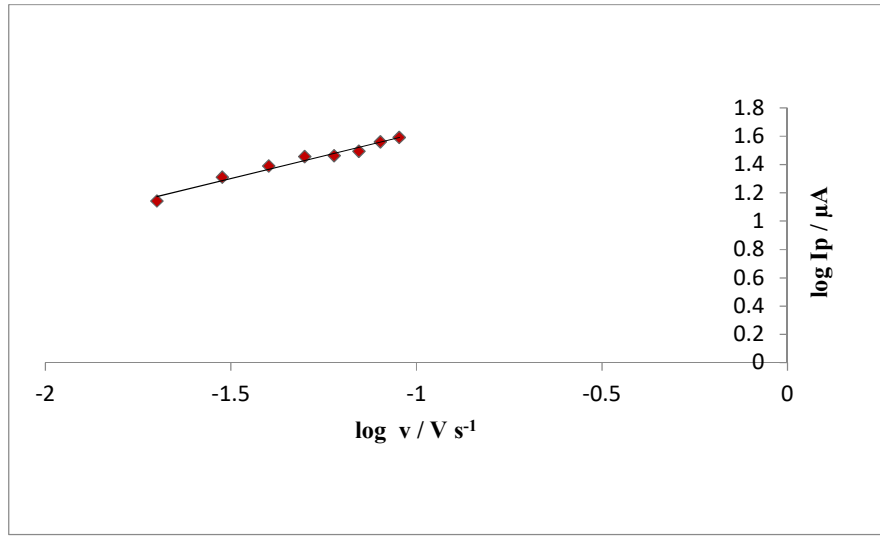


Fig. 3(b): log $I_{pa}$ vs log v

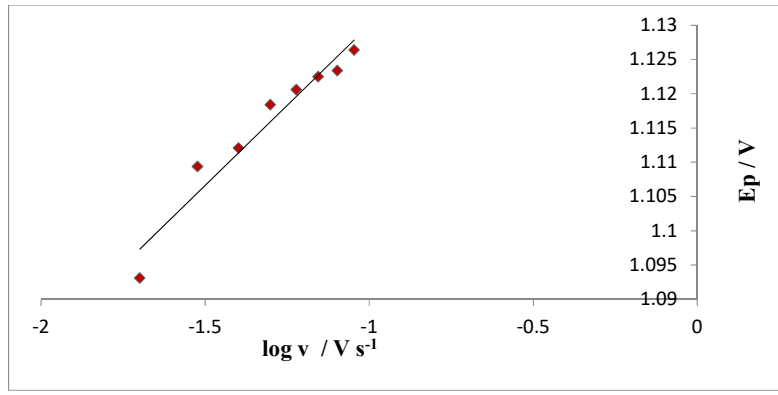


Fig. 3(c): $E_p$ vs log v

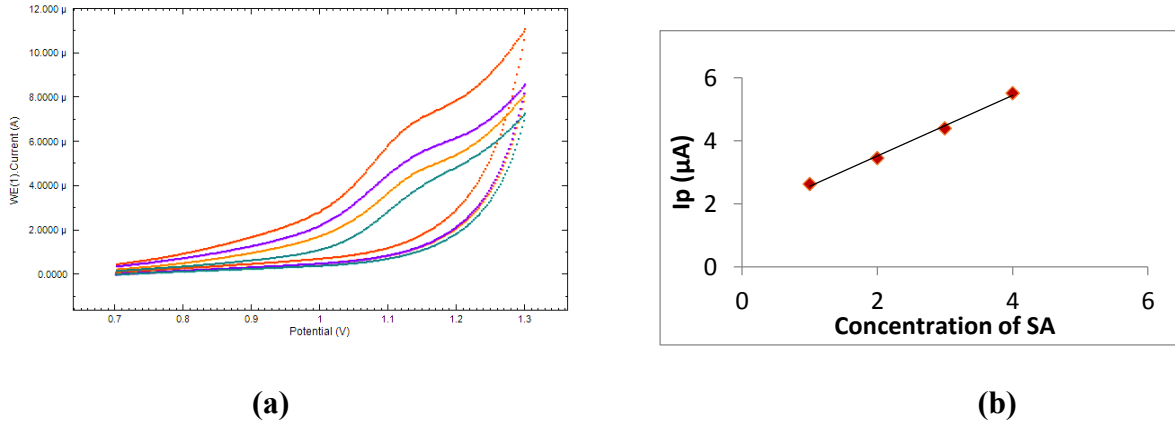


Fig. 4: (a) Cyclic voltammograms with increasing concentration of SA in pH 2.2 buffer solution on a platinum electrode with SA concentration: (i) 1.0, (ii) 2.0, (iii) 3.0, (iv) 4.0 mM (b) Plot of peak current versus concentration of SA.

1.26. In our system taking R=8.314 $JK^{-1}mol^{-1}$, T=298 K, and F=96480 C $mol^{-1}$.

α can be expressed by Bard and Faulkner (Allen & Ferry 2001) as:

$$\alpha = \frac{47.7}{Ep - Ep/2} \text{ mV}$$

Where $Ep_{/2}$ is the potential at half-peak current. So, the average value of the electron transfer coefficient of reaction ($\alpha$) was calculated as 0.673. Further, the number of the transferred electron (n) was calculated from the αn value as 1.88~2 in the SA electro-oxidation. The value of the standard heterogeneous rate constant ($k^0$) can be calculated by knowing the value of the formal potential ($E^0$) (from the intercept of the plot Ep versus ν by extrapolating to the vertical axis at ν=0) (Fotouhi et al. 2012, Wu et al. 2004). The formal potential ($E^0$) and the standard heterogeneous rate constant ($k^0$) for the reaction were obtained as 1.0937 and 2.468 × $10^3$ $s^{-1}$ respectively. The electron transfer rate constant ($k_{ox}$) can be calculated from the equation (Benschoten et al. 1983).

$$k_{ox} = k^0 \times \exp\{-(1-\alpha)\, nF(E - E^0)/(RT)\}$$

So the, $k_{ox}$ was obtained as $2.507 \times 10^3 s^{-1}$

**Effect of Concentration**

The effect of varying concentrations of SA was also studied at Pt electrode in 0.04 M BR buffer, pH 2.2 at the scan rate of 10 $mVs^{-1}$. With increasing concentrations of SA, the cyclic voltammogram revealed that the peak current was linearly increasing as shown in Fig. 4(a). A linear SA calibration curve was obtained in the range from 1 mM to 4 mM (Fig. 4(b)). The linear equation was

Ipa (µA) = 0.9625 C + 1.5947 (r= 0.9977)

The limit of detection (LOD) (Rageh et al.2015) and limit of quantification (LOQ) (Harisha et al.2018) were 0.0031 mM and 0.0103 mM respectively. It was calculated by the below equations.

$$LOD = 3\ s/m$$

$$LOQ = 10\ s/m$$

Where m is the slope of the calibration plot and s is the standard deviation of the peak current of three blank measurements.

Table 1: Comparison of potential window range, concentration, and limit of detection (LOD) obtained for salicylaldehyde using the proposed method with the previously reported methods.

| S.No | Method | Potential window range | Concentration range | LOD | References |
|---|---|---|---|---|---|
| 1 | Uv/ Vis Spectroscopy | – | 30 ppm | – | (Matyasovszky et al. 2009) |
| 2 | Spectroelectrochemistry | - 0.4 to 1.2 V | 100 µm | – | (Wang et al. 2014) |
| 3 | Electrochemical | 0 to 3 V | 10 mM | – | (Kiss & Kunsági-Máté 2019) |
| 4 | Photoelectrochemical | -0.4 to 1.2 V | 30 ppm | – | (Tian et al.2009) |
| 5 | Cyclic voltammetry | 0.7 to 1.3 V | 1-4 mM | 0.0031 mM | Present work |

## CONCLUSION

The aim of this research was to degrade toxic salicylaldehyde with the help of an eco-friendly cyclic voltammetry technique. Salicylaldehyde was discovered to have an irreversible two-electron transfer, diffusion-controlled reaction. This work will help in the clinical and safety development of the environment.

## ACKNOWLEDGEMENT

The author would like to thank the Department of Chemistry, Gurukula Kangri (Deemed to be University) Haridwar, India for providing all the necessary facilities for completing this work.

## REFERENCES

Alasmi, A. and Merza, J.2017.Synthesis and characterization of novel dialdehydes based on SN2 reaction of aromatic aldehyde. Inorg. Chem. Ind. J., 12(1): 111.

Allen, J.B. and Larry, R.F. 2001. Electrochemical Methods Fundamentals and Applications. John Wiley & Sons, New York.

Benschoten, J.J.V., Lewis, Y.T., Heineman, W. R., Roston, D.A. and Kissinger, P.T. 1983. Cyclic voltammetry experiments. J. Chem. Educ., 60(9): 772-76.

Chatterjee, A. 2017. Different electrodes for paracetamol estimation using cyclic voltammetry technique: A Review. Res. J. Pharmacol. Pharmacody., 9(2): 88-92.

Compton, R.G. and Banks, C.E. 2018. Understanding Voltammetry. World Scientific Publishing, Singapore.

Crompton, T.R. 1999. Determination of Organic Compounds in Natural and Treated Waters. CRC Press, Boca Raton, Florida.

Farghaly, O.A., Hameed, R.A. and Abu-Nawwas, A.A.H. 2014. Analytical application using modern electrochemical techniques. Int. J. Electrochem. Sci., 9(1) : 3287-3318.

Fotouhi, L., Fatollahzadeh, M. and Heravi, M.M. 2012. Electrochemical behavior and voltammetric determination of sulfaguanidine at a glassy carbon electrode modified with a multi-walled carbon nanotube. Int. J. Electrochem. Sci., 1(7): 3919-3928.

Harisha, KzV., Swamy, B.K. and Ebenso. E.E. 2018. Poly (glycine) modified carbon paste electrode for simultaneous determination of catechol and hydroquinone: A voltammetric study. J. Electroanal. Chem., 823: 730-736

Kiss, L., Bősz, D., Kovács, F., Li, H., Nagy, G. and Kunsági-Máté, S. 2019. Investigation of phenol electrooxidation in aprotic non-aqueous solvents by using cyclic and normal pulse voltammetry. Polymer Bull., 76(11): 5849-5864.

Kiss, L. and Kunsági-Máté S. 2019. Electrochemical oxidation of benzaldehyde and hydroxybenzaldehydes in acetonitrile on platinum and glassy carbon electrodes. Comptes Rendus Chimie, 22(8): 557-61

Laviron, E. 1979. The general expression of the linear potential sweep voltammogram in the case of diffusionless electrochemical systems. J. Electroanal. Chem. Interf. Electrochem., 101(1): 19-28.

López, L.J. M., Mochón, M.C., Sánchez, J.C.J. and Pérez, A.G. 1996. Differential pulse polarographic determination of salicylaldehyde as its Girard-P derivative. Microchim. Acta, 124(3-4)1: 87-194.

Matyasovszky, N., Tian, M. and Chen, A. 2009. Kinetic study of the electrochemical oxidation of salicylic acid and salicylaldehyde using UV/vis spectroscopy and multivariate calibration. J. Phys. Chem. A, 113(33): 9348-9353

Martinez-Huitle, C.A. and Ferro, S. 2006. Electrochemical oxidation of organic pollutants for the wastewater treatment: direct and indirect processes. Chem. Soc. Rev., 35(12): 1324-1340.

Monk, P. 2001. Fundamentals of Electroanalytical Chemistry. John Wiley & Sons, New York.

Nicholson, R.S. and Shain, I. 1964. Theory of stationary electrode polarography. Single scan and cyclic methods are applied to reversible, irreversible, and kinetic systems. Anal. Chem., 36(4): 706-723.

Nicholson, R.S. 1965. Theory and application of cyclic voltammetry for measurement of electrode reaction kinetics. Anal. Chem., 37(11): 1351-1355.

Nonoyama, R., Naito, T., Takayanagi, M., Goto, S. and Yashiro, T. 1987. Colorimetric determination of salicylaldehyde with 1, 3-diphenyl-2-thiohydantoin. Chem. Pharm. Bull., 35(3): 1281-1284.

Pouramini, Z. and Moradi, A. 2012. Structural and ortho selectivity study of 2-hydroxybenzaldehyde using spectroscopic analysis. Arab. J. Chem., 5(1): 99-102.

Rageh, H.M., Abou-Krisha, M.M., Abo-Bakr, A.M. and Abd-Elsabour, M. 2015. Electrochemical behavior and the detection limit of ascorbic acid on a Pt-modified electrode. Int. J. Electrochem. Sci., 10: 4105-4115.

Rasalingam, S., Peng, R. and Koodali, R.T. 2014. Removal of hazardous pollutants from wastewaters: applications of TiO2-SiO2 mixed oxide materials. J. Nanomater., 2014.

Tian, M., Adams, B., Wen, J., Asmussen, R.M. and Chen, A. 2009. Photoelectrochemical oxidation of salicylic acid and salicylaldehyde on titanium dioxide nanotube arrays. Electrochim. Acta, 54(14) : 3799-3805.

Wang, J. 2000. Analytical Electrochemistry. 2nd edition. Wiley- VCH & Sons, New York.

Wang, Y., Jiang, H., Tian, J.J. and He, J.B. 2014. Spectroelectrochemistry of salicylaldehyde oxidation. Electrochim. Acta, 125: 133-140.

Wudarska, E., Chrzescijanska, E., Kusmierek, E. and Rynkowski, J. 2013. Voltammetric studies of acetylsalicylic acid electro-oxidation at platinum electrode, Electrochim. Acta, 93: 189-94

Wu, Y., Ji, X. and Hu, S. 2004. Studies on the electrochemical oxidation of azithromycin and its interaction with bovine serum albumin. Bioelectrochemistry, 64(1): 91-97.

Nature Environment and Pollution Technology
An International Quarterly Scientific Journal

p-ISSN: 0972-6268
(Print copies up to 2016)
e-ISSN: 2395-3454

Vol. 20 | No. 5 (Suppl) | pp. 1973-1980 | 2021

Original Research Paper

https://doi.org/10.46488/NEPT.2021.v20i05.013

Open Access Journal

# Biodiesel-Alkaline Transesterification Process for Methyl Ester Production

**U.S.P.R. Arachchige†, K.A. Viraj Miyuranga, D. Thilakarathne, R. A. Jayasinghe and N. A. Weerasekara**
Department of Civil and Environmental Technology, Faculty of Technology, University of Sri Jayewardenepura, Homagama, Sri Lanka
†Corresponding author: U.S.P.R. Arachchige; udara@sjp.ac.lk

**Nat. Env. & Poll. Tech.**
**Website: www.neptjournal.com**

*Received:* 13-05-2021
*Revised:* 22-06-2021
*Accepted:* 15-07-2021

**Key Words:**
Biodiesel production
Coconut oil
Esterification
Free fatty acid
Renewable energy

## ABSTRACT

The world needs to increase renewable and alternative fuel sources such as Biomass, Bioethanol, and Biodiesel to compete with fossil fuels. Biodiesel is an important renewable fuel source since it can be used in regular diesel vehicles without requiring engine modifications. Conventional biodiesel production takes around 90 min of reaction time. A longer reaction time is not suitable for commercial production. Furthermore, traditional products such as oil react with biodiesel methoxide to produce a maximum of 90% biodiesel yield. As the catalyst is not involved with the reaction, pure methanol and methoxide (methanol with KOH catalyst) are separately added to the system to enhance the pre-reaction step. By changing the methanol to methoxide ratio, biodiesel is produced, and yield is calculated. The highest yield, which is 95%, is obtained with a 5:15% methanol to methoxide ratio. The total reaction time with the new experimental procedure is only 20 min. That is a significant reduction by saving operating costs such as energy consumption. Produced biodiesel show similar properties to that of standard biodiesel.

## INTRODUCTION

Global warming and environmental pollution are alarming today due to fossil fuel combustion in the power generation and the transport sector. The atmospheric carbon dioxide ($CO_2$) concentration hit 417 ppm (parts per million) in May 2020, which was 414 ppm in May 2019 (Andrew & Chris 2020). $CO_2$ levels have reached unprecedented heights in human history, as shown in Fig. 1.

The impact of man on the environment through his daily activities is complex and irreversible. Most of the intentional or unintentional causes are contributing to environmental pollution and changes in the ecosystem. There is no single cause that can be considered the main reason for environmental pollution, as most of them are interrelated. However, the following causes can be viewed as the main contributors to ecological damage and environmental pollution (Manisalidis et al. 2020).

- Population growth and deforestation
- Industrialization and urbanization

### Vehicle emissions

There is a considerable impact of population growth on the environment. With the population increase, we consume more and more natural resources and deplete the resources faster than before. Simultaneously, more and more waste is generated and disposed of in the open environment polluting the water, air, and soil. Both ways, the negative impact on the environment is significant (Manisalidis et al. 2020).

The population growth rates are not at an environmentally sustainable level. The increasing demands for the consumables such as food, water, land, power, and energy lead to devastating conditions worldwide. It should be addressed immediately to avoid resource depletion and irreversible impact on the environment. According to Fig. 1, it is clear that around 37 billion tons of $CO_2$ are emitted into the atmosphere annually (Our World in Data n.d).

$CO_2$ emissions from vehicles account for a substantial part of $CO_2$ emissions due to fossil fuel combustion. Even though fossil fuel resources are depleting and the prices are escalating, it does not discourage the usage as they are easily accessible to consumers. The use of fossil fuels such as coal, oil, and gas, over many years, directly causes global warming and climate change (Ogunwole 2012, Swapan & Bablu 2020).

To stabilize the concentration of $CO_2$ in the atmosphere, the world needs to increase the usage of renewable and alternative fuel sources such as biomass, bioethanol, and biodiesel to compete with fossil fuels. Biodiesel is an important renewable fuel source since it can be used in regular diesel vehicles without requiring engine modifications.

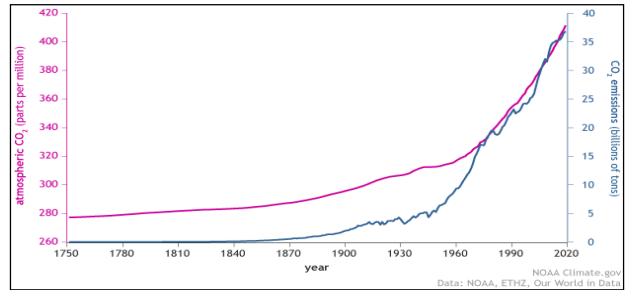


Fig. 1: Atmospheric $CO_2$ Concentration from the year 1750-2020. (Our World in Data n.d)

## Bio-Diesel Production

Several edible and non-edible raw materials are used to produce biodiesel around the world (Onyinyechukwu et al. 2018). Edible oils can be categorized as coconut oil, palm oil, sunflower oil, rapeseed oil, etc., and non-edible oils can be classified as rubber seed oil, algal oil, Jatropha oil, and waste cooking oil.

There are multiple ways of producing biodiesel and alkaline esterification on the top of the list due to flexibility, simplicity, and the production yield with readily available raw materials. Biodiesel's manufacturing cost is the most important factor in its ability to compete with fossil diesel. To minimize the production cost, raw material cost, operating cost, and the energy requirement to produce biodiesel have to be minimized. The cost of the raw material has a direct promotional relationship with the overall biodiesel cost (Braga et al. 2015).

## Alkaline Esterification

Alkaline esterification is the process by which the glycerides present in the oil react with alcohol (methanol, ethanol) in the presence of an alkaline catalyst (KOH, NaOH) to form esters and glycerol as a byproduct (Banerjee & Chakraborty 2009, Enweremadu & Mbarawa 2009). To perform the forward reaction, it is essential to perform the reaction with the catalyst present (Fig. 2).

The catalyst is prepared by adding potassium hydroxide (KOH) into alcohol (methanol) and stir it properly until it dissolves completely. The ultimate goal of the catalyst preparation step is to produce methoxide ($CH_3O^-$), which may then be processed with triglycerides in the oil sample. The active catalyst for the production of methyl esters is methoxide ion, $–OCH_3$, which attacks triglyceride molecules and creates methyl esters. It is regenerated at the end of each reaction step when a hydrogen ion is stripped from a nearby methanol molecule.

If ethanol is being used, then the corresponding catalyst is called ethoxide, $–OCH_2CH_3$. During the catalyst preparation step, OH- ions abstract the hydrogen ion to form water ($H_2O$). Water will increase the formation of soap when free fatty acids are available, eventually reducing the yield of the biodiesel production process. It is important to process the oils with low free fatty acids (FFA) (<2% of the oil weight) to avoid soap formation by saponification reaction. To maintain the FFA% below 2, oils with higher FFA have to go through an acid esterification reaction before the alkaline esterification (Paraj et al. 2019).

It has been reported that the transesterification process depends on many factors, such as reaction temperature, mixing speed, reaction time, catalyst, alcohol percentage, and FFA in the oil. Therefore, base case experiment is performed

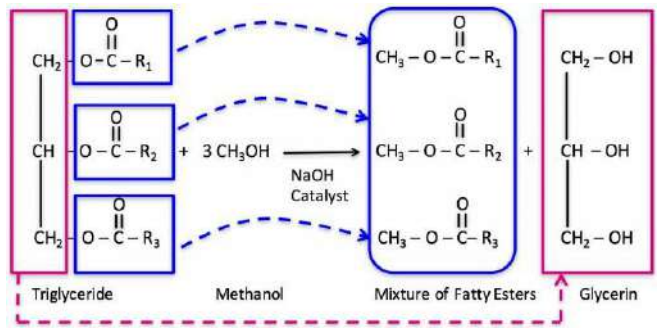


Fig. 2: Graphical representation of the esterification reaction.

with the operating conditions which are given in the literature without any changes such as 60°C operating temperature, 600RPM mixing speed, KOH as a catalyst and 1% of oil weight, <2% FFA content in the oil, methanol as alcohol and 20% of oil volume (Wanodya & Arief 2013, Phan & Phan 2008, Corro et al. 2011, Endang et al. 2018).

## MATERIALS AND METHODS

Pure coconut oil is used as the feedstock for this study. The total methanol amount taken is 20 mL since the oil sample is 100 mL. To meet the 1% W/W of the oil weight, 1 g of KOH is used. The operating temperature is 60°C with 600 RPM, and 90 min reaction time is selected for the present experiment. The FFA% of coconut oil is 0.5% with the titration method. Considering previous studies, a homogeneous base catalyst such as KOH is used. At first, the oil sample is preheated to remove any oil moisture to avoid soap formation during the reaction. The exact amount of KOH is added to the methanol and mixed well to prepare the methoxide. The prepared methoxide is then added to the heated oil sample while the stirring process continues.

## RESULTS AND DISCUSSION

The properties of the fresh coconut oil and the oil sample composition are given in Table 1 and Table 2. According to Table 2, it can be clearly seen that coconut oil majorly comprises Lauric acid ($C_{12}H_{24}O_2$). Coconut oil's physical properties were tested by the Petroleum and Lubricant Testing Laboratory, Industrial Technology Institute (ITI), Colombo 07, Sri Lanka. The fatty acid composition analysis was carried out by the Chemical and Microbiological Laboratory, Industrial Technology Institute (ITI), Colombo 07, Sri Lanka. Using the fatty acid composition, the molecular mass of the fresh coconut oil can then be estimated. In this research, the molecular mass of fresh coconut oil is estimated as 679.3 $g.mol^{-1}$.

The transesterification reaction was performed in the batch reactor. After 90 min of reaction time, the reacted oil sample was moved to the separation funnel and kept overnight for separation. After 24 hours of separation, the top layer fatty acid methyl ester (FAME) and the bottom layer glycerin (glycerol) were identified (Fig. 3).

The top layer of FAME is separated and washed with distilled water which is 50% of the FAME sample. The

Table 1: Properties of fresh coconut oil.

| Property | Test Method | Unit | Value[a] |
|---|---|---|---|
| Specific gravity at 60ºF | Gravity Bottle Method | - | 0.9331 |
| Kinematic Viscosity at 40ºC | ASTM D 445 - 01 Using Cannon - Fenske Routine Viscometer | cSt | 27.71 |
| Flash Point | ASTM D 92 - 05a Using COC | ºC | 309.0 |
| Water Content | ASTM D 4377 - 00 | % by mass | 0.12 |
| Total Sulphur Content | ASTM D 129 - 00 | % by mass | 0.42 |

a: Tested by the Petroleum and Lubricant Testing Laboratory, Industrial Technology Institute (ITI), Colombo 07, Sri Lanka

Table 2: Fatty acid composition of fresh coconut oil.

| Acid type | Formula | Method | Composition %[a] |
|---|---|---|---|
| Caproic acid | $C_6H_{12}O_2$ | CML/MM/05/51/003 | 0.38 |
| Caprylic acid | $C_8H_{16}O_2$ | | 6.81 |
| Capric acid | $C_{10}H_{20}O_2$ | | 5.45 |
| Lauric acid | $C_{12}H_{24}O_2$ | | 48.28 |
| Myristic acid | $C_{14}H_{28}O_2$ | | 19.50 |
| Palmitic acid | $C_{16}H_{32}O_2$ | | 9.12 |
| Stearic acid | $C_{18}H_{36}O_2$ | | 2.70 |
| Oleic acid | $C_{18}H_{34}O_2$ | | 6.18 |
| Linoleic acid | $C_{18}H_{32}O_2$ | | 1.51 |
| Arachidic acid | $C_{20}H_{40}O_2$ | | 0.07 |

a: Tested by the Chemical and Microbiological Laboratory, Industrial Technology Institute (ITI), Colombo 07, Sri Lanka

washing process is carried out at 60°C with constant stirring. After completion of washing, the washed sample is added to the separation funnel for further separation. The upper layer is taken and the pH value is analyzed. The lower layer is discarded to remove all the residual by-products like excess alcohol, excess catalyst, glycerine, and soap. If the pH of washed biodiesel is less than 7, we must repeat the washing process until pH reaches 7 (Fig. 4). The washed biodiesel sample was heated to 110°C while being stirred to remove further moisture. Pure biodiesel is used for further testing and composition analyses to verify the quality of the biodiesel.

## Parameter Optimization

The parameters' effects on the biodiesel production process are important to 2optimize the process.

*a. Effect of reaction time*

Effect of the reaction time for alkaline esterification is vital as it counts the energy consumption and the efficiency of the process. By maintaining 60°C reaction temperature and 600 RPM as the mixing speed, reaction time varied from 5 min to 120 min. During the analysis, oil volume of 100 mL, 20% of methanol by volume of oil, and 1% KOH (Methoxide) by weight of the oil are maintained to evaluate the single parameter effect. The effect of reaction time on the coconut oil conversion efficiency is shown in Fig. 5. The percent yield of biodiesel is calculated on a weight basis concerning the initial oil used for transesterification. With reaction times ranging from 5 to 50 min, the FAME production yield increased rapidly; after that, the conversion efficiency increased slowly and remained stable at around 85% at 60 min. Based on the results, it can be assumed that the reaction rate is steady and in equilibrium after 80 min.

*b. Effect of reaction temperature*

Methyl esterification of coconut oil was carried out at 30, 40, 50, 55, and 60°C to determine the effect of reaction temperature on the formation of the methyl ester. The methanol and KOH were maintained at a constant value of 20% and 1 wt.% for all these experiments. As can be seen from Fig. 6, for the same final reaction time, the ester formation yield increases with the temperature. Because methanol has a boiling point of 64.7°C, temperatures above 60°C are not used in the study. When the reaction temperature closes to the boiling point of methanol, it will start to vaporize and form a bubble to inhibit the reaction. Higher temperatures can be maintained by changing the operating pressure, which will increase the operating cost. The maximum yield of FAME is achieved at the 60°C reaction temperature and selected as the best operating temperature for further analysis.

*c. Effect of reaction stirring speed (RPM)*

In alkaline esterification, the mixing speed (RPM) is critical. To investigate the effect, the mixing speed is varied between 0 and 800 RPM while maintaining constant values of 60oC reaction temperature, 80 min working duration, 20% methanol, and 1% KOH. The reaction at the 0 RPM, which is without mixing, is very slow as the reaction occurs in oil and alcohol interfaces such as methanol. The yield of biodiesel at different mixing speeds is recorded and given in Fig. 7. As it can be seen from Fig. 7, the highest yield, which is 86%, is obtained with 600 RPM.

## Process Optimization

*a. Methanol to oil ratio*

The most effective variable for the biodiesel production yield is identified as methanol to oil molar ratio for transesterification reaction. As transesterification is an equilibrium

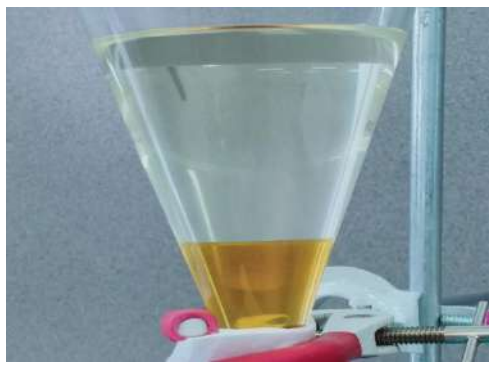

Fig. 3: Separation funnel - FAME at the upper layer and glycerine at the bottom layer.

Fig. 4: Two layers after washing the FAME with distilled water 50% by FAME volume, the top layer is washed biodiesel.

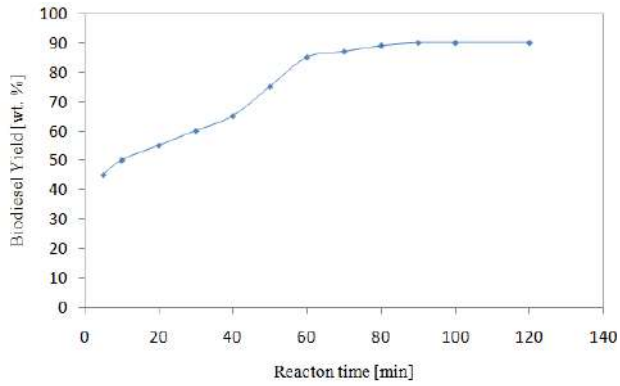


Fig. 5: Effect of reaction time on oil conversion efficiency, under 20 vol% methanol, 1 wt.% KOH at 60°C and 600 RPM.

reaction, an excess amount of alcohol is required to move the reaction forward (Bournay et al. 2005).

The biodiesel production is analyzed by changing the methanol volume with the fixed amount of 100 mL oil sample and 1% KOH by weight. The methanol amount varies from 10% to 30% by oil volume (2.3: 1 to 7:1 molar ratio of methanol to oil). It has been recorded that with the increase of methanol, the yield of the FAME also increased, and the result is given in Fig. 8. However, because there is insufficient Methanol for the reaction, the methanol to oil ratio of 2.3 results in the formation of a unique and opaque layer due to the presence of unreacted triglycerides. However, 20% methanol amount is selected by considering the yield and the cost of methanol, which will directly affect the production cost.

*b. Effect of catalyst concentration*

The most commonly and widely used catalyst is KOH, which is used for the reaction as they react with the triglycerides to break them apart and form the methyl ester. A wide concentration range of KOH from 0.5% to 2.5% (wt/wt of oil) has been tested as a catalyst that was premixed with methanol to

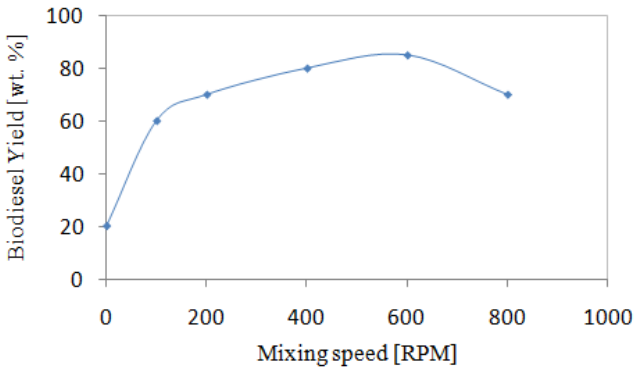


Fig. 7: Effect of stirring speed (RPM) on oil conversion efficiency, under 20 vol% methanol, 1 wt.% KOH, at 80 min reaction time and 60ºC temperature.

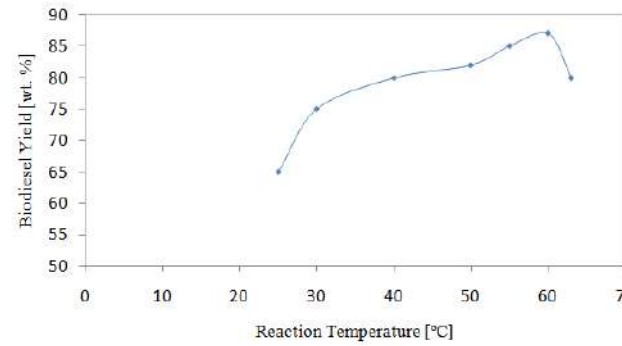


Fig. 6: Effect of reaction temperature on oil conversion efficiency, under 20 vol% methanol, 1 wt.% KOH at 80min reaction time and 600 RPM.

form sodium methoxide ($CH_3ONa$). The behavior of NaOH concentration regarding the biodiesel production yield is shown in Fig. 9.

The highest biodiesel yields (86%) were obtained with a 1% catalyst concentration. However, as the concentration of KOH increased over 1%, biodiesel production decreased due to the formation of an emulsion, which increased the viscosity of the product.

*c. Effect of methanol to methoxide ratio*

KOH is the catalyst of the alkaline esterification reaction to produce biodiesel. It has been followed all the time to used Methoxide to the oil to produce the biodiesel. However, changing the pure Methanol and Methoxide separate samples added to the oil for biodiesel production seems promising. The methanol 5% and Methoxide 15%, 10% of Methanol with 10% of Methoxide and 15% of Methanol and 5% of Methoxide were added separately into oil samples to check the reaction performance of the biodiesel yield. Based on the observations, biodiesel was formed with each case, and yield was analyzed for further processing (Fig. 10).

The maximum yield was achieved at the 5% Methanol and 15% Methoxide sample, around 95%. Other operating

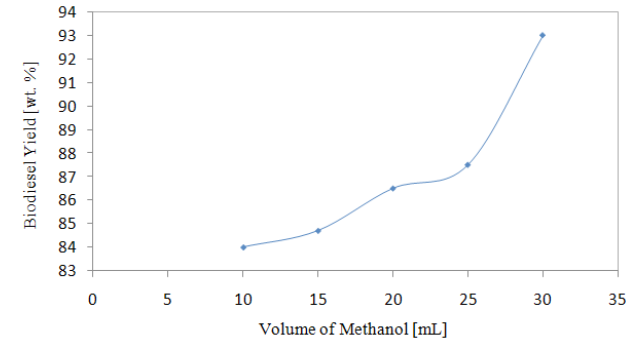


Fig. 8: Effect of Methanol to oil ratio on oil conversion efficiency, under 1 wt.% KOH, at 80min reaction time and 60ºC temperature.

parameters were maintained at the fixed condition during the process, such as reaction time, temperature, KOH concentration, and the RPM of the mixer as base case values. The yield obtained with the new raw material setup was much higher than the conventional methoxide reaction with the oil sample.

*d. Effect of the time interval between methanol and methoxide*

The KOH is not the reactant of the transesterification process; it is only the catalyst. As a result, it is critical to examine catalyst activity to comprehend the catalyst's true significance. It was done by maintaining the time interval between the addition of pure methanol to the oil sample and the addition of methoxide to the reactor constant. The biodiesel process was performed and the yield of the process was examined by varying the time interval. The 'x' axis of Fig. 11 indicates the time between methanol to methoxide feeding. However, the total reaction time was maintained as 90 min for the production process. Fig. 11 shows no significant variation of the yield with the different time intervals of methanol and methoxide. For the reaction to begin, methanol and methoxide must be added to the oil sample at the same time. The methanol sample was introduced to the oil sample at a 70-minute interval for methoxide addition, with a maximum yield of 95%. Following that, the biodiesel yield decreased. Therefore, 20 min of reaction time (90min-70min) is sufficient for biodiesel production with a 95% yield.

Therefore, the experiment is repeated to identify the optimum reaction time with the selected 5% methanol +15% methoxide mixer as the biodiesel process catalyst. The experimental setup we used to develop Fig. 5 is repeated to identify the optimum reaction temperature. Fig. 12 represents the maximum yield that is obtained at 20 min reaction time.

## Biodiesel Quality comparison

The optimum final product of methyl ester developed by optimized parameters was tested for its composition, as shown in Table 3. The methyl ester's primary fatty acid composition

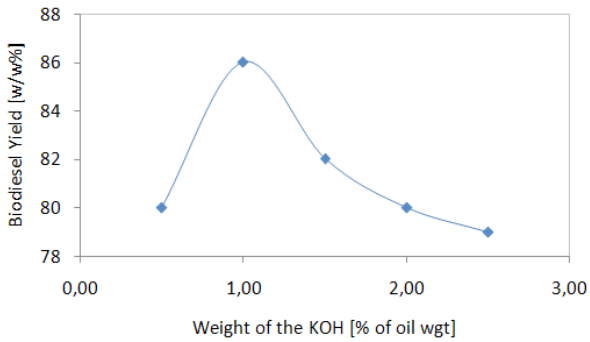


Fig. 9: Effect of catalyst concentration on oil conversion efficiency, under 20 vol% methanol, at 80min reaction time and 60ºC temperature.

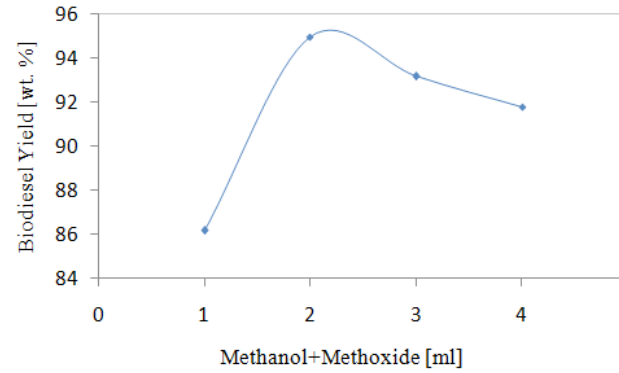


Fig. 10: Effect of methanol to methoxide ratio on oil conversion efficiency, under 20 vol% total methanol, 1 wt.% KOH, at 80min reaction time and 60ºC temperature.
1: 0%Methanol+20% methoxide, 2: 5% methanol+15% methoxide, 3: 10% methanol+ 10% methoxide, 4: 15% methanol+5% methoxide

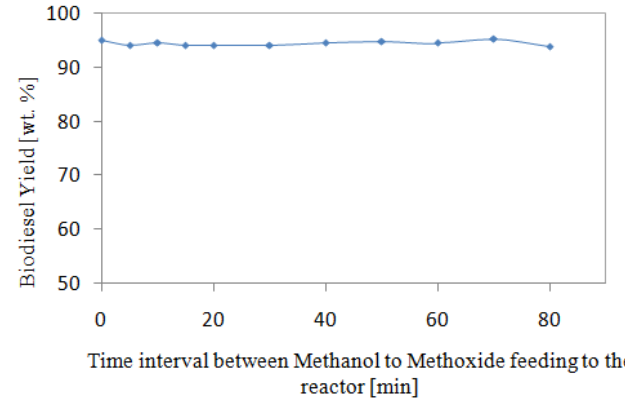


Fig. 11: Effect of the time interval between methanol to methoxide feeding on Oil conversion efficiency, under 20 vol% total methanol, 1 wt.% KOH, at 90min total reaction time and 60ºC temperature.

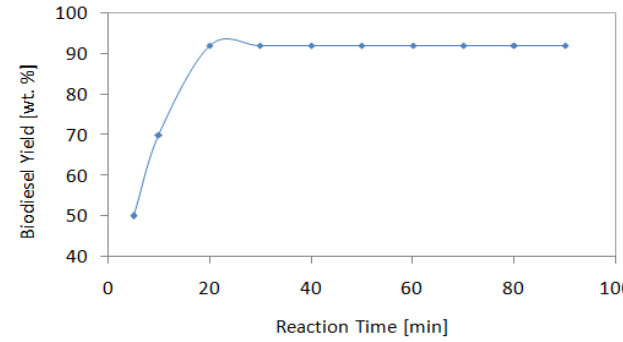


Fig. 12: Effect of reaction time on Oil conversion efficiency, under 5 vol% Methanol + 15%Methoxide, 1 wt.% KOH, at 60 °C and 600 RPM.

Table 3: Fatty acid composition of methyl ester (biodiesel).

| Acid type | Formula | Method | Composition %[a] |
|---|---|---|---|
| Caproic acid | $C_6H_{12}O_2$ | CML/MM/05/51/003 | 0.34 |
| Caprylic acid | $C_8H_{16}O_2$ | | 6.94 |
| Capric acid | $C_{10}H_{20}O_2$ | | 5.68 |
| Lauric acid | $C_{12}H_{24}O_2$ | | 46.72 |
| Myristic acid | $C_{14}H_{28}O_2$ | | 19.45 |
| Palmitic acid | $C_{16}H_{32}O_2$ | | 9.31 |
| Stearic acid | $C_{18}H_{36}O_2$ | | 2.98 |
| Oleic acid | $C_{18}H_{34}O_2$ | | 6.78 |
| Linoleic acid | $C_{18}H_{32}O_2$ | | 1.65 |
| Arachidic acid | $C_{20}H_{40}O_2$ | | 0.09 |
| Linolenic acid | $C_{18}H_{30}O_2$ | | 0.04 |
| Behenic acid | $C_{22}H_{44}O_2$ | | 0.02 |

a: Tested by the Chemical and Microbiological Laboratory, Industrial Technology Institute (ITI), Colombo 07, Sri Lanka

Table 4: Analysis of physical and chemical properties of biodiesel and petroleum diesel.

| Parameter | Test Method | Values achieved in this study[a] | Petroleum diesel[b] | Standard Biodiesel - EN14214[b] |
|---|---|---|---|---|
| Density [15ºC, $kg.m^{-3}$] | ASTM D 1298- 99 | 884.3 | NA | 860-900 |
| Flash Point [ºC] | ASTM D 3278-96 | 109 | >65 | >101 |
| Cloud Point [ºC] | ASTM D 2500 - 99 | 8.0 | NA | NA |
| Kinematic Viscosity at [40ºC, cSt] | ASTM D 445 - 01 | 3.842 | 3.0 - 8.0 | 3.5 - 5.0 |
| Total sulfur content [wt. %] | ASTM D 129-00 | 0.003 | <0.05 | <0.01 |
| Moisture content [wt. %] | ASTM D 4377 - 00 | 0.20 | NA | <0.05 |
| Gross calorific value moisture free basis [$MJ.kg^{-1}$] | ASTM D 240 - 06 | 39.3 | 41.8 | NA |
| Micro carbon residue [m/m%] | ASTM D 4530-06 | 0.06 | 0.3 | 0.3 |
| Total acid number [mg $KOH.g^{-1}$] | ASTM D 664/18 | 0.20 | <0.1 | <0.5 |
| Cetane index | ASTM D - 91 | 39.5 | >49 | >51 |

a: Tested by the Petroleum and Lubricant Testing Laboratory, Industrial Technology Institute (ITI), Colombo 07, Sri Lanka
[b]: Meng et. al, 2008.

is methyl laurate, 46.72%, methyl myristate 19.45%, and methyl palmitate, 9.31%. The fatty acid type and composition analysis influence the cetane number, affecting ignition quality in the engine.

The physical and chemical properties play a vital role in the qualifying process of diesel engines' operation. Biodiesel derived from coconut oil was analyzed by Petroleum and Lubricant Testing Laboratory, Industrial Technology Institute, Sri Lanka, and the results are shown in Table 4.

Biodiesel, as an alternative fuel, should have some physical and chemical properties that make it suitable for use in diesel engines. These properties play a vital role in quality control in the petroleum industry. Biodiesel derived from fresh coconut oil was analyzed at the Petroleum and Lubricant Testing Laboratory, Industrial Technology Institute (ITI), Colombo 07, Sri Lanka, and the results are shown in Table 4. As is indicated, the biodiesel sample meets EN14214 standards for density, kinematic viscosity, carbon residue, and acid value. The increased flashpoint of the biodiesel sample produced is advantageous for safe operation The decreased sulfur concentration is beneficial since it lowers $SO_2$ emissions during the combustion process.

## CONCLUSION

The following values were obtained for the maximum yield; Reaction time: 20 min, Reaction temperature: 60ºC,

RPM: 600, Methanol: 20 vol%, KOH: 1 wt.%, Methanol + Methoxide: 5%+15%. A maximum biodiesel yield of 95% is achieved with the optimized operating conditions. It has been shown that adding fresh methanol and methoxide into the coconut oil sample produces a higher yield of biodiesel with minimum reaction time. Rather than the conventional biodiesel production method, this process of biodiesel production has less energy consumption as well. The yielded methyl ester was tested for its fuel properties and was in good agreement with the standard biodiesel. However, the use of edible oil for biodiesel production is not encouraging due to the crisis of the food industry. As a result, the results of the experiments are used to improve the production process and operating parameters. Other sources of biodiesel production such as waste cooking oil, algal oil, non-edible oil should be implemented with the optimized operating conditions.

## ACKNOWLEDGMENT

The authors express their gratitude to the AHEAD project (RIC-2) of the World Bank for the financial support provided for this study.

## REFERENCES

Andrew, F. and Chris, M. 2020. Earth's Carbon Dioxide Levels Hit a Record High, Despite Corona Virus-Related Emissions Drop. https://www.washingtonpost.com/weather/2020/06/04/carbon-dioxide-record-2020/.

Banerjee, A. and Chakraborty, R. 2009. Parametric sensitivity in transesterification of waste cooking oil for biodiesel production: A review. Resour. Conserv. Recycl., 53: 490-497.

Bournay, L., Casanave, D., Delfort, B., Hillion, G. and Chodorge, J.A. 2005. New heterogeneous process for biodiesel production: A way to improve the quality and the value of the crude glycerin produced by biodiesel plants. Catal. Today, 106(1-4): 190-192.

Braga, E.A.S, Malveira, J.Q, Milhome, M.A.L, Aquino M.D. and Nascimento, R.F. 2015. Characterization of the fatty acids present in wastewaters from the production of biodiesel tilapia. J. Chem., 4: 1-6.

Corro, G., Tellez, N., Jimenez, T., Tapia, A., Banuelos, F. and Vazquez-Cuchillo O. 2011. Biodiesel from waste frying oil: Two step process using acidified SiO2 for esterification step. Catal. Today, 166: 116-122.

Endang, S.R., Yerizam, M. and Martha, P. 2018. Biodiesel production from waste cooking oil. Indones. J. Fundam. Appl. Chem., 3(3): 77-82.

Enweremadu, C.C. and Mbarawa, M.M. 2009. Technical aspects of production and analysis of biodiesel from used cooking oil: A review. Renew. Sustain. Energy Rev., 13: 2205-2224

Manisalidis, I., Stavropoulou, E., Stavropoulos, A. and Bezirtzoglou, E. 2020. Environmental and health impacts of air pollution: A review. Front. Public Health, 8: 14.

Meng, X., Chen, G. and Wang, Y. 2008. Biodiesel production from waste cooking oil via alkali catalyst and its engine test. Fuel Process. Technol., 89: 851-857.

Ogunwole, O.A. 2012. Production of biodiesel from jatropha oil (curcas oil). Res. J. Chem. Sci., 2(11): 30-33.

Onyinyechukwu, J.C., Christiana, N.O., Chukwudi, O. and James, C.O. 2018. Lipase in biodiesel production. Afr. J. Biochem. Res., 12(8): 73-85.

Our World Data. n.d. Research and Data to Make Progress Against the World's Largest Problems. https://ourworldindata.org/

Paraj, R.K., Nikul, K.P. and Mehul, P.B. 2019. Design and development of small-scale biodiesel production unit. Int. J. Fluid Thermal Eng. Peer-Rev. J., 4(1): 8-13.

Phan, A.N. and Phan, T.M. 2008. Biodiesel production from waste cooking oils. Fuel, 87: 3490-3496.

Swapan, K.G. and Bablu, K.G. 2020. Fossil fuel consumption trend and global warming scenario: Energy overview. Glob. J. Eng. Sci., 5(2): 606

Wanodya, A.K. and Arief, B. 2013. Synthesis of biodiesel from second-used cooking oil. Energy Procedia, 32: 190-199.

Nature Environment and Pollution Technology
An International Quarterly Scientific Journal

p-ISSN: 0972-6268
(Print copies up to 2016)
e-ISSN: 2395-3454

Vol. 20 | No. 5 (Suppl) | pp. 1981-1987 | 2021

Original Research Paper

https://doi.org/10.46488/NEPT.2021.v20i05.014

Open Access Journal

# Groundwater Recharge Planning Using Field Survey for Talupula Mandal in Anantapur District, Andhra Pradesh, India

**K. Nagamani*†, Prabhu Dass Batvari**, S. Packialakshmi***, C. Sai Kumar Reddy*** and B. Anuradha******

*Center for Remote Sensing & Geoinformatics, Sathyabama Institute of Science & Technology, Chennai, India
**Center for Earth and Atmospheric Science, Sathyabama Institute of Science & Technology, Chennai, India
***Department of Civil Engineering, Sathyabama Institute of Science & Technology, Chennai, India
****Chennai Institute of Technology, Chennai, India
†Corresponding author: K. Nagamani; nagamaniloganathan@gmail.com

**Nat. Env. & Poll. Tech.**
**Website: www.neptjournal.com**

*Received:* 30-07-2021
*Revised:* 25-08-2021
*Accepted:* 03-09-2021

**Key Words:**
Groundwater
Recharge
Resistivity
Pseudo graphs
Semi-arid area

## ABSTRACT

Groundwater is essential to the sustainability of India's environment, economy, and living conditions because it isn't just the primary source of domestic supply of water in rural areas, but it is also the major and most productive origin of the water. The increased demand for groundwater as a result of reduced rainfall has put a strain on groundwater resources in areas where groundwater is the primary supply of water. The main aim of this study is to identify and explore the groundwater potential zones in Talupula Mandal of 280.3 $km^2$ in Ananthapur district in Andhra Pradesh, India with semi-arid climatic conditions. Based on the field survey approach, groundwater availability is found out in the villages. Schlumberger Vertical Electrical Sounding (VES) survey technique was used to discover the resistivity and thickness of the unmistakable layers. It was carried out in 18 randomly selected sites where groundwater plays an important role in agricultural and domestic use. The thickness and resistivity of first- and second-layer crack sites of the various layers were separated from ground data using IPI2WIN programming. Using software, graphs were plotted and groundwater potential zones were identified for recharging the groundwater. Based on the results, different models of recharge structures for the study area are identified and recommended. Hence the management of groundwater paves the way for sustainable groundwater levels.

## INTRODUCTION

Groundwater is essential for the growth of the country's economy, ecosystem, and living standards. Groundwater movement in an area is influenced by topography, geological structure, lithology, the extent of the fracture, depth of weathering, slope, land use and land cover, drainage pattern, climatic conditions, and the interrelationships between these factors. Geology, soil texture, permeability, drainage intensity, soil depth, soil physiography, water holding capacity of the soil all influence the delineation of potential zones for both natural and artificial recharge (Alwathaf & Mansouri 2011, George et al. 2011, Chandramohan et al. 2017). In semi-arid and arid zones, the problem of getting a sufficient supply of groundwater has always been a major concern of social orders. Even in zones with more and more abundant rainfall, the problem of getting a sufficient supply of groundwater is often turning out to be tougher due to increasing population and industrialization (Srinivasamoorthy et al. 2014, Zeinelabidin et al. 2015). As a result, this investigation focuses on options, as surface water cannot be relied upon on a constant basis, necessitating the search for other options to improve surface water (Vidhya & Vinay 2018, Hammouri et al. 2013). As a result, the world is forced to rely on the most accessible source of high-quality freshwater, which is found underground as groundwater.

### Study Area

Talupula Mandal is located in the Anantapur District's southeastern part in Andhra Pradesh which lies between $77^0$30' - $78^0$15'E and $14^0$0' - $14^0$30'N and it belongs to the Rayalaseema region. It is bounded on the west by Kadiri Mandal, on the south by Gandlapenta Mandal, on the north by Vemula Mandal, and on the east by Vempalle Mandal. The total population of Talupula Mandal is 42,019 living in 10,377 Houses, Spread across a total of 115 villages and 16 panchayats. Males are 21,451 and Females are 20,568. The climate in Talupulamandal is semiarid, with a moisture index of 33.7%, with its monthly average temperatures ranging

from 15° C in winter to 39° C in summer. The district's average precipitation is 553 mm, which is the lowest in Andhra Pradesh when compared to other districts. The study area is shown in Fig.1.

## MATERIALS AND METHODS

The study area and base map were prepared using Survey of India Topographical sheet nos. 57 J/3, J/4, F/14, F/15. The Schlumberger Vertical Electrical Sounding (VES) method was used for the resistivity survey. The corresponding field study was conducted in 18 different locations. (Fig.2) in Talupula Mandal, where there is the availability of aquifers. The Schlumberger VES field survey was completed by dividing the electrode spacing by 100 m. The spacing between the current electrodes (AB/2) varied from 0.5 to 100 m, while the spacing between the potential electrodes (MN/2) varied from 0.5 to 10 m. IPI2WIN software was used to convert the collected data into graphs, and the thickness and resistivity of various layers were determined.

## RESULTS AND DISCUSSION

### Electric Resistivity

Resistivity is a measure of how difficult it is to make an electrical current flow through it. It is also known as specific electrical resistance or volume resistivity, though these terms are less commonly used. Despite the fact that some materials are better than others at resisting the passage of electricity,

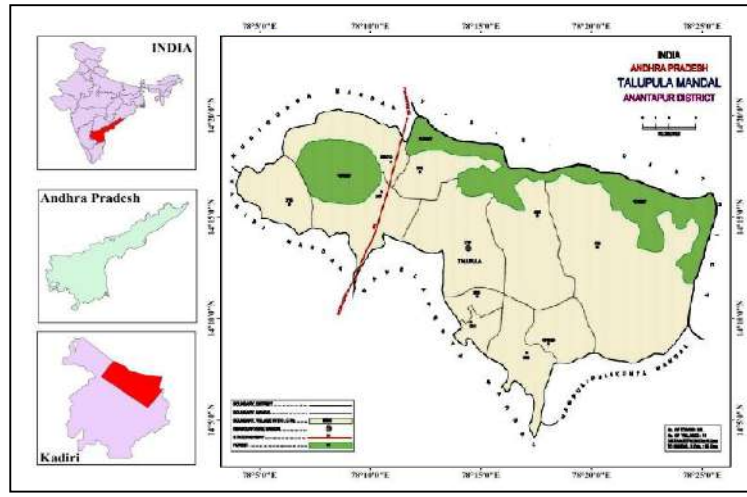


Fig. 1: Study area map of Talupula Mandal.

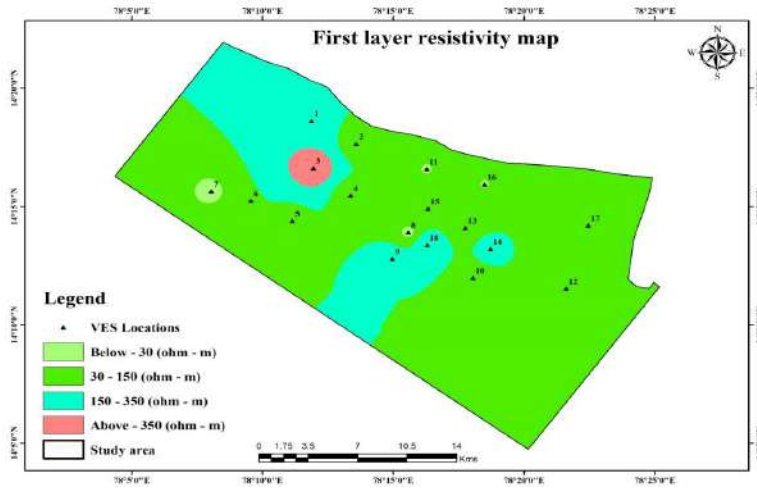


Fig. 2: First layer resistivity map.

some are better at leading it. Resistivity is an assumption that enables examinations of how various materials permit or oppose flow (Bera & Ahmad 2017, Singh et al. 2019). To make resistivity records meaningful, explicit units are used, and for a given size of material, there are equations for determining it and relating it to the obstruction in Ohms. Materials with a low resistivity that effectively lead electrical flow are known as channels (Arfan et al. 2020, Khan et al. 2018). Covers are those that do not effectively direct electrical flow, and these materials have a high resistivity.

**Electric Resistivity Survey**

Electrical resistivity surveys are carried out by passing a known electric current through the ground using two electrodes and calculating the potential differences between the other two potential electrodes. The potential variations may be changes due to the size, shape, and conducting capacity of the material in the subsurface, and the resistance is calculated based on the quantities of potential differences and the current applied (Abrams et al. 2018, Kaliraj et al.2018).

**Resistivity Layer Maps**

The resistivity of the study area has been separated into five layers. Each layer has its own significance and characteristics. It helps to identify the resistivity of each layer.

**Demarcating the Resistivity Layers in Groundwater Potential Region Using Resistivity Survey**

***First Layer Resistivity Map***

In the study area, the first layer is the topmost layer, which is the weathered material of basement rock. A low value of resistivity in the first layers is referred to as clayey formation and it is not good for surface recharge potential.

Resistivity ranges of 30-150 are good for surface recharge structures like percolation ponds and lakes. The first layer resistivity is shown in Fig. 2**.**

***Second Layer Resistivity Map***

The second layer is the weathered formation of basement rock. The second layer's low resistivity is associated with the presence of highly weathered areas and is suitable for recharging through injection wells. Highly weathered areas can be seen in the northern section of the study area. The second layer resistivity map is shown in Fig.3.

***Third Layer Resistivity Map***

The third layer is circulated by fractured formation. An injection well is used to place fluid underground into porous geologic formations. Water can be recharged directly into the location (subsurface) through deep injection wells. Most of the study area is occupied with higher resistivity areas and it is the base of the study area. Locations 6 and 12 may be recharged in third layer conditions. Fig. 4 shows the resistivity map of the 3rd layer.

***Fourth Layer Resistivity Map***

The fourth layer is the secondary fracture formation. A borewell structure can be built in this location. The entire study area has high resistivity; it is not suitable for recharging expect in location numbers 6, 13, and 14. The layer one by one defines the significant characteristic of the layer. The more it goes deeper the more the compacted layers are found. Fig. 5. shows the resistivity map of the fourth layer.

***Fifth Layer Resistivity Map***

The fifth layer is known as secondary fracture formation with

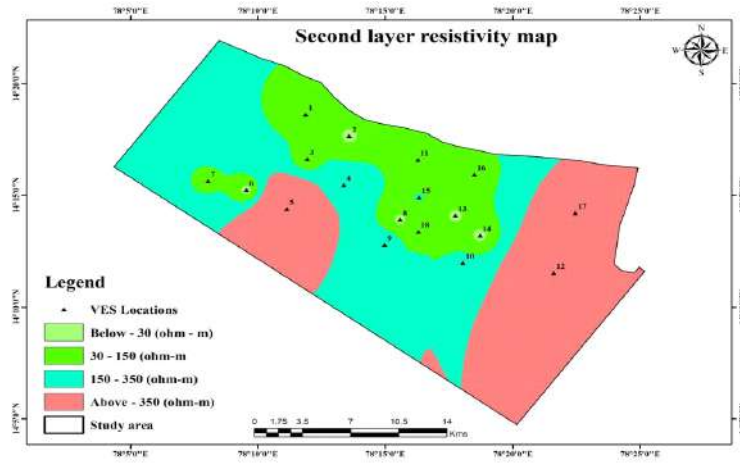


Fig. 3: Second layer resistivity map.

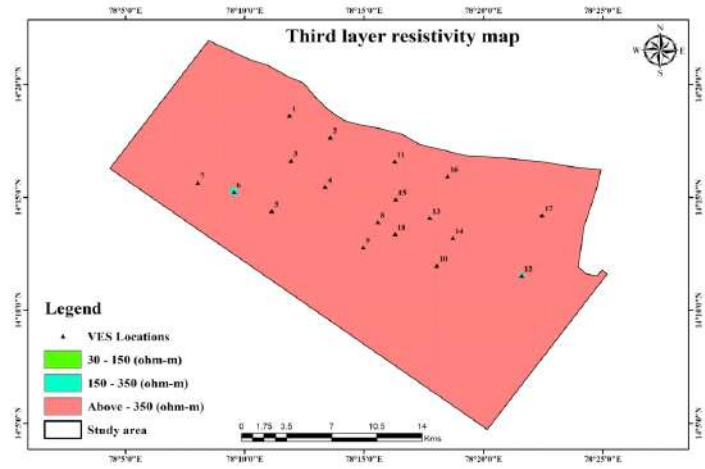


Fig. 4: Third layer resistivity map.

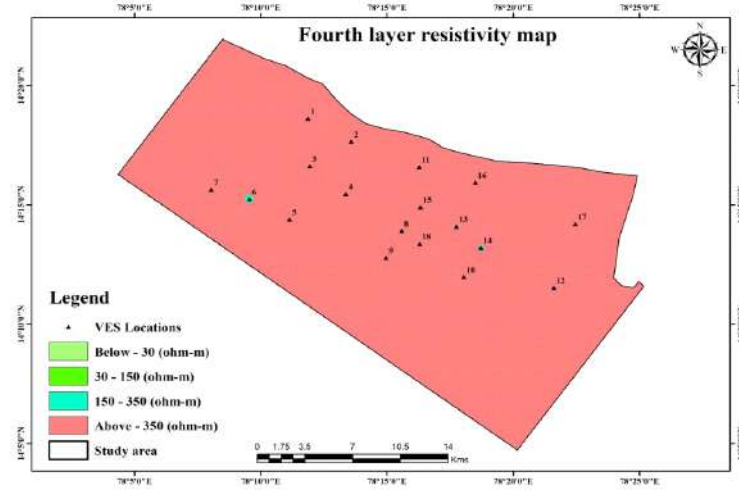


Fig. 5: Fourth layer resistivity map.

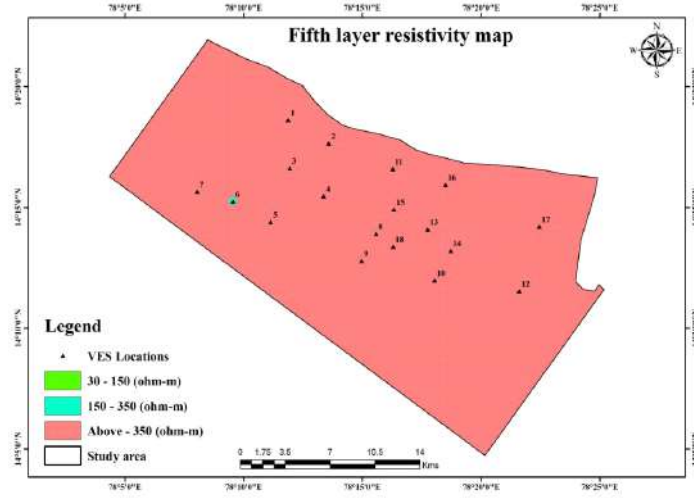


Fig. 6: Fifth layer resistivity map.

a non-potential stage, and it is also used to build a recharge bore well structure. This fracture exists at location number 13, and this zone can only be recharged. Fig. 6. shows the resistivity map of the fifth layer.

### *Thickness Layer Map*

Thickness is also an important aspect of groundwater recharge. The study area was divided into four layers based on its thickness. It defines the depth of each layer. Every layer has its own significance and characteristics.

### Demarcating the Thickness Layers in Groundwater Potential Region Using Resistivity Survey

### *First Layer Thickness Map*

Groundwater recharge is high in densely populated areas. Locations 15, 16, and 17 in this layer have a better chance of being recharged from surface resources. The thickness map of the first layer is shown in Fig. 7.

### *Second Layer Thickness Map*

The second layer shows the weathered zones. Thickness is more in this layer. Hence, this layer is good for groundwater recharge. Injection wells are the most effective method of recharging. The weathered zone is defined as the superficial layer of Earth's crust above the water table that is exposed to atmospheric destructive agents and where soils develop. Fig. 8 shows the thickness map of the second layer.

### *Third Layer Thickness Map*

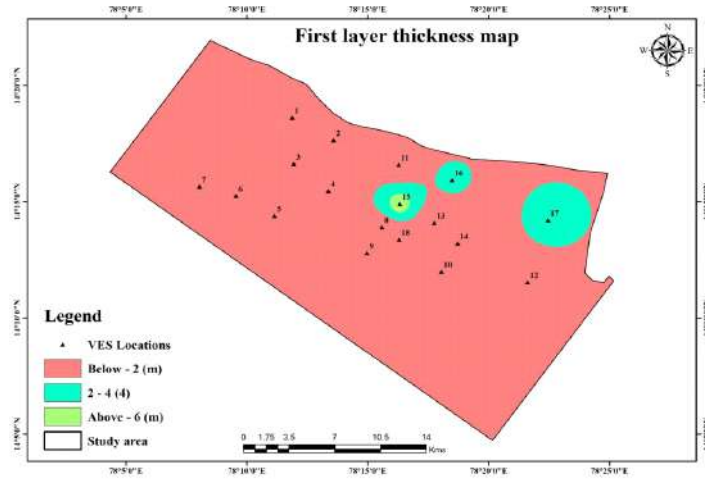


Fig. 7: First layer thickness map.

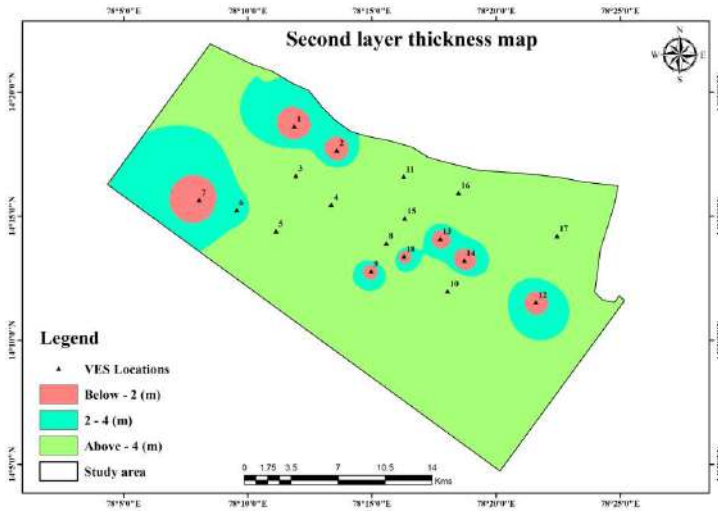


Fig. 8: Second layer thickness map.

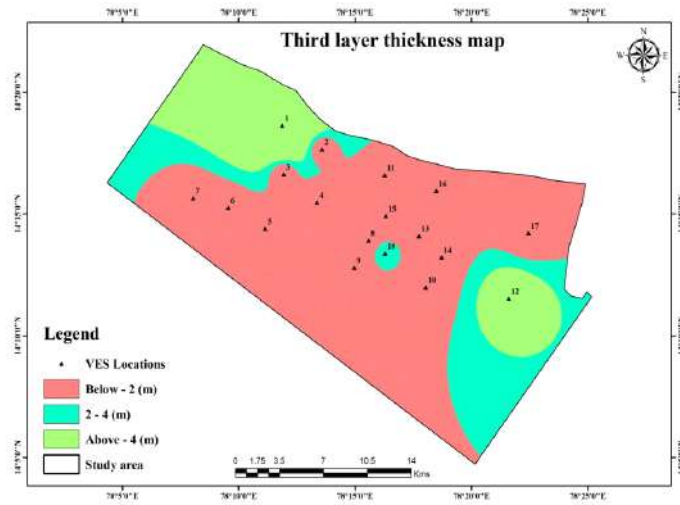


Fig. 9: Third layer thickness map.

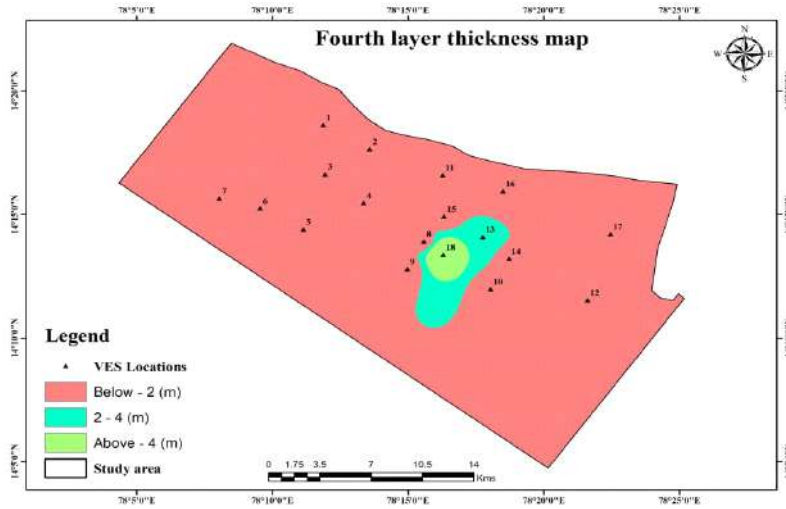


Fig. 10: Fourth layer thickness map.

In the third layer, recharging possibilities are very less because of its thickness. Location numbers 1, 12, and 18 are suitable for recharging. Fig**.** 9 shows the thickness map of the third layer.

### Fourth layer thickness map

Except at site number 18, the recharging is essentially unsuitable in this layer due to lesser fracture thickness. Fig.10 shows the thickness map of the fourth layer.

## CONCLUSION

This research has shown that a resistivity survey is useful to identify the groundwater potential zones in many possible ways. Several methodologies can be recommended for carrying out resistivity surveys of potential zones. Schlumberger's method is very easy and gives accurate output. As a result, groundwater potential zones for recharging groundwater structures were found among the 18 places in the study region, Talupulamandal of Toposheet Nos. 57 J/3, J/4, F/14, F/15. According to the resistivity survey, it is found that these seven locations Lakka Samudram, Gajjelappagaripalli, Bateripalli, Vepamanupeta, Gurramgundlapalli, Gangivaripalli, Poolavandlapalli, have more water potential for constructing groundwater recharge structures.

## REFERENCES

Abrams, W., Ghoneim, E., Shew, R., LaMaskin, T., Al-Bloushi, K., Hussein, S., AbuBakr, M., Al-Mulla, E., Al-Awar, M. and El-Baz, F. 2018.

Delineation of groundwater potential (GWP) in the northern United Arab Emirates and Oman using geospatial technologies in conjunction with simple additive weight (SAW), analytical hierarchy process (AHP), and probabilistic frequency ratio (PFR) techniques. J. Arid Environ., 157: 77-96.

Alwathaf, Y. and Mansouri, B.E. 2011. Assessment of aquifer vulnerability based on GIS and ARCGIS methods: A case study of the Sana'a Basin (Yemen). J. Water Resour. Prot., 3: 845-855.

Arfan, A., Zhijie, Z., Wanchang, Z. and Adil, D. 2020. Mapping favorable groundwater potential recharge zones using a GIS-based analytical hierarchical process and probability frequency ratio model: A case study from an agro-urban region of Pakistan. Geosci. Front., 11(5): 1805-1819.

Bera, S. and Ahmad, M. 2017. Delineation of groundwater potential zones in Dhanbad district, Jharkhand, using Remote Sensing and GIS Techniques. Int. Res. J. Eng. Technol., 03: 2395-0072.

Chandramohan, R., Kanchanabhan, T.E., Siva Vignesh, N. and Krishnamoorthy, R. 2017. Integrated techniques to identify groundwater potential region in Palani Taluk, Tamilnadu, India using electric resistivity, remote sensing, and GIS techniques. ARPN J. Eng. Appl. Sci., 12(22): 6309-6319.

George, N.J., Obianwu V.I. and Obot, I.B. 2011. Estimation of groundwater reserve in the unconfined frequently exploited depth of aquifer using a combined surficial geophysical and laboratory techniques in the Niger Delta, South Nigeria. Adv. Appl. Sci. Res., 2(1): 163-177.

Hammouri, N., Amoush, H.A., Raggad, M.A. and Harahsheh, S. 2013. Groundwater recharge zones mapping using GIS: A case study in Southern part of Jordan Valley. Arab J Geosci., 7: 2815-2829.

Kaliraj, S., Chandrasekar, N. and Magesh, N. 2014. Identification of potential groundwater recharge zones in Vaigai upper basin, Tamil Nadu, using GIS-based analytical hierarchical process (AHP) technique. Arab. J. Geosci., 7: 1385-1401.

Khan, A.D., Ashraf, M., Ghumman A.R. and Iqbal, N. 2018. Groundwater resource of Indusplain aquifer of Pakistan investigations, evaluation, and management. Int. J. Water Resour. Arid Environ., 7: 52-69.

Singh, S.K., Zeddies, M., Shankar, U. and George, A.G. 2019. Potential groundwater recharge zones within New Zealand. Geosci. Front., 10(3): 1065-1072.

Srinivasamoorthy, K., Chidambaram, S., Vasanthavigar, M., Anandhan, P. and. Sarma, V.S. 2014. Geophysical investigations for groundwater in a hard rock terrain, Salem district, Tamil Nadu, India, Bull. Eng. Geol. Environ., 73: 357-368.

Vidhya, L. and Vinay, K.R. 2018. Identification of groundwater potential zones using GIS and remote sensing. Int. J. Pure Appl. Math., 119(17): 3195-3210.

Zeinelabidin, E., Hassan, R., Garamoon, K., Ahmed, S., Al Matari, M., Khalil, F. and Ebraheem, A.M. 2015. Application of earth resistivity, hydrogeochemistry, and isotope hydrology methods for assessment of groundwater recharge in two drainage basins in Northeastern United Arab Emirates. IOSR J. Appl. Geol. Geophys., 3(6): 01-13.

Nature Environment and Pollution Technology
An International Quarterly Scientific Journal

p-ISSN: 0972-6268
(Print copies up to 2016)
e-ISSN: 2395-3454

Vol. 20 | No. 5 (Suppl) | pp. 1989-1995 | 2021

Original Research Paper

https://doi.org/10.46488/NEPT.2021.v20i05.015

Open Access Journal

# Consideration and Application of Evaluation Indicators of Regional Circular and Ecological Sphere (CES) for the Utilization of Woody Biomass

**Yajuan Li*†, Toru Matsumoto** and Atsushi Fujiyama****

*Course of Environmental and Ecological Systems, Graduate Programs in Environmental Systems Graduate School of Environmental Engineering, The University of Kitakyushu, Hibikino 1-1, Wakamatsu-ku, Kitakyushu-shi, Fukuoka 808-0135, Japan

**Faculty of Environmental Engineering, The University of Kitakyushu, Hibikino 1-1, Wakamatsu-ku, Kitakyushu-shi, Fukuoka 808-0135, Japan

†Corresponding author: Yajuan LI; liyajuan0107@gmail.com

**Nat. Env. & Poll. Tech.**
**Website: www.neptjournal.com**

*Received:* 13-07-2021
*Revised:* 06-09-2021
*Accepted:* 03-09-2021

**Key Words:**
Woody biomass energy
GIS
Regional circulation symbiotic area
SDGs

## ABSTRACT

The "Regional Circular and Ecological Sphere" takes advantage of the SDGs' concept of integrated solutions to numerous concerns, complementing and supporting resources based on the region's features while maximizing the utilization of local resources. This research makes a comprehensive evaluation of the three aspects of the environment, economy, and society. First, formulate the evaluation indicators of the regional circulation symbiosis zone. Then, choose the cutting conditions of trees according to geographical factors, use the thinning forecasting system and forest GIS data to evaluate the supply potential of thinned wood in the area, and calculate the heat and power generation of wood biomass. According to the above analysis and calculation, 12,000 tons of unused wood chips can be supplied per year for 36 years from 2016 to 2051. From the economic point of view, the purchase of wood chips of 146 million yen due to the local circulation of wood fuel is expected to save about 50 million yen in intermediate input. And it is estimated that if 12,000 tons of unused wood chips can be supplied in the city per year, and about 98.4 million yen can be saved annually. Finally, from a social perspective point of view, biomass power generation of unused thinned timber using materials worth about 146 million yen is expected to create about 20 jobs.

## INTRODUCTION

The "Regional CES" is one of the main initiatives of Japan's "Fifth Environmental Basic Plan," which was approved by the Cabinet in 2018, and each area uses its unique qualities to leverage its strengths. It entails establishing a larger network by establishing a self-sustaining and decentralized community in which resources circulate while coexisting and communicating with neighboring areas.

Since 2013, Kitakyushu City has been promoting a "regional energy base promotion project," and biomass utilization plays a vital role as a renewable energy source, but it also has a strong affinity with regional symbiotic sphere measures. Furthermore, attempts to accomplish the United Nations Sustainable Development Goals (SDGs) are widely recognized as significant, but biomass consumption has the potential to affect not only the environment but also many other fields. It needs to be considered as a goal to be considered. The purpose of this study is to estimate the availability of woody biomass in Kitakyushu City and to make a comprehensive evaluation from the three aspects of environment, economy, and society. First, we will evaluate the regional circulation symbiosis area's evaluation index. The amount of thinned timber supply potential in the region is assessed using the thinning harvest prediction system and forest GIS data, followed by power generation and heat consumption using woody biomass. Evaluate low carbon and resource-saving effects by substituting fossil resources and reducing long-distance transportation. Third, estimate the amount of direct job creation.

## MATERIALS AND METHODS

### Examination of Evaluation Index

**Environment:** In this study, evaluation indexes were examined from the three aspects of environment, economy, and society. In addition to the concept of the regional circulation symbiotic area, the evaluation index was set based on the evaluation index of SDGs. Although forests cover 38% of the Kitakyushu metropolitan area (approximately 18,598 ha), the forestry sector is dormant, and the trees

are still being cut down even after thinning, and the forests are not being used properly. From an environmental point of view, the planned use of unused thinned wood not only leads to the maintenance and management of healthy forests but also contributes to the maintenance and improvement of ecosystem services. Utilizing the woody biomass resources in the region can be regarded as a sustainable and ideal regional resource.

**Economy:** From the perspective of supporting the region such as city life and industrial activities, the purchase of fossil fuels has been reduced by shifting to a low carbon / decarbonized society, creating a sustainable economic society that embodies the SDGs and introducing renewable energy. It can also be expected to have the effect of reducing the amount of money that flows out of the region.

**Society:** By incorporating the perspective of a low-carbon society and a recycling-oriented society, the degree of contribution to a sustainable society will increase, so local companies and individuals will participate to build a regional economy and create new employment. Indexes are selected and evaluated in consideration of regional characteristics. The indicators set in Table 1 below are shown, and the indicators evaluated in this study were marked those indicators in blue.

## Forest Resources and $CO_2$ Absorption

**Estimating forest resources:** In the forest resource survey, the number of forest resources was estimated using the Kitakyushu City Forest Book (Kitakyushu City Forest Book 2016) and the GIS-based forest interpretation data.The area estimation results for each tree species are shown in Table 2.

The forest area of Kitakyushu City is 18,598 ha, of which the area covered by the regional forest plan (private forest area) is 15,727 ha and the forest ratio is about 38%. Of the privately owned forests, the planted forest is about 4,622 ha, and the area of Japanese cedar and Cypress occupies about 90.8%. The distribution ratio of each tree species is shown in Fig. 1.

It was also taken into consideration that about 70.5% of the total are 10 years old (Fukuoka Area Forest Plan 2016) or older and that the planted forest resources are mature and need to promote forest circulation when they reach the utilization period.The age distribution map of Japanese cedar and cypress is shown in Fig. 2.

**Setting thinning conditions:** For deforestation (including main deforestation, thinning, and deforestation), the presence or absence of forest roads, steep slopes and the situation of the surface, and the possibility of carrying out should be taken into consideration.

Table 1: Discussion on evaluation index.

| | Index | Building a Regional CES area | SDGs goal |
|---|---|---|---|
| | Forest resources | Contributing to the maintenance and improvement of ecosystem services by contributing to the maintenance and management of healthy forests. | 15.2 By 2020, promote the implementation of sustainable management of all types of forests and so on |
| | Land use change | | |
| | Carbon stock | | |
| | CO2 absorption | The transition to a low-carbon/decarbonized society and the creation of a sustainable economic society that embodies the SDGs. | 7.2 By 2030, increase substantially the share of renewable energy in the global energy mix |
| Environment | Fossil fuel consumption by use | | |
| Economy | Volume of thinned timber and amount that can be used as woody biomass | Proper thinning will produce high-quality timber while maintaining the biodiversity of the forests, while aiming to reduce CO2 by using thinned wood as heat energy. | 7.a enhance international cooperation to facilitate access to clean energy research and technology, including renewable energy, energy efficiency and advanced and cleaner fossil-fuel technology, and promote investment in energy infrastructure and clean energy technology |
| | Electricity/thermal efficiency of woody biomass and creation of economic value | Local resources are circulated by utilizing the woody biomass resources of the area.x | |
| | Collection and transportation costs for carrying out thinned wood, etc. | - | - |
| Society | Amount of food supply (such as bamboo shoots) | Including delicious food and materials, disaster prevention and mitigation functions, life culture and recreation, etc. | 2. End hunger, achieve food security and improved nutrition and promote |
| | Number of jobs created by forestry employees | local companies and individuals will participate to build a regional economy and create new jobs. | 8.9 By 2030, devise and implement policies to promote sustainable tourism that creates jobs and promotes local culture and products |

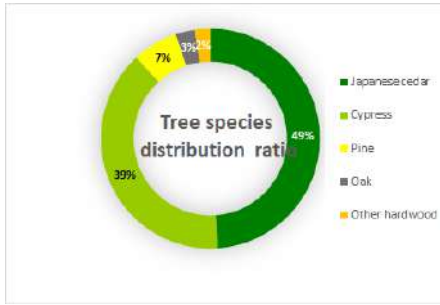


Fig. 1: Tree species distribution ratio.

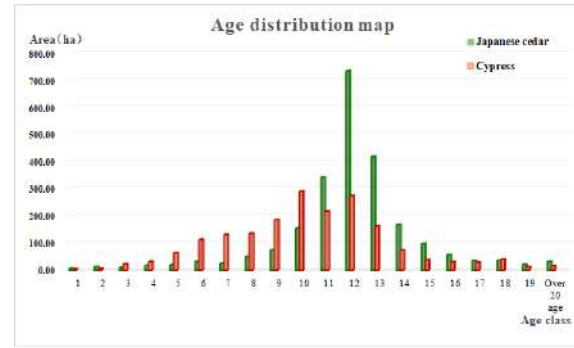


Fig. 2: Japanese cedar and cypress age distribution map.

In this study, set the thinning conditions for the maintenance of the planted forests:

- Inclination angle of planted forest (35 degrees or less)
- Distance from planted forest to a forest road (within 500m)
- Distance from plantation to the sawmill (within 30km)

The reason is that working in areas with an inclination angle of 35 degrees or more is dangerous and cutting a lot of trees affects the natural stability of the terrain. As a past record, the distance from the forest road is often within about 500 meters. Therefore, the priority of timber cutting is decided based on the above three geographical factors.

In the analysis of ArcGIS, the DEM data for the entire Kitakyushu city was downloaded from the official website of the Geographical Survey Institute of the Ministry of Land, Infrastructure, Transport, and Tourism. hen, using the downloaded data, take out the administrative divisions of Kitakyushu City. Because the raster data transformed by ArcGIS includes data from areas that aren't relevant to our study, the parts other than Kitakyushu City will be cut out using the ArcGIS clip tool.

Fig. 3 shows the use management tool in ArcGIS's Arc toolbox. Using ArcGIS, the raster data of the entire administrative area of Kitakyushu is completely extracted from the map of Fukuoka Prefecture

Fig. 4 shows all slope and shadow calculations are performed using the map algebra operation of the Arc toolbox

Table 2: Area of each tree species.

| Tree species | Area [ha] |
|---|---|
| Japanese cedar | 2,328.8 |
| Cypress | 1,868 |
| Pine | 318.2 |
| Oak | 135.72 |
| Other hardwood | 107.42 |

special analyst tool. Once the calculation is completed, the map algebra operation of the special analyst tool can be used to extract the terrain data of the slope above or below the specified value.

Fig. 5 shows the polyline data of the forest road is targeted, and the buffer map of the forest road is created by using the buffer analysis of ArcGIS to create the area around the forest road and the surrounding area of 500 me-

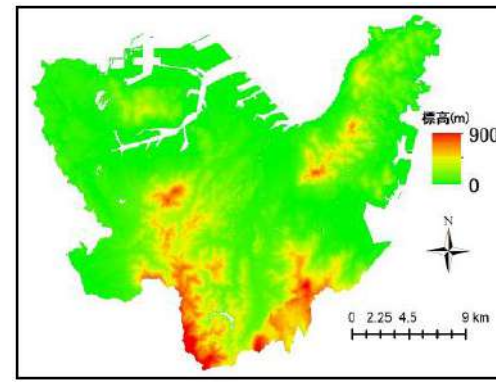


Fig. 3: Topographic raster data of Kitakyushu area.

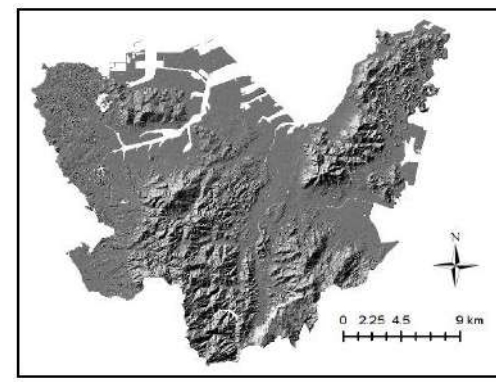


Fig. 4: Topographic shadow map of Kitakyushu area.

ters. Then combine the distribution map of the forest with a buffer map.

The forest composition of both Japanese cedar forest and cypress forest peaked at 51-60 years old, and 46-60 years old dominated when the forest area by tree type and age was validated from the forest book.

**Estimating thinned wood that can be harvested from plantations:** To estimate the available thinned wood, first, use the Kitakyushu City Forest Book Data (2016) and the Fukuoka Prefecture Japanese cedar/cypress Plantation Harvest Prediction System (Narasaki et al. 2015)

To determine the annual amount of thinned woodcut among unused wood, the author made a trial calculation.

In addition, to examine the study's long-term sustainability, the degree of growth was calculated using the artificial forest in Fukuoka Prefecture's stand density control chart (Narasaki et al. 2015) and the Fukuoka Prefecture's volume table (Forestry Agency 2018).

Looking at the results of the annual thinning possible amount estimation of Japanese cedar/cypress as shown in Fig. 6, we can see the trend of yearly decrease. According to the 2016 version of the forest book data, medium-aged Japanese cedar/cypress trees in the planted forest will be cut down in order from the 20th grade (older trees) to the 4th grade (young trees). Therefore, if thinning is done without proper forest management, the number of trees that can be collected will decrease steadily.

**Estimated $CO_2$ Absorption:** The carbon accumulation amount (C) is the bulk density (V) of the thinned wood by tree type obtained by 3-3, the volume density (D), the biomass expansion coefficient (BEF), and the ratio of the underground part to the above-ground part (R), Estimated by multiplying the carbon content (CF) per dry matter weight. The calculation formula is as shown in the following formula (1).

$$C = \sum_j \{[V_j \times D_j \times BEF_j] \times (1 + R_j) \times CF\} \quad \ldots(1)$$

C: Carbon stock amount

V: Volume

D: Bulk density

BEF: Biomass Expansion Factor

R: Ratio of the underground to above ground

CF: Carbon content per dry matter weight

j: Tree species

The amount of CO2 absorbed was calculated by considering its molecular composition (44/12) based on the amount of carbon accumulated.

Each parameter is quoted from the Japan Greenhouse Gas Inventory Report (National Institute for Environmental Studies) (Table 3).

The calculation results are shown in Table 4.

The total amount of carbon dioxide emissions in 2016 was 17,531 thousand tons, and the amount absorbed only for the thinned wood to be harvested was about 0.061%.

## RESULTS AND DISCUSSION

### The Economic Value of Woody Biomass Energy

**The economic value that wood fuel replaces fossil fuel:** Logs harvested from forests cannot be used directly as raw materials for power generation and are processed into wood chips as a type of fuel for woody biomass. Based on the

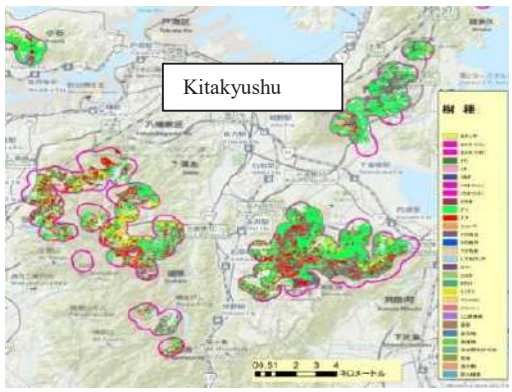


Fig.5: Distribution map of forests that can be felled.

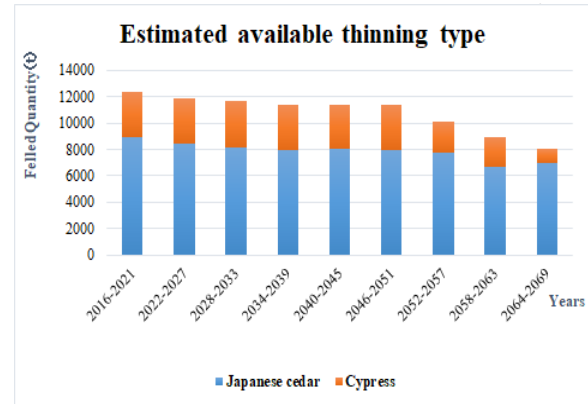


Fig. 6: Estimated available thinning type.

estimation results of the annual logging amount of 3-3, it was judged that about 123,000 tons of wood chips (Nakamura & Shibata 2013, Wood Chip Conversion Factor 2020) can be stably supplied every year in the five years from 2016 to 2021 as an example.

Compared with the conventional boiler using fuel oil A as fuel for heat utilization, when switching from fuel oil A to the use of wood chips, if the economic effect is better than fuel oil purchased from outside the city, it will reduce the cost of biomass users. By replacing fossil fuels with wood fuel, which has excellent thermal efficiency, industries that purchase wood fuels can save intermediate inputs. The estimation was based on the following formula.

Reduction in fossil fuel interim input due to purchase of wood fuel-fuel purchase amount

= (Available amount of wood chips in the city ×0.17× Unit price of fuel oil A) - Purchase amount of wood chips

= 38.5 million yen

Calculation of $CO_2$ reduction when used as an alternative fuel:

Fuel consumption x calorific value per unit calorific value x carbon emissions per unit calorific value x 44/12

= 2,040 t x 48.875 GJ / t x 0.0189 t C / GJ x 44/12

= 99,705 GJ x 0.0189 t C / GJ x 44/12

= 6,909.56 t-CO2

In this case, if wood chips were used as an alternative fuel to the boiler instead of fuel oil A, the annual $CO_2$ reduction was calculated to be 6,909.56 t-$CO_2$.

**Power generation of wood chips for fuel:** From the calculation results (Table 6), in this case, the annual power generation is equal to a small-scale (100-500 kW class) wood biomass power plant with an output of 400 kW.

On the other hand, according to the business plan of the woody biomass burning power plant in Kitakyushu City, there is a plan to import fuel chips from overseas, which requires about 100 thousand tons to 320 thousand tons per year.

According to the Ministry of Finance's "Trade Statistics" data and the Japan Woody Biomass Energy Association's statistical data (Statistical data of Japan Woody Biomass Energy Association 2019) (Fig.7), the average purchase price of imported wood chips is 20,000 yen.ton$^{-1}$, or 2 to 6.4 billion yen per year if all imported chips are used overseas. It is estimated that supplying the city with 12,000 tonnes of unused wood chips per year will save the city approximately 98.4 billion yen annually.

### Creating Jobs for Forestry Workers

In addition to direct job creation such as logging and transportation associated with the processing of wood into fuel, indirect and multifaceted job creation effects are expected as a ripple effect. The Input-output analysis was used for the estimation, and the calculation was made quantitatively. In this study, the employment coefficient was calculated in EXCEL with reference to the input-output table of Kitakyushu (Kitakyushu City Input-Output Table 2011).

The sum of the employment induction factors for the forestry industry in Kitakyushu is 0.0472, and if demand for combustion chips of 147.6 million yen is generated for power plants, the employment of 6 people will be indirect and rippled.

Furthermore, if a job is created in the processing of fuel chips and a new woody biomass power plant is constructed, an operator will be required. In the chip processing industry, it is estimated to be about 12 people when calculated from the employment coefficient (0.0831) in the input-output table.

In addition, about 1 to 2 people are required for the output of 400 kW. Summing up the above results, it is expected that the biomass power generation of unused thinned wood, which

Table 3: Biomass expansion coefficient by tree type, the ratio of aboveground to belowground, volume density, etc.

| | | BEF | | R [-] | D [t-d.m./m3] | CF [t-C./t-d.m] |
|---|---|---|---|---|---|---|
| | | ≤20 | >20 | | | |
| | Japanese cedar | 1.57 | 1.23 | 0.25 | 0.314 | |
| | Cypress | 1.55 | 1.24 | 0.26 | 0.407 | |
| | Red pine | 1.63 | 1.23 | 0.26 | 0.451 | |
| | Black pine | 1.39 | 1.36 | 0.34 | 0.464 | |
| softwood | Other | 2.55 | 1.32 | 0.34 | 0.352 | 0.51 |
| hardwood | Oak | 1.36 | 1.32 | 0.26 | 0.668 | |
| | Other | 1.37 | 1.37 | 0.26 | 0.469 | 0.48 |

Table 4: Estimates of carbon accumulation and $CO_2$ absorption.

| Year | Volume growth ($m^3$) | Carbon stock (t-C) | $CO_2$ absorption (t-$CO_2$) |
|---|---|---|---|
| 2016-2021 | 57,990 | 13,427.63 | 49,234.63 |
| 2022-2027 | 34,065 | 7,898.20 | 28,960.08 |
| 2028-2033 | 29,785 | 7,762.98 | 28,464.27 |
| 2034-2039 | 28,815 | 7,081.18 | 25,964.34 |
| 2040-2045 | 24,245 | 6,130.59 | 22,478.83 |
| 2046-2051 | 22,640 | 5,873.48 | 21,536.08 |
| 2052-2057 | 34,465 | 8,363.74 | 30,667.04 |
| 2058-2063 | 24,475 | 5,583.05 | 20,471.17 |
| 2064-2069 | 25,635 | 5,643.88 | 20,694.21 |


Fig. 7: Imported coniferous and non-coniferous chips, monthly customs.

Table 5: Alternative ratio of wood chip fuel and fossil fuel.

| classification | Generated heat: Wood fuel L | Generated heat: fuel oil A L | A heavy fuel oil→1 ton of wood fuel | Price of fuel oil A this year | Wood fuel price | Amount of wood fuel equivalent to the purchase price of fuel oil A |
|---|---|---|---|---|---|---|
| | ① | ② | ③ = ① / ② | ④ | ⑤ | ⑥ = ③ × ④ |
| chips→fuel oil A | 8,380MJ/t | 48,875MJ/t | 0.171 | 74.8Yen/L | 1,2000 Yen/t | 15,507.3 t |
| Interim input reduction:38.5million Yen | | | | | | |

uses about 147.6 million yen of material, will have the effect of creating employment for about 20 people.

## CONCLUSION

In this study, we estimated the availability of unused woody biomass in Kitakyushu City.

According to the calculation results, it was found that 12,000 tons of unused wood chips can be supplied annually for 36 years from 2016 to 2051. During this period, the total amount of new carbon accumulated due to tree growth was estimated to be about 68,000 tons, and the amount of $CO_2$ absorbed was estimated to be about 249,000 t-$CO_2$. To evaluate the utilization of woody biomass, it is necessary to compare the amount of carbon accumulated and the amount of $CO_2$ absorbed depending on whether or not it is utilized, which is a future issue. On the other hand, to provide a constant supply, a road network that can enter the forest and transport timber, the selection of an effective harvesting method, staffing, and forest management planning for continuous harvesting, among other things, are required. There are additional challenges.

From the economic point of view, the purchase of wood chips of 147 million yen due to the local circulation of wood fuel is expected to save about 38.5 million yen in intermediate input. It was also estimated that there would be a $CO_2$ reduction effect of approximately 7,000 t-$CO_2$ by replacing heavy oil A with woody biomass fuel. The average purchase price of imported wood chips is 20,000 yen.ton$^{-1}$, and it is estimated that if 12,000 tons of unused wood chips can be supplied in the city per year, about 98.4 million yen can be saved annually.

Table 6: Annual power generation (Japanese cedar & Cypress)

| W.B.(%) | LHV(kcal/kg) | Thermal efficiency (%) | Ideal calorific value(kcal/kg) | Power generation efficiency(%) | Ideal annual power generation(kWh) |
|---|---|---|---|---|---|
| 0 | 4,562 | 20 | $1.13\times10^{19}$ | 34 | $4.44\times10^{6}$ |
| 10 | 4,020 | 20 | $9.92\times10^{9}$ | 34 | $3.91\times10^{6}$ |
| 20 | 3,476 | 20 | $8.58\times10^{9}$ | 34 | $3.38\times10^{6}$ |
| 30 | 2,937 | 20 | $7.25\times10^{9}$ | 34 | $2.86\times10^{6}$ |
| 40 | 2,395 | 20 | $5.91\times10^{9}$ | 34 | $2.33\times10^{6}$ |
| 50 | 1,853 | 20 | $4.57\times10^{9}$ | 34 | $1.80\times10^{6}$ |

Finally, from the social point of view, it was revealed that the employment creation effect related to the power generation of unused wood biomass in the region will revitalize the local economy by increasing the number of employees, although there is a difference in the calculation.

## ACKNOWLEDGEMENT

In carrying out this research, we received the cooperation of the people involved in the Agriculture and Forestry Division of Kitakyushu City Hall and the Yahata Agriculture and Forestry Office, such as providing data. We would like to express our sincere gratitude to Professor Zhou Guoyun of Nishinippon Institute of Technology for guidance on GIS operation, and Professor Toru Matsumoto and Professor Atsushi Fujiyama for guidance and correction of this treatise.

## REFERENCES

Forestry Agency. 2018. http://www.rinya.maff.go.jp/j/riyou/biomass/hatudenriyou_guideline.html

Fukuoka Area Forest Plan. 2016. Fukuoka Prefecture Rural Fisheries Promotion Division. https://www.rinya.maff.go.jp/kyusyu/keikaku/chikibetu/pdf/129_hukuokak_an_261028.pdf

Kitakyushu City Forest Book. 2016. Kitakyushu City Agriculture and Forestry Division Kitakyushu City Input-Output Table. 2011 https://www.city.kitakyushu.lg.jp/files/000780681.pdf

Nakamura, R. and Shibata, H. 2013, Economic revitalization effect of regional circulation of woody biomass-biomass energy utilization in Maniwa City, Okayama Prefecture. J. Econ. Soc. Okayama Univ., 45(1): 19-31

Narasaki, K., Maeda, M. and Sasaki, S. 2015. Adjustment of Sugi Stand Density Control Chart And Status Index Curve for Preparation of Fukuoka Prefecture Version System Harvest Table. Fukuoka Prefectural Agriculture and Forestry Research Institute Research Report 1. Japan

National Institute for Environmental Studies. 2018. Japan Greenhouse Gas Event Report, pp.6-11. https://www.nies.go.jp/gio/archive/nir/jqjm1000000pck2j-att/NIR-JPN-2018-v4.1_web.pdf

Statistical data of Japan Woody Biomass Energy Association. 2019. https://www.jwba.or.jp/database/price-transition01/

Wood Chip Conversion Factor. 2020. National Wood Chip Industry Association https://www.rinya.maff.go.jp/kanto/apply/publicsale/wood/attach/pdf/sisutemu20200225-5.pdf

Nature Environment and Pollution Technology
An International Quarterly Scientific Journal

p-ISSN: 0972-6268
(Print copies up to 2016)
e-ISSN: 2395-3454

Vol. 20 | No. 5 (Suppl) | pp. 1997-2005 | 2021

Review Research Paper | https://doi.org/10.46488/NEPT.2021.v20i05.016 | Open Access Journal

# Toxicity, Monitoring, and Biodegradation of Cypermethrin Insecticide: A Review

**Ramandeep Kaur† and Joginder Singh**
Department of Microbiology, Lovely Professional University, Phagwara-144411, Punjab, India
†Corresponding author: Ramandeep Kaur; ramandeepk709@gmail.com

**Nat. Env. & Poll. Tech.**
**Website: www.neptjournal.com**

*Received:* 14-03-2021
*Revised:* 13-05-2021
*Accepted:* 25-05-2021

**Key Words:**
Cypermethrin
Pyrethroid
Insecticide
Biodegradation
Toxicity

## ABSTRACT

Cypermethrin insecticide is widely used to prevent and control pest and crop diseases though, its residues have caused significant damage to the environment and living organisms. Microbial remediation becomes a popular approach to counter the toxicity of cypermethrin in both aquatic as well as terrestrial life. Cypermethrin can be effectively degraded to nontoxic compounds by bacterial and fungal strains. Various bacterial and fungal strains such as *Ochrobactrum lupini* DG-S-01, *Bacillus* sp. strain SG2, *Azoarcus indigens* strain HZ5, *Streptomyces aureus* strain HP-S-01, and *Aspergillus oryzae* M-4 are used for the cypermethrin degradation. Extensive usage of cypermethrin has caused problems such as surface water contamination, reduced fertility of the soil, detrimental effects on soil microbiota and non-targeted species. Due to environmental concerns associated with the cypermethrin in groundwater and food products, there is a crucial need to develop economical, rapid, and reliable techniques that can be used for field applications. An in-depth understanding of cypermethrin is explored in this review paper and possible solutions to mitigate its environmental toxicity are suggested.

## INTRODUCTION

In India, crop production is increased with the usage of pesticides, however, increased usage of pesticides resulted in affecting adversely the aquatic ecosystem and selected body parts of non-target organisms (Agarwal & Shahi 2015, Singh et al. 2010). Cypermethrin has been classified by WHO as a slightly hazardous type II pesticide (WHO 1994-95). Cypermethrin insecticide has more commercial applications in agriculture as well as domestic products (Zhang et al. 2011). Mostly when cypermethrin is degraded it breaks down into various metabolites such as 3-PBA. In India, cypermethrin is registered by CIBRC for use in eight specified crops, such as cabbage, wheat, cotton, rice, sugarcane, brinjal, sunflower, and okra. In India, the cypermethrin production appeared to be 6.5 MT in 2005-2006 and 2473 MT during 2009-2010. (State of Pesticide Regulations in India 2013) Cypermethrin is frequently used by Indian farmers to prevent insects in jute, wheat, paddy, and vegetables (Tendulkar & Kulkarni 2012). Nontarget organism like L. marginalis (Raksheskar 2012, Pugazhendy et al. 2012, Pankaj et al. 2015) was reported to be more vulnerable to cypermethrin toxicity than the target organisms. During monsoon, the agricultural runoff loaded with cypermethrin contaminates the natural habitat of *L. marginalis*. Thus they are exposed to cypermethrin present in their natural habitat. Cypermethrin toxicity was recorded in West Bengal by different workers including (Raghavendra et al. 2014, Goswami et al. 2013). Even at very low concentration pyrethroids are highly effective, therefore, it is the most important pesticide. They are used against flies, mosquitoes, stored grain insects, and aphids. They are mostly used for pest controlling and eradicating the disease-causing vector in developing countries such as China (Chen et al. 2011a). Synthetic pyrethroids have been used in agricultural fields to control pests on a variety of crops for over 20 years. They gained popularity, however, after the use of cholinesterase inhibitor insect repellents was banned completely (Zhang et al. 2011). Although cypermethrin is an effective pesticide, it is toxic to non-targeted creatures. As a result, reducing the environmental impact of cypermethrin, as well as the risks to human health, is critical. Among various approaches, the biological approach is a more effective and promising strategy. And in this review, we have summarized the data available regarding the toxicity and degradation of cypermethrin which will help further help others to know about the different microbes involved in the bioremediation of cypermethrin.

## TOXICITY OF CYPERMETHRIN ON NON-TARGETED ORGANISMS

Cypermethrin has shown toxic effects against various aquatic organisms like fish, daphnia, mussel, etc., goats, lizards, and human cells (Akinrotimi et al. 2012, Chen et al. 2016, Dawar et al. 2016). Cypermethrin adversely affects the central nerv-

ous system (Tallur et al. 2008), leads to endocrine toxicity (Jin et al. 2011a), tumor promoter (Chen et al. 2011b), and has an immuno-toxic effect (Jin et al. 2011b) in nontargeted species. In females, several oral intakes of cypermethrin have shown detrimental effects on the uterus and ovaries and lead to loss of oocytes and follicular cells in ovaries formed by cypermethrin at the dosage of 20 $mg.kg.day^{-1}$ (Grewal et al. 2010). A reduction in mass of ovaries was detected after 4 weeks of cypermethrin intake although the length and weight of uterus and myometrium thickness improved at the dosage of 50 $mg.kg^{-1}$ body mass at 2 and 4 weeks (Sangha et al. 2013). The liver plays an essential role in the detoxification and decomposition of harmful chemicals like pesticides. In the removal of metabolic wastes from the body, the kidney plays a significant role. But cypermethrin has been shown to cause toxicity in the liver and kidney (Sushma & Devasena 2010).

**CypermethrinToxic Effect on Aquatic Life**

Cypermethrin is a broad-spectrum insecticide. Like the targeted species, it also kills the other beneficial insects and animals. Fish are particularly affected by cypermethrin (Stephenson 1982) (Fig. 1). When exposed to cypermethrin, the amount of lipid peroxidation and glutathione peroxidase was elevated in the gills, kidneys, and liver of the *Cyprinus carpio* fish (Meenambal et al. 2012). The superoxide dismutase (SOD) and catalase activities were reported more when treated with cypermethrin *Cyprinus carpio* compared to untreated controls (Meenambal et al. 2012). It was stated that cypermethrin exposed fish have gradually lost antioxidant defense ability along the exposure time. The authors reported the first evidence of cypermethrin-induced glutathione-S-transferase activity in a crustacean specimen. Cypermethrin treatment resulted in a reduction in the glycogen content of gill, mantle, foot, and gonads of clams Marcia opima (Tendulkar & Kulkarni 2012). Nowadays, for ecotoxicological studies organism models are used for studying pesticide toxicity. In the aquatic environment, fish, mollusks, and amphibians (Johnson et al. 2017) are used as model organisms. Amphibians are considered as good indicators as they have a biphasic cycle and they encounter pesticides in both aquatic and terrestrial environments. As compared to larvae, the embryos were more resistant to cypermethrin. During embryo mobility assays, it was observed that cypermethrin causes spasmodic contractions (Macagnan et al. 2017). Cypermethrin deposits were recently detected in soil and water, and it poses a possible threat to aquatic species and humans (Kuivila et al. 2012). Alpha cypermethrin has a chronic toxic effect on channa fish. Lactate dehydrogenase (LDH), catalase, DNA, RNA, and protein have been investigated in the liver, gills, skeletal muscles, and brain of the *Channa punctatus* freshwater fish (Tripathi & Singh 2013). In another research on zebrafish, a

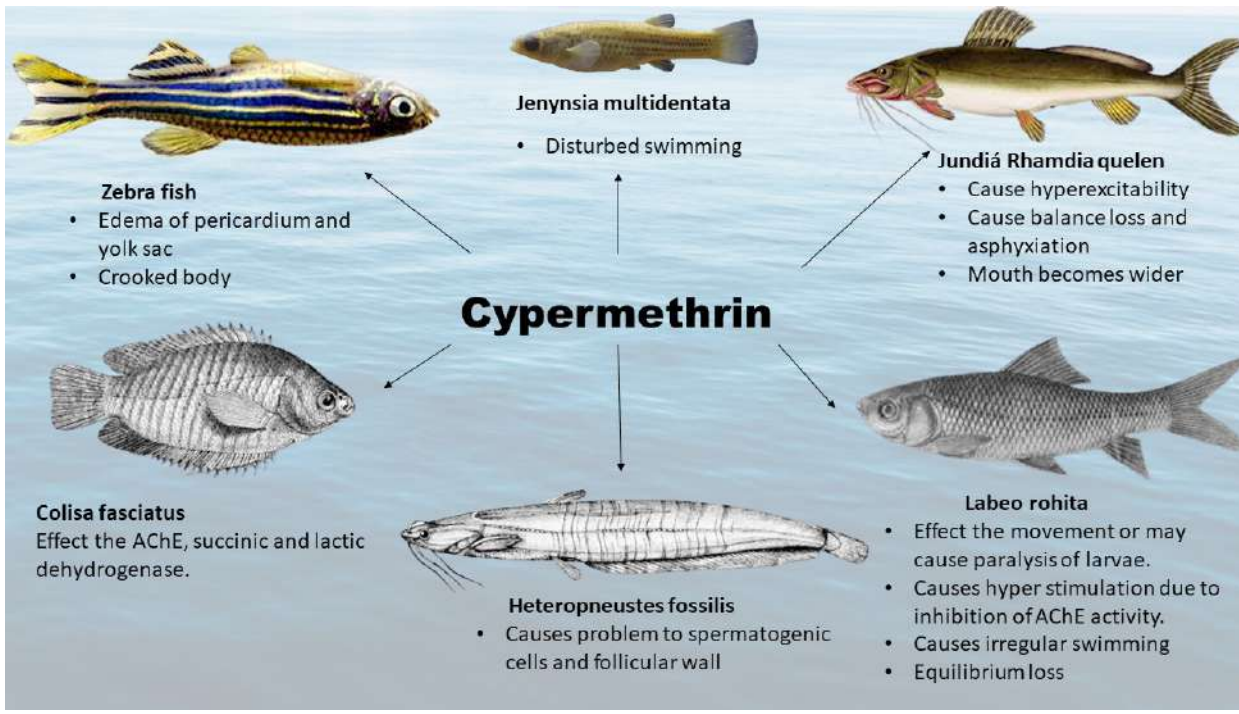


Fig. 1: Effect of cypermethrin on aquatic life.

notable reduction was observed in activities of catalase and level of GSH in the liver and gills, on the other hand, there was an increase in LPO in both the tissues (Ansari & Ansari 2014). The cypermethrin effect differently on the larvae than on the embryo of Gangetic mystus. In *Mystus cavasius* the hatching rate is decreased and larvae mortality is increased significantly due to increased concentration of cypermethrin. When exposed to high cypermethrin concentrations, different abnormalities occur in embryos and larvae. The observed abnormalities in larvae were edema and notochord fracture when exposed to various concentrations of cypermethrin. All these malfunctioning in *Mystus cavasius* embryo and larvae were due to high cypermethrin exposure (16 and 32 $\mu g.L^{-1}$) (Ali et al. 2018).

As per the studies, cypermethrin has the potential to control the secretion of HPG (hypothalamic-pituitary-gonadal) and similar hormones by channels of sodium (Na) and calcium (Ca) (Ye et al. 2017). According to research conducted by (Zhang & Li 2018) on zebrafish, beta-cypermethrin can damage its reproductive system. But, the mechanisms behind the toxicity caused by beta-cypermethrin in the fish reproductive system are not yet clear. It has been observed that due to beta-cypermethrin there is a huge reduction in the production of eggs. However, the mechanisms behind the toxicity caused by beta-cypermethrin in the reproductive system of fish are not yet clear. As shown in the study, beta-cypermethrin has the potential to minimize the reproductive capability of zebrafish. Even previous research has shown that beta cypermethrin significantly decreases the rate of pregnancy in female rats, suggesting that beta cypermethrin can harm the mammalian reproductive organs (Zhou et al. 2018a, 2018b). The study concluded that beta cypermethrin could potentially target both fish and mammalian reproductive systems.

### Toxicity of Cypermethrin on Terrestrial Life

Data signified that cypermethrin interfered with the energy transformation process in the same specimen. Cypermethrin has various effects in rats as mentioned in Fig 2. It shows the harmful impact on the reproductive system of male rodents. The androgen receptor and serum testosterone amounts were reduced significantly due to a regular dosage of 15 days. The study suggested the potent role of cypermethrin in initiating disfigurement of seminiferous tubules and adversely affecting spermatogenesis in male rodents at high dosages (Hu et al. 2011). Aside from the negative impact on males, (Zhou et al. 2018c) the likely role of beta-cypermethrin in inhibiting reproductive hormones and affecting female rats' fertility by blocking the endometrium, as well as, causing developmental delays in endometrial pinopodes was established. Due to daily cypermethrin exposure, dopaminergic neurodegeneration was initiated in rodents during their adulthood, while postpartum exposure increased the sensitivity of animals to dopaminergic neurodegeneration when challenged further in adulthood (Singh et al. 2012). Reports have also shown developmental delays in the progeny of rodents that were exposed to cypermethrin during pregnancy. The abnormal sperm count increased in male rodents due to exposure to cypermethrin. The experiment to investigate the potential impact on rat physiology of cypermethrin-treated lettuce, showed increased plasma concentrations of ALT, AST, and total biurubin and decreased plasma protein concentrations along with decreased body weight (Adjrah et al. 2013).

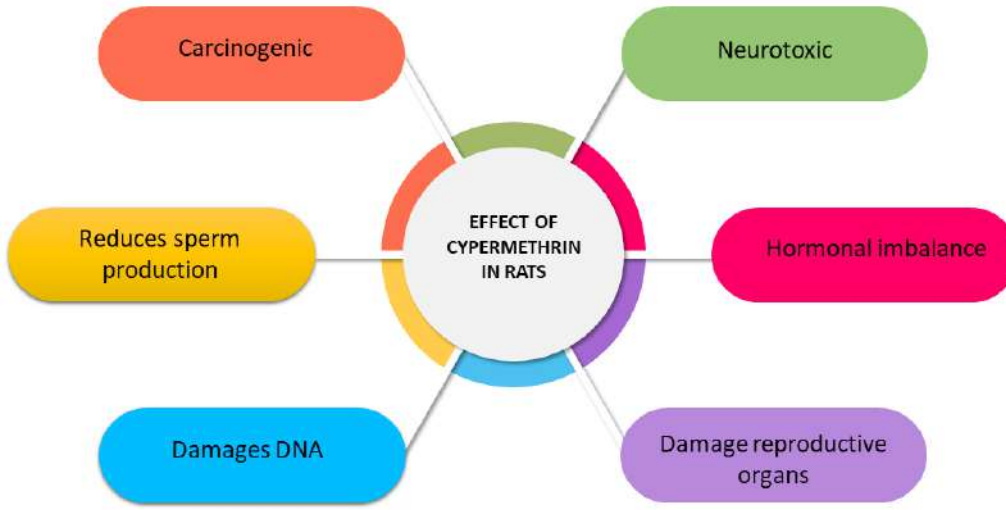


Fig. 2: Toxicological effect of cypermethrin in rats.

In rats, 28 days of administration of cypermethrin resulted in a substantially increased number of micronuclei formation in bone marrow cells and dge ti DNA in blood cells (Sankar et al. 2010). Due to the combined effect of cytotoxic cytostatic, alpha-cypermethrin along with acetamiprid with different doses in human peripheral blood lymphocyte culture contribute to a substantial decrease in the mitotic, proliferation, and nuclear division indexes (Kocaman & Topaktaş 2010). Exposure to cypermethrin contributes to follicular atresia by influencing angiogenesis pathologically, disrupting endocrine capacity, and increasing oxidative stress throughout the rat ovary (Molavi et al. 2016). Cypermethrin insecticide is neurotoxic in nature which acts on sodium (Na), potassium (K), and calcium (Ca) channels for exerting neurotoxicity (Singh et al. 2012). In various papers, cypermethrin toxicity was reported to affect mammalian reproductive systems. According to studies, cypermethrin in male mice reduces the weight of reproductive organs, damages seminiferous tubules, decreased the production of sperms, and interferes with the hormone secretions (Huang & Li 2014). In females, cypermethrin may reduce the follicle numbers and successful pregnancy rates by destroying the endometrium and may also disturb hormone secretions like estrogen and follicle-stimulating hormones (Sangha et al. 2013). Cypermethrin treatment in mice has shown a huge reduction in sperm count and testicular testosterone. The protein level in the testis was significantly reduced in cypermethrin-treated mice. An oral study in mice showed that cypermethrin induces neurotoxicity by damaging sciatic nerves, axonal degeneration by myelin sheet fragmentation, and axoplasm shrinkage (Kamel 2011).

The neurotoxicity data states the role of cypermethrin in damaging the ion channels (sodium, calcium, and chloride) of brain synaptosomes in rats. Also, recent data had shown that in mitochondrial membranes, the cypermethrin can damage the ion channels (Paravani et al. 2019, Kaisarevic et al. 2019, Gao et al. 2018). Currently, enough attention has been given to the impact of cypermethrin in reproductive organs. Cypermethrin subjection alters the amount of sex hormone in males, on the other hand, it has decreased reproductive production in females and triggers histopathological alterations in reptiles. Mitochondrial-associated apoptosis protein expression was estimated to find out the potential mechanism of apoptosis. Research to date has shown that pyrethroids have more harmful effects on vertebrates, affect the ion channels of the neuronal membrane and mitochondrial membrane (Lidova et al. 2016, Gao et al. 2018, Kaisarevic et al. 2019). Excessive cypermethrin use leads to the possibility of human exposure to many environmental pollutants (Romero et al. 2015). It also has unnecessary side effects on the non-targeted species, involving vertebrates (Vardavas et al. 2016). Cypermethrin raises serum glucose in rats and drops the levels of serum triglycerides. The liver and kidney effects of cypermethrin have been studied in rats for both biochemical and histopathological effects (Sankar et al. 2012, Bhushan et al. 2013). As per the recent research done by Huang et al. (2018), it was discovered that exposure to cypermethrin can lead to metastasis of lung cancer by modulating macrophage polarization; cypermethrin treatment with macrophages has facilitated the growth of lung cancer cells in both in-vivo and in-vitro models. According to the findings, cypermethrin can inhibit M1 polarisation and enhance M2 phenotypes in macrophages, which is important for tumor metastasis.

## ADVANCE TECHNOLOGY USED FOR CYPERMETHRIN DETECTION

Mostly cypermethrin degradation is studied by using gas chromatography, mass spectroscopy, and HPLC (Castellarnau et al. 2016). The most widely used methods for the identification of cypermethrin and its residues in various samples, such as crops, soil, and other samples depend on the extraction of the organic solvent residues. These methods are capable of detecting cypermethrin metabolites up to ng.gm-1 of soil, efficiently following microbial degradation (Braganca et al. 2018). HPLC is used for the quantification of cypermethrin. It is quick, easy, reliable, and has a low cost. Different types of detectors like UV and a photodiode are used for the detection of cypermethrin. During cypermethrin degradation, different metabolites are produced which can be observed by using GC-MS analysis. Each degraded metabolite is represented by different peaks in the gas chromatogram and these techniques are used due to their high sensitivity; however, they are very expensive as well as tedious. Furthermore, these techniques are highly selective and sensitive, and they generally require elaborate procedures, costly, and time-consuming sample pretreatment steps. Traditional chromatography-based techniques, which need complicated sample preparation protocols, and experts, and specialized instruments, are being replaced by newer approaches like electrochemical sensors and optical sensors which reduce sample preparation costs and time and can allow on-site pesticide detection. Therefore, advanced technologies are invented which are highly accurate, simple, less time-consuming.

### Microfluidic Paper-Based Analytical Device

A Microfluidic paper-based analytical device is used for the identification of type II pyrethroids present in various water samples, and the detection depends on the cyanide formation from the hydrolysis of type-II pyrethroid. This detection method comes up with an alternative way for

rapid, semi-quantitative analysis of pesticide-contaminated samples by permitting low-cost testing, mobility, and low sample utilization. (Pengpumkiat et al. 2020)

### Electrochemical Sensing

Various techniques are used for cypermethrin detection include HPLC, GC-MS, immunoassay, etc. (Zhou et al. 2018c). However, due to a few drawbacks, such as false-positive reactions, laborious pretreatment, high turnaround times, and high costs, it limits their uses (Li et al. 2016, Zhang et al. 2014). This helps scientists to find the latest and effective method for cypermethrin testing. Whereas electrochemical sensor has edge over other methods as it has simple preparation, low detection limit, high sensitivity, and convenient operation. As compared to the methods described above, trace analytes can be traced rapidly and instantly in a simple manner (Ng & Khor 2017). Detection of cypermethrin from real samples was rapid and accurate with an electrochemical sensor. Different electrochemical sensors like DMMIP-Ag-N@ ZnO/CHAC have immense capabilities in the detection of drug residues, food safety, and environmental detection (Li et al. 2019).

### Optical Sensing

Intensive research is being conducted in the domains of optical sensing and pesticide monitoring in water. With the scarcity of freshwater, the development of these kinds of optical sensors is in high demand. Optical detection of pesticides has several benefits over other detection approaches since it uses simple routes and does not require complex equipments or environmental limitations. Taking into account the improvement of sensing process constraints such as sensitivity, selectivity, quick and adaptable approach for pesticide detection is of great importance to us. As a result, this method of identification and monitoring might be used to precisely monitor pesticides. Although there have been several reports on the detection of various pesticides, no or few attempts to produce optical sensor film as an analytical approach for pesticide detection have been made too far. Fluorescence, ultraviolet-visible, Raman, and chemiluminescence are some of the techniques used in optical sensors to investigate signal modifications. It consists of an identification element that interacts precisely with the target analyte, as well as a part of the transducer for signaling the interactions. Simple procedures, fast detection, wide linearity range, high sensitivity, simple operation, and cost-effectiveness are some of its advantages (Pang et al. 2016).

In contrast, the artificially manufactured molecularly imprinted polymer (MIP) is able to work as an excellent detecting option for the development of specialized sensing signals because of its special characteristics like simple manufacture, high stability, cost-effectiveness, and resistance to environmental effects (Capoferri et al. 2018, Zhang et al. 2018, Zhang et al. 2015). Electrochemical probes need electrical signal indicators for their functioning, however, MIP-based sensors are not dependent on the electrochemical activities of the analytes and hence have many applications. (Gupta et al. 2016, Li et al. 2018, Wei et al. 2017). Electrochemical polymerization is the most common approach for creating a molecularly imprinted electrochemical sensor, which allows for fine control of the polymer film thickness and produces a stable and consistent imprinted membrane. A single type of functional monomer is used in most MIP preparations (Li et al. 2016). According to research, MIPs made with multiple functional monomers outshines the performance of a single monomer (Wu et al. 2016), because of the integral function and combined effect that different monomers have on molecular recognitions. Because of the rise of polymer-template interaction groups and a variety of functional groups, selectivity and adsorption capacity of MIPs may be increased to some amount when properly chosen multi-monomers are associated with the generation of the polymeric skeleton (Geng et al. 2014, Zhao et al. 2017). MIPs nanoparticles were used as an alternative to antibodies in the fabrication of enzyme-linked immunosorbent assays since it was the simplest method. According to research by Xiao et al. (2016), MIP coat was applied to the surface of QDs to form MIP-QDs composites, which were used as sensing nanoparticles in the preparation of an ELISA like the technique for cypermethrin detection.

## CYPERMETHRIN DEGRADATION BY MICROORGANISMS

In the detoxification and degradation of pesticides, microbes play a major role and the list of such microbes are listed in Table 1. The functional class of pesticides requires specific genes and enzymes to cleave them. The optimum environmental conditions are required for the functioning of microbes which helps in the effective biodegradation of pesticides (Chishti et al. 2013). The organic pollutants are degraded with help of microbial collaborations. *Pseudomonas mendocina* and *P. putida* strains have the ability to degrade cypermethrin up to 90% within 15 days (Mendoza et al. 2011). As reported by Chen et al. (2012), *Streptomyces aureus* HP-S01 can degrade β-cypermethrin and its 3-PBA metabolite from agricultural land. In the agricultural land, 80.5% and 73.1% of the dose of β-cypermethrin and 3PBA (50 $mg.kg^{-1}$) were removed from the sterile soil within 10 days. The elimination rate of beta-cypermethrin and 3-PBA in non-sterile soils was comparatively maximum 87.8% and

Table 1: Different microorganisms involved in the degradation of cypermethrin.

| Microorganisms Name | Location | Intermediate products | Source | References |
|---|---|---|---|---|
| *Ochrobactrum lupini* DG-S-01 | Zhongshan,China | 3-phenoxybenzoic acid | Activated sludge | Chen et al. (2011a) |
| *Bacillus* sp. strain SG2 | Uttarakhand, India | 3-phenoxybenzoic acid and 3-phenoxybenzaldehyde | Soil | Sharma et al. (2016) |
| *Bacillus subtilis* strain 1D | Uttarakhand, India | cyclododecylamine, phenol | Soil | Gangola et al. (2018) |
| *Bacillus thuringiensis* strain SG4 | Uttarakhand, India | 3-phenoxybenzaldehyde | Soil | Bhatt et al. (2020) |
| *Bacillus* sp. DG-02 | China | 3-phenoxybenzoic acid | Sewage treatment system | Chen et al. (2014) |
| *Bacillus thuringiensis* strain ZS-19 | China | 3-phenoxybenzoic acid | Activated sludge | Chen et al. (2015) |
| *Azoarcus indigens* strain HZ5 | Hangzhou, China | 3-phenoxybenzoic acid and 3-phenoxybenzaldehyde | Activated sludge | Ma et al. (2013) |
| *Bacillus megaterium* JCm2, *Rhodococcus* sp. JCm5 and *Ochrobactrum anthropi* JCm1 | Punjab, India | 3-phenoxybenzoic acid, catechol, and phenol | Soil | Akbar et al. (2015) |
| *Streptomyces aureus* strain HP-S-01 | Zhongshan, China | α-hydroxy-3-phenoxybenzeneacetonitrile and 3-phenoxybenzaldehyde | Activated sludge | Chen et al. (2011c) |
| Pseudomonas aeruginosa CH7, | China | 3-(2,2-dichloroehtenyl)-2,2-dimethyl cyclopropanecarboxylic acid and 3-phenoxybenzoic acid | Activated sludge | Zhang et al. (2011) |
| *Catellibacterium* sp. strain CC-5 | Chengdu, China | 3-phenoxybenzaldehyde and α-hydroxy-3-phenoxybenzeneacetonitrile | Soil | Zhao et al. (2013) |
| *Acinetobacter baumannii* ZH-14 | Singapore | 3-Phenoxybenzaldehyde | Sewage sludge | Zhan et al. (2018) |
| *Aspergillus oryzae* M-4 | China | 3-Phenoxybenzoic acid, Phenol, and Catechol | Soil | Zhao et al. (2016) |
| *Pseudomonas fulva* P31 | Zhongshan, China | 3-Phenoxybenzaldehyde | Activated sludge | Yang et al. (2018) |

79.3% respectively. The bacterial strain CC5 was cultivated from polluted soil and identified as *Catellibacterium* sp. It utilizes cypermethrin as the primary source of carbon and degrades cypermethrin (100 $mg.mL^{-1}$) up to 97% within 7 days. The optimum degradation was at 30 temperature and pH 7. The cypermethrin elimination was higher in cypermethrin-treated soil inoculated with CC5 strain than in non-inoculated soil. This study shows that the bacterial strain can be used in the degradation of an environment contaminated with a pyrethroid (Zhao et al. 2013). According to Zhang et al. (2011), isolated *Pseudomonas aeruginosa* CH-7 strain from activated sludge which utilizes cypermethrin as a carbon source for its growth was not able to degrade cypermethrin. Thus, the CH7 strain may have the ability to remediate the sewage and soil contaminated with cypermethrin. At 25-35 and pH of 7, the photosynthetic bacterium GJ-22 was able to degrade cypermethrin. Metabolic products were observed after performing gas chromatography-mass spectrometry, and degradation was done by oxidative and hydrolytic pathways producing 5 metabolites (Yin et al. 2012).

The SG4 strain of Bacillus thuringiensis has been isolated from the soil that degrades cypermethrin. SG4 has successfully degraded cypermethrin under various conditions. Degradation was greatly improved by bioaugmentation of cypermethrin-contaminated soil and strain SG4 (83.3%). Degradation products research has resulted in the discovery of nine different cypermethrin metabolites, which demonstrates that cypermethrin can be degraded by binding its ester, then its benzene ring, and another metabolism (Bhatt et al. 2020). The isolated bacteria *Bacillus subtilis* strain 1D completely degrade cypermethrin within 15 days under laboratory conditions. The study indicated the action of the laccase enzyme in the degradation of cypermethrin. The isolated bacteria follow a metabolic pathway for detoxifying and degrading cypermethrin without any toxic metabolite. The isolated bacteria consume cypermethrin as a carbon source for their growth (Gangola et al. 2018). According to a study carried by (Narayanan et al. 2020), *Bacillus cereus* was isolated from BT cotton and soil contaminated with pesticide. *B. cereus* shows great resistance towards

beta-cypermethrin at a concentration of 100 mg.$L^{-1}$. First, by using thin-layer chromatography they confirmed the presence of beta-cypermethrin. SDS-PAGE analysis identified the pyrethroid hydrolase enzyme which was effective in metabolizing beta-cypermethrin. GC-MS analysis confirmed that Benzylamine and similar components were formed by beta-cypermethrin in degradation by *B. cereus.* As per the research on the degradation of cypermethrin by immobilization of *Micrococcus* sp. cells of strain CPN 1, PUF-immobilized cells have shown a higher degradation capability than other used matrices. PUF-immobilized cells could maintain the degradation capability after reusage for 32 cycles or more without losing their degradation capability (Tallur et al. 2015). Therefore, it could be used in the biodegradation of cypermethrin polluted water.

## CONCLUSION

Cypermethrin insecticide is a type II pyrethroid that is broadly used in agricultural fields, and which contaminates the soil, water, and other environments. The toxicity of cypermethrin has recently been investigated in aquatic and terrestrial life. Therefore, cypermethrin degrading microbes were isolated and studied for many years for bioremediation. In the future, microorganisms that help in the decomposition of cypermethrin within a short period under various environmental conditions must be detected or isolated. The consortium-based approach to degrade pesticides is highly acceptable but cypermethrin degradation has not been significantly studied. Metagenomic techniques are time-saving compared to conventional culture-dependent strategies. The advancing omics-based technology will also promote the isolation and classification of contaminated sites of cypermethrin degrading microorganisms. It is a safe and efficient remediation technique that focused on cypermethrin residue contamination in natural environments.

## REFERENCES


Adjrah, Y., Karou, S.D., Agbonon, A., Ameyapoh, Y. and Gbeassor, M. 2013. Effect of cypermethrin-treated lettuce (Lactuca sativa) on Wistar rat liver. J. Appl. Pharm. Sci., 3(1): 128-132

Agarwal, N. and Shahi, S.K. 2015. An environmental cleanup strategy-microbial transformation of xenobiotic compounds. Int. j. Curr. Micr. Appl. Sci., 4: 429-461.

Akbar, S., Sultan, S. and Kertesz, M. 2015. Bacterial community analysis of cypermethrin enrichment cultures and bioremediation of cypermethrin contaminated soils. J. Basic Microbiol., 55(7): 819-829.

Akinrotimi, O.A., Gabriel, U.U. and Ariweriokuma, S.V., 2012. Haematotoxicity of cypermethrin to African catfish (Clarias gariepinus) under laboratory conditions. J. Environ. Eng. Technol. 1 (2): 13-19.

Ali, M.H., Sumon, K.A., Sultana, M. and Rashid, H. 2018. Toxicity of cypermethrin on the embryo and larvae of Gangetic mystus, Mystus cavasius. Environ. Sci. Pollut. Res., 25(4): 3193-3199.

Ansari, S. and Ansari, B.A. 2014. Temporal variations of CAT, GSH, and LPO in gills and livers of zebrafish, Danio rerio, exposed to dimethoate. Arch. Polish Fish., 22(2): 101-109.

Bhatt, P., Huang, Y., Zhang, W., Sharma, A. and Chen, S. 2020. Enhanced cypermethrin degradation kinetics and metabolic pathway in Bacillus thuringiensis strain SG4. Microorganisms, 8(2): 223.

Bhushan, B., Saxena, P.N. and Saxena, N., 2013. Biochemical and histological changes in rat liver caused by cypermethrin and beta-cyfluthrin. Arh. Hig. Rada. Toksikol., 64, 57-67.

Braganca, I., Lemos, P.C., Barros, P., Delerue-Matos, C. and Domingues, V.F. 2018. Phytotoxicity of pyrethroid pesticides and their metabolite towards Cucumis sativus. Sci. Total Environ., 619-620, 685-691.

Capoferri, D., Álvarez-Diduk, R., Del Carlo, M., Compagnone, D. and Merkoçi, A. 2018. Electrochromic molecular imprinting sensor for visual and smartphone-based detections. Anal. Chem., 90(9), 5850-5856.

Castellarnau, M., Azcon, J.R., Lopez, J.F., Grimalt, J.O., Marco, M.P. and Nieuwenhuijsen, M.. 2016. Assessment of analytical methods to determine pyrethroids content of bednets. Trop. Med. Int. Health, 22: 41-51.

Chen, L., Xu, P., Diao, J., Di, S., Li, R. and Zhou, Z. 2016. Distribution, metabolism, and toxic effects of beta-cypermethrin in lizards (Eremias argus) following oral administration. J. Hazard. Mater., 306: 87-94.

Chen, S., Deng, Y., Chang, C., Lee, J., Cheng, Y., Cui, Z. and Zhang, L. H. 2015. Pathway and kinetics of cyhalothrin biodegradation by Bacillus thuringiensis strain ZS-19. Sci. Rep., 5(1): 1-10

Chen, S., Chang, C., Deng, Y., An, S., Dong, Y.H., Zhou, J. and Zhang, L.H. 2014. Fenpropathrin biodegradation pathway in Bacillus sp. DG-02 and its potential for bioremediation of pyrethroid-contaminated soils. J. Agric. Food Chem., 62(10): 2147-2157.

Chen, L., Guan, L.M., Wu, Y.N., Xu, L.J. and Fu, F.F. 2012. Study on the residue and degradation of fluorine-containing pesticides in Oolong tea by using gas chromatography-mass spectrometry. Food Control 25: 433-440.

Chen S., Kaiping, L., Yanan, L., Meiying, H., Yanbo, Z. and Yong, Z. 2011a. Biodegradation of deltamethrin and its hydrolysis product3-phenoxybenzaldehyde by a newly isolated Streptomyces aureus strain HP-S-01. Appl. Microbiol. Biotechnol., 90: 1471-1483.

Chen, S., Hu, Q., Hu, M., Luo, J., Weng, Q. and Lai, K. 2011b. Isolation and characterization of a fungus able to degrade pyrethroids and 3-phenoxybenzaldehyde. Bioresour. Technol., 102(17): 8110-8116.

Chen, S., Hu, M., Liu, J., Zhong, G., Yang, L., Rizwan-ul-Haq, M. and Han, H. 2011c. Biodegradation of beta-cypermethrin and 3-phenoxybenzoic acid by a novel Ochrobactrum lupini DG-S-01. J. Hazard. Mater., 187(1-3): 433-440.

Chishti, Z., Hussain, S., Arshad, K.R., Khalid A. and Arshad, M. 2013. Microbial degradation of chlorpyrifos in liquid media and soil. J. Environ. Manage., 114: 372-380.

Dawar, F.U., Zuberi, A., Azizullah, A. and Khattak, M.N.K. 2016. Effects of cypermethrin on survival, morphological and biochemical aspects of rohu (Labeo rohita) during early development. Chemosphere, 144: 697-705.

Gangola, S., Sharma, A., Bhatt, P., Khati, P. and Chaudhary, P. 2018. The presence of esterase and laccase in Bacillus subtilis facilitates biodegradation and detoxification of cypermethrin. Sci. Rep., 8(1): 1-11.

Gao, Y., Kim, K., Kwon, D.H., Jeong, I.H., Clark, J.M. and Lee, S.H., 2018. Transcriptome-based identification and characterization of genes commonly responding to five different insecticides in the diamondback moth, plutella xylostella. Pestic. Biochem. Physiol., 144: 1-9.

Garoiaz, H., Berrabah, M., Elidrissi, A., Hammouti, B. and Ríos, A. 2012. Analysis of cypermethrin residues and its main degradation products in soil and formulation samples by gas chromatography-electron impact-mass spectrometry in the selective ion monitoring mode. International Journal of Environmental Analytical Chemistry, 92(12):1378-1388.

Geng, H., Kong, S.F. and Wang, Y. 2014. NiS nanorod-assembled nanoflowers grown on graphene: morphology evolution and Li-ion storage applications. J. Mater. Chem. A, 2(36): 15152-15158.

Grewal, K.K., Sandhu, G.S., Kaur, R., Brar, R.S. and Sandhu, H.S., 2010. Toxic impacts of cypermethrin on behavior and histology of certain tissues of albino rats. Toxicol. Int., 17(2): 94-98.

Goswami, M.R., Pati, U.K., Chowdhury, A. and Mukhopadhyay, A. 2013. Studies on the effect of cypermethrin on soil microbial biomass and its activity in alluvial soil. Int. J. Agric. F. Sci., 3(1): 1-9.

Gupta, B.D., Shrivastav, A.M. and Usha, S.P. 2016. Surface plasmon resonance-based fiber optic sensors utilizing molecular imprinting. Sensors, 16(9): 1381.

Hu, J. X., Li, Y.F., Li J., Pan, C., He, Z., Dong, H.Y. and Xu L. C. 2011. Toxic effects of cypermethrin on the male reproductive system: With the emphasis on the androgen receptor. J. Appl. Technol., 54: 619-650.

Huang, C. and Li, X. 2014. Maternal cypermethrin exposure during the perinatal period impairs testicular development in C57BL male offspring. PLoS One, 9(5): e96781.

Huang, F., Chen, Z., Chen, H., Lu, W., Xie, S., Meng, Q. H. and Xia, D. 2018. Cypermethrin promotes lung cancer metastasis via modulation of macrophage polarization by targeting MicroRNA-155/Bcl6. Toxicol. Sci., 163(2): 454-465.

Jin, Y.X., Wang, L.G., Ruan, M., Liu, J.W., Yang, Y.F., Zhou, C., Xu, B. and Fu, Z.W. 2011a. Cypermethrin exposure during puberty induces oxidative stress and endocrine disruption in male mice. Chemosphere 84: 124-130.

Jin, Y.X., Zheng, S.S. and Fu ZW. 2011b. Embryonic exposure to cypermethrin induces apoptosis and immunotoxicity in zebrafish (Danio rerio). Fish Shellfish Immunol., 30: 1049-1054.

Johnson, M.S., Aubee, C., Salice, C.J., Leigh, K.B., Liu, E., Pott, U. and Pillard, D. 2017 A review of ecological risk assessment methods for amphibians: comparative assessment of testing methodologies and available data. Integr. Environ. Assess. Manage., 18: 91-114.

Kaisarevic, S., Tenji, D., Mihajlovic, V., Micic, B., Francija, E., Periz-Stanacev, J., Krnic Skiljo, B., Brkic, D. and Teodorovic, I. 2019. Comparative analyses of cellular physiological responses of non-target species to cypermethrin and its formulated product: contribution to the mode of action research. Environ. Toxicol. Pharmacol., 65: 31-39.

Kamel, A.M. 2011. Histologic study on the protective effect of α-lipoic acid in sciatic nerve neurotoxicity induced by cypermethrin in albino rats. Egypt. J. Histol., 34(2): 218-230

Kocaman, A.Y. and Topaktaş, M. 2010. Genotoxic effects of a particular mixture of acetamiprid and β-cypermethrin on chromosome aberration, sister chromatid exchange, and micronucleus formation in human peripheral blood lymphocytes. Environ. Toxicol.: Int. J., 25(2): 157-168.

Kuivila, K.M., Hladik, M.L., Ingersoll, C.G., Kemble, N.E., Moran, P.W., Calhoun, D.L., Nowell, L.H. and Gilliom, R.J. 2012. Occurrence and potential sources of pyrethroid insecticides in stream sediments from seven US metropolitan areas. Environ. Sci. Technol., 4: 4297-4303.

Li, Y., Zhang, L., Dang, Y., Chen, Z., Zhang, R., Li, Y. and Ye, B. C. 2019. Robust electrochemical sensing of the molecularly imprinted polymer prepared by using bifunctional monomer and its application in detection of cypermethrin. Biosens. Bioelectron., 127: 207-214.

Li, Y., Liu, J., Zhang, Y., Gu, M., Wang, D., Dang, Y.Y. and Li, Y. 2018. A robust electrochemical sensing platform using carbon paste electrode modified with molecularly imprinted microsphere and its application on methyl parathion detection. Biosens. Bioelectron.,106: 71-77.

Li, Y., Song, H., Zhang, L., Zuo, P., Ye, B.C., Yao, J. and Chen, W. 2016. Supportless electrochemical sensor based on molecularly imprinted polymer-modified nanoporous microrod for determination of dopamine at trace level. Biosens. Bioelectron., 78, 308-314.

Lidova, J., Stara, A., Kouba, A. and Velisek, J. 2016. The effects of cypermethrin on oxidative stress and antioxidant biomarkers in marbled crayfish (Procambarus fallax f. Virginalis). Neuro. Endocrinol. Lett., 37(1): 53-59.

Ma, Y., Chen, L. and Qiu, J. 2013. Biodegradation of beta-cypermethrin by a novel Azoarcus indigens strain HZ5. J. Environ. Sci. Health B, 48(10): 851-859.

Macagnan, N., Rutkoski, C.F., Kolcenti, C., Vanzetto, G.V., Macagnan, L.P., Sturza, P.F. and Hartmann, M.T. 2017. Toxicity of cypermethrin and deltamethrin insecticides on embryos and larvae of Physalaemus gracilis (Anura: Leptodactylidae). Environ. Sci. Pollut. Res., 24(25): 20699-20704.

Meenambal, M., Pugazhendy, K., Vasantharaja, C. and Venkatesan, S. 2012. Chelating properties of Delonix elata against cypermethrin induced oxidative stress and antioxidant enzyme activity in Cyprinus carpio (Linn). IJPBA., 3(1): 237-243.

Mendoza, J. C., Perea, Y. and Salvador, J. A. 2011. Bacterial biodegradation of permetrina and cipermetrina pesticides in a culture assemblage. Avances en Ciencias e Ingenieria, *2*(3): 45-55.

Molavi, M., Razi, M., Cheraghi, H., Khorramjouy, M., Ostadi, A. and Gholirad, S. 2016. Protective effect of vitamin E on cypermethrin-induced follicular atresia in rat ovary: Evidence for energy-dependent mechanism. Vet. Res. Forum, 7(2): 125.

Narayanan, M., Kumarasamy, S., Ranganathan, M., Kandasamy, S., Kandasamy, G. and Gnanavel, K. 2020. Enzyme and metabolites attained in degradation of chemical pesticides ß Cypermethrin by Bacillus cereus. Mater. Today, 64: 555-571.

Ng, K.L. and Khor, S.M. 2017. Graphite-based nanocomposite electrochemical sensor for multiplex detection of adenine, guanine, thymine, and cytosine: A biomedical prospect for studying DNA damage. Anal. Chem. 89(18): 10004-10012.

Pang, S., Yang T. and He, L. 2016 Review of surface-enhanced Raman spectroscopic (SERS) detection of synthetic chemical pesticides. TrAC Trends Anal. Chem., 85: 73-82.

Pankaj, G.N., Gangola, S., Khati, P., Srivastava, A. and Sharma, A. 2015. Optimization of sulfosulfuron biodegradation through response surface methodology using indigenous bacterial strain isolated from contaminated agriculture field. Int. J. Curr. Microbiol. Appl. Sci., 4: 105-112.

Paravani, E.V., Simoniello, M.F., Poletta, G.L. and Casco, V.H. 2019. Cypermethrin induction of DNA damage and oxidative stress in zebrafish gill cells. Ecotoxicol. Environ. Saf., 173: 1-7.

Pengpumkiat, S., Nammoonnoy, J., Wongsakoonkan, W., Konthonbut, P. and Kongtip, P. 2020. A microfluidic paper-based analytical device for type-II pyrethroid targets in an environmental water sample. Sensors, 20(15): 4107.

Pugazhendy, K., Meenambal, M. and Vijayan, P. 2012. Chelating property of Delonix elata against the toxic impact of cypermethrin on hematological changes in fresh fish Cyprinus carpio (Linn). J. Pharmacol. Res., 5(5): 2610- 2614.

Raghavendra, K., Barik, T.K., Sharma, S.K., Das, M.K., Dua, V.K., Pandey, A., Ojha, V.P., Tiwari, S.N., Ghosh, S.K. and Dash, A. P. 2014. A note on the insecticide susceptibility status of principal malaria vector Anopheles culicifacies in four states of India. J. Vector Borne Dis., 51: 230- 234.

Raksheskar, G.A. 2012. Influenced of cypermethrin on DNA, RNA/ DNA ratio in gills of the freshwater fish Channa striata. Biol. Dis., 3(1): 17-19.

Romero, A., Ares, I., Ramos, E., Castellano, V., Martinez, M., Martinez-Larranaga, M.R., Anadon, A. and Martinez, M.A. 2015. Evidence for dose-additive effects of a type II pyrethroid mixture. In vitro assessment. Environ. Res., 138: 58-66.

Sankar, P., Telang, A.G. and Manimaran, A. 2010. Curcumin protects against cypermethrin-induced genotoxicity in rats. Environ. Toxicol. Pharmacol., 30(3): 289-291.

Sankar, P., Telang, A.G. and Manimaran, A. 2012. Protective effect of curcumin on cypermethrin-induced oxidative stress in Wistar rats. Exp. Toxicol. Pathol., 64(5): 487-493.

Sangha, G.K., Kaur, K. and Khera, K.S. 2013. Cypermethrin induced pathological and biochemical changes in reproductive organs of female rats. J. Environ. Biol., 34(1): 99.

Sharma, A., Gangola, S., Khati, P., Kumar, G. and Srivastava, A. 2016. A novel pathway of cypermethrin biodegradation in a Bacillus sp. strain SG2 isolated from cypermethrin-contaminated agriculture field. 3. Biotech, 6(1): 45.

Singh, R.N., Kumar, P., Singh, V.K. and Singh, D. K. 2010. Toxic effects of Deltamethrin on the levels of biochemical changes in the snail Lymnaea acuminata. J. Pharmacol. Res., 3(8): 1739- 1742.

Singh, A.K., Tiwari, M.N., Upadhyay, G., Patel, D.K., Singh, D., Prakash O. and Singh M.P. 2012. Long-term exposure to cypermethrin induces nigrostriatal dopaminergic neurodegeneration in adult rats: Postnatal exposure enhances the susceptibility during adulthood. Neurobiol. Aging, 33: 404-15.

State of Pesticide Regulations in India. 2013. Centre for Science and Environment, New Delhi.

Stephenson, R.R. 1982. Aquatic toxicology of cypermethrin. I. Acute toxicity to some freshwater fish and invertebrates in laboratory tests. Aqua. Toxicol., 2: 175-185.

Sushma, N. and Devasena, T. 2010. Aqueous extract of Trigonella foenum graecum (fenugreek) prevents cypermethrin-induced hepatotoxicity and nephrotoxicity. Hum. Exp. Toxicol., 29: 311-319.

Tallur, P.N., Megadi, V.B. and Ninnekar, H.Z. 2008. Biodegradation of cypermethrin by Micrococcus sp. strain CPN 1. Biodegradation, 19(1): 77-82.

Tallur, P.N., Mulla, S.I., Megadi, V.B., Talwar, M. P. and Ninnekar, H.Z. 2015. Biodegradation of cypermethrin by immobilized cells of Micrococcus sp. strain CPN 1. Braz. J. Microbiol., 46(3): 667-672.

Tendulkar, M. and Kulkarni, A. 2012. Cypermethrin-induced toxic effect on glycogen metabolism in estuarine clam, Marcia opima (Gmelin, 1791) of Ratnagiri Coast, Maharashtra. J. Toxicol., 6: 1-3.

Tripathi, G. and Singh, H. 2013. Impact of alphamethrin on biochemical parameters of Channa punctatus. J. Environ. Biol., 34(2): 227-230.

Vardavas, A.I., Fragkiadaki, P., Alegakis, A.K., Kouretas, D., Goutzourelas, N., Tsiaoussis, J., Tsitsimpikou, C., Stivaktakis, P.D., Carvalho, F. and Tsatsakis, A.M. 2016. Downgrading the systemic condition of rabbits after long-term exposure to cypermethrin and piperonyl butoxide. Life Sci., 145: 114-120.

Wei, Y., Zeng, Q., Bai, S., Wang, M. and Wang, L. 2017. Nanosized difunctional photo responsive magnetic imprinting polymer for electrochemically monitored light-driven paracetamol extraction. ACS Appl. Mater. Interfaces, 9(50): 44114-44123.

WHO Recommended Classification of Pesticides by Hazard 1994-95, WHO, Geneva.

Wu, L., Liu, F., Wang, G., Guo, Z. and Zhao, J. 2016. Bifunctional monomer molecularly imprinted polymers based on the surface of multiwalled carbon nanotubes for solid-phase extraction of tartrazine from drinks. RSC Adv., 6(1): 464-471.

Xiao, T.T., Shi, X.Z., Jiao, H.F., Sun, A.L., Ding, H., Zhang, R.R. and Chen, J. 2016. Selective and sensitive determination of cypermethrin in fish via enzyme-linked immunosorbent assay-like method based on molecularly imprinted artificial antibody-quantum dot optosensing materials. Biosens. Bioelectron., 75: 34-40.

Yang, J., Feng, Y., Zhan, H., Liu, J., Yang, F., Zhang, K. and Chen, S. 2018. Characterization of a pyrethroid-degrading Pseudomonas fulva strain P31 and biochemical degradation pathway of D-phenothrin. Front. Microbiol., 9: 1003.

Ye, X., Li, F., Zhang, J., Ma, H., Ji, D., Huang, X., Curry Jr., T.E., Liu, W. and Liu, J. 2017. Pyrethroid insecticide cypermethrin accelerates pubertal onset in male mice via disrupting the hypothalamic-pituitary-gonadal axis. Environ. Sci. Technol., 51 (17): 10212-10221.

Yin, L., Li, X., Liu, Y., Zhang, D., Zhang, S. and Luo, X. 2012. Biodegradation of cypermethrin by pseudomonas palustris GJ-22 isolated from activated sludge. Fresenius Environ. Bull. A, 21: 397-405.

Zhan, H., Wang, H., Liao, L., Feng, Y., Fan, X., Zhang, L. and Chen, S. 2018. Kinetics and novel degradation pathway of permethrin in Acinetobacter baumannii ZH-14. Front. Microbiol., 9: 98.

Zhang C., Wang S. and Yan Y. 2011. Isomerization and biodegradation of betacypermethrin by Pseudomonas aeruginosa CH7 with biosurfactant production. Bioresour. Technol., 102: 7139-7146.

Zhang, W., Li, B., Chen, L., Wang, Y., Gao, D., Ma, X. and Wu, A. 2014. Anal. Methods, 6 (7): 2066–2071.

Zhang, Y., Zhou, Y., Tang, Q., Hu, F., Feng, L., Shen, J. and Huang, B. 2018. The protective effects of selenium-enriched spirulina on the reproductive system of male zebrafish (Danio rerio) exposed to beta-cypermethrin. Food Funct., 9(11): 5791-5804.

Zhang, Y., Zuo, P. and Ye, B.C. 2015. A low-cost and simple paper-based microfluidic device for simultaneous multiplex determination of different types of chemical contaminants in food. Biosens. Bioelectron., 68: 14-19.

Zhang, Z. and Li, L. 2018. Efficient synthesis of molecularly imprinted polymers with bio-recognition sites for the selective separation of bovine hemoglobin. J. Sep. Sci., 41(11), 2479-2487.

Zhao H., Geng Y., Chen L., Tao K. and Hou T. 2013. Biodegradation of cypermethrin by a novel Catellibacterium sp. strain CC-5 isolated from contaminated soil. Can. J. Microbiol., 59: 311-17.

Zhao, J., Chi, Y., Xu, Y., Jia, D. and Yao, K. 2016. Co-metabolic degradation of β-cypermethrin and 3-phenoxybenzoic acid by co-culture of Bacillus licheniformis B-1 and Aspergillus oryzae M-4. PLoS One, 11(11): e0166796.

Zhao, W.R., Kang, T.F., Lu, L.P., Shen, F.X. and Cheng, S.Y. 2017. A novel electrochemical sensor based on gold nanoparticles and molecularly imprinted polymer with binary functional monomers for sensitive detection of bisphenol A. J. Electroanal. Chem., 786: 102-111.

Zhou, Y.J., Huang, H.R., Zhou, J. and Wang, L.Q. 2018a. Beta-cypermethrin exposure affects female reproduction by enhancing oxidative stress in mice uterine tissue. Regul. Toxicol. Pharmacol., 98: 284-290.

Zhou, Y.J., Wang, J.H., Wang, L.Q., Xiao, S., Wang, X.D., Yan, H.L., Li, C.F. and Zhu, H.Q. 2018b. Effect of beta-cypermethrin exposure on embryo implantation in mice. Reprod. Toxicol., 76: 1-11.

Zhou, J.W., Zou, X.M., Song, S.H. and Chen, G.H. 2018c. Quantum dots applied to methodology on detection of pesticide and veterinary drug residues. J. Agric. Food Chem., 66(6): 1307-1319.

Nature Environment and Pollution Technology
An International Quarterly Scientific Journal

p-ISSN: 0972-6268
(Print copies up to 2016)
e-ISSN: 2395-3454

Vol. 20 | No. 5 (Suppl) | pp. 2007-2015 | 2021

Original Research Paper

https://doi.org/10.46488/NEPT.2021.v20i05.017

Open Access Journal

# Coal Mining Energy Utilization and Environmental Impact Management Strategy Using the LCA Method

**Frances Roi Seston Tampubolon*†, Arief Sabdo Yuwono**, Armansyah Halomoan Tambunan*** and Noer Azam Achsani******

*Natural Resources and Environmental Management, IPB University, 16177, Indonesia
**Department of Civil and Environmental Engineering, IPB University, Bogor, 16680, Indonesia
***Department of Mechanical and Biosystems Engineering, IPB University, Bogor, 16680, Indonesia
****School of Business, IPB University, Bogor, 16151, Indonesia
†Corresponding author: Frances Roi Seston Tampubolon; roipb19frances@apps.ipb.ac.id

**Nat. Env. & Poll. Tech.**
**Website: www.neptjournal.com**

*Received:* 08-05-2021
*Revised:* 02-07-2021
*Accepted:* 15-07-2021

**Key Words:**
Coal mining
Global warming
Heavy equipment
Life cycle assessment

## ABSTRACT

Coal mining processing and the clearing of land require that materials which have been removed be carefully inspected before it is reused. In this study, the boundary of our model starts with excavation and ends with material recovery. Therefore, further processing of the material to be recovered (recycling, reprocessing) is excluded from the model. In this study, the topsoil layer was collected in three pits numbered one, two, and three, from January to December 2020. The use of the LCA method gives results after the inventory data is carried out, which results in global warming. The results showed material removal unit process generated a total $CO_2$ value of 32.44 kg $CO_2$- eq.tonne$^{-1}$ of coal, and the coal mining unit process generated a total $CO_2$ value of 255.99 kg $CO_2$- eq.tonne$^{-1}$ of coal, for the impact of global warming. When compared to the material removal process, the results of the coal mining unit process show the highest global warming impact. Coal processing gives a yield of 25.61 kg $CO_2$- eq.tonne$^{-1}$ of coal. So that the resulting impact as a whole is 314 kg $CO_2$- eq.tonne$^{-1}$ of coal. The total emissions resulting from B30 fuel (314 kg $CO_2$- eq.tonne$^{-1}$ of coal) are smaller than B20 fuel (320 kg $CO_2$- eq.tonne$^{-1}$ of coal), 6 kg $CO_2$-eq.tonne$^{-1}$ of coal. The coal mining process includes fuel used in coal extraction, coal hauling, coal stockpiling, blasting, water pumps, and water tracks.

## INTRODUCTION

Before extracting coal mining materials, the first thing that must be done is land clearing (Arinaldo & Adiatama 2019). Land clearing requires the use of heavy equipment based on the conditions and shape of the land. In the land clearing process, materials which have been removed must be carefully inspected before it is reused (Hogland et al. 2018). We specifically assessed the impacts of climate change on desertification, land degradation, and food security, and these impacts are evaluated separately (Hogland et al. 2018). In this study, the boundary of our model starts with excavation and ends with material recovery.

Therefore, further processing of the material to be recovered (recycling, reprocessing) is excluded from the model (Gusca et al. 2015). Dozers are one type of heavy equipment used for land clearance. After the land has been prepared for the next process, the heavy equipment for the excavation stage is designed according to the specifications and purpose. For the removal of topsoil layers, the heavy equipment that will be combined for excavating process are excavators, dozers, graders, dump trucks, and compactors (vibrators) (Katta et al. 2020). Before the heavy equipment is used, the production department's manager prepares the necessary combinations to match the specifications, keeping in mind the difficulties of removing the topsoil layer (Agwa-Ejon &Pradhan 2018). The heavy equipment that can be used are excavator (PC 700) and dump truck (DT 740 and DT 741) This equipment's specifications are also essential so that the removal of the topsoil layer is carried out more efficiently and on time. Furthermore, it can minimize the amount of fuel needed in the process (Farjana et al. 2020). It has been shown that different forms of energy derived from fossil fuels can be combined, known as e-fuel (Mahmud et al. 2018, Ioakimidis et al. 2019, Andersson & Börjesson 2021). It is important to combine heavy equipment used at the mine site. (Shaddad 2017, Lodhia 2018). In addition to reducing fuel use, it will also save time when removing the topsoil layer. In this study, the topsoil layer was collected from three pits numbered one, two, and three, from January to December 2020.

For each pit, there are several fleets on each front that it makes. The front is defined as a location where heavy equipment transports topsoil to a temporary stockpile. Usually, on one front, there are about 2 or 3 fleets. A combination of heavy equipment is used at every fleet. Apart from heavy equipment, other supporting heavy equipment such as graders and vibrators will also be used. The graders and vibrators will improve the condition of the mine road so that it may be traversed more easily.

The primary activity in the coal mining industry is coal extraction. Coal extraction is a continuation of the waste reduction process. The areas to be mined are decided once the topsoil and subsoil layers have been properly removed. Thus, the coal is extracted for sending to the stock pile. It is important to have coal cleaning activity in order to mine the coal (coal obtaining). The purpose of coal cleaning is to remove impurities off the surface of coal (coal face) in the form of minor waste material soil, as well as other impurities caused by precipitation agents (surface water, rainwater, avalanches). Following that, the coal extraction process continues until the coal is loaded onto the vehicle.

The use of heavy equipment requires energy for removing/extracting topsoil layers. The average energy needed for seven mines is summarized where the energy requirement is broken down into six components: crushing, grinding, processing, tailings, process water, general plant (Jeswiet & Szekeres 2016). Energy requirements for both open pit and underground mines include electricity and a variety of carbon fuels: natural gas, propane gas and diesel fuel. Both open pit and underground operations are very different and have different energy needs, for instance, underground mines have HVAC energy needs, whereas open pit mines do not. (Jeswiet & Szekeres 2016). The energy source for this study is the same as that used by dump trucks, excavators, graders, and vibrators. Biodiesel B30 is the fuel used. B30 energy is used in coal production by only a few mining businesses. The use of B30 energy has a number of advantages and disadvantages. In this study, the advantages and disadvantages will be examined further using the LCA technique. Compared to 100% diesel, it will be seen which part gives an excess efficiency in the excavation process.

Life cycle assessment or LCA is a methodology for assessing environmental impacts associated with all the stages of the life cycle of a commercial product, process, or service (ISO14044 2006). Biodiesel and electricity energy sources will be input data in the LCA. The final stage is to interpret the impact category study that has been carried out. The LCA stages follow (SNI ISO14004 2016) standards that contain general information, namely: goal and scope of LCA, LCI phase, LCIA phase, interpretation phase, report and critical review, limitations, relationship phase, conditions for the use of value choices, and optional elements (Fig. 1).

Stages, such as interpretation, will be carried out using the LCA technique. This part of the process uses a systematic approach to identify, test, study, evaluate, and deliver conclusions based on the findings of the LCA. It's done to meet the application requirements outlined in the study's objectives and scope.

## MATERIALS AND METHODS

The research was conducted at PT. Bukit Asam Tbk (Persero), located in the village of Tanjung Enim Market, Lawang Kidul District, Muara Enim Regency, South Sumatra. The investigation began in August 2020. LCA is used to achieve the objective of this study. The LCA method is carried out based on the LCA principles and framework in (ISO14040 2006). The objective is to estimate the environmental impact of coal mining management using biodiesel (B30) as a substitute for fuel and an energy source to produce 1 ton of Coal (functional unit) as the final product.

### Goal and Scope

This study uses the LCA method to estimate coal mining management's environmental impact using electricity, biodiesel (B30), and blasting material as an energy source to produce 1 ton of coal (function unit) as the final product.

### Inventory Data Collection

There are three types of data in the life cycle inventory (LCI): primary data, generic data, and estimation data, as presented in Fig. 1.

### Primary Data

Primary data was obtained directly from the company and then entered as inventory data. Data obtained directly from the company can be used immediately and does not undergo data processing, but some must be processed to get the same unit (unit) as the entry system used in the LCA. The data obtained from the company is in the form of input and output of the coal production per month during 2020 from the material removal process unit. The data obtained from the material removal process is fuel (B30) used by heavy equipment. For example, open-pit transportation (rock removal) uses 30% energy for waste and 24% energy for ore disposal (Jeswiet et al. 2015, Jeswiet & Szekeres 2016). Heavy equipment used in the material removal process includes dozers, excavators, graders, compactors, and several other supporting heavy equipment (Fig. 2 & Fig. 3).

In addition to input and output data for the coal production process, input, output, and emission data is also obtained from the coal mining process unit, including coal extracting, coal hauling and coal stockpiling (Fig. 3 and Fig. 4). The data obtained from the material removal process will provide results of the process using alternative fuels (biodiesel B30) and the resulting emissions. First, the LCA assesses the environmental costs (Zhou et al. 2021, Ezeokoli et al. 2021). Second, it is linked to a product, process, or activity by identifying and quantifying the amount of energy and materials used, as well as the waste that is released into the environment.

## Generic Data

Generic data is an average value that represents a value based on the preliminary information that has been obtained. In this process, the initial data acquired will be processed to have a relationship with data originating from the material removal process unit to produce a production process flow.

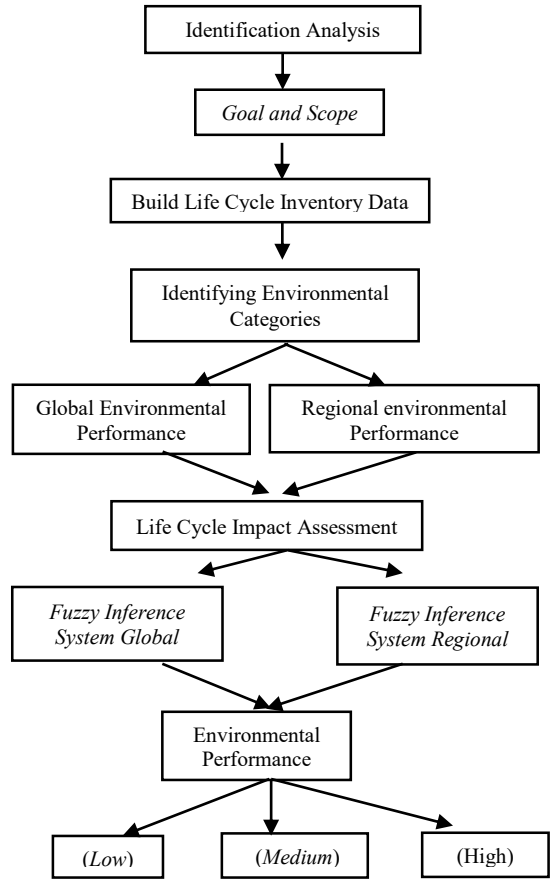


Fig. 1: Stages of the LCA method and fuzzy inference system.

Fig. 2: Dump truck and excavator in Pit 1.

Fig. 3: Grader (coal hauling).

The data of the production flow will be modified into one process flow based on the process unit data.

**Estimated Data**

The data that has been collected from the industry can be done by estimation. It is because not all data can be obtained from industry. To obtain a complete data flow, we estimate by completing the current values. At this stage, an estimate is made to determine energy use during the mining process. The estimation process is carried out by using reports and obtaining data online from employees.

**Data Analysis**

It consists of four stages, namely the goals and scope (goal and scope definition), analysis of input and output inventories (life cycle inventory analysis), environmental impact assessment from inventory data (life cycle impact assessment), and life cycle interpretation. The Open LCA database is used to achieve goal 1 in this study, as presented in Table 1 (Intergovernmental Panel on Climate Change 2014)(USEPA AP 42 1995).

The initial stage of LCA analysis is determines the goal and scope (goal and scope definition) of the analysis (study). The purpose here is to estimate the environmental impact of coal mining management using biodiesel (B30) as a fuel and energy source to generate 1 tonne of coal (functional unit) (Fig. 5). The aim of the LCA study will be decided, as well as the limitations or scope of the LCA implementation. The LCA study will be carried out more systematically and directly if a clear purpose and scope is established. Finally, the use of LCA as a comparison in various cases was carried out as per ISO 14044 2006.

The coal products that will be used by users (consumers) are PLN and PLTU. The restrictions imposed will limit the raw materials that can be used in the final product.

The data that we have obtained and have become inventory data will be factored using a characterization factor. The factor derived from the characterization model is to convert the life cycle inventory results into general units of category indicators (SNI ISO14004 2016). The goal is to see the flow diagram of each unit process carried out at the mine site, and there is a process flow, as shown in Fig. 5 below. The unit process starts from stripping, blasting, overburden hauling, mining, coal processing, and the final coal product with a functional unit of 1 ton of coal.

The relationship between impact indicators, inventory data, and characterization factors is shown in the table presented in Table 1.

The next stage is to carry out normalization and to get an impact indicator. Normalization is the calculation of the size of a category indicator relative to some reference information. The purpose of normalization is to better understand each indicator's comparable magnitude from the product system under study. It is an optional element that can be useful. Some of the normalizations that can be done include: checking for inconsistencies, providing and communicating relatively important indicator result information, and preparing additional procedures, such as grouping, weighting, or life cycle interpretation. The definition of weighting is converting indicators from different impact categories using numerical factors based on choice values. Therefore, weighting methodologies should play an essential role in simplifying LCA output, which would

Fig. 4: Compactor (coal mining).

Table.1: The relationship between inventory data and characterization factors.

| Amount | Emissions | Characteristic Factors | Equivalents |
|---|---|---|---|
| The amount consumed by the process (input) | Emissions released per input unit | Characterization factors of impact categories (IPCC, GWP) | Total kg eq. |

ultimately help identify priorities and define environmental strategies (Vargas-Gonzalez et al. 2019). It can include the aggregation of the results of the weighted indicators. Weighting is an element of choice with two possible procedures: converting the development of the indicator or normalization using the selected weighting factor or combining the corrected or normalized indicator results from all impact categories. Weighting measures are based on choice values and are not scientific. Weighting, one of the steps in LCIA, integrates the various environmental impacts by assigning relative importance to each impact category (Ji & Hong 2016, Curran 2015).

It can be done by analyzing the impact of the data on the number of inputs entered into the inventory data to see the effect on the environment (McKone et al. 2011, Berrill et al. 2016). The material removal process unit will enter input data, such as fuel for topsoil (overburden) and electricity, as previously stated. In a mining operation, LCA can be used to identify the conditions that need to be improved in order to improve the environment (Pell et al. 2019). For the fuel used in this process unit and topsoil removal and transportation of the top layer, B30 biodiesel fuel is also used for watering roadways at the mine site.

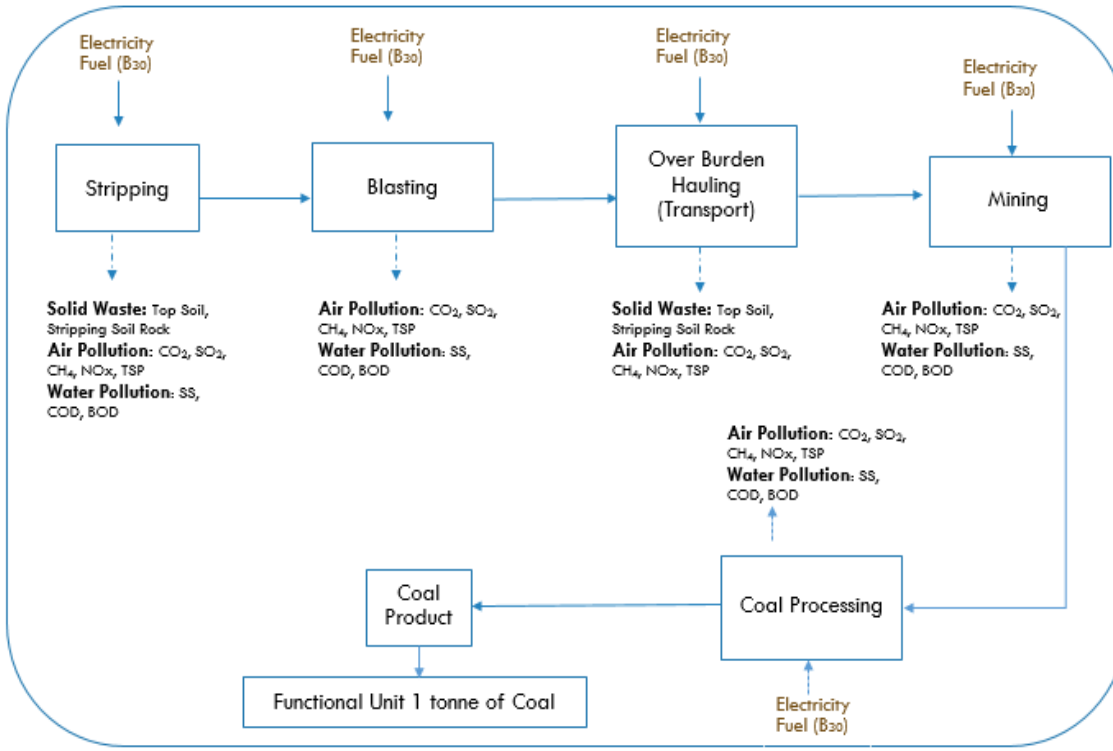


Fig. 5: Boundary system of the LCA process unit.

Fig. 6: Watering for mine road.

After the material removal process unit, the next process unit is coal mining. The processing unit data was fed into the inventory data (coal extracting, coal hauling, and coal stockpiling, transportation for blasting material, explosive material for blasting, electricity, and mine watering and pump for water treatment) as shown in Fig. 6. This process unit produces a coal product as its output.

We use distinguishing factors to determine the impact category from the inventory data entered in the LCA stage. Distinguishing characteristics can use data from databases from both open LCA, Gabi and Simapro.

## RESULTS AND DISCUSSION

The percentage and contribution of the heavy equipment used are shown in Table 2 below. These figures show the kg $CO_2$-equivalent emissions produced by each process unit. These figures show the kg.$CO_2$-eq.tonne$^{-1}$ emissions produced by each process unit. Each processing unit has uses a type of heavy equipment. Meanwhile, the energy source required is electricity taken from the State Electricity Company (PLN), B30 biodiesel fuel, and blasting material used for blasting. Each of these energy sources has different categorical factors. The (Intergovernmental Panel on Climate Change 2014)(EPA and Standards 2003) database was used as definite factors (David & Khanda 2001). The loading and transportation of iron ore (67 percent of total mining emissions) produces the largest GHG emissions, as diesel-powered loaders and trucks are needed to extract ore from the mine for further extraction. According to Tarnoczi (2013), the LCA transportation model was constructed for transportation of oil sands products by pipeline and rail.

The second-largest contributor is vegetation and soil removal, which includes GHG emissions from microbial decomposition of removed biomass and soil, as well as a decrease in photosynthetic productivity over the mine's life. The contribution to the loading and transportation of coal was 255.99 kg.$CO_2$-eq.tonne$^{-1}$ or 81.5% of the total emissions of 314 kg.$CO_2$-eq.tonne$^{-1}$. In this study, the identical results for the second contribution are material removal or those related to soil removal, as shown in Tables 2 and 3.

The amount of emissions produced by the coal-hauling process unit is also shown in Table 2. It means that the process of transporting waste and coal materials requires quite a large amount of biodiesel fuel. Another thing that is very important and needs to be considered is the condition of the mine road (Wolfgang & Burgess-Limerick 2014). Before each assessment and consequently, each measurement, the road is classified according to one of three categories: maintained, which occurs in graded surfaces, rough which is usually found in new exploitation areas or after wet weather

Table 2: Impact category each proses unit (B30) (The year 2020).

| No | Process Unit | Impact Category | | | Total kg $CO_2$-eq. tonne$^{-1}$ of coal |
|---|---|---|---|---|---|
| | | kg $CO_2$ | kg $CH_4$ | kg $N_2O$ | |
| 1 | Fuel for Top Soil and Waste | 27.74 | 0.04 | 0.44 | 28.22 |
| 2 | Electricity for Mine Site Lighting Lamps (Material Removal) | 3.33 | | | 3.33 |
| 3 | Water Truck for Watering the Mine Road | 0.87 | 0.00 | 0.01 | 0.89 |
| 4 | Total kg $CO_2$-eq.tonne$^{-1}$ of Coal (Material Removal) | | | | 32.44 |
| 5 | Coal Extraction, Coal Hauling, Coal Stockpiling | 3.10 | 0.01 | 0.07 | 3.18 |
| 6 | Transportation for Blasting Material | 0.21 | 0.00 | 0.00 | 0.21 |
| 7 | Explosive Material for Coal Blasting | 0.54 | | | 0.54 |
| 8 | Electricity for Mine Site Lighting Lamps (Coal Mining) | 5.61 | | | 5.61 |
| 9 | Water Truck for Watering the Mine Road | 0.96 | 0.00 | 0.02 | 0.98 |
| 10 | Water Pump for Water Treatment | 1.56 | 0.00 | 0.02 | 1.59 |
| 11 | Coal Operation | | 243.88 | | 243.88 |
| 12 | Total kg $CO_2$-eq. tonne$^{-1}$ of Coal (Coal Mining) | | | | 255.99 |
| 13 | Fuel (Coal Crusher, Coal Stacking as Product) | 2.33 | 0.00 | 0.04 | 2.37 |
| 14 | Electricity for Mine Site Lighting Lamps (Coal Processing) | 3.12 | | | 3.12 |
| 15 | Coal As Received (Pasca Mining) | | 20.12 | | 20.12 |
| | Total kg $CO_2$-eq.tonne$^{-1}$ of Coal (Coal Processing) | | | | 25.61 |
| | Total of all | | | | 314 |

conditions or combination, which means the variety of both maintained and uneven (Duarte et al. 2020).

In general, the results from the unit process made the most significant contribution, especially during the coal transportation operation, which generated 255.99 kg.$CO_2$-eq. tonne$^{-1}$ of coal.

The results given from the impact analysis give a value of 32.44 tonnes of $CO_2$-eq.tonne$^{-1}$ coal for material removal process. The activity describes the biodiesel fuel used in the process unit for each tonne of coal produced. Energy is needed to extract topsoil and waste, to light the mine site during excavation using electricity, to remove and dispose waste material, and watering the mine road that the dump truck traverses.

Furthermore, the findings from the coal mining process unit, shows a yield value of 255.99 kg.$CO_2$.eq.tonne$^{-1}$ coal.

Table 3: Impact category each process unit (B20 &B30) (The Year.2020).

| No | Process Unit | $B_{20}$ | | | | $B_{30}$ | | | |
|---|---|---|---|---|---|---|---|---|---|
| | | Impact Category | | | Total kg $CO_2$-eq. tonne$^{-1}$ of coal | Impact Category | | | Total kg $CO_2$-eq. tonne$^{-1}$ of coal |
| | | kg $CO_2$ | kg $CH_4$ | kg $N_2O$ | | kg $CO_2$ | kg $CH_4$ | kg $N_2O$ | |
| 1 | Fuel for Top Soil dan Over Burden | 32.42 | 0.04 | 0.44 | 32.90 | 27.74 | 0.04 | 0.44 | 28.22 |
| 2 | Electricity for Mine Site Lighting Lamps (Material Removal) | 3.33 | | | 3.33 | 3.33 | | | 3.33 |
| 3 | Water Truck for Watering for the Mine Road | 1.02 | 0.00 | 0.01 | 1.04 | 0.87 | 0.00 | 0.01 | 0.89 |
| 4 | Total kg $CO_2$-eq/tonne of Coal (Material Removal) | | | | 37.26 | | | | 32.44 |
| 5 | Coal extracting, Coal Hauling, Coal Stockpiling | 3.62 | 0.01 | 0.07 | 3.70 | 3.10 | 0.01 | 0.07 | 3.18 |
| 6 | Transportation for Blasting Material | 0.24 | 0.0003 | 0.003 | 0.24 | 0.21 | 0.00 | 0.00 | 0.21 |
| 7 | Explosive Material for Coal Blasting | 0.54 | | | 0.54 | 0.54 | | | 0.54 |
| 8 | Electricity for Mine Site Lighting Lamps (Coal Mining) | 5.61 | | | 5.61 | 5.61 | | | 5.61 |
| 9 | Water Truck for Watering for the Mine Road | 1.12 | 0.00 | 0.02 | 1.14 | 0.96 | 0.00 | 0.02 | 0.98 |
| 10 | Water Pump for Water Treatment | 1.82 | 0.0021 | 0.03 | 1.85 | 1.56 | 0.00 | 0.02 | 1.59 |
| 11 | Coal Operation | | 243.88 | | 243.88 | | 243.88 | | 243.88 |
| 12 | Total kg $CO_2$-eq/ tonne of Coal (Coal Mining) | | | | 256.96 | | | | 255.99 |
| 13 | Fuel (Coal Crusher, Coal Stacking as Product) | 2.58 | 0.00 | 0.04 | 2.62 | 2.33 | 0.00 | 0.04 | 2.37 |
| 14 | Electricity for Mine Site Lighting Lamps (Coal Processing) | 3.12 | | | 3.12 | 3.12 | | | 3.12 |
| 15 | Coal As Received (Pasca Mining) | | 20.10 | | 20.10 | | 20.12 | | 20.12 |
| 16 | Total kg $CO_2$-eq/ tonne of Coal (Coal Processing) | | | | 25.84 | | | | 25.61 |
| | Total of all | | | | 320 | | | | 314 |

This result demonstrates the greatest impact. Coal haulage, coal stockpiling, and coal operations in the coal extraction process require the most fuel. Table 3 shows the final result of the coal extracting process, which shows a yield of 25.61 $kg.CO_2.eq.tonne^{-1}$ of coal. The majority of heavy equipment used in the coal mining process is for tasks such as coal hauling, coal extraction, water rails, and water pumps.

This tool uses biodiesel fuel and uses electricity obtained from the state electricity company (PLN). Transportation used is a dump truck to deliver materials. The blasting process also requires material for detonating and transportation to provide the material to the blasting site.

Energy consumption data for the loading and hauling fleet was collected as part of this study. Much of the equipment used in mining for material movement or haulage is powered by diesel engines. Diesel technologies demand a lot of energy, accounting for 87 percent of the energy used in materials handling (Norgate & Haque 2010).

The results obtained in this study show a value of 7.6 $kg.CO_2.eq.tonne^{-1}$ of coal in materials handling compared to a previous study that showed a value of 6.0 $kg.CO_2.eq.tonne^{-1}$ of ore in materials handling (Norgate & Haque 2010). We compare the results obtained in this study, namely 81.5% of the total emissions from the cradle to gate activity. The result is almost similar to Norgate & Haque (2010).

The results of the impact categories presented in table 3 illustrate the impacts they can have on human health, the environment, and other resources (Munawer 2018). According to Munawer (2018), the effect that is acceptable to humans is due to continuous $CO_2$ emissions and underlying climate change; global warming is correlated with an increase in flood incidence and overall storm activity (Farjana et al. 2018, Hurlbert et al. 2019).

## CONCLUSION

The results of the LCA process contribute to each of the processes that have been completed. However, some data related to material removal, coal mining, and coal processing is evaluated and estimated according to the conditions in the field. Although some data cannot be processed, the inventory data input process and categorical factors yield an approximate value.

The impact of metal production processes, particularly those linked to energy content and greenhouse gas emissions, on the environment can be seen from the value of the contribution of the mining and mineral processing phases to the environment.

The results that have been obtained from each process unit are:

1. Total material removal is 32.44 $kg.CO_2$ $eq.tonne^{-1}$ of coal.
2. Total coal mining is 255.99 $kg.CO_2.eq.tonne^{-1}$ of coal.
3. Total coal processing is 25.61 $kg.CO_2.eq.tonne^{-1}$ of coal.

The results obtained in the coal mining process unit gave 81.5% of the total emission produced. Therefore, the total emissions resulting from B30 fuel (314 $kg.CO_2.eq.tonne^{-1}$ of coal) are smaller than B20 fuel (320 $kg.CO_2.eq.tonne^{-1}$ of coal), 6 $kg.CO_2.eq.tonne^{-1}$ of coal. The coal mining process includes fuel used in coal extracting, coal hauling, coal stockpiling, blasting, water pumps, water tracks. Meanwhile, the state electrical corporation provides electricity for mining street lighting (PLN).

## ACKNOWLEDGEMENT

This research was funded by the Education Fund Management Agency (LPDP) from the Ministry of Finance of the Republic of Indonesia.

## REFERENCES

Agwa-Ejon, J.F. and Pradhan, A. 2018. Life cycle impact assessment of artisanal sandstone mining on the environment and health of mineworkers. Environ. Impact Assess. Rev., 72(10): 71-78..

Andersson, Ö. and Börjesson, P. 2021. The greenhouse gas emissions of an electrified vehicle combined with renewable fuels: Life cycle assessment and policy implications. Appl. Energy, 289: 6621.

Arinaldo, D. and Adiatama, J.C. 2019. The dynamics of Indonesian coal: Towards a fair energy transition. Inst. Essent. Serv. Reform, 4(5): 31-49

Berrill, P., Anders, A., Yvonne, S., Hans, C.G. and Edgar, G.H. 2016. Environmental impacts of high penetration renewable energy scenarios for Europe. Environ. Res. Lett., 11(1): 12-40

Curran, M.A. 2015. Life cycle assessment: A systems approach to environmental management and sustainability. Chem. Eng. Prog., 111(10): 26-35.

David, C.W. and Khanda, D. 2001. Application of life cycle assessment. Energy, 11(3): 1-20 https://doi.org/10.1201/9780203907931.ch16.

Duarte, J., Branco, J.C., Matos, M.L. and Santos, J.B. 2020. Understanding the whole-body vibration produced by mining equipment as a role-player in workers' well-being: A systematic review. Extr. Indust. Soc., 7(4): 1607-23.

EPA, U.S. and Office of Air Quality Planning and Standards. 2003. Wood Residue Combustion In Boilers. AP 42, Compilation of Air Pollutant Emission Factors, Volume 1 Stationary Point and Area Sources, pp. 1-20.

Ezeokoli, O.T., Oluwatosin, G., Oladipo, C., Bezuidenhout, C., Adeleke, R.A. and Maboeta, M.S. 2021. Assessing the ecosystem support function of South African coal mining soil environments using earthworm (Eisenia Andrei) bioassays. Appl. Soil Ecol., 157(5): 103771.

Farjana, S.H., Nazmul H., and Parvez Mahmud,M.A. 2018. Life-Cycle environmental impact assessment of mineral industries. IOP Conf. Series: Mater. Sci. Eng., 351(1): 0-7.

Farjana, S.H., Parvez, M. and Nazmul, H.. 2020. Solar process heat integration in the lead mining process. Case Stud. Thermal Eng., 22(10): 100768.

Gusca, J., Maksims, F. and Indra, M. 2015. Life cycle assessment of landfill mining project. Energy Procedia, 72: 322–328.

Hogland, M., Dace, Ā, Mait, K., Yahya, J., Fabio, K. and André Luís, D.S.K.O. 2018. Remarks on four novel landfill mining case studies in Estonia and Sweden. J. Mater. Cycles Waste Manag., 20(2): 1355–1363.

Hurlbert, M., Krishnaswamy, J., Davin, E., Johnson, F.X., Mena, C.F., Morton, J., Myeong, S., Viner, D., Warner, K. and Wreford, A.

2019. Risk Management and Decision-Making in Relation to Sustainable Development Coordinating. In Shukla, P.R., Skea, J.,

Calvo Buendia, E., Masson-Delmotte, V., Pörtner, H.O., Roberts, D.C., Zhai, P., Slade, R., Connors, S., Van Diemen, R., Ferrat,

M., Haughey, E., Luz, S., Neogi, S., Pathak, M., Petzold, J., Portugal Pereira, J., Vyas, P., Huntley, E., Kissick,

K., Belkacemi, M. and Malley, J. (eds.), Climate Change and Land: An IPCC Special Report on Climate Change, Desertification, Land Degradation,

Sustainable Land Management, Food Security, and Greenhouse Gas Fluxes in Terrestrial Ecosystems . In Press, pp.673-800.

Intergovernmental Panel on Climate Change. 2014. Climate Change 2014 Mitigation of Climate Change. Climate Change 2014 Mitigation of Climate Change. https://doi.org/10.1017/cbo9781107415416.

Ioakimidis, C.S., Alberto, M., Ali, B.D., Dimitrios, T. and Konstantinos, N.G. 2019. Life cycle assessment of a lithium iron phosphate (LFP) Electric vehicle battery in second life application scenarios. Sustainability, 11(9): 52.

ISO14040. 2006. Standard, International Organization.

ISO14044. 2006. Standard, International Organization.

Jeswiet, J., Archibald, J., Thorley, U. and. De Souza, E. 2015. Energy use in premanufacture (mining). Procedia CIRP, 29: 816-21.

Jeswiet, J. and Alex Szekeres, A. 2016. Energy consumption in mining comminution. Procedia CIRP, 48:140-45.

Ji, C. and Hong, T. 2016. New Internet search volume-based weighting method for integrating various environmental impacts. Environ. Impact Assess. Rev., 56: 128-38.

Katta, A.K., Matthew, D. and Kumar, A. 2020. Development of disaggregated energy use and greenhouse gas emission footprints in Canada's iron, gold, and potash mining sectors. Resour. Conserv. Recycl., 152: 104485.

Lodhia, S.K. 2018. Mining and Sustainable Development: Current Issues. Routledge, England, UK.

Mahmud, M.A.P., Nazmul, H., Shahjadi, H.F. and Candace, L. 2018. Environmental impacts of solar-photovoltaic and solar-thermal systems with life-cycle assessment. Energies, 11(9): 46. https://doi.org/10.3390/en11092346.

McKone, T.E., Nazaroff, W.W., Berck, P., Auffhammer, M., Lipman, T., Torn, M.S. and Masanet, E. 2011. Grand challenges for life-cycle assessment of biofuels. Environ. Sci. Technol., 45(5): 1751-56.

Munawer, M.E. 2018. Human health and environmental impacts of coal combustion and post-combustion wastes. J. Sustain. Mining, 17(2): 87-96.

Norgate, T. and Haque, N. 2010. Energy and greenhouse gas impacts of mining and mineral processing operations. J. Cleaner Prod., 18(3): 266-74.

Pell, R., Laurens, T., Palmer, L.W.H, Glass, X.Y., Frances,W., Xianlai, Z. and Jinhui, L. 2019. Environmental optimization of mine scheduling through life cycle assessment integration. Resour. Conserv. Recycl., 142(12): 267-76.

Shaddad, A. 2017. Analysis of the compatibility of mechanical equipment (match factor) for increased productivity. J. Geo., 4(3): 74.

SNI ISO14004. 2016. SNI ISO 14004 Sistem Manajemen Lingkungan – Pedoman Umum Dalam Penerapan Environmental Management Systems – General Guidelines on Implementation, pp. 1-122.

USEPA AP 42. 1995. AP 42, Fifth Edition Compilation of Air Pollutant Emission Factors, Volume 1: Stationary and Point Sources, pp. 1-10.

Tarnoczi, T. 2013. Life cycle energy and greenhouse gas emissions from transportation of Canadian oil sands to future markets. Energy Policy, 62: 107-17.

Vargas-Gonzalez, M., François, W., Patricia, M., Laurent, G., Sébastien, H., Olivier, J., Rosalie, V.Z and Jacques, L. 2019. Operational life cycle impact assessment weighting factors based on planetary boundaries: applied to cosmetic products. Ecol. Indicators, 107(4): 105498.

Wolfgang, R. and Burgess-Limerick, R. 2014. Whole-body vibration exposure of haul truck drivers at a surface coal mine. Appl. Egron., 45(6): 1700-1704.

Zhou, Y., Feng, L. and Tao, Z. 2021. An experience-based mining approach to supporting urban renewal mode decisions under a multi-stakeholder environment in China. Land Use Policy, 106: 105428.

Nature Environment and Pollution Technology
An International Quarterly Scientific Journal

p-ISSN: 0972-6268
(Print copies up to 2016)
e-ISSN: 2395-3454

Vol. 20 | No. 5 (Suppl) | pp. 2017-2021 | 2021

Original Research Paper

https://doi.org/10.46488/NEPT.2021.v20i05.018

Open Access Journal

# Biosynthesis of Xanthan Gum by *Xanthomonas campestris* Using Cane Molasses as a Carbon Source

**Bhumi Rajyaguru*, Ajit Varma*, Amit Kharkwal*† and Jasvir Singh****
*Department of Microbiology, Amity Institute of Microbial Technology, Amity University, Noida-201313, India
**Global Regulatory Affairs, Danisco (India) Private Limited, Gurgaon- 122002, India
†Corresponding author: Amit Kharkwal; ackharkwal@amity.edu

**Nat. Env. & Poll. Tech.**
**Website: www.neptjournal.com**

*Received:* 16-04-2021
*Revised:* 15-05-2021
*Accepted:* 25-05-2021

**Key Words:**
*Xanthomonas campestris*
Cane molasses
Xanthan gum
Cauliflower leaf

## ABSTRACT

The objective of the present study was to study the optimization conditions for the production of xanthan by *Xanthomonas campestris* from pre-treated sugarcane molasses. In the study, the optimization was carried out for different parameters including pH, temperature, and incubation time for the pre-treated sugarcane molasses. The age of inoculums and time of culture growth (6, 12, 18 and 24 hrs), size of inoculums (2%, 5%, 7.5% and 10%), pH (6.6, 6.8, 7.0 and 7.2) and temperature (25°C, 28°C, 30°C, 32°C and 37°C) were studied. It was observed that the xanthan production was maximal with 7.5% (v/v) inoculums, pH. 7 at 30°C for 48 hrs. The study suggested that cane molasses is an appropriate agro-industrial substrate for xanthan gum fermentations, and further scale-up study is needed for gum production in the stirred fermenter.

## INTRODUCTION

Polysaccharides are important natural products usually obtained through plant sources. The manufacture of polysaccharides by the fermentation process, instead of their extraction from plant sources, is a newly developed industry (Murugesan et al. 2012, Kleinitz et al. 1989). xanthan gum is one of the polysaccharides that can be produced by culturing microorganisms belonging to the Xanthomonas genus (Sutherland 1998, Becker et al.1998). The natural synthesis in bacteria is a dual-stage method wherein first stage growth of the microorganism is ideal and in second stage biosynthesis of the polysaccharide takes place with considerably no growth of the microorganism (Amanullah et al.1998). The polysaccharide or gums with novel properties are in high demand in food processing and many industrial operations. FDA allowed use of xanthan gum for general use in foods e.g., in cream cheese as a thickening and stabilizing agent (Chi-Liang et al.1996, FDA 2020).

Xanthan gum is also widely used in the oil industry, the pharmaceutical industry, and a variety of other industries. (Hassler 1990). However, commercially procured xanthan is relatively expensive. The higher cost is due to the costly substrate such as glucose or sucrose and high purity required for use in food products. For example, in the synthesis of food-grade xanthan, almost half of the cost is capitalized in its downstream processing. The cost of large-scale xanthan synthesis can be reduced by a significant amount if we use waste agricultural products as substrate (Frank & Somkuti 1979, Jean-Claude et al. 1997).

One of the best available agricultural wastes is molasses. It is a by-product of sugar production, both from sugar beet as well as from sugarcane (Pinches & Pallent 1986). Molasses is the surfeit syrup from the final stage of crystallization, from which further crystallization of sugar is profligate (Silva et al. 2009, Gumus et al. 2010). In contrast to sugar beet molasses, cane molasses differs in nitrogen levels. Also, cane molasses is a virtuous source of sucrose (almost 90%) (Cadmus et al. 1978).

Using molasses as a substrate helps to reduce the cost of xanthan production and also help address bio-waste management issue and pollution (Honart et al. 1985). In the present study, we have attempted to produce xanthan gum using cane molasses bio-waste as a carbon source. Hence, we tried to optimize the growth conditions of Xanthomonas strains to maximize xanthan gum production.

## MATERIALS AND METHODS

### Microorganism and Culture Conditions

The Xanthomonas strains capable of producing xanthan gums were isolated from infected cauliflower leaves. The isolated strains were screened further for xanthan gum production

and the isolate was identified based on cultural, morphological, Biochemical characteristics and molecular identification (accession number SUB9292907 16_rRNA_Xanthomonas MW741556. NCBI BLAST (http://www.ncbi.nlm.nih.gov/Blast). A standard strain of *Xanthomonas campestris* (NCIM 5028) bacteria procured from NCIM-Pune was also used as a Reference Culture. The isolated *X. campestris* was grown in 50 mL LB sucrose media (Sucrose: 1 g/L, Yeast Extract: 0.1g/L, Peptone: 0.5 g/L, NaCl: 0.3 g/L) for 48 h at 34°C. The isolated *X. campestris* strain was adapted to high molasses concentrations and maintained in submerged cultures on MGYP medium (Malt Extract: 0.3g, Glucose: 1g, Yeast Extract: 0.3g, Peptone: 0.5g, Water: 100mL, Agar: 2g, pH: 6.4-6.8).

**Collection and Analysis of Sugarcane Molasses**

The sugarcane molasses was purchased from a local source. The physico-chemical characteristics of sugar cane molasses such as color, odour, pH, biochemical oxygen demand (BOD), chemical oxygen demand (COD), acidity, total Kjeldahl nitrogen, total suspended solids (TSS), oils and grease total dissolved solids (TDS) and sulphides were conducted using the standard method (APHA 2005).

**Pre-treatment of Sugarcane Molasses**

The cane molasses was pre-treated by the addition of 4 g/L K2HPO4 to the medium to obtain better xanthan gum yield and biomass production (Murugesan et al. 2012).

**Growth Adaptation of *X. campestris* in Molasses**

To achieve quick growth and thereupon higher productivity, the organism was adapted to high molasses environments by successive sub-culturing (4 passages). The pure culture obtained possessed improved characteristics in terms of growth and xanthan gum manufacture (Stavros et al. 2003).

**Culture Medium and Optimization**

The culture Medium used was 8 % molasses pre-treated with 4 g/L $K_2HPO_4$. Growth parameters, viz. pH, temperature, effect of inoculum, aeration, agitation and incubation period were standardized at bench scale for the *Xanthomonas campestris* strain (isolated from cauliflower leaves) to get maximum gum production. Various parameters such as age of inoculums time of culture growth (6, 12, 18, 24 hrs), size of inoculums (2%, 5%, 7.5%, 10%), pH (6.6, 6.8, 7.0, 7.2) and temperature (25°C, 28°C, 30°C, 32°C, 37°C) and the incubation period (12, 24, 48, 72 hrs) were observed and optimized for best growth. Other factors such as aeration and agitation of culture flasks were also optimized. It was pragmatic that shaker flasks provided better aeration to the culture and agitation is required for better mass transfer.

**Assay of Xanthan Gum**

The final product in form of xanthan Gum was obtained in the optimized culture of *Xanthomonas campestris*. The presence of xanthan gum was determined by test method as per Indian Pharmacopoeia, 1996. Briefly, the solution was lysed with 0.1 M hydrochloric acid, the supernatant was treated with dinitrophenyl hydrazine- hydrochloric solution followed by methyl acetate and then sodium carbonate. An absorption maximum was measured at 375 nm using sodium carbonate as the compensation liquid.

**Xanthan Gum Recovery**

Precipitation of xanthan gum was done with isopropanol (2x volume of supernatant) to which 1 % (w/v) of potassium chloride was added. The dried biomass and xanthan gum produced were determined by drying in an oven at 105°C and 40°C, respectively and measured using Brookfield Viscometer (LABPRO, Model No. LMDV-60) at 25°C (Carignatto et al. 2011).

## RESULTS AND DISCUSSION

The "xanthan gum" is produced in dual stages by *Xanthomonas campestris*. The bacterium is cultivated in Nutrient Agar and the biomass formed is used as inoculum for the subsequent stage in which the gum is formed by batch process. The biomass and xanthan gum formed were determined by drying in an oven at 105°C and 40°C. Xanthomonas strains capable of producing gums were isolated from infected plants (*Brassica oleracea* var. *botrytis*). Morphological and biochemical characterization of *Xanthomonas campestris* was done (Fig. 1).

To obtain a good yield of xanthan gum, various parameters such as carbon source, pH, temperature and incubation time were optimized. It was established that xanthan gum was attained in the best quantity at 30°C temperature (Fig. 2). The cell dissociation enhanced metabolite production giving high continuous yield (Psomas et al. 2007, Esgalhado et al. 1995, Garcia-Ochoa et al. 1996). A comparable observation has been made in other optimization studies wherein xanthan production was increased with a change in physical parameters (Kerdsup et al. 2011, Borges et al. 2008, Kalogiannis et al. 2003). Amongst other growth parameters, it was found that xanthan production was maximal with 7.5% (v/v) inoculums, pH.7 at 30°C at 48 hrs. (Figs. 3 and 4).

The parameters were standardized at bench scale for the effect of inoculums and age of Inoculums at different incubation time points including 6, 12, 18, 24 and 48 hrs. culture respectively. It was found that 48 hrs. were optimal for a good yield of xanthan gum. Also, the ideal size of inoculums

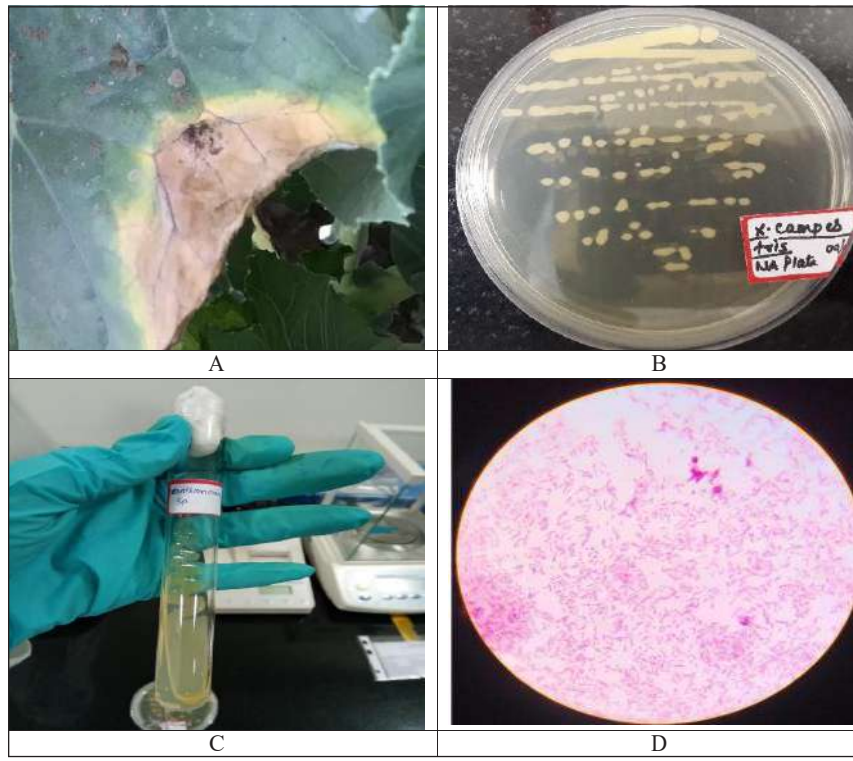


Fig. 1: A-infected Cauliflower leaf with *Xanthomonas*, B and C- isolated *Xanthomonas* strains, capable of producing gums, from infected plants (Cauliflower), D-The bacterial genus *Xanthomonas* are small, motile, Gram-negative rods, aerobic, and produce Cremish/yellow pigments and characteristically parasitize plants.

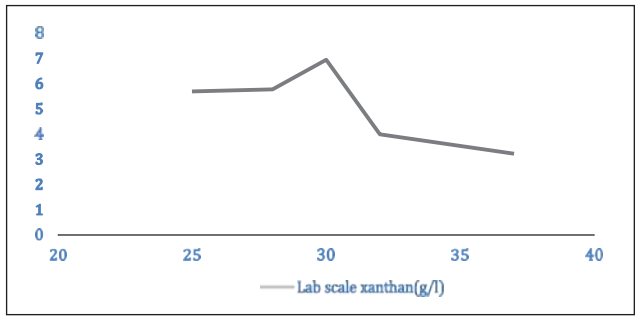


Fig. 2: Temperature variation of different quantity of xanthan production.

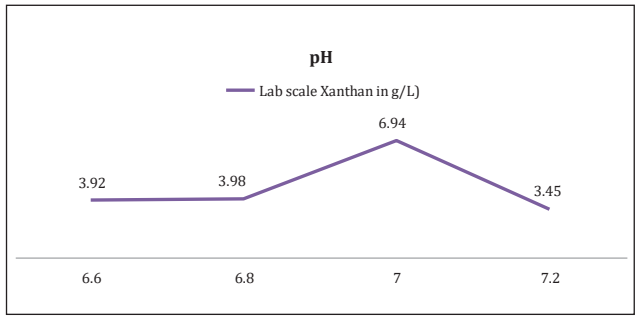


Fig. 3: Production of xanthan at different pH.

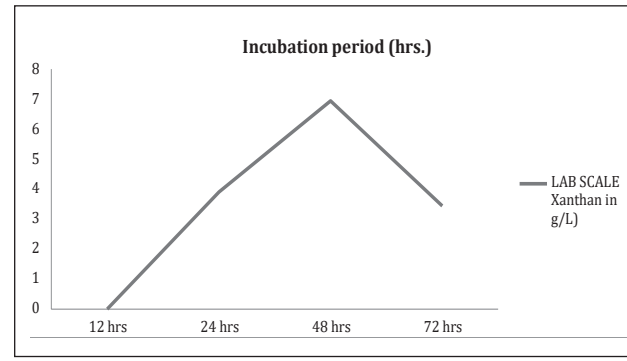


Fig. 4: Production of xanthan at different incubation time points.

was tested to find the appropriate amount. It was observed that 12 hrs of culture as ideal age of inoculum and size of inoculums 7.5% of were best for gum yield as mentioned in Table 1. Aeration plays a vital role in determining the yield of any product in closed culture. It was observed that shaker flasks provide the right amount of aeration to *X. campestris* culture. Agitation of culture flasks is also required for better mass transfer.

This study looked into the possibility of making xanthan gum from cane molasses (8 % molasses pre-treated with 4

Table 1: Effect of ioculum.

| Age of inoculum, 12 hrs culture is optimum | |
|---|---|
| Age of inoculum | Lab Scale (Xanthan gum g/L) |
| 6 hrs | ND |
| 12 hrs | 6.94 |
| 18 hrs | 4.32 |
| 24 hrs | 2.34 |

| Size of inoculum: 7.5 % is optimum | |
|---|---|
| Size of Inoculum | Lab Scale (Xanthan gum g/L) |
| 2 | 3.72 |
| 5 | 3.96 |
| 7.5 | 6.94 |
| 10 | 2.1 |

g/L $K_2HPO_4$). In most cases, using low-cost substrates can help biological processes run more efficiently (Yoo & Harcum 1999, Stredansky & Conti 1999, Psomas et al. 2007). Glucose syrup is currently produced primarily from starchy materials. Because of the cost and availability of starch, the use of glucose syrup as a substitute for pure glucose is favored in a variety of industries, including the beverage and ethanol industries. (Kobayashi & Nakamura 2004). Cane molasses was used as a carbon source for the production of xanthan gum in this study. Indeed, this work is a first step toward increasing the efficiency of the xanthan gum manufacturing process.

The purity of xanthan gum is generally an important consideration, particularly when the product is intended for use in the food industry. The use of cane molasses in this study could help to reduce the presence of unwanted substrate ingredients in the final product (García et al. 2000, Funahashi et al.1987). *Xanthomonas campestris* grew well on LB sucrose media and was maintained on MGYP medium and cane molasses was pre-treated by addition of K2HPO4 to the medium to obtain better xanthan gum yield and biomass production. The strain

*Xanthomonas campestris* performed better in xanthan production because it had a higher maximum growth rate.

Few reports are showing different culture conditions for xanthan production using *Xanthomonas campestris* (Shu & Yang 1990). The conditions and parameters vary in each indicating that there is always a good scope of experimenting with the best conditions producing xanthan gum. This might be due to varied carbon sources and slight differences in the culture of *Xanthomonas campestris* used for inoculation.

## CONCLUSION

In the current study, the *Xanthomonas* strains capable of producing gums from infected cauliflower were isolated and screened further for xanthan gum production. The potent isolated strain was used for gum production using cane molasses as a carbon source. The study concluded that xanthan production was maximum with 7.5% (v/v) inoculum, 12 hrs culture, pH.7 at 30°C for 48 hrs with the isolated strain. Further, scale-up studies of gum production in the stirred fermenter (10 L) are underway.

## ACKNOWLEDGEMENTS

The authors are highly grateful to the Faculty of Microbiology, Amity Institute of Microbial Technology, Amity University, Noida for their support and guidance, special thanks to Dr. Rahul Singh and Ms. Madhulika Ganguly from Emami Ltd. for their support and Dr. Meghna Singh for her immense help and support.

## REFERENCES

Amanullah, A., Satti, S. and Nienow, A.W. 1998. Enhancing xanthan fermentation by different modes of feeding. Biotechnology Progress, 14: 265-269.

APHA 2005. Standard Methods for the Examinations of Water and Wastewater, 21th edition. American Public Health Association, Washington D.C.

Becker, A., Katzen, F., Puhler, A. and Ielpi, L. 1998. Xanthan gum biosynthesis and application: A biochemical/genetic perspective. Applied Microbiology Biotechnology, 50: 145-152.

Borges, C.D., da Moreira, A.S., Vendruscolo, C.T. and Ayub, M.A.Z. 2008. Influence of agitation and aeration in xanthan production by *Xanthomonas campestris* pv pruni strain 101. Revista Argentina de Microbiologia, 40: 81-85.

Cadmus, M.C., Knutson, C.A., Lagoda, A.A., Pittsley, J.E. and Burton, K.A. 1978. Synthetic media for production of quality xanthan gum in 20 liter fermentors. Biotechnol Bioeng., 20: 1003- 1014.

Carignatto, Cíntia, Oliveira, Kassandra Sussi, Lima, Valéria and de Oliva Neto, Pedro 2011. New culture medium to xanthan production by *Xanthomonas campestris* pv. campestris. Indian Journal of Microbiology, 51: 283-288.

Chi-Liang, W., Ka, T.C., Nien-Tsung, L. and Yi-Hsiung, T. 1996. Increase of xanthan production by self-cloning of a 3.0-kb EcoRI-KpnI chromosomal fragment in *Xanthomonas campestris*. Biotechnology Letter, 18: 1301-1304.

Esgalhado, M.E., Roseiro, J.C. and Amaral, C.M.T. 1995. Interactive effects of pH and temperature on cell growth and polymer production by *Xanthomonas campestris*. Process Biochemistry, 30: 667-671.

FDA 2020. Code of Federal Regulations, Food and Drugs, Chapter I--Food and Drug Administration, Food Additives Permitted for Direct Addition to Food For Human Consumption (https://www.accessdata.fda.gov/scripts/cdrh/cfdocs/cfcfr/cfrsearch.cfm?fr=172.695).

Frank, J.F. and Somkuti, G.A. 1979. General properties of beta-galactosidase of *Xanthomonas campestris*. Appl. Environ. Microbiol., 38: 554-556.

Funahashi, H., Yoshida, T. and Taguchi, H. 1987. Effect of glucose concentration on xanthan gum production by *Xanthomonas campestris*. J. Ferment. Technol., 65: 603-606.

García, O.F., Castro, E.G. and Santos, V.E. 2000. Oxygen transfer and uptake rates during xanthan gum production. Enzyme Microb. Technol., 27: 680-90.

Garcia-Ochoa, F., Santos, V.E. and Alcon, A. 1996. Simulation of xanthan gum

production by a chemically structured kinetic model. Mathematics and Computers in Simulation, 42: 187-195.

Gumus, T., Demirci, A.S., Mirik, M., Arici, M. and Aysan, Y. 2010. Xanthan gum production of Xanthomonas spp. isolated from different plants. Food Sci. Biotechnol., 19: 201-206.

Hassler, R.A. 1990. Genetic engineering of polysaccharide structure: Production of variants of xanthan gum in *Xanthomonas campestris*. Biotechnology Progress, 6: 182-187.

Honart, P., Paquot, M., Hermans, L., Alaoui, H. and d'Ippolito, P. 1985. Xanthan production by *Xanthomonas campestris* NRRL B-1459 and interfacial approach by zeta potential measurement. Enzyme and Microbial Technology, 7: 235-238.

Indian Pharmacopoeia 1996. Vol. 1. New Delhi: Controller of Publication, Government of India, Ministry of Health and Family Welfare, 736.

Jean-Claude, M.G.T., Roland, H.F.B. and Benedicte, L.T.W. 1997. Production of xanthan gum by fermenting a feedstock containing a mixture of mannose and glucose. Biotechnol. Adv., 15: 267.

Kalogiannis, S., Iakovidou, G., Liakopoulou-Kyriakides, M., Kyriakidis, D. and Skaracis, G. 2003. Optimization of xanthan gum production by *Xanthomonas campestris* grown in molasses. Process Biochem., 39: 249-256.

Kerdsup, P., Tantratian, S., Sanguandeekul, R. and Imjongjirak, C. 2011. Xanthan production by mutant strain of *Xanthomonas campestris* TISTR 840 in raw cassava starch medium. Food and Bioprocess Technology, 4: 1459-1462.

Kleinitz, W., Littman, M. and Herbst, H. 1989. Screening of xanthan biopolymer for a high salinity oil reservoir, Proc. Fifth European Symposium on improved oil recovery, Budapest, pp. 25-27.

Kobayashi, F. and Nakamura, Y. 2004. Mathematical model of direct ethanol production from starch in immobilized recombinant yeast culture. Biochem. Eng. J., 21: 93-101.

Murugesan, A.G., Dhevahi, B., Gowdhaman, D., Bala Amutha, K. and Sathesh Prabu, C. 2012. Production of xanthan employing *Xanthomonas campestris* using sugarcane molasses. American Journal of Environmental Engineering, 2(2): 31-34.

Murugesan, A.G., Dhevahi, B., Gowdhaman, D., Bala Amutha, K. and Sathesh Prabu, C. 2012. Production of xanthan employing *Xanthomonas campestris* using sugarcane molasses. American Journal of Environmental Engineering, 2(2): 31-34.

Pinches, A. and Pallent, L.J. 1986. Rate and yield relationships in the production of xanthan gum by batch fermentations using complex and chemically defined growth media. Biotechnol. Bioeng., 28: 1484-1496.

Psomas, S.K., Kyriakides, M.L. and Kyriakidis, D.A. 2007. Optimization study of xanthan gum production using response surface methodology. Biochem. Eng. J., 35: 273-80.

Psomas, S.K., Liakopoulou-Kyriakides, M. and Kyriakidis, D.A. 2007. Optimization study of xanthan gum production using response surface methodology. Biochemical Engineering Journal, 35: 273-280.

Shu, C.H. and Yang, S.T. 1990. Effect of temperature on cell growth and xanthan production in batch culture of *Xanthomonas campestris*. Biotechnol. Bioeng., 35: 454-468.

Silva, M.F., Fornari, R.C.G., Mazutti, M.A., Oliveira, D., Padilha, F.F. and Cichoski, A.J. 2009. Production and characterization of xanthan gum by *Xanthomonas campestris* using cheese whey as sole carbon source. Journal of Food Engineering, 90: 119-123.

Stavros, K., Gesthimani, I., Maria, L.K., Dimitrios, A. K. and George, N. S. 2003. Optimization of xanthan gum production by *Xanthomonas campestris* grown in molasses. Process Biochemistry, 39: 249-256.

Stredansky, M. and Conti, E. 1999. Xanthan production by solid-state fermentation. Process Biochem., 34: 581-587.

Sutherland, I.W. 1998. Novel and established applications of microbial polysaccharides.
Trends in Biotechnology, 16: 41-46.

Yoo, S.D. and Harcum, S.W. 1999. Xanthan gum production from waste sugar beet pulp. Bioresour. Technol., 70: 105-109.

Nature Environment and Pollution Technology
An International Quarterly Scientific Journal

p-ISSN: 0972-6268
(Print copies up to 2016)
e-ISSN: 2395-3454

Vol. 20 | No. 5 (Suppl) | pp. 2023-2030 | 2021

Original Research Paper

https://doi.org/10.46488/NEPT.2021.v20i05.019

Open Access Journal

# Evaluation of Fluoride Contamination Using GIS in Thirukkazhukundram Block, Tamil Nadu, India

**A. Amuthini Sambhavi*, K. Nagamani†** and B. Gowtham*****
*Sathyabama Institute of Science and Technology, Chennai, India
**Centre for Remote Sensing and Geo-informatics, Sathyabama Institute of Science and Technology, Chennai, India
***Department of Geology, Presidency College, Chennai, India
†Corresponding author: K.Nagamani; nagamani@sathyabama.ac.in

**Nat. Env. & Poll. Tech.**
**Website: www.neptjournal.com**

*Received:* 26-07-2021
*Revised:* 29-08-2021
*Accepted:* 03-09-2021

**Key Words:**
Fluoride contamination
Health hazard
Groundwater
Hydro-geology

## ABSTRACT

The presence of fluoride in the groundwater in the Thirukkazhukundram Block in south India is now becoming an increasingly alarming issue. With the semi-arid climatic conditions, charnockite and gneiss rocks form the basement, contributing to the geology of the study area. The pre-monsoon (August 2016) and post-monsoon (February 2017) fluoride concentrations have an average output of 1.3 $mg.L^{-1}$ and 0.72 $mg.L^{-1}$ respectively. As of date, only in Neikuppi, the fluoride contamination is found to be 2 $mg.L^{-1}$ in pre-monsoon which is beyond the accepted limit as per the WHO standards. Other 29 locations taken up for study have fluoride value fluctuation from 1 $mg.L^{-1}$ to 2 $mg.L^{-1}$ in the pre-monsoon and from 0 to 1.5 $mg.L^{-1}$ in the post-monsoon. The main factor responsible for this fluoride contamination lies in the study area's hydro-geological condition which must be attended to immediately to prevent a public health problem in the future.

## INTRODUCTION

All developing countries across the world depend upon the subsurface lithology water to meet up their consumption needs. The quality of the groundwater has been steadily deteriorating due to normal or anthropogenic means, as it happened in cases of worldwide groundwater fluoride contamination and even in our South Indian Thirukkazhukundram block. Fluorine reacting with rock minerals yield fluoride, which though found as a minor trace element in water are very noxious when their concentration is beyond the acceptable limit. Even when the fluoride concentration is very low below the normal limit, the latent effects disturb the public's health after prolonged intake. Thapa et al. (2009) showed the occurrence of high fluoride in drinking water of the study area, maximum mobilization of fluoride associated with na-$hco_3$ water type, chemical weathering along with ion-exchange bearing the blueprint of fluoride release, inverse geochemical modeling indicating under-saturation of fluoride, and alkaline aquifer condition accelerates the F-accumulation in groundwater. Kalpana et al. (2018) developed a Fluoride Index for mitigation of geogenic contamination by Managed Aquifer Recharge (FIMAR). Groundwater fluoride contamination could be judged by taking into account the temperature, pH, fluorine-containing minerals solubility, anion exchangeability of the minerals present in the aquifer, the geological and geomorphological texture of the study area through which the water is drained, and also the time of contact with a specific lithological unit (Thapa et al. 2009). To avoid dental cavities and mineralization of bone and formation of teeth enamel, a small amount of fluoride is always required. (Thapa et al. 2009). Overconsumption of fluoride causes dental fluorosis, skeletal fluorosis, and nonskeletal fluorosis in humans (WHO 2006). As per WHO, 0.5 $mg.L^{-1}$ is apt to stop dental fluorosis. Fluoride's desirable limit is 1 $mg.L^{-1}$ and the allowed limit is 1.5 $mg.L^{-1}$ as per BIS (1991) and ICMR. High fluoride concentrations in groundwater cause fluorosis in rural, dry, and semi-arid regions, areas with granite and gneiss, and advanced stages of groundwater development (Handa 1988, Balkema et al. 2013, Handa 1975, Narasayya 1970, CSME 1997, Garg et al. 2008, Tchobanoglous & Burton 1995, Saha 2015, Jothivenkatachalam et al. 2010, Ramesh & Soorta 2012, Dar et al. 2011, Balakrishnan et al. 2008, Kamalanandhini et al. 2016, Senthilkumar & Elango 2013, Mondal et al. 2008, Rao et al. 1997, Rama et al. 1982, Whitehead et al. 2009, PHED 2009, Ghazavi et al. 2012, Sinha 1986, Jadhav 2012, Mitharwal et al. 2009, Shrestha & Kazama 2007, Bharadwaj et al. 2011, Saxena & Ahmed 2001, WHO 2006, Chen Ching et al. 2015).

### Study Area

Groundwater samples collected from 30 locations of the Thirukkazhukundram Block were tested for fluoride contamina-

tion in the field itself using the color indicator method. This study area belongs to the Kanchipuram district of Tamil Nadu (Fig. 1). The geology of the study area (Fig. 2) has three segregations viz. coastal aeolian deposits, sand, and silt followed by basement charnockite in certain regions and gneiss in certain other parts. Ultrabasic intrusives of the archaean age and charnockites mainly comprise biotite and hornblende and are intruded by amphibolite, dykes of dolorite, and alluvial deposits are the youngest formation consisting of sands and clays and have deposits of quartz and pegmatites. The shale and clay of the Gondwana age occur on the bank of the Palar river. The Palar alluvium comprises coarse sands and gravels. The average thickness of alluvium is about 10 m to 30 m. The general trend of the gneiss is NE-SW direction. During the Jurassic period, Gondwana rocks, sedimentary rocks, faulted troughs, and rugged topography of crystalline 6 rocks, were deposited. The in-situ soils, laterites, and alluvial deposits were deposited along the Palar river during the quarternary period. The geomorphology of the study area (Fig. 3) also provides a clear picture of the subsurface lithology, which helps us understand the underlying soil's water-holding and yielding capacity, as well as their chemical environment and interaction, which plays a vital role in the presence or absence of fluoride and other contaminants. Fig. 4 shows the transport network of the study area.

Groundwater occurs mostly under water table or phreatic conditions in weathered, fractured, jointed, and faulted portions of granitic rocks and under artesian conditions in fractured zones located below impervious hard rocks. The pore spaces developed in the weathered mantle acts as shallow granular aquifers and forms the potential water-bearing zones. The water table is shallow in ayacut regions whereas it is relatively deeper in other regions. The groundwater of the charnockite type is found in shallow depths only when weathering is intense, and it develops much more slowly than gneissic formations.

The alluvium is the most important formation that carries a significant amount of groundwater. Groundwater is found below the water table or in semi-confined areas. The best aquifer is alluvium, which is primarily made up of stones, gravel, or coarse sand with little or no silt or clay. While silt or clay with a little or no boulders gravel or sand is a very poor aquifer. The thickness of these aquifers ranges from 10 m to nearly 80 m. One another mode of occurrence of groundwater in the alluvium is in the form of perched aquifers. Groundwater is met in these perched aquifers at a depth of 10 m from the ground level. In the Gondwana formation area, the groundwater yield is very poor. Groundwater is available under perched water table conditions along the coast. This is quite precious, and it should be used sparingly, as overlapping causes seawater intrusion in the area. The occurrence and movement of groundwater in hard rock formations are restricted to weathered and jointed portions. The intensity of weathering is not uniform and varies from place to place. Generally weathering and fractures are common at shallow depth. The sub-surface conditions can be studied by open-well inventories and by geophysical investigation.

In difficult situations, exploratory boreholes can be used to determine the subsurface conditions. Aquifer test or yield test can also be tried where ever large quantity of groundwater is needed. The SG & SWRDC has drilled 190 boreholes for investigation purposes throughout the entire district to get a comprehensive idea of the subsurface conditions. The complexity of the geological formations in this district is very well determined by drilling a series of bore wells all along the Palar river course. The thickness of alluvium is about 10 m near the confluence of the Cheyyar and Palar rivers. The maximum thickness of alluvium (30 m -40 m in flood plain area) is noted near Panakattucheri village of Thirukkazhukundram block. Based on the field study carried out and interpretations made from aerial photographs and satellite imageries, favorable

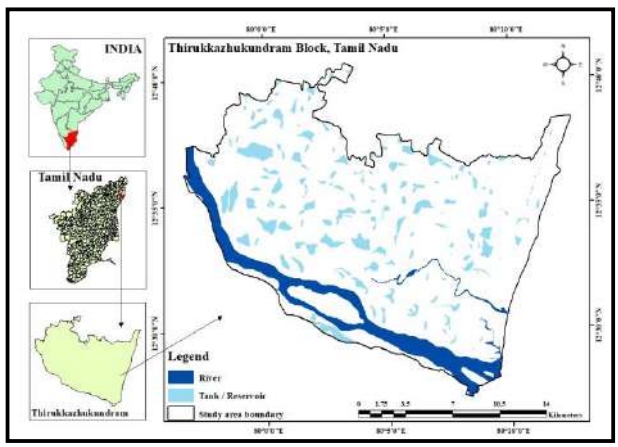


Fig. 1: Location of the study area.

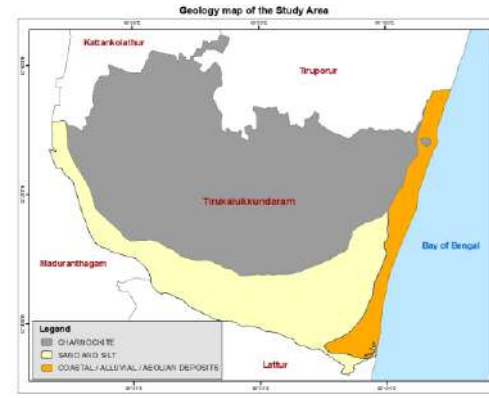


Fig. 2: Geology map of the study area.

locations are selected for exploratory boreholes. Subsurface hydrogeological characteristics are determined to evaluate the groundwater potential of the area. More than 46 boreholes have been handed over to user agencies like Municipality, TWAD Board and Panchayat Unions, etc., for drinking water purposes. The main aim of this study is to check out the existence and spatial fluctuation of fluoride contagion in pre-monsoon and post-monsoon under surface water, to thoroughly look into the nature of the fluoride concentration and hence to assess the resulting effect on human health on account of fluoride contaminated drinking water.

## MATERIALS AND METHODS

To have clear knowledge regarding the fluoride concentration in groundwater, 30 samples from dug wells and bore wells were collected for examination and were tested in the field using the color indicator method both for pre-monsoon and post-monsoon from the research area, Thirukkazhukundram Block. The outputs were compared with drinking water quality standards as specified in the World health organization (WHO 2006). For every location, before and after the monsoon period, the comparison with the WHO standards was done and the respective spatial maps were prepared. As per WHO standards, fluoride concentration range in groundwater fluoride lies between 1 $mg.L^{-1}$ (acceptable limit) and 1.5 $mg.L^{-1}$ (permissible limit). The majority of the study area is unaffected by groundwater fluoride concentration contamination, but in a few areas, contamination has started, posing a serious threat to society.

## RESULTS AND DISCUSSION

Fluoride, pH, EC, and total hardness were keenly studied. The final mean value of fluoride, pH, EC, and total hardness is provided in Table 1. The groundwater specimen data shows significant variations. Table 1 and Table 2 exhibits the pre-monsoon and post-monsoon period's fluoride distribution and limit of occurrence. Pre-monsoon fluoride varies from 1 to 2 $mg.L^{-1}$ with a mean value of 1.3 $mg.L^{-1}$ and post-monsoon fluoride concentration fluctuates from 0 to 1.5 $mg.L^{-1}$ with a mean value of 0.72 $mg.L^{-1}$. pH varies from 7.2 to 8.2 in the pre-monsoon with a mean value of 7.7 and from 7 to 8.1 in the post-monsoon with a mean value of 7.6. EC varies from 616.9 to 2766.5 $mg.L^{-1}$ in the pre-monsoon with an average of 1310.7 $mg.L^{-1}$ and from 100.8 to 1219.4 $mg.L^{-1}$ in the post-monsoon with a mean value of 525.1 $mg.L^{-1}$. TH varies from 134.541 to 890.1 $mg.L^{-1}$ in the pre-monsoon with an average limit of 379.1 $mg.L^{-1}$ and from 25.5 to 344.4 $mg.L^{-1}$ in the post-monsoon with a mean value of 144 $mg.L^{-1}$. The samples were classified into five classes for depicting the frequency distribution (Fig. 5). During the post-monsoon period alone, 17% of the samples are below the detectable level (<0.25 $mg.L^{-1}$). Taking the level 0.25-0.5 $mg.L^{-1}$, 33% of the samples are observed only during the post-monsoon season. When it comes to the 0.75 $mg.L^{-1}$, 37% and 40% of the samples are observed during pre- and post-monsoon respectively. Then, for the level 1.25-1.5 $mg.L^{-1}$, 60% samples are observed during pre-monsoon and 10% are observed during post-monsoon. Between the two categories, there appears to be a positive trend with fluoride concentration, implying higher pre-monsoon fluoride content in the groundwater of the study area (Fig. 6 and Fig. 7). Also, we found that for value 1.5 $mg.L^{-1}$, we only observed 3% of the samples during the pre-monsoon period and nil observation during the post-monsoon period. Up to 0.5- 0.75 $mg.L^{-1}$ level and between 1-1.25 $mg.L^{-1}$ level, pre-monsoon observations are nil. Only, in Neikuppi, we find fluoride concentration

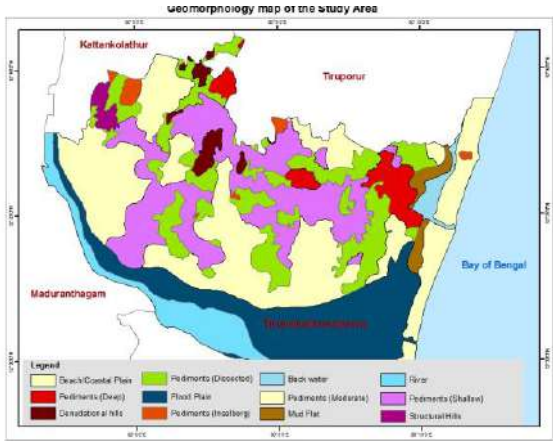


Fig. 3: Geomorphology map of the study area.

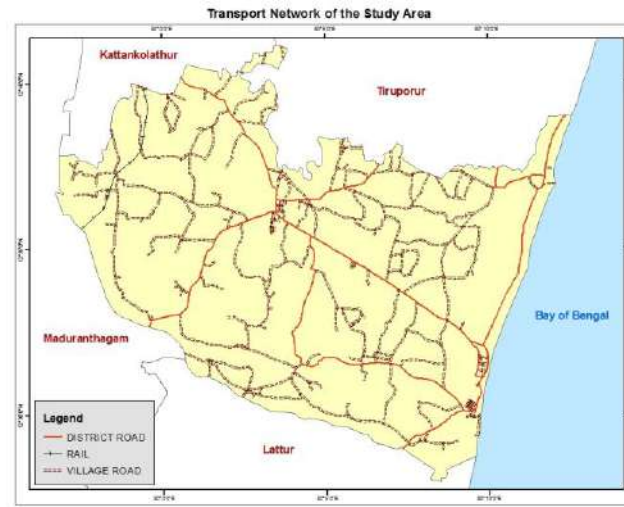


Fig. 4: Transport network of the study area.

Table 1: Pre-monsoon and post-monsoon concentrations of fluoride (mg.$L^{-1}$), pH, EC (mg.$L^{-1}$), and total hardness (mg.$L^{-1}$) in thirty places of groundwater in Thirukkazhukundram block.

| No. of samples | Locations | Pre-monsoon | | | | Post-monsoon | | | |
|---|---|---|---|---|---|---|---|---|---|
| | | F | pH | EC | TH | F | pH | EC | TH |
| 1 | Nenmeli | 1.00 | 8.1 | 746.21 | 224.52 | 0.00 | 7.96 | 272.06 | 98.36 |
| 2 | Thirumani | 1.00 | 7.6 | 650.85 | 214.92 | 0.00 | 7.69 | 215.89 | 70.09 |
| 3 | Alagusamudram | 1.00 | 7.6 | 773.97 | 178.18 | 0.50 | 7.92 | 200.39 | 59.99 |
| 4 | Keerapakkam | 1.00 | 7.8 | 2402.5 | 787.56 | 0.50 | 7.83 | 883.3 | 191.9 |
| 5 | Mosivakkam | 1.00 | 7.5 | 1086.2 | 330.87 | 0.50 | 7.03 | 509.15 | 152.2 |
| 6 | Thazhambedu | 1.00 | 7.8 | 1617.4 | 357.13 | 1.00 | 7.42 | 367.1 | 120.1 |
| 7 | Manapakkam | 1.50 | 7.8 | 2740.2 | 734.32 | 1.00 | 7.84 | 1098.3 | 295.4 |
| 8 | Kuzhipanthandalam | 1.50 | 7.9 | 1108.2 | 340.05 | 1.00 | 7.29 | 241.38 | 58.01 |
| 9 | Pulikundram | 1.50 | 7.8 | 2126.2 | 667.88 | 1.50 | 7.84 | 1219.4 | 344.4 |
| 10 | Mamallapuram | 1.00 | 8.2 | 748.04 | 200.27 | 0.00 | 7.33 | 100.79 | 25.54 |
| 11 | Ponvilayanthakalathur | 1.50 | 7.2 | 2036.5 | 579.61 | 1.00 | 7.65 | 670.08 | 205.8 |
| 12 | Thirukazhukundram | 1.50 | 7.7 | 2766.5 | 890.13 | 1.00 | 7.45 | 1104.8 | 321.8 |
| 13 | Igai | 1.00 | 7.7 | 1084.6 | 316.14 | 0.50 | 7.29 | 512.06 | 149.7 |
| 14 | Navalur | 1.00 | 7.6 | 922.92 | 242.33 | 0.50 | 7.5 | 332.03 | 96.81 |
| 15 | Kadambadi | 1.50 | 7.8 | 676 | 166.99 | 1.00 | 7.61 | 236.99 | 79.16 |
| 16 | Salur | 1.50 | 7.7 | 1011.1 | 260.06 | 1.00 | 7.55 | 373.94 | 109.1 |
| 17 | Pattikadu | 1.50 | 7.7 | 1127 | 338.7 | 1.50 | 8.09 | 312.34 | 102.1 |
| 18 | Thathalur | 1.50 | 7.8 | 977.59 | 273.43 | 0.50 | 7.54 | 466.08 | 130.3 |
| 19 | Amaipakkam | 1.50 | 7.7 | 935.27 | 201.94 | 1.00 | 7.61 | 368 | 116.9 |
| 20 | Kunnathur | 1.50 | 7.9 | 1363.2 | 416.48 | 1.00 | 7.84 | 495.89 | 149.2 |
| 21 | Veerapuram | 1.00 | 7.7 | 1260.7 | 335.67 | 0.50 | 7.33 | 523.38 | 160 |
| 22 | Kilapakkam | 1.50 | 7.7 | 2647.1 | 882.7 | 0.50 | 7.48 | 1079.7 | 270.1 |
| 23 | Neikuppi | 2.00 | 7.8 | 830.55 | 245.27 | 1.50 | 7.35 | 227.18 | 32.89 |
| 24 | Vilagam | 1.50 | 7.9 | 1797.1 | 639.23 | 1.00 | 7.05 | 617.01 | 227.5 |
| 25 | Pandur | 1.50 | 7.6 | 729.48 | 179.48 | 1.00 | 7.94 | 458.73 | 102.6 |
| 26 | Sadurangapatnam | 1.50 | 7.5 | 1186.8 | 282.02 | 0.50 | 7.33 | 621.89 | 121.5 |
| 27 | Lathur | 1.50 | 7.6 | 1523.1 | 431.56 | 0.50 | 7.7 | 551.41 | 108.8 |
| 28 | Irumbilicheri | 1.50 | 7.9 | 1158.9 | 347.82 | 1.00 | 7.57 | 682.96 | 200.4 |
| 29 | Nallathur | 1.50 | 7.3 | 671.01 | 134.48 | 0.00 | 7.34 | 796.62 | 146.3 |
| 30 | Voyalur | 1.00 | 7.3 | 616.94 | 172.57 | 0.00 | 7.53 | 213.83 | 72.98 |

Table 2: Pre-monsoon and post-monsoon concentrations of fluoride(mg/L) pH, EC (mg/L) and total hardness (mg/L) (maximum and mean) in the study place groundwater.

| | Pre-monsoon | | Post-monsoon | |
|---|---|---|---|---|
| | Max | Mean | Max | Mean |
| F | 2 | 1.3 | 1.5 | 0.72 |
| pH | 8.2 | 7.7 | 8.1 | 7.6 |
| EC | 2767 | 1311 | 1219.4 | 525.1 |
| TH | 890.1 | 379.1 | 344.4 | 144 |

in groundwater to be above the permissible level and that particular value is 2 mg.$L^{-1}$.

### The Hydro-Chemical Environment of Thirukkazhukundram's Relation with Groundwater Fluoride

The relation between environment hydrochemistry and groundwater fluoride is well analyzed. The scatter diagrams in Fig. 8 explain the pre-monsoon and post-monsoon pH, EC, and TH's relation with fluoride. PH, EC, and total hardness (TH) administer the correlated plotting. The pH and fluoride levels have a negative correlation. The main source of fluoride in groundwater is natural contamination, however, the dissolution process is still not well understood (Handa 1975, Saxena & Ahmed 2001). Fluoride is present in fluorite, granite, gneisses, and pegmatite (Rama 1982), all of which include fluoride. Granite, gneisses, basalts, dolerites, quartzites, pegmatites, hornblende, syenites, biotite, muscovite, fluorite, fluoromica, cryolite, villanite, etc., (Saxena & Ahmed 2001) are rock varieties that have high fluoride contagion in hard rock terrain. The study area is characterized by three to four layers namely basement gneiss or charnockite hard rock overlain by fractured charnockite or gneissic rocks sedimentary subsurface and on the top we have alluvium. According to Thapa et al. (2009), water level variations, as well as fluoride contamination of groundwater in alluvial zones, are unusual. The majority of the dug wells along with sub-surface water

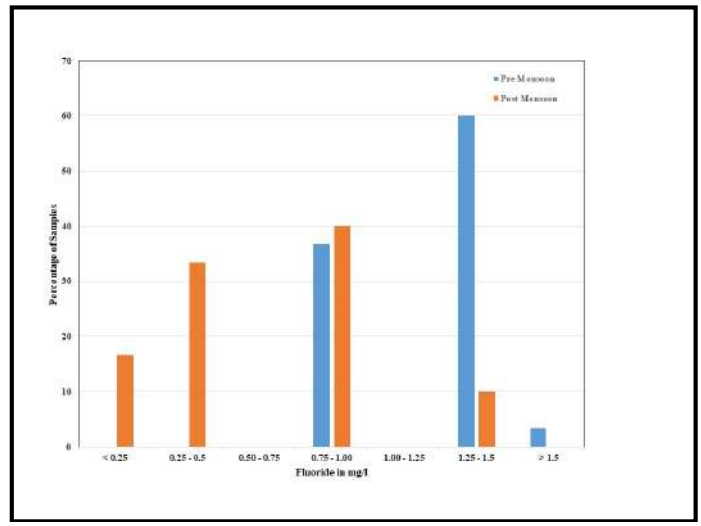


Fig. 5: Frequency distribution of fluoride during pre-monsoon season (August 2016) and post-monsoon season (February 2017).

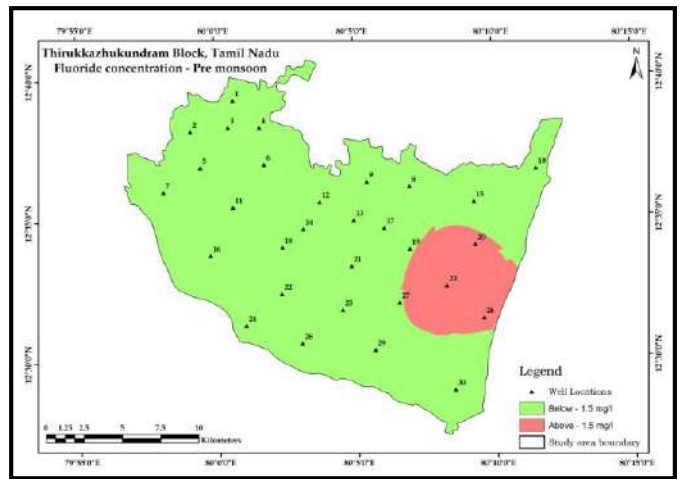


Fig. 6: Spatial map of pre-monsoon groundwater fluoride concentration of the study area.

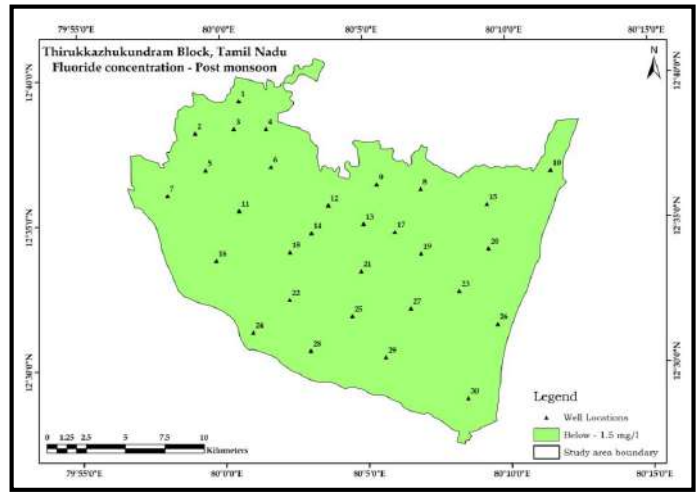


Fig. 7: Spatial map of post-monsoon groundwater fluoride concentration of the study area.

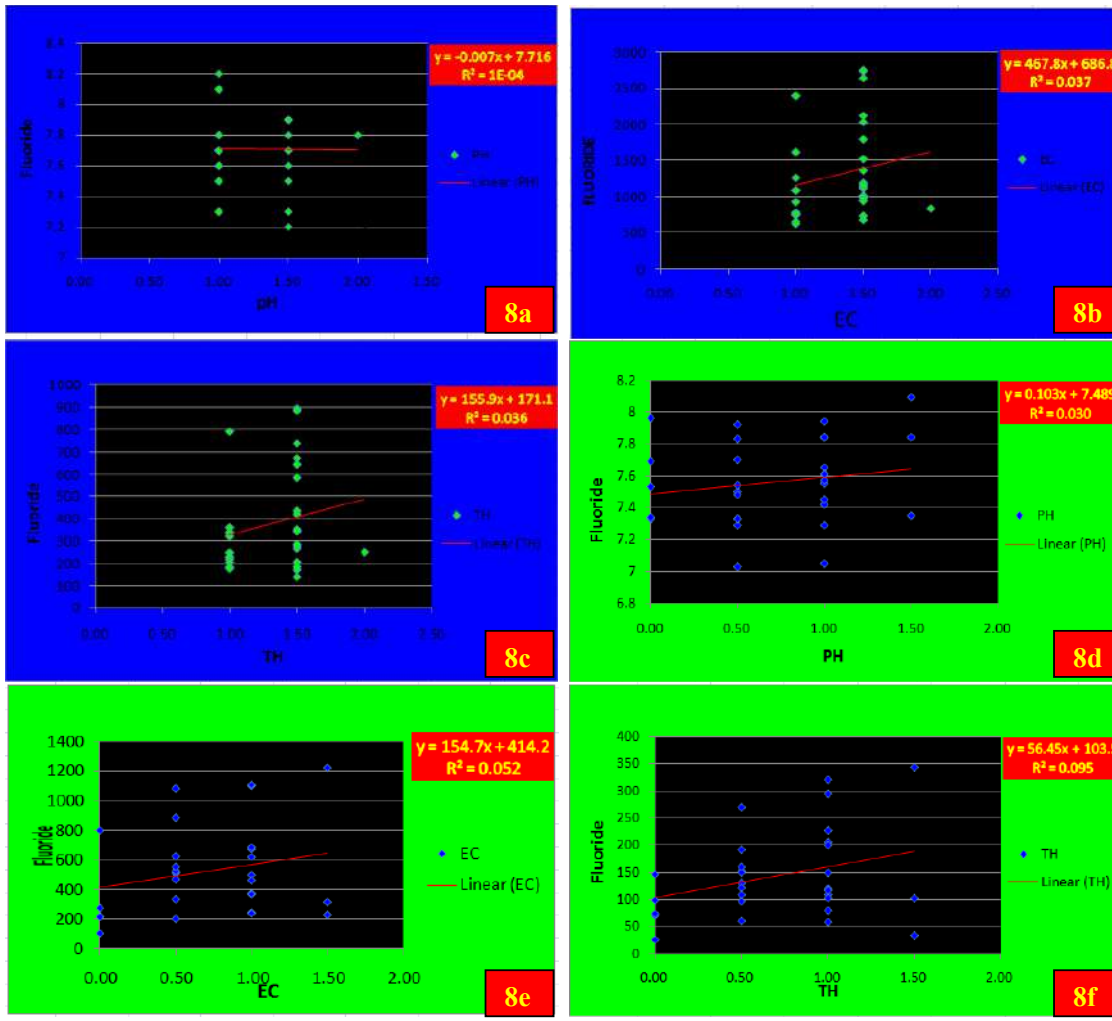


Fig. 8 (a to f): Scatter diagrams showing the relationship of the study area groundwater fluoride and pH, EC and total hardness.

bodies get depleted. The enrichment process, as well as the rapid decline of the water table, are made more effective by the soil and water reaction, and the gradual and steady casual leaching of fluoride into subterranean flowing water is aided by regional groundwater over-pumping. Because groundwater serves all of the public's domestic needs in the study area, special attention must be paid to fluoride contamination in the groundwater, which could eventually lead to all types of dental and skeletal fluorosis, posing a serious threat to future generations (Kamalanandhini et al. 2016).

**Fluoride's Impact on Health Factor**

In terms of the reproductive system (Naseem et al. 2016), there is a decrease in female fertility rates, as well as testosterone reduction, follicle stimulating hormones, and inhibin B quantity reduction in males (OrtizPérez et al. 2003). Fluoride also influences the shape and mobility of sperm in males (Chinoy & Narayana 1994). When it comes to neurobehavior (Trivedi et al. 2007), intellectual quotient (IQ) and thinking capacity loss occur. Children's mental abilities are impaired. Children's developing brain is subjected to neurotoxicity. (Grandjean & Landrigan 2006). The central nervous system's energy needs are met by interrupting the glycolysis cycle (ValdezJiménez et al. 2011). Fluoride has an effect on enzyme function, protein structure, brain functioning, hence, defective cognition and memory occurs (Spittle 1994). When it comes to the cardiovascular system, excessive fluoride intake causes oxidative stress, which leads to inflammatory mechanisms, atherosclerosis, vascular stiffness, myocardial cell damage, Bradycardia, abnormal heart rhythms, reduced myocardial function, hypothyroidism, diabetes mellitus, and obesity (Xu et al. 1997). Hypocalcemia and hypercalcemia are also caused by excessive fluoride6 (Nureddin 2018). Loss of mucus layer, hyperaemia, oedema, haemorrhage, and stomach lining rupture are all common gastrointestinal complications (Pratusha et al. 2011), also nausea, vomiting, and stomach pains occur (Nabavi et al. 2013). Thyroid gland structural changes and dysfunctions occur as endocrine system-based effects of abnormal fluoride intake (Kheradpisheh et al. 2018). There is an increase in parathyroid and calcitonin activity, as well as secondary hyperparathyroidism and impaired glucose tolerance (Doull et al. 2006). With respect to the renal system, fluoride concentration abnormality increases the kidney stone risks (Doull et al. 2006). Metabolic, histopathological, and pathological variations in the glomeruli are seen (Bouaziz et al. 2006).

## CONCLUSION

Natural sources constitute the main site of groundwater fluoride in the study area, with a higher concentration during the pre-monsoon season than during the post-monsoon season. The geology, hydrology, and geochemistry of the environment, as well as the weathering of fluoride-containing rocks and significant ups and downs in the water table level, all contribute to the presence of fluoride. Fluoride in groundwater exceeds allowed limits, posing a reasonable concern that is slowly increasing due to delays in the implementation of water treatment schemes. Also, the public relies on groundwater for drinking and other household works. The majority of the public suffers from a lack of proper water supply. Due to the numerous health issues associated with fluoride concentration level abnormalities, care must be taken to ensure that fluoride content does not exceed the permissible limit, and necessary steps must be taken to protect the lives of those who live in this area.

## REFERENCES

Balakrishnan, M., Arul Antony, S., Gunasekaran, S. and Natarajan, R.K. 2008. Impact of dyeing industrial effluents on the groundwater quality in Kancheepuram (India). Indian J. Sci. Technol., 1(7): 1-8.

Balkema, A. A., Rotterdam, M., Chakrabarti, S. and Bhattachary, H.N. 2013. Inferring the hydro-geochemistry of fluoride contamination in Bankura District, West Bengal: A case study. J. Geol. Soc. India, 82: 379-391.

Bharadwaj, V., Dhruv, M. and Singh, S. 2011. Surface and ground-water quality characterization of Deoria district, Ganga Plain, India. Environ. Earth Sci., 63: 383-395.

Bouaziz, H., Ketata, S., Jammoussi, K., Boudawara, T., Ayedi, F., Ellouze, F. and Zeghal, N. 2006. Effects of sodium fluoride on hepatic toxicity in adult mice and their suckling pups. Pestic. Biochem. Physiol., 86: 124-130.

Bureau Of Indian Standards (BIS). 1991. Drinking-Water Specification, (First Revision) IS 10500. India

Calderon, J., Machado, B., Navarro, M., Carrizales, L., Ortiz, M.D. and Diaz-Barriga, F. 2000. Influence of fluoride exposure on reaction time and visuospatial organization in children. Epidemiology, 11(4): S153.

Chen Ching, Y., Heng Lee, Y., Ekhwan Toriman, M., Abdullah, M. and Bin Yatim, B. 2015. Effect of the big flood events on the water quality of the Muar River, Malaysia. Sustain. Water Resour. Manag., 1(2): 97-110.

Chinoy, N.J. and Narayana, M.V. 1994. In vitro fluoride toxicity in human spermatozoa. Reprod. Toxicol., 8: 155-159.

CSME. 1997. Report submitted to NRDMS, DST, GOI, Centre for Study of Man and Environment 1997. http://nrdms.gov.in/ assessment. groundwater.asp.

Dar, M.A., Sankar, K. and Dar, I.A. 2011. Fluorine contamination in groundwater: a major challenge. Environmental Monitoring Assessment, 173(1-4): 955- 68.

Doull, J., Boekelheide, K., Farishian, B.G., Isaacson, R.L., Klotz, J.B., Kumar, J.V. and Thiessen, K.M. 2006. Fluoride in Drinking Water: A Scientific Review of EPA's Standards, Committee on Fluoride in Drinking Water, Board on Environmental Studies and Toxicology, Division on Earth and Life Sciences. National Research Council of the National Academies, National Academies Press, Washington, DC, pp.530.

Garg, D., Kaur, R., Chand, D., Kumar Mehla, S. and Singh, R. 2008. Analysis of water quality of Bharatpur area in post-monsoon season, January 2007. Rasayan J. Chem., 1(4): 743.

Ghazavi, R., Ali, A.B. and Eslamian, S. 2012. Impact of flood spreading on groundwater level variation and groundwater quality in an arid environment. Water Resour. Manag., 26: 1651-1663.

Grandjean, P. and Landrigan, P.J. 2006. Developmental neurotoxicity of industrial chemicals. Lancet, 368: 2167-2178.

Handa, B.K. 1975. Geochemistry and genesis of fluoride-containing groundwater in India, groundwater, Groundwater, 13: 275-281.

Handa, B.K. 1988. Fluoride occurrence in natural waters in India and its significance. Bhu-Jal News, 3(2): 31-37.

Jadhav, S.D., Sawant, R.S., Godghate, A.G., Patil, S.R. and Patil, R.S. 2012. Assessment of groundwater quality of Ajara Tahsil from Maharashtra. Rasayan J. Chem., 5(2): 246 -249.

Jothivenkatachalam, K., Nithya, A. and Chandra Mohan, S. 2010. Correlation analysis of drinking water quality in and around Perur block of Coimbatore district, Tamil Nadu, India. Rasayan J. Chem., 3(4): 649.

Kalpana, L., Brindha, K. and Elango, L. 2018. FIMAR: A new Fluoride Index for identification of sites to mitigate geogenic contamination by managed aquifer recharge. Chemosphere, 220: 381-390.

Kamalanandhini, M., Nagalakshmi, R., Srividhya, S. and Golda Percy, V.P. 2016. Water quality monitoring in selected observation wells in coastal areas of Chennai and Tiruvallur Districts, Tamil Nadu, India: A case study. Int. J. Pure Appl. Math., 118(20): 4343-4354.

Kheradpisheh, Z., Mirzaei, M., Mahvi, A.H., Mokhtari, M., Azizi, R., Fallahzadeh, H. and Ehrampoush, M.H. 2018. Impact of drinking water fluoride on human thyroid hormones: A case-control study. Sci. Rep., 8(1): 2674

Mitharwal, S., Yadav, R.D. and Angasaria, R.C. 2009. Water quality analysis in Pilani of Jhunjhunu district (Rajasthan): The place of Birla's origin. Rasayan J. Chem., 2(4): 920 -923.

Mondal, N.C., Saxena, V.K. and Singh. V.S. 2008. Occurrence of elevated nitrate in groundwaters of Krishna delta, India. Afr. J. Environ. Sci. Technol., 2(9): 265-271.

Nabavi, S.M., Habtemariam, S., Nabavi, S.F., Sureda, A., Daglia, M., Moghaddam, A.H. and Amani, M.A. 2013. Protective effect of gallic acid isolated from Peltiphyllum peltatum against sodium fluoride-induced oxidative stress in rat's kidney. Mol. Cell. Biochem., 372(1-2): 233-239.

Narasayya, B.L. 1970. Mineralogy of chromite, magnetite, and apatite deposits of the parts of Eastern Ghats, Andhra Pradesh, India. PhD thesis, Andhra University, Andhra Pradesh, India.

Naseem, M., Khurshid, Z., Khan, H.A., Niazi, F., Zohaib, S. and Zafa, M.S. 2016. Oral health challenges in pregnant women: recommendations for a dental care professional. Saudi J. Dent. Res., 7: 138-146.

Nureddin, A. 2018. Adverse effects of fluoride. Adv. Dent. Oral Health, 8(5): 555746.

Ortiz-Pérez, D., Rodríguez-Martínez, M., Martínez, F., Borja-Aburto, V.H., Castelo, J., Grimaldo, J.I., De la Cruz, E., Carrizales, L. and Díaz-Barriga, F. 2003. Fluoride-induced disruption of reproductive hormones in men. Environ. Res., 93: 20-30.

PHED 2009. Report. http://www.wbphed.gov.in/saticpages/ fluoride.html

Pratusha, N.G., Banji, O.J.F., Banji, D., Ragini, M. and Pavani, B. 2011. Fluoride toxicity: A harsh reality. Int. Res. J. Pharm., 2(4): 9-85.

Rama, R.N.V. 1982. Geo Chemical Factors Influencing The Distribution Of Fluoride In Rocks, Soils, And Water Sources Of Nalgonda District. Doctoral Thesis, Osmania University, India.

Ramesh, K. and Soorta, V. 2012. Fluoride contamination in drinking water in Palacode Region, Tamil Nadu. Int. J. Res. Chem. Environ., 2(1): 116-123.

Rao, N.S. 1997. The occurrence and behavior of fluoride in the groundwater of the Lower Vamsadhara river basin, India, Hydrol. Sci. J., 6(42): 877-892.

Saha, J. 2015. Groundwater quality of Purulia district: A microlevel study on Purulia-I block, Purulia district, West Bengal. Int. J. Human Resour. Social Sci., 2(7): 40-48.

Saxena, V.K. and Ahmed, S. 2001. Dissolution of fluoride in groundwater: A water-rock interaction study. Environ. Geol., 40: 1084-1087.

Senthilkumar, M. and Elango, L. 2013. Geochemical processes controlling the groundwater quality in the lower Palar river basin, southern India. J. Earth System Sci., 122(2): 419-432.

Shrestha, S. and Kazama, F. 2007. Assessment of surface water quality using multivariate statistical techniques: A case study of the Fuji river basin, Japan. Environ. Model. Software, 22(4): 464-475.

Sinha, R.K. 1986. Industrial Minerals. 2nd edition. Oxford & FBH, New Delhi, p. 379.

Spittle, B. 1994. Psychopharmacology of fluoride: A review. Int. Clin. Psychopharmacol., 9: 79-82.

Tchobanoglous, G. and Burton, F.L. 1995. Wastewater Engineering: Treatment, Disposal, and Reuse. Tata McGraw-Hill Publishing Company Limited, New Delhi.

Thapa, R., Gupta, S., Kaur, H. and Baski, R. 2019. Assessment of groundwater quality scenario in respect of fluoride and nitrate contamination in and around Gharbar village, Jharkhand, India. HydroResearch, 09: 2-14

Trivedi, M.H., Verna, R.J., Chinoy, N.J., Patel, R.S. and Sathawara, N.G. 2007. Effect of high fluoride water on intelligence of school children in India. Fluoride, 40: 178-183.

Valdez-Jiménez, L., Fregozo, C.S., Beltrán, M.M., Coronado, O.G. and Vega, M.P. 2011. Effects of the fluoride on the central nervous system. Neurologia, 26: 297-300.

Whitehead, P.G., Wilby, R.L., Battarbee, R.W., Kernan, M. and Wade, A.J. 2009. Hydrol. Sci. J., 54(1): 101-123.

WHO. 2006. Guidelines for Drinking Water Quality. 3rd Edition. World Health Organization, Geneva.

Xu, R.Q., Wu, D.Q. and Xu, R.Y. 1997. Relations between environment and endemic fluorosis in a hot region, Inner Mongolia. Fluoride, 302: 6-28.

Nature Environment and Pollution Technology
An International Quarterly Scientific Journal

p-ISSN: 0972-6268
(Print copies up to 2016)
e-ISSN: 2395-3454

Vol. 20 | No. 5 (Suppl) | pp. 2031-2040 | 2021

Original Research Paper

https://doi.org/10.46488/NEPT.2021.v20i05.020

Open Access Journal

# Implementation of Eco-Industrial Park for Effectual Establishment of Circular Economy in Russia

**Ipsita Saha*(**)†, Tatiana S. Smirnova***(****) and Vladimir A. Maryev******

*Department of Mechanical Engineering, Jadavpur University, India
**Department of Computer Science & Engineering, Guru Nanak Institute of Technology, India
***Gubkin Russian State University of Oil and Gas (National Research University), Moscow region, Russian Federation
****Environmental Industrial Policy Center - Federal Autonomous Institution, Moscow Region, Russian Federation
†Corresponding author: ipsita.saha49@gmail.com

**Nat. Env. & Poll. Tech.**
**Website: www.neptjournal.com**

*Received:* 07-07-2021
*Revised:* 20-09-2021
*Accepted:* 01-10-2021

**Key Words:**
Eco-industrial park (EIP)
Innovative infrastructure
Industrial symbiosis
Waste management
Secondary resources
Sustainable development
Resource efficiency

## ABSTRACT

In recent years, waste management has become a major concern in Russian cities. This can be addressed through the circular economy. Developing Eco-Industrial Parks (EIP) can be considered an innovative infrastructure of a circular economy. EIP is based upon the principles of industrial symbiosis involving the exchange of material and energy flows, sharing of infrastructural facilities, and provision of municipal utility and other services. Researchers have found that most industrial symbiotic interconnections originated spontaneously, the main driver being the increasing commercial benefits of such interchange. Still, the authors were able to identify pre-designed EIP through their examination of global practices. This paper proposes a five-stage methodological approach to EIP organization. This methodology was applied to create a model of an EIP in the Voronezh Region, one of the fastest developing regions in Russia. Implementation of this model is intended to help solve a set of environmental, economic, and social problems of a region. The approach to creating EIPs described in this study can be used in other places to improve resource efficiency and reduce waste disposal. Because Russia's garbage disposal rate currently exceeds 90% per year, this is one of the country's top sustainable development priorities.

## INTRODUCTION

Innovative infrastructure based on a circular economy is a concern of many cities around the world. This demand is mainly driven by the lack of raw materials, an increasing volume of hazardous waste, intensifying unplanned landfills, and the lack of energy resources. Disposal of waste is a problem in many cities of Russia and a solution is immediately required towards the establishment of energy-efficient infrastructure. Developing a circular economy for industrial processes will reduce resource consumption and eliminate unauthorized landfills and dumps. EIP in Russia integrates the concept of circular economy, which is crucial for the sustainable development of the country (Zhou et al. 2017, Pakhomova et al. 2017).

The basic premise of ensuring an ecosystem's sustainability is to keep its constituents in a closed loop. Despite the fact that the entire biosphere is enveloped in a circle of intense global currents and changes, these currents and changes are almost perfectly balanced; in other words, they are looped. Everything that a living organism has produced, including itself, is consumed by organisms of other species, chain-wise. These processes are cyclical and do not result in the creation of "surplus" matter due to the use of solar energy.

Metabolic (within an organism) and physical (natural circuit of matter) cycles in the biosphere ensure chemical and physical continuity of the environment. The law of equilibrium of cycles may be termed the "principle of cyclical circularity", or "circularity principle". Looped metabolic and physical cycles help to maintain the continuity of chemical and physical properties of the biosphere, which is called sustainability (Mashukova 2016, Skobelev 2020).

**Based on various research gaps and research questions the following research objective have been set for the study,** objective 1: Analyze the possibility of organizing an industrial system by analogy with the natural system through the creation of eco-industrial parks, objective 2: Develop an algorithm for organizing eco-industrial parks and objective 3: To put the developed algorithm to the test on a real-world problem in one of Russia's regions. The project's major goal is to create a mechanism for putting a circular economy into practice in eco-industrial parks by closing resource cycles. For Russia's sustainable development, improving resource efficiency and decreasing waste disposal at landfills are top priorities.

The paper presents a methodological approach towards the organization of EIP, with five main stages:

Step 1 – Assessment of the current situation in the field of waste and secondary resources management in the region

Step 2 – Collecting the main flows directed to the EIP

Step 3 – Defining the object composition of the EIP and the list of technological solutions

Step 4 – Selection of a land area for EIP location

Step 5 – Defining the EIP performance indicators

This is an aggregative method, but it does not allow for the formulation of a comprehensive concept for the creation of eco-industrial parks. Each level can be detailed in the future based on the unique design conditions of eco-industrial parks.

This principle of natural ecosystems organization is the foundation of the circular economy concept (Tyrganova & Makhashkeeva 2014). Similarly, to a natural ecosystem, the industrial and utility system may be regarded as a spatially defined aggregate of production components (cells), including production sites, facilities, factories, etc., and natural objects, all integrated with material, energy, and information interconnections (Smirnova et al. 2018). Within such a system waste generation is the result of the production processes. Waste management, existing in such systems, requires the collection, transportation, recycling, decontamination, or landfilling (Ayres & Simonis 1994). Material and energy flows are transported between components (objects) of the industrial realm and the environment in municipal/industrial ecosystems, just as they are in natural ecosystems. There is an informal interaction between these objects.

The analogy between natural and municipal/industrial ecosystems can be described as "industrial symbiosis". Industrial symbiosis, as a part of the new area of the industrial ecology, implies combining of the material and energy flows via local and regional economics. This symbiosis draws the attention of traditionally autonomous industries to collaborate to achieve a competitive advantage in the physical exchange of materials, energy, and water (Fischer-Kowalski 1998). The core elements of the industrial symbiosis are active collaboration and symbiotic opportunities ensured by the geographical proximity of industrial enterprises (Albino et al. 2016).

For optimal implementation, the concept of creating an eco-industrial park should be based on an interdisciplinary approach. Several terminologies and definitions are used by organizations to refer to EIPs and similar related concepts. Fig. 1 presents combinations of commonly used terms relating to EIPs. As per World Bank 2021 International Framework for Eco-Industrial Parks, broadly, EIPs can be defined as, "managed industrial areas that promote cross-industry and community collaboration for common benefits related to economic, social and environmental performance". The concept of EIP has evolved to address additional and interrelated aspects, including, resource-efficient and cleaner production, climate change, pollution, industrial symbiosis, social standards, shared infrastructure, and management of risks and shared resources at higher echelon, land, and ecosystem services.

In worldwide practice, such interconnections have been evolved into Eco-Industrial Parks (EIP). The generally accepted definition of EIPs is currently based on the wording by Ernest Lowe published in 2001 in the "Eco-Industrial Handbook" prepared with the assistance of the Asian Development Bank - "An Eco-Industrial Park is a community of manufacturing and service businesses seeking enhanced environmental and economic performance through collaboration in managing environmental and resources issues including energy, water, and materials. By working together, the community of businesses seeks a collective benefit that is greater than the sum of the individual benefits each company would have realized if it optimized its individual interests" (Ernest 1995).

However, other definitions exist, emphasizing specific features and components of an EIP. Below there are some examples of them.

According to Smirnova et al. (2019), the term eco-industrial park is used to define both eco-industrial parks and eco-innovative areas combining residential and industrial activities, such as eco-cities or eco-industrial zones. Eco-innovation parks are designed with the environment in mind (e.g., piloting installations and processes, designing new goods) and actively work with research and development institutions.


Fig. 1: Combinations of terms used internationally in relation to Eco-Industrial Parks (Source: World Bank 2021)

Côté and Cohen-Rosenthal present the following definitions (Côté & Cohen-Rosenthal 1998, Coté & Hall 1995), "An Eco-Industrial Park is a community of businesses aiming at the improvement of their environmental and economic performance through co-operation inefficiently sharing resources including efficient consumption of energy, water, and materials. An EIP is created to improve the economy of its participants while minimizing their environmental impact. Components of this approach involve a new or redefined design of parking infrastructure and installations, prevention of pollution, increasing energy efficiency, and other areas of collaboration between the companies in and EIP. Such form of cooperation may be defined as an industrial ecosystem."

"An Eco-Industrial Park is an industrial system which conserves natural and economic resources; reduces production, material, energy, insurance, and treatments costs and liabilities; improves operating efficiency, quality, worker health, and public image; and provides opportunities for income generation from use and sale of wasted materials".

In their publications Chertow (2007), Smirnova et al. (2019), and Côté and Cohen-Rosenthal (1998), the authors claim that the key factor of EIP operation is establishing material and energy flows between businesses both on the local and regional economy levels. The key element of all the above definitions of the concept of "eco-industrial park" is the organization of "closed cycles of materials" between enterprises in EIPs. Such exchanges of material and energy flows are called industrial symbiosis.

As a result, EIPs apply a set of industrial ecology system components, presenting another definition of an EIP as "an industrial unity of businesses aimed at more efficient use of natural resources, also via industrial symbiosis" (Kiseleva et al. 2018).

By physically exchanging materials, energy, water, and by-products, industrial symbiosis encourages industries that operate separately to come together in sharing material and energy flows in areas with essential and technological options, gaining a competitive economic and environmental edge for all participants (Neves et al. 2016). New "unexpected" connections between various facilities operating in different production (among others) industrial areas may appear in EIPs thanks to the geographical proximity of such facilities. For instance, some authors define an EIP as "a set of manufacturing and service businesses located within one site and employing the same infrastructure" (Hein et al. 2016).

EIPs can be developed via two approaches, the first one is based on self-organization of companies into an EIP and the second one could be based on an analysis of the production processes of the potential EIP participants as well as local/regional material and energy flows, implying a dedicated design of an EIP.

The second approach is more holistic. Owners of business organizations may have an interest in forming (participating in) an EIP as soon as they discover the prospects for maximizing operational efficiency through symbiosis (Alejandro et al. 2018).

Table 1 demonstrates a few examples of eco-industrial parks with the main benefits that have been achieved in their operation.

Designing the organization of an EIP requires methodological approaches and template technical and administrative solutions. Many authors proposed different approaches for this task (Chew et al. 2017, Tiejun 2010, Park & Behera 2014, Leeuwen et al. 2003). Still, the analysis of the solutions proposed by Chew et al. (2017), Tiejun (2010), Park and Behera (2014), and Leeuwen (2003) indicates the need to consider national specifics of economics in the regions where the EIP should be established. This paper attempts to take into account such specific features.

The assessment of material flows that can be directed to the eco-industrial park is the general step of the analyzed approaches to the organization of EIPs and the established methodology. At the same time, in addition to identifying material flows, an important stage in the established technique is determining the location of the eco-industrial park, taking into account the possibilities of the subsequent sale of its products.

## MATERIALS AND METHODS

The study is divided into two parts.

The first part describes the developed methodology for organizing eco-industrial parks. The creation of EIPs is a multi-step process that starts with an analysis of the current situation "before the organization of an EIP" to an assessment of its operation. The key steps in the process for organizing Eco-Industrial Parks were formulated after an analysis of socioeconomic factors and environmental indicators in the regions of potential EIP locations. The EIP guide scheme is shown in Fig. 2.

In the second part of the study, the developed approach was applied to create a model of an Eco-Industrial Park in the Voronezh Region, one of the developing regions of the Russian Federation.

The article is based on the analysis of literature sources, official regional data, and case studies of the authors.

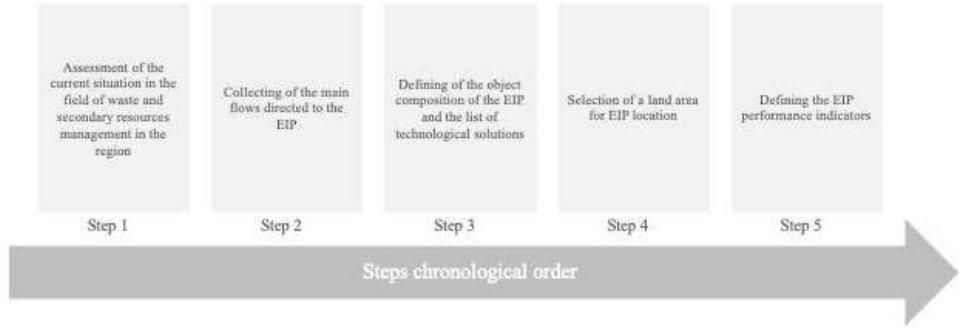


Fig. 2: Schematic Diagram of EIP guide

## RESULTS AND DISCUSSION

### The EIP Methodology

The entire process is viewed as an algorithm accelerator, allowing for the rapid identification and analysis of relevant IS opportunities (Fig. 3). Each individual step's methodology, as well as the required inputs and expected outputs, are detailed below.

*Step 1 – Assessment of the current situation in the field of waste and secondary resources management in the region*

Table 1: Examples of Eco-Industrial Parks implemented on the principles of industrial symbiosis in the world

| Country/ Region | Number of enterprises | Network scope (local/ regional/ national) | Supported/ planned / self-organized | Economic benefits | Social benefits (job creation) | Environmental benefits | References |
|---|---|---|---|---|---|---|---|
| Denmark/ Kalundborg | 9 | Regional | Self-organized | No data | 4614 | Waste Prevention (1997): 1 mln.$m^{-3}$ of sewage sludge 200,000 tons of fly ash and boiler slag 80,000 tons of sludge from gas cleaning 2800 tons of sulfur 300,000 tons - annual reduction of $CO_2$ emissions | (Smirnova et al. 2019) |
| Austria/ Styrian recycling network | 28 | Regional | Self-organized, supported | No data | 22943 | 1 mln tons of by-products collected, 780,000 tons recycled, 200,000 tons thermal recycled. Reached 70% waste recycling rate, reduced 42% of $CO_2$ emissions, 25% of energy resources are renewable | (Smirnova et al. 2019) |
| Finland/ Harjavalta | 13 | local | self-organized | No data | 1000 | Waste utilization rate - 81.8%. 351 tons/year of energy waste 181 tons/year of metal waste 124 tons/year of hazardous waste 15 tons/year of paper waste 16 tons/year of MSW | (Cooperation Fostering Industrial Symbiosis Market 2018) |
| South Korea, Ulsan Mipo, and Onsen Industrial Park | 1000 | Local | Supported, planned | US$ 65 million.$year^{-1}$ from selling by-products and waste for recycling purposes. US$ 78.1 million.$year^{-1}$ from energy and material savings (in 2016) | 35 | saved 279,761 tons of oil equivalent in energy use reduction of 665,712 tons of $CO_2$ emissions and 4052 tons of toxic gases during 2005–2016 79,357 tons of water and 40,044 tons of by-products and waste were reused | (World Bank 2021) |

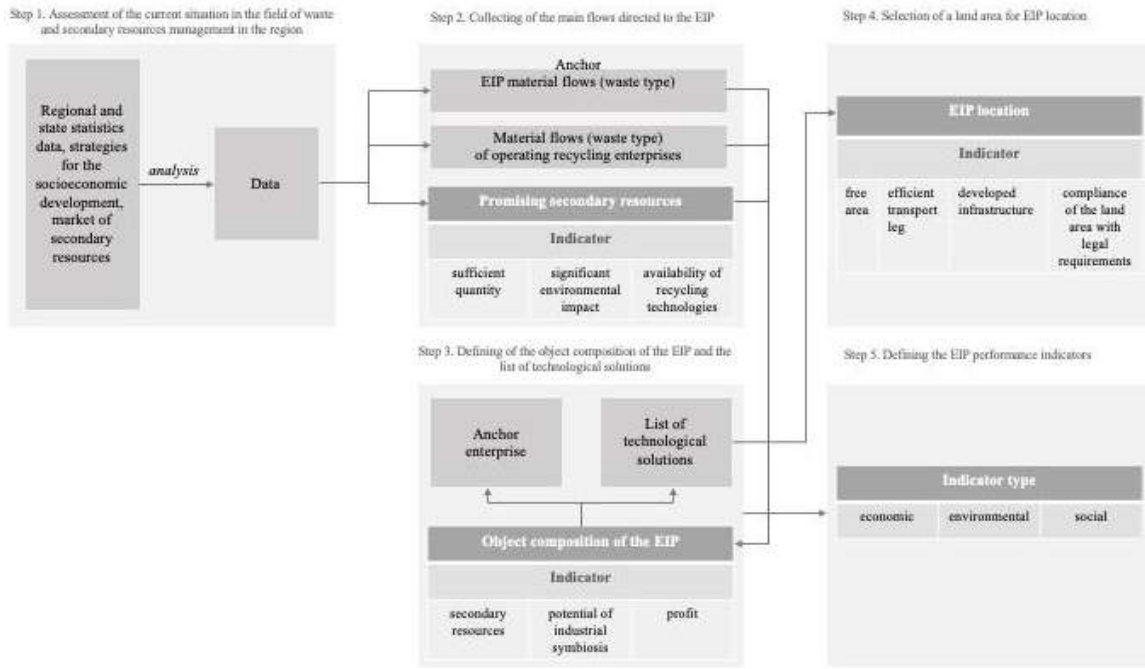


Fig. 3: EIP organization methodology

Input data analysis is the cornerstone of creating an EIP in a given region. This stage envisages evaluation of all available data on waste management in the region and its bordering regions; regional and national statistical accounts; data from environmental reference guides and databases; strategies for aerial and socioeconomic development; strategies for the development of certain industries; and marketing research reports on secondary resources markets.

These activities provide information on the following:

- amount of municipal solid waste (MSW) and industrial waste generated in the region;
- presence of the facilities for treatment, recycling, and landfilling of waste, if any, and the rate of capacity utilized;
- number of prospective sites for collecting, recycling, and decontamination and their location;
- Options for the development of industrial symbiosis;
- Opportunities for the interregional collaboration;
- Problems in waste management in bordering regions.

This set of data is the baseline for the next step.

*Step 2 –Collecting the main flows directed to the EIP*

At this stage, the analysis focuses on raw material flows of the potential EIP, including MSW, industrial waste, and prospective secondary resources to be probably generated during EIP operations including waste sorting and waste recycling.

The criteria for the selection of prospective secondary resources include their sufficient weight or volume; significant environmental impact; and the availability of recycling technologies.

The design of an EIP project requires drawing a plan to combine enough physical resources to enable reaching target rates of recycling and producing a strategy for collecting such resources.

A prospective increase in estimated capacity due to a possible increase in future waste flows resulting from interregional interaction or the elimination of objects of accumulated environmental damage, among other causes, must be considered in addition to the forecast average level of material flows towards a planned EIP.

*Step 3 – Defining the object composition of the EIP and the list of technological solutions*

Following the creation of the EIP's list of material resources, one must then create a list of technological solutions for the treatment, recycling, and decontamination of industrial and municipal waste/secondary resources to use in the manufacturing process. The analysis and marketing for the output based on secondary resources must be the following step.

Selection of technologies requires envisaging the interconnectivity of technologies for the realization of symbiotic industrial connections between industrial facilities.

Technologies for treatment, recycling, and decontamination of industrial and municipal waste/secondary resources shall meet the following requirements:

- waste generated within the EIP operations process shall be safe or present minimal risks to the environment and human health;
- most of the waste shall be returned to the production cycle or must be securely disposed of as environmentally safe objects;
- the amount of landfilled waste must be minimized.

*Step 4 – Selection of a land area for EIP location*

The composition of the prospective EIP objects defines the requirements for the land area to locate the EIP. Its selection is a standalone task that also needs a multifactor approach.

The main criteria for the s*election of a land area for EIP* include:

- available area;
- effective transportation leg, from the source of waste generation through the waste storage places to the recycling and utilization facilities;
- suitable infrastructure (water supply and removal, energy and thermal power supply, good surface transport network);
- the land area's compliance with the current regulations and demands.

Other meaningful factors are the potential for the development of neighboring urban and rural communities, their functional zoning and development pattern, utility and transport infrastructures, rational management of natural resources, and environmental protection. It's essential to consider the efficient material sources while deciding where to locate EIPs. As a result, it is vital to select places with the maximum concentration of material flow sources, as well as factors affecting the region's development, such as physiographic, socioeconomic, transportation, and logistical.

EIPs' infrastructure is built in accordance with legislation governing industrial and technological infrastructure, operational profiles, and material and energy inputs.

The design of EIPs and implementation plans for innovative solutions shall account for reliability, ease of use, and the operational and maintenance efficiency of infrastructural facilities, as well as their reorganization and reconstruction, to ensure sustainable cost efficiency and the opportunity for technical upgrades.

There is the option to use economically and technically viable decentralized facilities.

In the design of an EIP, the transport and utility infrastructure shall ensure the following:

- possibility for the cooperation between utility facilities such as water supply and wastewater disposal, power and heating and gas supply, communications, etc.;
- interaction between industry facilities;
- transport links between urban and rural communities;
- separation of cargo and passenger traffic, the building of parking areas and networks of walkways and bicycle lanes;
- rational organization of pedestrian and automobile traffic towards workplaces, minimization of distances from operation support infrastructure.

*Step 5 –Defining the EIP performance indicators*

At this stage, we apply specially designed performance indicators to assess the efficiency of the EIP project in three main aspects, environmental, economic, and social.

As the key part of the circular economy, an EIP primarily aims at creating closed-loop supply chains to maximize the return of waste and secondary resources to new production. This approach enables efficient preservation and augmentation of natural resources and streamlining production processes, increasing resource and energy efficiency, which helps to scale down environmental problems and improve the region's economic efficiency and sustainability. Symbiotic connections between EIP participants allow addressing a number of diverse tasks as follows:

- reducing landfill areas;
- reducing emissions, dumping, and generation of waste;
- reducing energy and material costs;
- increasing resource and energy efficiency;
- returning secondary material resources to the production cycle and reducing consumption of natural resources;
- strengthening climate resilience by reducing greenhouse gas emissions from landfills;
- boosting capex efficiency while reducing operating costs;
- creating new jobs;
- raising the quality of life, also by improving environmental and economic conditions;
- supporting the region's transition to the development in the circular economy model.

Below are the results of the evaluation of the described methodology applied to the organization of an EIP in the Voronezh Region of the Russian Federation.

## Case Study

Voronezh Region, located in the Central European part of Russia, has an area of 52,216 sq.km, with a population of 2.4 million. The region comprises eight administration clusters: Voronezhsky, Liskinsky, Rossoshansky, Bogucharsky, Paninsky, Buturlinovsky, Borisoglebsky, and Kalacheevsky. The climate is continental. Economically, the region focuses on agriculture, industrial manufacturing, and construction. The main sources of waste generation are manufacturing facilities, MSW and food production, animal farms, and agricultural farms. Combined, they account for 4/5 of the region's total industrial output. Leaders by waste generation in Voronezh Region are animal farms, sugar factories, and vegetable processors (The Strategy of Socio-Economic Development of the Voronezh Region 2018).

*Step 1 – Assessment of the current situation in the field of waste and secondary resources management in the Voronezh Region*

### The amount of MSW generation

According to the waste inventory register of the Voronezh Region, the Voronezhsky inter-municipal cluster generates the greatest amount of waste, standing at 755.5 thousand tons (66% of the total in Voronezh Region), due to a significant concentration of population in the Voronezh agglomeration and a higher level of industrial and business activity. In each of the other seven inter-municipal clusters of the Voronezh Region, the amounts of annually disposed of MSW are meaningfully lower (Voronezh waste management system 2016).

### Waste disposal facilities

There are 30 facilities on the list of waste disposal sites in the Voronezh Region. Over 80% (24 facilities) are landfills. 17 of them deal with MSW and seven deal with industrial waste. Six facilities are dumpsites.

The majority of MSW landfills in the Voronezh Region are located in the Voronezhsky inter-municipal cluster. The capacity of landfills (filled with wastes) in the Voronezh Region ranges from 14% up to 115 %.

### MSW treatment facilities

The sites for MSW treatment in the Voronezh Region are waste sorting facilities, five are in operation and are located in the Voronezhsky cluster (Novosumansky and Semilukinsky Districts), Borisoglebsky cluster (Povorinsky District), and Rossoshansky cluster (Rossoshansky District) (Voronezh Waste Management System 2016).

### Waste recycling facilities

These are concentrated mainly in the Voronezhky cluster, in the City of Voronezh, and recycle all fractions of MSW.

### Interregional co-operation

To assess the options for interregional collaboration in the operation of an EIP, we analyzed waste management systems in neighboring regions. Voronezh Region borders the Lipetsk, Tambov, Volgograd, Belgorod, Kursk, Rostov, and Saratov Regions. This analysis helped to define prospective districts from which waste (secondary resources) flows could be directed to the Voronezh EIP. Selection criteria included geographical proximity to the Voronezh Region and the absence of facilities for treatment, recycling, decontamination, and landfilling of MSW. The authors advise directing MSW flows from Terbunsky, Khlevensky, and Umansky Districts of Lipetsk Region as well as from Rovensky District of Belgorod Region (Belgorod Waste Management System 2016, Lipetsk Waste Management System 2019).

### Industries and industrial waste

The industrial sector of the Voronezh Region is dominated by agriculture (The Strategy of Socioeconomic Development of the Voronezh Region 2018). As of 2018, the breakdown of industrial waste by volume in the Voronezh Region was as follows:

- food production – 3,810.23 thousand tons;
- animal farms waste – 2,852 thousand tons;
- mineral fertilizer production – 287.33 thousand tons.

Voronezh Region has no facilities for demercurization. Being a major logistical hub, Voronezh is the main producer of mercury-containing waste, while also accumulating the residue of such type delivered from other municipalities. It handles redirection of waste for decontamination outside of the region: to Moscow and the Regions of Moscow, Kursk, Ryazan, and Ulyanovsk.

The results of the analysis of the current situation in waste management in the Voronezh Region and bordering regions are presented in Table 2.

The Voronezhsky cluster is the primary source of MSW in the Voronezh Region. In Semiluksky Municipal District, there are three garbage disposal sites, facilities for recycling all MSW fractions, and a waste sorting facility with a used capacity of 440 thousand tons.year$^{-1}$ (Voronezh Waste Management System 2016). The MSW sorting plant has a design capacity of 900 thousand tons.year$^{-1}$.

*Step 2 –Collecting the main flows directed to the EIP*

We believe that recycling potential secondary resources

such as scrap paper, plastic trash, and scrap glass have the most potential.

The establishment of a chain of interactions from waste generation to the manufacturing of products from waste and secondary resources is an example of how the methodological approach to the formation of material flows can be used to the EIP. (see Table 3).

Agriculture has the highest industrial load in Voronezh Region. Organic waste, manure, and food producers' waste could be generated by producers of meat, sugar, oils, fats, canned vegetables, and fruits, etc.

*Step 3 – Defining the object composition of the EIP and the list of technological solutions*

The agricultural sector defines the base for the prospective EIP. We advise building a complex for composting organic waste that would act as the anchor facility of the EIP. Produced compost shall be used for reclamation (remediation) of full landfills and unauthorized dumps. In the future, the complex may be converted to generate energy for the construction of other facilities within the EIP. Based on the analysis in steps one to three, we propose locating two sites of the Voronezh EIP in the Semiluksky and Rossoshansky districts. The proposed composition of the EIP by the example of Semiluksky District is presented in Fig. 4.

*Step 4 – Selection of a land area for EIP location*

The assessment based on our methodological approach resulted in the selection of two sites for the creation of the EIP:

- in Semiluksky District, with the area of 30.88 hectares and the developed infrastructure in the distance of 1.7 km from the MSW sorting plant;
- in Rossoshansky District, with an area of 4.6 hectares and the developed infrastructure in the distance of 3 km from the MSW sorting plant.

*Step 5 – Defining the EIP performance indicators*

The evaluation of the efficacy of the EIP activities was facilitated by the identification of three areas and the development of specific and quantitative performance indicators for each of them (Table 4).

The cornerstone of industrial symbiosis, according to leading Russian and worldwide specialists in the circular economy, is established by the combination of resource exchange between companies, recycling of secondary resourc-

Table 2: The results of data analysis.

| Waste generation | Voronezh cluster 755.5 thousand tons (65% of the total education in the Voronezh Region) |
|---|---|
| Waste disposal facilities, percentage of filling | Only 30, of which 14 are 115% filled |
| Current MSW recycling facilities | Recycling companies of all MSW fractions (Voronezh cluster) |
| Planned waste recycling facilities | 8 |
| MSW processing facilities | 7 waste sorting facilities |
| Interregional interaction | Belgorod region (Rivne district)<br>Lipetsk region (Terbunsky, Khlevensky, and Umansky districts) |
| Industrial waste | Waste from food production, farm animal waste, garden waste, mercury lamps, used oils |

Table 3: Chains of relationships from waste generation to the final consumer of products.

| Material flow (waste type) | Waste recycling company | Secondary resources | Recycled products | Potential consumers of secondary resources |
|---|---|---|---|---|
| Plastic waste | Voronezh-Polymer LLC<br>LLC Polymer-Chernozemye<br>LLC "Contact"<br>LLC "Management Company Region-Resource"<br>Voronezhvtorma LLC | Crusher, agglomerate, granules, flex | Polyethylene film, garbage bags, polyethylene granules, LDPE film, plastic packaging | Producers of PET bottles and other plastic packaging, bristles for cleaning equipment, building materials |
| Paper waste | Eco Liner LLC<br>LLC "Kharti"<br>LLC "Kivo Market"<br>LLC "KartonChernozemye" | Pressed sorted waste paper, cellulose wool | Sanitary and hygienic products, corrugated board, cardboard | Producers of cardboard, sanitary products |
| Scrap glass | "Branch of LLC RASCO"<br>Voronezh glass container plant"<br>LLC "Sferastek" | Sorted scrap glass | Foam glass, fiberglass, glass crystal materials, road marking materials | Producers of glass containers, building materials |
| | | Processed containers | Reusable packaging | Producers of drinks, food |

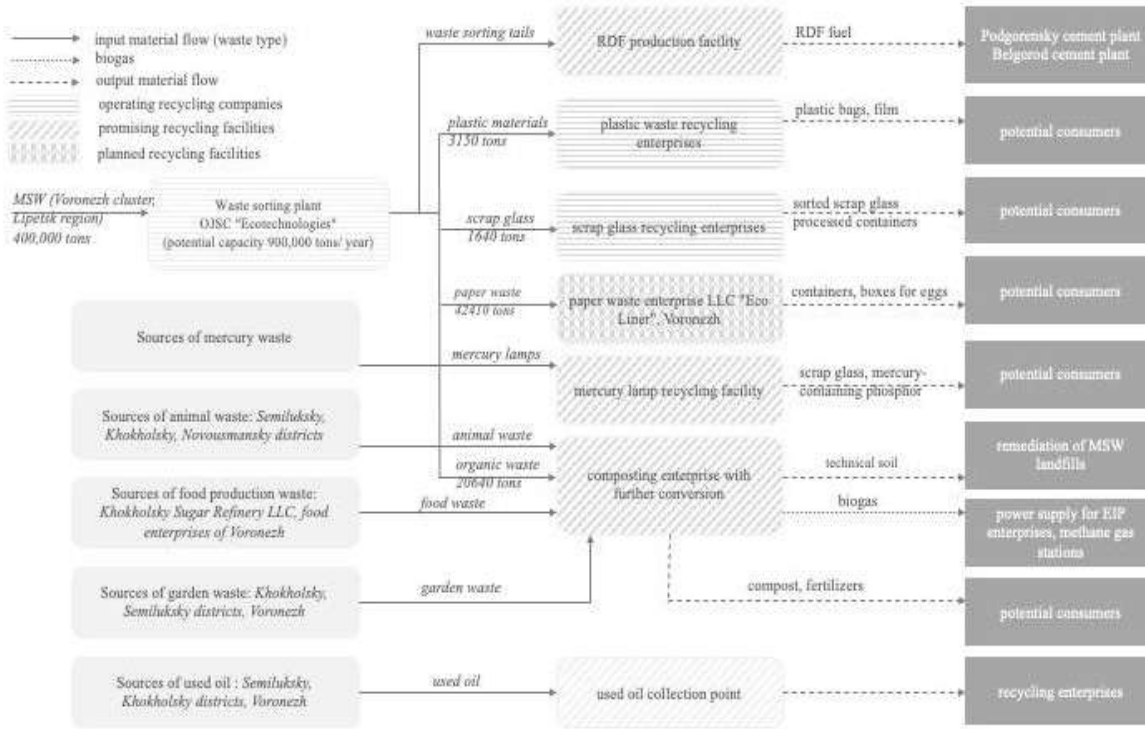


Fig. 4: Model of the object composition of the EIP in the Semiluksky district

es, involvement of many enterprises, and manufacture of competitive goods. The proposed methodological approach reflects this viewpoint.

The findings of the work on the EIP model's organization have been approved, and the Voronezh Region Administration is considering them further. The approach is planned for possible replication in other regions.

Thus, using the Voronezh Region of Russia as an example, the five stages of EIP organization proposed in the study make it possible to close waste streams to recycling firms operating and developed within the eco-industrial park.

Table 4: Assessment of compliance with the criteria for sustainable development of performance indicators of the EIP

| Indicator type | Indicator |
|---|---|
| Economic | Increasing share of secondary resources usage in production |
| | Increasing investments in waste recycling and recovery and use of secondary resources |
| | Decreasing fees for the negative impact of waste disposal |
| | Decreasing operating costs |
| Environmental | Reducing landfill disposal |
| | Increasing waste recycling rate |
| | Decreasing emission of greenhouse gases |
| | Increasing the secondary resources recovery rate |
| | Increasing volume of production using waste and secondary resources |
| | Improving resource and energy efficiency |
| | Increasing number of facilities implementing the best technologies available |
| Social | Increasing public satisfaction with the quality of the environment |
| | Increasing the number of jobs involved in waste recycling and using secondary resources |

This is in line with the primary goals of establishing an eco-industrial park: improving resource efficiency and reducing landfill waste disposal.

## CONCLUSION

The authors presented a methodological approach based on classification and algorithmization of operations that must be followed to create an Eco-Industrial Park. In steps One and Two, initial data is processed to evaluate and calculate material flows to the prospective EIP. In step 3, the data collected and processed is used for designing the project composition of the EIP and choosing the required technological solutions. Step four sets the requirements for the land area and infrastructure for the EIP. In the final step, five performance indicators of the EIP are defined. This approach aims at delivering a comprehensive solution to the problem of waste management and reuse of secondary resources in regional economics. Implementing this technology to construct an EIP in the Voronezh Region could help to streamline trash flows and raise recycling rates by increasing capacity, all while lowering the negative environmental impact of waste landfilling. Implementing the circular economy in the appropriate region is one of the EIP's core ideas.

This paper gives a general outline of the methodology for the Eco-Industrial Parks organization. The authors continue refining the approaches to develop more detailed operations at each step and produce template technological solutions for EIPs.

## REFERENCES


Albino, V., Yazan, D.M. and Romano, V.A. 2016. The design of industrial symbiosis: An input-output approach. J. Cleaner Prod., 129: 537-547.

Alejandro, M., Gómeza, M., Gonzáleza, F.A. and Bárcena, M.M. 2018. Smart eco-industrial parks: A circular economy implementation based on industrial metabolism. Resour. Conserv. Recycl., 135: 58–69.

Ayres, R.U. and Simonis, U.E. 1994. Industrial Metabolism: Theory and Policy. In: Ayres, R.U. and Simonis, U.E. (eds), Industrial Metabolism: Restructuring for Sustainable Development. United Nations University Press, Cham, Switzerland, pp.3-20.

Chertow, M.R. 2007. "Uncovering" industrial symbiosis. J. Ind. Ecol., 11(1): 11-30.

Chew, I.M.L., Leong, Y.T., Lee. J.Y., Tan. R.R. and Foo, J.J. 2017. Multi-objective optimization for resource network synthesis in eco-industrial parks using an integrated analytic hierarchy process. J. Cleaner Prod., 143: 1268-1283.

Cooperation Fostering Industrial Symbiosis Market 2018. Potential, good practice, and policy actions: Final report. Available at: URL: http://trinomics.eu/project/industrial-symbiosis (accessed 20 April 2021).

Côté, R.P. and Hall J. 1995. Industrial parks as ecosystems. J. Cleaner Prod., 3: 41-46.

Côté, R.P. and Cohen-Rosenthal, E. 1998. Designing eco-industrial parks: A synthesis of some experiences. J. Cleaner Prod., 6: 181-188.

Ernest, L.A. 1995. The Eco-Industrial Park: A Business Environment for a Sustainable Future. Paper presented at Conference on Designing, Financing and Building the Industrial Park of the Future," sponsored by the U.S. EPA, Research Triangle Institute, and the University of California at San Diego, San Diego, May 4–5.

Fischer-Kowalski, M. 1998. Society's metabolism: The intellectual history of material flow analysis, Part I, 1860–1970. J. Ind. Ecol., 2(1): 61-78.

Hein, A.M., Farel, R., Jankovic, M. and Yannou, B. 2016. A data- and knowledge-driven methodology for generating eco-industrial park architectures. In ASME 2016 International Design Engineering Technical Conferences and Computers and Information in Engineering Conference, Charlotte, North Carolina, USA, 21-24 August 2016, pp. 1-12.

Kiseleva, S.P., Smirnova, T.S. and Maryev, V.A. 2018. Transition to a Circular Economy: A Way to Improve the Ecological Situation In Russia. In Priority And Promising Directions Of Scientific and Technological Development of the Russian Federation, Materials from the Seminar of the 1st Russian Scientific and Practical Conference, Moscow, Russian Federation, 11 April 2018, pp. 240–245.

Leeuwen, M.G., Vermeulen, W.J.V. and Glasbergen, P. 2003. Planning eco-industrial parks: An analysis of Dutch planning methods. Bus. Strategy Environ., 12: 147-162.

Mashukova, B.S. 2016. Basic principles of a circular economy. Euro. Sci., 7: 14-16

Neves, A., Godina, R., Azevedo, S.G., Pimentel, C. and Matias J.C.O. 2016. The potential of industrial symbiosis: Case analysis and main drivers and barriers to its implementation. Sustainability, 11(24): 1-68.

Belgorod Waste Management System 2016. On approval of the territorial waste management system, including solid municipal waste, in the Belgorod Region (2016) Regulatory Act. Available at: URL: http://belgkh.ru/media/site_platform_media/2020/2/28/postanovlenie-pravitelstva-belgorodskoj-obl-ot-26092016-350-pp.pdf (accessed 20 April 2021).

Voronezh Waste Management System 2016. On approval of the territorial waste management system, including solid municipal waste, in the Voronezh Region. Regulatory Act. Available at: URL: https://docs.cntd.ru/document/453149000 (accessed 20 April 2021).

Lipetsk Waste Management System 2019. On approval of the territorial waste management system, including solid municipal waste, in the Lipetsk Region. Available at: URL: http://ekolip.ru/territorialnaya-skhema-obrash-cheniya-s-otkhodami.php?clear_cache=Y (accessed 20 April 2021).

Pakhomova, N.V., Richter, K.K. and Vetrova, M.A. 2017. Transition to the circular economy and closed supply chains as a factor of sustainable development. J. Bul. St. Pet. State Univ., 33(2): 244-268.

Park, H.S. and Behera, S.K. 2014. Methodological aspects of applying eco-efficiency indicators to industrial symbiosis networks. J. Cleaner Prod., 64: 478-485.

Skobelev, D.O. 2020. Formation of the infrastructure of resource-technological transformation of industry. Eco. Sust. Develop., 1(41): 162-167.

Smirnova, T.S., Maryev, V., Guz, L. and Mankulova, J. 2018. Industrial symbiosis as an instrument of sustainable development in the modern world. Interdiscip. Sci. Pract. J: Ecol. Ind. Prod., 3: 64-68.

Smirnova, T.S., Evtukhov, V.L. and Maryev, V.A. 2019. Analysis of the World Experience: The Organization f Eco-Industrial Parks and the Implementation of the Principles of the Circular Economy. INFRA-M., Cham, Switzerland

The Strategy of Socio-economic Development of the Voronezh Region. 2018. Regulatory Act: For the Period Up to 2035. Available at: URL: https://docs.cntd.ru/document/550300779 (accessed 20 April 2021).

Tiejun, D. 2010. Two quantitative indices for the planning and evaluation of eco-industrial parks. Resour. Conserv. Recycl., 54: 442-448.

Tyrganova, A.A. and Makhashkeeva, A.Y. 2014. Circular economy as a new model of the world economy: Foreign experience and Russian practice. Eco. Sci. Appl. Res., 18(22): 301-304.

World Bank. 2021. International Framework for Eco-Industrial Parks v.2. World Bank, Washington, DC.

Zhou, L., Pang, M., Sikorski, J., Garud, S., Kleinelangshorst, M., Karimi, I. and Kraft, M. 2017. System development for eco-industrial parks using ontological innovation. J. Energy Procedia, 105: 2239–2244.

Nature Environment and Pollution Technology
An International Quarterly Scientific Journal

p-ISSN: 0972-6268
(Print copies up to 2016)
e-ISSN: 2395-3454

Vol. 20 | No. 5 (Suppl) | pp. 2041-2050 | 2021

Original Research Paper

https://doi.org/10.46488/NEPT.2021.v20i05.021

Open Access Journal

# Development of Eco-friendly Adsorbent Pellets from Low Fire Clay and Potato Starch for Potential Use in Methylene Blue Removal in Aquaculture

**Priyanka Sharma and Kushal Qanungo†**
Division of Chemistry, Institute of Science, Chandigarh University, Gharuan, Distt. Mohali, Punjab, India
†Corresponding author: Kushal Qanungo; kushalq@rediffmail.com

**Nat. Env. & Poll. Tech.**
**Website: www.neptjournal.com**

*Received:* 04-05-2021
*Revised:* 13-05-2021
*Accepted:* 01-07-2021

**Key Words:**
Clay
Aquaculture
Methylene blue
Potato starch
Adsorption

## ABSTRACT

Mesoporous clay-starch ceramic pellets have been prepared using silica-rich low fire clay and potato starch as a pore-forming agent. The ceramic pellets prepared using 30% starch, showed the highest porosity and lowest compressive strength among all the different pellets. Batch mode studies using the pellets showed higher methylene blue adsorption capacity with an increase in time and increased initial dye concentration. The adsorption capacity was found to decrease with increasing pellet dose, while pH had a negligible effect on methylene blue removal which makes them a suitable adsorbent in both acidic and basic mediums. Adsorption isotherm analysis of the process was followed by the Langmuir adsorption isotherm whereas the kinetics analysis fitted well with the pseudo-second-order kinetic model. A low-cost, simple device was made from a stainless-steel wire mesh with mesoporous ceramic pellets enclosed in it, which can easily be dipped and taken out of an aquarium and can remove methylene blue from water.

## INTRODUCTION

A number of drugs, dyes, and chemicals are widely used to treat various problems and diseases in fish. Different chemicals used in aquaculture, when get mixed with environmental components, cause various harmful effects (Mabel et al. 2019). Many of the dyes are toxic and carcinogenic in nature, causing threats to humans and other living organisms (Abdel-Halim 2013). Due to their synthetic origin, high molecular weight, and complex structures they are resistant to biodegradation. Discharge of dye-containing water, even in the low concentration affects the process of photosynthesis, chemical oxygen demand, and the quality of water which in turn disturbs the ecological balance (Yemendzhiev et al. 2009).

Methylene Blue (MB) is a cationic dye belonging to an azo group and characterized by an N=N bond. The structure of MB is shown in Fig. 1a:

MB is commonly used for dyeing textiles, leather, and paper. Exposure to MB results in an increased heartbeat, vomiting, jaundice, Heinz body formation, and tissue necrosis in humans (Zeynolabedin et al. 2015) in the long term. MB is also used for the removal of external parasites as well as for fungal infections in fishes at a concentration of 0.15 to 1-2 ppm. Most aquariums are fitted with activated carbon filters before a mechanical filter to filter out the odor and color causing contaminants that accumulate over time. This activated carbon filter has to be removed before MB treatment, otherwise, the filter would absorb MB, rendering it useless and the treatment would also be ineffective. Post MB treatment, the aquarium water has to be changed to remove the MB before putting in the activated carbon filter back. Discharging a large volume of dye-containing water into the environment, even at low concentrations is an ecological risk. Therefore, it is important to remove MB from the aquarium water post-MB treatment.

Among different techniques of dye removal from water, adsorption is a widely used process due to its effectiveness, cost, simple design, and easy operation (Ahmed et al. 2010). Ceramics are an effective adsorbent for the removal of dyes and chemicals from aqueous systems due to their low cost and natural availability. The use of different additives helps in transforming clay minerals into porous materials and these can be stabilized through calcination. Increased porosity makes them useful to control environmental pollution in relation to dye adsorption (Elimbi et al. 2019).


Fig. 1a. Chemical structure of Methylene Blue.

In this paper, we report the preparation of mesoporous ceramic pellets using low fire clay and potato starch and the testing of an MB removal device containing these ceramic pellets. This device can be used in aquariums to conveniently remove MB, remaining after antifungal treatment of fishes at ultralow concentrations at an extremely low cost.

## MATERIALS AND METHODS

### Preparation of Mesoporous Ceramic Pellets

For making the ceramic pellets, 5 mm holes were drilled into a mild steel plate of 5 mm thickness. The plates were then cleaned and painted to protect from corrosion and these plates were then used as molds for making pellets. Low fire clay was purchased from Bhoomi Pottery, Mumbai, Maharashtra, and was used as such. All chemicals used were of AR grade.

The clay powder and starch were mixed in defined proportion (Table 1) in a pestle mortar for 15 min with a minimum quantity of distilled water to make it plastic (e.g., 8 g clay, 2 g starch, and 5 mL distilled water). The wet clay was poured into the mold and left to dry in shade. The green pellets were then removed with the help of a cotton-tipped steel rod and placed in a silica crucible. The ceramic pellets were now fired in a muffle furnace and the temperature was raised in stages to reach 850°C. After heating, the furnace was turned off and pellets were left to cool overnight. Ceramic pellets made from clay, starch, and water are named clay-starch ceramic pellets (Fig. 1b). The compressive strength was determined using EI Digital Tablet Hardness Tester, Model No. 3956 (range 2 mm to 28 mm).

### Characterization of Starch-Clay Ceramics

XRF analysis was carried out by BRUKER WDXRF Model S8 Series 2, TIGER Spectrometer, IR using the Perkin Elmer 4000 FTIR Spectrometer. Surface morphology by JEOL, IT 500 SEM., determination of pore size, BET surface area, and pore volume of pellets was done with $N_2$ adsorption/desorption isotherm at a temperature 77K using Quanta Chrome, Nova Surface Area Analyser (ver. 11.05).

### Water Adsorption Capacity

To check water absorption capacity ($W_{ad}$., eqn.1), of pellets,

Table 1: Composition and compressive strength of prepared mesoporous pellets.

| S.No. | Clay [% ] | Starch [%] | Compressive Strength [$N.m^{-2}$] |
|---|---|---|---|
| 1 | 100 | 0 | 214 |
| 2 | 90 | 10 | 110 |
| 3 | 80 | 20 | 90 |
| 4 | 70 | 30 | 71 |
| 5 | 60 | 40 [crumbled on firing] | - |

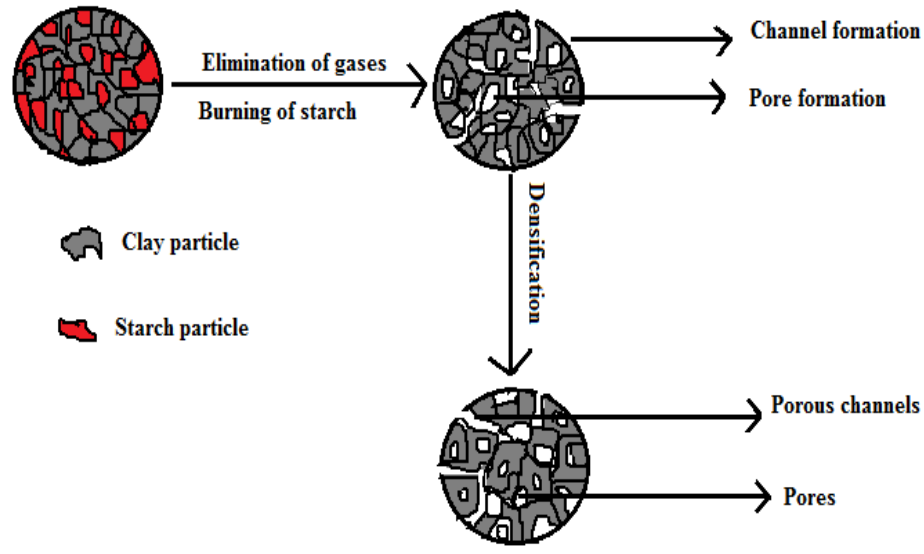


Fig. 1b: Formation of clay ceramic pellets using starch as a pore-forming agent.

Fig. 1c: Prepared ceramic pellets.

dried pellets (3 Nos.) were weighed ($W_1$) and immersed in boiling water for a time of 2 h, and then heating was turned off and the pellets remained immersed in water to cool for 4 h. The pellets were removed from the water, the extra moisture present on the surface of pellets surfaces was removed using a soft cloth, and was re-weighed ($W_2$).

$$Wad.(\%) = \frac{(W2 - W1)}{W1} X100 \quad \ldots(1)$$

### MB Adsorption Experiment

MB adsorption experiment was done using batch mode studies. For this, 0.5 g of ceramic pellets were added to MB solution of different concentrations (0.25,0.5,1.0 ppm). The resultant solution was stirred at a speed of 200 rpm. All experiments were carried out at room temperature. The absorbance of the solution was then determined at a wavelength of 680 nm using a microprocessor-controlled colorimeter (D.S. Scientific Instruments). In this study ceramic pellets with initial starch content of 30% (sample no. 4, with the highest porosity) were used to analyze the MB adsorption process.

### Tap Water Trials of MB Removal Device

Tap water was used to understand the MB adsorption behavior of ceramic pellets in water suitable for aquarium use. Analysis of different water quality parameters was done at Eco Laboratory Pvt. Ltd. (Mohali) (Table 5) by standard methods. The pellets in specified quantities (0.5, 0.75, 1.0 g) were taken in a stainless-steel tea ball wire mesh of 4 cm dia. and dipped in 100 mL of 1 ppm MB solution in tap water. The solution was then stirred at a speed of 20 rpm at room temperature to replicate the actual aquarium conditions.

## RESULTS AND DISCUSSION

### Temperature Selection and Preparation of Mesoporous Pellets

Firing is the most critical stage of the ceramic formation as any temperature variation can lead to unsatisfactory results in ceramic durability and color. If fired too high, clay can deform or even melt, if fired too low, ceramics will be dry, rough, and potentially unsolidified. Low fire clays reach maturity at lower temperatures as they need less energy during the firing process. The clay sintering process involves the bonding of clay minerals and the change of clay to ceramics. For making ceramic pellets, the temperature was raised at a rate of 1°C.min$^{-1}$ to reach 240°C, 2°C.min$^{-1}$ to reach 490°C, and finally, 3°C. min$^{-1}$ to reach 850°C

### Characterization of Pellets

The spectrum of fired pellets shows bands at ≈1057 cm$^{-1}$ are associated with stretching of Si-O bonds (Aroke et al. 2013). The doublet of quartz was observed at 778 cm$^{-1}$ (Saikia et al. 2008), and Si-O-Si bonds were observed at 685 cm$^{-1}$ (Fig. 2).

XRF analysis of clay showed that it is mainly composed of $SiO_2$ (64.21%), $Al_2O_3$ (24.36%), CaO (4.70%) MgO (4.31%), $K_2O$ (1.22%).

The surface morphology of pellets before and after MB is shown in Fig. 3a and 3b. The specific surface areas and pore diameters ceramic pellets as determined by the BET method and $N_2$ adsorption/desorption isotherm are shown in Fig.4a and 4b. It was found that the specific surface area of the ceramics was 3.332 m$^2$.g$^{-1}$ with a density of 3.659 g.cc$^{-1}$. The pore volume was found to be 0.008 g.cc$^{-1}$ and a pore diameter of 2.453 nm, showing the mesoporous nature of the ceramic pellets. The nitrogen adsorption-desorption isotherms of the samples were classified as a typical type IV isotherm characteristic (Yan et al. 2018, Ambroz et al. 2018) suggesting capillary condensation after multilayer adsorption at mesopores. Water adsorption capacity (Fig. 5) of ceramic pellets was found to increase with an increase in starch content due to an increase in porosity of the ceramic pellets.

### Reaction Parameters and Their Effect on Adsorption Behavior of Pellets

### Effect of Contact Time

Contact time studies correlate the amount of dye adsorbed onto a fixed mass of adsorbent. It is used to find out the equilibration time for adsorption. The effect of contact time was studied in a time range of 1500 min. Following equations (eqn. 2, 3, 4) were used to determine $q_t$, $q_e$, and percentage removal.

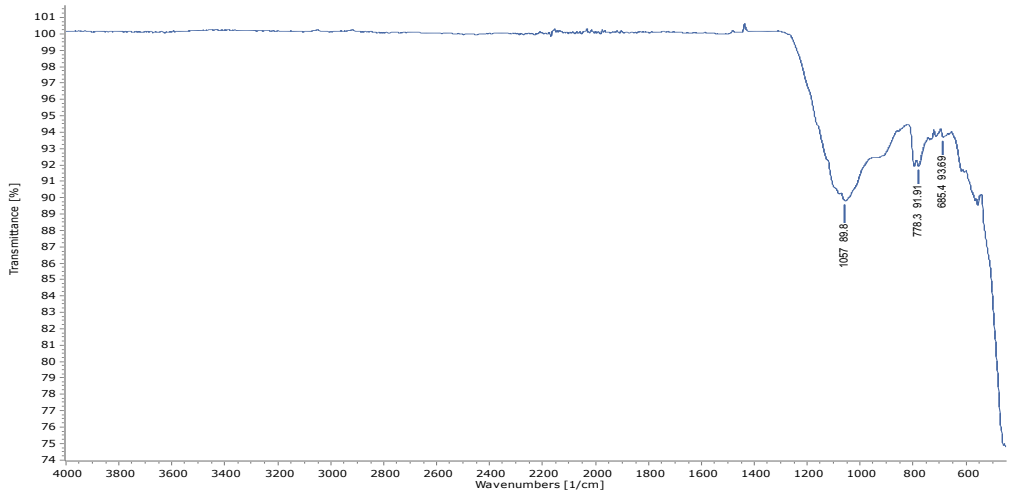


Fig. 2: FTIR Spectra of clay ceramic pellets (sample no.4).

$$qe = \frac{(Co - Ce)}{m} \times V \quad \ldots(2)$$

$$qt = \frac{(Co - Ct)}{m} \times V \quad \ldots(3)$$

$$\%removal = \frac{(Co - Ct)}{Co} \times 100 \quad \ldots(4)$$

The terms $C_o$, $C_t$, and $C_e$ indicate the MB concentration during the initial time, at time t and equilibrium, respectively. $q_t$ and $q_e$ ($mg.g^{-1}$) indicate the amount of MB adsorbed at time t and equilibrium time.

A quick increase in MB adsorption capacity was observed during the first 130 min of reaction time followed by a gradual increase in dye adsorption. Percentage removal was also found to increase with an increase in starch content.

**Effect of Pellet Dose**

Initial adsorbent dose controls adsorption via available surface area and binding sites. The adsorbent dose was varied from 5 to 40 $g.L^{-1}$ and adsorption capacity was found to be reduced as the dosage increased (Fig. 6). This decrease in adsorption capacity with an increase in dose may be due to

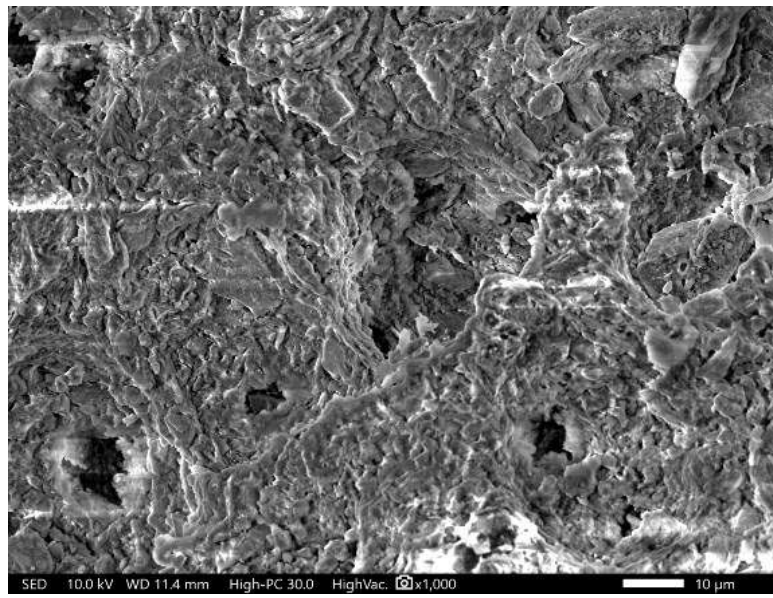


Fig. 3a: SEM images of ceramic pellets (sample no.4) before MB adsorption.

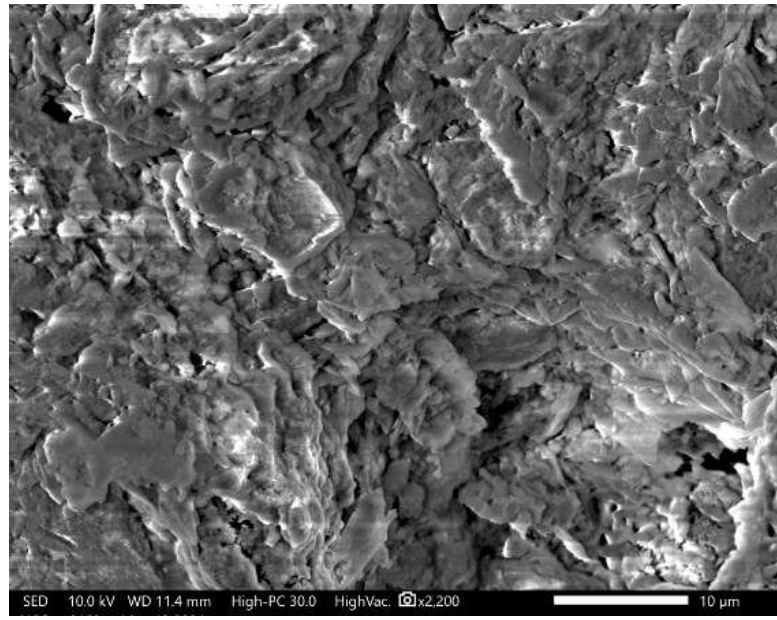


Fig. 3b: SEM images of ceramic pellets (sample no.4) after MB adsorption.

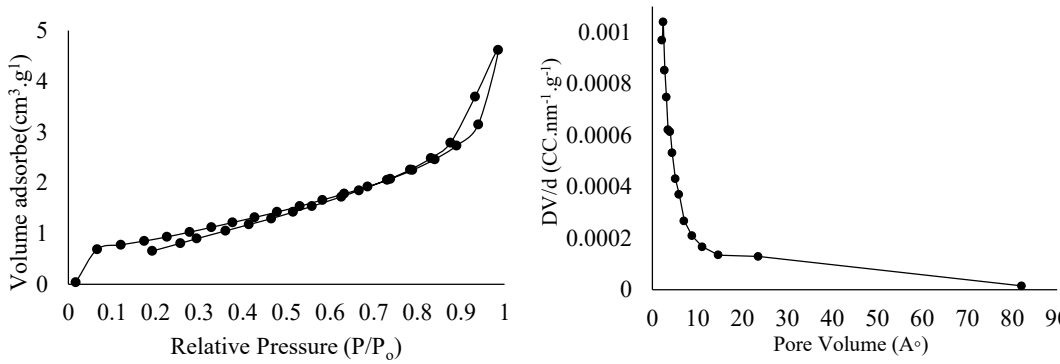


Fig. 4: a) BET surface area and b) pore size distribution of ceramic pellets (sample no.4).

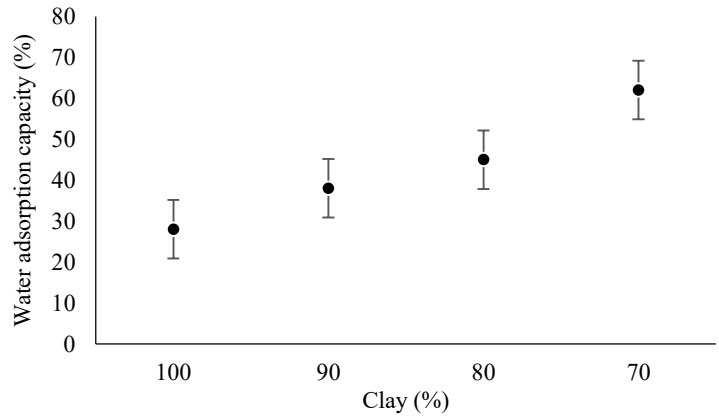


Fig. 5: Water adsorption capacity of ceramic pellets with increased starch content in the green body.

saturation of adsorption sites through the sorption process or due to aggregation resulting from a higher dose.

**Effect of Initial Dye Concentration**

Initial dye concentration plays a crucial role as it drives the solute transfer rate under a higher concentration gradient between MB solution and pellet surface. The adsorption capacity of pellets was shown to increase when the initial MB concentration increased (Fig. 7), as at lower concentration the ratio of the initial number of MB molecules to the available surface area is low, and subsequently, the fractional adsorption becomes independent of initial concentration. Similar results were also obtained for MB adsorption using natural clay (Bentahar et al. 2017).

**Effect of pH**

The pH of the aqueous solution is an important parameter that controls the adsorption process. The effect of solution pH on the adsorption capacity of MB dye on the pellet surface was performed at different pH levels (pH 2–12) with a fixed dose of 1g.100 $mL^{-1}$ at room temperature. 0.1M HCl/0.1M NaOH was used for pH adjustment. The pH-independent behavior of ceramic pellets makes them suitable to use over a wide pH range (2 to 12), (Fig. 8). Similar results were also noticed during the adsorption of MB on mesoporous Iraqi red Kaolin clay (Jawad & Abdulhameed 2020).

**Effect of Co-existing ions**

The co-ions reduce the adsorption of MB marginally in the

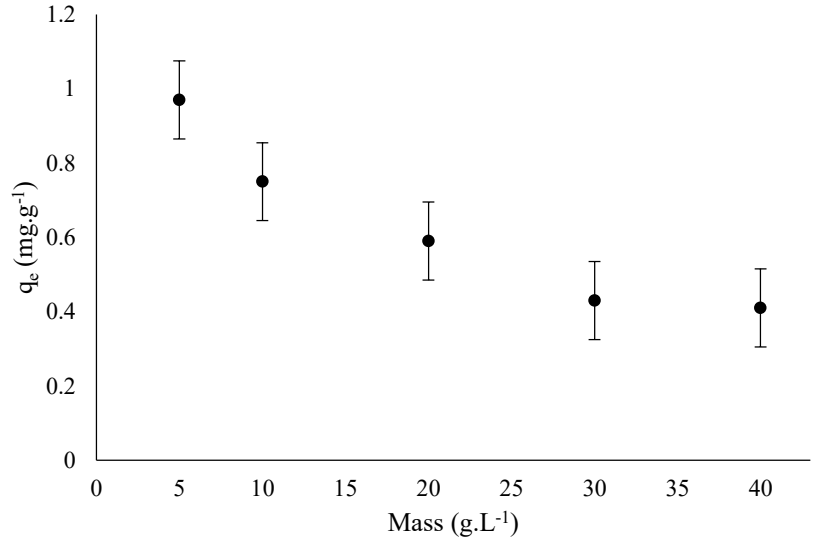


Fig. 6: Variation of MB adsorption with increasing pellet dose.

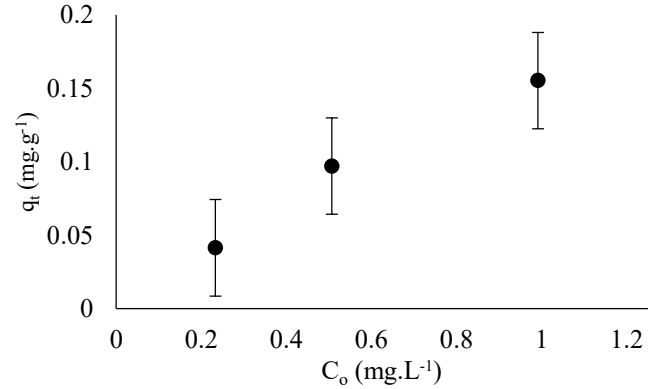


Fig. 7: Variation of MB adsorption with an increase in dye concentration.

order of $CO_3^{2-}$ $SO_4^{2-}$< $HCO_3^-$<$NO_3^-$ < $Cl^-$ (Fig.9). This was accounted for by the competition for active sites between MB molecules and co-ions present in the solution.

### Adsorption Isotherm Studies

### Langmuir Isotherm

The linearized Langmuir equation (eqn. 5, 6) was used to show the surface binding properties of MB with the mesoporous ceramic pellets.

$$\frac{c_e}{q_e} = \left(\frac{1}{bQmax}\right) + \frac{c_e}{Qmax} \quad \ldots(5)$$

$$R_L = \frac{1}{1+bc_0} \quad \ldots(6)$$

Where b is the Langmuir isotherm constant representing affinity between adsorbate and adsorbent (Huang et al. 2020). Qmax is the maximum adsorption capacity. Feasibility of isotherm can be calculated by using a dimensionless separation factor (Mckay et al. 1982), $R_L$; $R_L > 1$ is unfavorable; $R_L = 1$ is linear; $0 < R_L < 1$ is favorable; and $R_L = 0$ is irreversible. The value of $R_L$ between 0-1 indicates the favorable nature of the adsorption process (Tahir et al. 2010) (Table 2).

### Freundlich Isotherm

The Freundlich equation (eqn. 7) is based upon the assumption that the logarithmic value of enthalpy of adsorption decreases with an increase in the number of occupied sites and it is used to describe the adsorption involving the heterogeneous surfaces. $K_F$ is the Freundlich constant corresponding to the binding energy (Akkaya & Ozer 2005) (Table 2).

$$ln\ ln\ q_e = ln\ ln\ k_F + \frac{1}{n} ln\ ln\ c_e \quad \ldots(7)$$

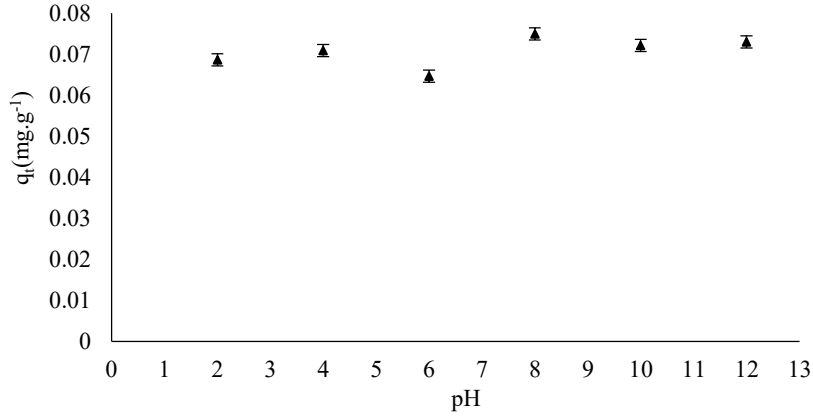


Fig. 8: Effect of initial pH on MB adsorption by pellets (initial MB conc.1ppm, pH:7).

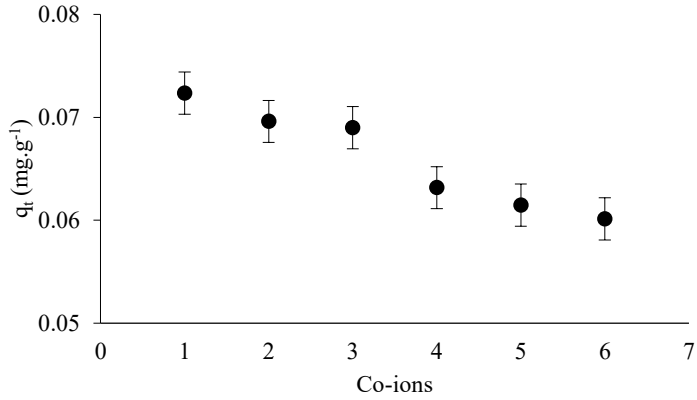


Fig. 9: Effect of co-ions on MB adsorption (initial MB conc.1ppm, initial co-ion conc.1 ppm, pH:7).

**Temkin Isotherm**

The Temkin model (eqn. 8) is used to explain the effect of adsorbate adsorbent interactions. It assumes that the heat of adsorption of all molecules in the adsorbent layers decreases linearly with coverage of the surface.

$$q_e = B\ ln\ ln\ A\ + B\ ln\ ln\ C_e\ ,\ \left(B = \frac{RT}{b}\right) \quad \ldots(8)$$

Where R is the gas constant, (8.314 J.mol $K^{-1}$), T is reaction temperature in kelvin. A plot between $q_e$ and $lnc_e$ gives the values of constants A and B. The Temkin constant b is related to the heat of adsorption (Mohebali et al. 2018) (Table 2).

On comparing the $R^2$ for different adsorption isotherms used, it was found that the Langmuir isotherm and Temkin model are best suited for the description of the adsorption mechanism.

**Kinetic Study of MB Adsorption**

Kinetic models can give valuable insight into the adsorption rate and adsorption mechanism. To determine the rate-determining step and to study the kinetics of MB adsorption by pellets, five kinetics models; pseudo-first-order,(PFO) (eqn.9), pseudo-second-order, (PSO) (eqn.10), Bangham (BKM) (eqn.11), Elovich (EKM) (eqn.12), and Intraparticle Diffusion (IPD), (eqn.13), models were applied.

$$log\ (q_e - q_t)\ = log\ q_e - \frac{K_1}{2.303}t \quad \ldots(9)$$

$$\frac{t}{q_t} = \frac{1}{K_2 q_e^2} + \frac{t}{q_t} \quad \ldots(10)$$

$$log.log\left(\frac{Ci}{Ci - qt.m}\right) = log\left(\frac{K.m}{2.303V}\right) + \alpha log(t) \quad \ldots(11)$$

$$qt = \frac{1}{\beta}\ ln\ ln(\alpha\beta) + \frac{1}{\beta}l(t) \quad \ldots(12)$$

$$q_t = K_{diff}\ t^{\frac{1}{2}} + C \quad \ldots(13)$$

$K_1$ and $K_2$ are PFO and PSO kinetic rate constants (Dang et al. 2015). $K_{diff.1}$ and $K_{diff.2}$ are the intra-particle rate constants (Balasubramaniam et al. 2018). α and $\frac{1}{\beta}$, the Elovich equation represents the rate of MB adsorption and available adsorption sites respectively (Sarma et al. 2019). α (<1) and $K_O$ are Bangham's constant (Junghare et al. 2020).

The kinetic parameters of both models are summarized in Table 3a-b. The $R^2$ value obtained for second-order kinetic ($R^2$=0.99) is higher than that of other kinetic models for MB adsorption on the pellet surface. For the intra-particle diffusion model, a deviation of the straight line from the origin was observed which indicates involvement of the pore diffusion during rate-controlling step along with intra-particle diffusion during adsorption of dye. Second-order kinetics along with pore and intraparticle diffusion is predominantly followed for MB adsorption by several clay-based adsorbents (Sharma & Qanungo 2021). Furthermore stastical analysis of experimental data (Table 4) using Mean Absolute Deviation (MAD), Mean Squared Error (MSE), Root Mean Square Error (RMSE) and Normalized Standard Deviation (NSD) also indicates second order kinetic model to be well followed.

**MB Removal Device Containing Pellets**

For MB removal from tap water, a stainless-steel tea ball wire mesh containing the mesoporous pellets was used and all experiments were carried in duplicate (three trials). To study the complete decolorization time using the MB removal device, three sets of experiments were carried out using 5 $g.L^{-1}$, 7.5 g. $L^{-1}$, and 10 $g.L^{-1}$ of pellet dose (Fig.10) using 100 mL, 1ppm MB solution. The increase in MB removal by the increase in pellet dose is due to the increase in surface area and the number of active sites. This leads to lower decolorization times. Further increase in pellet dose leads to higher decolorization times due to aggregation and reduction in active sites for adsorption. From this study, it is indicated that the MB removal device containing mesoporous ceramic pellets can be conveniently used in practical settings (post antifungal treatment, transport of fishes, and in aquariums).

## CONCLUSION

Mesoporous porous clay-starch ceramic pellets from low fire clay and starch (up to 30 %) were successfully prepared. The mesoporous nature of the pellets was confirmed by BET surface area analysis. The absence of starch in prepared ceramics pellets was confirmed by IR studies. Analysis of the adsorption isotherm and the kinetic data was found to

Table 2: Isotherm data for the MB adsorption by mesoporous pellets.

| Langmuir | | | | Freundlich | | | | Temkin | | | |
|---|---|---|---|---|---|---|---|---|---|---|---|
| $R^2$ | Q [$mg.g^{-1}$] | B [$l.mg^{-1}$] | $R_L$ | $R^2$ | 1/n | n | $K_f$ [$l.g^{-1}$] | $R^2$ | b [$K.Cal.mol^{-1}$] | B | A [$l.g^{-1}$] |
| 0.99 | 0.2331 | 11.539 | 0.079 | 0.97 | 0.6017 | 1.661 | 2.117 | 0.99 | 11.4018 | 0.0519 | 1.235 |

Table 3a: Kinetic data for the MB adsorption by pellets.

| Conc. (ppm) | Pseudo1st order | | Pseudo 2nd order | | Bhangham | | | Elovich | | |
|---|---|---|---|---|---|---|---|---|---|---|
| | $R^2$ | $K_1$ [$g.mg^{-1}.min^{-1}$] | $R^2$ | $K_2$ [$g.mg^{-1}.min^{-1}$] | $R^2$ | K [$mL.g^{-1}.L^{-1}$] | α [$min^{-1}$] | $R^2$ | β [$g.mg^{-1}$] | α [$mg.g^{-1}min^{-1}$] |
| 0.25 | 0.967 | 0.0078 | 0.99 | 0.2829 | 0.941 | 198.437 | 0.463 | 0.917 | 125 | 0.00376 |
| 0.5 | 0.986 | 0.0087 | 0.99 | 0.0236 | 0.917 | 84.8641 | 0.35 | 0.943 | 58.823 | 0.00509 |
| 1.0 | 0.947 | 0.0055 | 0.99 | 0.0519 | 0.955 | 203.200 | 0.429 | 0.906 | 36.363 | 0.01402 |

Table 3b: Kinetic data intra-particle parameters for pellets.

| Conc. [ppm] | $R_1^2$ | $R_2^2$ | $K_{diff.1}$ [$g.mg^{-1}.min^{-1}$] | $K_{diff.2}$ [$g.mg^{-1}.min^{-1}$] | $C_1x10^2$ [$mg.g^{-1}$] | $C_2x10^2$ [$mg.g^{-1}$] |
|---|---|---|---|---|---|---|
| 0.25 | 0.9926 | 0.6112 | $2.2 x10^{-4}$ | $1x10^{-4}$ | $6x10^{-4}$ | $3.64x10^{-2}$ |
| 0.5 | 0.9696 | 0.8292 | $4.9x10^{-3}$ | $2x10^{-4}$ | $1.2x10^{-2}$ | $9.12x10^{-2}$ |
| 1.0 | 0.9836 | 0.7276 | $6.6x10^{-3}$ | $1x10^{-4}$ | $3.4 x10^{-2}$ | $1.16x10^{-1}$ |

Table 4: Statistical analysis for kinetic models.

| [Vol.100mL, dose: 5 $g.l^{-1}$] | | MAD $\frac{\sum qexp-qcal}{n}$ | MSE $\frac{\sum(qexp-qcal)2}{n}$ | RMSE $\frac{\sqrt{\sum(qexp-qcal)2}}{n}$ | NSD(Δq%) $100\sqrt{\frac{\sum\left[(qexpexp-q_{Cal})/qexp\right]2}{n-1}}$ |
|---|---|---|---|---|---|
| 0.25 ppm | PFO | 0.0020 | 5.74E-06 | 0.0023 | 14.924 |
| | PSO | 0.0018 | 4.87E-06 | 0.0022 | 10.680 |
| | BKM | 0.0019 | 6.38E-06 | 0.0025 | 6.99 |
| | EKM | 0.0026 | 0.00066 | 0.0258 | 164.111 |
| | IPD | 0.0012 | 2.32E-06 | 0.0015 | 8.4798 |
| 0.5 ppm | PFO | 0.0178 | 0.00032 | 0.01813 | 34.3168 |
| | PSO | 0.0030 | 1.4E-05 | 0.0037 | 7.1947 |
| | BKM | 0.0025 | 7.49E-06 | 0.0027 | 4.0098 |
| | EKM | 0.025 | 0.000656 | 0.0256 | 49.45 |
| | IPD | 0.0029 | 1.987E-05 | 0.00445 | 6.8106 |
| 1.0 ppm | PFO | 0.0094 | 0.00012 | 0.01105 | 21.03 |
| | PSO | 0.0069 | 7.262E-05 | 0.0085 | 13.003 |
| | BKM | 0.0072 | 0.00011 | 0.0108 | 9.3193 |
| | EKM | 0.07212 | 0.0053 | 0.073 | 131.35 |
| | IPD | 0.0077 | 0.00016 | 0.0124 | 8.83 |

be of Langmuir type and the pseudo-second-order reaction, respectively. Processes like boundary layer and pore diffusion were found to be involved during the rate-determining step of the adsorption. Error analysis of different kinetic models also favored pseudo-second-order reaction kinetics. The application of these ceramic pellets as a viable MB adsorbent at ultra-low concentrations in aquaculture has been demonstrated.

## REFERENCES

Abdel-Halim, E.S. 2013. Preparation of starch/poly (N, N-Diethylamino-ethyl methacrylate) hydrogel and its use in dye removal from aqueous solutions. React. Funct. Polym., 73(11): 1531-1536.

Ahmed, T., Rafatullah, M., Ghazali, A., Sulaiman, O., Hashim, R. and Ahmad, A. 2010. Removal of pesticides from water and wastewater by different adsorbents: A review. J. Environ. Sci. Health, Part C., 28(4): 231-271.

Akkaya, G. and Özer, A. 2005. biosorption of acid red 274 (ar 274) on

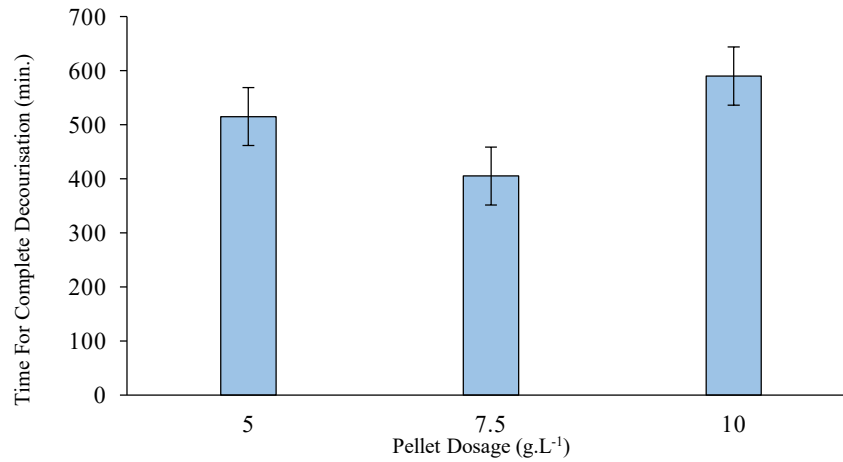


Fig.10: Time taken by ceramic pellets for complete decolorization of solution.

dicranella varia: Determination of equilibrium and kinetic model parameters. Process Biochem., 40(11): 3559-3568.

Ambroz, F., Macdonald, T.J., Martis, V. and Parkin, I.P. 2018. Evaluation of the BET theory for the characterization of meso and microporous MOFs. Small Methods, 2(11): 1800173.

Aroke, U.O., Abdulkarim, A. and Ogubunka, R.O. 2013. Fourier-transform infrared characterization of kaolin, granite, bentonite, and barite. ATBU J. Environ. Techno., 6(1): 42-53.

Balasubramaniam, P., Venkateswaran V. and Rathinavelu A. 2018. Adsorption of methylene blue on to fire clay - mno2 nanocomposite materials. Int. J. Res. Advent Techno., 6(10):2753-2763.

Bentahar, S., Dbik, A., El Khomri, M., El Messaoudi, N. and Lacherai, A. 2017. Adsorption of methylene blue, crystal violet, and congo red from binary and ternary systems with natural clay: Kinetic, isotherm, and thermodynamic. J. Environ. Chem. Eng., 5(6): 5921-5932.

Dang, A.Y., Boansi, A.O. and Pedevoah, M. 2015. Reduction of fluorine in water using clay mixed with hydroxyapatite. Int. J. App. Sci. Techno., 5: 45-55.

Elimbi, A., Njouonkou, S., Nsami, J.N., Belibi, P.B. and Mbadkam, J.K. 2019. Adsorption test of methylene blue onto porous powdered ceramics obtained from mixtures of kaolin–bauxite and kaolin–oyster shell. Int. J. Environ. Sci. Techno., 16(3): 1337-1350.

Huang, K., Li, W., Wang, Y., Liu, B., Xu, R., Dai, J., Zheng, X., Yang, N., Qiu, M. and Han, L. 2020. Adsorption of acid orange 7 in aqueous solution by biochar from peanut shell supported with clay mineral kaolinite. Nature Environ. Pollut. Techno., 19(4): 1657-1662.

Jawad, A.H. and Abdulhameed, A.S. 2020. Mesoporous Iraqi red kaolin clay as an efficient adsorbent for methylene blue dye: adsorption kinetic, isotherm and mechanism study. Surf. Interfaces., 18(3): 100422.

Junghare, K., Kodape, S. and Jadhao, V. 2020. Adsorption study of F–ions onto ultrasonified electrochemically generated ultrafine particles. Desal. Water Treat., 173(1): 243-254.

Mabel, M., Sundararaman, T. R., Parthasarathy, N. and Rajkumar, J. 2019. Chitin beads from peneaus sp. shells as a biosorbent for methylene blue dye removal. Pol. J. Environ. Stud., 28(4): 2253-2259.

Mckay, G.B.H.S., Blair, H.S. and Gardner, J.R. 1982. Adsorption of dyes on chitin. i. equilibrium studies. J. App. Polym. Sci., 27(8): 3043-3057.

Mohebali, S., Bastani, D. and Shayesteh, H. 2018. Methylene blue removal using modified celery (apium graveolens) as a low-cost biosorbent in batch mode: kinetic, equilibrium, and thermodynamic studies. J. Mol. Struct., 1173: 541-551.

Njoya, D., Nsami, J. N., Rahman, A. N., LekeneNgouateu, R. B., Hajjaji, M. and Nkoumbou, C. 2017. Adsorption of methylene blue from aqueous solution onto cordierite based ceramic., J. Mat. Environ. Sci., 8(5): 1803-1812.

Sharma, P. and Qanungo, K., 2021. Clay and ceramics as sustainable and green materials to remove methylene blue from water: a critical analysis, Chapter 13, in The Handbook of Sustainable Development Through Green Engineering and Technology, Ed. Bali, P. et.al., CRC Press, Taylor and Francis, Boca Raton, USA. ISBN:0367650959(in press).

Rehman, M.S.U., Munir, M., Ashfaq, M., Rashid, N., Nazar, M. F., Danish, M. and Han, J.I. 2013. Adsorption of brilliant green dye from aqueous solution onto red clay. Chem. Eng. J., 228: 54-62.

Saikia, B.J., Parthasarathy, G., and Sarmah, N. C. 2008. Fourier transform infrared spectroscopic estimation of crystallinity in $SiO_2$ based rocks. Bull. Mater. Sci., 31(5): 775-779.

Sarma, G.K., Gupta, S.S. and Bhattacharyya, K.G. 2019. Removal of hazardous basic dyes from aqueous solution by adsorption onto kaolinite and acid-treated kaolinite: kinetics, isotherm, and mechanistic study. SN App. Sci., 1(3):211.

Tahir, H., Hammed, U., Sultan, M. and Jahanzeb, Q. 2010. Batch adsorption technique for the removal of malachite green and fast green dyes by using montmorillonite clay as adsorbent. Afr. J. Biotechnol., 9(48): 8206-8214.

Yan, S., Pan, Y., Wang, L., Liu, J., Zhang, Z., Huo, W., Yang, J. and Huang, Y. 2018. Synthesis of low-cost porous ceramic microspheres from waste gangue for dye adsorption. J. Adv. Ceramics., 7(1):30-40.

Yemendzhiev, H., Alexieva, Z. and Krastanov, A. 2009. Decolorization of synthetic dye reactive blue 4 by a mycelial culture of white-rot fungi trametes versicolor 1. Biotechnol. Equip., 23(3): 1337-1339.

Zeynolabedin, R., Marjani, A., Shokri, A., Saghi, M. and Bigtan, M.H. 2015. Removal of methylene blue dye from aqueous solutions by elaeagnusan gastifolial as an adsorbent. Orient J. Chem., 31: 271-276.

Nature Environment and Pollution Technology
An International Quarterly Scientific Journal

p-ISSN: 0972-6268
(Print copies up to 2016)
e-ISSN: 2395-3454

Vol. 20 | No. 5 (Suppl) | pp. 2051-2059 | 2021

Original Research Paper

https://doi.org/10.46488/NEPT.2021.v20i05.022

Open Access Journal

# Application of Remote Sensing and GIS Techniques for the Analysis of Lake Water Fluctuations: A Case Study of Ugii Lake, Mongolia

**Amgalan Magsar*†, Toru Matsumoto**, Altanbold Enkhbold*** and Nandintsetseg Nyam-Osor******

*Faculty of Environmental Engineering, The University of Kitakyushu, Hibikino 1-1, Wakamatsu-ku, Kitakyushu-shi, Fukuoka 808-0135, Japan

**Institute of Environmental Science and Technology, The University of Kitakyushu, Hibikino 1-1, Wakamatsu-ku, Kitakyushu-shi, Fukuoka 808-0135, Japan

***Department of Geography, School of Art & Sciences, National University of Mongolia, Ikh Surguuliin Gudamj-1, P.O.X-46A/523, 210646 Ulaanbaatar, Mongolia

****Institute of Geography and Geoecology of Mongolia, Baruunselbe 15-4, 4th Khoroo, Chingeltei district 15170, Ulaanbaatar, Mongolia

†Corresponding author: Amgalan Magsar; a-magsar@kitakyu-u.ac.jp

**Nat. Env. & Poll. Tech.**
**Website: www.neptjournal.com**

*Received:* 01-07-2021
*Revised:* 27-08-2021
*Accepted:* 03-09-2021

**Key Words:**
Lake water fluctuation
Climate change
Ugii lake
Water index

## ABSTRACT

Ugii Lake is a freshwater lake located in the steppe region of Mongolia and is an important breeding and staging area for a wide variety of waterfowl. Remote sensing and geographic information system techniques were used to estimate fluctuations in the surface area and water balance of Ugii Lake. To estimate the changes in lake water balance, lake water fluctuations should be analyzed using the most accurate methods. A different water extraction technique was applied, and the results were compared with field surveys conducted in May, July, and September 2020. The lake surface area using both NDWI and MNDWI-1 showed a strong, positive correlation (R=0.93, R=0.94, $p < 0.01$) with the water level of Ugii Lake. A topographic map of Ugii Lake was provided by the project (P2018-3568) conducted in August 2019 and used to estimate the volume of Ugii Lake in ArcGIS 10.1. This result was consistent with that of a previous study by JICA in 2005. Finally, the water balance of Ugii Lake was estimated, and the results proved that the influence of both surface and groundwater on Ugii Lake are valuable parameters, which are completely dependent on hydrological regime changes mostly due to local climate change in steppe regions. This study provides valuable insight into the most suitable water extraction methods for lakes in semi-arid steppe regions in Mongolia.

## INTRODUCTION

Lakes are essential components of the hydrological cycle, affecting many aspects of ecosystems and human activity. Lakes remain sensitive to natural changes and serve as an important proxy of global climate change and regional environmental variations (Mason et al. 1994). Lake area is an important indicator of climate change and is related to climatic factors that are critical for understanding the mechanisms that control changes in water levels (Kang et al. 2015). The water of most inland lakes in arid regions is supplied by seasonal snowmelt water and rainfall. As a result, these lakes are sensitive to the volume of water flowing into the lake and evaporation loss from their surface (Bai et al. 2011). In Mongolia, global warming occurs more rapidly than the global average. The time taken for the accumulated snow to disappear has advanced by approximately one month in our study area, which is evidence of the impact of climate change on hydrological processes. Due to changes in precipitation and temperature, the hydrological regime of the surface water body is likely to be affected, especially in semi-arid regions. Several studies have examined the dynamics of climate and hydrological systems in semi-arid regions of Mongolia. Significant decreases in river discharges have occurred in the past three decades, while the annual precipitation has remained relatively stable (Dorjsuren et al. 2018). Ugii Lake is surrounded by the small mountains of eastern Khangay, which is a steppe zone area in terms of climate and landscape. The water level of Ugii Lake is influenced by the surface and groundwater flow of the Orkhon, Tamir, and Khugshin Orkhon Rivers (Batchuluun 2021). Ugii Lake was first registered as an International Ramsar Convention site in 1998 and is an ecologically important lake located in the semi-arid region of Mongolia.

In recent years, the water level of Ugii Lake has fluctuated. Several environmental problems have occurred due to changes in the hydrological regime, local climate changes,

and increased human activities around the lake. Sumiya et al. (2020) concluded that the surface area of Ugii Lake has fluctuated by 10 percent in the last three decades because of global warming.

Mapping lake areas using remote sensing (RS) images is key for detecting changes in the size of lakes and understanding the relationship between lake variations and climate change. RS is a rapidly growing technology that provides low-cost and reliable information for environmental changes at local, regional, and global scales, providing long-collected repeatable and even real-time data (Melesse et al. 2007). Various water indices have been applied to extract surface water bodies from the surrounding land using RS imagery based on their spectral characteristics (Acharya et al. 2019, Herndon et al. 2020, Liu et al. 2016, Zhai et al. 2015). The accuracy of the surface water extraction method is important for the estimation of lake water fluctuation and to understand the impact of hydrometeorological factors on lakes in semi-arid regions. The objectives of this study were to apply the most common water index ratios in the multi-spectral RS water identification method, which includes the normalized difference vegetation index (NDVI), normalized difference water index (NDWI), modified normalized difference water index-1 (MNDWI-1), and modified normalized difference water index-2 (MNDWI-2), to extract the lake surface area, to verify with *in-situ* measured data, and to suggest the most suitable method for surface water extraction in semi-arid regions of Mongolia. Furthermore, the extracted surface area and topographic map of Ugii Lake are proposed to estimate the changes in the water balance of the lake.

## MATERIALS AND METHODS

### Study Area

According to the climate zone classification by Jambaajamts (1989) in Mongolia, Ugii Lake is located in the sub-humid-cool zone, 1332 m above sea level. Sumiya et al. (2020) reported that Ugii Lake was formed by the meandering of the Khugshin Orkhon River, which is a unique surface inflow into the Ugii Lake. The outlet is located northwest of the inlet and joins the Orkhon River after 7 km (Schwanghart et al. 2008). For numerous years, the outflow river (Narini Gol) has been dry, and it only becomes an issue when the water level of Ugii Lake reaches a certain level. Ugii Lake is 7.4 km long, 5.3 km wide (mean width 3.4 km), and covers an area of 25.7 $km^2$ with a maximum depth of 15.3 m and a mean depth of 6.6 m (Tserensodnom 2000). More than half of the lake is less than 3 m deep. The lake has a shoreline of 24.7 km and carries a water volume of approximately 0.171 $km^3$ (Fig. 1). The mean annual temperature is approximately –2°C, and the mean annual precipitation ranges from 250 to 300 mm, with the majority of the precipitation occurring in June, July, and August.

## MATERIALS AND METHODS

### Field Survey

The field survey was conducted three times in May, July, and September 2020 using a Garmin eTrex10 handy GPS. The measured coordinates were used to calculate the lake surface area using ArcMap 10.1.

### Data Collection

**Hydrological station data:** Discharge of Khugshin Orkhon River was obtained from the Ugii Lake gauging station between 2002 and 2019. Daily lake water level data was obtained from Ugii Lake Hydrological Station (~102.77°E, 47.75°N) between 2002 and 2019. Global daily precipitation gridded data (102.71º-102.82º E, 47.74º-47.79º N) with a spatial resolution of 0.5º latitude by 0.5º longitude from the Global Precipitation Climatology Centre (GPCC) was obtained from the Physical Science Laboratory (PSL) at the National Oceanographic Atmospheric Administration (NOAA) from their website (https://psl.noaa.gov/). Daily evaporation data for Ugii Lake was compiled from previous research (Magsar et al. 2020) between 2002 and 2019 in order to estimate the water balance of Ugii Lake. A topographic map of Ugii Lake was provided by the literature.

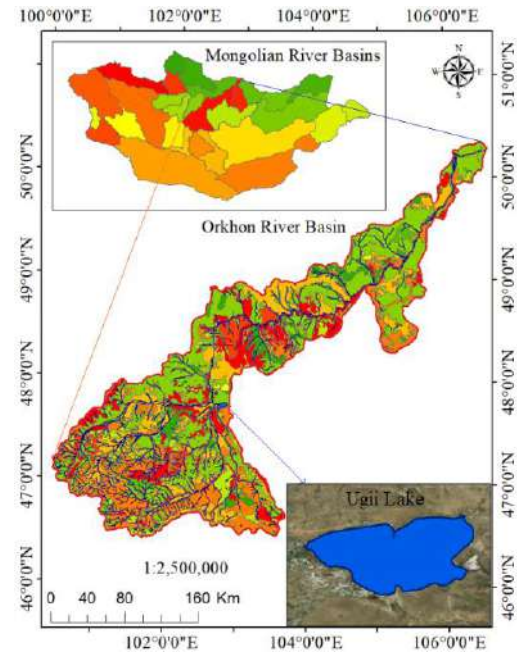


Fig. 1: Location of the study area.

**Satellite remote sensing images:** RS is an effective technology for the monitoring of water resources. Both Landsat 5 TM and Landsat 8 OLI satellite RS imagery data was used to derive the surface area of the Ugii Lake. Since its inception on March 1, 1984, until its decommission on June 5, 2013, Landsat 5 has provided Earth-imaging data for approximately 29 years. Landsat-8 Operational Land Imager (OLI) and Thermal Infrared Sensor (TIRS) satellite were launched in February 2013. Satellite data (pixel size of 30 m) was downloaded from the Earth Explorer at https://earthexplorer.usgs.gov/, which was developed by the United States Geological Survey (USGS). The differences in band range and resolution between the OLI and TM sensors are listed in Table 1.

**Satellite image processing and analysis:** Satellite images were preprocessed before conducting any analyses because they contained noise and digital number value offsets that result from the viewing geometry of the satellite, and the atmospheric depth due to the viewing angle of the sun's incoming radiation (Alparslan et al. 2007). Landsat 5 satellite images were preprocessed with the radiometric calibration tool in ENVI 4.7, which converted the digital number (DN) images to top of atmosphere (TOA) reflectance.

The Landsat 8 images were also preprocessed using Equation (1) and Equation (2):

$$\rho\lambda' = M_\rho * Q_{cal} + A_\rho \quad \ldots (1)$$

Where,

$\rho\lambda'$ TOA planetary spectral reflectance, without correction for solar angle,

$M_r$ Reflectance multiplicative scaling factor for the band,

$Q_{cal}$ Quantized and calibrated standard product pixel value in DN,

$A_r$ Reflectance additive scaling factor for the band.

TOA reflectance with a correction for the sun angle was denoted by:

$$\rho\lambda = \frac{\rho\lambda'}{\cos(\theta_{SZ})} = \frac{\rho\lambda'}{\sin(\theta_{SE})} \quad \ldots (2)$$

where

$\rho\lambda$ TOA planetary reflectance,

$\theta_{SZ}$ Local solar zenith angle,

$(\theta_{SZ} = 90^\circ - \theta_{SE})$,

$\theta_{SE}$ Local sun elevation angle (degrees).

After the conversion of the scene center sun elevation angle provided in the metadata, the lake water surface was delineated using the most common water indices such as NDVI, NDWI, MNDWI-1, and MNDWI-2. Then, the surface area of Ugii Lake was calculated using ArcMap 10.1.

Table 2 shows the multiband indices used for water feature extraction in this study. NDVI is an index of plant greenness since plants absorb red light and reflect NIR. Its value ranges from −1 to +1. By contrast, water absorbed the majority of the NIR light; hence, NDVI could be used to delineate surface water features (Acharya et al. 2019). NDWI is one of the most commonly used water indices to detect surface water bodies and was first created by the green and near-infrared (NIR) spectral bands of Landsat TM, introduced by McFeeters in 1994. NDWI is designed

Table 1: Differences in band ranges and resolutions between the OLI and TM sensor.

| № | Landsat 8 OLI (Gabr et al. 2020) | | | № | Landsat 5 TM/ETM+ (Zhai et al. 2015) | | |
|---|---|---|---|---|---|---|---|
| | Band | Wavelength (μm) | Resolution (m) | | Band | Wavelength [μm] | Resolution [m] |
| 1 | Coastal aerosol (CA) | 0.435–0.451 | 30 m | 1 | Blue | 0.450–0.515 | 30 m |
| 2 | Blue | 0.452–0.512 | | 2 | Green | 0.525–0.605 | |
| 3 | Green | 0.513–0.590 | | 3 | Red | 0.630–0.690 | |
| 4 | Red | 0.636–0.673 | | 4 | NIR | 0.775–0.900 | |
| 5 | Near Infrared (NIR) | 0.851–0.879 | | 5 | Mid Infrared (MIR) | 1.550–1.750 | |
| 6 | Shortwave NIR1 (SWIR1) | 1.566–1.651 | | 6 | Thermal Infrared Sensor (TIRS) | 10.40–12.50 | 60 m |
| 7 | Shortwave NIR2 (SWIR2) | 2.107–2.294 | | 7 | MIR | 2.080–2.350 | 30 m |
| 8 | Pan | 0.500–0.680 | 15 m | 8 | Pan | 0.520–0.900 | 15 m |
| 9 | Panchromatic | 1.363–1.384 | 15 m | | | | |

to: (1) maximize the reflectance of water by using green wavelengths, (2) minimize the low reflectance of NIR by water features, and (3) take advantage of the high reflectance of NIR by vegetation and soil features (Xu 2006). Xu noted that the threshold 0 was not an appropriate distinguishing feature and proposed the MNDWIs (Zhai et al. 2015).

Lake water fluctuations provide important information regarding the water balance of lakes in arid and semi-arid regions and are necessary to understand the conditions of local climate change, the hydrological regime, and the ecological status of important lakes.

The water balance of Ugii Lake can be expressed by Equation (3):

$$P - E + Y_{SI} \pm \Delta V - Y_{SO} = \Delta Y_{GW} \quad \ldots (3)$$

Where,

$\Delta V$ - Changes of the lake volume,

P - Precipitation over the lake,

E - Evaporation over the lake,

$Y_{SI}$ - Surface inflow,

$Y_{SO}$ - Surface outflow,

$\Delta Y_{GW}$ - Groundwater change,

The topographic map of Ugii Lake and the lake depth measurement results were provided by the implemented project (P2018-3568) at Ugii Lake in August 2019 and used to estimate the changes in lake volume. The surface area of each depth was calculated using ArcGIS, and the volume of the lake was calculated using Equation (4):

$$V = \sum_{i=1}^{n} [(A_i - A_{i+1}) \times d_i] \quad \ldots (4)$$

Where,

$V$ - Volume of the lake,

$A$ - Surface area,

$d$ - Depth of the lake level,

$n$ - Number of each water depth,

$i = 1, 2, \ldots n$

## RESULTS AND DISCUSSION

According to the station data, the average annual water level of Ugii Lake fluctuated. The highest water level was observed in 2004 (3.53 m); however, the lake water level decreased gradually between 2004 and 2011. The lowest water level was observed in 2011 (1.79 m), which increased steadily until 2017 (3.23 m) and decreased by 0.63 m in 2018. Ugii Lake has only one surface inflow to lake. The annual average discharge of the Khugshin Orkhon River was 0.5 $m^3.s^{-1}$ in 2003, which was the highest level during the study period. Since 2003, the annual average discharge decreased gradually until 2011 (0.079 $m^3.s^{-1}$) and increased in 2016 (0.463 $m^3.s^{-1}$). The changes in discharge of the Khugshin Orkhon River are relevant to the fluctuation of the Ugii Lake water level (Fig. 2). In the case of Ugii Lake, water flows out from the lake on the northwestern side and joins the Orkhon River when the water level of the lake increases. However, due to fluctuations in the water level in recent decades, outflow rivers from lakes have dried out. Therefore, the amount of surface outflow from the lake could be excluded from further lake water balance calculations.

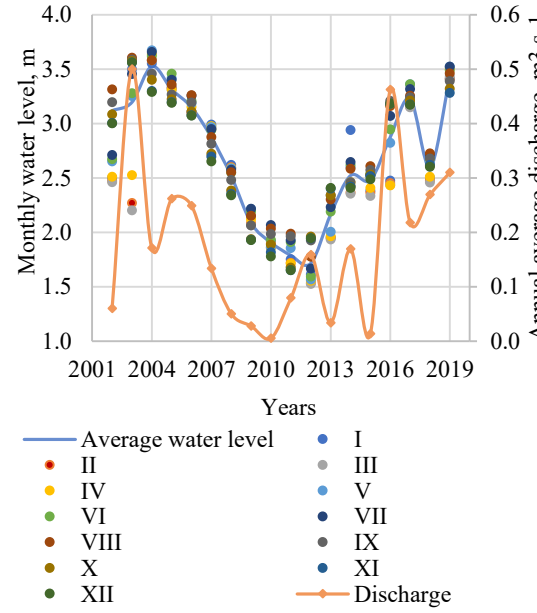


Fig. 2: Comparison of annual average discharge and monthly water level of Ugii Lake.

### Estimation of Changes in the Surface Area of Ugii Lake Using Satellite Remote Sensing

**Field survey result:** Surface area and water level are interrelated parameters of lake morphometry. As mentioned above, data on the water level of Ugii Lake was available between 2002 and 2019. Therefore, above mentioned water indices were applied to estimate the lake surface area using the monthly RS images of both Landsat 5 TM and Landsat 8 OLI. To assess the extraction accuracy of the water indices, the length of the lake shoreline was measured three times between May and September 2020. Table 3 provides detailed information on satellite images and field survey dates.

Cloudless satellite images from paths 134 and 27 with 30 m resolution were collected, and each water index was estimated accordingly. The comparison between the water indices and *in-situ* measurements are shown in Table 4 and Fig. 3.

According to the estimated lake water surface area, both NDWI and MNDWI-1 had closer estimates than NDVI and MNDWI-2. A total of 68 satellite images were used to estimate the monthly lake water surface area using both NDWI and MNDWI-1 within the study period from May to October (2002-2019). The results of the estimated lake water surface area were compared with the water level data from the Ugii Lake station. Fig. 4 shows that the estimated surface area of the lake had a strong, positive correlation (R=0.93, R=0.94, $p < 0.01$) with the water level of the lake. Therefore, the NDWI and MNDWI-1 methods are recommended for lake water extraction in steppe regions.

As shown in Fig. 5, the surface area of the lake changed slightly each month during the study period, increasing in August and September each year, which may contribute to the increases in both surface and groundwater discharge during the summer (rainy) season. From the beginning of November, the lake surface area was covered by ice with a thickness of 1–1.5 m during the winter season until mid-April. Once the snow and ice cover melted, the surface water discharge and lake water level increased depending on the amount of snow accumulated during the winter months.

Since 2016, changes in the surface area of the lake have steadily increased. The highest value of lake surface area was estimated in September of each year. Fig. 6 shows the difference between each year in September. Water flowed out from the lake when the lake surface area increased. Magsar et al. (2020) concluded that annual total evaporation from the lake mostly exceeds the total amount of precipitation since 1995. The summer precipitation consisted predominantly of total annual precipitation, the majority of which occurred during the months of July and August each year during the study period. The highest recorded monthly precipitation was in July 2018 (113.25), which may have contributed to an increase in the lake's surface area by 0.95 km$^2$ in the following month (August 27, 2018). The lowest recorded monthly precipitation was in July 2017 (26.45 mm), which may have contributed to a decrease in the lake surface area by 0.04 km$^2$ in the following month (August 01, 2017). As seen in Table 5, the surface area of Ugii Lake fluctuates each month. Depending on the weather condition, the surface area increases mostly in August and September.

Table 2: Multiband indices used for water feature extraction.

| Multib-and index | Equation | Water value | Refer-ence |
|---|---|---|---|
| NDVI | NDVI=(NIR-Red)/(NIR+Red) … (5) | - | (Rouse et al. 1974) |
| NDWI | NDWI=(Green-NIR)/(Green+NIR) … (6) | + | (Mc-Feeters 1996) |
| MNDWI | MNDWI1=(Green-SWIR1)/(Green+SWIR1) … (7)<br>MNDWI2=(Green-SWIR2)/(Green+SWIR2) … (8) | +<br>+ | (Xu 2006) |

## Estimation of the Water Balance of the Ugii Lake

According to the results described in the previous section, the surface area of Ugii Lake had fluctuated, which is an indicator of changes in the local hydrological regime as a result of several factors, including local climate change. In

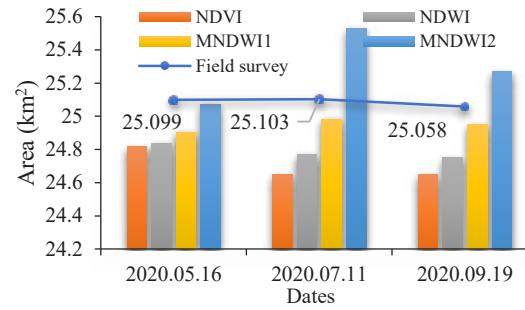


Fig. 3: Comparison of different water indices.

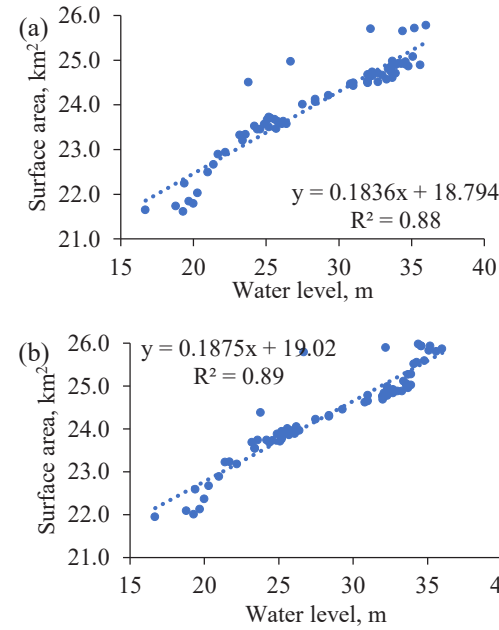


Fig. 4: Correlation between lake level and surface area (a) NDWI, (b) MNDWI-1.

Table 3: Details of Landsat 8 OLI images and field survey dates.

| Field survey | Acquisition date | Landsat product ID | Path | Row | Resolution [m] |
|---|---|---|---|---|---|
| 2020.05.16 | 2020.05.12 | LC08_L1TP_134027_20200512_20200526_01_T1 | 134 | 27 | 30 |
| 2020.07.11 | 2020.07.15 | LC08_L1TP_134027_20200715_20200715_01_RT | 134 | 27 | 30 |
| 2020.09.19 | 2020.09.17 | LC08_L1TP_134027_20200917_20201006_01_T1 | 134 | 27 | 30 |

Table 4: Comparison between *in situ* measurements and different water indices for estimating the surface area of Ugii Lake.

| Field survey date | Area [km$^2$] | Satellite name | Acquisition date | Area [km$^2$] | | | |
|---|---|---|---|---|---|---|---|
| | | | | NDVI | NDWI | MNDWI1 | MNDWI2 |
| 2020.05.16 | 25.099 | Landsat 8 OLI | 2020.05.12 | 24.818 | 24.837 | 24.905 | 25.072 |
| 2020.07.11 | 25.103 | | 2020.07.15 | 24.647 | 24.767 | 24.984 | 25.528 |
| 2020.09.19 | 25.058 | | 2020.09.17 | 24.65 | 24.75 | 24.95 | 25.27 |

Table 5: Monthly average lake surface area fluctuation (km$^2$) using MNDWI-1.

| Years | Months | | | | | |
|---|---|---|---|---|---|---|
| | May | Jun | Jul | Aug | Sep | Oct |
| 2002 | - | 25.79 | - | 25.04 | 24.83 | 24.61 |
| 2003 | - | - | 25.27 | 25.86 | 25.98 | 25.89 |
| 2004 | - | - | - | 25.81 | 25.55 | 25.51 |
| 2005 | - | - | - | 24.95 | 24.88 | 24.77 |
| 2006 | - | - | - | 24.83 | 24.69 | 24.78 |
| 2007 | - | - | 24.45 | - | 24.22 | - |
| 2008 | - | - | - | 23.88 | 23.73 | 24.38 |
| 2009 | - | - | - | 23.22 | 22.89 | 22.58 |
| 2010 | - | - | - | 22.67 | 22.12 | 22.08 |
| 2011 | - | - | - | 22.37 | 22.00 | 21.94 |
| 2012 | - | - | 23.34 | 23.38 | 23.46 | - |
| 2013 | - | 23.23 | 23.18 | 23.69 | 23.54 | 23.74 |
| 2014 | - | 23.89 | 23.96 | 23.86 | 23.68 | 23.73 |
| 2015 | 23.70 | 23.76 | 24.00 | 24.05 | 23.96 | 23.85 |
| 2016 | 24.29 | - | 24.65 | 24.76 | 24.76 | - |
| 2017 | 25.02 | 25.01 | 24.88 | 24.92 | 24.9 | - |
| 2018 | 24.82 | 24.76 | 24.98 | 25.93 | 25.93 | - |
| 2019 | 25.93 | 25.83 | - | 25.59 | 25.11 | - |

addition, the changes in lake water volume are interdependent on the hydrometeorological conditions.

As shown in Fig. 7, the lake water depth increased while the surface area of the lake decreased. For instance, the estimated lake surface area was 25.49 km$^2$, 23.59 km$^2$, and 21.71 km$^2$ at a depth of 0.5 m, 1 m, and 2 m, respectively (Table 6).

Based on the morphometric parameters of the lake, the volume of the lake in August, 2019 was estimated using Equation (4); (Table 6), the results of which were similar to those reported by JICA in 2005. The estimated surface area (2002-2019) and topographic map (August 2019) of Ugii Lake were used to calculate the volume of the lake. During the study period, the volume of the lake decreased by $0.6 \times 10^{-3}$ km$^3$, $1.4 \times 10^{-3}$ km$^3$, and $1.5 \times 10^{-3}$ km$^3$ in 2009, 2010, and 2011, respectively, compared to the data reported by JICA in 2005. Since 2013, the volume of the lake steadily increased until 2018, and then decreased by $0.4 \times 10^{-3}$ km$^3$ in 2019, compared to the previous year (Table 7).

As mentioned above, fluctuations in lake water are related to the hydrological regime. This is a primary indicator of local climate change, which results in the ecological condition of shallow lakes in the steppe region. As described earlier, the

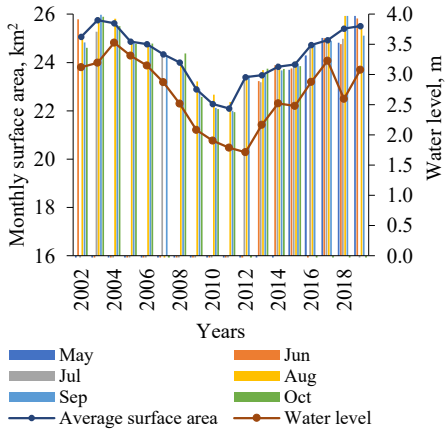


Fig. 5: Monthly fluctuations in surface area of the lake between 2002 and 2019.

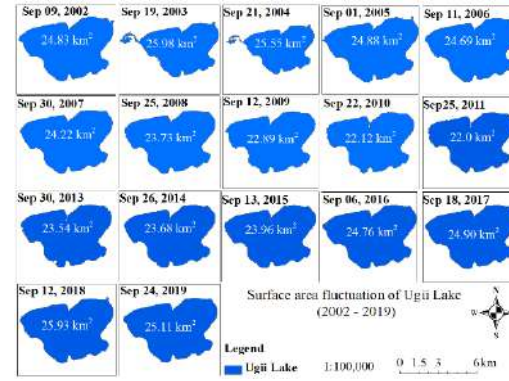


Fig. 6: Mapping of the surface area of Ugii Lake in September of every year between 2002 and 2019.

Table 6: The morphometric parameters of Ugii Lake (August 2019).

| No | Reference lake depth [m] | Surface area of each depth [km$^2$] | Lake volume [km$^3$] |
|---|---|---|---|
| 1 | 0.5 | 25.49 | 0.00095 |
| 2 | 1 | 23.59 | 0.00188 |
| 3 | 2 | 21.71 | 0.00362 |
| 4 | 3 | 19.90 | 0.00474 |
| 5 | 4 | 18.32 | 0.0056 |
| 6 | 5 | 16.92 | 0.0081 |
| 7 | 6 | 15.30 | 0.0141 |
| 8 | 7 | 12.95 | 0.01645 |
| 9 | 8 | 10.60 | 0.01248 |
| 10 | 9 | 9.04 | 0.01602 |
| 11 | 10 | 7.26 | 0.0196 |
| 12 | 11 | 5.30 | 0.01188 |
| 13 | 12 | 4.22 | 0.012 |
| 14 | 13 | 3.22 | 0.01833 |
| 15 | 14 | 1.81 | 0.0126 |
| 16 | 15 | 0.91 | 0.00825 |
| 17 | 15.3 | 0.36 | 0.00551 |
| Total volume of the lake [km$^3$] 0.1721 | | | |

water balance of Ugii Lake can be expressed by Equation (3). Based on available hydro-meteorological data, changes in the main parameters relating to Ugii Lake's water balance were investigated, and it was estimated how these factors are linked to changes in the lake's water volume.

The total amount of evaporation, precipitation, and surface inflow to the lake between the satellite acquisition dates of each September between 2002 and 2019, were compiled and used to derive the water balance of Ugii Lake (Table 8).

The volume of the lake was estimated at $172.3 \times {}^{3-}10$ km$^3$ in 2003 and 2018, which is the highest volume during the study period. As shown in Table 8, the annual total surface inflow was high, when the total amount of precipitation was closer to the amount of water evaporated from the lake.

For instance, the surface inflow was $15.77 \times 10^{-3}$ km$^3$.year$^{-1}$, $14.02 \times {}^{3-}10$ km$^3$.year$^{-1}$, and $11.34 \times {}^{3-}10$ km$^3$.year$^{-1}$ in 2003, 2016, and 2018, respectively, which resulted in an increase in the volume of the lake at the highest value. The

Table 7: Changes on volume of Ugii Lake in September between 2002 and 2019.

| Years | [km$^2$] | [km$^3$] | | [$10^{-3}$ km$^3$] |
|---|---|---|---|---|
| 2002 | 24.83 | 0.1717 | | ** |
| 2003 | 25.98 | 0.1723 | | 1.3 |
| 2004 | 25.55 | 0.1721 | 0.171* | 1.1 |
| 2005 | 24.88 | 0.1718 | | 0.8 |
| 2006 | 24.69 | 0.1717 | | 0. 7 |
| 2007 | 24.22 | 0.1715 | | 0. 5 |
| 2008 | 23.73 | 0.1712 | | 0. 2 |
| 2009 | 22.89 | 0.1704 | | -0. 6 |
| 2010 | 22.12 | 0.1696 | | -1.4 |
| 2011 | 22.0 | 0.1695 | | -1.5 |
| 2012 | 23.46 | 0.1710 | | 0 |
| 2013 | 23.54 | 0.1711 | | 0. 1 |
| 2014 | 23.68 | 0.1712 | | 0. 2 |
| 2015 | 23.96 | 0.1713 | | 0. 3 |
| 2016 | 24.76 | 0.1717 | | 0. 7 |
| 2017 | 24.90 | 0.1718 | | 0. 8 |
| 2018 | 25.93 | 0.1723 | | 1.3 |
| 2019 | 25.11 | 0.1719 | | 0. 9 |

Note: * Reference value by JICA in 2005
** Indicates no value

Table 8: Characteristics of the water balance of Ugii Lake.

| Years | P | E | $Y_{SI}$ | $\Delta Y_{GW}$ | V | ΔV |
|---|---|---|---|---|---|---|
| | [$10^{-3}$ km$^3$.year$^{-1}$] | | | | [$10^{-3}$ km$^3$] | |
| 2002 | 2.87 | 6.67 | 1.90 | ** | 171.7 | ** |
| 2003 | 7.07 | 7.97 | 15.77 | 14.27 | 172.3 | 0.6 |
| 2004 | 4.59 | 7.88 | 5.39 | 2.31 | 172.1 | -0.2 |
| 2005 | 4.76 | 7.50 | 8.25 | 5.81 | 171.8 | -0.3 |
| 2006 | 6.46 | 8.17 | 7.86 | 6.25 | 171.7 | -0.1 |
| 2007 | 6.23 | 8.79 | 4.22 | 1.85 | 171.5 | -0.2 |
| 2008 | 5.54 | 8.04 | 1.59 | -0.62 | 171.2 | -0.3 |
| 2009 | 3.99 | 7.85 | 0.88 | -2.18 | 170.4 | -0.8 |
| 2010 | 5.41 | 8.41 | 0.17 | -2.03 | 169.6 | -0.8 |
| 2011 | 6.49 | 7.31 | 2.50 | 1.78 | 169.5 | -0.1 |
| 2012 | 6.97 | 7.83 | 5.01 | 2.65 | 171 | 1.5 |
| 2013 | 6.10 | 6.68 | 1.07 | 0.39 | 171.1 | 0.1 |
| 2014 | 6.40 | 8.33 | 5.34 | 3.31 | 171.2 | 0.1 |
| 2015 | 6.32 | 7.92 | 0.43 | -1.27 | 171.3 | 0.1 |
| 2016 | 8.54 | 7.52 | 14.02 | 14.65 | 171.7 | 0.4 |
| 2017 | 6.38 | 8.61 | 9.15 | 6.82 | 171.8 | 0.1 |
| 2018 | 8.26 | 8.71 | 11.34 | 10.38 | 172.3 | 0.5 |
| 2019 | 6.08 | 8.29 | 7.31 | 5.50 | 171.9 | -0.4 |

volume of the lake remained higher for the following year after increasing, and it was decreased because of the high amount of evaporation and decreased surface inflow to the lake for the following years. According to the estimated lake volume and Equation (4), it can be concluded that the fluctuation of Ugii Lake contributes to hydrometeorological parameters and groundwater flow. For instance, the surface inflow to the lake gradually decreased, and evaporation from the lake was higher than the precipitation between 2008 and 2010. However, the volume of the lake decreased slightly, which was not balanced. This imbalance was because the remaining changes in lake volume are fed by groundwater. Therefore, there is a need to study the potential groundwater of the Ugii Lake Basin in further studies.

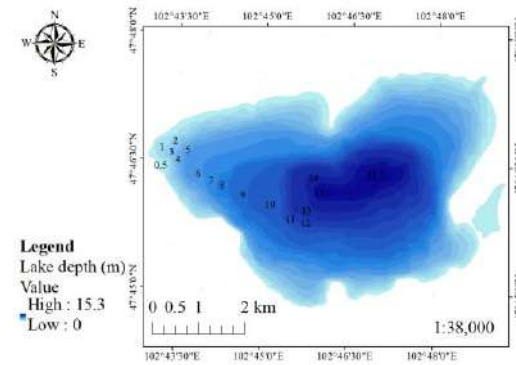


Fig. 7: Topographic map of Ugii Lake.

## CONCLUSION

The lake water surface area calculated using both NDWI and MNDWI-1 showed a strong, positive correlation (R=0.93, R=0.94, $p < 0.01$) with the water level of Ugii Lake. The accuracy of both NDWI and MNDWI-1 methods makes them feasible for lake water extraction in steppe regions. The estimated volume of Ugii Lake was consistent with that reported in a previous study by JICA in 2005. The water balance of Ugii Lake was calculated, and the results proved that the influence of both surface and groundwater on the water balance of the lake are valuable parameters, which can be seen from the difference between the estimated lake volume and the total inflow and outflow to the lake. This study provides valuable information on water extraction methods using satellite images that can be used for further studies, on the influence of climate change on the lakes of the steppe region in Mongolia.

## ACKNOWLEDGMENT

The authors gratefully acknowledge the project (P2018-3568) members who provided the lake morphometric data.

## REFERENCES

Acharya, T.D., Anoj, S., He, H. and Dong. H.L. 2019. Application of water indices in surface water change detection using Landsat imagery in Nepal. Sens. Mater., 31(5):1429-47.

Alparslan, E., Cihangir, A., Vildan, T. and Hüseyin, T. 2007. Water quality assessment at Ömerli dam using remote sensing techniques. Environ. Monit. Assess., 135(1-3): 391-398.

Bai, J., Xi, C., Junli, L., Liao, Y. and Hui, F. 2011. Changes in the area of inland lakes in arid regions of Central Asia during the past 30 years. Environ. Monit. Assess. 178(1-4): 247-56.

Batchuluun, Y. 2021. The physical geography of Mongolia. Springer Nature, 6: 2-19.

Dorjsuren, B., Denghua, Y., Hao, W., Sonomdagva, C., Altanbold, E., Xu, Y., Abel, G., Mohammed, G. and Asaminew, A. 2018. Observed trends of climate and river discharge in Mongolia's Selenga sub-basin of the Lake Baikal basins. Water (Switzerland), 10(10): 1-18.

Gabr, B., Mostafa, A. and Yehia, M. 2020. Planet scope and Landsat 8 imageries for bathymetry mapping. J. Marine Sci. Eng., 8(2): 65-73.

Herndon, K., Rebekke, M., Emil, C. and Robert, G. 2020. An assessment of surface water detection methods for water resource management in the Nigerien Sahel. Sensors (Switzerland), 20(2): 1-14.

Jambaajamts, B. 1989. Climate of Mongolia. Ulsiin hevlel Publishers: 1-271 (in Mongolian)

Kang, S., Gyoungbin, L., Chuluun, T. and Keunchang, J. 2015. Characterizing regional precipitation-driven lake area change in Mongolia. J. Arid Land., 7(2): 146-58.

Liu, Z., Zhijun, Y. and Rui, W. 2016. Assessing methods of identifying open water bodies using Landsat 8 OLI imagery. Environ. Earth Sci., 75(10): 1-13.

Magsar, A., Matsumoto, T., Ulaanbaatar, T., Nandintsetseg, N., Erdenesukh, S., Sandelger, D. and Altanbold, E. 2020. Estimation of evaporation from Ogii Lake using the energy budget method. J. Glob. Environ. Eng., 6: 31-51

Mason, I. M., Guzkowska, M., Rapley, C.G. and Street-Perrott, F.A. 1994. The response of lake levels and areas to climate change. Climatic Change, 27(2): 161-97.

McFeeters, S.K. 1996. The use of the normalized difference water index (NDWI) in the delineation of open water features. Int. J. Remote Sens., 17(7): 1425-32.

Melesse, A.M., Qihao, W., Prasad, T. and Gabriel, B.S Senay. 2007. Remote sensing sensors and applications in environmental resources mapping and modeling. Sensors 7(12): 3209-41.

Rouse J.W., Haas, R.H., Schell, J.A. and. Deering, D.W. 1974. Monitoring Vegetation Systems in the Great Plains with ERTS. In S.C. Freden and E.P. Mercanti (eds.), Third Earth Resources Technology Satellite-1 Symposium. National Aeronautics and Space Administration, Washington D.C: 309-19.

Schwanghart, W., Brigitta, S. and Michael, W. 2008. Holocene climate evolution of the Ugii Nuur Basin, Mongolia. Adv. Atmos. Sci., 25(6): 986-98.

Sumiya, E., Batsuren, D., Denghua, Y, Sandelger, D., Hao, W., Altanbold, E., Baisha, W., Tianlin, Q., Kun, W., Tuvshin, G., Oyunbaatar, D., Wuxia, B., Yuheng, Y., Byambabayar, G., Mohammed, G., Asaminew, A. and Abel, G. 2020. Changes in water surface area of the lake in the steppe region of Mongolia: A case study of Ugii Nuur lake, Central Mongolia. Water (Switzerland), 12(5): 14-27.

Tserensodnom, J. 2000. Catalog of Lakes of Mongolia. Ulaanbaatar.

Xu, H. 2006. Modification of normalized difference water index (NDWI) to enhance open water features in remotely sensed imagery. Int J. Remote Sens., 27(14): 3025-33.

Zhai, K., Xiaoqing, W., Yuanwei, Q. and Peipei, D. 2015. Comparison of surface water extraction performances of different classic water indices using OLI and TM imageries in different situations. Geo-Spatial Inform. Sci., 18(1): 32-42

Nature Environment and Pollution Technology
An International Quarterly Scientific Journal

p-ISSN: 0972-6268
(Print copies up to 2016)
e-ISSN: 2395-3454

Vol. 20 | No. 5 (Suppl) | pp. 2061-2067 | 2021

Original Research Paper

https://doi.org/10.46488/NEPT.2021.v20i05.023

Open Access Journal

# Removal of Mefenamic Acid from Aqueous Solution by Fenton Process: Optimization Using Response Surface Methodology with Central Composite Design

**R. Deepa*, G. Madhu*†, Roy M Thomas* and V. Sivanandan Achari****
*School of Engineering, Cochin University of Science and Technology, Kochi-682 022, Kerala, India
**School of Environmental Studies, Cochin University of Science and Technology, Kochi-682 022, Kerala, India
†Corresponding author: G. Madhu; profmadhugopal@gmail.com

**Nat. Env. & Poll. Tech.**
**Website: www.neptjournal.com**

*Received:* 07-05-2021
*Revised:* 25-06-2021
*Accepted:* 01-07-2021

**Key Words:**
Mefenamic acid
Fenton process
Hydroxyl radical
Response surface methodology

## ABSTRACT

In the present study, the three main process parameters in the Fenton process for the removal of pharmaceutical compound Mefenamic acid from an aqueous solution were optimized using response surface methodology (RSM). Central composite design (CCD) was used for process optimization. The primary and secondary interaction effects of the selected parameters such as $H_2O_2$, $Fe^{2+}$ and pH on the removal of mefenamic acid were examined. A mathematical model for the removal process based on the selected variables was developed. The interaction effect between the chosen parameters shows that the removal of mefenamic acid was enhanced in the acidic pH range at a high concentration of $H_2O_2$ and in a medium concentration level of the catalyst $Fe^{2+}$. The removal efficiency of 81.24% was obtained for mefenamic acid at the optimized condition of variables such as 9.36 mM $H_2O_2$, 0.058 mM $Fe^{2+}$and at a pH value of 2.1.

## INTRODUCTION

Pharmaceuticals compounds are one of the emerging contaminants, the presence of which even in trace levels in water sources can cause lethal effects on human beings and aquatic organisms. By the development of modern analytical techniques, various categories of pharmaceutical compounds such as analgesics/anti-inflammatory, β-blockers, psychiatric drugs, antibiotics, lipid regulators, contrast agents, anti-cancer agents, and hormones have been identified in municipal and hospital wastewaters and even in surface and groundwater sources (Wang et al. 2014, Bu et al. 2016). To remove these non-biodegradable and persistent compounds, in addition to the conventional treatment methods, various advanced treatment techniques such as adsorption, reverse osmosis, microfiltration, advanced oxidation, and nano filtration techniques are under research (Rivera-Utrilla et al. 2013).

Among the advanced treatment techniques, advanced oxidation processes (AOPs) are found to be promising. AOPs are based on the formation of highly reactive and non-selective oxidants such as hydroxyl radical (•OH), superoxide radical ($•O_2$), hydroperoxyl radicals ($•HO_2$), sulfate radicals ($•SO_4^-$) and peroxyl radical (•ROO) generated under atmospheric or subcritical conditions of temperature and pressure, with or without catalyst and/or energy. These oxidants degrade the persistent organic compounds into carbon dioxide and water or convert them into metabolite forms (Deng & Zhao 2015). There are several types of AOPs based on the techniques used for the in situ formation of oxidant radicals such as chemical, photochemical, sonochemical, microwave-assisted, and electrochemical AOPs (Andreozzi et al. 1999). Fenton process is a chemical AOP method in which •OH radicals are produced by the catalytic decomposition of $H_2O_2$ by iron salts in an acidic medium (Oturan & Aaron 2014). The advantage of this process is its simple operation principle, environmentally safe nature, short reaction time, and the absence of mass transfer limitation (Naveed et al. 2017). The removal efficiency of the Fenton process depends on various factors such as initial pH, reaction time, initial pollutant concentration, the dosage of Fenton reagent, reagent mole ratio, mode of addition of $H_2O_2$, and temperature (Roudi et al.2018).

Mefenamic acid (MEF) is a nonsteroidal analgesic and anti-inflammatory drug (NSAID). It is commonly used to reduce pain, menstrual pain, dysmenorrhea, migraine and is also used in the treatment of rheumatoid arthritis and other muscular-skeletal diseases (Idrees 2015). In European Union (EU), mefenamic acid is considered a third-class priority pollutant as its concentration in various environmental compartments has been detected larger than the no-effect concen-

tration value of 0.428μg.$L^{-1}$ (Chang et al.2012). The removal of mefenamic acid by photolysis, adsorption on activated carbon, and ozonation showed that 60% removal efficiency in 120 min was achieved by applying a combination of UV and ozone. Also, it reveals that the activated carbon addition did not enhance the removal of the compound (Gimeno et al. 2010). Nitrite-induced photo transformation studies of MEF showed that intermediate photo transformation products are formed and they were found more toxic than mefenamic acid (Chen et al. 2016). Different oxidative processes such as UV, UV/$H_2O_2$, Fenton, and photo Fenton were investigated and optimized using fractional factorial design and found photo Fenton process using ferric oxalate and hydrogen peroxide at a pH of 6.1 gives a maximum removal of 95.95% in 60 min (Colombo et al. 2016).

Polyurea formaldehyde-Bentonite was tested as an adsorbent for mefenamic acid from water and found maximum adsorption of 16mg.$g^{-1}$ achieved at 47°C at pH 1.5 (Majeed et al. 2017). For practical application of the removal process, it is necessary to optimize the various important factors using experimental design techniques.

The aim of this study is to apply a statistically based technique named the central composite design method to optimize the Fenton process for removal of mefenamic acid from aqueous solutions by varying the selected three main experimental variables such as concentration of oxidant $H_2O_2$, catalyst $Fe^{2+}$, and pH, and to develop a model to examine the single and combined effect of these variables on the removal process of the compound.

## MATERIALS AND METHODS

### Materials

Mefenamic acid ($C_{15}H_{15}NO_2$, 2-[(2,3dimethyl phenyl) amino] benzoic acid, 99%, (Sigma -Aldrich, India), $H_2O_2$ (30.0% w/v), ferrous sulfate heptahydrate $FeSO_4.7H_2O$ (FS), NaOH, $Na_2S_2O_3$, and sulphuric acid from Merk (India) were used as such without further purification. All chemicals used were of analytical grade unless indicated otherwise. HPLC grade acetonitrile (ACN), 98% formic acid, and isopropanol (Merck) were used for the analysis.

### Experiments

In a typical Fenton experiment, an aqueous solution of mefenamic acid having a concentration of 15 ppm was prepared using Milli Q water and mixed with appropriate concentrations of $FeSO_4.7H_2O$ and $H_2O_2$ in liquid form in a 250 mL closed pyrex glass reactor. The reactor was placed in a dark chamber to avoid any photochemical reaction. The reaction volume was maintained as 100 mL and stirred continuously using a magnetic stirrer at 500 RPM. The pH of the sample was maintained by using NaOH and $H_2SO_4$ solutions as necessary. One drop of 0.1 N sodium sulfite solution was added to each sample taken to quench the action of any excess $H_2O_2$ present in the sample. All samples taken were filtered through 0.45μm syringe filters before the analysis. The removal of the compound was monitored by analyzing the initial samples and samples taken after 60 min of the interval by using HPLC.

### HPLC Analysis

The quantitative determination of mefenamic acid was carried out with an HPLC-UV system on LC2030 plus liquid chromatograph (Shimadzu, Prominence *i*) equipped with a binary solvent gradient pump and an automatic injection system. The compounds were eluted off the C-18 column (250 mm x 4.6 mm packed with 5 μm particle size) with two solvents as mobile phases. The mobile phase consists of solvent A 0.1% formic acid in milliQ water and solvent B 100% acetonitrile. The elution started at 0% B and was then linearly increased to 100% B over 10 minutes at a flow rate of 1.0 mL.$min^{-1}$ then kept isocratic for 3minutes and B concentration reached to initial level in the last 2 min. The total run time of the gradient flow method was 15 min. The injection volume was 20 μL and the UV detection wavelength was at 275 nm. The signal acquired from the detector was recorded by Lab Solution software.

### Experimental Design

#### Central Composite Design (CCD)

The CCD was used to optimize the pH, the concentration of $H_2O_2$ and $Fe^{2+}$ and to evaluate the interaction among these three variables on the removal of Mefenamic acid. CCD is a very efficient design tool for fitting second-order models and optimizing the effective parameters with a minimum number of experimental runs (Bezerra et al. 2008). A CCD consists of cube points made up of design points from a $2^k$ factorial or $2^{(k-1)}$ fractional factorial design with 2k axial or "star" points, and $n_c$ center points (where k is the number of factors) (Im et al. 2012).

In this work, the CCD design consists of 8 cube points (all possible combinations of +1 and -1 for the 3 factors), 5 replicates of central points (coded as 0 for all 3 factors), and 6 axial points (+1.68,-1.68, and 0 for three factors). Thus there is a total of nineteen experiments with three factors coded at five levels.

A regression design is used to mathematically model the response as a function of the independent factors. The following general model equation is used to obtain the optimal response.

$$Y = \beta_0 + \sum_{i=1}^{k} \beta_i X_i + \sum_{i=1}^{k} \beta_{ii} X_i^2 + \sum_{i=1}^{k} \sum_{j=1}^{k} \beta_{ij} X_i X_j + \epsilon \quad \ldots(1)$$

Where Y represents the response variable i.e., the percentage removal of the compound and 'k' is the number of factors, $X_i$ to $X_k$ represents the independent variables, $\beta_i$ represents the regression coefficients for the linear or primary effect, $\beta_{ii}$ represents the quadratic coefficients or the squared effect, $\beta_{ij}$ represent the interaction effect coefficients and $\varepsilon$ is the random error (Chauhan et al. 2013).

In this study, three independent variables were considered and the quadratic polynomial equation for the response in terms of coded independent variables can be represented as

$$y = \beta_0 + \beta_1 X_1 + \beta_2 X_2 + \beta_3 X_3 + \beta_{11} X_1^2 + \beta_{22} X_2^2 + \beta_{33} X_3^2 + \beta_{12} X_1 X_2 + \beta_{13} X_1 X_3 + \beta_{23} X_2 X_3 \quad \ldots(2)$$

MINITAB 16 was used to obtain the linear, squared, and interaction regression coefficients, and also the response surface and contour plots of the response model.

## RESULTS AND DISCUSSION

Preliminary experiments were conducted by univariate method to fix the range of variables and the time interval for the process. The variables $X_1$ $X_2$ and $X_3$ were the concentration of added $H_2O_2$, $Fe^{2+}$ and the pH maintained at the start of

Table 1: Experimental range and levels of selected independent factors.

| Independent factors | Range and Levels | | | | |
|---|---|---|---|---|---|
| | -α | -1 | 0 | 1 | α |
| $H_2O_2$ concentration (mM) ($X_1$) | 2.64 | 4 | 6 | 8 | 9.36 |
| $Fe^{2+}$ concentration (mM) ($X_2$) | $6.4x10^{-3}$ | $2.0x10^{-2}$ | $4.0x10^{-2}$ | $6.00x10^{-2}$ | $7.36x10^{-2}$ |
| pH ($X_3$) | 0.96 | 3 | 6 | 9 | 11.04 |

Table 2: CCD matrix in terms of coded units along with the observed and predicted removal values of the compound after 1 hour Fenton process.

| Run | Coded variables | | | % Removal of Mefenamic acid | |
|---|---|---|---|---|---|
| | $X_1$ | $X_2$ | $X_3$ | Observed values | Predicted values |
| 1 | 0.00 | -1.68 | 0.00 | 27.31 | 29.38 |
| 2 | -1.00 | -1.00 | -1.00 | 58.65 | 56.32 |
| 3 | 0.00 | 0.00 | 0.00 | 60.65 | 60.54 |
| 4 | 1.00 | -1.00 | -1.00 | 61.43 | 59.16 |
| 5 | -1.00 | 1.00 | -1.00 | 52.75 | 51.66 |
| 6 | -1.00 | 1.00 | 1.00 | 22.70 | 23.82 |
| 7 | -1.68 | 0.00 | 0.00 | 36.43 | 37.09 |
| 8 | 1.68 | 0.00 | 0.00 | 64.50 | 65.47 |
| 9 | 0.00 | 0.00 | 0.00 | 60.80 | 60.54 |
| 10 | 0.00 | 0.00 | 0.00 | 60.46 | 60.54 |
| 11 | 0.00 | 0.00 | 1.68 | 23.41 | 21.38 |
| 12 | 1.00 | 1.00 | 1.00 | 53.57 | 54.75 |
| 13 | -1.00 | -1.00 | 1.00 | 16.84 | 17.09 |
| 14 | 0.00 | 0.00 | 0.00 | 60.52 | 60.54 |
| 15 | 0.00 | 0.00 | -1.68 | 70.82 | 74.49 |
| 16 | 1.00 | 1.00 | -1.00 | 80.16 | 78.75 |
| 17 | 0.00 | 0.00 | 0.00 | 60.54 | 60.54 |
| 18 | 1.00 | -1.00 | 1.00 | 23.85 | 23.78 |
| 19 | 0.00 | 1.68 | 0.00 | 51.92 | 51.48 |

the reaction. The range of variables $H_2O_2$ (4 - 8 mM), $Fe^{2+}$ ($2\times10^{-2}$ - $6\times10^{-2}$ mM), and pH (3 to 9) was fixed based on preliminary studies and the five different levels of each variable were selected based on the central composite design. Table 1 shows the various levels of selected independent factors and Table 2 is the list of coded variables and the observed and predicted removal values of the response.

The model equation obtained for the removal of mefenamic acid in terms of coded variables was as follows:

$$Y = 60.536 + 8.445X_1 + 6.578X_2 - 15.807X_3 - 3.279X_1^2 - 7.123X_2^2 - 4.466X_3^2 + 6.061X_1X_2 + 0.961X_1X_3 + 2.843X_2X_3 \quad ...(3)$$

Where: Y is the percentage removal of mefenamic acid and $X_1$ and $X_2$ were the initial concentration of $H_2O_2$ and $Fe^{2+}$ in mM and $X_3$ is the initial pH value.

## Statistical Analysis

The quality of the proposed model was checked by the coefficient of determination ($R^2$) and adjusted $R^2$. The coefficient of determination ($R^2$) indicates the proportion of variation in the response described by the model. If the value of $R^2$ is closer to 1, it indicates that the model is good to describe the variation in response as a function of independent variables (Ishak & Malakahmad 2013). Adjusted $R^2$ is another useful statistical tool to evaluate the model adequacy; it is a modified $R^2$ value by taking into account the number of covariates or predictors in the model. The 'F value' was the ratio of the mean sum of square due to the model variance and error variance, and is used to test the null hypothesis (Chauhan et al. 2013). The statistical significance was assessed by the lack of fit test. The result of the analysis of variance (ANOVA) was presented in Table 3.

The ANOVA result shows that the linear, quadratic, and interaction terms are significant since the corresponding p-values are <0.05. A high $R^2$ value of 0.9936 and an adjusted $R^2$ value of 0.9873 indicates the significance of the model and its adequacy to predict the response. A normal probability plot of residuals versus response is shown in Fig. 1. The normal probability plot is a graphical method for determining residuals' normality. Fig. 1 shows that the points are close to the straight line and the model is sufficient to describe the response.

Table 3: ANOVA result of the quadratic model for percentage removal of Mefenamic acid.

| Source | | Sum of squares | Df | Square mean | F value | P value | Remarks |
|---|---|---|---|---|---|---|---|
| Regression | | 6238.4 | 9 | 693.16 | 156.08 | 0.000 | Significant |
| Linear | | 4972.64 | 3 | 1657.55 | 373.23 | 0.000 | |
| Square | | 899.77 | 3 | 299.92 | 67.53 | 0.000 | |
| Interaction | Residual | 366.00 | 3 | 122.00 | 27.47 | 0.000 | |
| Error | | 39.97 | 9 | 4.44 | | | |
| Lack-of-Fit | | 39.90 | 5 | 7.98 | | | |
| Pure Error | | 0.07 | 4 | 0.02 | | | |
| Total | | 6278.37 | 18 | | | | |

$R^2$ = 0.9936, $R^2$ (adjusted) = 0.9873

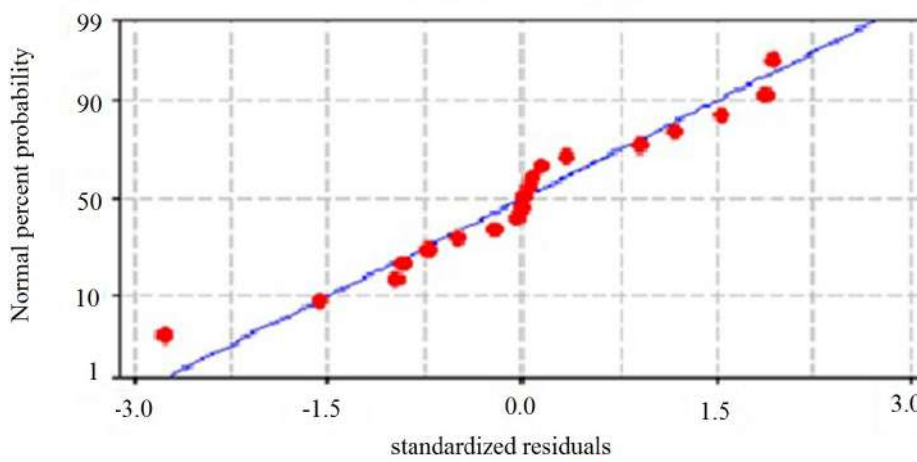


Fig. 1: Normal Probability Plot, % removal of mefenamic acid.

### Effect of Independent Variables on the Removal of the Compound

The plot in Fig. 2. shows the effect of independent variables $H_2O_2$, $Fe^{2+}$ and pH on the mean removal of mefenamic acid in 19 experiments conducted based on the central composite design. Fig. 2 shows a sharp increase in the average removal value from 4 to 9.36 mM concentration of $H_2O_2$. This may be due to the more •OH radicals produced during the more concentration of $H_2O_2$ and thus enhancing the removal of the compound (Rezaee et al. 2014). The second curve shows that the mean removal value of mefenamic acid increases up to 55% when the iron concentration changes from 0.0064 to 0.040. Further increase in iron concentration did not show an increase in the removal efficiency. This shows that a high concentration of metal ions was not favoring the removal of this compound. This may be due to the ferrous ion inhibition that occurs at a high concentration of $Fe^{2+}$ in the system. The excess metal ion increases the yield of $Fe^{2+}$ ions which act as a scavenger by quenching the hydroxyl ions formed (Wang et al. 2014). The higher concentration of $Fe^{2+}$ in the system can also result in the production of hydroperoxyl radical (•HO ) which has less oxidation potential than hydroxyl radicals (Karale et al. 2014). Effect of pH indicates that the mean removal of mefenamic acid was more favorable at the acidic pH range than at alkaline pH. Mefenamic acid shows more than 50 % average removal efficiency in neutral pH but the removal was less than 30% in alkaline pH.

### Combined Effect Among the Independent Variables on the Removal Efficiency

To understand the interaction effect among the independent variable, contour plots and 3D response surface curves were considered. Fig. 3. shows the profile for the quadratic response surface and the contour plots of % removal of mefenamic acid versus various coded independent variables.

From the contour plot Fig. 3(a), it was evident that more than 70% removal of mefenamic acid was obtained at a higher concentration of added $H_2O_2$ and $Fe^{2+}$ at a neutral pH range. Fig. 3(b) indicates that a removal value above 60% was obtained at medium concentration levels of $H_2O_2$ with varying $Fe^{2+}$ concentrations in the acidic pH range of the solution. Interaction between pH and $H_2O_2$ at medium $Fe^{2+}$ concentration was shown in Fig. 3(c). It shows that removal of mefenamic acid was more than 75% at medium to high levels of $H_2O_2$ concentration in acidic pH values. This was due to more production of •OH radicals from added oxidants resulting in the degradation of the compound (Im et al. 2012).

### Optimization of Operating Parameters

The optimal value of the independent variable for maximizing the response was obtained by using the Minitab Response optimizer. The value of the process variable obtained corresponding to the optimum response is presented in Table 4. Accordingly, the maximum removal of 82.36% for the mefenamic acid was obtained at optimum conditions of 9.36 mM of $H_2O_2$, 0.058 mM $Fe^{2+}$ and at a pH of 2.08. The experimental test was conducted in triplet using the predicted value of independent variables and it shows that the average experimentally observed removal value of 81.24% is very close to the predicted value using the model. It implies that the RSM is a good tool for optimizing the operating parameters in this Fenton process for the removal of mefenamic acid.

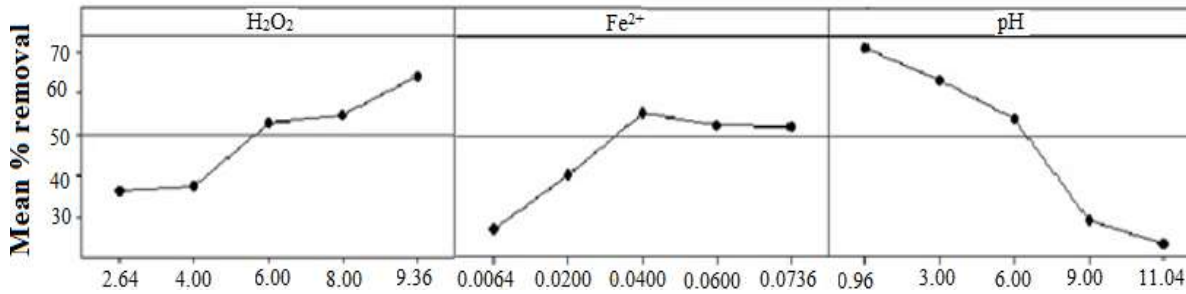


Fig. 2: Primary effect of independent variables $H_2O_2$, $Fe^{2+}$ and pH on the removal of mefenamic acid.

Table 4: Optimum value of process variables for maximum removal of Mefenamic acid and its predicted and observed values.

| Response | $H_2O_2$ (mM) | $Fe^{2+}$ (mM) | pH | Predicted Removal (%) | Observed Removal (%) |
|---|---|---|---|---|---|
| Removal of Mefenamic acid | 9.36 | 0.058 | 2.1 | 82.36 | 81.24 |

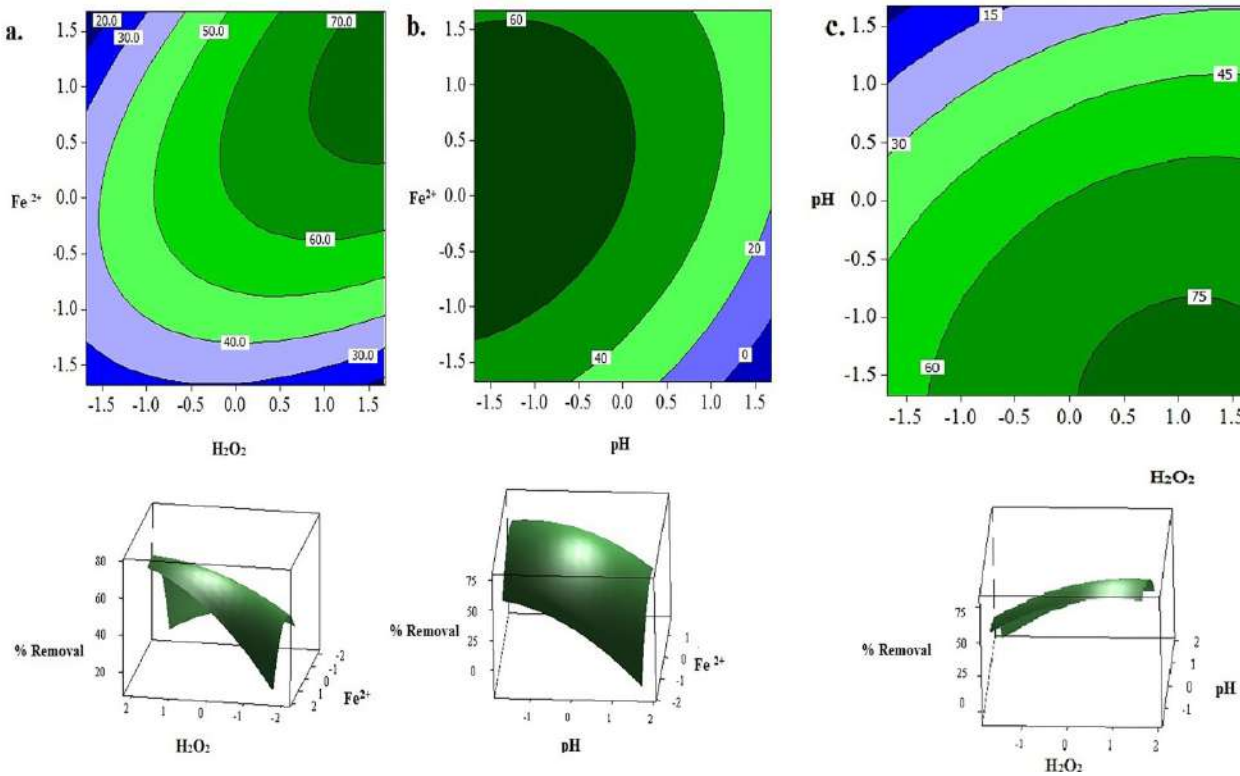


Fig. 3: Contour plots and Response surface plots for mefenamic acid removal versus coded independent variables a) $H_2O_2$ with $Fe^{2+}$ b) pH with $Fe^{2+}$ and c) $H_2O_2$ with pH.

## CONCLUSION

In this work, RSM was used to optimize the removal of mefenamic acid by using the Fenton process. By using the central composite method, three main operating parameters in the Fenton process including the pH, the initial $H_2O_2$, and $Fe^{2+}$ concentration were examined. Based on the experimental results and the relationship between the selected independent variables, a quadratic model was obtained. Statistical test by ANOVA showed a high coefficient of determination value ($R^2$= 0.9936) which indicates a good agreement of the model with experimental data. The interaction effect of experimental parameters on the response was established by response surface curves and contour plots. A high percentage removal value of 82.36% was obtained under the optimal value of variables in the process. Further confirmation experiment under the optimized condition results in a maximum removal value of 81.24%. This indicates that the model is in accordance with the experimental data. Our study implies that RSM based on the central composite method is a useful tool for optimizing the operating parameters for the Fenton removal process of mefenamic acid.

## ACKNOWLEDGMENT

The authors are thankful to Kerala State Council for Science, Technology, and Environment for the financial support extended to this research work.

## REFERENCES

Andreozzi, R., Caprio,V., Insola, A. and Marotta, R. 1999. Advanced oxidation processes for water purification and recovery, Cataly. Today., 53: 51-53.

Bezerraa, M.A., Santelli, R.E., Oliveiraa, E.P., Villara, L.S. and Escaleiraa, L.A. 2008. Response surface methodology ( RSM ) as a tool for optimization in analytical chemistry. Talanta, 76: 965-977.

Bu, Q., Shi, X., Yu, G., Huang, J. and Wang, B. 2016. Assessing the persistence of pharmaceuticals in the aquatic environment: challenges and needs. Emerg. Contam., 2(3): 145-147.

Chang, E.E., Liu, T.Y., Huang, C.P., Liang, C.H. and Chiang, P.C. 2012. Degradation of mefenamic acid from aqueous solutions by the ozonation and $O_3$/UV processes. Sep. Purif. Technol., 98: 123-129.

Chauhan, V.S., Bhardwaj, N.K. and Chakrabarti, K.S. 2013. Application of response surface methodology and central composite design for the optimization of talc filler and retention aid in papermaking. Indian J. Chem. Technol., 20(2): 121-127.

Chen, P., Wang, F.L., Yao, K., Ma, J.S., Li, F.H., Lv, W.Y. and Liu, G.G. 2016. Photodegradation of mefenamic acid in aqueous media: kinetics,

toxicity and photolysis products. Bull. Environ. Contam. Toxicol., 96(2): 203-209.

Colombo, R., Ferreira, T.C.R., Ferreira, R.A. and Lanza, M.R.V. 2016. Removal of mefenamic acid from aqueous solutions by oxidative process: optimization through experimental design and HPLC/UV analysis. J. Environ. Manage., 167: 206-213.

Deng, Y. and Zhao, R. 2015. Advanced oxidation processes (AOPS) in wastewater treatment. Curr. Pollut. Rep., 1: 167-176.

Gimeno, O., Rivas, J., Encinas, A. and Beltran, F. 2010. International application of advanced oxidation processes to mefenamic acid elimination. Int. J.Chem. Mol. Nuc. Mater. Metall. Eng., 4(6): 399-401.

Idrees, U. 2015. Estimation and analysis of mefenamic acid suspension ; a proportional investigation. SOJ Pharm. Pharm. Sci., 3(2): 2-4.

Im, J.K., Cho, I.H., Kim, S.K. and Zoh, K.D. 2012. Optimization of carbamazepine removal in O3/UV/H2O2 system using a response surface methodology with central composite design. Desalination, 285: 306-314.

Ishak, S. and Malakahmad, A. 2013. Optimization of Fenton process for refinery wastewater biodegradability augmentation. Korean J. Chem. Eng., 30(5): 1083-1090.

Karale, S.R., Manu, B. and Shrihari, S. 2014. Fenton and photo-Fenton oxidation processes for degradation of 3-aminopyridine from water. APCBEE Procedia, 9: 25-29.

Majeed, B.A.A., Muhseen, R.J. and Jassim, N.J. 2017. Adsorption of mefenamic acid from water by bentonite poly urea-formaldehyde composite adsorbent. J. Eng., 23(7): 50-73.

Naveed, S., Qamar, F., Abbas, S.S., Safdar, S., Ameer, S., Matavos-Aramyan, S. and Moussavi, M. 2017. Advances in Fenton and Fenton-based oxidation processes for industrial effluent contaminants control-A review. Int. J. Environ. Sci. Nat. Resour., 2(4): 1-18.

Oturan, M.A. and Aaron, J.J. 2014. Advanced oxidation processes in water/wastewater treatment: principles and applications. A review. Crit. Rev. Environ. Sci. Technol., 44(23): 2577-2641.

Rezaee, R., Maleki, A., Jafari, A., Mazloomi, S., Zandsalimi, Y. and Mahvi, A.H. 2014. Application of response surface methodology for optimization of natural organic matter degradation by the advanced oxidation process. J. Environ. Health Sci. Eng., 12(67): 1-8.

Rivera-Utrilla,J., Sánchez-Polo,M., Ferro-García, M, A., Prados-Joya,G.and Ocampo-Pérez, R. 2013. Pharmaceuticals as emerging contaminants and their removal from water. A review. Chemosphere, 93(7): 1268-1287.

Roudi, M.A., Chelliapan, S., Mohtar, W.H.M.W. and Kamyab, H. 2018. Optimization of the fenton process for the treatment of landfill leachate using an artificial neural network. Water, 10(595): 1-12.

Wang, C., Zhang, S., Zhang, Z., Zeng, M. and Yuji, S. 2014. Optimization and interpretation of Fenton and UV/Fenton processes for degradation of syringyl lignin. J. Environ. Anal. Chem., 01(02): 2-6.

Nature Environment and Pollution Technology
An International Quarterly Scientific Journal

p-ISSN: 0972-6268
(Print copies up to 2016)
e-ISSN: 2395-3454

Vol. 20 | No. 5 (Suppl) | pp. 2069-2078 | 2021

Original Research Paper

https://doi.org/10.46488/NEPT.2021.v20i05.024

Open Access Journal

# Hydrochemistry and Application of GIS in Groundwater Quality in Nagalapura Taluk, Bellary District, Karnataka, India

**Maradi Sangrama Nayaka*, T. Suresh*, S. Manjappa** and B. Suresh***†**

*Department of Chemistry, Vijayanagara Sri Krishnadevaraya University, Bellary-583104, Karnataka, India

**Department of Chemistry, University BDT College of Engineering, Davangere-577005, Karnataka, India

***Department of Civil Engineering, Bapuji Institute of Engineering & Technology, Davangere-577 005, Karnataka, India

†Corresponding author: B. Suresh; drbssmg@gmail.com; drbssmg@bietdvg.edu

**Nat. Env. & Poll. Tech.**
**Website: www.neptjournal.com**

*Received:* 18-05-2021
*Revised:* 23-06-2021
*Accepted:* 04-07-2021

**Key Words:**
Groundwater quality,
Gibbs graphs
Wilcox diagram
GIS
Pollution
Drinking water source

## ABSTRACT

The assessment of groundwater quality is essential for the conservation of natural resources. Hence, this study aims to assess the hydrochemistry of groundwater in and around the Nagalapura Taluk in Bellary district, Karnataka, India. The groundwater quality variables are mapped using a Geographic Information System (GIS). For the hypothesis, the mean value of ten groundwater quality variables was obtained from 50 bore well samples (2016-2018). To assess the lead ions and type of water, the USSL, SAR, and Na% were measured. Ionic ratio and Gibbs graphs were used to demonstrate the chemical reactions in the water samples. ArcGIS was used for spatial analysis of the quality variables. The results showed the order of $Cl^- > SO_4^{2-} > HCO_3^-$ with water types $Na^+$-$Cl^-$ and $Cl^-$, and the order of $Na^+ > Mg^{++} > Ca^{++} > K^+$ with $Na^+$ and $Mg^{++}$ as the dominant anion and cation, respectively. The hydrochemistry of groundwater is determined by the geological structure in 64 percent of the water samples examined. The Wilcox diagram shows that no-alkali exposure to the crops is expected. Forty one samples (82%) fit within the C3-S1 group; this category is fit for irrigational needs. Only 01 and 03 samples showed maximum SAR during two seasons like pre-monsoon and post-monsoon periods. The maps showed that groundwater in the selected sites is usually of higher quality, whereas the presence of dolomite indicates a reduction in water quality.

## INTRODUCTION

Groundwater is the water present beneath Earth's surface in rock and soil pore spaces and the fractures of rock formations (Freeze 1979). Water enters the ground in the lower layer where the discharge ends, which contains wells, springs, rivers, lakes, and the ocean. The world's freshwater supply contains 62% groundwater, which is 0.65% of the total amount of water on Earth (EPA 2009). Man-made activities on land, land use, changes in the soil layer, and ground-water percolation impact the quality of ground-water. Although groundwater testing and drilling, which includes strata analysis, are good methods for determining the depth of the aquifer and the ideal site for a bore-well, they take time and often require skilled manpower (Madan et al. 2010, Mukherjee et al. 2012, Mallick et al. 2015). On the other hand, using GIS, remote sensing, and satellite images to assess groundwater resources is beneficial and cost-effective (Adiat et al. 2012, Verma & Singh 2013). Honarbakhsh et al. (2019) used a GIS-based approach with the Groundwater Quality Index (GWQI) to analyze ground-water quality in Marvdasht located in the semi-arid region of Iran. For this purpose, they used groundwater quality data that were collected in a five-year period (2010-2015). During the study period, the groundwater quality index (GWQI) indicated that only 3% of the total area ($10km^2$) was of low quality. $Mg^{++}$, total hardness (TH), and Na+ were predicted to be the most sensitive water quality variables. Elubid et al. (2019) reported the spatial distribution of groundwater quality parameters in some parts of Gedare State by using GIS and the total water quality index (TWQI). Major cations and anions were found in 38 bore wells identified in this study. Furthermore, the groundwater quality is controlled by sodium and bicarbonate ions that defined the composition of the water type to be Na-$HCO_3$.

Furthermore, as reported by Hemant and Limaye (2012), Kesari et al. (2016), and Madan et al. (2010) in several parts of India, groundwater quality is deteriorating due to massive industrial effluent dumping and mining activities. The reduction in precipitation in arid places leads to an increase in the public's use of water for drinking and irrigation purposes (Mallick et al. 2015). Groundwater resources can be defined as the only vital and alternative resource for the people in dry

areas, particularly to encourage human life through agriculture activities. With the above literature review, the present work is undertaken to generate groundwater level zonation image-based thematic maps utilizing remote sensing and GIS for improved groundwater resource utilization, planning, and management.

Seasonal maps are used to evaluate field experts' opinions and data analysis. Several experiments to assess the quality and hydrochemistry of groundwater were conducted in and around Nagalapura Taluk, Bellary district, using Pie, Schoeller, and Piper diagrams, as well as maps, to assess groundwater quality in and around Nagalapura Taluk.

## MATERIALS AND METHODS

### Geology of Hospet, India

Geologically, rocks of granodiorite and granite are associated with iron and manganese ore bands. These rocks are joined and intruded by doleritic dykes. Unlike hard rocks, which are partially weathered up to 5 meters below the surface, schist and phyllite can weather up to 20 meters deep.

### Experimental Work

The groundwater samples obtained from twenty-five different locations in and around the Nagalapura taluk were examined and analyzed and interpreted for this study. The sampling locations in this study were identified in five different zones of the city, and groundwater samples were taken. In a GIS model, interpretation strategies that integrate ground-based and remote sensing data are developed. Critical steps include acquiring all relevant data, processing, and constructing the database. Capacity levels and data are required in assessing the study area to generate GIS data. Geologic, hydrologic, topographic, vegetation, and soil maps are among the data types available, and so are satellite imagery, geological logs, bore well locations with latitude and longitude, and hydrological data such as water quality, aquifer test data, and reports from local and regional study areas.

### Collection of Samples

Groundwater samples are collected in five-liter plastic cans that have been washed and rinsed twice with distilled water. All samples were carried to the laboratory using ice-boxes and kept refrigerated at 4°C APHA, 2005. The Fig. 1 gives the sampling location map and details of the locations are given in Table 1. Samples were analyzed for physico-chemical variables, using respective methods as per APHA, 2005. Statistical analysis was also applied to the results and tabulated.

## RESULTS AND DISCUSSION

According to preliminary research, Nagaralapura district provided the best opportunity to collect the most relevant data across the study area. 50 bore wells were chosen from a GPS field survey of the study area, and water samples were collected from these 50 locations. Hydrochemistry and all other data have been entered into the GIS. The spatial pattern of various water quality variables is discussed in this paper. During the present investigation, thematic map hardness of groundwater revealed that 80% of the groundwater samples in the pre-monsoon period, 76% of the groundwater samples during the monsoon period, and 75% of the groundwater samples during the post-monsoon period had hardness in the range of 300 to 600 $mg.L^{-1}$. During the pre-monsoon season, 6% of the groundwater samples (Fig. 2(a)), 5% of the groundwater samples during monsoon (Fig. 2(b)) and 4% of the groundwater samples during the post-monsoon period (Fig. 2(c)) had hardness less than 300 $mg.L^{-1}$ (Hemant & Limaye 2012). It was observed that 28% and 22% of the groundwater samples during pre- and post-monsoon periods had hardness above 600 $mg.L^{-1}$. In both seasons, it was evident that more than 20% of the groundwater samples exceeded the permissible limit set by BIS and WHO drinking water standards. The hardness of water is caused due to occurrence of carbonates and bi-carbonates of $Ca^{++}$ and $Mg^{++}$, $Cl^{-}$, $NO_3^{-}$, and $SO_4^{2-}$ of $Ca^{++}$ and $Mg^{++}$. The maximum content of TH was found in HW-41 (M.M.Halli near Anjinappa home), which is above the permissible limit. Most of the selected locations had TH content within the permissible limit. Spatial distribution of TH during pre- and post-monsoon periods, and monsoon periods are given in Fig. 2(a), 2(b), and 2(c) respectively.

Maximum hardness was observed at HW-41 (M.M.Halli near Anjinappa home) (1280 $mg.L^{-1}$) in all the seasons during the study period, while it was 143 $mg.L^{-1}$ in HW-43 (D.N.Keri Devalapura near Shayari Durugamma Temple) during post-monsoon and monsoon periods. However, it was 195 $mg.L^{-1}$ in HW-42 (D.N.Keri near Nandibanda) during the pre-monsoon season. Pujari, et al. (2012) recorded TH of 808 $mg.L^{-1}$ during the rainy season in Kovaya, the coastal area of Gujarat whereas Champidi et al. (2011) recorded 1685 $mg.L^{-1}$ of TH in the Erasinos area of eastern Attica.

The perusal map of the $Ca^{++}$ content showed that 82% and 81% of groundwater samples have calcium concentrations in the range of 75 $mg.L^{-1}$ to 200 $mg.L^{-1}$ during pre- and post-monsoon periods, and monsoon periods.

Table 1: Location of the bore-well samples in the Hospet Taluk, Bellary District.

| Sl. No. | Village | location | Latitude and Longitude | Sl. No. | Village | Location | Latitude and Longitude |
|---|---|---|---|---|---|---|---|
| HW-1 | Hossur | Kichadi Net | $15^0$16'08.20N $76^0$23'26.82E | HW-26 | Bylavaddigeri | Dharmasagara | $15^0$14'55.55N $76^0$31'53.64E |
| HW-2 | Hossur | Near Railway Gate | $15^0$16'08.10N $76^0$23'26.50E | HW-27 | Bylavaddigeri | Kakubalu | $15^0$14'55.43N $76^0$31'53.60E |
| HW-3 | Nagenahalli | Nagenahalli | $15^0$17'50.23N $76^0$24'12.59E | HW-28 | P K Halli | Ganesh Tample | $15^0$16'22.58N $76^0$28'37.77E |
| HW-4 | Nagenahalli | Basavadurga | $15^0$17'50.17N $76^0$24'12.30E | HW-29 | P K Halli | Ingalagiri | $15^0$16'22.17N $76^0$28'37.41E |
| HW-5 | Kamalapaura | Opp SriKari College | $15^0$18'21.53N $76^0$28'27.34E | HW-30 | P K Halli | P K Halli | $15^0$16'22.38N $76^0$28'37.52E |
| HW-6 | Seetharam Tanda | Seetharam Tanda Cross | $15^0$16'30.48N $76^0$24'15.63E | HW-31 | Hosapete (T B Dam) | Muttumariyamma Temple | $15^0$16'27.64N $76^0$21'10.28E |
| HW-7 | Seetharam Tanda | Mustafa Darga | $15^0$16'30.17N $76^0$24'15.10E | HW-32 | Hosapate | Industrial Area | $15^0$16'27.81N $76^0$21'10.40E |
| HW-8 | Seetharam Tanda | N R Camp | $15^0$16'30.22N $76^0$24'15.30E | HW-33 | Hosapete | Sanaki veerabadra temple | $15^0$16'27.79N $76^0$21'10.38E |
| HW-9 | Bukkasagara | 76 Venkarta-pura | $15^0$21'03.28N $76^0$31'50.64E | HW-34 | Hosapete | Chittavadigeppa temple | $15^0$16'27.75N $76^0$21'10.26E |
| HW-10 | Bukkasagara | Near Anjaneya Temple | $15^0$21'03.36N $76^0$31'50.22E | HW-35 | Kallahalli | Vyasanakere Station | $15^0$13'05.08N $76^0$24'14.94E |
| HW-11 | Bukkadagara | SC-ST Keri | $15^0$21'03.14N $76^0$31'50.10E | HW-36 | Kallahalli | Kaniverayan Gudi | $15^0$13'05.29N $76^0$24'14.82E |
| HW-12 | Ramasagara | near Renu-kamma House | $15^0$16'03.02N $76^0$23'04.68E | HW-37 | Kallhalli | Jambaiah Hola | $15^0$13'05.31N $76^0$24'14.41E |
| HW-13 | Ramasagara | near Shi-vamurthy House) | $15^0$16'03.20N $76^0$23'04.41E | HW-38 | Danaapura | Galemma temple Hola | $15^0$19'29.73N $76^0$35'32.63E |
| HW-14 | Sanaapura | near Narasim-ha House | $15^0$16'03.36N $76^0$23'04.22E | HW-39 | Danaapura | Hampinkatte | $15^0$19'29.52N $76^0$35'32.38E |
| HW-15 | Sanaapura | near Kurugo-su Basappa House | $15^0$16'03.08N $76^0$23'04.12E | HW-40 | Danaapura | Ayyanhalli | $15^0$19'29.81N $76^0$35'32.42E |
| HW-16 | Devasamudra | near Health Centre | $15^0$20'49.07N $76^0$38'07.89E | HW-41 | M M Halli | Anjinappa Home | $15^0$09'29.33N $76^0$20'48.93E |
| HW-17 | Devasamudra | Krishna Naga-ra Camp | $15^0$20'49.28N $76^0$38'07.52E | HW-42 | D N Kere | Nandi Banda | $15^0$35'41.24N $76^0$53'52.60E |
| HW-18 | Devasamudra | Harejayagnuru | $15^0$20'49.32N $76^0$38'07.49E | HW-43 | D N Kere (De-valapura) | Shyari Durgammana Gudi | $15^0$35'41.48N $76^0$53'52.77E |
| HW-19 | Hampadevan-ahalli | Chikka Jaya-ganuru | $15^0$19'38.45N $76^0$41'35.41E | HW-44 | D N Kere (Gol-larahalli) | near Gowdru Ven-katesh House | $15^0$06'67.54N $76^0$22'20.30E |
| HW-20 | Hampadevan-ahalli | Near Dugu-lamma Temple | $15^0$19'38.45N $76^0$41'35.34E | HW-45 | Nagalapura | Hullinamane | $15^0$08'36.55N $76^0$23'54.98E |
| HW-21 | Devalapura | opp Ma-hadevana House | $15^0$35'42.10N $76^0$53'52.99E | HW-46 | Nagalapura | Byalakundi | $15^0$08'36.17N $76^0$23'54.60E |
| HW-22 | Devalapura | Nallapur | $15^0$35'42.26N $76^0$53'52.54E | HW-47 | Nagalapura (Gunda) | Near gowri Swami | $15^0$08'36.24N $76^0$23'54.76E |
| HW-23 | Gadiganuru | Opp Mallikar-juna House | $15^0$12'24.40N $76^0$35'21.35E | HW-48 | Chilakanahatti | Thimlapura | $15^0$04'33.23N $76^0$21'02.73E |
| HW-24 | Gadiganuru | Opp Hospital | $15^0$12'24.20N $76^0$35'21.41E | HW-49 | Chilakanahatti | Pootalakatte | $15^0$04'33.17N $76^0$21'02.51E |
| HW-25 | Bylavaddigeri | Opp Hospital | $15^0$14'55.68N $76^0$31'53.66E | HW-50 | Chilakanahatti | Ajanta Nagalinga mata | $15^0$04'33.29N $76^0$21'02.61E |

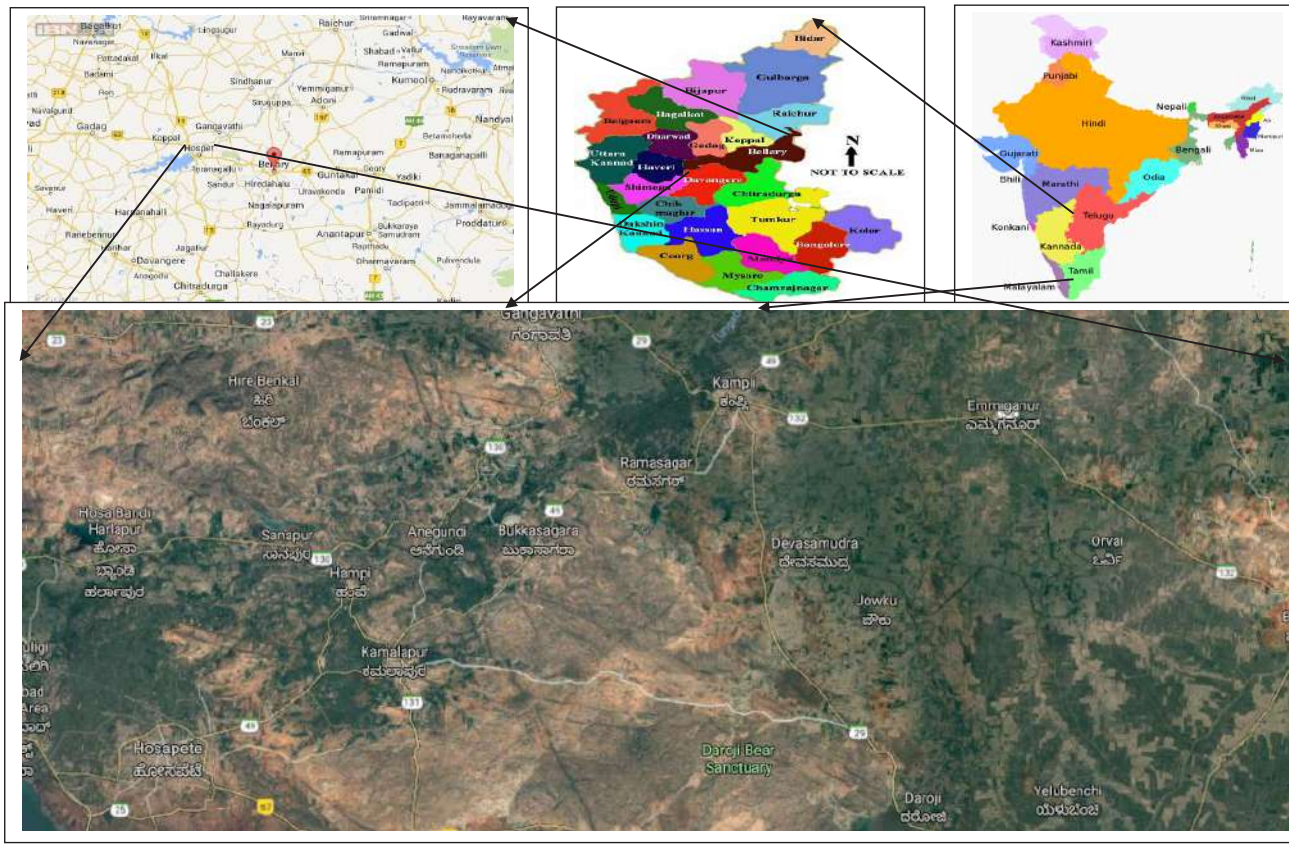


Fig. 1: Location map of the north-east of the Hospet Taluk, Bellary region.

Calcium content in the groundwater samples (Fig. 3(c)) ranged from a minimum of 40 $mg.L^{-1}$ in HW-17 (Ramasagara near Sugandi Renukamma House) to a maximum of 412 $mg.L^{-1}$ in HW-27 (Byluvaddigere near Kakubaal) during post-monsoon season. In the monsoon period (Fig. 3(b)), the calcium content ranged from a minimum of 42 $mg.L^{-1}$ in HW-42 (D.N.Keri near Nandibanda) to a maximum of 412 $mg.L^{-1}$ in HW-50 (Chilakanahatti near Ajatha Nagalinga Mata). In the pre-monsoon season (Fig. 3(a)), the calcium content ranged from a minimum of 20 $mg.L^{-1}$ in HW-48 (Chilakanahatti near Thimmalapura)) to a maximum of 421 $mg.L^{-1}$ in HW-27 (Byluvaddigere near Kakubaal).

The BIS permissible limit for calcium is 200 $mg.L^{-1}$. However, in the current work, 81% of the groundwater samples were within the permissible limit of drinking water guidelines of BIS. The remaining 18% of the groundwater samples in the pre-monsoon period and 17% of groundwater samples in the post-monsoon period are above the prescribed limit. The calcium content of 1% of water samples is below 75 $mg.L^{-1}$ during three seasons (Fig. 3(a), 3(b), and 3(c)). In the present study, thematic maps of $Mg^{++}$ of the study area showed that 67% of pre-monsoon and 74% of post-monsoon seasons groundwater samples have magnesium concentration below 30 $mg.L^{-1}$. 19% of the groundwater samples have magnesium content above 50 $mg.L^{-1}$ in both seasons. The remaining samples were in the range of 30 $mg.L^{-1}$ to 50 $mg.L^{-1}$. This study revealed that during both seasons almost all the groundwater samples were within the permissible level and suitable for drinking purposes owing to low magnesium content. $Mg^{++}$ content in the assessed groundwater samples (Fig. 4(c)) ranged from a minimum of 12.6 $mg.L^{-1}$ in HW-17 (Ramasagara (Sugandi Renukamma House) to a maximum of 153 $mg.L^{-1}$ in HW-27 (Byluvaddigere near Kakubaal) during post-monsoon season. In the monsoon period in Fig. 4(b), magnesium content ranged from a minimum of 7.0 $mg.L^{-1}$ in HW-2 (Hosuru Near Railway gate) and a maximum of 68 $mg.L^{-1}$ in HW-41 (M.M.Halli near Anjinappa home). In the pre-monsoon season (Fig. 4(a)), magnesium content ranged from a minimum of 11.4 $mg.L^{-1}$ in HW-48 (Chilakanahatti near Thimmalapura) and a maximum of 78 $mg.L^{-1}$ in HW-27 (Byluvaddigere near Kakubaal).

The spatial values in the map of the study area revealed that 1% of the groundwater samples in the pre-monsoon peri-

od and 6% of the groundwater samples in the post-monsoon period have $SO_4^{2-}$ content less than 50 mg.$L^{-1}$. 87% of the groundwater samples in the pre-monsoon period and 81% of the groundwater samples in the post-monsoon period have sulfate content in the range of 50-100 mg.$L^{-1}$. 12% of the groundwater samples in the pre-monsoon period and 13% of the groundwater samples in the post-monsoon season have $SO_4^{2-}$ content more than 100 mg.$L^{-1}$. Swarna Latha (2010) also found the same trend of $SO_4^{2-}$ concentration in her studies.

In the present study, the $SO_4^{2-}$ concentration varied between a minimum of 10.9 mg.$L^{-1}$ in HW-40 (Danapura near Iyyanahalli) to a maximum of 82 mg.$L^{-1}$ in HW-10 (Bukkasagara (76 Venkatapura Main road near Hanuman Temple) during the post-monsoon season (Fig. 5(c)). In the monsoon season (Fig. 5(b)), the $SO_4^{2-}$ content in the groundwater samples ranged from a minimum of 9.3 mg.$L^{-1}$ in HW-40 (Danapura near Iyyanahalli) and a maximum of 84 mg.$L^{-1}$ in HW-10 (Bukkasagara (76 Venkatapura Main road near Hanuman Temple). In the post-monsoon period (Fig. 5(a)), the $SO_4^{2-}$ content in the groundwater samples ranged from a minimum of 8.9 mg.$L^{-1}$ in HW-40 (Danapura near Iyyanahalli) and a maximum of 83 mg.$L^{-1}$ in HW-10 (Bukkasagara (76 Venkatapura Main road near Hanuman Temple).

Agricultural Indices that were adopted in the present study are SH, MC, $Na^+$, SAR, RSC and PI, Gibbs class I and II (anion and cation) ratio, which are relevant variables for assessing the suitability of groundwater for agricultural purposes. The irrigation indicators are adopted to categorize ground-water quality into excellent to unfit. Equations for the various hazards are adapted from Asante-Annor et al. (2018).

A salinity hazard is a major constituent of irrigation water quality that reflects crop growth and yields. The SAR values using the USSL diagram show that all the samples have less SAR value. Out of 50 samples, 03, 04, and 03 samples come under the C1-S1 category; 33, 35, and 25 samples come under the C2-S1 category in pre-monsoon, monsoon, and post-monsoon periods. Correspondingly 08, 06, and 04 samples come under the C1-S2 category; and 05, 06, and 12 samples come under the C2-S2 category (Fig. 3). The C3-S1 group in the USSL diagram (Fig. 6) is considered as a moderate water category for irrigation. These imply that

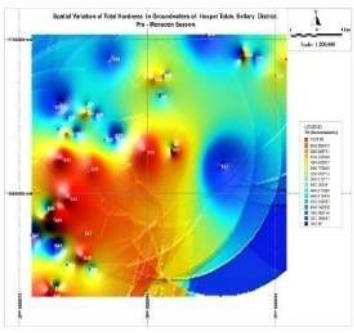

Fig. 2(a):

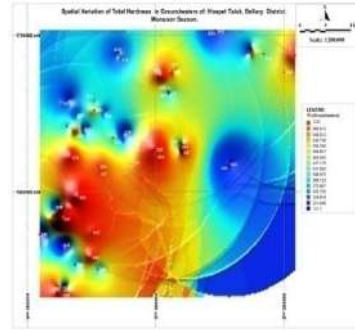

Fig. 2(a):

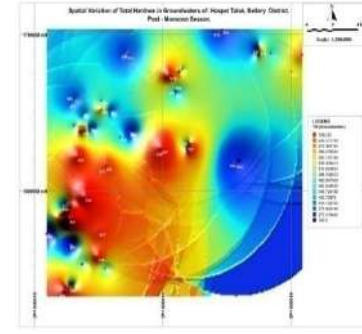

Fig. 2(a):

Average of three seasons level of TH (mg/L) at selected areas of Hospet Taluk.

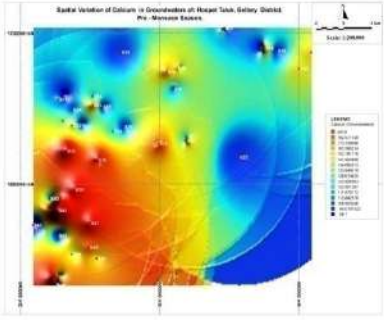

Fig. 3(a):

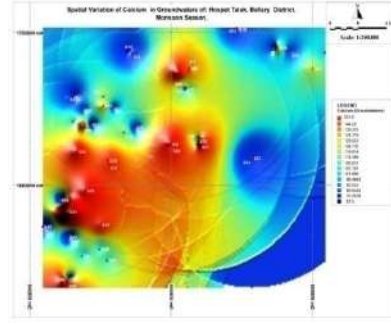

Fig. 3(a):

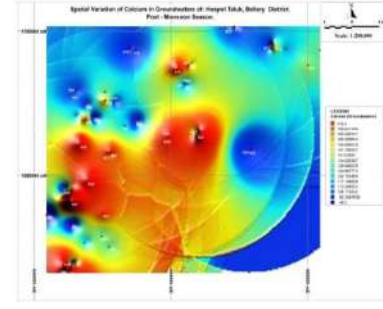

Fig. 3(a):

Average three seasons level of Ca++ (mg.L-1) at selected areas of Hospet Taluk.

no alkali hazard to the crops is expected. 41 Location (82%) samples come under the C3–S1 category and this category is fit for irrigational needs.

In the pre-monsoon and post-monsoon seasons, only 01 and 03 samples had the highest SAR. Irrigation water affects permeability on shrinking types in clay-type soils if the SAR is >6 to 9 (Karuppannan & Kawo 2018). Overall in the entire study period, SAR value percentage comes under C2-S1 during pre-monsoon (60%), monsoon (70%), and post-monsoon (50%) periods respectively. The source of salt in water can be introduced to the water either manually or by natural processes such as the weathering of rocks when the water permeates through them. EC or TDS are commonly used to calculate SH hazards. When the EC is increased, the amount of water available to the crops is reduced, leading to a deficit and low crop yield.

Sodium adsorption ratio (SAR) is a measure of the amount of sodium ($Na^{+}$) relative to calcium ($Ca^{++}$) and magnesium ($Mg^{++}$) in the water extract from saturated soil paste (Kesari et al. 2016). It gives the sodicity of the soil through quantitative chemical assessment of water in contact with it. According to Richards (1954), categorization of SAR values is: < 10 (Low sodium in water, little danger), 10 to 18 (affects the texture of the soil as the soil is sensitive to $Na^{+}$), 18 to 26 (maximum $Na^{+}$; affects the entire soil), and > 26 (unsatisfactory and high sodium). As per the classification, SAR values in the study area varied from 4.86 meq.$L^{-1}$ in HW-41 (M.M.Halli near Anjinappa home) to 48.82 meq.$L^{-1}$ in HW-34 (Hosapete near Chittavadigeppa temple) during the post-monsoon period, and in the monsoon period, SAR values varied between 4.07 meq.$L^{-1}$ in HW-41 (M.M.Halli near Anjinappa home) to 17.82 meq.$L^{-1}$ in HW-2 (Hosuru Near Railway gate). During pre-monsoon season SAR values varied from 0.64 meq.$L^{-1}$ in HW-35 (Kallahalli near Vysyanakeri Station) to 8.82 meq.$L^{-1}$ in HW-05 (Kamalapura Opp to Vet. Hospital). SAR values of three periods were shown in decreasing order: pre-monsoon (48.82 meq.$L^{-1}$) > monsoon (17.82 meq.$L^{-1}$) > post-monsoon season (8.82 meq.$L^{-1}$). Seasonal distribution of values of groundwater samples predicts a relatively low minimum value of SAR in the post-monsoon period, and hence, the samples can be used for irrigation on almost any soil type and have only a slight risk of sodium permeating in the soil (Bozdag 2015 & Shammi et al. 2016).

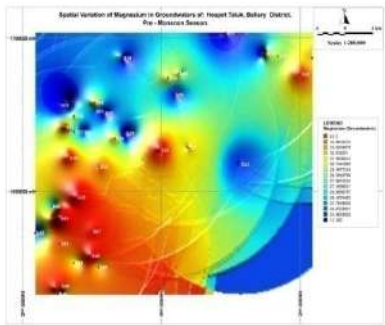

Fig. 4(a):

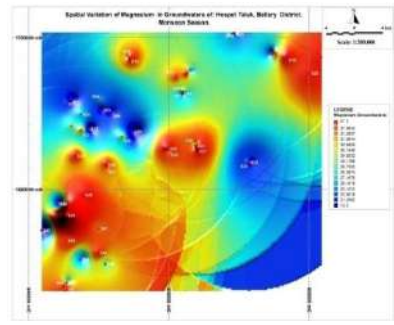

Fig. 4(a):

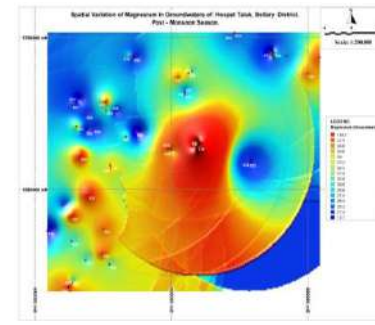

Fig. 4(a):

Average three seasons level of Mg++ (mg/L) at Selected Areas of Hospet Taluk.

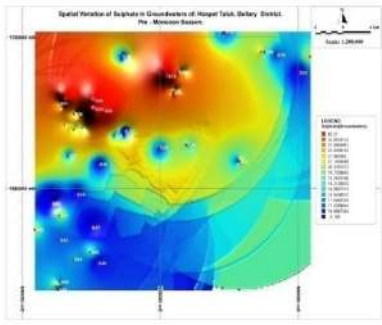

Fig. 5(a):

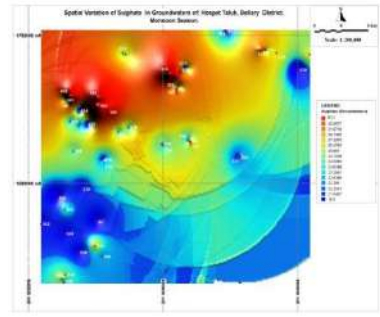

Fig. 5(a):

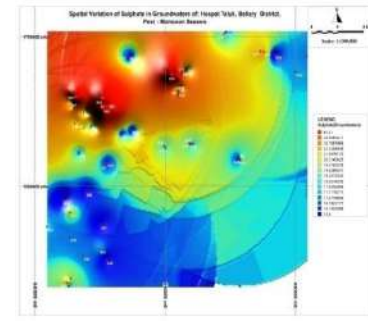

Fig. 5(a):

Average three season level of SO42- (mg/L) at Selected Areas of Hospet Taluk.

According to SAR, the samples from the study area were classified as having a medium level of risk of sodium in the soil. If the SAR values are more than 10 and 26, the irrigation water permeability reduces in clayey soil, causing plant and soil degradation (Bozdag et al. 2015). The higher the SAR values in the water, the higher the sodium (Vasanthavigar et al. 2016).

Seasonal observation during the post-monsoon period shows that 18% of the groundwater samples fall under the good category, and 82% of groundwater samples fall under the excellent category. In the pre-monsoon period, all the samples fall under the excellent category. During the monsoon season, 8% of the groundwater samples fall under the good category, 92% of the groundwater samples fall under the excellent category. However, none of the groundwater samples are within the permissible, doubtful, and unsuitable categories. This may be because of agricultural activities. Based on Na% (Table 2 and 3), all the groundwater samples < 20 falls under the excellent to good Class-I irrigation water. Table 3 shows the suitability of irrigation water based on $Na^{+}$%.

Excess of $Mg^{++}$ in the soil effects easily the crop yield. In three periods $Mg^{++}$ value is more than the permissible limit except for one location. In the pre-monsoon period, the groundwater samples have a minimum value of 14.71 meq.$L^{-1}$ in HW-50 (Chilakanahatti near AjathaNagalinga Mata) and a maximum value of 40.25 meq.$L^{-1}$ in HW-48 (Chilakanahatti near Thimmalapura). During the monsoon season, the groundwater samples have a maximum value of 41.30 meq.$L^{-1}$ in HW-43 (D.N.Keri, Devalapura near Shayari Durugamma Temple) and a minimum value of 14.67 meq.$L^{-1}$ in HW-50 (Chilakanahatti near AjathaNagalinga Mata), and in the post-monsoon period, the groundwater samples have a maximum value of 43.41 meq.$L^{-1}$ in HW-43 (D.N.Keri, Devalapura near Shayari Durugamma Temple) and a minimum value of 16.60 meq.$L^{-1}$ in HW-50 (Chilakanahatti near AjathaNagalinga Mata). The spatial allocation of MH in groundwater shows that almost all the samples are within the

Table 2: SAR values for the selected groundwater samples in Hospet Taluk during three seasons.

| | HW-1 | HW-2 | HW-3 | HW-4 | HW-5 | HW-6 | HW-7 | HW-8 | HW-9 | H W - 10 | HW-11 | H W - 12 | HW-13 |
|---|---|---|---|---|---|---|---|---|---|---|---|---|---|
| Pre | 2.396 | 1.821 | 6.399 | 1.491 | 8.820 | 1.453 | 7.155 | 7.177 | 5.103 | 5.195 | 6.772 | 4.918 | 4.691 |
| Monsoon | 12.612 | 17.179 | 5.495 | 5.952 | 6.406 | 12.200 | 15.897 | 8.560 | 7.012 | 6.151 | 8.905 | 15.517 | 7.171 |
| Post | 12.996 | 16.393 | 5.909 | 6.164 | 6.669 | 12.539 | 15.781 | 9.076 | 6.963 | 6.007 | 9.488 | 15.868 | 7.607 |
| | HW-14 | H W - 15 | HW-16 | HW-17 | H W - 18 | HW-19 | HW-20 | HW-21 | HW-22 | H W - 23 | HW-24 | H W - 25 | HW-26 |
| Pre | 5.897 | 2.267 | 1.425 | 1.854 | 1.089 | 1.335 | 3.160 | 1.985 | 2.130 | 2.357 | 4.365 | 6.985 | 6.250 |
| Monsoon | 8.627 | 9.721 | 8.640 | 11.185 | 9.797 | 7.163 | 6.584 | 8.052 | 8.974 | 9.828 | 11.321 | 11.785 | 9.173 |
| Post | 9.104 | 9.889 | 8.605 | 13.140 | 9.501 | 7.387 | 7.077 | 8.178 | 8.814 | 10.449 | 12.421 | 12.452 | 9.482 |
| | HW-27 | H W - 28 | HW-29 | HW-30 | H W - 31 | HW-32 | HW-33 | HW-34 | HW-35 | H W - 36 | HW-37 | H W - 38 | HW-39 |
| Pre | 4.328 | 1.729 | 1.799 | 1.469 | 1.058 | 0.806 | 1.747 | 1.942 | 0.644 | 1.138 | 1.350 | 0.801 | 1.663 |
| Monsoon | 8.547 | 7.010 | 9.332 | 5.081 | 6.687 | 5.950 | 7.205 | 11.328 | 9.090 | 6.511 | 6.929 | 12.100 | 8.851 |
| Post | 5.102 | 6.863 | 9.758 | 5.681 | 7.912 | 6.029 | 8.172 | 18.823 | 6.207 | 7.039 | 6.928 | 12.656 | 8.773 |
| | | H W - 40 | HW-41 | HW-42 | H W - 43 | HW-44 | HW-45 | HW-46 | HW-47 | H W - 48 | HW-49 | H W - 50 | |
| | Pre | 4.838 | 2.559 | 8.042 | 5.634 | 3.711 | 1.296 | 3.086 | 4.057 | 1.013 | 0.940 | 4.838 | |
| | Monsoon | 8.783 | 4.074 | 8.162 | 7.381 | 8.263 | 5.430 | 5.017 | 4.882 | 5.531 | 6.471 | 8.783 | |
| | Post | 9.907 | 4.156 | 9.294 | 9.005 | 8.330 | 5.520 | 5.668 | 5.407 | 5.363 | 8.178 | 5.115 | |

Table 3: Suitability of irrigation water based on Na %.

| Parameters | Range | Classification | Number of Samples | | |
|---|---|---|---|---|---|
| | | | Pre-Monsoon | Monsoon | Post- Monsoon |
| %$Na^+$ Wilcox 1955 | < 20 | Excellent | All most all the groundwater locations | HW-1, HW-3, HW-10, HW-11, HW-13, HW-14, HW-15, HW-16, HW-18, HW-19, HW-20, HW-21, HW-22, HW-23, HW-24, HW-25, HW-26, HW-27, HW-28, HW-29, HW-30, HW-31, HW-32, HW-33, HW-34, HW-35, HW-36, HW-37, HW-38, HW-39, HW-40, HW-41, HW-42, HW-43, HW-44, HW-45, HW-46, HW-47, HW-48, HW-49, HW-50 | HW-3, HW-4, HW-5, HW-6, HW-8, HW-9, HW-10, HW-11, HW-13, HW-14, HW-15, HW-16, HW-18, HW-19, HW-20, HW-21, HW-22, HW-23, HW-26, HW-27, HW-28, HW-29, HW-30, HW-31, HW-32, HW-33, HW-35, HW-36, HW-37, HW-38, HW-39, HW-40, HW-41, HW-43, HW-44, HW-45, HW-46, HW-47, HW-48, HW-49, HW-50 |
| | 20 – 40 | Good | - | HW-2, HW-7, HW-12, HW-17 | HW-1, HW-2, HW-7, HW-12, HW-17, HW-24, HW-25, HW-34, HW-42 |
| | 40 – 60 | Permissible | - | - | - |
| | 60 – 80 | Doubtful | - | - | - |
| | > 80 | Unsuitable | - | - | - |

range of 50 meq.$L^{-1}$ and are fit for irrigation. The maximum magnesium ratio value of the observed samples is 43.41 meq.$L^{-1}$ in HW-43 at D.N.Keri, Devalapura near Shayari Durugamma Temple) on magnesium ratio.

The MH values of the study area range from 14.67 at HW-50 (Chilakanahatti near Ajatha Nagalinga Mata) to 43.41 meq.$L^{-1}$ at HW-43 (D.N.Keri, Devalapura near Shayari Durugamma Temple) with a mean value of 32.06). Almost all the groundwater samples (100%) are within magnesium hazard of 50 which are considered beneficial and fit for irrigation use. In the present work, Gibbs ratio I (Anion) values in the pre-monsoon period vary from 0.05 to 0.40, in the monsoon period varies from 0.05 to 0.42, and in the post-monsoon period varies from 0.06 to 0.42. Gibbs ratio

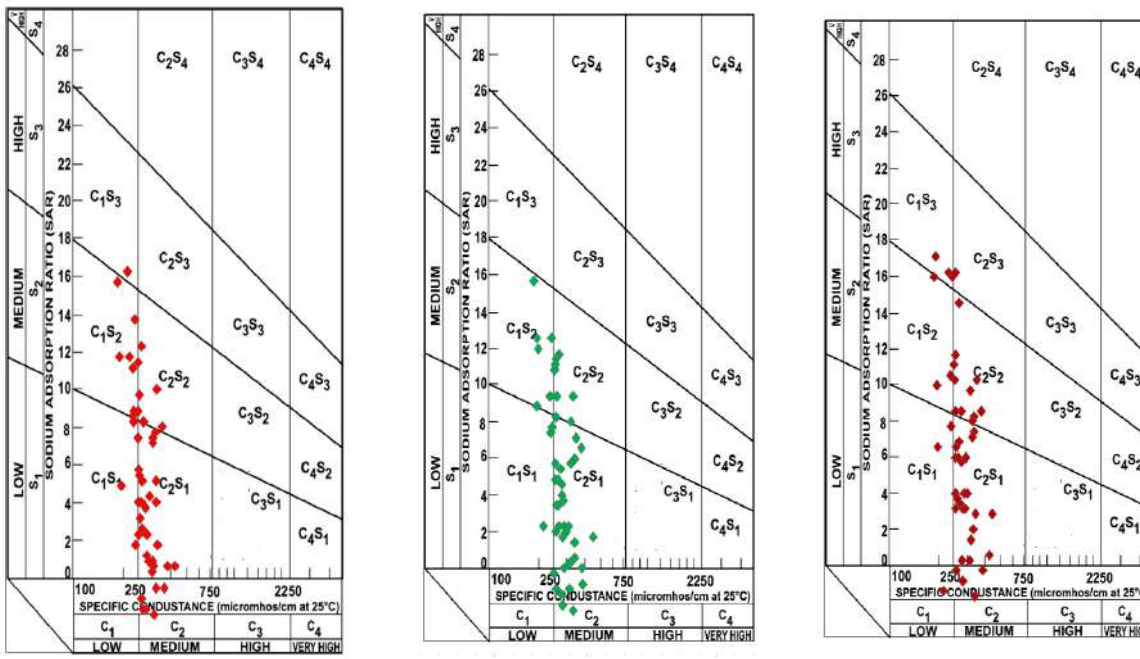


Fig. 6: SH classification of the groundwater locations according to the USSL diagram for pre- and post-monsoon and monsoon seasons.

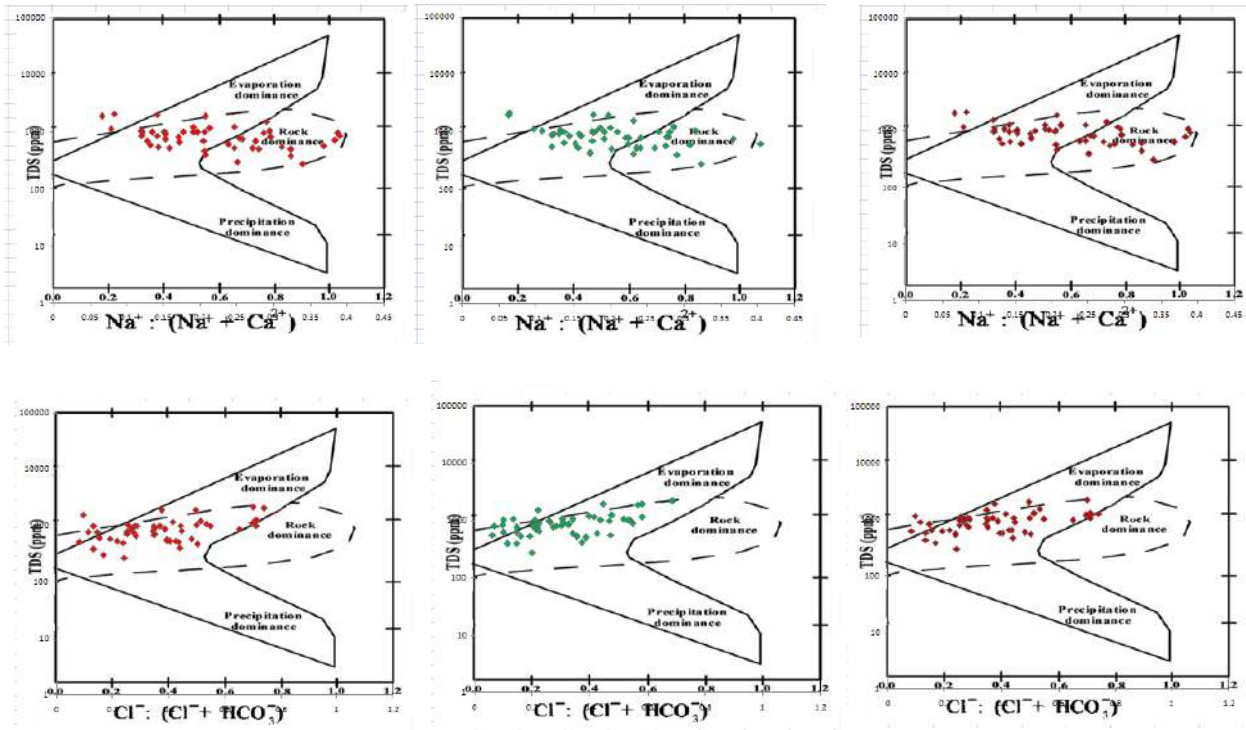


Fig. 7: Seasonal variations in mechanism controlling the quality of groundwater.

II (Cation) values vary from 0.12 to 0.78, 0.11 to 0.72, and 0.21 to 0.81 during three seasons respectively According to Fig. 7, the samples in the study area fall into the rock dominance area, indicating rocks in the groundwater in the aquifers. This affects the hydrochemistry of groundwater in alluvial plains and rock–water contact (Wu et al. 2015).

## CONCLUSION

Most of the selected locations had TH content within the permissible limit. The results showed the order of $Cl^- > SO_4^{2-} > HCO^{3-}$ with water types Na-$Cl^-$ and $Cl^-$, and the order of $Na^+ > Mg^{++} > Ca^{++} > K^+$ with $Na^+$ and $Mg^{++}$ as the dominant anions and cations, correspondgly. As per the Wilcox diagram no-alkali exposure to the crops is expected. Forty one samples (82%) fit within the C3–S1 group; this category is fit for irrigational needs. Only 01 and 03 samples showed maximum SAR during two seasons like pre-monsoon and post-monsoon periods. The GIS maps of the respective variables indicated that groundwater are usually of higher quality, whereas the presence of dolomite indicates a reduction in water quality.

## REFERENCES

Adiat, K.A.N., Nawawi, M.N.M. and Abdullah, K. 2012. Assessing the accuracy of GIS-based elementary multicriteria decision analysis as a spatial prediction tool: A case of predicting potential zones of sustainable groundwater resources. J. Hydrol., 440–441: 75-89.

APHA. 2005 Standard Methods for the Examination of Water and Wastewater. 21st Edition, American Public Health Association/American Water Works Association/Water Environment Federation, Washington DC.

Asante-Annor, A., Bewil, P.N. and Boateng, D. 2018. Evaluation of groundwater suitability for irrigation in the Lambussie-Karni district of Ghana. Ghana Mining J., 18(1): 9-19.

Bozdag, A. 2015. Combining AHP with GIS for assessment of irrigation water quality in Cumra irrigation district (Konya), Central Anatolia, Turkey. Environ. Earth Sci., 73: 8217-8236.

Champidi, P., Stamatis, G. and Zagana, E. 2011. Groundwater quality assessment and geogenic and anthropogenic effect estimation in Erasinos Basin (E. Attica). European Water, 33: 11-27.

Elubid, A.B., Tao Huang, T., Ekhlas, H., Ahmed, E.H., Zhao, J., Elhag, K.M., Abbass, W. and Babiker, M.M. 2019. Geospatial distributions of groundwater quality in Gedaref State using geographic information system (GIS) and drinking water quality index (DWQI). Int. J. Environ. Res. Public Health, 16(5): 2-20.

EPA. 2009. The United States Environmental Protection Agency. http://www.epa.gov/ogwdw000/kids/wsb/pdfs/9124.pdf. Accessed on 30 December 2009.

Freeze, R.A. and Cherry, J.A. 1979. Groundwater. Prentice-Hall, Upper Saddle River.

Hemant, P. and Limaye, S. N. 2012. Assessment of physico-chemical quality of groundwater in a rural area nearby Sagar city, MP, India. Adv. Appl. Sci. Res., 3(1); 555-562.

Honarbakhsh, A., Tahmoures, M., Tashayo, B., Mousazadeh, M., Ingram, B., and Ostovari, Y. 2019. GIS-based assessment of groundwater quality for drinking purposes in the northern part of Fars Province, Marvdasht. J. Water Supply: Res. T-Aqua., 68(3): 187-196

Kawo, N.S. and Karuppannan, S. 2018. Groundwater quality assessment using water quality index and GIS technique in Modjo River Basin, Central Ethiopia. J. Afr. Earth Sci., 147: 300-311.

Kesari, T., Ramakumar, K.L., Chidambaram, S., Pethperumal, S. and Thilagavathi, R. 2016. Understanding the hydro-chemical behavior of groundwater and its suitability for drinking and agricultural purposes in Pondicherry area, South India: A step towards sustainable development. Groundwater Sustain. Dev., 2-3: 143-153.

Madan, K.J., Chowdary, V.M. and Chowdhury, A. 2010. Groundwater assessment in Salboni Block, West Bengal (India) using remote sensing, geographical information system, and multi-criteria decision analysis techniques. Hydrogeol. J., 18(7): 1713-1728.

Mallick, J., Singh, C.K., Al Wadi, H., Ahmed, M., Rahman, A., Shashtri, S. and Mukherjee S. 2015. Geospatial and geostatistical approach for groundwater potential zone delineation. Hydrol. Process., 10: 153.

Mukherjee, P., Singh, C.K. and Mukherjee, S. 2012. Delineation of groundwater potential zones in the arid region of India: A remote sensing and GIS approach. Water Resour. Manag., 26(9): 2643-2672

Pujari, P.R., Padmakar, C., Labhasetwar, P.K., Mahore, P. and Ganguly, A.K. 2012. Assessment of the impact of on-site sanitation systems on groundwater pollution in two diverse geological settings: A case study from India. Environ. Monit. Assess., 184(1): 251-263.

Richards, L.A. 1954. Diagnosis and Improvement of Saline Alkali Soils. Agriculture, 160, Handbook 60, US Department of Agriculture, Washington DC.

Shammi, M., Karmakar, B., Rahman M.M., Islam, M.S., Rahman, R. and Uddin M.K. 2016 Assessment of salinity hazard of irrigation water quality in the monsoon season of Batiaghata Upazila, Khulna District, Bangladesh, and adaptation strategies. Pollution, 2: 183-197.

Swarna Latha, P. 2010. Studies on spatial and temporal changes of land use and land cover groundwater quality and shoreline of greater Vishakapatanum municipal corporation, Andrpradesh, India using remote sensing and GIS techniques. Ph.D, thesis, Andra University, Vishakapatanum.

Vasanthavigar, M., Srinivasamoorthy, K., Rajiv Gandhi, R., Vijayaraghavan, K. and Sarma, L.S. 2016. Characterization and quality assessment of groundwater with a special emphasis on irrigation utility: Thirumanimuttar sub-basin, Tamil Nadu, India. Arab. J. Geosci., 5(2): 245-258.

Verma, A.K. and Singh, T.N. 2013 Prediction of water quality from simple field parameters. Environ. Earth Sci., 69(3): 821-829.

Wu, J., Li, P. and Qian, H. 2015 Hydrochemical characterization of drinking groundwater with special reference to fluoride in an arid area of China and the control of aquifer leakage on its concentrations. Environ. Earth Sci., 73: 8575-8588.

Nature Environment and Pollution Technology
An International Quarterly Scientific Journal

p-ISSN: 0972-6268
(Print copies up to 2016)
e-ISSN: 2395-3454

Vol. 20 | No. 5 (Suppl) | pp. 2079-2086 | 2021

Original Research Paper

https://doi.org/10.46488/NEPT.2021.v20i05.025

Open Access Journal

# Evaluation of Waste Plastic Pyrolysis Oil Performance with Diethyl Ether Additive on Insulated Piston Diesel Engine

**S. Padmanabhan*†, C. Joel**, Linda Joel***, Obulareddy Yuvatejeswar Reddy*, K.G.D. Sri Harsha* and S. Ganesan******

*School of Mechanical and Construction, Vel Tech Rangarajan Dr. Sagunthala R&D Institute of Science and Technology, Chennai, India

**Department of Mechanical Engineering, Easwari Engineering College, Chennai, India

***Department of Mathematics, SRM Institute of Science and Technology, Ramapuram, Chennai, India

****Department of Mechanical Engineering, Sathyabama Institute of Science and Technology, Chennai, India

†Corresponding author: S. Padmanabhan; padmanabhan.ks@gmail.com

**Nat. Env. & Poll. Tech.**
**Website: www.neptjournal.com**

*Received:* 21-05-2021
*Revised:* 24-06-2021
*Accepted:* 04-07-2021

**Key Words:**
Thermal barrier coating
Coated piston
Diethyl ether
Diesel engine
Waste plastic pyrolysis oil

## ABSTRACT

Considering the amount of waste plastics has risen significantly, energy may be extracted from it. Not only is it possible to dispose of waste plastics by converting them to fuel, but it is also possible to extract energy from them. Our research is motivated by the prospect of using waste plastics as a source of energy through waste plastic pyrolysis oil (WPPO). The innovation of this research is that it will assess the efficiency of plastic pyrolysis oil derived from Low-Density Polyethylene (LDPE) on a Thermal Barrier Coated (TBC) piston engine. The incremental ratio of WPPO to pure diesel with the addition of diethyl ether (DEE) was determined and its output and exhaust emission standards were evaluated using a direct injection single cylinder low heat rejection diesel engine. The results for the WPPO blends were promising as with TBCW20DEE10 demonstrating a 5 to 15% increase in carbon monoxide under different load conditions. TBCW20DEE10 confirmed a greater reduction of hydrocarbons varying from 5 to 12 %. At half load condition, TBCW20DEE10 emits approximately 3.5 % less unit of smoke.

## INTRODUCTION

The world's use of plastics is increasing daily, and the world is yet to discover a suitable substitute. Disposal of plastic products after use poses a significant risk. The most environmentally friendly way to dispose of waste plastics is to turn them into energy fuel. Rajan et al. (2016) examined the efficiency and combustion characteristics of a diesel engine fueled by recycled plastics. The results indicated that the engine would run on waste plastic oil and its mixtures without modification can be used as a substitute for diesel fuel. Gungor et al. (2015) analyzed waste plastic oil and contrasted it to fuel in a multi-cylinder diesel engine. Thermal performance significantly decreased when pure WPPO was used. The concentrations of carbon monoxide and nitrogen oxides increased.

Mangesh et al. (2017) conducted an exhaustive analysis of waste plastic oil conversion methodology, research, and property characteristics, resulting in a greater understanding of waste plastic oil fuel conversion as an alternate fuel. Bridjesh et al. (2018) made an effort to replace diesel with half the amount of WPPO and the additives diethyl ether and methoxyethyl acetate. Sachuthananthan et al. (2019) combined different ratios of magnesium oxide nanoparticles with plastic pyrolysis oil. The investigation was conducted to determine the effect of compression ignition on the physicochemical properties of the engine. Singh et al. (2020) developed pure plastic pyrolytic oil without using a catalyst and analyzed the fuel properties. The plastic oil blends were checked on the engine and it was determined that using 50% blends results in a marginal loss of performance and a nominal rise in emissions. Mani et al. (2011) investigated the oxidation of plastic oil in a diesel engine. It has been compared to the performance of diesel engines. The exhaustive pollution findings demonstrated a greater spectrum of emissions than standard diesel.

Mangesh et al. (2020b) investigated a novel method for converting unsaturated compounds to saturated compounds through pyrolysis oil hydrogenation. The research investigated the combustion, production, and emission of hydrogenated polypropylene pyrolysis oil mixed with diesel. Das et al. (2020) investigated the performance and emission of a single-cylinder DI four-stroke diesel engine using waste plastic oil (WPO) derived from pyrolysis of waste plastics using Zeolite-A as the catalyst. The engine study revealed improved brake thermal performance up to 20% blends at full load. The NOx and

HC emission is found lower under low load conditions and became higher by increasing the load as compared to diesel. Fuel exergy was significantly increasing after blending WPO with pure diesel, but the exergetic efficiency of the blended fuels followed the reverse trend. However, an increase in load of the engine improved the exergetic efficiency. Hariram et al. (2017) contrasted the properties of plastic pyrolysis oil to those of diesel and also tabulated the properties of blended fuels containing cetane and ethanol. Damodharan et al. (2017) found that the addition of n-butanol reduced diesel pollution while increasing HC emission. Due to the inclusion of 10% n-butanol by volume in comparison to WPPO and diesel, the WPPO blend reduces NOx pollution significantly. However, NOx emissions from higher volume n-butanol blends exceeded the applicable WPPO.

Sivakumar and Bridjesh (2019) and Sambandam et al. (2020) had used a low-heat diesel engine with blended waste plastic oil. WPPO's low-heat engine has proven to have stronger performance than diesel but for NOx emissions. Gnanamoorthi and Jayaram (2018) observed an improvement in frequency thermal performance and a decrease in real fuel consumption for diesel engines covered by thermal barriers. With the exception of hydrocarbon emissions, there was a significant reduction in nitrogen oxide and carbon monoxide emissions with a coated engine. Ramalingam et al. (2016) conducted a preventative study in a diesel engine using copper and cadmium nanocatalyst coated pistons, as contrasted to an uncoated engine. The results showed that a coated piston reduced nitrogen oxide, carbon monoxide, and hydrocarbon emissions significantly.

The primary objective of this study is to evaluate the feasibility of using WPPO as an alternate energy source in the automotive industry. To combat the high-value emissions of WPPO in a diesel engine, a thermal barrier coating on the combustion chamber components is highly desirable. The thermal barrier coated piston is used in this investigation on a single-cylinder diesel engine to evaluate waste plastic oil and to minimize exhaust pollution and increase engine performance, resulting in lower fuel consumption. The incremental ratio of WPPO with oxygenated additive DEE was blended with pure diesel for the experiment, and its output and exhaust emission standards were evaluated on the TBC piston engine.

## MATERIALS AND METHODS

### Thermal Barrier Insulation

Many researchers are actively innovating to boost engine efficiency by changing the engine components. The thermal barrier coating (TBC) on the combustion chamber components is a safer way of keeping heat resistant in the chamber to improve combustion efficiency. Coating materials should have a good thermal expansion coefficient to survive the heat shock during combustion (Patnaik et al. 2017). Thermal barrier coating engines are engines that reduce thermal rejection and recover combustion energy. Piston heat insulation has been incorporated into engines to further minimize heat loss during combustion and thereby improve the thermal performance of diesel engines. Ceramic insulation methods are gaining traction as the planet strives to meet stricter pollution standards while still saving money on diesel. Ceramic materials can exhibit desirable properties such as a strong coefficient of thermal expansion, a greater Poisson's ratio, low thermal conductivity, and a stable phase structure at elevated combustion temperatures (Sivakumar & Senthil Kumar 2014). Among the various coating techniques, some researchers used the plasma spray coating method to avoid heat loss from high-temperature surroundings. Joel et al. (2018) evaluated piston coatings utilizing CAE methods rather than physical experiments. Zirconia and alumina stabilized with yttria are commonly utilized in thermal-barrier components, both of which were left unattended (Thibblin et al. 2018).

### Waste Plastic Pyrolysis Oil

Catalytic pyrolysis may be used to convert used waste plastics into alternative energy fuel for diesel engines. The chemical properties of the plastic pyrolysis fuel vary according to the grade of used plastics and the pyrolysis process used. The low calorific value and excessive viscosity of the plastic pyrolysis oil are the primary drawbacks of using plastic oil as a diesel engine replacement. Mangesh et al. (2020a) studied the properties of four related pyrolysis oils derived from a variety of plastics, including high-density polyethylene, low-density polyethylene, polypropylene, and styrene.

Due to its affordability, Low-Density Polyethylene (LDPE) was used as a type of waste plastic in this study. LDPE is available in a variety of forms, which results in lower intermolecular resistance and, thus, lower tensile strength and stiffness as compared to High-Density Polyethylene (HDPE). Although polyethylene with a low density exhibits far greater elasticity than HDPE, its lateral branching results in a less crystalline shape. It is very resistant to water and is used in a variety of other applications, including garbage containers, garbage cans, covering paper, and packaging. These goods are widely used in daily life, so LDPE waste is collected daily to serve as the second-largest plastic waste stream in solid waste.

Table 1 summarizes the properties of waste plastic pyrolysis oil. WPPO's fuel properties are very close to those of diesel fuel in many critical respects. However, the formulated fuel's combustion and pollution properties must be determined. Additionally, very few experiments have been conducted on the behavior of plastic pyrolysis oil with additives in a thermal coated engine. The current article

Table 1: Properties of waste plastic pyrolysis oil.

| Sl. No. | Properties | Diesel | WPPO | ASTM standards |
|---|---|---|---|---|
| 1 | Calorific Value, kcal/kg | 10952 | 11507 | ASTM D 240 |
| 2 | Kinematic Viscosity at 40°C, cSt | 2.59 | 4.89 | ASTM D 445 |
| 3 | Density @15°C , kg/m$^3$ | 838 | 798 | ASTM D 1298 |
| 4 | Flash Point , °C | 74 | 23 | ASTM D 93 |
| 5 | Fire Point , °C | 85 | 32 | - |
| 6 | Cetane Index | 53 | 65 | ASTM D 613 |

discusses the usage of waste plastic oil derived from LDPE as a possible replacement fuel for existing diesel engines. As a result, the analysis is conducted using different fuel blend percentages and a coated piston to determine the efficiency, combustion, and emission characteristics.

### Experimental Details

The engine investigation was evaluated using a constant speed single-cylinder water-cooled direct injection diesel engine with a power of 4.2 kW. The hand-cranking method was used to start the test engine, and the diesel engine was connected to an eddy current dynamometer. A dynamometer can be used to manually load the engine from zero to maximum load in increments of 25% to 100%, depending on the engine power generated. The test engine was permitted to run under normal test conditions. The engine spins at 1500 rpm and has an 18:1 compression ratio. The AVL di gas analyzer and AVL smoke meter were used to observe the exhaust pollution characteristics.

The use of WPPO was explored by engine efficiency and pollution characteristics measurements. The test was conducted using diesel as the baseline fuel. The blends were prepared on the volume based on 70% diesel and 20% of WPPO and 10 % of DEE as TBCW20DEE10. Similarly, TBCW30DEE10 and TBCW40DEE10 were prepared with 30% and 40% WPPO volume for the testing. The test was carried out on a diesel engine with a coated piston using WPPO blend diesel. The gases emitted by the engines are determined, and they include unburned hydrocarbons (HC), carbon monoxide (CO), nitrogen oxides (NOx), and smoke.

## RESULTS AND DISCUSSION

### Performance Characteristics

**Brake thermal efficiency:** Engine output was determined by the brake thermal efficiency (Fig. 1). The thermal performance of the brakes is determined by the ratio of brake engine power to fuel energy, with fuel energy being

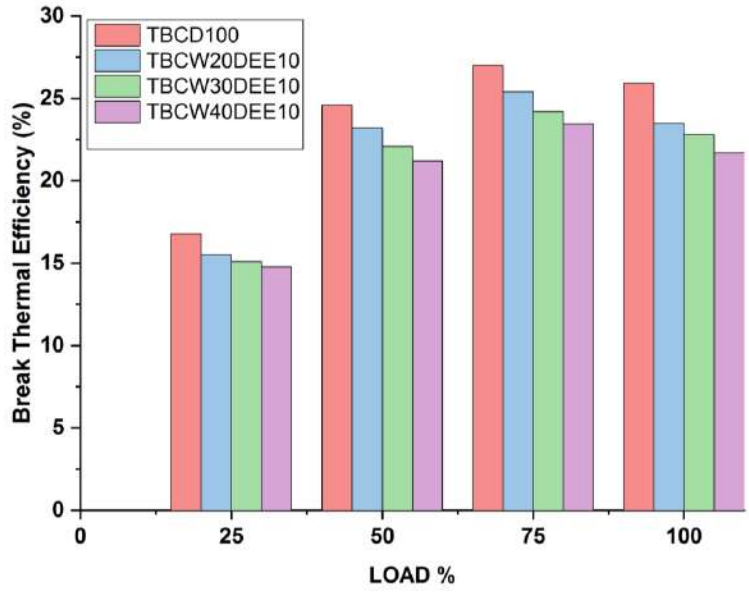


Fig. 1: Evaluation of WPPO's brake thermal efficiency on engine load.

determined by fuel usage and the calorific benefit of fuel blends. At maximum load, the TBCW20DEE10 brake thermal efficiency increased and approached that of the TBCW30DEE10 brake thermal efficiency. A lower exhaust temperature indicates less heat loss during combustion, which results in a better thermal performance of the brakes. When comparing an uncoated TBC engine to one coated with unblended WPPO, similar findings of an increase in brake thermal performance at full load were discovered (Sivakumar & Bridjesh 2019).

WPPO exhibits up to an 80% increase in thermal performance at maximum load (Mani et al. 2011). Due to improved vaporization and air-fuel atomization, the TBC coated engine achieves higher thermal performance, maintains optimum in-cylinder temperatures, improves combustion efficiency, and maintains a consistent ignition pace. Additionally, the TBC coating reduces the reject rate of the combustion chamber, increasing the strength available to generate a unit kW for a limited volume of diesel, resulting in increased brake thermal performance.

**Specific Fuel Consumption:** The engine has a unique specific fuel consumption (SFC) value that varies with speed and load. For example, a reciprocating engine operates at full efficiency only when it absorbs unthrottled air and travels near its torque peak. However, only a few turbines were able to operate at optimum performance. Brake-specific fuel consumption falls by approximately 1.5% to 7.5% for TBCW20DEE10 at various load conditions as compared to TBCD100 as represented in Fig. 2. The coating combustion parts result in a shorter ignition delay time, which results in a lower SFC rating than a conventional diesel engine. SFC rises as the amount of blends containing WPPO increases. This is attributed to WPPO's low atomization owing to its increased viscosity and density.

## Emission Characteristics

**Unburned hydrocarbons:** The majority of hydrocarbons emitted originate from a tested diesel, while others have changed structures as a result of chemical processes occurring within the combustion chamber. When the diesel engine is started or warmed up, HC emissions normally reach the maximum value due to vaporization, a slower oxidation rate, and the fuel mixture (Hariram et al. 2020). In Fig. 3, TBCW20DEE10 demonstrated a higher hydrocarbon reduction efficiency of 5% to 12 %, under different load conditions. Sivakumar and Bridjesh (2019) found that TBC engines emit less hydrocarbons than diesel engines due to the increased amount of heat produced inside the combustion chamber and the results of a ten ppm lower WPPO value than an

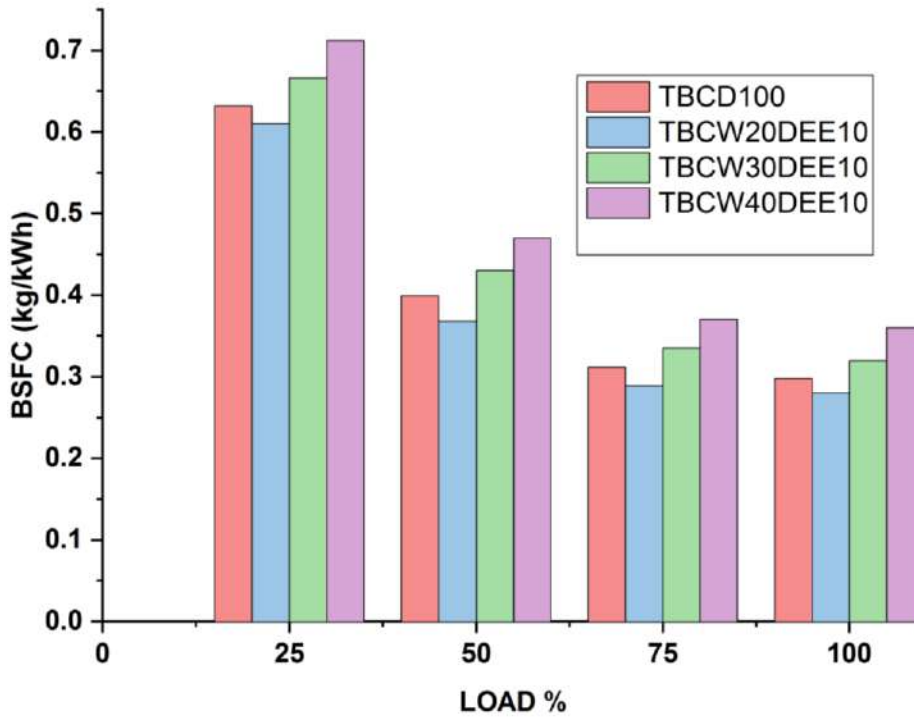


Fig. 2: Evaluation of WPPO's specific fuel consumption on engine load.

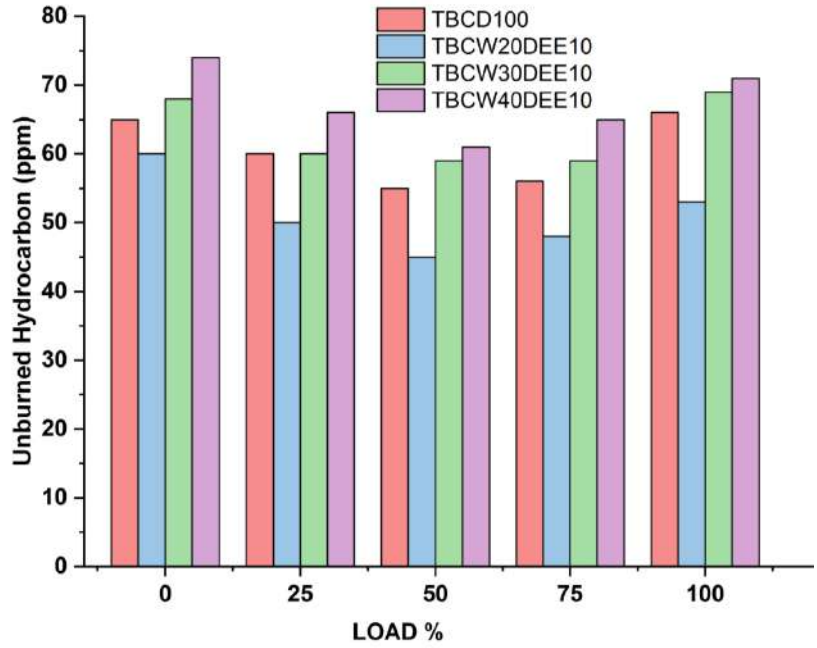


Fig. 3: Evaluation of WPPO's Unburned Hydrocarbons on engine load.

uncoated engine. As the percentage of WPPO increased, HC pollution increased as a result of incomplete combustion and unreacted hydrocarbons. The fuel blends do not extend out through the combustion chamber, and therefore do not burn down around the cylindrical wall or across crevices. The WPPO's low cetane number and reduced auto-ignition characteristics enhance the quenching impact in the leaner mixture area of the cylinder, which increases HC emissions. Additionally, unreactive hydrocarbons do not degrade into saturated compounds through combustion, which are released as exhaust (Singh et al. 2020). The indestructible essence of waste plastic is a product of the presence of unsaturated aromatic mixtures, which increases hydrocarbon emissions.

**Carbon monoxide:** Carbon Monoxide is formed as an intermediate compound during hydrocarbon combustion. The equivalence ratio proportions are the critical element in CO development. The elevated CO concentration is due to increased fuel intake at higher loads. The lower equivalence ratio, along with the increased in-cylinder temperatures, leads to extremely low CO emissions at initial loads. Carbon monoxide emission decreases gradually from low to half load and then increases sharply to maximum load for all the blends shown in Fig. 4. TBCW20DEE10 demonstrated an increase in carbon monoxide elimination of 5% and 15% under different load conditions. Sivakumar and Bridjesh (2019) discovered that TBC engines emit less CO at maximum load than traditional engines. WPPO contains about four percentage oxygen, which helps in full combustion and results in a greater decrease in carbon monoxide production. CO pollutants for the research fuel are reduced in the ceramic coated engine as opposed to the uncoated engine (Aydin et al. 2015).

Additionally, the TBC coating improves the combustion performance of WPPO mixtures by allowing for larger cylinders, which results in slightly increased cylinder pressure, combustion temperature, and air-fuel mixing, as well as oxygen quality. The higher fuel quantity used in combustion, along with the same amount of gas enclosed within a cylinder, results in a rich mixture that produces more CO emissions at maximum engine load. The primary cause of increased CO emissions is fuel-rich combustion inside the cylinder, which results in an insufficient evaporation period for the fuel mixture and an insufficient concentration of oxygen for combustion.

**Nitrogen oxides:** As shown in Fig. 5, all tested fuels exhibit a growing pattern in terms of NOx emission levels. Sivakumar and Bridjesh (2019) found increased NOx emissions in uncoated engines for WPPO and TBC diesel engines, with NOx emissions increasing more for WPPO. This is attributed to the use of larger cylinders and the melting of a thermal film coated with YSZ in the combustion chamber. Mani et al. (2011) found that waste plastic oil generated 25% more NOx as compared to pure diesel at maximum

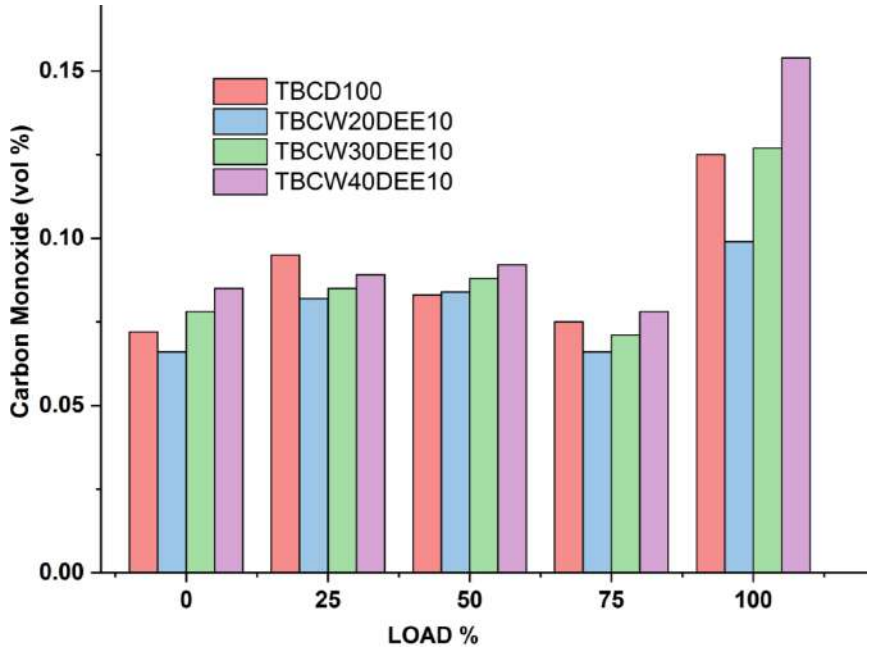


Fig. 4: Evaluation of WPPO's carbon monoxide on engine load.

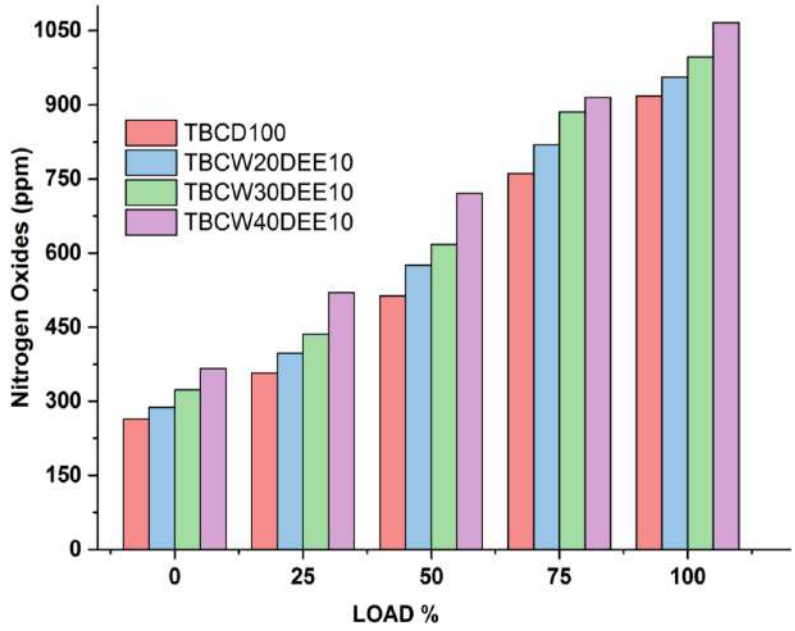


Fig. 5: Evaluation of WPPO's nitrogen oxides on engine load.

load. The primary factor contributing to NOx emission is the increased temperature within the cylinder and the overall peak temperature during the combustion cycle as a result of the lean fuel mixture (Hoang & Pham 2019). NOx development occurs only at the point of combustion termination at increased gas levels, as N2 reacts with O2 at these increased temperatures in the soil. O2 also plays a major part in the formation of NOx.

When oxygen molecules appear at a lean mixing scale, NOx levels rise, resulting in higher combustion temperatures. The Zeldovich process undoubtedly governs the kinetics of NOx production, and some of the differences in NOx are due to oxygen concentration, combustion chamber temperature, surplus air coefficient, and residence time (Nam Cao et al. 2020). The combustion temperature, which increases NOx generation, is another variable that aids in the reaction between N2 and O2 molecules. Temperature, engine revolutions per minute, fuel mixture density, and combustion chamber homogeneity are only a few of the variables that influence NOx output.

**Smoke emission:** Smoke is formed in engines at the diffusion combustion period, where all the fuel atomized droplets are separated into elementary carbon atoms which are later oxidized in the combustion region. WPPO comprises a higher proportion of aromatic elements, it develops an inappropriate fuel mixture and forms a spray, resulting in incomplete combustion and significant smoke emission. Smoke concentrations often arise in the combustion-rich region due to a shortage of oxygen, a higher C/H ratio, a higher viscosity of the fuel, insufficient atomization, and an unnecessary concentration of fuel inside the combustion chamber.

As shown in Fig. 6, TBCD100 emits less smoke than TBCW20DEE10, while TBCW20DEE10 emits approximately 3.5% less HSU smoke at half load. Sivakumar and Bridjesh (2019) found that TBC engines emit less smoke than traditional diesel engines due to the combustion chamber accumulating more heat. Mani et al. (2011) found that waste plastic oil generated 40% more smoke than pure diesel at maximum load. WPPO blends produce more smoke than diesel oil does. As a result, the engine cylinder does not receive a homogeneous charge. The explanation for the increased smoke strength is that the combustion time and flame spreading rate have been decreased. At full load, smoke production occurs as a result of insufficient oxygen and irregular combustion. The intensity difference in smoke is caused by a partial exhaust gas replacement caused by combustion instability. Increased hydrocarbon burning will result in full combustion and a reduction in smoke levels. Alternatively, increasing the fuel injection pressure results in improved atomization of the fuel blends, resulting in complete, safer combustion and a decrease in smoke (Nam Cao et al. 2020). The inclusion of TBC laminates mitigates the negative consequences by raising cylinder temperature and thereby reducing ignition centers and smoke, which is the product of the diesel blend's larger mean droplet size being broken.

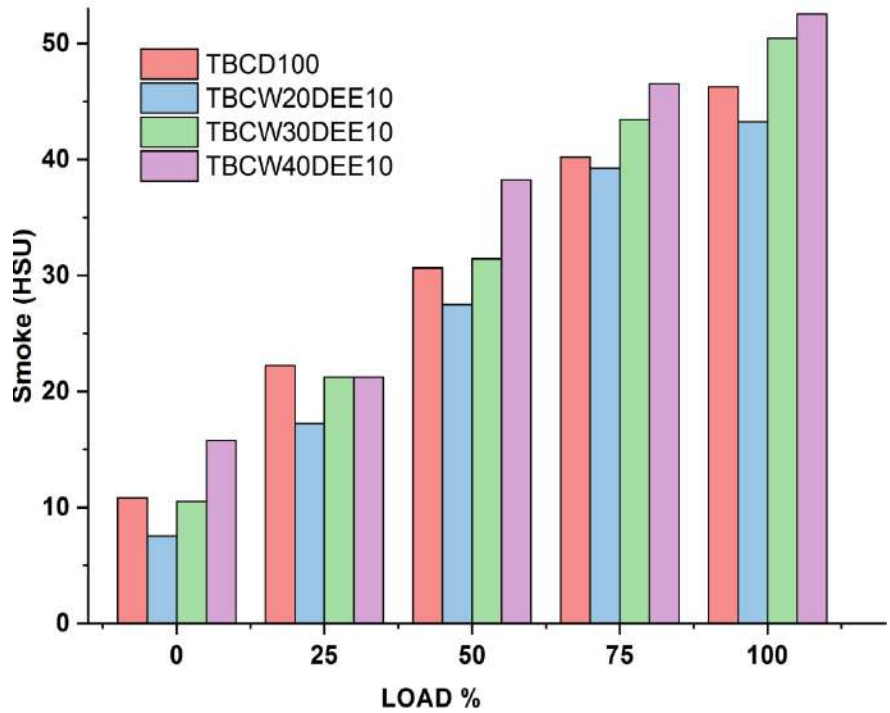


Fig. 6: Evaluation of WPPO's smoke on engine load.

## CONCLUSION

Consumable plastic materials accumulate during daily operations, and the world is yet to develop a better method of disposing of non-biodegradable plastics. The most difficult aspect of waste plastic recycling is that it may be converted into electricity. The primary purpose of this study is to demonstrate the feasibility of using WPPO as an alternate energy source in the automotive industry. To address the high-value emissions of WPPO in a diesel engine, a thermal barrier coating was created as a test rig for the evaluation of exhaust pollution reduction and engine performance enhancement, resulting in lower fuel consumption. On the TBC engine's WPPO blends, the following observations were made: At different load conditions, TBCW20DEE10's specific fuel consumption decreases by approximately 1.5% to 7.5%. At the maximum load, WPPO blends increased the thermal performance achieved the nearer to the value of Diesel. TBCW20DEE10 demonstrated an increase in carbon monoxide elimination of between 5 to 15% under different load conditions. For different load conditions, TBCW20DEE10 demonstrated a greater reduction of hydrocarbons varying from 5% to 12 %. At half load condition, TBCW20DEE10 emits approximately 3.5% less unit of smoke. On this evaluation, based on the results, WPPO can be utilized as an alternative energy source for fossil fuels.

## REFERENCES


Aydin, S., C. Sayin, and H. Aydin. 2015. Investigation of the usability of biodiesel obtained from residual frying oil in a diesel engine with a thermal barrier coating. Applied Thermal Engineering, 80: 212-219.

Bridjesh, P., Periyasamy, P., Chaitanya, A.V.K. and Geetha, N.K. 2018. MEA and DEE as additives on diesel engines using waste plastic oil diesel blends. Sustain. Environ. Res., 28(3): 142-147.

Damodharan, D., Sathiyagnanam, A.P., Rana, D., Kumar, B.R. and Saravanan, S. 2017. Extraction and characterization of waste plastic oil (WPO) with the effect of n-butanol addition on the performance and emissions of a DI diesel engine fueled with WPO/diesel blends. Energy Conv. Manage., 131: 117-126.

Das, A.K., Hansdah, D., Mohapatra, A.K. and Panda, K. 2020. Energy, exergy, and emission analysis on a DI single-cylinder diesel engine using pyrolytic waste plastic oil diesel blend. J. Energy Inst., 93(4): 1624-1633.

Gnanamoorthi, V. and Jayaram, M. 2019. Experimental investigation of Al2O3/8YSZ and CeO2/8YSZ plasma sprayed thermal barrier coating on the diesel engine. Ceramics Int., 4(3): 3166-3176.

Gungor, C., Serin, H., Ozcanli, M., Serin, S. and Aydin, K. 2015. Engine performance and emission characteristics of plastic oil produced from waste polyethylene and its blends with diesel fuel. Int. J. Green Energy, 12(1): 98-105.

Hariram, V., Balakarthikeyan, N., Seralathan, S. and Micha Premkumar, T. 2020. Effect of variable compression ratios on performance and emission phenomena of DI CI engine fuelled with palm stearin biodiesel-diesel blends. Nature Environ. Pollut. Technol., 19(4): 1517-1526.

Hariram, V. Seralathan, S. and Mohammed Raffiq, A. 2017. Formulation and characterization of pyrolytic oil from waste tire and waste plastic: a comparative study. Nature Environ. Pollut. Technol., 16(4): 1183-1188.

Hoang, A.T. and Pham, V.V. 2019. Impact of Jatropha oil on engine performance, emission characteristics, deposit formation, and lubricating oil degradation. Combustion Sci. Technol., 191(3): 504-519.

Joel, C., Anand, S., Padmanabhan, S. and Prasanna Raj Yadav, S. 2018. Thermal analysis of carbon-carbon piston for commercial vehicle diesel engine using CAE tool. Int. J. Amb. Energy, 42(2): 163-167.

Mangesh, V.L., Sambandam, P., Tamizhdurai, P., Narayanan, S. and Ramesh, A. 2020b. Combustion and emission analysis of hydrogenated waste polypropylene pyrolysis oil blended with diesel. J. Hazard. Mater., 386: 121453.

Mangesh, V.L., Padmanabhan, S., Tamizhdurai, P. and Ramesh, A. 2020a. Experimental investigation to identify the type of waste plastic pyrolysis oil suitable for conversion to diesel engine fuel. J. Cleaner Prod., 246: 119066.

Mangesh, V.L., Padmanabhan, S., Ganesan, D., Prabhudev, R. and Dinesh Kumar Reddy, T. 2017. Prospects of pyrolysis oil from plastic waste as fuel for diesel engines: A review. IOP Conf. Ser.: Mater. Sci. Eng., 197: 012027.

Mani, M., Nagarajan, G. and Sampath, S. 2011. Characterization and effect of using waste plastic oil and diesel fuel blends in compression ignition engine. Energy, 36(1): 212-219.

Nam Cao, D., Hoang, A.T., Luu, H.Q., Bui, V.G. and Huong Tran, T.T. 2020. Effects of injection pressure on the NOx and PM emission control of diesel engine: A review under the aspect of PCCI combustion condition. Energ. Sources Part A - Recovery Utilization Environ. Effects, 15: 1-18.

Patnaik, P.P., Jena, S.P., Acharya, S.K. and Das, H.C. 2017. Effect of FeCl3and diethyl ether as additives on compression ignition engine emissions. Sustain. Environ. Res., 27(3): 154-161.

Rajan, K., Mishra, M.K., Singh, S.K. and Kumar, A. 2016. Experimental evaluation of waste plastic oil and its blends on a single-cylinder diesel engine. J. Mech. Sci. Technol., 30: 4781-4789.

Ramalingam, S., Rajendran, S. and Ganesan, P. 2016. Performance improvement and emission control in a direct injection diesel engine using nanocatalyst coated pistons. Biofuels, 7(5): 529-535.

Sachuthananthan, B., Krupakaran, R.L. and Balaji, G. 2019. Exploration on the behavior pattern of a DI diesel engine using magnesium oxide nano additive with plastic pyrolysis oil as an alternate fuel. Int. J. Amb. Energy, 12: 44-59.

Sambandam, P., Venu, H. and Narayanaperumal, B.K. 2020. Effective utilization and evaluation of waste plastic pyrolysis oil in a low heat rejection single-cylinder diesel engine. Energ. Source Part A- Recovery, Utilization Environ. Effects, 18: 34-53

Singh, R.K., Biswajit Ruj, A.K., Gupta, S.P. and Tigga, V.P. 2020. Waste plastic to pyrolytic oil and its utilization in CI engine: Performance analysis and combustion characteristics. Fuel, 262: 116539.

Sivakumar, E. and Bridjesh, P. 2019. Utilization of unattended waste plastic oil as fuel in low heat rejection diesel engine. Sustain. Environ. Res., 29: 2.

Sivakumar, G. and Senthil Kumar, S. 2014. Investigation on the effect of Yttria stabilized zirconia coated piston crown on performance and emission characteristics of a diesel engine. Alex. Eng. J., 53 (4): 787-794.

Thibblin, A., Jonsson, S. and Olofsson, U. 2018. Influence of microstructure on thermal cycling lifetime and thermal insulation properties of yttria-stabilized zirconia thermal barrier coatings for diesel engine applications. Surf. Coat. Technol., 350: 1-11.

Nature Environment and Pollution Technology
An International Quarterly Scientific Journal

p-ISSN: 0972-6268
(Print copies up to 2016)
e-ISSN: 2395-3454

Vol. 20 | No. 5 (Suppl) | pp. 2087-2097 | 2021

Original Research Paper

https://doi.org/10.46488/NEPT.2021.v20i05.026

Open Access Journal

# Estimating the Potential of Carbon Sequestration in Tree Species of Chintapalle Forest Range, Narsipatnam Division, Visakhapatnam, Andhra Pradesh, India

**Korra Simhadri*, Syam Kumar Bariki**† and A.V.V.S. Swamy***
*Department of Environmental Sciences, Acharya Nagarjuna University, Guntur, A.P, India
**† N S Raju Institute of Technology, Sontyam Visakhapatnam, A.P, India
†Corresponding author: Syam Kumar Bariki; syamemmanuel@gmail.com

**Nat. Env. & Poll. Tech.**
**Website: www.neptjournal.com**

*Received:* 29-05-2021
*Revised:* 28-06-2021
*Accepted:* 04-07-2021

**Key Words:**
Carbon sequestration
Tree species
Sequestration potential
Soil organic carbon

## ABSTRACT

The potential of carbon sequestration of tree species in the Chintapalle forest range, of Narsipatnam Division, was estimated by using a non-destructive method. The sequestration of 6033 trees belonging to 22 species was investigated; the approximate height of tree species and the diameter at breast height (DBH) were measured for the estimation of $CO_2$ sequestration. The maximum weight of carbon was observed in *Pongamia pinnata* (L.) Pierre species i.e (37987.06 kg) and the minimum weight of carbon was noted in *Phyllanthus emblica* L. species i.e is (61.8kg). The total carbon sequestrated by the entire tree species was (2370614.0 kg), The average carbon sequestered was (39865.81 kg). The highest sequestration was noted in the species *P. pinnata* (L.) Pierre i.e. (139271.95 kg) and the lowest (226.79 kg) was noted in the species *P. emblica* L. The maximum average DBH with maximum carbon sequestration potential was observed in *Ficus benghalensis* L. species, with higher total green (AGW) observed in all sites, whereas minimum average DBH with minimum carbon sequestration potential was noted in *Bambusa vulgaris* species. The regression analysis tests the relationship between two variables. The height of trees has no significant impact on the amount of $CO_2$ sequestered F (32085087175.84, 12946607900) = 2.478262; P ≥ 0.05, which indicates that the tree height plays an insignificant role in $CO_2$ sequestration (β = 2713.28 P ≥ 0.05). The dependent variable $CO_2$ sequestered was also regressed on the predictor variable soil organic carbon (SOC) to test the relationship. SOC insignificantly predicted $CO_2$ sequestrated F (5.83, 2.62) = 0.2236; P ≥ 0.25, indicating that the SOC has an insignificant role in $CO_2$ sequestration (β = 102780.3 P ≥ 0.05). Insignificant relation was observed between the parameters SOC and height of tree species to the rate of carbon dioxide sequestered, and gave a regression equation of y = 10278x + 50863 with $R^2$ = 0.100; y=2713.285803x-209800.8762 with $R^2$ = 0.553 respectively.

## INTRODUCTION

The forests absorb CO from the atmosphere and store it in the form of carbon, while green plants act as a sink for atmospheric CO by fixing carbon during the photosynthesis process, and excess carbon is stored as biomass. Terrestrial Carbon sequestration is one of the processes of (a) transforming atmospheric $CO_2$ into components of biomass such as shrubs, trees, and Soil Organic Matter (SOM), through the process of photosynthesis and (b) assimilation of biomass into the soil as humus, which, involves the storing of atmospheric $CO_2$ in these components of biomass successfully. According to IPCC (2003) and Gorte (2009), as photosynthesis occurs more, maximum $CO_2$ is converted to biomass, lessening the carbon levels in the environment and sequestering it in plant tissues above and below ground, resulting in the growth of different parts (Chavan & Rasal 2010). There is a great interest, in balancing the atmospheric $CO_2$ concentration and decreasing $CO_2$ emissions by using diverse types of land use patterns to increase the carbon sink of forestry. The role of forests (trees) in carbon cycles is quite predictable (Singh & Lal 2000). Haripriya (2000, 2001, 2003), Manhas et al. (2006), Ravindranath et al. (1997), Chhabra and Dadhwal (2004), Gupta (2009), and Kaul et al. (2009) investigated changes in stratum and regional forest area as part of the study on the national forest carbon balance. According to the findings of Chhabra and Dadhwal (2004), forests are the largest suppliers of carbon, as well as a large sink for atmospheric carbon. Carbon dioxide emissions attributed to plants' vegetative mechanisms have increased significantly over the past decade. The use of existing $CO_2$ from the atmosphere for photosynthetic processes provides a natural sink for excess carbon dioxide created by human activities. It is well known that global carbon dioxide emissions have increased to 18%, reaching their first peak level after 1750. In the past, there has been an annual increase of 1.5 ppb in

1990-2000, 2 ppb in 2001-2009, and 2.3 ppb in 2009-2010, which was the maximum (Chavan & Rasal 2010).

According to the Food and Agricultural Organization (FAO), deforestation is responsible for 70% of all emissions in Africa (FAO 2005). Deforestation of tropical forests also destroys worldwide important carbon sinks that are presently sequestering $CO_2$ from the atmosphere, and are crucial for climate stabilization (Stephens et al. 2007). The present models of global climate forecast a gradual rise in the atmospheric concentrations of greenhouse gases over the next century and associated increases in global temperature. Increased global temperatures have a number of negative consequences, including negative effects on human health, the spread of pathogenic illnesses, forest fires, heatstroke, salinity rises, glacier melting, and so on. It is therefore very important to stabilize the increase of temperature by regulating the carbon dioxide intensity in the atmosphere. Through the sequestration of carbon in producer communities, atmospheric carbon dioxide can be condensed by utilizing the carbon stored in all biomass in living vegetation, including woody and herbaceous plants above the soil as well as stems, branches, bark, seeds, and flora, as well as dead organic matter and Soil Organic Carbon (SOC). Some of the more stable compounds found in the humus may not turn over for hundreds to thousands of years. Scientists can enhance the sequestration process by applying agricultural methods that lessen the erosion of soil by wind, water, and oxidation of soil. The ecosystem in the terrestrial part is the main resource of carbon as well as a sink. The increase of carbon content in the US is due to erosion by water and wind, and uncultivated land contains an average of 1329 MMTC of carbon while poor agricultural practices contribute five percent of the global greenhouse gas emissions. The 90-230 MMTC emitted annually from arable land and pastures in the tropics accounts for the largest portion of that global amount (Crookshank 1999). Trees in urban and rural settings provide a two-fold advantage: direct carbon storage and natural ecosystem stability with increased nutrient recycling, as well as the maintenance of climatic conditions by biogeochemical processes in the carbon reduction process of the atmosphere.

Estimations of biomass and stored carbon for the main tree species in the forest areas of the Eastern Ghats of Visakhapatnam, located in the state of Andhra Pradesh, India, were carried out in this study (taken during 2019-20) using three vital parameters namely Diameter at Breast Height (DBH), the height of the tree (h), and form factor (ratio of the square of radius at breast height to the radius of the tree at base). To combat global warming, the Kyoto Protocol proposed that carbon emissions be minimized by reducing fossil fuel emissions or by accumulating carbon in terrestrial ecosystem foliage and soil. For estimating the tree biomass, a non-destructive technique i.e., regression or allometric equations were used. Carbon sequestration can be achieved by accumulating all components of the ecosystem's carbon pool, such as SOC (soil organic carbon) content at 0 to 15 cm depth, as well as carbon can be stored in aboveground biomass (AGB), and belowground biomass (BGB). In the process, tree biomass is directly estimated by using the Diameter at Breast Height (DBH) values (Brown 1997). Throughout the world, allometric equations have been used for the determination of AGB and BGB and the carbon stored within the ecosystem components. Carbon sequestration through planted forests serves as a sizeable sink for atmospheric $CO_2$ both in temperate and tropical regions (Houghton et al. 2000, Houghton 1985, 1990, Fang et al. 2001). As a result of its total commoditization, $CO_2$ sequestration has garnered a significant amount of attention in the present and past. The accurate measurement of forest carbon sink is complex without the precise assessment of biomass. Therefore, the objective of this study is to calculate, approximately, the $CO_2$ sequestration potential of different types of tree species of the reserve forest blocks of Chintapalle, forest range of Narsipatnam Division, Visakhapatnam, Andhra Pradesh, India.

## MATERIALS AND METHODS

### Study Area

The Chinthapalli forest range, of Narsipatnam, is located on the northeast of Visakhapatnam district, Andhra Pradesh. It lies between $17^0$44'22'' North latitude to $18^0$04'29'' North and $82^0$16'00'' East to $82^0$38'04'' East. Temperatures in hill track villages range from $2^o$ to $30^o$C, as measured at the local agriculture research station in Chintapalle, Lambasingi area, and travelers refer to this place as Andhra Kashmir as temperatures are as low as $0^o$C in December and January. Depending on topographical conditions, the block and its surroundings can be divided into four categories viz. mountainous region, highlands tracks, rising and falling plains, and plains. The main hill ranges of the study area are Chintooru forest, Lothugedda and Chintapalli town, and Thanjangi.

### Sampling

For this investigation, sampling locations were identified in the Chintaaplle block of the Narsipatnam forest division region, namely: Chinrooru (Lothu Gedda Junction), Tajangi, Chinnagedda, and St. Ann's School colony. These sites were selected as the sampling area due to their wide green forest with low rural anthropogenic emission of carbon components. A total of six thousand and thirty-three (6033) trees belonging to twenty-two (22) different tree species were selected for the study. They are: *Ficus hispida* L.f,

*Trichilia connaroides* (Wight & Arn.) Bentv*, Bombax ceiba* L.*, Artocarpus heterophyllus* Lam.*, Tamarindus indica* L.*, Mangifera indica* L., *Eucalyptus globules, Grevillea robusta, Ficus religosa, Semecarpus anacardium* L.f., *Bambusa vulgaris, Caryota urens* L.*, Pongamia pinnata* (L.) Pierre*, Tectona grandis* L.f, *Delonix regia, Ficus benghalensis* L.*,* and *Syzygium cumini* (L.) Skeels.

**Analytical Methods**

The non-destructive method was used for the determination of the above-ground weight (total green) dry weight, and $CO_2$ Sequestration (kg), and the total organic carbon of each tree species was evaluated. SOC was determined in the forest sites by the IS2720 & ASTM methods (Table 5). There are two approaches for evaluating the biomass concentration of tree species. (a) The biomass density was directly estimated through biomass regression or allometric equations. (b) By converting wood volume estimations to biomass density using biomass factors (Brown 1997). The use of allometric equations is a central step in evaluating above and below-ground biomass (Brown et al. 1989, 1991). In India, several authors had published biomass estimations using allometric equations for a few tree species and the diameter above 10 cm at breast height (Lodhiyal et al. 2002, Lodhiyal & Lodhiyal 2003). The methodology used included statistics and linear regression models and figures.

**Tree Height (TH) and Diameter at Breast Height (DBH)**

For measuring the circumference of a tree to determine the (DBH) Diameter at Breast Height of the tree species, the circumference of the tree trunk at 1.3 m from the ground level was considered, while for trees with a circumference less than or equal to 10 cm, direct measurement leaving the height from the ground level was performed (Fig. 1). The total height of the tree species was estimated by measuring with a tape by climbing, and by straight measurement aided by a pole and the affirmation by calculating the Thiodolite angle and sides.

The angle between the top of the tree and the view of the eye at breast height () angle was used to determine the tree height of the species. The angle ACB between the top of a tree and the distance (b) at the observer point at DBH is considered. Hence the height of the tree species was calculated if (α) is the angle between the top of the tree and the eye view, (H) is the tree height in meters/inches, (c) is the slope between eye view and the treetop, (b) is the distance between observer and tree and (h) is the height of horizontal plane of Thiodolite instrument. Therefore, tree species height was calculated by the below formula:

$$H = h + b \tan \alpha$$

**Determination of Carbon Sequestration Potential and Biomass of Tree Species**

The method suggested by Chavan and Rasal (2010) was directly applied, five stages as follows:

- The total (green) weight of a tree is calculated as follows: W = Above-ground weight of the tree in kilogram (kg); D = Diameter of the trunk in inches; H = Height of tree in meters. $W = 0.25 \times D^2 \times H$ for trees with D ⊴ 0 and $W = 0.15 \times D^2 \times H$ for trees with D 11. The root system of a tree weighs about 120% of the tree's above-ground weight. Therefore, for determining the total green weight of the tree, multiply the above-ground weight of the tree by 120%.

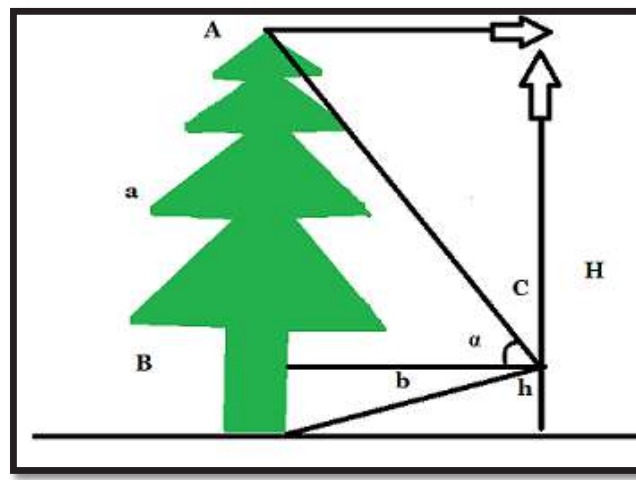


Fig. 1: Determination of tree height by thiodolite at DBH.

- The dry weight of a tree is based on a University of Nebraska publication (Chavan & Rasal 2010). The tree's dry weight was determined by multiplying the tree's weight by 72.5 percent.
- The average carbon content of a tree is 50 percent of its total volume (weight of carbon). As a result, the dry weight of carbon in the tree was determined by multiplying the dry weight of carbon in the tree.
- Carbon dioxide sequestration weight ($CO_{2)}$ is composed of one molecule of carbon and 2 molecules of oxygen and the atomic weight of Carbon is 12.001115; the atomic weight of Oxygen is 15.9994 As a result, the weight of $CO_2$ is C + (2 X O) = 43.999915, and the $CO_2$ to C ratio is 43.999915/12.001115 = 3.6663. To calculate the weight of carbon dioxide sequestered in the tree, multiply the weight of carbon in the tree by 3.6663.
- The weight of $CO_2$ sequestered in the tree per year was calculated by dividing the weight of carbon dioxide sequestered in the tree by the age of the tree. Hence, in the present study, we used the allometric equation using tree diameter to estimate above-ground biomass following Brown et al. (1989).

Table 1: $CO_2$ Sequestration of tree species at Chintooru, Lothugedda Junction in (Block-6).

| S.No. | Vernacular Name | Scientific Name of Trees | Number of Trees | Average DBH (Inches) | Average Height meter | Weight from tree species (kg) | | | | |
|---|---|---|---|---|---|---|---|---|---|---|
| | | | | | | Total Green (AGW) | Dry weight | Carbon Estimated | Amount of $CO_2$ sequestered | Average $CO_2$ sequestered |
| 1 | Boddechettu | *Ficus hispida* L.f | 42 | 15.74 | 7.5 | 334.45 | 242.47 | 121.23 | 444.46 | 10.58 |
| 2 | Usiri | *Phyllanthus emblica* L. | 25 | 13.77 | 5 | 170.65 | 123.72 | 61.86 | 226.79 | 9.07 |
| 3 | Peddaturayi | *Delonix regia* | 17 | 106.30 | 12 | 24407.33 | 17695.31 | 8847.65 | 32438.13 | 1908.12 |
| 4 | Neredu | *Syzygium cumini* (L.) Skeels | 46 | 104.33 | 16 | 31348.07 | 22727.35 | 11363.67 | 41662.62 | 905.70 |
| 5 | Teku | *Tectona grandis* L.f | 450 | 82.67 | 18 | 22143.22 | 16053.83 | 8026.91 | 29429.06 | 65.39 |
| 6 | Panasa | *Artocarpus heterophyllus* Lam. | 73 | 133.85 | 17 | 54822.41 | 39746.24 | 19873.12 | 72860.81 | 998.10 |
| 7 | Chinta | *Tamarindus indica* L. | 67 | 92.51 | 16.5 | 25417.55 | 18427.72 | 9213.63 | 22779.93 | 339.99 |
| 8 | Mamidi | *Mangifera indica* L. | 98 | 122.04 | 21 | 56298.41 | 41273.09 | 20636.54 | 75659.74 | 772.03 |
| 9 | Neelagiri | *Eucalyptus globulus* | 41 | 66.92 | 28 | 22570.56 | 16363.65 | 8181.82 | 29997.0 | 731.63 |
| 10 | Silver Oak | *Grevillea robusta* | 200 | 47.24 | 23 | 9238.89 | 6698.19 | 3349.09 | 12278.76 | 61.39 |
| 11 | Nallajeedi | *Semecarpus anacardium* L.f. | 32 | 17.71 | 8 | 451.64 | 327.43 | 163.71 | 600.20 | 18.20 |
| 12 | Veduru | *Bambusa vulgaris* | 27 | 7.87 | 11 | 204.39 | 148.18 | 74.09 | 271.63 | 10.06 |
| 13 | Jeelugu | Caryotaurens L. | 35 | 90.55 | 17.5 | 25827.80 | 18725.15 | 9362.57 | 34325.99 | 980.74 |
| 14 | Nalla Maddi | *Terminalia alata* Roth. | 43 | 59.05 | 19.5 | 12239.02 | 8873.28 | 4436.91 | 16267.04 | 378.30 |
| 15 | Tella Maddi | *Terminalia arjuna* (Roxb. ex DC.) Wight &Arn. | 38 | 47.24 | 18 | 7230.44 | 5242.1 | 2621.09 | 9609.70 | 252.88 |
| 16 | Kanugu | *Pongamia pinnata* (L.) Pierre | 7 | 62.99 | 12 | 8570.31 | 6213.47 | 3106.47 | 11389.25 | 1627.03 |
| 17 | Sampangi | *Micheliachampaca* (L.) Baill. ex Pierre | 5 | 66.92 | 17.5 | 14106.60 | 10227.28 | 5113.64 | 18748.13 | 3749.62 |
| 18 | Gumpena | *Lanneacoro mandelica* (Houtt.) Merr. | 23 | 20.07 | 8 | 580.03 | 420.52 | 210.26 | 770.87 | 33.51 |
| TOTAL | | | 1269 | 1157.77 | 275.5 | 315961.8 | 229529 | 114764.3 | 409760.1 | 12852.34 |

### Soil Sampling

To determine the SOC (Soil organic Carbon) from the study sites, the soil samples were collected from the sites by using standard sampling procedures, given for soil sampling. All the soil samples were collected from the depth of 0-15 cm with two replicates. The physicochemical parameters such as – soil texture, pH, and soil organic carbon, were analyzed by standard methods, as per IS2720 & ASTM methods.

## RESULTS AND DISCUSSION

The carbon dioxide sequestration and carbon storage capability of (6033) tree species belonging to (22) tree species were assessed. The evaluation was divided into four sections, as shown in Tables 1- 4. Fig. 2. shows the relationship between above-ground weight and below-ground weight (AGW). Fig. 2 also shows the relationship between the total carbon dioxide sequestered and the above-ground weight (AGW) and dry weight of the studied trees in the sites.

The total carbon dioxide sequestered and calculations of carbon dioxide sequestered at the study locations are shown in Tables 1 to 4. The amount of $CO_2$ sequestered in block-1, Chintooru is (409,760.1 kg); block-2 Chinnagedda is (568,891.3 kg); St.Anns School Colony Chintapalli, Block-3 is (659,853 kg) and block-4 Tajangi is (732,109.2 kg). A large amount of $CO_2$ sequestration was recorded at block-4 Tajangi site, which may be due to the presence of more tree species, and the long age of species. A large amount of $CO_2$ sequestered was found in the species *P. pinnata* (L.) Pierre, and *F. benghalensis* L, and a low amount of carbon dioxide sequestrated was observed in block-1 Chinnagedda in *P. emblica* L. species. The maximum weight of carbon was observed in *P. pinnata* (L.) Pierre) species, i.e. (37987.06 kg) and minimum weight of carbon was noted in the species *P. emblica* L. species i.e is (61.8 kg). The maximum assessment of carbon dioxide sequestration is especially noted in *F. benghalensis* species, because of its higher (AGW) compared to other species. In an earlier study by Chavan and Rasal (2010), similar findings were recorded. The estimated average C-stock of *P. pinnata* was 23.52 tC ha-1 in Site-1 and 72.70 tC ha-1 in Site-2 and an average equivalent of 86.34 $tCO_2$ ha-1 and 266.84 $tCO_2$ ha-1 has been stored (Annissa Muhammed et al. 2013). A similar study performed by Cox (2012), in California State University, Northridge (CSUN), showed that the total carbon dioxide sequestered by the trees in the campus was 154 tons per year. Haghparast (2013) also recorded a whole of 1694.5 tons of carbon sequestered in seventy-six plots of Pune University. De Villiers et al. (2014) reported the sequestration potential of 4139 trees to be 5809 tons in New Zealand University. Vucetich et al. (2000) and Pussinen et al. (2002) reported that the carbon stock depends upon the type of tree species, location properties, spacing, environment conditions, age class distribution, etc. The three dominant species of the entire site are *T. grandis* L.f, *M. indica* and *T. indica* L. In contrast to it, a study conducted by Kaur and Sharma (2014) in the agricultural fields of block Ramgarh revealed *M. indica* as the densest tree species with a density value of 1.9 trees per hectare. Rowntree and Nowak, (1991) stated that the broader the leaves, the thicker the crown cover, and consequently the denser the cluster, the more $CO_2$ sequestered by trees.

From the results obtained, it clearly indicates that the native species like *P. pinnata* (L.) Pierre, *F. benghalensis,* L., *T. grandis* L.f, *M. indica,* and *T. indica* L. have a maximum

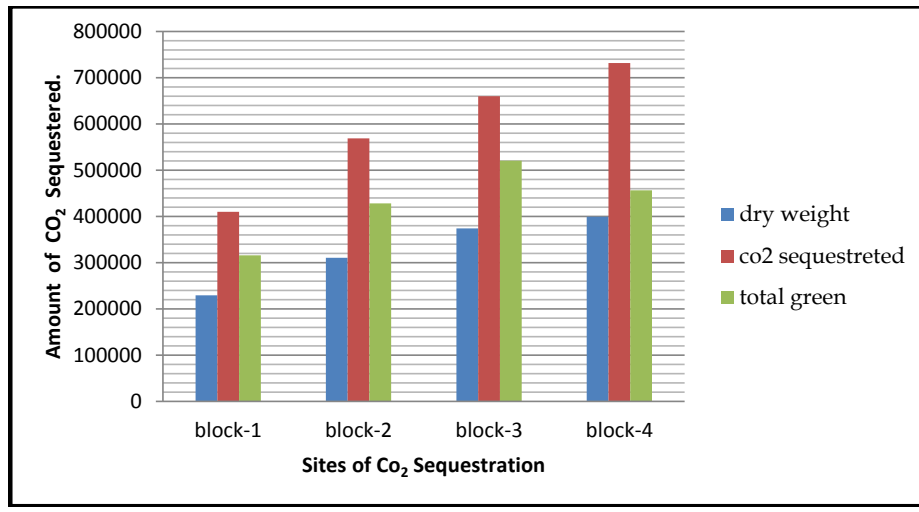


Fig. 2: Relationship between dry weight and the total amount of sequestered $CO_2$.

Table 2: $CO_2$ Sequestration of tree species at Chinnagedda, (Block-7).

| S.No. | Vernacular Name | Scientific Name of Trees | Number of Trees | Average DBH (Inches) | Average Height (meters) | Weight from tree species (kg) | | | | |
|---|---|---|---|---|---|---|---|---|---|---|
| | | | | | | Total Green (AGW) | Dry weight | Carbon Estimated | Amount $CO_2$ sequestered | Average $CO_2$ sequestered |
| 1 | Garugu | *Trichilia connaroides* (Wight & Arn.) Bentv | 78 | 14.96 | 5 | 201.42 | 146.42 | 73.01 | 267.69 | 3.43 |
| 2 | Bodda chettu | *Ficus hispida* L.f. | 56 | 21.65 | 8 | 674.96 | 489.34 | 244.67 | 897.04 | 16.01 |
| 3 | Peddaturayi | *Delonix regia* | 47 | 90.55 | 12 | 17710.49 | 12840.10 | 6420.05 | 23537.84 | 500.80 |
| 4 | Teku | *Tectona grandis* L.f | 850 | 98.42 | 17.5 | 30512.46 | 22121.53 | 11060.76 | 40552.09 | 47.70 |
| 5 | Panasa | *Artocarpus heterophyllus* Lam. | 284 | 102.36 | 16 | 30175.40 | 21877.16 | 10938.58 | 40104.12 | 141.211 |
| 6 | Chinta | *Tamarindus indica* L. | 105 | 96.45 | 15.5 | 25954.26 | 18816.83 | 9408.41 | 34494.88 | 328.51 |
| 7 | Mamidi | *Mangifera indica* L. | 368 | 151.57 | 21 | 86839.69 | 62958.78 | 31479.39 | 115412.88 | 313.62 |
| 8 | Neelagiri | *Eucalyptus globulus* | 250 | 62.99 | 32 | 22854.18 | 16569.28 | 8284.64 | 30373.98 | 121.49 |
| 9 | Silver Oak | *Grevillea robusta* | 325 | 49.21 | 24 | 10461.41 | 7584.52 | 3792.26 | 13903.57 | 42.78 |
| 10 | Ravi | *Ficus religiosa* L. | 24 | 108.26 | 20 | 42192.81 | 30589.79 | 15294.89 | 56075.68 | 2336.48 |
| 11 | Nallajeedi | *Semecarpus anacardium* L.f. | 30 | 26.77 | 7.50 | 967.45 | 701.40 | 350.70 | 1285.77 | 42.859 |
| 12 | Veduru | *Bambusa vulgaris* | 102 | 7.87 | 11 | 204.39 | 148.18 | 74.09 | 271.63 | 2.66 |
| 13 | Jeelugu | *Caryota urens L.* | 50 | 72.51 | 14.5 | 13722.59 | 9948.88 | 4974.44 | 18237.79 | 364.75 |
| 14 | Sampangi | *Michelia champaca* (L.) Baill.ex Pierre | 18 | 88.20 | 16 | 22404.21 | 16243.05 | 8121.52 | 29775.95 | 1654.21 |
| 15 | Marri Chettu | *Ficus benghalensis* L. | 6 | 177.16 | 18 | 101689.55 | 73724.92 | 36862.46 | 135148.85 | 22524.80 |
| 16 | Neredu | *Syzygiumcumini* (L.) Skeels | 87 | 89.2 | 15 | 21482.92 | 15575.12 | 7787.56 | 28551.53 | 328.17 |
| | TOTAL | | 2680 | 1258.13 | 253 | 428048.2 | 310335.3 | 155167.4 | 568891.3 | 28769.48 |

amount of carbon dioxide sequestration potential than all the other tree species. Fig. 2, shows the relationship between the dry weights of tree species of diverse sampling sites with the amount of carbon dioxide sequestered. From this figure, it was observed that the total green obtained is the AGW (Above ground weight) (kg) is directly proportional to the amount of $CO_2$ sequestered, and dry weight obtained (kg) is also directly proportional to the amount of carbon dioxide sequestered. This phenomenon was mostly observed in block-4 Thajangi, where the number of tree species is more compared to all the other blocks is (732,109.2 kg). In block-01, the numbers of trees are scanty which declines the total green (AGW) and dry weight of the tree and shows a deviation in the quantity of $CO_2$ sequestrated i.e. (409,760.1 kg.). Gibbs et al. (2007) provided similar findings, finding a progressive direct link between total green (AGW), the dry weight of the tree, and the amount of carbon dioxide sequestered by trees. In the four sampling sites, it was observed from Tables 1-4, that the species like *P. pinnata* (L.)*, A. heterophyllus* Lam, *T. indica* L. *M. indica* L. *F. religiosa* L., *F. benghalensis* L. Pierre, *and T. grandis* are with maximum $CO_2$ sequestration. Similarly, the lowest $CO_2$ sequestration was recorded in *B. vulgaris and P. emblica* L.*,* species. (70.72; 226.79 kg) respectively.

Fig. 3 and Table 6 interpret the relationship between the heights of the tree to the amount of $CO_2$ sequestrated. Fig. 3 shows the tree height carries an insignificant impact on $CO_2$ sequestered. The dependent variable $CO_2$ sequestered was regressed on the predicting variable tree height to test the relationship. The height of tree species insignificantly pre-

Table 3: $CO_2$ Sequestration of tree species from Chintapalli, St. Ann's School, (Block-8).

| S.No. | Vernacular Name | Scientific Name of Trees | Number of Trees | Average DBH (Inches) | Average Height meter | Weight from tree species (kg) | | | | |
|---|---|---|---|---|---|---|---|---|---|---|
| | | | | | | Total Green (AGW) | Dry Weight | Carbon Estimated | Amount $CO_2$ sequestered | Average $CO_2$ sequestered |
| 1 | BoddaChettu | *Ficus hispida* L.f | 20 | 30.70 | 9.5 | 1611.65 | 1168.45 | 584.22 | 2141.94 | 107.09 |
| 2 | Burugu | *Bombax Ceiba* L. | 15 | 84.64 | 14 | 18053.10 | 13088.59 | 6544.24 | 23993.18 | 1599.54 |
| 3 | Chinta | *Tamarindus indica* L. | 78 | 114.17 | 17 | 39886.45 | 28917.67 | 14458.83 | 53010.43 | 679.62 |
| 4 | Mamidi | *Mangifera indica* L. | 86 | 127.95 | 22.5 | 66303.37 | 48069.94 | 24034.97 | 88119.41 | 1024.64 |
| 5 | Neelagiri | *Eucalyptus globulus* | 52 | 64.96 | 31 | 23546.59 | 17071.20 | 8535.60 | 31294.08 | 601.80 |
| 6 | Silver Oak | *Grevillea robusta* | 180 | 59.05 | 26.5 | 16632.52 | 12058.58 | 6029.29 | 22105.18 | 122.80 |
| 7 | Ravi | *Ficus religiosa* L. | 21 | 106.29 | 22 | 44738.35 | 32435.30 | 16217.65 | 59458.77 | 2831.37 |
| 8 | Jeelugu | *Caryotaurens* L. | 15 | 98.42 | 16 | 27897.10 | 20225.40 | 10112.70 | 37076.20 | 2471.74 |
| 9 | Kanugu | *Pongamia pinnata* (L.) Pierre | 10 | 84.64 | 11.5 | 14829.33 | 7414.66 | 10751.26 | 39417.37 | 3941.73 |
| 10 | Panasa | *Artocarpus heterophyllus* Lam. | 52 | 127.95 | 18 | 53042.69 | 38455.95 | 19227.97 | 70495.53 | 1355.68 |
| 11 | Marri Chettu | *Ficus benghalensis* L. | 9 | 167.32 | 19 | 95746.25 | 69416.03 | 34708.01 | 127250.01 | 14138.89 |
| 12 | Teku | *Tectona grandis* L.f | 55 | 74.80 | 19.5 | 12549.79 | 9098.60 | 4549.30 | 16679.10 | 303.25 |
| 13 | Medi | *Ficus racemosa* L. | 18 | 25.59 | 8 | 942.98 | 683.66 | 431.83 | 1253.25 | 69.62 |
| 14 | Neredu | *Syzygium cumini* (L.) Skeels | 15 | 85.82 | 17 | 22537.12 | 16339.41 | 8169.70 | 29952.59 | 1996.83 |
| 15 | Gumpena | *Lannea coromandelica* (Houtt.) Merr. | 25 | 19.68 | 8.5 | 592.57 | 429.61 | 214.80 | 787.54 | 31.50 |
| 16 | Nalla Maddi | *Terminalia alata* Roth. | 18 | 102.36 | 18 | 33947.32 | 24611.81 | 12305.90 | 45117.14 | 2506.50 |
| 17 | Tella Maddi | *Terminalia arjuna* (Roxb. ex DC.) | 23 | 109.44 | 21 | 45273.48 | 32823.27 | 16411.63 | 8205.81 | 30084.99 |
| 18 | Mulu maddi | *Bridelia retusa* (L.) A. Juss. | 15 | 11.O2 | 8 | 174.87 | 126.78 | 63.39 | 232.41 | 15.49 |
| 19 | Karaka | *Terminalia chebula* Retz | 27 | 33.85 | 12 | 2455.23 | 1780.04 | 890.02 | 3263.09 | 120.85 |
| TOTAL | | | 734 | 1517.63 | 319 | 520760.8 | 374215 | 194241.3 | 659853 | 64003.93 |

dicted $CO_2$ sequestrated F (32085087175.84, 12946607900) = 2.478262; $P \geq 0.05$, which indicates that the tree height has an insignificant role in $CO_2$ sequestration ($\beta = 2713.28$ $P \geq 0.05$). The regression analysis indicates clearly that there is no direct relationship of the tree height, moreover, $R^2 = 0.553$, which indicates the regression model explains 55.3% of the variance. Most of the research works revealed that AGB is strongly correlated with tree diameter (Brown 1997, Brown & Lugo 1984, Clark et al. 2001). Also, it is accepted that a simple model with the only diameter as the input is a good estimator of above-ground biomass (Brown 1997, Nelson et al. 1999, Clark et al. 2001, Djomoa et al. 2010). There

Table 4: $CO_2$ Sequestration Assessment of tree species at Thajangi, (Block-9).

| S.No. | Vernacular Name | Scientific Name of Trees | Number of Trees | Average DBH (Inches) | Average Height meter | Weight from the tree (kg) | | | | |
|---|---|---|---|---|---|---|---|---|---|---|
| | | | | | | Total Green (AGW) | Dry Weight | Carbon Weight | Amount $CO_2$ sequestered | Average $CO_2$ sequestered |
| 1 | Bodda Chettu | *Ficus hispida* L.f | 38 | 26.77 | 7.5 | 967.45 | 701.40 | 350.70 | 1285.77 | 33.83 |
| 2 | Garugu | *Trichilia connaroides* (Wight & Arn.) Bentv. | 60 | 19.68 | 6 | 418.28 | 303.25 | 151.62 | 555.91 | 9.26 |
| 3 | Burugu | *Bombax ceiba* L. | 45 | 84.64 | 14 | 18053.10 | 13088.49 | 6544.24 | 23993.18 | 533.18 |
| 4 | Panasa | *Artocarpus heterophyllus* Lam. | 158 | 127.95 | 16 | 47149.06 | 34183.07 | 17091.53 | 62662.69 | 396.59 |
| 5 | Chinta | *Tamarindus indica* L. | 125 | 94.48 | 15.5 | 24904.85 | 18056.01 | 9028.0 | 33099.38 | 264.79 |
| 6 | Mamidi | *Mangifera indica* L. | 180 | 124.06 | 20 | 55407.18 | 40170.20 | 20085.10 | 73638.01 | 409.10 |
| 7 | Neelagiri | *Eucalyptus globulus* | 55 | 70.87 | 32 | 28929.92 | 20974.19 | 10.487.09 | 38448.85 | 699.07 |
| 8 | Silver Oak | *Grevillea robusta* | 150 | 53.14 | 26.5 | 13469.81 | 9765.61 | 4882.80 | 17901.83 | 119.34 |
| 9 | Ravi | *Ficus religosa* | 6 | 98.42 | 18 | 31384.24 | 22753.58 | 11376.79 | 41710.72 | 6951.78 |
| 10 | Nallajeedi | *Semecarpus anacardium* L.f. | 12 | 17.71 | 7.50 | 423.41 | 306.97 | 153.48 | 562.73 | 46.89 |
| 11 | Veduru | *Bambusa vulgaris* | 95 | 7.87 | 10.5 | 195.10 | 141.44 | 70.72 | 259.29 | 2.272 |
| 12 | Jeelugu | *Caryota urens* L. | 24 | 53.14 | 17 | 8641.01 | 6264.73 | 3132.36 | 11484.19 | 478.50 |
| 13 | Kanugu | *Pongamia pinnata* (L.) Pierre | 15 | 66.92 | 13 | 10479.19 | 75974.12 | 37987.06 | 139271.95 | 9284.79 |
| 14 | Sampangi | *Micheliachampaca* (L.) Baill.ex Pierre | 8 | 45.27 | 18 | 6639.96 | 4813.97 | 2406.98 | 8824.74 | 1103.09 |
| 15 | Teku | *Tectona grandis* L.f | 250 | 70.86 | 17.5 | 15816.58 | 11467.02 | 5733.51 | 21020.78 | 84.083 |
| 16 | Peddaturayi | *Delonix regia* | 10 | 90.55 | 12.5 | 18448.43 | 13375.11 | 6687.55 | 24518.58 | 2451.85 |
| 17 | Marri Chettu | *Ficus benghalensis* L. | 5 | 177.16 | 17 | 96040.13 | 69629.09 | 34814.54 | 127640.58 | 25528.11 |
| 18 | Neredu | *Syzygium cumini* (L.) Skeels | 16 | 92.51 | 16 | 24647.32 | 17869.31 | 8934.65 | 32757.13 | 2047.32 |
| 19 | Nalla Maddi | *Terminalia alata* Roth. | 27 | 88.58 | 18 | 25422.38 | 18431.23 | 9215.61 | 33787.21 | 1251.37 |
| 20 | Tella Maddi | *Terminalia arjuna* (Roxb. ex DC.) | 32 | 93.30 | 17.5 | 27420.40 | 19879.79 | 9939.89 | 36442.64 | 2024.59 |
| 21 | Rela | *Cassia fistula* L. | 18 | 26.77 | 8 | 1031.95 | 748.16 | 374.08 | 1371.49 | 76.194 |
| 22 | Pampini | *Oroxylum indicum* (L.) Kurz. | 21 | 22.04 | 7.5 | 655.77 | 475.43 | 237.71 | 871.55 | 41.50 |
| TOTAL | | | 1350 | 1552.69 | 335.5 | 456545.5 | 399372.2 | 189198.9 | 732109.2 | 53837.5 |

is no direct relationship between the height of the tree and the $CO_2$ sequestration in the sampling locations. Rowntree (1984) revealed that the height of the tree contributes to the volume of the tree which can be related to the mass and consequently the relative $CO_2$ sequestration potential of the tree. The linear regression equation of y= 2713.285803x-209800.8762 with $R^2$ = 0.553 demonstrates the height of tree species with carbon dioxide sequestered**,** indicating the insignificant variations between the tree species height with the rate of $CO_2$ sequestered at $P > 0.05$. The number of trees is also the major contributor to the rate of sequestration of carbon, followed by the size of the tree, which increases quickly as the number of individuals in a species increases, and then stabilizes. According to Vishnu and Patil (2016), the tree with the highest DBH has higher carbon stock. Baishya et al. (2009) found that biomass and carbon sequestration

vary with DBH, with maximum trees during the regeneration stage and high biomass of larger trees. Fast-growing trees capture more carbon than slow-growing trees (Montagnini & Porras 1998, Redondo- Brenes 2007).

### Soil Organic Carbon

Carbon sequestered in the soil is called hummus, giving maximum storage of carbon than the biomass. The SOC of Chinthuru Lothugedda Junction, block-1 is (0.93%), Chinnagedda village, block-2 is (0.22%), Near St.Ann's School, block-3 is (0.88%) and Thajangi village, block-4 is (1.24). The observations show only little amount of SOC was noted in the sampling blocks, except for Thajangi village (block-4), which had (1.24%) maximum SOC compared to all the other locations.

Depending on land use management, the soil could be a source of ($CO_2$, $CH_4$, and $N_2O$) or a sink ($CO_2$ and $CH_4$) of global greenhouse gases (Lal & Bruce 1999, Lal & Kimble 1998)**.** SOC in this study sites would not be a major contributor to carbon dioxide sequestration due to the negligible levels of SOC. Bouwman (1990) showed the size has been estimated between 700 to 3,000 Gt carbon as organic carbon and 780 to 930 Gt C as Calcium carbonate ($CaCO_3$). Other carbon pools are the oceans (38,000 Gt C), fossils carbon reserves (6,000 Gt c), and $CO_2$ in the atmosphere (720 Gt c).

The linear regression presented in Fig. 4 and Table 6 reveals that SOC has an insignificant impact on $CO_2$ sequestered. The Dependent Variable $CO_2$ sequestered was regressed on Predicting variable SOC to the test the relationship, SOC insignificantly, predicted $CO_2$ sequestrated F (5.83,2.62) = 0.2236; $P \geq 0.25$, which indicates that the SOC play an insignificant role in $CO_2$ sequestration ($\beta$ = 102780.3 $P \geq 0.05$). It was discovered that there was no direct relationship between the SOC and R2 = 0.100, indicating that the regression model explains 100% of the variance. Table 6 below shows the summary of the findings and the results of linear regression. Table 6 reveals that both SOC and the rate of $CO_2$ sequestration in trees have a regression equation of y = 10278x + 50863 with R2 = 0.100, indicating that there are no significant differences between tree height and $CO_2$ sequestration at $P > 0.05$ of the tree species' $CO_2$ sequestration rate.

## CONCLUSION

The total average potential of carbon sequestration of various tree species was calculated in four different sites (Block1 to 4) and was 12852.34 kg, 28769.48 kg, 64003.93 kg, and 53837.5 kg respectively.

Therefore, it is concluded that the local trees of the forest have a large carbon concentration and stocks of carbon. In this study, the native tree species *T. grandis* L.f, *M. indica,* and *T. indica* L., *P. pinnata* (L.)*, A. heterophyllus* Lam, L. *M. indica* L.*, F. religiosa* L., and *F. benghalensis* L. Pierre, recorded the maximum amount of carbon dioxide sequestration and carbon storage, which facilitate to build up the ecological services, thereby reducing global warming.

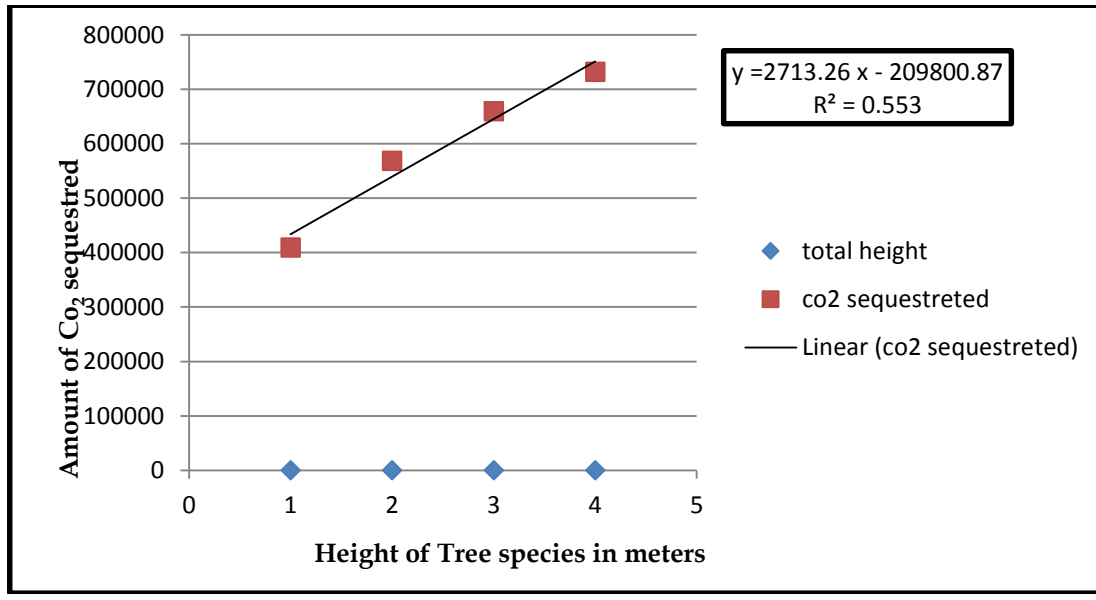


Fig. 3: Relationship between heights of the tree to the total amount of $CO_2$ sequestered

Table 5: The physico-chemical parameters, pH, Soil texture, and SOC.

| S.No. | Sampling Station | pH | Soil Texture | | | Organic Carbon% |
|---|---|---|---|---|---|---|
| | | | Sand% | Silt% | Clay% | |
| 1. | Chinthuru Lothugedda Junction- (block-1) | 6.28 | 71 | 12 | 17 | 0.93 |
| 2. | Chinnagedda village-(block-2) | 6.22 | 61 | 15 | 25 | 0.22 |
| 3. | Near St.Anns School, (block-3) | 7.81 | 45 | 26 | 29 | 0.88 |
| 4. | Thajangi village (block-4) | 6.78 | 66 | 16 | 16 | 1.24 |

Note: All the above parameters are analyzed as per IS2720 & ASTM methods.

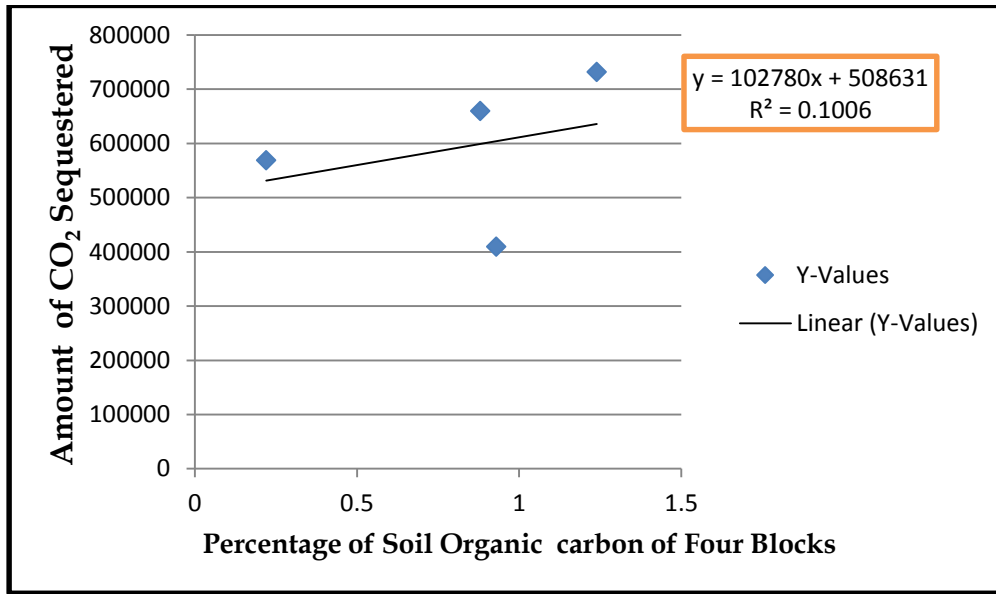


Fig. 4: Relationship soil organic carbon against the total amount of $CO_2$ sequestered.

Furthermore, because these trees protect the Earth from the greenhouse effect and climatic change, they must be protected against deforestation, and sustainable forest management with the goal of carbon sequestration should be mandated. Plantation initiatives can be used to generate carbon credits, which can help developing countries generate income (Niles et al. 2002).

Because there is a need for proper organization and protection of biodiversity in the hilly forest areas which are the major source of carbon sinks, the findings of this study may assist future planning and decision-making by the forest department regarding native species selection and plantation, which would be the major contributors of high $CO_2$ sequestration for the ecological balance of the Eastern Ghats reserve forest. Due to its high elevation from sea level, thick green forest, and low rural anthropogenic emissions of carbon components, the temperature of this area may drop to 0ºC, especially in the winter season, and hence it is the coolest hill station of Andhra Pradesh.

## REFERENCES

Annissa Muhammed, A., Surendra, B., Keredin, T.S. and Solomon Raju,

Table 6: The Regression Analysis of the height of tree and SOC to $CO_2$ sequestrated.

| S.No. | Regression weights | β- coefficient | $R^2$ Value | F Value | P-Value | Hypothesis supported |
|---|---|---|---|---|---|---|
| 1. | Height of tree – $CO_2$ Sequestered | 2713.286 | 0.553 | 2.478262 | 0.256093 | No |
| 2. | Soil Organic Carbon - $CO_2$ Sequestered | 102780.3 | 0.1005 | 0.2236 | 0.682343 | No |

A.J. (2013), Assessment of biomass and carbon sequestration potentials of standing Pongamia pinnata in Andhra University, Visakhapatnam, India. Biosci. Discov., 4(2): 143-148

Baishya, R.S., Barik, K. and Upadhya, K.2009. Distribution pattern of above-ground biomass in natural and plantation forests of humid tropics in northeast India. Trop. Ecol., 50(2): 295-304.

Bouwman, A.F. 1990. Soils and greenhouse effect. John Willey and Sons, New York, USA.

Brown S. and Lugo, A.E. 1982. The storage and production of organic matter in tropical forests and their role in the global carbon cycle. J. Biotropica., 14: 161-187.

Brown, S. 1997. Estimating Biomass Change of Tropical Forests: A Primer. Forestry, Paper, FAO, Rome, Italy, p. 134.

Brown, S., Gillespie, A.J.R. and Lugo, A.E. 1989. Biomass estimation methods for tropical forests with applications to forest inventory data. For. Sci., 35: 881-902.

Brown, S., Gillespie, A.J.R. and Lugo, A.E. 1991. Biomass of tropical forests of South and Southeast Asia. Can. J. For. Res., 21: 11-117.

Chavan, B.L. and Rasal, G.B. 2010. Sequestered standing carbon stock in selective tree species grown in University campus at, Aurangabad, Maharashtra, India. Int. J. Eng. Sci. Technol., 2 (7): 3003- 3007.

Chhabra A and Dadhwal, V.K. 2004. Assessment of major pools and fluxes of carbon in Indian forests. Climate Change, 64: 341-360.

Clark, D.A., Brown, S., Kicklighter, D.W., Chambers, J.Q., Thomlinson, J.R., Ni, J. and Holland, E.A. 2001. Net primary production in tropical forests: An evaluation and synthesis of existing field data. Ecol. Appl., 11: 371-384.

Cox, H.M. 2012. A sustainability initiative to quantify carbon sequestration by campus trees. J.Geogr., 20: 111-138.

Crookshank, S.L. 1999. Carbon Sinks and the Kyoto Protocol. Discussion Paper No. 091, American Petroleum Institute, Washinton DC, USA.

De Villiers, C., Chen, S. and Zhu, Y. 2014. Carbon sequestered in trees on a University campus: A case study. Sustain. Account. Manag. Policy J., 5: 149-171.

Djomoa, A.N., Ibrahima, A., Saborewskic, J. and Gravenhorsta, J. 2010. Allometric equations for biomass estimations in Cameroon and pan moist tropical equations including biomass data from Africa. 260(10): 1873-1885.

Fang, J., Chen, A., Peng, C., Zhao, S., and Ci, L. 2001. Changes in forest biomass carbon storage in China between 1949 and 1998. Science, 292: 2320 – 2322.

Food and Agricultural Organization (FAO). 2005. State of the World's Forests. FAO, Rome.

Gibbs, H.K., Brown, S., Niles, J.O. and Foley, J.A. 2007. Monitoring and estimating tropical forest carbon stocks: Making REDD a reality. Environ. Res. Lett., 2: 045023

Gorte, R. 2009. Carbon sequestration in forests, Congressional Research Service Report for Congress. 1-5

Gupta, H.S. 2009. Forest as a carbon sink: Temporal analysis for Ranchi district. Indian J. For., est 32(1): 7–11

Haghparast, H., Delbari, A. and Kulkarni, D.K. 2013. Carbon sequestration in Pune university campus with special reference to Geographical Information System (GIS). Ann. Biol. Res., 4: 169–175.

Haripriya, G.S. 2000. Estimate of biomass in Indian forests. Biomass Bioenerg., 19: 245–258

Haripriya, G.S. 2001. A framework for the carbon stored in Indian wood products. Environ. Dev. Sustain., 3: 229– 251

Haripriya, G.S. 2003.Carbon Budget of the Indian Forest Ecosystem. Climate Change, 56: 291-391.

Houghton, R.A. 1985. Net flux of carbon dioxide from tropical forest in 1980. Nature, 316.

Houghton, R.A., Skole, D.L., Nobre, C.A., Hackler, J.L., Lawrence, K.T. and Chomentowski, W.H. 2000. Annual fluxes of carbon from deforestation and regrowth in the Brazilian Amazon. Nature, 403: 301–304.

Houghton, R.A. 1990. The future role of tropical forest in affecting the carbon dioxide concentration of the atmosphere. Ambio, 19: 204-209.

IPCC. 2003. Good Practice Guidance for Land Use, Land-Use Change, and Forestry. IPCC National Greenhouse Gas Inventories Programme, Kanagawa, Japan.

Kaul, M., Dadhwal, V.K. and Mohren, G.M.J. 2009. Land use change and net C flux in Indian forests. For. Ecol. Manage., 258: 100–108

Kaur, K. and Sharma, S. 2014. Potential of agroforestry, inventorization, distribution pattern, and phytosociological analysis of tree species in block Ramgarh, Samba (J&K), India. Int. J. Adv. Agric. Sci. Technol., 2(6):19-25

Lal, R. and Bruce, J.P. 1999. The potential of world cropland soils to sequester C and mitigate the greenhouse effect. Environ. Sci. Policy, 2: 177-185.

Lal, R., Kimble, J.M. and Follett, R.F. 1998. Land use and soil C pools in the terrestrial ecosystem, Environ. Sci. Policy, 7: 1-10.

Lodhiyal, N. and Lodhiyal, L.S. 2003. Biomass and net primary productivity of Bhabar Shisham forests in central Himalaya, India. For. Ecol. Manage., 176(1-3): 217-235.

Lodhiyal, N., Lodhiyal, L.S. and Pangtey, Y.P.S. 2002. Structure and function of Shisham forests in Central Himalaya, India: Dry matter dynamics. Ann. Bot., 89(1): 41-54.

Manhas, R.K., Negi, J.D.S., Kumar, R., Chauhan P.S. 2006. temporal assessment of growing stock, biomass and carbon stock of Indian forests. Climatic Change, 74: 191–221

Montagnini, F. and Porras, C. 1998. Evaluating the role of the plantation as carbon sinks: An example of an integrative approach from the humid tropic. Environ. Manage., 22: 459-470.

Niles, J.O., Brown, S., Pretty, J., Ball, A.S. and Fay, J. 2002. Potential carbon mitigation and income in developing countries from changes in use and management of agricultural and forest lands. Philos. Trans. A Math. Phys. Eng. Sci., 360(1797):1621-1639.

Pussinen, A., Karjalainen, T., Makip, R., Valsta, L. and Kellom, A. 2002. Forest carbon sequestration and harvests in a Scots pine stand under different climate and nitrogen deposition scenarios. For. Ecol. Manage., 158(1–3): 103–115

Ravindranath, N.H. Somashekhar, B.S. and Gadgil, M. 1997. Carbon flow in Indian forests, submitted to the Ministry of Environment and Forest. Climate Change, 35(3): 297-320.

Redondo-Brenes, A. 2007. Growth, carbon sequestration, and management of negative tree plantation in the humid region of Costa Rica. New Forest, 34: 253-268.

Rowntree, R.A. 1984. Forest, canopy cover and land use in four eastern United States Cities. Urban Ecol., 8: 55-67.

Rowntree, R.A. and Nowak, D.J. 1991. Quantifying there of urban forest N removing atmospheric carbon dioxide. J. Arbori., 17: 269-275.

Singh, R. and Lal, M. 2000. Sustainable forestry in India for carbon mitigation. Curr.Sci., 78: 563-567.

Stephens, B.S. 2007. Weak northern and strong tropical land carbon uptake from vertical profiles of atmospheric $CO^2$. Science, 316: 1732-1735.

Vishnu, P.R. and Patil, S.S. 2016. Carbon storage and sequestration by trees in and around the university campus of Aurangabad city, Maharashtra. Int. J. Innov. Res. Sci. Eng. Technol., 5(4): 5459-5468

Vucetich, J.A. Reed, D.D., Breymeyer, A., Deg´orski, M., Mroz, G.D., Solon, J., Roo-Zielinska, E. and Noble, R. 2000. Carbon pools and ecosystem properties along a latitudinal gradient in northern Scots pine (Pinus sylvestris) forests. For. Ecol. Manage., 136: 135–145

Nature Environment and Pollution Technology
An International Quarterly Scientific Journal

p-ISSN: 0972-6268
(Print copies up to 2016)
e-ISSN: 2395-3454

Vol. 20 | No. 5 (Suppl) | pp. 2099-2110 | 2021

Original Research Paper

https://doi.org/10.46488/NEPT.2021.v20i05.027

Open Access Journal

# Comparative Life Cycle Assessment Analysis of Sewage Sludge Recycling Systems in China

**Jiawen Zhang† and Toru Matsumoto**
Graduate School of Environmental Engineering, The University of Kitakyushu, 808-0135, Japan
†Correspongding author: Jiawen Zhang; a9dac402@eng.kitakyu-u.ac.jp

**Nat. Env. & Poll. Tech.**
**Website: www.neptjournal.com**

*Received:* 14-07-2021
*Revised:* 02-09-2021
*Accepted:* 03-09-2021

**Key Words:**
Sewage sludge
Recycling
Life cycle assessment
ReCiPe method
Sustainability

## ABSTRACT

With the acceleration of economic development and urbanization in China, sewage sludge generation has sharply increased. To maximize energy regeneration and resource recovery, it is crucial to analyze the environmental impact and sustainability of different sewage sludge recycling systems based on life cycle assessment. This study analyzed four sewage sludge recycling systems in China through life cycle assessment using the ReCipe method, namely aerobic composting, anaerobic digestion and biomass utilization, incineration, and heat utilization and using for building materials. In particular, the key pollution processes and pollutants in sewage sludge recycling systems were analyzed. The results demonstrated that aerobic composting is the most environmentally optimal scenario for reducing emissions and energy consumption. The lowest environmental impact and operating costs were achieved by making bricks and using them as building materials; this was the optimal scenario for sludge treatment and recycling. In contrast, incineration and heat utilization had the highest impact on health and marine toxicity. Anaerobic digestion and biomass utilization had the highest impact on climate change, terrestrial acidification, photochemical oxidant formation, and particulate matter formation. In the future, policy designers should prioritize building material creation for sludge treatment and recycling.

## INTRODUCTION

With the rapid development of the economy and urbanization in China, municipal sewage has gradually become a huge environmental problem that needs to be urgently solved. To maintain ecological sustainability, the improvement of wastewater treatment focuses on saving energy and resources, recovering nutrients, and reducing waste production (Linderholm et al. 2012). Sewage sludge, as the main solid waste after wastewater treatment, increases with an increase in sewage treatment volume annually. Sewage sludge disposal and management have become an inescapable problem after wastewater treatment. In wastewater treatment systems, the "heavy sewage light sludge" phenomenon is common, and the environmental impact of wastewater cannot be entirely eliminated.

Sludge generation in China steadily rose annually from 11 million tons in 2005 to 21 million tons in 2010, with sludge having 80% water content. The dry sludge production in China is summarized in Fig. 1; it showed an average annual growth of 9% from 2011 to 2017. Sewage sludge treatment has previously been considered secondary to wastewater treatment but is gradually becoming one of the most significant challenges facing municipal wastewater management worldwide, particularly in China (Yang et al. 2015). Currently, the main methods include aerobic sludge fermentation for agricultural waste, anaerobic digestion to recover biomass, incineration, or production of building materials or fuel (Mininni et al. 2015, Hong et al. 2009, Zhang et al. 2017). In fact, the large quantity of sewage sludge should not be considered a heavy burden to municipal management but rather a great source of bioenergy and recovered material (Raheem et al. 2018, Tyagi & Lo 2013).

Life cycle assessment (LCA) is a technique used to assess the environmental impacts associated with all stages of a product's life from raw material extraction through material processing, manufacturing, distribution, use, repair and maintenance, and disposal or recycling (Ekvall et al. 2017, ISO 2006, Pasqualino et al. 2009). At present, LCA, as a management evaluation to analyze the environmental impact, is used for technical comparison of certain methods of sludge treatment to identify technological improvement in the further (Huppes & Oers 2011, Kelessidisa & Stasinakis 2012, Scheutz 2018, Schrijvers et al. 2016, Suh & Rousseaux 2002, Xiao et al. 2018, Xu et al. 2014). Simultaneously, the environmental impact of different sludge treatment methods is evaluated by LCA, especially greenhouse gas emissions and energy efficiency (Houillon et al. 2005, Li et al. 2017, Li & Feng 2018, Liu et al. 2011, Mill et al. 2014, Li & Feng 2018). Yoshida et al. (2018) reviewed 35 published studies

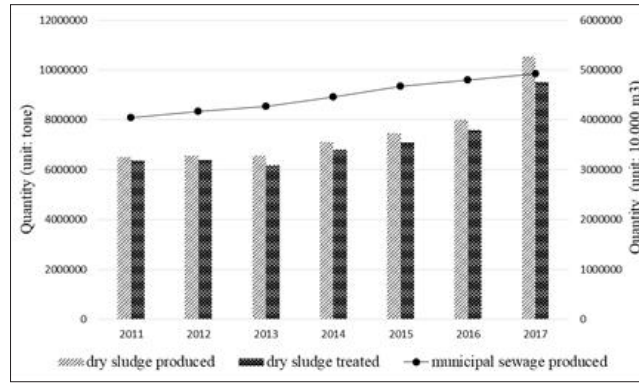


Fig. 1: Dry sludge produced, dry sludge treated, and municipal sewage produced in China

on life cycle assessment (LCA) of sewage sludge for their methodological and technological assumptions. Overall, LCA has been providing a flexible framework to quantify the environmental impacts of wastewater and sewage sludge treatment and disposal processes for multiple scales, ranging from process selection to policy evaluation. The results of LCA are, in principle, unique to the goal and scope of each study, reflecting its local conditions, and comparison between different LCAs is not intended. Furthermore, the assessments are limited by the methodological development of the life cycle impact assessment (LCIA) and the advancement of research in quantifying environmental emissions associated with wastewater and sewage sludge treatment processes. With the significant impact of global warming, accurate calculation of greenhouse gas (GHG) emissions is essential, including direct emissions and indirect emissions (Ding et al. 2021). The direct emissions of GHGs are incomplete in environmental impact assessments (EIAs), which unaccounted for direct $CO_2$ emissions.

Furthermore, Hospido et al. (2010) evaluated the reuse of anaerobically digested sludge in agriculture from an environmental point and specifically quantified the potential impacts of emerging micropollutants such as pharmaceuticals (Hospido et al. 2010, Xu et al. 2014). In a later comparative study, Heimersson et al. (2017) identified and explored several scenarios to handle multi-functionality in the LCA of a sludge handling system (Ekvall et al. 2007, Heimersson et al. 2017). The authors used LCA to examine the environmental impact of strategic sludge treatment and end-use decisions. The authors also modeled resource recovery and accounted for different possibilities for secondary functions such as biogas and sludge used in agriculture. In contrast, Linderholm et al. (2012) investigated the environmental impact of sewage sludge as a phosphorus alternative for agriculture. Their study focused on secondary functions, such as nutrient input to soil (Johansson et al. 2008, Linderholm et al. 2012).

In the case of comparative "Waste LCAs", as the amount of waste treated can be equal in the different scenarios, a simplification is done by excluding the upstream materials and processes from the system boundaries. This means that the system is focused only on waste treatment. This concept is called the "zero burden assumption" and is also known as the cut-off approach. This "zero burden assumption" concept was first used on an LCA system simplification for a comparative "Waste LCA" analysis (Huppes & Oers 2011, Piao et al. 2016). While some of these technologies exist only at laboratory or pilot scales, others are fully functional at the industrial scale, and there is a growing willingness to increase the sustainability of sludge management via recovery processes that extract potentially marketable value-added products. In this study, sewage sludge was considered "waste"—free of environmental impact—where the sewage sludge recycling process was designed to produce a product with high added value in the recycling system (Pradel et al. 2016). This created uncertainty in the comparative LCA of the system that produced the value-added products used by sewage sludge. The limitations of this study include incomplete accounting of GHG emissions and uncertainty caused by ignoring the environmental impact of sewage sludge.

The aim of this study was to identify the environmental and economic impacts of four sewage-sludge recycling systems to determine the optimal system in China. This research contributes to the field by evaluating the sustainability of sludge management based on the recovery and reuse of potential value-added products and modeling the sludge as waste to assess the environmental impact of sludge treatment. Moreover, the main environmental impacts and corresponding pollution phases of the four systems were identified as suggestions for technology or management improvements in the future.

## MATERIALS AND METHODS

### Goal and Scope

The goal of this study was to compare and assess four sewage sludge recycling systems from an environmental and economic viewpoint, to obtain clear results about the environmental preferences of both viewpoints to enable decision-makers to develop a sustainable sewage sludge disposal policy. The LCA of scenarios was performed from a 'gate to gate' perspective and comprises all environmentally relevant processes from sludge as waste to the finished energy recovery or material substitution. The functional unit of this LCA was 1 ton of sewage sludge, including 80% moisture.

### System Boundary

The boundary of Scenario 1 (S1), the incineration process using fluidized bed combustion technology, includes partial drying of sludge to achieve 40% dry matter content using the heat of the incineration of flue gases, incineration of sludge, heat and electricity generation, and exhaust gas purification. Aerobic composting (Scenario 2 (S2)) using high-temperature fermentation includes mixing with conditions and fermentation bacteria to achieve a 60% moisture rate, primary fermentation to reduce the moisture rate to 50%, and secondary fermentation to obtain a fertilizer substitute and purify exhaust gas. Scenario 3 (S3) proposed the use of sewage sludge as a raw material substitute in brick production, including mixing with other raw materials; the brick-making process, including making bricks, drying bricks, and roasting bricks; exhaust gas purification, and brick production. Scenario 4 (S4), which was the anaerobic digestion process in an AAe anaerobic digestion reactor that reacts at high solid concentration, includes conditioning with reflux sludge, anaerobic digestion, biogas, and heat generation, and exhaust gas purification. The overall scope of this study, comprising the most important processing stages involved in sewage sludge treatment and recycling and included in LCA, is shown in Fig. 2.

### Life-Cycle Inventory

This study was based on data from both sewage sludge treatment processes. Thus, the processes of the four scenarios are based on the EIA of each sludge disposal plant. The difference in sludge composition used in the four scenarios is not taken into account in this study to compare four different methods. The significant variations in data are attributed to the waste-water treatment plants in China because they do not send proper reports on the treatment and final disposal of their sewage sludge. To carry out the inventory, data was mainly collected from EIAs for projects using four sludge treatment technologies and from the Chinese Life Cycle Database (CLCD). The overall inputs and outputs to be measured in the study should be elementary flows. To evaluate the function of sludge treatment and recycling systems, a large amount of basic data is necessary. Energy and raw material use, as well as emissions from energy production activities such as electricity generation, are among them.

The use of sludge and other solid waste will not exacerbate the intensity of consumption of natural resources; hence, the analysis of inventory data only considers the energy consumption and pollutant emissions of raw materials, such as crude and iron, in the process. First, we established the energy-material balance for each unit process based on the function of the unit. Then, we created the inventories for each

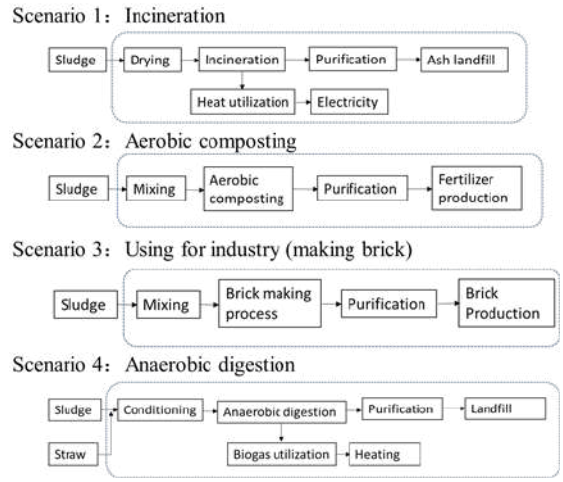


Fig. 2: System boundaries of the cradle-to-gate for both energy recovery or material substitution scenarios using treated urban sewage sludge.

scenario based on the functioning of units in each scenario shown in Table 1. The life cycle inventory of the scenarios includes the following aspects (Wang et al. 2015):

1) Main technical indicators of scenarios, including production and specifications;
2) Consumption of various raw materials in the scenarios, including the use of waste;
3) Energy consumption;
4) Water consumption;
5) The amount of pollutants contained in the ecology system;
6) The amount of pollutants produced by conventional production was reduced by sludge recycling.

## RESULTS AND DISCUSSION

To analyze the outstanding environmental impact category and evaluate the environmental impact of each scenario, the normalization results, as presented in Table 2, were calculated using the world reference values and characterization results. Using the midpoint environmental impact weights, we calculated the endpoint environmental impact; the results showed that the endpoint environmental impact was S2 < S4 < S1 < S3.

An environmental load of each scenario on different environmental impact categories was analyzed based on the characterization results. As the impact of S2 for every environmental category was significantly lower than that of the other three scenarios, the characterization results of S1, S3, and S4 were compared and analyzed. The environmental load of S1 in TT was significantly higher than that of the other two scenarios. In terms of CC, AP, MEP, HT, FT, MT, POFP, and PMFP, the environmental load of S4 was the most obvious of the three scenarios. Climate change, human toxicity, photochemical oxidant formation, particulate matter formation, and ozone depletion were the impact categories that affect human health. S2 had a positive value for each of these categories. S4 should focus on the environmental impact categories of CC, HT, POFP, and PMFP. S1 had a significant impact on each category, especially ozone depletion.

Paying attention to the greenhouse gas emissions during the sludge disposal process can reduce other pollutants caused by energy consumption, and alternatively, it can

Table 1: Inventory of main energy and materials consumption of the four scenarios.

| Inventory flow | Unit | S1 | S2 | S3 | S4 | Inventory flow | Unit | S1 | S2 | S3 | S4 |
|---|---|---|---|---|---|---|---|---|---|---|---|
| **Input** | | | | | | | | | | | |
| Electricity | kWh | 108.18 | -73.413 | 1.09 | 294.81 | Crude | kg | -0.14 | - | 24.552 | - |
| Gas | kg | 20.60 | - | | - | Water | kg | 33.70 | 1305 | 72.5 | 1.9 |
| Coal | kg | -5.57 | -10.2 | 65.2 | -0.546 | Iron | kg | - | - | -8.23E-06 | - |
| **Output** | | | | | | | | | | | |
| $NH_3$ | kg | 0.01 | -12.75 | | 0.01 | As | kg | -2E-05 | -3.28E-02 | - | - |
| $H_2S$ | kg | 4E-04 | 0.03 | 5E-04 | 0.02 | Cr | kg | -1.62E-06 | -8.28E-03 | - | - |
| HCl | kg | 0.01 | - | 0.007 | - | Ni | kg | -2.3E-05 | -1.23E-05 | - | - |
| HF | kg | 0.002 | -0.017 | 0.007 | - | V | kg | -2.76E-05 | -1.42E-04 | - | - |
| $SO_2$ | kg | 0.105 | -1 | 0.41 | -0.002 | Zn | kg | -2.3E-05 | -1.42E-04 | - | - |
| $CH_4$ | kg | -0.025 | -0.128 | - | -0.005 | Dioxin | kg | 2E-08 | - | - | - |
| NMVOC | kg | -0.0047 | -0.024 | - | - | $COD_{cr}$ | kg | 1.4 | 0.049 | 0.03 | 2.3 |
| CO | kg | 0.025 | -0.437 | - | - | $NH_3$-N | kg | 0.14 | -4.047 | 0.003 | 2 |
| $CO_2$ | kg | 139.728 | -654 | -2.85E-05 | -0.947 | CxHy | kg | - | -0.075 | - | - |
| $NO_x$ | kg | 0.548 | -0.99 | 0.29 | 0.0183 | $SO_4^{2-}$ | kg | - | -0.025 | - | - |
| Dust | kg | 38.47 | 5.55 | 1 | -0.15 | $N_2O$ | kg | - | -1.656 | | - |
| Hg | kg | 8.92E-05 | -4.32E-06 | - | - | NOx-N | kg | - | -0.166 | | - |
| Cd | kg | 8.99E-05 | -8.64E-04 | - | - | TN | kg | - | - | - | 2.7 |
| Pb | kg | 1.83E-04 | -3.88E-03 | - | - | TP | kg | - | - | - | 0.3 |

Table 2: ReCiPe midpoint normalization results for all scenarios (Values are presented per functional unit).

| Categories | Unit | S1 | S2 | S3 | S4 |
|---|---|---|---|---|---|
| Climate change [CC] | p/yr | 4.94E-03 | -1.53E-01 | 6.96E-04 | 7.41E-05 |
| Terrestrial acidification [AP] | p/yr | 5.18E-03 | -2.03E+00 | 4.37E-02 | 1.26E-04 |
| Marine Eutrophication [MEP] | p/yr | 2.25E-03 | -3.83E-01 | 5.58E-03 | 7.24E-04 |
| Human toxicity [HT] | p/yr | 1.70E-02 | -3.31E+01 | 3.28E-03 | 3.69E-04 |
| Terrestrial toxicity [TT] | p/yr | 2.34E-03 | -7.78E-02 | 1.34E-04 | 1.56E-05 |
| Freshwater toxicity [FT] | p/yr | 9.67E-05 | -2.87E-02 | 2.48E-05 | 2.89E-06 |
| Marine toxicity [MT] | p/yr | 2.06E-02 | -2.48E+00 | 2.74E-03 | 3.19E-04 |
| Photochemical oxidant formation [POFP] | p/yr | 2.40E-03 | -9.05E-02 | 1.70E-02 | 4.52E-05 |
| Particulate matter formation [PMFP] | p/yr | 2.04E-02 | -3.81E-01 | 2.37E-01 | 5.93E-04 |
| Water depletion [WDP] | p/yr | 1.21E-03 | 6.51E-03 | 7.12E-02 | 8.03E-07 |
| Fossil fuel depletion [FDP] | p/yr | 2.50E-03 | -4.39E-02 | 3.20E-02 | 3.97E-05 |
| Freshwater eutrophication [FEP] | p/yr | 0 | -1.32E+01 | 0 | 1.27E-03 |
| Metal depletion [MDP] | p/yr | 0 | 0 | -3.84E-07 | 0 |
| Ozone depletion [ODP] | p/yr | 2.05E-04 | 0 | 6.55E-03 | 0 |

motivate people to develop new clean energy technology. Therefore, climate change is an impact category that is specifically considered in research.

Fig. 3 presents the relative constituents of the impact on the climate change category. From the results of the climate change impact, S2 had a positive environmental impact. The reason for the positive environmental impact of S2 was the reduction in $N_2O$. $N_2O$ is produced in mineral fertilizer production, and it has a huge influence on climate change. $N_2O$ was not significantly generated in S2 compared with

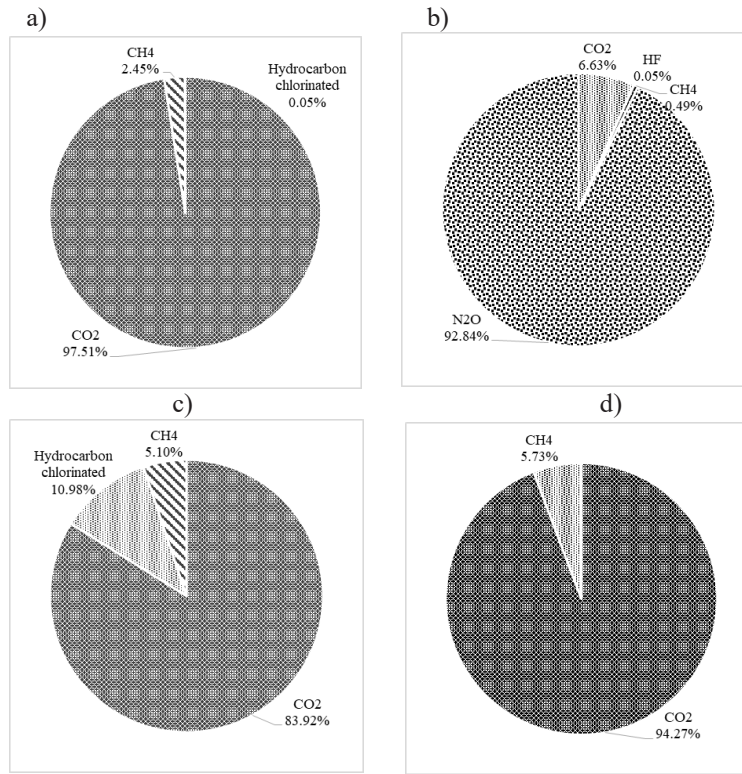


Fig. 3: The relative constituents about the impact category of climate change a) scenario 1, b) scenario 2, c) scenario 3, d) scenario 4.

mineral fertilizer production. According to the analysis of the contributors to climate change, the main pollutant driving climate change is $CO_2$. Organic matter content and energy utilization are the main sources of $CO_2$. Therefore, the organic matter content in the sludge should be reduced. Additionally, sludge treatment and recycling should focus on energy conservation.

Fig. 4. shows the proportion of each environmental impact category in the four scenarios. S2 presents an obvious positive environmental impact. In addition to certain environmental impacts in WDP, S2 was beneficial to the environment in other impact categories. From the normalization results (Fig. 4), the most obvious midpoint environmental impact category was human toxicity, followed by freshwater eutrophication, marine toxicity, and terrestrial acidification.

The main normalization results of different processes in S2, as shown in Fig. 5, were reflected in the reduction of environmental load by replacing the mineral fertilizer. The most obvious midpoint environmental impact category of S2 was HT and FEP. Heavy metals, such as As, Cd, Pb, and Cr, are produced during mineral fertilizer production. As a result, heavy metal resources are derived solely from indirect emissions caused by energy use. The environmental impact of human toxicity in S2 was significantly reduced, showing an overall impact on the environment.

These normalization results indicated the relative magnitude of the environmental impacts of aerobic composting on sludge-based fertilizer production compared to mineral fertilizer manufacture at a global level. In the midpoint environmental impact categories of human toxicity and freshwater eutrophication, there were impacts that were significantly beneficial to the environment, and the environmental impact was also relatively reduced in terms of marine toxicity and terrestrial acidification. During the entire life cycle of the

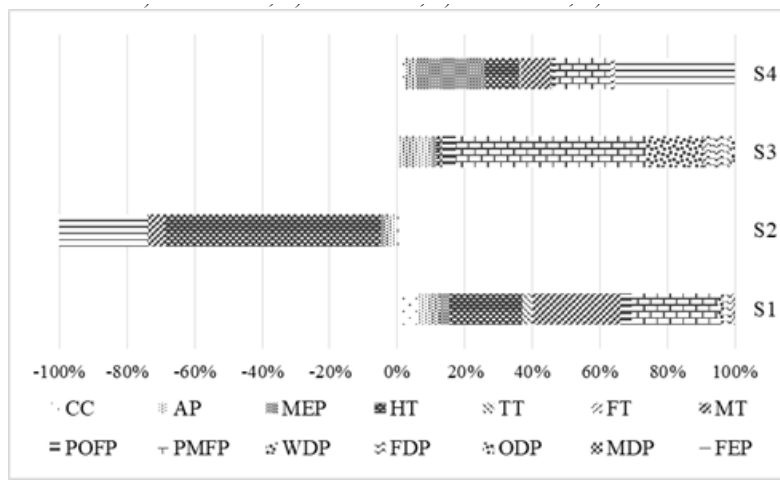


Fig. 4: The proportion of each impact category in four scenarios.

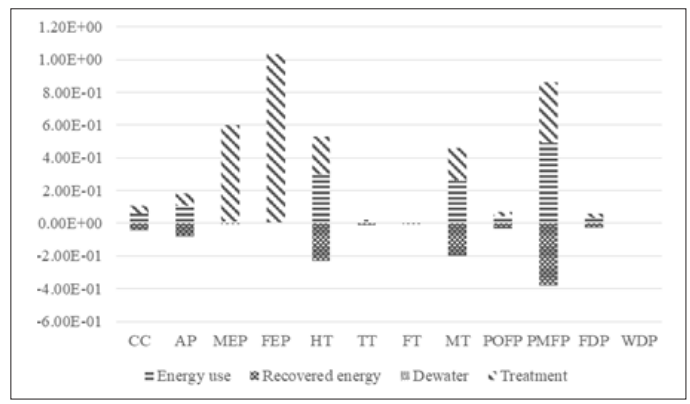


Fig. 5: The normalization results of aerobic composting (S2) as well as the offset caused by material substitution.

mineral fertilizer production process, the stages included ore extraction, transportation, energy consumption, and mineral fertilizer production. In S2, sewage sludge—considered "waste"—was free of any environmental burden when used for sludge-based fertilizer production. Therefore, the production of sludge-based fertilizers instead of mineral fertilizers should be promoted in the fertilizer industry.

The environmental impacts of the other three sludge treatment and recycling systems were mainly from energy consumption and sludge treatment and recycling processes, and the environmental impacts during the pretreatment process were negligible.

From the perspective of environmental assessments, S3 had the greatest number of negative environmental impacts of the four sludge treatments and recycling systems. According to the normalization results shown in Fig. 6, PMFP and WDP had significant negative environmental impacts during S3, which was 4-200 times that of other environmental impact categories such as CC. Dust, $SO_2$, and NOx lead to particulate matter formation during the treatment process of S3. The process of making bricks causes water depletion.

On the other hand, FDP, AP, and POFP also showed obvious environmental impacts. The main sources of FDP, AP, and POFP, which are shown in Fig. 7, are treatment processes including SO2, CO, CH4, non-methane volatile organic compounds (NMVOC), NOx, HF, HCl, and dust. They are derived from emissions during the production of raw materials and the brick-making process. POFP and PMFP are the major midpoint environmental impact categories affecting human health in S3. According to the analysis of the released constituents (Fig. 7), NOx (87.77%) and SO2 (10.07%) were the principal sources of PMFP. In addition, dust (87.24%) was the principal source of POFP. Therefore, in S3, the sludge treatment and recycling process should improve the production technology to reduce water use and carry out clean production to reduce the environmental im-

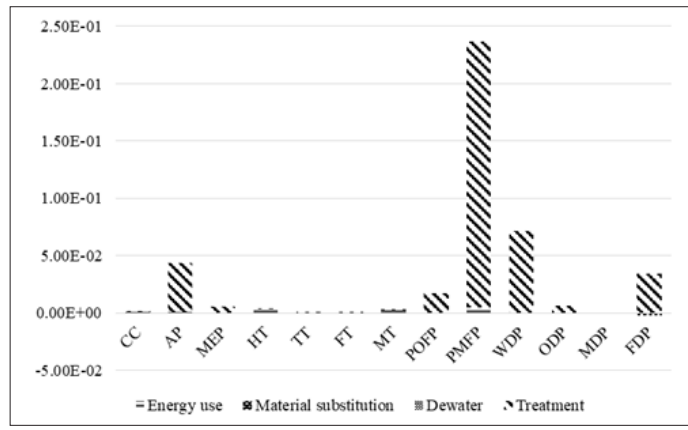


Fig. 6: The normalization results of using in industry (S3) as well as the offset caused by material substitution.


Fig. 7: The relative constituents about midpoint environmental impact of human health in Scenario 3 a) PMFP, b) POFP.

pact of the treatment process. According to the normalization results of S1 shown in Fig. 8, HT, MT, FDP, and PMFP are obvious impact categories in which S1 has the most serious environmental impact.

In the environmental impact categories of CC, AP, and FDP, S1 also had significant negative environmental impacts. CC, HT, and PMFP were the major midpoint environmental impact categories of human health in S1. Fig. 9 presents the relative constituents of each environmental impact category. From the perspective of CC, the environmental impact mainly comes from the use of fossil energy and the emission of $CO_2$ (98%) during sludge incineration. The main sources of human toxicity were heavy metals, hydrocarbons, and dioxins, of which Cr (53.89%) and Hg (32.91%) are the main influences. Cr is mainly derived from energy consumption and Hg is in the process of sludge incineration. However, the mechanism of dioxin production is complicated. For example, dioxin is easily produced when the incineration temperature is less than 800°C during the burning of domestic garbage. Among them, PMFP pollutants come from dust (81.39%) during energy consumption and incineration.

Therefore, according to the above analysis, energy consumption is the main cause of HT, MT, POMF, AP, and CC. In S1, pollutants were mainly derived from energy consumption, and heavy metal and dust emissions were high because China still relies mainly on thermal power generation. Therefore, in future production processes, the use of clean energy should be gradually promoted to reduce the proportion of thermal power generation. At the same time, the incineration process should focus on the collection and treatment of dust in S1.

From the normalization results of S4 shown in Fig. 10, FEP, MEP, HT, MT, and PMFP were the most serious environmental impacts in the environmental impact categories, followed by AP, CC, POFP, and FDP. Among them, the environmental impact of TT, FT, and WDP was almost zero, and the impact of S4 on these environmental impact categories can be neglected.

The source of the FEP is the production of TP during anaerobic digestion. The main causes of MEP are $NH_3$-N

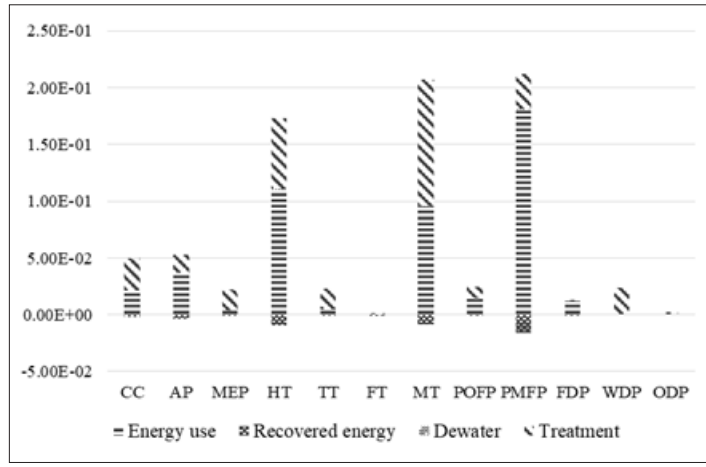


Fig. 8: The normalization results of incineration (S1) as well as the offset caused by recovered energy.

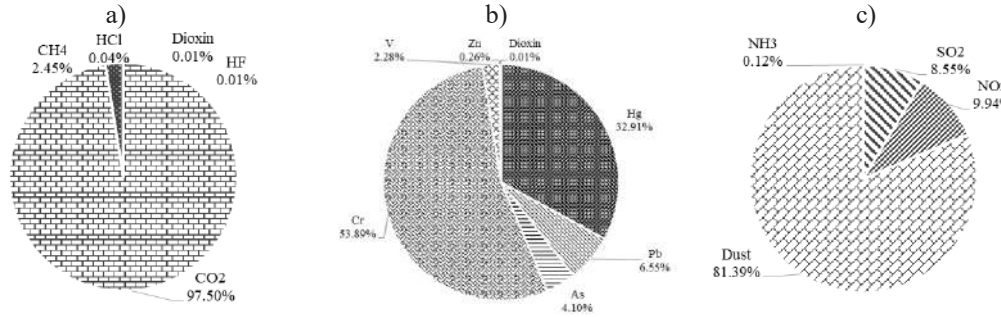


Fig. 9: The relative constituents about midpoint environmental impact of human health in S1
a) CC, b) HT, c) PMFP.

and TN, which are produced during anaerobic digestion, and NOx from energy production. CC, HT, PMFP, AP, and MT pollution sources are mainly derived from pollutants generated during and after energy production and use and are the most obvious midpoint environmental impact categories of human health in S1, followed by CC and POFP. The main constituent of HT was AS (87.94%), as shown in Fig. 11. The main reason for PMFP was PM10 (85.17%) during the process of energy production and consumption. The main influencing constituent of CC was $CO_2$ (94.27%), similar to S1. TN (62.27%) and $NH_3$-N (35.98%) caused the impact of POFP during the energy consumption and treatment process of S4.

In view of this, the main pollution from S4 comes from heavy metals and dust in energy production and pollutants of N and P in the process of anaerobic digestion. Therefore, the utilization of clean energy should be promoted, and technology should be improved to reduce the pollutant emissions of N and P in the future. The other three scenarios, in addition to S2, had the greatest impact on the midpoint of particulate

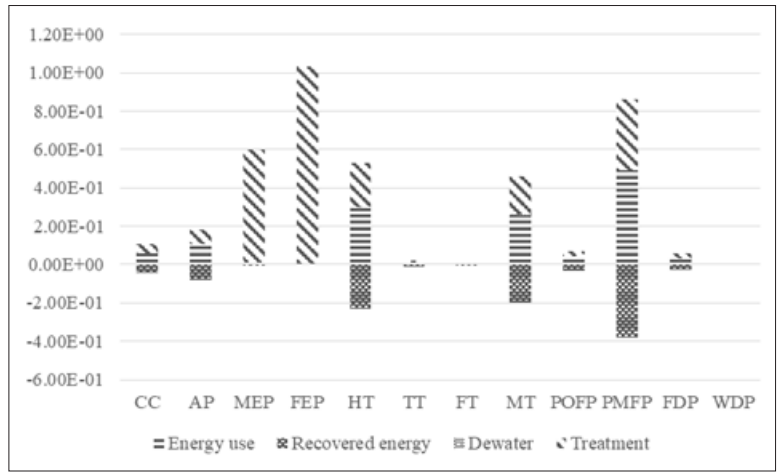


Fig. 10: The normalization results of anaerobic digestion (S4) as well as the offset caused by recovered energy.

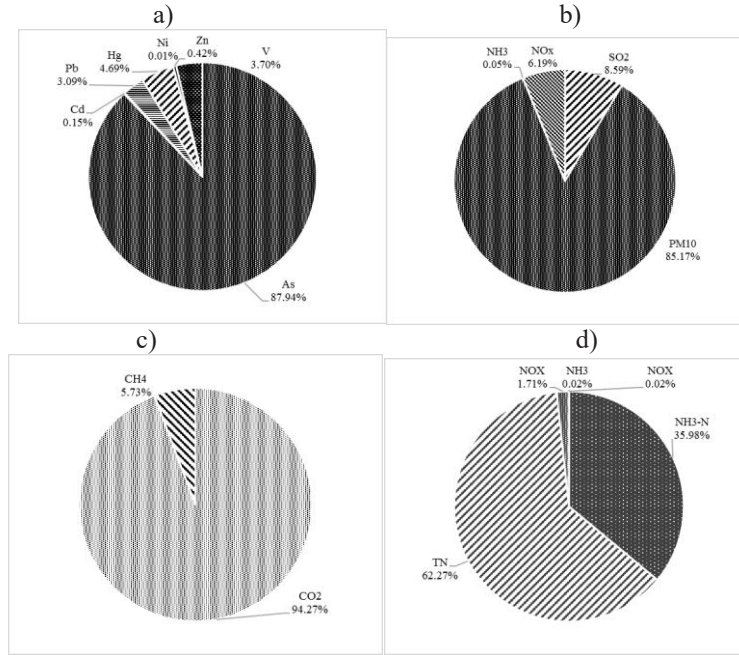


Fig. 11: The relative constituents about midpoint environmental impact of human health in scenario 4 a) HT, b) PMFP, c) CC, d) POFP

matter generation due to emissions from sludge treatment and recycling operations, as well as indirect emissions from energy use. Incineration and anaerobic digestion have obvious environmental impacts in the four midpoint environmental impact categories of global warming, human toxicity, marine toxicity, and fossil fuel depletion.

The operating costs of the sludge treatment and recycling system were estimated using the functional units of the four scenarios. China's subsidy policy for sludge recycling has not been well defined. In fact, each province has its own detailed subsidy policy. Jiangsu Province has a clear subsidy policy for the four scenarios involved in this study (Liu et al., 2013). Therefore, this study adopted Jiangsu's subsidy policy for sludge recycling. Based on the statistical results, the operating costs under the subsidies for each program are listed in Table 3.

The operating costs and the environmental and economic impacts of the various programs are basically the same. Combined with the environmental assessment results of the four schemes, S2 had the highest operating cost and the lowest environmental impact. Among the other three options, S3 had the least environmental impact and the lowest operating cost, as shown in Fig. 12, which is similar to the findings of Han et al. (2021). Compared with Liu et al. (2013), incineration was the optimal method, followed by anaerobic digestion and aerobic composting. The theoretical value of incineration and actual operation may have caused the differences in the results (Liu et al. 2013). In Xiao et al. (2018), hydrothermal-pyrolysis technology as a new method demonstrated the best performance with the lowest consumption of land resources, a relatively small environmental impact, and high economic benefits compared with other methods. The scenario of creating building materials (bricks) was not considered in Xu et al. (2014), and anaerobic digestion was a suitable alternative for sewage sludge treatment (Xu et al. 2014). In sum, it is similar to the comparison of the results obtained with previous literature.

## CONCLUSION

This study shows which scenarios of sludge treatment and recycling systems are more sustainable during the period of operation from an environmental perspective. Human health is the primary impact category of the overall environmental impact. S2 was the most environmentally friendly scenario, with the fewest emissions and lowest energy consumption. S3 was the optimal scenario, based on the lowest environmental impact and operating costs. According to the analysis of pollutant sources and composition, treatment and recycling processes mainly account for the environmental impacts. According to the endpoint environmental impact results, human health was the primary endpoint environmental impact category for the scenarios. In the midpoint characterization results of human health, S1 had significantly higher environmental impacts on CC and HT than other scenarios, and S3 had obvious environmental impacts on POFP and PMFP.

In S1, pollutants were mainly derived from energy consumption, and heavy metal and dust emissions were high because China still relies mainly on thermal power gener-

Table 3: The cost under subsidy of four scenarios (Values are presented per functional unit).

| | S1 | S2 | S3 | S4 |
|---|---|---|---|---|
| Cost ($) | 34 | 79 | 20 | 37 |

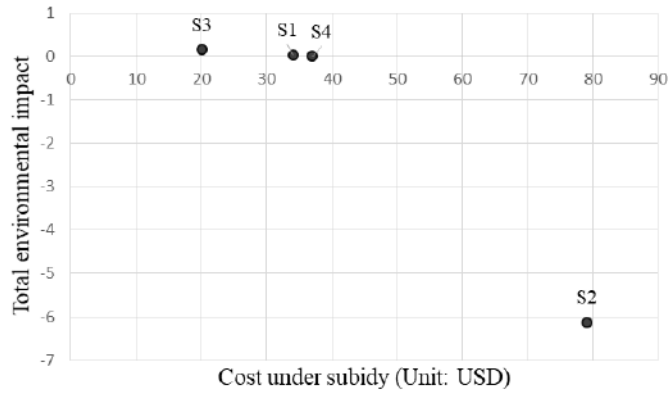


Fig. 12: Total environmental impact and operating cost of four scenarios.

ation. Therefore, in future production processes, the use of clean energy should be gradually promoted to reduce the proportion of thermal power generation. At the same time, the incineration process should focus on the collection and treatment of dust in S1.

Considering the environmental assessment results of the four schemes, S2 had the highest operating cost and the lowest environmental impact. The reason for the minimal environmental impact of S2 was that sewage sludge—considered "waste"—was free of any environmental burdens when used for sludge-based fertilizer production. In the future, the operating costs of S2 should be minimized. Therefore, the production of sludge-based fertilizers instead of mineral fertilizers should be promoted in the fertilizer industry.

In view of the above analysis, S3 was the optimal solution among the four scenarios because of its minimal operating costs and relatively small environmental impact. When comparing the human health impact, PMFP, POFP, and ODP were major impact categories. The treatment process was the main source of these environmental impacts. The treatment plants should carry out clean production to reduce dust and nitrogen oxides during the treatment process.

S4 should focus on CC, HT, POFP, and PMFP, which cause damage to human health. MEP and FEP are also obvious impact categories in S4. In view of the above analysis, the main pollution in S4 comes from heavy metals, NMVOC, and dust in energy production and pollutants of N and P in the process of anaerobic digestion. Therefore, the utilization of clean energy should be promoted, and the technology should be improved to reduce the environmental impact, especially pollutant emissions of N and P.

The following limitations of the study should be noted when considering the conclusions of the study. This study investigated the environmental performance of the systems investigated during their operation and does not consider the effect of their construction. Due to methodological issues with their classification and normalization, some impact categories, such as land occupation and the indirect effect of the avoided fertilizer on agricultural land application, were not considered. Finally, the data and assumptions used in this study were based on the Chinese context.

In future research, life cycle cost analysis will be added to the study, and the economic evaluation of the four programs will be considered more completely. Local factors such as economic level and industrial structures in various regions of China should be considered in future studies on the planning of sewage sludge reuse in various regions of China.

## REFERENCES

Ding, A., Zhang, R.R., Ngo, H.H., He, X., Ma, J., Nan, J. and Li, G.B. 2021. Life cycle assessment of sewage sludge treatment and disposal based on nutrient and energy recovery: A review. Sci. Total. Environ., 769: 144451.

Ekvall, T., Assefa, G., Björklund, A., Eriksson, O. and Finnveden, G. 2007. What life-cycle assessment does and does not do in assessments of waste management. J. Waste Manag., 27: 989-996.

Han, W., Jin, P.K., Chen, D.W., Liu, X.K., Jin, H., Wang, R. and Liu, Y.J. 2021. Resource reclamation of municipal sewage sludge-based on local conditions: A case study in Xi'an, China. J. Cleaner Prod., 316: 128189.

Heimersson, S., Svanström, M., Cederberg, C. and Peters, G. 2017. Improved life cycle modeling of benefits from sewage sludge anaerobic digestion and land application. Resour. Conserv. Recycl., 122: 126-134.

Hong, J.L., Otaki, M. and Jolliet, O. 2009. Environmental and economic life cycle assessment for sewage sludge treatment processes in Japan. J. Waste Manag., 29: 696-703.

Houillon, G. and Jolliet, O. 2005, Life cycle assessment of processes for the treatment of wastewater urban sludge: energy and global warming analysis. J. Cleaner Prod., 13: 287-299.

Hospido, A., Carballa, M., Moreira, M., Omil, F. and Feijoo, G. 2010. Environmental assessment of anaerobically digested sludge reuse in agriculture: Potential impacts of emerging micropollutants. Water Res., 44: 3225-3233.

Huppes, G. and Oers, L.V. 2011. Background Review of Existing Weighting Approaches in Life Cycle Impact Assessment (LCIA), JRC Scientific and Technical Reports.

ISO. 2006. 14040 Environmental Management - Life Cycle Assessment - Principles and Framework.

Johansson, K., Perzon, M., Fröling, M., Mossakowska, A. and Svanström, M. 2008. Sewage sludge handling with phosphorus utilization – life cycle assessment of four alternatives. J. Cleaner Prod., 16: 135-151.

Kelessidisa, A. and Stasinakis, A.S. 2012. Comparative study of the methods used for treatment and final disposal of sewage sludge in European countries. J. Waste Manag., 32: 1186-1195.

Li, H. and Feng, K. 2018. Life cycle assessment of the environmental impacts and energy efficiency of integration of sludge anaerobic digestion and pyrolysis. J. Cleaner Prod., 195: 476-485.

Li, H., Jin, C., Zhang, Z.Y., O'Hara, I. and Mundree, S. 2017. Environmental and economic life cycle assessment of energy recovery from sewage sludge through different anaerobic digestion pathways. Energy, 126: 649-657.

Linderholm, K., Tillman, A.M. and Mattsson, J.E. 2012. Life cycle assessment of phosphorus alternatives for Swedish agriculture. Resour. Conserv. Recycl., 66: 27-39.

Liu, B.B., Wei, Q., Zhang, B. and Bi, J. 2013. Life cycle GHG emissions of sewage sludge treatment and disposal options in Tai Lake Watershed. Sci. Total. Environ, 447: 361-369.

Liu, Q., Jiang, P.P., Zhao, J., Zhang, B., Bian, H.D. and Qian, G.R. 2011. Life cycle assessment of an industrial symbiosis based on energy recovery from dried sludge and used oil. J. Cleaner Prod., 19: 1700-1708.

Mill, N., Pearce, P., Farrow, J., Thorpe, R.B. and Kirkby, N.F. 2014. Environmental and economic life cycle assessment of current and future sewage sludge to energy technologies. J. Waste Manag., 34: 185-195

Mininni, G., Blanch, A.R., Lucena, F. and Berselli, S. 2015. EU policy on sewage sludge utilization and perspectives on new approaches of sludge management. Environ. Sci. Pollut. Res., 22: 7361-7374.

Pasqualino, J.C., Meneses, M., Abella, M. and Castells, F. 2009. LCA as a decision support tool for the environmental improvement of the operation of a municipal wastewater treatment plant. Environ. Sci. Technol., 43(9): 3300-3307.

Piao, W.H., Kim, Y.J., Kim, H.S., Kim, M.S. and Kim, C.W. 2016. Life cycle assessment and economic efficiency analysis of integrated management of wastewater treatment plants. J. Cleaner Prod., 113: 325-337.

Pradel, M., Aissani, L., Villot, J., Baudez J.C. and Laforest, V. 2016. From waste to added value product: towards a paradigm shift in life cycle assessment applied to wastewater sludge: A review. J. Cleaner Prod., 131: 60-75.

Raheem, A., Sikarwar, V.S., He, J., Dastyar, W., Dionysiou, D.D., Wang, W. and Zhao, M. 2018. Opportunities and challenges in sustainable treatment and resource reuse of sewage sludge: A review. Chem. Eng. J., 337: 616-641.

Scheutz, C. 2018. Life cycle assessment of sewage sludge management options including long-term impacts after land application. J. Cleaner Prod., 174: 538-547.

Schrijvers, D.L., Loubet, P. and Sonnemann, G. 2016. Developing a systematic framework for consistent allocation in LCA. Int. J. Life Cycle Assess., 21: 976-993.

Suh, Y.J. and Rousseaux, P. 2002. An LCA of alternative wastewater sludge treatment scenarios. Resour. Conserv. Recycl., 35: 191-200.

Tyagi, V.K. and Lo, S.L. 2013. Sludge: A waste or renewable source for energy and resources recovery? Renew. Sustain. Energy Rev., 25: 708-728.

Wang, X., Zhao, B., Zhang, A. and Sha, Z. 2015. The present situation and research progress of treatment of sludge from city sewage treatment plant. Tian. Daxue Xue., 30: 165.

Xiao, L.S., Lin, T., Wang, Y., Ye, Z.L. and Liao, J.F. 2018. Comparative life cycle assessment of sludge management: A case study of Xiamen, China. J. Cleaner Prod., 192: 354-363.

Xu, C.Q., Chen, W. and Hong, J.L. 2014. Life-cycle environmental and economic assessment of sewage sludge treatment in China. J. Cleaner Prod, 67: 79-87.

Yang, G., Zhang, G. and Wang, H. 2015. The current state of sludge production, management, treatment, and disposal in China. Water Res., 78: 60-73.

Yoshida, H., Hoevea, M., Christensen, T.H., Bruun, S. and Jensen, L.S. 2013. Life cycle assessment of sewage sludge management: A review. Waste Manag., 31: 1083-1101.

Zhang, Q.G., Hu, J.J., Lee, D. J., Chang, Y.J. and Lee Y.J. 2017. Sludge treatment: Current research trends. Bioresour. Technol., 243: 1159-1172.

Nature Environment and Pollution Technology
An International Quarterly Scientific Journal

p-ISSN: 0972-6268
(Print copies up to 2016)
e-ISSN: 2395-3454

Vol. 20 | No. 5 (Suppl) | pp. 2111-2116 | 2021

Original Research Paper

https://doi.org/10.46488/NEPT.2021.v20i05.028

Open Access Journal

# Optimization of *Chlorella* Culture Conditions with Response Surface Methodology to Increase Biomass

**R. Kanimozhi*, D. Arvind Prasath*†, R. Dhandapani** and Santhosh Sigamani****

*Medical Microbiology Laboratory, Department of Microbiology, School of Biosciences, Periyar University, Salem-636011, India

**Fermentation Technology Laboratory, Department of Microbiology, School of Biosciences, Periyar University, Salem-636011, India

†Corresponding author: D. Arvind Prasath; prasanthvi@periyaruniversity.ac.in

**Nat. Env. & Poll. Tech.**
**Website: www.neptjournal.com**

*Received:* 11-06-2021
*Revised:* 05-07-2021
*Accepted:* 12-07-2021

**Key Words:**
Response surface methodology
Biomass
optimization
*Chlorella* sp.

## ABSTRACT

Microalgae is gaining popularity as a major ingredient in nutrition supplements. To mass cultivate, it is imperative to improve the biomass yield hence optimization of cultures conditions becomes paramount. In this work, an attempt has been made to optimize the microalgal production using response surface methodology (RSM) and validate further the optimized parameters. The optimum conditions for the cultivation of *Chlorella* sp. KPU016 under optimized nutrient conditions were pH 8.2, the light intensity of 3100 lx, glycerol 1.44 g.L$^{-1}$ (under pre-set conditions of 12 h lighting, the temperature at 27±1°C. With these RSM-driven optimum conditions, the yield of microalgal biomass achieved was 282.50 mg.L$^{-1}$. For larger-scale microalgal harvesting, the validated optimal conditions can be inferred as the best for enhanced microalgal production. The isolate was partially sequenced and submitted to the NCBI database and the GenBank accession number is MZ348364.

## INTRODUCTION

Cyanobacteria (CBs) are valuable mining sources to harness beneficial metabolites (proteins, fatty acids, carbohydrates, pigments, and antimicrobials), which can be augmented as feed-additives and health-care products. Among CBS, *Chlorella* is one among the most preferred for generating larger capacities of biomass yield owing to its high cell growth rate and the convenience to procure its biomass (Chinnasamy et al. 2009). Subsequently, they can be cultivated in an alkaline environment, thus eliminating or mitigating bacterial and fungal contamination (Ak 2011). However, the elevated cost impact in microalgae cultivation has hampered the large-scale harvesting of biomass for further commercial exploitation. The vast majority of the costs for larger-scale harvesting of microalgae cultivation are attributed to extensive consumption of media and water (Luo et al. 2016, Ortiz Montoya et al. 2014). Hence, using recycled water is deemed economical with promising potentials for harvesting biomass; simultaneously using by-products of other appliances as the substrate has added advantage, since this would decrease the cost and serve as a waste management step (Zamani et al. 2012). A variety of microalgae like *Chlorella vulgaris*, *Scendesmus obliques* and *Spirulina platensis* have been explored for cultivations in recycled water and a system with recycled nutrients (Ebrahimian et al. 2014). Amidst the explored microalgae, *Chlorella* has been acknowledged as the prominent one to be cultivated in different recycled waters, and it can sustain as well in simulated water with artificial media components (Chaiklahan et al. 2010). Many credible research works have established that the medium components impact the microalgal growth directly, thus the biomass output (Zhang et al. 2014). Meanwhile, the optimum growth conditions for mass cultivation of *Chlorella* were proven as pH 9.0 to10.0, temperature 25 to 30°C, light intensity (4000lx) (at a constant 12 h of light illumination under micro-aeration) (Daliry et al. 2017). However, these proven optimum conditions were under surplus and tailor-made nutrient conditions for *Chlorella* harvesting. It can be thus postulated that in a large-scale commercial platform for harnessing *Chlorella,* the parameters and factors involved has to be optimized. Regarding the *Chlorella* cultivated in recycled water, there are very limited credible works on the strategic enhancement of *Chlorella* biomass production, and of optimization of environmental conditions using response surface methodology (RSM) (Wang et al. 2021, Elyemni et al. 2021). Additionally, more research knowledge on the impact of recycled waste or organic carbon effects on *Chlorella* growth needs to be deeply investigated. Hence, in this study, *Chlorella* is cultivated in recycled water for biomass yield with glycerol

(a by-product) as recycled-waste treatment. The optimum conditions for *Chlorella* cultivation were proven with the aid of Box-Behnken RSM, and the optimized conditions were further validated through an independent run. The interactive effects of pH, light intensity, and glycerol were explored based on biomass generation. *Chlorella* has also been strongly established over the years as a worthy source of nutraceuticals owing to their rich composition in terms of vitamins, antioxidants, etc., (Matos et al. 2019, Andrade et al. 2018). Hence this current work's proven optimum growth conditions can be further explored in a large-scale commercial application to procure biomass in higher volume so that it can be commercially exploited as a nutraceutical.

## MATERIALS AND METHODS

### Microalgal Strain, Media and Cultivation

The microalgal strain used in this study was isolated from Nangavalli lake, Salem, Tamilnadu, India (Latitude 11.7622ºN, Longitude 77.8898 ºE). Microalgal cells that were grown in BG 11 medium were used for the isolation of cyanobacteria. 1.0 mL of the cyanobacterial samples were transferred to sterile 100 mL of BG 11 medium in 250 mL conical flasks, in a growth chamber at 28±2ºC with the illumination of 2000lx with the aid of cool white 40 W fluorescent tubes (Philips). After 15 days of incubation, algae was harvested and used for further experiments (Yang et al. 2015). Glycerol was obtained as a waste residue from a biodiesel production facility and used in the optimization experiments.

### Evaluation of Effective Parameters on Microalgae Growth

The RSM Box-Behnken design through Design Expert software (Version 11) was employed to investigate the effects of the parameters on the microalgal biomass yield; pH, Light intensity (lx), glycerol ($g.L^{-1}$) to predict the optimum conditions. The RSM is a combination of mathematical and statistical tools adequate for the analysis, modeling, and prediction of a particular response or multi-responses based on Design of Experiments (DOE) in which the interaction of several variables contributes to the outcome. In this work, the experimental runs were designed and performed involving the variables in ranges (pH, light intensity, glycerol load) as exhibited in Table 1. The original polynomial models based on the various parameters were fitted to experimental data

Table 1: RSM Box-Behnken design with the actual and predicted response.

| | Factor 1 | Factor 2 | Factor 3 | Response actual Vs Predicted | |
|---|---|---|---|---|---|
| Run | A: pH | B: Light intensity (lx) | C: Glycerol ($g.L^{-1}$) | Biomass ($mg.L^{-1}$) | Biomass ($mg.L^{-1}$) |
| 1 | 9 | 3000 | 0.5 | 200.5 | 200.99 |
| 2 | 8 | 4000 | 2 | 266.6 | 264.11 |
| 3 | 8 | 3000 | 1.25 | 245.5 | 245.7 |
| 4 | 7 | 3000 | 0.5 | 198.2 | 197.41 |
| 5 | 8 | 3000 | 1.25 | 246.2 | 245.7 |
| 6 | 9 | 3000 | 2 | 254.2 | 254.99 |
| 7 | 8 | 4000 | 0.5 | 205.5 | 203.31 |
| 8 | 9 | 2000 | 1.25 | 233.6 | 230.62 |
| 9 | 9 | 4000 | 1.25 | 225.8 | 227.5 |
| 10 | 8 | 2000 | 2 | 268.4 | 270.59 |
| 11 | 7 | 4000 | 1.25 | 230.1 | 233.08 |
| 12 | 7 | 2000 | 1.25 | 238.9 | 237.2 |
| 13 | 8 | 3000 | 1.25 | 244.9 | 245.7 |
| 14 | 7 | 3000 | 2 | 271.2 | 270.71 |
| 15 | 8 | 3000 | 1.25 | 246.1 | 245.7 |
| 16 | 8 | 2000 | 0.5 | 201.6 | 204.09 |
| 17 | 8 | 3000 | 1.25 | 245.8 | 245.7 |

Model prediction $R^2$ for the quadratic polynomial equation is 0.9877

using the least-squares method and analysis of variance techniques in Design-Expert software (Version 11) (Zhai et al. 2017, Wang et al. 2021). The models for microalgal biomass yield, for the autotrophic cultivation of the microalga, could be obtained by Eq. (1)

$$Y=\beta 0 + \Sigma\beta iXi + \Sigma\beta ijXiXj + \Sigma\beta iiX2i, \quad \ldots(1)$$

Where $Y$ is the predicted response, $\beta_0$ is the intercept term, $\beta_i$ is the linear coefficient, $\beta_{ij}$ is the quadratic coefficient, $\beta_{ii}$ is the interaction coefficient, and $X_i X_j$ represent the independent variables (Onumaegbu et al. 2019).

### Analytical Methods

The *Chlorella* biomass was accumulated and measured once in 24 h by measuring the optical density at 560 nm. The dry biomass weight was measured by filtering 10 mL of each sample through a pre-weighed 0.45 nm membrane filter, drying in a drying chamber at 110°C for 2 h, and reweighing the filter using an electronic-balance (Zhai et al. 2017).

## RESULTS AND DISCUSSION

### Determination of the Optimum Levels of the Factors

The range of pH, light intensity and glycerol, all impacted *Chlorella* biomass yield, significantly ($p < 0.01$) (Table 2). These three variables also positively impact the biomass yield individually (equation 1). The pH and daily illumination positively interacted with each other and also affected positively the response. PH and glycerol interacted negatively with each other, so did the light intensity, and glycerol $pH^2$, Light intensity$^2$, Glycerol$^2$ also interacted slightly negatively on the biomass yield even though pH x glycerol, $pH^2$, Light intensity$^2$, Glycerol$^2$ were significant at ($p < 0.01$) (Table 2) (Tork et al. 2017, Zhai et al. 2017).

### Equations

Biomass = -478.837 + 149.054 x pH + 0.0258625 x Light intensity + 124.6 x Glycerol + 0.00025 x pH x Light intensity + -6.43333 x pH x Glycerol + -0.0019 x Light intensity x Glycerol + -9.05 x pH^2 + -4.55e-06 x Light intensity$^2$ + -10 x Glycerol$^2$ …(2)

In this current work, the optimum levels for the cultivation of *Chlorella* in recycled water with waste substrate glycerol were optimal, in contrast to other established results reported in previous studies. The pH, light intensity, and glycerol significantly impacted the *Chlorella* biomass output ($P < 0.01$). Previous research has also suggested that pH, light intensity, and carbon source play a significant influence in determining the outcome (Dorling et al., 1997, Fan et al. 2020, Zhai et al. 2017). When the pH value is more alkaline, the form of carbon shifts to form carbonates, hence the assimilation of glycerol is better suited at this pH range for *Chlorella*. Thus, the predicted optimum pH value between 8.2-8.6 is best suited for the cultivation of *Chlorella* in recycled wastewater under simulated conditions (Fig. 1a, 1b, & 1c). Regarding the light intensity, earlier published data has established that the microalgal composition, as well as the biomass, dwindle with respect to the extremes of light intensity (Pandey & Tiwari, 2010). Congruent results were achieved in our investigation. The *Chlorella* growth and biomass output were obtained at the optimum light inten-

Table 2: ANOVA of factors involved in the experiment.

| Source | Sum of Squares | df | Mean Square | F-value | p-value |
|---|---|---|---|---|---|
| Model | 8928.18 | 9 | 992.02 | 143.94 | < 0.0001 |
| A-pH | 73.81 | 1 | 73.81 | 10.71 | 0.0136 |
| B-Light intensity | 26.28 | 1 | 26.28 | 3.81 | 0.0918 |
| C-Glycerol | 8102.64 | 1 | 8102.64 | 1175.70 | < 0.0001 |
| AB | 0.2500 | 1 | 0.2500 | 0.0363 | 0.8544 |
| AC | 93.12 | 1 | 93.12 | 13.51 | 0.0079 |
| BC | 8.12 | 1 | 8.12 | 1.18 | 0.3136 |
| $A^2$ | 344.85 | 1 | 344.85 | 50.04 | 0.0002 |
| $B^2$ | 87.17 | 1 | 87.17 | 12.65 | 0.0093 |
| $C^2$ | 133.22 | 1 | 133.22 | 19.33 | 0.0032 |
| Residual | 48.24 | 7 | 6.89 | | |
| Lack of Fit | 47.14 | 3 | 15.71 | 57.14 | 0.0010 |
| Pure Error | 1.10 | 4 | 0.2750 | | |
| Cor Total | 8976.42 | 16 | | | |

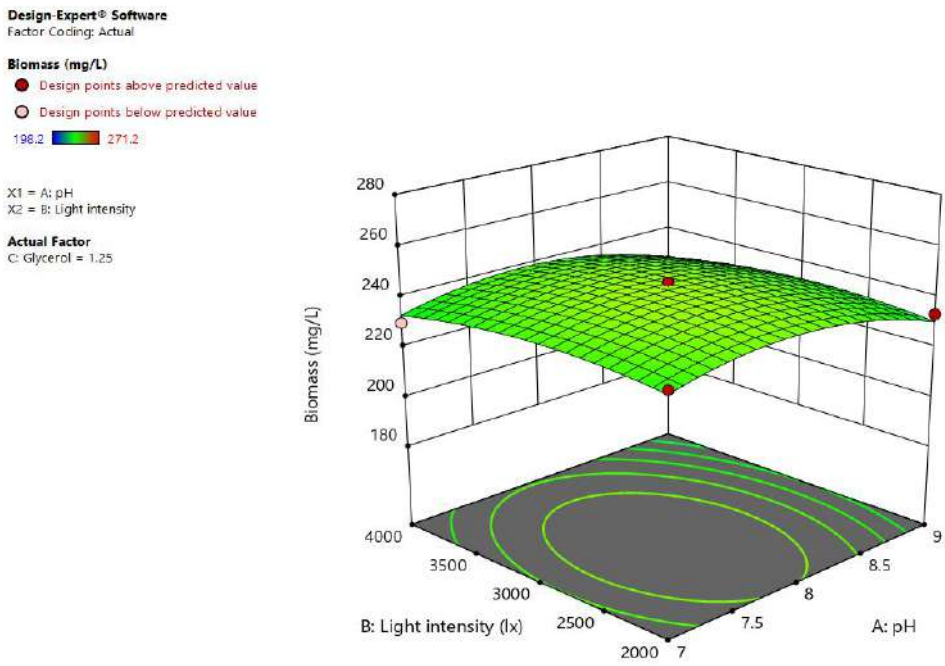


Fig. 1a: 3D contour plot of interaction between pH vs light intensity effect on biomass.

sity between 3100–3300lx in the current work; lesser than 4000lx as established in other published works. This result suggests that the current optimized level of light intensity could be economically viable via lesser energy consumption (Skorupskaite et al. 2015, Zhai et al. 2017).

The medium used for the cultivation of microalgae can be the prime factor when the culture conditions are to be optimized. In our work also glycerol levels were significant at concentrations 1.35 to 1.45 g.L$^{-1}$. Deep investigations have elucidated that the nutrients concentration and their forms

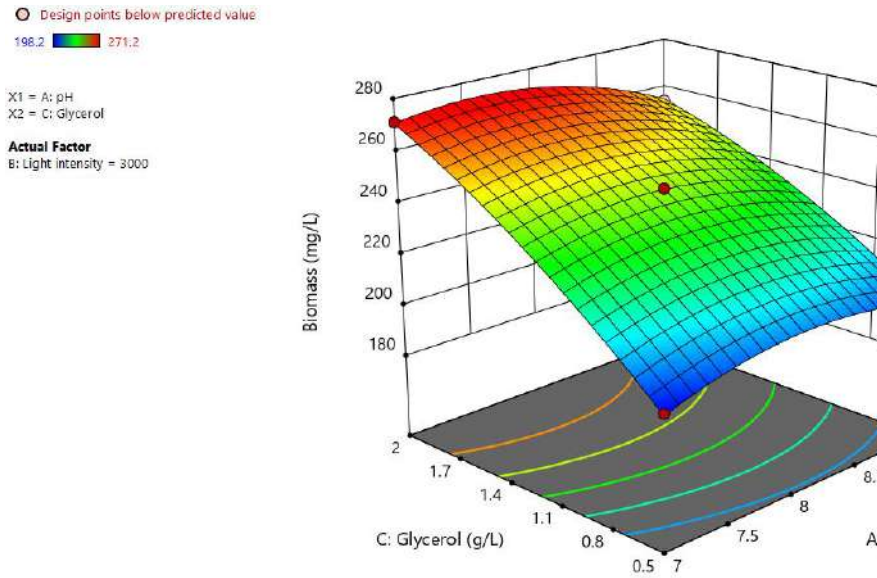


Fig. 1b: 3D contour plot of interaction between pH vs glycerol; their effect on biomass.

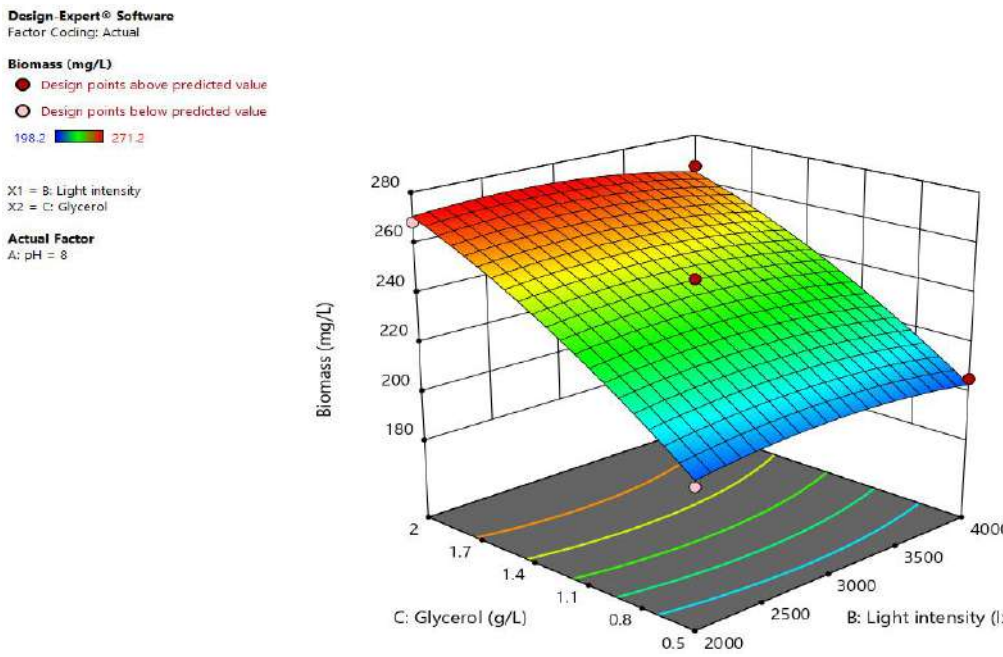


Fig. 1c: 3D contour plot of interaction between glycerol vs light intensity effect on biomass.

impacted the growth of *Chlorella* and other microalgae, and thus directly impacted *Chlorella* biomass generation and harvest.

### Validated Run

The optimized values ascertained via RSM are pH 8.2, the light intensity of 3100 lx, glycerol 1.44 $g.L^{-1}$; when validated with an independent run, yielded 282.50 $mg.L^{-1}$ of *Chlorella* biomass.

## CONCLUSION

In this work, the optimum levels of variables involved for the cultivation of *Chlorella* sp. KPU016 in simulated recycled water were envisioned and forecasted by RSM Box-Behnken and were further validated through an independent experimental run. All 17 runs projected minimal or no variation between the predicted values and experimental outcomes. Under the optimum conditions, pH 8.2, the light intensity of 3100 lx, glycerol 1.44 $g.L^{-1}$, when validated with an independent run, yielded 282.50 $mg.L^{-1}$ of *Chlorella* biomass. These optimal conditions could be strategies that can be a better endorsement for the advancement of *Chlorella* or other similar cyanobacteria cultivation so that the biomass can be harnessed in large-scale commercial applications. The isolate was partially sequenced and submitted to the NCBI database and the GenBank accession number was procured as MZ348364.1.

## REFERENCES

Andrade, L.M., Andrade, C.J., Dias, M., Nascimento, C.A.O. and Mendes, M.A. 2018. Chlorella and spirulina microalgae as sources of functional foods, nutraceuticals, and food supplements; an overview. MOJ Food Process. Technol., 6(1): 45-58.

Ak, I. 2011. Effect of organic fertilizer on growth of blue-green alga *Spirulina platensis*. Aquacult. Int., 20: 413-422.

Chaiklahan, R., Chirasuwan, N., Siangdung, W., Paithoonrangsarid, K. and Bunnag, B. 2010. Cultivation of *Spirulina platensis* using pig wastewater in a semi-continuous process. J. Microbiol. Biotechnol., 20(3): 609-614.

Chinnasamy, S., Ramakrishnan, B., Bhatnagar, A. and Das, K.C. 2009. Biomass production potential of a wastewater alga *Chlorella vulgaris* ARC 1 under elevated levels of $CO_2$ and temperature. Int. J. Mol. Sci., 10(2): 518-532.

Daliry, S., Hallajisani, A., Roshandeh, J.M., Nouri, H. and Golzary, A. 2017. Investigation of optimal condition for *Chlorella vulgaris* microalgae growth. Global J. Environ. Sci. Manage., 3(2): 217-230.

Dorling, M., McAuley, P.J. and Hodge, H. 1997. Effect of pH on growth and carbon metabolism of maltose-releasing Chlorella (Chlorophyta). Eur. J. Phycol., 32(1): 19-24.

Ebrahimian, A., Kariminia, H.R. and Vosoughi, M. 2014. Lipid production in mixotrophic cultivation of *Chlorella vulgaris* in a mixture of primary and secondary municipal wastewater. Renew. Energy, 71: 502-508.

Elyemni, M., Louaste, B., Ouadrhiri, F.E., Bouia, A. and Eloutassi, N. 2021. Application of response surface methodology to optimize the extraction of essential oil from *Rosmarinus officinalis* using microwave-assisted hydrodistillation. J. Appl. Pharm. Sci., 11(01): 129-136.

Fan, H., Wang, K., Wang, C., Yu, F., He, X., MA, J. and Li, X. 2020. A comparative study on growth characters and nutrients removal from wastewater by two microalgae under optimized light regimes. Environ. Technol. Innov., 19: 100849.

Luo, L., He, H., Yang, C., Wen, S., Zeng, G., Wu, M., Zhou, Z. and Lou,

W. 2016. Nutrient removal and lipid production by *Coelastrella* sp. in anaerobically and aerobically treated swine wastewater. Bioresour. Technol., 216: 135-141.

Matos, J., Cardoso, C.L., Falé, P., Afonso, C.M. and Bandarra, N.M. 2019. Investigation of nutraceutical potential of the microalgae *Chlorella vulgaris* and *Arthrospira platensis*. Int. J. Food. Sci. Technol., 55: 303-312.

Onumaegbu, C., Alaswad, A., Rodriguez, C. and Olabi, A. 2019. Modeling and optimization of wet microalgae *Scenedesmus quadricauda* lipid extraction using microwave pre-treatment method and response surface methodology. Renew. Energy, 132: 1323-1331.

Ortiz Montoya, E.Y, Casazza, A.A, Aliakbarian, B., Perego, P., Converti, A. and de Carvalho, J.C. 2014. Production *of Chlorella vulgaris* as a source of essential fatty acids in a tubular photobioreactor continuously fed with air enriched with $CO_2$ at different concentrations. Biotechnol. Prog., 30(4): 916-22.

Pandey, J.P. and Tiwari, A. 2010. Optimization of biomass production of *Spirulina maxima*. J. Algal. Biomass Util., 1(2): 20-32.

Skorupskaite, V., Makarevicien, V. and Levisauskas, D. 2015. Optimization of mixotrophic cultivation of microalgae *Chlorella* sp. for biofuel production using response surface methodology. Algal Res., 2015: 7:45-50.

Tork, M.B., Khalilzadeh, R. and Kouchakzadeh, H. 2017. Efficient harvesting of marine *Chlorella vulgaris* microalgae utilizing cationic starch nanoparticles by response surface methodology. Bioresour. Technol., 243: 583-588.

Wang, Q., Oshita, K. and Takaoka, M. 2021. Evaluation of flocculation performance of amphoteric flocculant when harvesting microalgae *Coccomyxa* sp. KJ by response surface methodology. J. Environ. Manage., 277: 111449.

Yang, C.C., Wen, R.C., Shen, C.R. and Yao, D-J. 2015. Using a Microfluidic Gradient Generator to Characterize BG-11 Medium for the Growth of Cyanobacteria *Synechococcus elongatus* PCC7942. Micromachines, 6: 1755-1767.

Zamani, N., Noshadi, M., Amin, S., Niazi, A. and Ghasemi, Y. 2012. Effect of alginate structure and microalgae immobilization method on orthophosphate removal from wastewater. J. Appl. Phycol., 24(4): 649-656.

Zhai, J., Li, X., Li, W., Rahaman, H., Zhao, Y., Wei, B. and Wei, H. 2017. Optimization of biomass production and nutrients removal by *Spirulina platensis* from municipal wastewater. Ecol. Eng., 108: 83-92.

Zhang, C., Zhang, Y., Zhuang, B. and Zhou, X. 2014. Strategic enhancement of algal biomass, nutrient uptake, and lipid through statistical optimization of nutrient supplementation in coupling *Scenedesmus obliquus*-like microalgae cultivation and municipal wastewater treatment. Bioresour Technol., 171: 71-79.

Nature Environment and Pollution Technology
An International Quarterly Scientific Journal

p-ISSN: 0972-6268
(Print copies up to 2016)
e-ISSN: 2395-3454

Vol. 20 | No. 5 (Suppl) | pp. 2117-2123 | 2021

Original Research Paper

https://doi.org/10.46488/NEPT.2021.v20i05.029

Open Access Journal

# GIS-Based Surface Runoff Modeling Using Empirical Technique For A River Basin In South India

**B. Prabhu Dass Batvari* and K. Nagamani**†**

*Centre for Earth and Atmospheric Sciences, Sathyabama Institute of Science and Technology, Chennai-600119, India

**Centre for Remote Sensing & Geoinformatics, Sathyabama Institute of Science and Technology, Chennai-600119, India

†Corresponding author: K. Nagamani: nagamani@sathyabama.ac.in

**Nat. Env. & Poll. Tech.**
**Website: www.neptjournal.com**

*Received:* 14-07-2021
*Revised:* 26-08-2021
*Accepted:* 03-09-2021

**Key Words:**
Rainfall runoff
Curve number
GIS
Land use

## ABSTRACT

Precipitation is the primary source of fresh water in the world. Surface runoff will happen when the amount of rainfall is greater than the soil's infiltration capacity. In most water resource applications, runoff is the most important hydrological variable. Aside from these rainfall characteristics, there are a number of catchment-specific elements that have a direct impact on runoff amount and volume. This research focuses on estimating surface runoff over the lower Vellar basin, a river basin in the southern part of India, by integrating Soil Conservation Service-Curve Number (SCS-CN) method with GIS. This technique is one of the most common methods used by hydrologists for estimating surface runoff. Curve Number (CN) is an index established by the Natural Resource Conservation Service (NRCS) to denote the potential for stormwater runoff. The nature of the watershed is explored first by creating land use and land cover pattern followed by the preparation of slope, drainage, and location maps. The area taken for this study is the lower Vellar basin situated in the Cuddalore District of Tamil Nadu, India. The curve number is analyzed using the rainfall data of 15 years (2001-2015) and the runoff is being calculated. The watershed pattern of the study area is also explored being analyzed and executed. Preservation of the runoff water is also discussed.

## INTRODUCTION

Water is the most important element for all living things; without water, there would be no vegetation on the Earth, no oxygen for animals to breathe, and the world would look very different than it does now. Water is required for human health and the preservation of the environment, and it should be valued and protected as a valuable resource. However, as a result of pollution, clean water is becoming increasingly scarce (Gagan et al. 2016).

The oceans hold around 97 percent of the world's water. Saltwater covers about 1.4 billion cubic kilometers. Freshwater makes up only 3% of the total, and it is found in rivers, glaciers, and lakes. Even though there is abundant fresh water all across the world, there are some areas that are too dry and do not receive enough rain. Water scarcity is a prevalent issue in developing countries due to population expansion. Many areas lack sufficient water because people exhaust it. Water moves in a continuous cycle, never disappearing or ceasing to exist, but shifting from solid to liquid to gas. While some rainwater returns to the atmosphere, the majority of it enters the ground through aquifers.

Runoff is the most significant hydrological factor used in more applications of water resources. Its incidence and amount are based on the features of rainfall occurrence, i.e. the length, intensity and circulation. In addition to these rainfall features, there are numerous catchment-specific variables that directly affect the incidence and quantity of runoff. There are several methods existing for rainfall-runoff modeling. Soil Conservation Services and Curve Number (SCS-CN) techniques offer an empirical relationship to estimate original abstraction and runoff as soil type and land use function. Curve Number (CN) is an index created by the Natural Resource Conservation Service (NRCS) to represent the potential of a drainage region for stormwater runoff (Hailu et al. 2018, Sishah 2021). The U.S. Soil Conservation Service at the Department of Agriculture initially created the SCS-CN technique (Van Dijk 2010, Abon et al. 2011, Steenhuis et al. 1995).

The CN for a watershed is evaluated using a mixture of land use, antecedent soil moisture condition (AMC), and soil. There are four types of hydrologic soils: A, B, C, and D. Group A has a high rate of infiltration, while Group D has a low rate of infiltration. The Soil Conservation Service Curve Number (SCS-CN) method is widely used to forecast direct runoff volume for a specific rainfall event (Mishra & Singh 1999, King & Balogh 2008, Elhakeem & Papanicolaou 2009, Romero et al. 2007).

Recent sophisticated methods such as remote sensing and the Geographic Information System (GIS) are therefore involved in the compilation, storage, and evaluation of spatial and temporal allocation information. These techniques are currently being used to address watershed-related challenges such as watershed planning, growth, and management, with the goal of harnessing all-natural resources for long-term development (Verma et al. 2016, Rawat & Singh 2017, Tiwari et al. 2017). Thus, Geographic Information Systems (GIS) and Remote Sensing is the main tool to provide the foundation for effective water resource management. (Gupta et al. 2004, Frevert & Singh 2002, Siddi Raju et al. 2018, Mahboubeh et al. 2012, Sharma et al. 2008, Ruslin Anwar 2011).

## MATERIALS AND METHODS

### Study Area

The Vellar River is situated in the Cuddalore district which lies in the coastal belt of Tamil Nadu. It is one of the many ephemeral rivers in the area; it runs from west to east and blends with the sea south of Porto-Novo. The lower Vellar sub basin comprises the Perumal Eri (lake) watershed and is connected by the Bay of Bengal to the east. The parts of the lower Vellar watershed (Study area) comprise the catchment and command areas of Perumal 'Eri' extended up to the Bay of Bengal in the East. Cuddalore is the district headquarters, which is well connected by both rail and roadways. The study area (lower Vellar watershed) is bounded to the north by the Ponnaiyar watershed, to the south by the Vellar watershed, and to the east by the Bay of Bengal. The pilot study area (lower Vellar watershed) lies between north latitudes 11° 30' 10' and 11° 42' 16" and east longitudes 79°30'00" and 79°46' 6" and is covered by the survey of India toposheet No.58 M/10. The total study area taken is said to be 1784 $km^2$, and a Google Earth snapshot of the entire study area is shown in Fig.1.

### Data Sources

IRS LISS-III data was used for the LULC classification. Land use/land cover classes in the current study region have been identified, and the LULC map is shown in Fig. 2. Daily rainfall data ((2001– 2015) was used in this study, and the data was collected from IMD, Chennai. Soil information was obtained from the National Bureau of Soil Survey and Land Use Planning (NBSS & LUP). The study area's Digital Elevation Model (DEM) and slope and elevation map were obtained from SRTM (Shuttle Radar Terrain Mission) and is shown in Fig. 3 and 4.

### Runoff Calculation

The equation of the runoff curve number is:

$$Q = \frac{(P-I_a)^2}{P-I_a} + S \quad P > I_a \qquad ...(1)$$

$$Q = 0 \qquad P \le I_a$$

Where: Q = Actual Direct Runoff (mm), P = Total Rainfall (mm), I = Initial Abstraction, S = Watershed Retention (mm). IA (I) and WR (S) can be related to each other by analyzing rainfall-runoff data for the sub-watersheds. The empirical relation between I and S may be stated as follows:

$$I = 0.2S \qquad ...(2)$$

Therefore, applying Equation 2 on Equation 1

$$Q = \frac{(P-0.2S)^2}{P+0.8S} \quad P \ge 0.2S \qquad ...(3)$$

Retention parameter (S) is dependent upon soils, land use, and slope, and it is defined as-

$$S = 25.4\left(\frac{1000}{CN-10}\right) \qquad ...(4)$$

Where CN is the day's Curve Number, a dimensionless runoff index determined by land use, hydrological soil groups (HSG), and antecedent moisture content (AMC).

The curve number (CN) depends on the permeability of the soil, its usage, and its previous moisture content. The daily retention value adjusted according to water content is calculated by rearranging equation 4 and inserting the retention parameter (explained in detail below) calculated for the soil which is completely saturated.

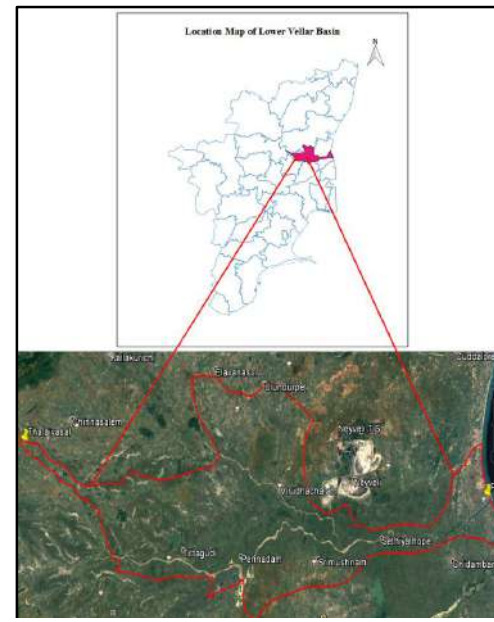


Fig. 1: Study Area-Vellar River Basin

$$S = \left(\frac{25400}{CN}\right) - 254 \quad ...(5)$$

The curve number (CN) depends on the permeability of the soil, its usage, and its previous moisture content. The equation for the derivation of CN is:

$$CN = \frac{\sum(P1A1+P2A2+\cdots+PnAn)}{\sum A} \quad ...(6)$$

This equation calculates CN values based on land use and land cover classes and hydrological soil groups, where a 5% slope is under consideration.

The present equation calculates CN for AMC 2. Variability in CN consequences related to moisture conditions of the soil, precipitation duration and intensity, total precipitation, cover density, temperature, and growth stage. These sources of variableness are collectively named as Antecedent Runoff Condition (ARC). The ARC is classified into three classes: CN2 for normal conditions, CN1 for arid conditions, and CN3 for humid conditions. CN1 and CN3 can be calculated with the following mathematical equations.

$$CN1 = \frac{4.2\ CN2}{10-0.058\ CN2} \quad ...(7)$$

$$CN3 = \frac{23\ CN2}{10+0.13\ CN2} \quad ...(8)$$

$$S = \left(\frac{25400}{CN1}\right) - 254 \text{ AMC} \leq 13 \quad ...(8)$$

$$S = \left(\frac{25400}{CN3}\right) - 254 \text{ AMC} > 28 \quad ...(9)$$

$$S = \left(\frac{25400}{CN2}\right) - 254 \text{ 28<AMC>13} \quad ...(10)$$

Either CN1/CN2/CN3 is used for the calculation of Watershed Retention (S) using Equation 5 based on the AMC values.

The run-off relationship was calculated using a number of retention criteria. The initial abstraction, Ia, may be regarded as the borderline between the size of the storm that creates runoff and the size of the storm that creates no runoff. Retention at its highest level, S, is dependent upon the soil cover compound and, in principle, must not differ from one storm to the next. It is greater than the initial abstraction, so Ia + S gives the maximum potential loss. The difference between rainfall and runoff (P – Q) is used to calculate the loss. When equation (9) is substituted for Q, the result is

$$\boldsymbol{Loss = P - Q = P - \frac{(P-I_a)^2}{(P-I_a)+S}} \quad \ldots (11)$$

Following the multiplication of both terms on the right-hand side by: $\mathbf{1} = \frac{(P-I_a)+S}{(P-I_a)+S}$

With certain manipulation this becomes:

$$\boldsymbol{Loss} = \frac{\left((S+I_a)-\left(\frac{I_a^2}{P}\right)\right)}{}\left(1 - \left(\frac{I_a}{P}\right) + \left(\frac{S}{P}\right)\right) \quad \ldots(12)$$

The terms in the denominator with P in the denominator approach zero as P approaches large, where large is defined as P being significantly greater than the maximum possible retention (S).

$$Loss = S + I_a \quad \ldots(13)$$

The parameter F is the storm's true retention, which is higher than the early abstraction. That is, the total actual retention is equal to the sum of the initial abstraction and the actual retention (Ia + F).

### Model Calculation

Let the Rainfall for five days be 40.9, 60.4, 70.2, 0, and 30.8. The rainfall on the 6th day is 25.5.

AMC (Antecedent Moisture Content) for day 6 can be calculated using the following formula (weighted average)

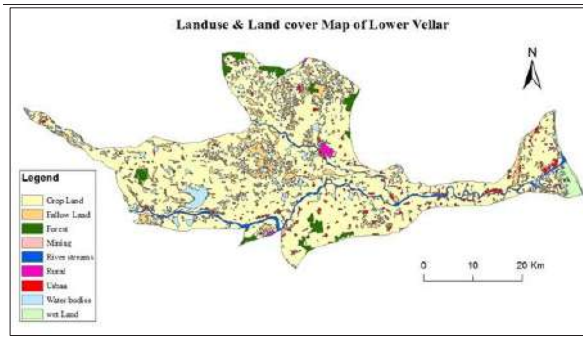


Fig. 2: Land use and Land cover classification of the Vellar

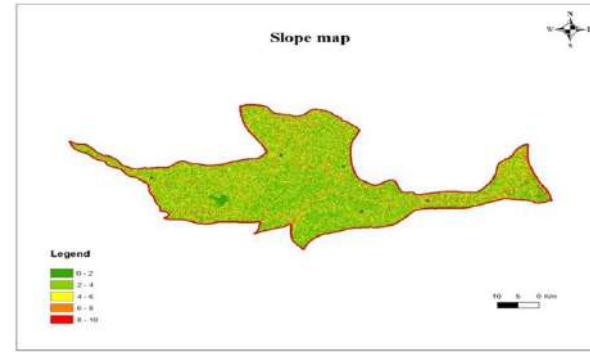


Fig. 3: Lower Vellar basin Slope map

AMC = (0.9*R1) + ((0.9) ^2*R2) +….+ ((0.9)^n*Rn)

Here, R1, R2, Rn represents rainfall in mm

= (0.9*40.9)+(0.9^2*60.4)+(0.9^3*70.2)+(0.9^4*0)+(0.9^5*30.8) = 142.68

Now, AMC > 28, we consider CN3 (wet) (CN3 = 91.89)

S = (25400/91.89)-254 = 22.42

I = 0.2*22.42 = 4.48

P-I = Daily rainfall – 4.48 = 25.5-4.48= 21.02

$Q = (P-I)^2/P+0.8*S = 21.02^2/25.5+0.8*22.42 = 10.17$ mm

The runoff of day 6 is **10.17mm**.

## RESULTS AND DISCUSSION

### Land Use

According to the LULC map of the lower Vellar basin, the majority of the area was classified as fallow land and cropland, implying that there may be more infiltration and consequently lesser runoff. Out of the overall area (1784 $km^2$), 2 $km^2$ have been designated as mining areas (Fig. 2), which will manage surface runoff.

### Slope Map

The slope is one of the deciding factors in surface runoff. SRTM elevation data acquired from USGS Earth Explorer was used. ArcMap 10.3 is the software used. The slope map findings for the chosen research area are less than 5%. As a result, it is not taken into account. Fig. 3 shows the slope map of the research area.

### Elevation Map

The most common type of map used to depict elevation is a topographical map. In Geographic Information Systems (GIS), digital elevation models (DEM) are commonly used to represent the surface (topography) of a location using a raster (grid) dataset of elevations. The color difference in the map depicts the study area's high to low elevation values. The elevation map is created using SRTM elevation data. Fig. 4 shows an elevation map of the research area.

### Contour Map

A contour map represents the elevation of the particular area within the elevation lines drawn on it. The contour interval is the difference in height between successive contour lines on a contour map. A two-variable function's contour line is often a curve that connects points where the function has the same value. The presented map's contour interval is 20 m. The study area's western side is sloppier than the lower Vellar basin's east side, and the distance between each contour is higher, implying that the study area is practically plain. Fig. 5 shows the contour map of the research region.

### Rainfall and Runoff Kuppanatham

The total rainfall recorded at Kuppanatham is 18191.4 mm, with a runoff of 8787.48 mm. Rainfall and runoff averages 1212.8 mm and 585.83 mm, respectively. In 2015, the largest rainfall was recorded, as well as the highest runoff. In the year 2012, the lowest rainfall was recorded, and the lowest runoff was recorded in the year 2003. This was because of the driest period, which lasted from 2001 to 2003. As a result, the actual amount of rain that fell throughout these years would sweep in. Despite the fact that rainfall was minimal in 2012, the rainfall in 2011 was adequate to recharge the groundwater potential. The runoff in 2012 is higher than in 2003. Data 2 contains the yearly runoff table for station Kuppanatham, while Fig. 6 and Fig. 7 depict the rainfall-runoff distribution and relationship.

### Rainfall and Runoff Memathur

The total rainfall in Memathur is 17613.6 mm, with an

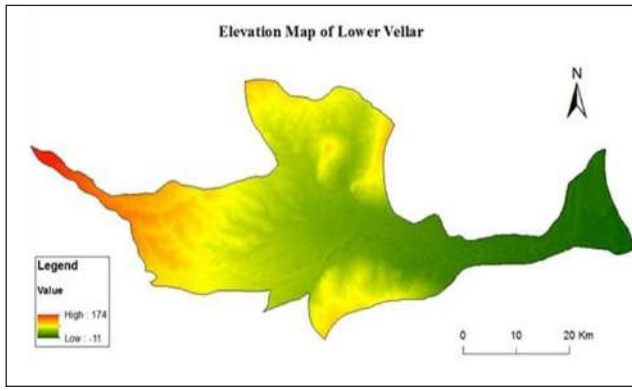


Fig. 4: Elevation Lower Vellar basin

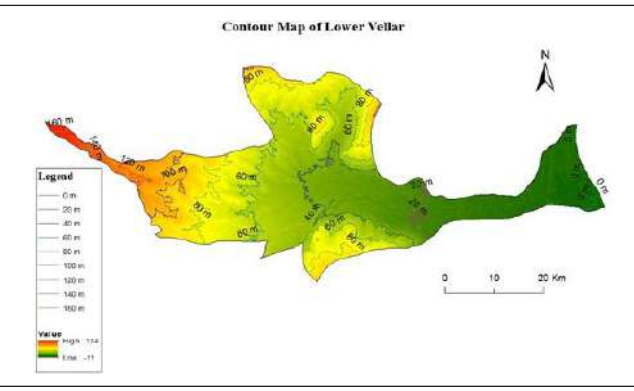


Fig. 5: Contour Lower Vellar basin

equivalent runoff of 8091.09 mm. Rainfall and runoff averages 1174.2 mm and 539.41 mm, respectively.

The year with the high rainfall was 2015, and the year with the highest runoff was 2005. In the year 2012, the lowest rainfall was recorded, as well as the lowest runoff. Because the rainfall in Memathur was higher in all of the years from 2001 to 2005, the year 2005 had the largest runoff (Fig. 8 & 9).

### Rainfall and Runoff Sethiyathope

The total rainfall at Sethiyathope is 21150 mm, while the runoff is also 21150 mm. The average rainfall is 1410 mm, while the average runoff is 716.02 mm. In 2005, the largest rainfall was recorded, as well as the highest runoff. The year 2012 saw the lowest rainfall, while 2001 saw the lowest runoff. Table 2 contains the yearly runoff table for station Sethiyathope, as well as graphs depicting the rainfall-runoff relationship and distribution. Fig. 10 and 11 show the graphs depicting the rainfall-runoff relationship and distribution.

### Rainfall and Runoff Srimushnam

In Srimushnam, the total rainfall reported is 17510.3 mm, with a runoff of 8531.86 mm. Rainfall and runoff average 1167.4 mm and 568.79 mm, respectively. The maximum rainfall and runoff were both recorded in the year 2003. The lowest rainfall and runoff were both recorded in the year 2012 (Fig. 12 & 13).

### Rainfall and Runoff Virudhachalam

The total amount of rainfall in Virudhachalam is 18815.1 mm, with a runoff of 8744.22 mm. The average rainfall is 1254.3 mm, while the average runoff is 582.95 mm. In 2005, the largest rainfall was recorded, as well as the highest runoff. In the year 2014 the lowest rainfall, as well as the lowest runoff has been recorded (Fig. 14 & 15).

### Rainfall and Runoff relationship in Lower Vellar basin

In 2005, the lower Velar basin received the most average rainfall (1758.92 mm). In 2012, the lower Vellar basin's average rainfall was at its lowest (750.84 mm). The highest

Table 1: Land Use and Land Cover

| S.No | Land Use | Area [$km^2$] |
|---|---|---|
| 1 | Water bodies | 91.5 |
| 2 | Fallow Land | 161.4 |
| 3 | Forest | 49.5 |
| 4 | Urban | 77.5 |
| 5 | Rural | 9 |
| 6 | Crop Land | 1321.8 |
| 7 | River Stream | 47.7 |
| 8 | Mining | 2 |
| 9 | Wet Land | 23.8 |

Table 2: Rainfall and Runoff in Vellar Basin

| | Kuppanatham | | Memathur | | Seithiyathope | | Srimushnam | | Virudhchalam | |
|---|---|---|---|---|---|---|---|---|---|---|
| Year | Rainfall | Runoff | Rainfall | Runoff | Rainfall | Runoff | Rainfall | Runoff | Rainfall | Runoff |
| 2001 | 867.50 | 384.13 | 1186.00 | 516.16 | 927.70 | 309.98 | 962.80 | 446.00 | 989.10 | 386.62 |
| 2002 | 918.70 | 411.69 | 1164.60 | 582.65 | 1141.10 | 594.46 | 1417.00 | 835.89 | 827.80 | 335.44 |
| 2003 | 895.60 | 317.71 | 1200.00 | 447.80 | 954.40 | 315.02 | 2281.00 | 1569.95 | 932.50 | 330.73 |
| 2004 | 1599.00 | 938.44 | 1149.00 | 550.98 | 1593.70 | 898.94 | 1801.00 | 1107.68 | 1503.70 | 755.39 |
| 2005 | 1660.20 | 898.94 | 1576.00 | 919.93 | 2021.00 | 1177.52 | 1788.50 | 992.67 | 1748.90 | 938.67 |
| 2006 | 897.00 | 330.11 | 905.00 | 335.09 | 1685.00 | 886.82 | 1292.00 | 596.86 | 1029.30 | 362.06 |
| 2007 | 1156.00 | 618.04 | 1021.00 | 469.63 | 1578.00 | 935.95 | 1046.00 | 417.79 | 1139.10 | 596.58 |
| 2008 | 1365.70 | 607.00 | 1248.00 | 533.29 | 1848.00 | 1134.72 | 1252.50 | 559.72 | 1511.70 | 677.10 |
| 2009 | 1150.90 | 466.48 | 1245.00 | 632.20 | 1388.50 | 635.56 | 755.00 | 282.67 | 1294.20 | 538.57 |
| 2010 | 1615.80 | 784.16 | 1557.00 | 750.21 | 1562.50 | 787.27 | 1106.00 | 482.37 | 1711.10 | 872.05 |
| 2011 | 1456.00 | 805.43 | 961.00 | 496.21 | 1207.00 | 632.81 | 853.00 | 299.01 | 1374.60 | 740.76 |
| 2012 | 752.80 | 325.42 | 747.00 | 304.74 | 832.00 | 392.89 | 414.00 | 119.64 | 1008.40 | 475.35 |
| 2013 | 1236.70 | 601.32 | 952.00 | 310.82 | 1161.70 | 453.09 | 650.00 | 129.19 | 1224.10 | 541.18 |
| 2014 | 873.90 | 343.98 | 936.00 | 339.29 | 1256.80 | 500.21 | 832.00 | 298.54 | 831.30 | 306.45 |
| 2015 | 1745.60 | 954.64 | 1766.00 | 902.10 | 1992.60 | 1085.03 | 1059.50 | 393.88 | 1689.30 | 887.27 |

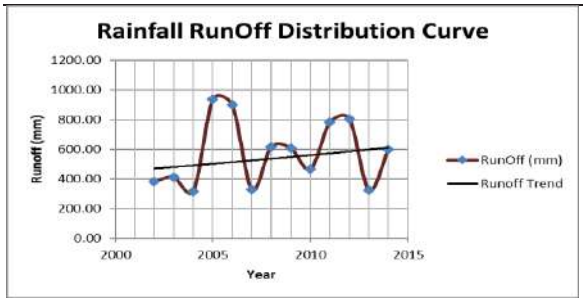


Fig. 6: Trend line of runoff Kuppanatham.

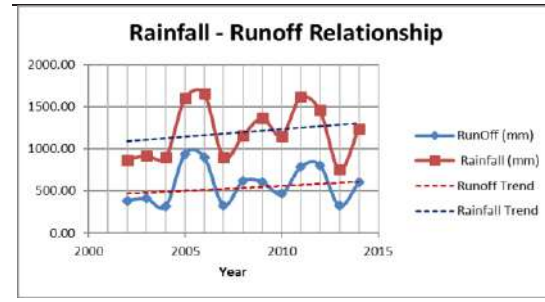


Fig.7: Positive correlation between rainfall and runoff in Kuppanatham.

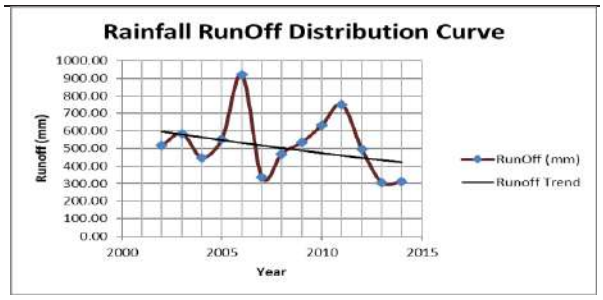


Fig. 8: Trend line of runoff decreased over years in Memathur.

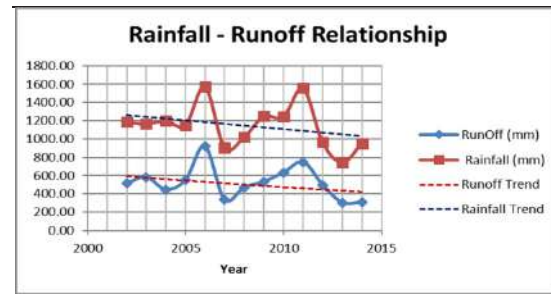


Fig. 9: Positive correlation between rainfall and runoff Memathur.

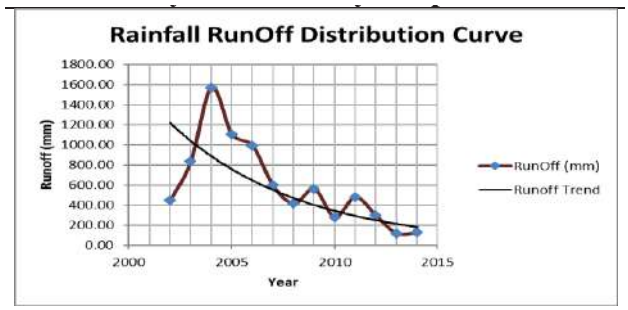


Fig. 10: Trend line of runoff increased over years in Sethiyathope.

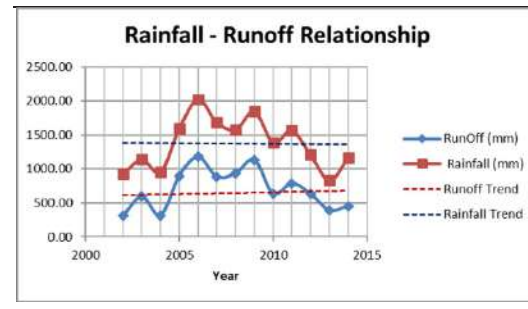


Fig. 11: Positive correlation between rainfall and runoff in Sethiyathope.

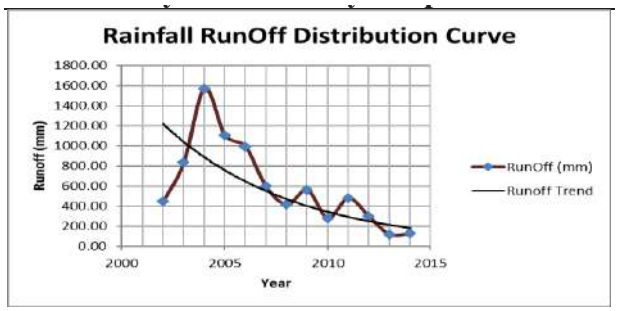


Fig. 12: Trend line of runoff tremendously decreased over years in Srimushnam.

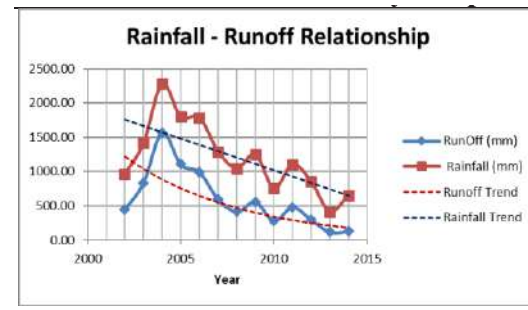


Fig. 13: Positive correlation between rainfall and runoff in Srimushnam.

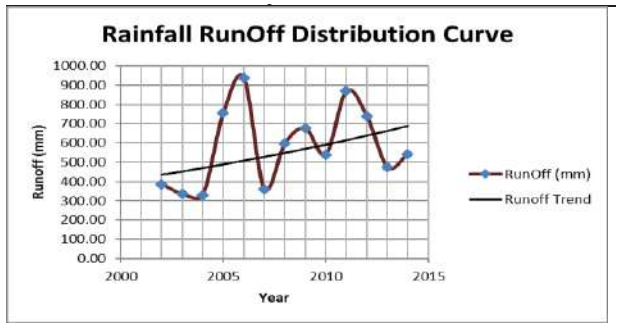


Fig. 14: The trend line of runoff increased over years in Virudhachalam

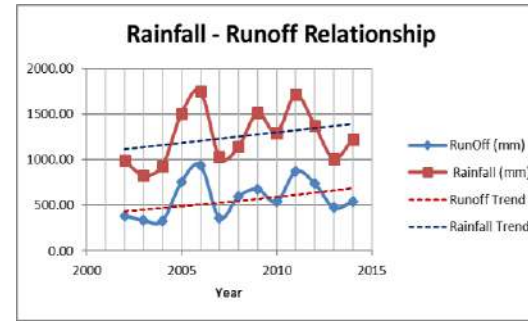


Fig. 15: Positive correlation between rainfall and runoff in Virudhachalam.

rainfall and runoff at Sethiyathope were both recorded at the same rainfall station. In Srimushnam, the Memathur rainfall station received the least rainfall and had the least drainage. In 2005, the lower Vellar basin's average runoff was at its highest (985.5445 mm). In 2012, the lower Velar basin's average rainfall was at its lowest (323.6096 mm).

## CONCLUSION

This study mainly focuses on the estimation of losses due to surface runoff, which is favorably based on the soil infiltration characteristics and the continuation of rainfall occurrences. Knowledge of runoff from individual rainfall is required to evaluate the runoff behavior of a catchment area, as well as a sign of both the runoff-peaks that the water harvesting scheme's structure must be able to withstand the elements, as well as the required capacity for temporary surface runoff storage, such as a micro catchment system, the size of an infiltration pit. The watershed as a whole receives a good amount of rainfall. But, when compared to runoff, recharge is relatively low, as the terrain is comprised of crystalline rocks. By building agricultural ponds at suitable locations, this runoff potential can be used for artificial recharge. Additionally, buildings such as check dams are being built to store water. It will be useful for drinking water as well as agricultural applications during the hot summer days.

## REFERENCES

Abon, C.C., David, C.P.C. and Pellejera, N.E.B. 2011. Reconstructing the tropical storm Ketsana flood event in Marikina River, Philippines. Hydrol. Earth Syst. Sci., 15: 1283–1289.

Elhakeem, M. and Papanicolaou, A.N. 2009. Estimation of the runoff curve number via direct rainfall simulator measurements in the state of Iowa, USA. Water Resour. Manag., 23: 2455–2473.

Frevert, D.K. and Singh, V.P. (ed). 2002. Mathematical Models of Large Watershed Hydrology. WRP, UK, pp.914.

Gagan, M., Amit, C., Avinash, K. and Ajendra, K. 2016. Impact of industrial effluent on groundwater and surface water quality: A case study of Dhampur region (UP), India. J. Chem. Pharm. Sci., 9(2): 709-713.

Gupta, H.V., Wagener, T. and Wheather, H.S. (ed). 2004. Rainfall-Runoff Modelling in Gauged and Ungauged Catchments. Imperial College Press, London, pp.306.

Hailu, R., Tolossa, D. and Alemu, G. 2018. Water institutions in the Awash basin of Ethiopia: The discrepancies between rhetoric and realities. Int. J. River Basin Manag., 16(1): 107–121.

King, K.W. and Balogh, J.C. 2008. Curve numbers for golf course watersheds. T. ASAE, 51: 987–996.

Mahboubeh, E., Ahmad, A., Nuruddin, B., Mohd Amin, B., Mohdsoom, A. and LiewJu, N. 2012. Runoff estimation in steep slope watershed with standard and slope-adjusted curve number methods. Pol. J. Environ. Stud., 21(5): 1191-1202

Mishra, S.K. and Singh, V.P. 1999. Another look at the SCS-CN method. J. Hydrol. Eng. ASCE., 4: 257–264.

Rawat, K.S. and Singh., S.K. 2017. Estimation of surface runoff from semi-arid ungauged agricultural watershed using SCS-CN method and earth observation data sets. Water. Conserv. Sci. Eng., 1: 233-247.

Romero, P., Castro, G., Go`ımez, J.A. and Fereres, E. 2007. Curve number values for olive orchards under different soil management. S. Sci. Soc. Am. J., 71: 1758–1769.

Ruslin Anwar, M. 2011. The rainfall-runoff model using the watershed physical characteristic approach. Int. J. Civil Environ. Eng., 11(6): 71-75.

Sharma, K.D., Sorooshian, S. and Wheater, H. (ed). 2008. Hydrological Modelling in Arid and Semi-Arid Areas.Cambridge University Press, New York, p. 223.

Siddi Raju, R., Sudarsana Raju, G. and Rajasekhar, M. 2018. Estimation of rainfall runoff using SCS-CN method with RS and GIS techniques for Mandavi Basin in YSR Kadapa District of Andhra Pradesh, India. Hydrospatial Anal., 2(1): 1-15.

Sishah, S. 2021. Rainfall runoff estimation using GIS and SCS-CN method for a wash river basin. Ethiopia. Int. J. Hydro., 5(1): 33-37.

Steenhuis, T.S., Winchell, M., Rossing, J., Zollweg, J.A. and Walter, M.F. 1995. SCS runoff equation revisited for variable-source runoff areas. J. Irrig. Drain. Eng. ASCE, 121: 234–238.

Tiwari, S., Kar, S.C., Bhatla, R. and Bansal, R. 2017. Annual Cycle of Temperature and Snowmelt Runoff in Satluj River Basin Using in Situ Data. In Pant, N.C., Ravindra, R., Srivastava, D. and Thompson, L.G. (eds), The Himalayan Cryosphere: Past and Present. Geological Society, London, Special Publications, pp. 1-20.

Van Dijk, A.I.J. M. 2010. Selection of an appropriately simple storm runoff model. Hydrol. Earth Syst. Sci., 14: 447–458.

Verma, D.K., Bhunia, G.S., Shit, P.K., Kumar, S., Mandal, J. and Padbhushan, R. 2016. Spatial variability of groundwater quality of Sabour block, Bhagalpur district (Bihar, India). Appl. Water Sci., 7(4): 1997-2008.

Nature Environment and Pollution Technology
An International Quarterly Scientific Journal

p-ISSN: 0972-6268
(Print copies up to 2016)
e-ISSN: 2395-3454

Vol. 20 | No. 5 (Suppl) | pp.2125-2136 | 2021

Review Research Paper | https://doi.org/10.46488/NEPT.2021.v20i05.030 | Open Access Journal

# Disaster Management: Tsunami and Remote Sensing Technology

**Sudhir Kumar Chaturvedi†**
School of Engineering, UPES, Dehradun-248007, India
†Corresponding author: Sudhir Kumar Chaturvedi; sudhir.chaturvedi@ddn.upes.ac.in

**Nat. Env. & Poll. Tech.**
**Website: www.neptjournal.com**

*Received:* 09-06-2021
*Revised:* 06-07-2021
*Accepted:* 12-07-2021

**Key Words:**
Remote sensing
Tsunami
Inundation
Energy movement
Earthquakes

## ABSTRACT

Remote sensing technology has changed the way disasters like earthquakes and tsunamis are detected, monitored, and mapped in recent years. This paper summarizes the general theoretical study of Tsunami generation, propagation, and its inundation for deep, intermediate, and coastal waters. Tsunami is a Japanese word, which is made up of two words: "tsu" means harbor, and "nami" means waves. It means that Tsunami is the coastal gravity waves, which propagate close to the coastline. This analysis presents a novel method to explore the effects of tsunami waves on coastal areas. The methodology includes remote sensing nearness examinations and alteration identification strategies in remote sensing to outline a number of support routes along the coast and divide them into four homogenous sub-regions. The adjustments in the land spread are then measured in these sub-regions when the tidal wave occurs. The proposed paper gives a more solid and exact method than ordinary strategies to assess spatial examples of harmful territories through various land qualities along the coastline. The generative phase of tsunami development comprises the creation of an early disruption at the surface of the ocean due to the earthquake-generated distortion on the seafloor. Various comparative studies are also carried out using spatial technology to examine tsunami routes around the globe, taking into account the most recent tsunami occurrences..

## INTRODUCTION

Tsunamis are long waves, which have wavelengths order magnitude up to 10km and amplitude order of 1m in Ocean, where the travel velocity is of 700-800km/hour. (Arii et al. 2014). Tsunamis are a dangerous threat that has no warning, cannot be predicted, and result in significant casualties and loss of life (Fig. 1).

The main cause of the Tsunami is underwater plate tectonics movements (Bryant 2001, Craig & Sulem 1993). Tsunami waves are similar to normal waves that propagate close to the surface. The geostrophic surface current streamlining for the Indian coastline region is shown in Fig. 2 (Dean & Dalrymple 1984).

Bottom pressure sensors can sense a tsunami of a few meters' fluctuations in the open sea (Dean 1986, Eze & Uko 2000) as shown in Fig. 3. The tectonic plate boundaries for convergent, divergent, and transform regions are also shown in the image.

The initial displacements of the free surface of various water wave conditions are induced by a strong earthquake with a magnitude greater than 9.0 on the Richter scale, in which the creation of N-type waves is more abundant. (Fig. 4).

In 1979, experts suggested that radars can be used to distinguish tsunamis based on their orbital wave speed as they approached the coast. The scattering of radars around the globe was scanty until the 1990s. In spite of the fact that there were no radars set up to see that occasion, work started to evaluate the radar tidal wave reaction. Numerous HF radars around the Pacific Rim with clear outcomes saw the Japan tidal wave signal from locations in Japan, the USA, and Chile. The 2012 Indonesia tidal wave and the 2013 US East Coast meteotsunami were two other weak tidal waves that were seen. An experimental strategy for the programmed discovery of a wave has been created. Over 350 HF radar sites located along the coast provide a consistent estimate of surface momentum speeds and waves. The basic model of tidal wave location programming can provide a warning before the wave reaches the coast.

### Remote Sensing Technology for Tsunami Signal Estimation

The seismic detection of an earthquake could be the most visible sign of a tidal wave. Nonetheless, not all subsea seismic tremors produce tidal waves, and thus the size of a quake cannot be used to conjecture the definite age or force of a subsequent tidal wave. DART systems are designed to sense pressure changes at the bottom of the ocean caused by passing tsunamis and to communicate these changes to the tsunami warning centers. Each DART system consists

of a bottom pressure recorder anchored to the ocean floor and a separately moored companion surface buoy. Because this system is located in the deep sea, DART (Deep-ocean Assessment and Reporting of Tsunamis) cannot detect all tidal waves, hence they are not included in the model before the beachfront effect. High frequency (HF) radar systems measure the speed and direction of ocean surface currents in near real-time The main problem with the buoy stations is that they are hard and expensive to maintain, and because they are located in a rather harsh environment, they have a fairly high failure rate. These radars can measure currents over a large region of the coastal ocean, from a few kilometers offshore up to 200 km, and can operate under any weather conditions. They are located near the water's edge, and need not be situated atop a high point of land. These radars, show the exact wave location that can otherwise be missed out. This can detect and warn of approaching tidal waves in the nearby shore district where these radars monitor the ocean surface. A sum of 21 disconnected radar discoveries of waves has been made to date. Tsunami periods lie normally somewhere in the range of 20 and 50 min. A tidal wave starts when there is a huge removal of water: The spatial sizes of water dislodging are as a rule of extraordinary even however little vertical measurements These include subsea seismic

Fig. 1: An aerial photo of the devastation in the Dongola area, north of Palou (Image source: BBC).

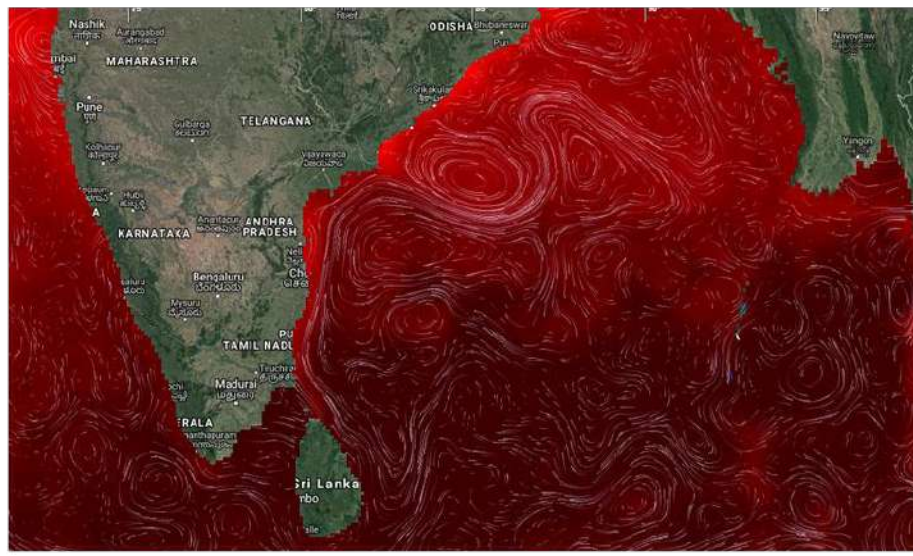


Fig. 2: Geostrophic surface current streamline (Glob current) of Indian coastal region (Source: ESA Ocean virtual laboratory).

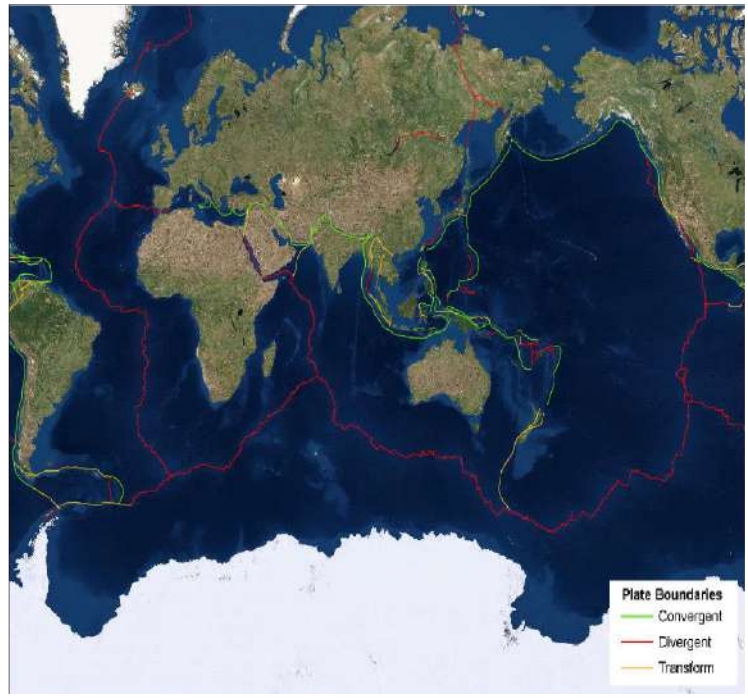


Fig.3: Tsunami plate boundaries (Source: NOAA National Centers for Environmental Information, Natural Hazards Viewer).

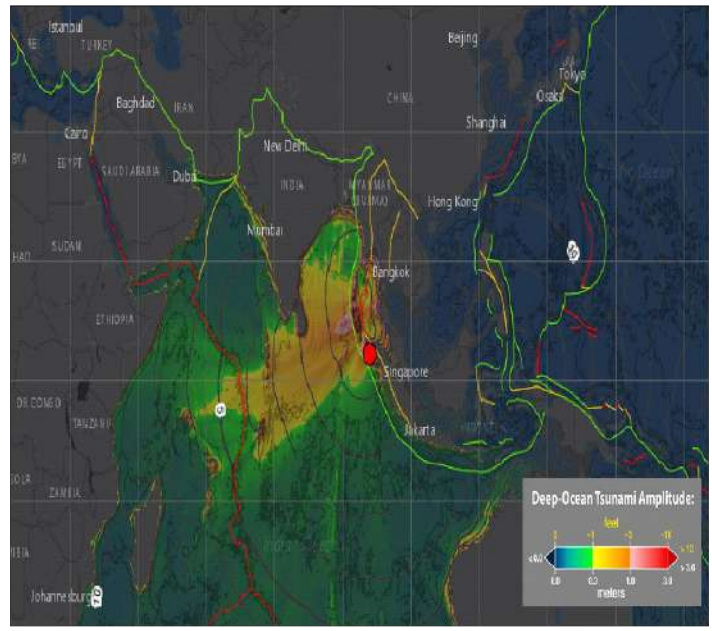


Fig. 4: Sumatra, Indonesia tsunami impact on 26th December 2004 (Source: NOAA National Centers for Environmental Information, Natural Hazards Viewer).

tremors where plates drive each other upward/descending, separately; subsea avalanches along soak submerged uneven slants; or quick-moving environmental inconsistencies (for example low-pressure focuses) that make "meteotsunami." The origins can be hundreds of kilometers away or very close to an impacted beachfront territory (where an HF radar may be located). As the dislodged water mass leaves its source area affected by gravity, it turns into a shallow-water wave. Tidal waves are shallow-water waves stretching out far into the ocean and continuously changing the ebb and flow pat-

terns. We describe a method for predicting tidal wave arrival at a coastline based on the projected speed of a simulated tidal wave. The factors that influence the radar location of tidal waves are discussed. The difficulties that can occur in wave detection, as well as reduction methods, are depicted.

Tsunamis are members of the same family as normal sea waves, which can be seen from a distance near beaches. The majority of big tsunamis have been caused by undersea earthquakes. The sudden displacement of the ocean surface is caused by spontaneous seafloor movement. By restoring gravitational forces, the sudden gain in potential energy is transferred to kinetic energy. The characteristics of tsunamis in the four oceans are detailed in Table 1 below.

Currently, ocean floor pressure sensors in the open sea may detect a tsunami of a few centimeters in height. To determine whether the tsunami was indeed formed, the tsunami

Table 1: **C**haracteristics of Tsunami for the 4 oceans (Source: NOAA National Centers for Environmental Information).

| Parameter | Pacific Ocean | Atlantic Ocean | Indian Ocean | Arctic Ocean |
|---|---|---|---|---|
| Area ($km^2$) | 166,241,000 | 86,557,000 | 73,427,000 | 9,485,000 |
| Average depth (m) | 4188 | 3735 | 3872 | 1038 |
| Deepest point (m) | Mariana Trench, 11,033 | Puerto Rico Trench, 8648 | Java Trench, 7725 | Eurasian Basin, 5450 |
| Number of trenches | 18 | 3 | 1 | None |
| Unpopulated area (%) – Southern Ocean | ~20 | 30 | 55 | Almost all of it |
| Length scale available (km). Half the size of an equivalent (in the area) square | 6447 | 4642 | 4284; if we omit the unpopulated area, it is about 2000 | 1540 |
| Ocean-wide tsunamis | Yes | No | Yes | Rare – extremely strong dissipative influence by ice cover |
| Tectonic-converging plates producing tsunami genic earthquakes | Yes | No; at the mid-Atlantic ridge, the plates are diverging | Yes | Some, but not as strong as in the Pacific and Indian oceans |
| Frequency of tsunami occurrence | High | Rare | Rare | Rare |
| Frequency dispersion | High | N/A – since no ocean-wide tsunamis | Low | Small |
| Amplitude dispersion (nonlinear effects at the coast) | High | High | High | Moderate; ice cover does not permit significant amplification of tsunami waves at the coast |
| Tsunami travel times | Up to 23 h | Only local tsunamis which travel within minutes | Up to 10 h to the most populated area | Local tsunamis; several minutes to almost a couple of hours |
| Available warning time to most populated areas | Generally sufficient | Because of local tsunamis, only several minutes | 1 to 4 h | Small – mostly several minutes |
| Importance of initial conditions | High | High | High | High |
| Importance of boundary reflections | Low | Low, since tsunamis originate close to the coast | High | Moderate; ice cover does not allow significant wave's reflection |
| Boundary conditions | Low | Medium | High | Medium |
| Coriolis force | Noticeable | Highly | Moderate | High |
| Nature of physical process | Hyperbolic (like astrology): everything is determined at birth | Parabolic: tsunamis travel slowly in shallow water near the coast. It is like a slow diffusion process | Elliptic: tsunami behavior everywhere in the ocean, including reflections at the boundaries, is relevant everywhere else | Halfway between parabolic and elliptic |

wave indicators are first based on the number of seismic tremors such as magnitude, sea depth, and location. A tsunami is a series of ocean gravitational waves that form as a result of large-scale disturbance of the seabed (Josheph 2010, Kânoglu & Synolakis 1998, Liu et al.1995). The Boussinesq equation is proposed as a tool for studying tsunami wave formation, dispersion, and run-up. The movement of a tsunami in the sea differs from that of other waves because it happens throughout the entire water column, from the surface to the ocean bottom. This phenomenon causes a tsunami to take on the shape of a solitary wave in shallow water. Little energy is dissipated because the wave's motion involves the entire water column, especially on steep coasts (Lin et al. 2013)

A tsunami wave motion distribution can be studied by examining the eigen functions with respect to depth variation at a given angular frequency. The values of the orbital velocity and distribution varied from the deep ocean to the coastal regions. In terms of their mode of generation, propagation, wavelength, time period, velocity, and distribution of the oceanic region to the coastal parts of the particular region, tsunamis are characterized differently (Madsen & Schäffer 2010). Hence, tsunamis have different consequences than normal wave propagation. Surface disturbances caused by seafloor movements can be examined using various analyses and mathematical models such as potential theory, power series Laplace Transform solutions, and Fourier Laplace Transforms for linear problems. The Boussinesq model results have shown excellent linear and non-linear properties, such as linear dispersion, shoaling, subharmonics, and super harmonics transmissions (Filloux 1970)

The generation stage of the tsunami includes the formation and evolution of initial ocean surface displacements due to the large earthquake triggered at the bottom of the seafloor. The generated water surface is transformed to the long gravity waves, which radiate from the earthquake source where it occurred at the time of evolution. The modeling of the tsunami is carefully related to further readings on the earthquake tools (Geist 1998)

The usefulness of early detection and warning systems has been demonstrated, particularly in the aftermath of the devastating tsunami that struck Japan in March 2011, as shown in Fig. 5. The objective of this study is to update and improve existing tsunami results to improve detection and early warning prediction accuracy (Okal 1988).

In this study, two major tasks have been carried out: (1) To calculate wave parameters, particularly Eigen functions (water wave number, angular frequency, horizontal and vertical orbital velocity, and acceleration, celerity of the waves) (2) Using radar data processing with q-factor estimation, the idea of an early warning system was developed. Since the work is primarily concerned with the development of radar remote sensing techniques for naval applications in tsunami detection and investigation of its early warning using radar technologies, the designed system may further be said as Integrated Tsunami Warning System (ITWS) (Martino et al. 2009)

Tsunami Modeling: Several models are currently used around the world for calculating stationary sea bottom distortions to calculate tsunami basic parameters. As a tool

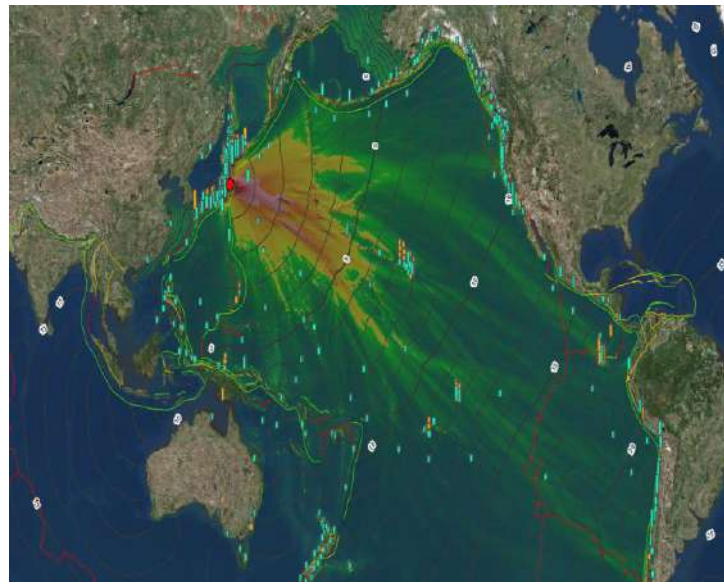

Fig.5: Tohoku-Japan tsunami impact on 11th March 2011 (Source: NOAA National Centers for Environmental Information, Natural Hazards Viewer).

for planning calamity relief and management strategies, numerical modeling of approaching tsunamis is considered essential since the information from previous tsunamis can be insufficient for planning either relief or management of a tsunami approaching from a regional or remote area. Models are digitized to account for any unfavorable conditions for tsunami origin/waves exactly offshore to determine the related impact on neighboring island shores (Murty et al. 2006). Models might even be computed with tiny origins to know the acerbity of disaster for lesser intense but more persistent events. This data then transforms the foundation to create tsunami drainage maps and methodologies.

Modeling techniques that have recently emerged need accurate inputs of bathymetry and topographic data for the modeled area/site (Prins 1958). Several numerical tools have been utilized to communicate tsunamis to distanced islands. For example, many numerical tools have been used to communicate the propagation of tsunamis among islands over long distances (Fig. 6) (Sirikulchayanon et al. 2005)

The accuracy of model predictions is directly related to the quality of the data used to create the bathymetry and topography of the model area. Coastal Bathymetry is the prime determinant of the height of the tsunami wave or storm surge as it approaches the coast (Tadepalli & Synolakis 1994,1996). High-resolution coastal bathymetry is thus the key input for various tsunami and storm surge prediction models. Bathymetric data provided by the National Hydrographic Office (NHO) has been used in tsunami modeling. In addition, the bathymetric survey is conducted for a few vulnerable areas of the Indian coast. CARTOSAT-1 data is being used for generating a Digital Elevation Model (DEM) of the coastal region. Tsunami Modeling is classified into three stages: (i) generation, (ii) propagation (iii) run-up (Inundation). The guidelines and varieties of models engaged at

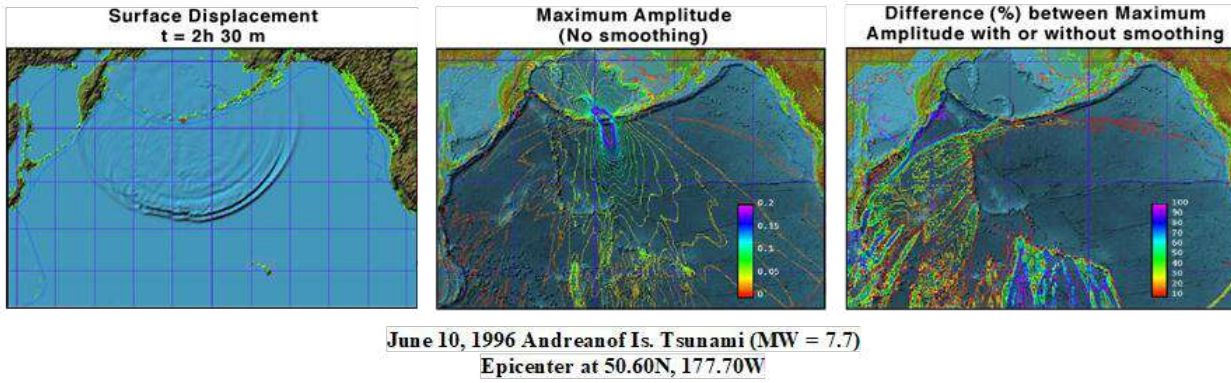


Fig. 6: Tsunami model simulation (Source: NOAA Centre for Tsunami Research).

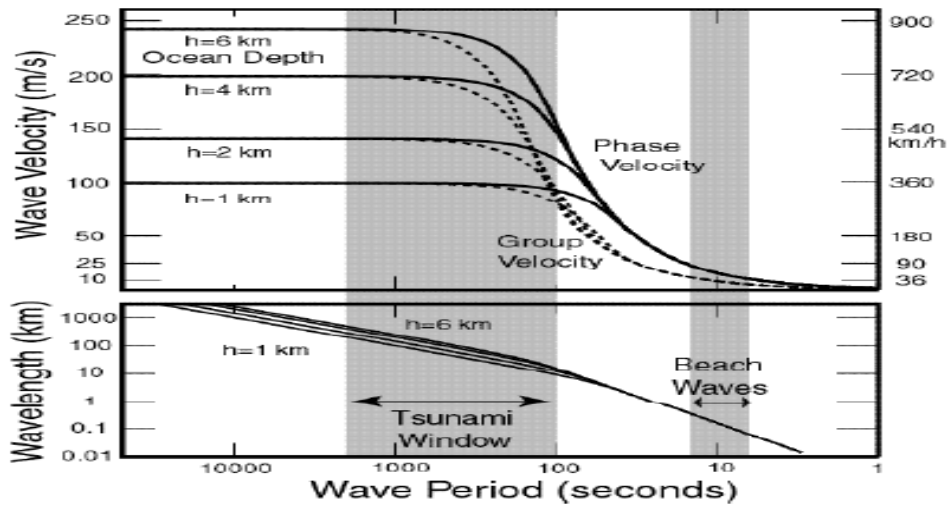


Fig. 7: (a) solid line indicates the phase velocity and dashed line represents group velocity of tsunami waves in the ocean for various depths of 1,2,4, and 6 km depth, (b) shows the variation of wavelength with wave period, tsunami windows appeared (Dean 1986).

these stages vary and depend on experimental site parameters (Titov 2000). The generation phase of tsunami comprises an early disruption at the surface of the ocean due to the earthquake-generated distortion on the seafloor. The long gravity wave searing from the earthquake's source causes this early water surface disturbance. The early phase of the tsunami's undulation is carefully modeled using several earthquake tools (Todorovska & Trifunac 2001, Ward 1980, Zielinski & Saxena 1983).

## CHARACTERISTICS OF TSUNAMIS

Tsunamis are defined by the wave dispersion theory, which envisions a hard seafloor overlain by an incompressible, homogeneous, and non-viscous ocean that is always subjected to a constant gravitational field. The effect of frequency dispersion is that the waves travel as a function of wavelength so that spatial and temporal phase properties of the propagating wave are constantly changing. The more specific variation in the water wave frequency with the wavelength charecterstics are mentioned in Fig. 7.Tsunami wave flow from Deep to intermediate and then to coastal (shallower) regions are shown in Fig. 8.

For example, under the action of gravity, water waves with a longer wavelength travel faster than those with a shorter wavelength. As per the theory (Dean 1980), the velocity $c$, and group velocity $u$ of the gravity waves with the uniform ocean depth of $d$ are

$$c = \sqrt{\frac{gh\tanh(kd)}{kd}} \quad \ldots(1)$$

and

$$u = c\left[\frac{1}{2} + \frac{(kd)}{\sin(2kd)}\right] \quad \ldots(2)$$

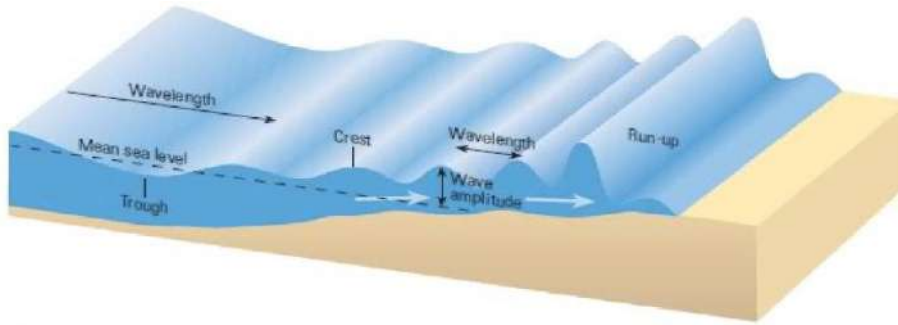


Fig. 8: Tsunami shoaling from deep to coastal region (Ward 1980).

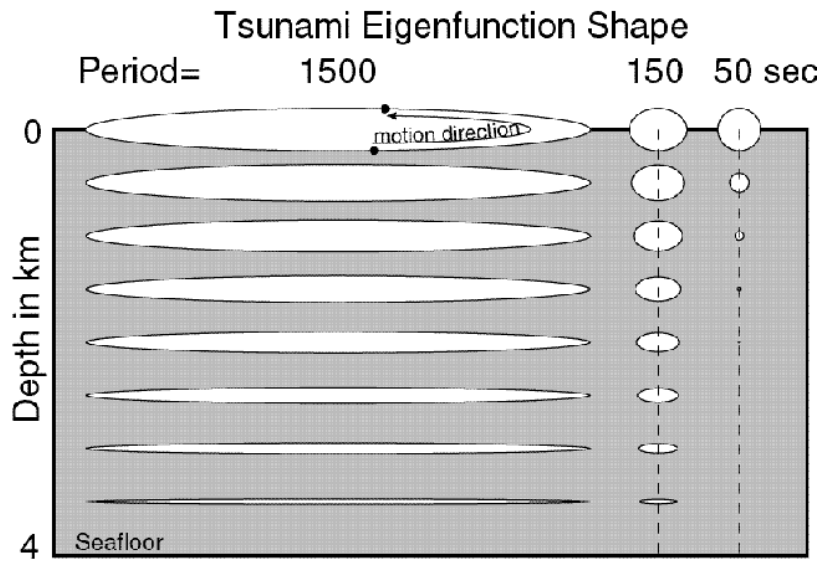


Fig. 9: Tsunami parameters (eigenfunctions) in various water depths with 1500s, 150s, and 50s of time duration.

Here, $g$ is the acceleration due to gravity and $k$ is the wave number associated with the sea wave of frequency ω. Wave number correlated with the wavelength is given by

$$L = \frac{2\pi}{k} \quad \ldots(3)$$

Wave number also satisfies the dispersion relationship, the basic and important equation used in the study of wave hydrodynamics especially to analyze the various type of waves and is given as

$$\omega^2 = gk \tanh(kd) \quad \ldots(4)$$

## TSUNAMI EIGEN FUNCTIONS

Consider a coordinate system $(x, y, z)$. Vertical $(u_z)$ and horizontal $(u_x)$ components of tsunami Eigen functions normalized to unit vertical displacement at the sea surface are (Chaturvedi et al. 2016)

$$u_z(\omega, z) = \frac{kg}{\omega^2} \frac{\sinh[k(d-z)]}{\cosh[kd]} e^{i[kx-\omega t]}$$

$$u_z(\omega, z) = \frac{kg}{\omega^2} \frac{\sinh[k(d-z)]}{\cosh[kd]} e^{i[kx-\omega t]} \quad \ldots(5)$$

$$u_z(\omega, z) = \frac{-ikg}{\omega^2} \frac{\cosh[k(d-z)]}{\cosh[kd]} e^{i[kx-\omega t]}$$

$$u_z(\omega, z) = \frac{-ikg}{\omega^2} \frac{\cosh[k(d-z)]}{\cosh[kd]} e^{i[kx-\omega t]} \quad \ldots(6)$$

Fig. 9 indicates the tsunami Eigenfunctions versus depth in a 4$km$ deep ocean at long (the 1500$s$), intermediate (150$s$), and short (50$s$) periods. The little ellipses can be thought of as tracing the path of a water particle as a wave of frequency ω passes. In the 1500$s$ period, the tsunami has a wavelength of $L$=297$km$ and it acts like a long wave (Chaturvedi et al. 2017). The vertical displacement peaks at the ocean surface and drops to zero at the seafloor. The horizontal displacement is constant through the ocean column and exceeds the vertical component by more than a factor of ten. The measurement and validation of the wave parameters are provided by Chaturvedi et al. 2019, 2020 for deep, intermediate, and shallower regions.

## COMPARATIVE STUDY ON RECENT TSUNAMIS ACROSS THE GLOBE

The results introduced for each location are merged in the following in a way that allows for future estimation of territorial tidal wave risk. A solitary wave risk map is created using this process by adding all of the extreme sea levels for each of the individual tidal wave occurrences. Only a few territories appear to be effectively protected against tidal waves (Fig. 10 & 11). Furthermore, it is concentrated in select areas, such as eastern Halmahera and the Makassar Strait; the combined hazard map is unlikely to include much of the risk (Helm & Stosius 2007, Chatterjee et al. 2008). A tidal wave may impact stretches of the coastline near the origins only a few minutes after it is generated, giving only a few minutes' notice and putting many inhabited areas at risk.

Tidal wave risks, in most parts, can be reduced or eliminated using predefined building construction plans. The guideline necessitates that buildings must be constructed within these areas, which must be evaluated to determine whether a risk exists in the area. If this is the case, major structural modifications must be undertaken before permission for private construction can be granted.

The simulation model in the study shows that significant stretches of the coastlines are subjected to extreme water levels in the range of 2–4 m, and at times exceeding 10 m. (Fig. 11). The wave metric (extreme water level) must be combined with the transient possibility of the situation to measure the risk, despite the fact that extreme water levels represent a high risk. (Westen & Soeters 2009)

Recent Tsunami registered datasets with UTC zones are also given in Table

Fig. 12 shows Tsunami events elaboration with symbols for cause or fatalities

The combination of broad immersion potential, short warning periods, and fairly short return times strongly suggests that the current hazards in these areas are disturbing; this could also indicate that the hazard is alarmingly high. This calls for prompt and coordinated activities needed for reducing the tsunami hazard.

## CONCLUSIONS

To summarize, the possibility of calamity reduction that utilizes remote sensing for improved tsunami detection and monitoring is that digitalization shortens the time between early warning and assessment of the hazard while increasing the period for evacuation, as well as providing precise data of the area and magnitude of the calamity. By using satellite remote sensing and rapid data analysis tsunami impact and occurrence interval can be determined. According to the findings of this study, current remote sensing techniques are helping the scientific community in mapping disasters' before and after impact using real-time data and simulation to plan solutions for future natural disasters.

Remote sensing is used to increase the precision of the data as well as the speed with which it is collected and processed. The Geographic Information System (GIS) offers a framework for managing and coordinating various geospatial

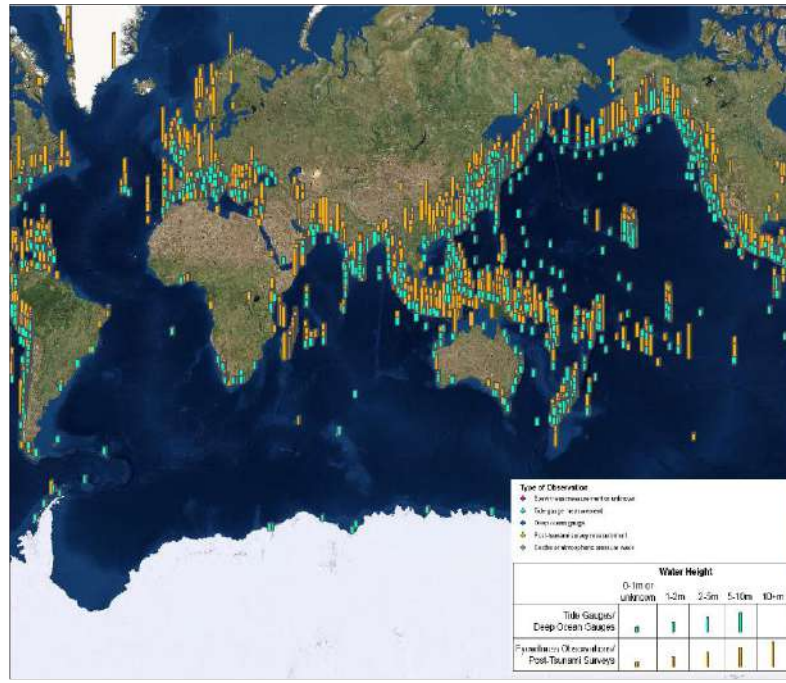


Fig. 10: Tsunami observations elaboration with vertical bars for wave height (NOAA National Centers for Environmental Information, Natural Hazards Viewer).

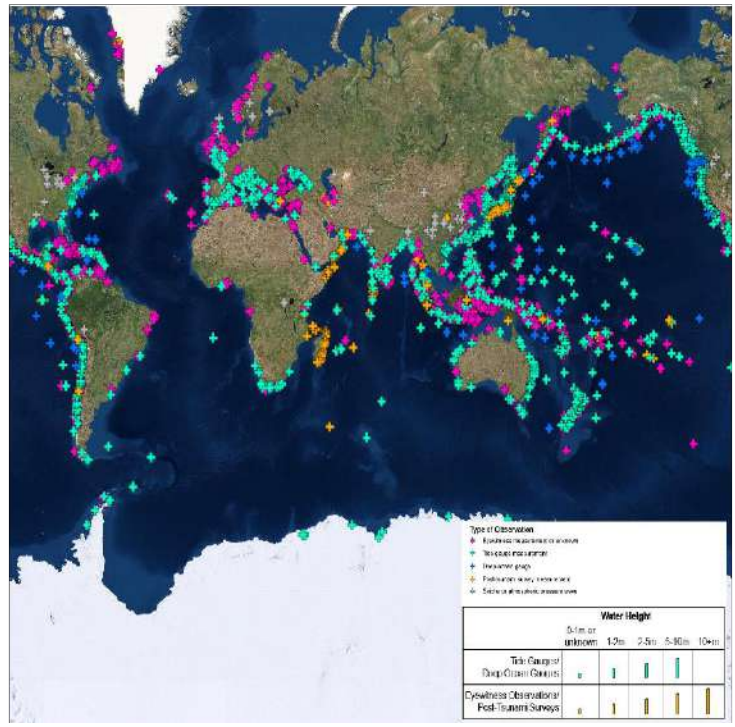


Fig. 11: Tsunami observations elaboration with color-coded by measurement type (NOAA National Centers for Environmental Information, Natural Hazards Viewer).

Table 2: Recent Tsunami registered datasets with UTC zones (NOAA/ National Service U.S. Tsunami Warning System).

| Tsunami data Issued | Origin Time | Mag | Depth | Lat | Lon | Location |
|---|---|---|---|---|---|---|
| 05-06-2019 21:25:57 | 05-06-2019 21:19:37 | 7.1 | 85 Mi. | 7° S | 146.4° E | IN THE EASTERN NEW GUINEA REGION, PNG |
| 05-06-2019 21:25:54 | 05-06-2019 21:19:37 | 7.1 | 85 Mi. | 7° S | 146.4° E | EASTERN NEW GUINEA REG PAPUA NEW GUINEA |
| 05-06-2019 21:25:42 | 05-06-2019 21:19:37 | 7.1 | 85 Mi. | 7° S | 146.4° E | EASTERN NEW GUINEA REG PAPUA NEW GUINEA |
| 05-06-2019 21:25:28 | 05-06-2019 21:19:37 | 7.1 | 85 Mi. | 7° S | 146.4° E | EASTERN NEW GUINEA REG PAPUA NEW GUINEA |
| 05-06-2019 21:25:05 | 05-06-2019 21:19:37 | 7.1 | 85 Mi. | 7° S | 146.4° E | EASTERN NEW GUINEA REG PAPUA NEW GUINEA |
| 05-05-2019 06:51:59 | 05-05-2019 06:46:59 | 4.7 | 6 Mi. | 40.6° N | 127.3° W | 165 MILES W OF EUREKA, CALIFORNIA |
| 05-02-2019 12:45:36 | 05-02-2019 12:40:17 | 4.5 | 11 Mi. | 18.1° N | 69.3° W | ABOUT 90 MILES WEST OF ISLA MONA |
| 05-02-2019 01:14:58 | 05-02-2019 01:10:25 | 4.4 | 6 Mi. | 18° N | 65.8° W | VICINITY OF PUERTO RICO |
| 04-29-2019 07:18:19 | 04-29-2019 07:16:08 | 4.2 | 12 Mi. | 39.3° N | 123.4° W | 110 MILES NW OF SACRAMENTO, CALIFORNIA |
| 04-28-2019 03:28:44 | 04-28-2019 03:26:01 | 4.1 | 20 Mi. | 19.3° N | 155.4° W | IN THE SOUTHWEST RIFT ZONE OF KILAUEA VOLCANO |
| 04-28-2019 01:01:19 | 04-28-2019 00:58:49 | 4 | 16 Mi. | 61.4° N | 149.9° W | 30 MILES SW OF PALMER, ALASKA |
| 04-23-2019 05:48:50 | 04-23-2019 05:37:57 | 6.6 | 53 Mi. | 11.9° N | 125.2° E | IN SAMAR, PHILIPPINE ISLANDS |
| 04-23-2019 05:47:46 | 04-23-2019 05:37:57 | 6.6 | 53 Mi. | 11.9° N | 125.2° E | SAMAR PHILIPPINES |
| 04-23-2019 05:47:25 | 04-23-2019 05:37:57 | 6.6 | 53 Mi. | 11.9° N | 125.2° E | SAMAR PHILIPPINES |
| 04-23-2019 05:47:03 | 04-23-2019 05:37:57 | 6.6 | 53 Mi. | 11.9° N | 125.2° E | SAMAR PHILIPPINES |
| 04-23-2019 05:46:18 | 04-23-2019 05:37:57 | 6.6 | 53 Mi. | 11.9° N | 125.2° E | SAMAR PHILIPPINES |
| 04-22-2019 21:50:09 | 04-22-2019 21:44:46 | 5.4 | 7 Mi. | 50.2° N | 130.1° W | 130 MILES W OF PORT ALICE, BRITISH COLUMBIA |
| 04-22-2019 20:32:31 | 04-22-2019 20:27:01 | 4.6 | 2 Mi. | 50.4° N | 129.8° W | 115 MILES W OF PORT ALICE, BRITISH COLUMBIA |
| 04-16-2019 10:36:14 | 04-16-2019 10:29:13 | 4.1 | 12 Mi. | 19° N | 62.3° W | ABOUT 132 MILES EAST OF ANEGADA |
| 04-14-2019 15:36:58 | 04-14-2019 15:30:39 | 5.6 | 26 Mi. | 51.9° N | 178° E | 50 MILES NW OF AMCHITKA, ALASKA |
| 04-14-2019 03:15:53 | 04-14-2019 03:09:04 | 5.5 | 2 Mi. | 19.8° N | 156.1° W | IN THE HUALALAI REGION OF THE BIG ISLAND |
| 04-12-2019 14:10:01 | 04-12-2019 14:06:27 | 5.4 | 7 Mi. | 40.4° N | 127° W | 155 MILES SW OF EUREKA, CALIFORNIA |
| 04-12-2019 12:35:04 | 04-12-2019 12:23:09 | 5.9 | 22 Mi. | 15.5° S | 172.5° W | ABOUT 111 MILES SOUTH OF UPOLU ISLAND |
| 04-11-2019 19:35:48 | 04-11-2019 19:31:35 | 4 | 16 Mi. | 19° N | 66.8° W | ABOUT 37 MILES NORTH OF PUERTO RICO |
| 04-09-2019 18:06:50 | 04-09-2019 17:53:57 | 6.7 | 71 Mi. | 58.7° S | 25.1° W | IN THE SOUTH SANDWICH ISLANDS REGION, SOUTH ATLANTIC OCEAN |
| 04-09-2019 18:06:20 | 04-09-2019 17:53:57 | 6.7 | 71 Mi. | 58.7° S | 25.1° W | SOUTH SANDWICH ISLANDS REGION |
| 04-09-2019 18:05:55 | 04-09-2019 17:53:57 | 6.7 | 71 Mi. | 58.7° S | 25.1° W | SOUTH SANDWICH ISLANDS REGION |
| 04-08-2019 23:43:05 | 04-08-2019 23:30:44 | 4.4 | 65 Mi. | 19° N | 69.8° W | ABOUT 135 MILES NORTHWEST OF ISLA MONA |
| 04-08-2019 23:36:39 | 04-08-2019 23:30:44 | 4.4 | 16 Mi. | 19.1° N | 69.7° W | ABOUT 135 MILES NORTHWEST OF ISLA MONA |

Table cont....

| Tsunami data Issued | Origin Time | Mag | Depth | Lat | Lon | Location |
|---|---|---|---|---|---|---|
| 04-08-2019 20:01:33 | 04-08-2019 19:57:43 | 4.6 | 12 Mi. | 56.4° N | 149.3° W | 155 MILES SE OF KODIAK CITY, ALASKA |
| 04-07-2019 03:04:17 | 04-07-2019 02:59:58 | 4.6 | 10 Mi. | 56.3° N | 154.4° W | 130 MILES SW OF KODIAK CITY, ALASKA |
| 04-05-2019 16:25:23 | 04-05-2019 16:14:20 | 6.6 | 38 Mi. | 55.5° S | 27.7° W | IN THE SOUTH SANDWICH ISLANDS REGION, SOUTH ATLANTIC OCEAN |
| 04-05-2019 16:24:03 | 04-05-2019 16:14:20 | 6.6 | 38 Mi. | 55.5° S | 27.7° W | SOUTH SANDWICH ISLANDS REGION |
| 04-05-2019 16:23:39 | 04-05-2019 16:14:20 | 6.6 | 38 Mi. | 55.5° S | 27.7° W | SOUTH SANDWICH ISLANDS REGION |
| 04-05-2019 16:22:50 | 04-05-2019 16:14:20 | 6.4 | 58 Mi. | 55.9° S | 27.9° W | IN THE SOUTH SANDWICH ISLANDS REGION, SOUTH ATLANTIC OCEAN |
| 04-02-2019 21:47:46 | 04-02-2019 21:36:00 | 6.5 | 19 Mi. | 52° N | 178° E | RAT ISLANDS ALEUTIAN ISLANDS ALASKA |
| 04-02-2019 21:47:28 | 04-02-2019 21:36:00 | 6.5 | 19 Mi. | 52° N | 178° E | RAT ISLANDS ALEUTIAN ISLANDS ALASKA |
| 04-02-2019 21:47:12 | 04-02-2019 21:36:00 | 6.5 | 19 Mi. | 52° N | 178° E | RAT ISLANDS ALEUTIAN ISLANDS ALASKA |
| 04-02-2019 21:46:49 | 04-02-2019 21:36:00 | 6.5 | 19 Mi. | 52° N | 178° E | RAT ISLANDS ALEUTIAN ISLANDS ALASKA |
| 04-02-2019 21:45:00 | 04-02-2019 21:36:00 | 6.5 | 19 Mi. | 52° N | 178° E | 55 MILES NW OF AMCHITKA, ALASKA |

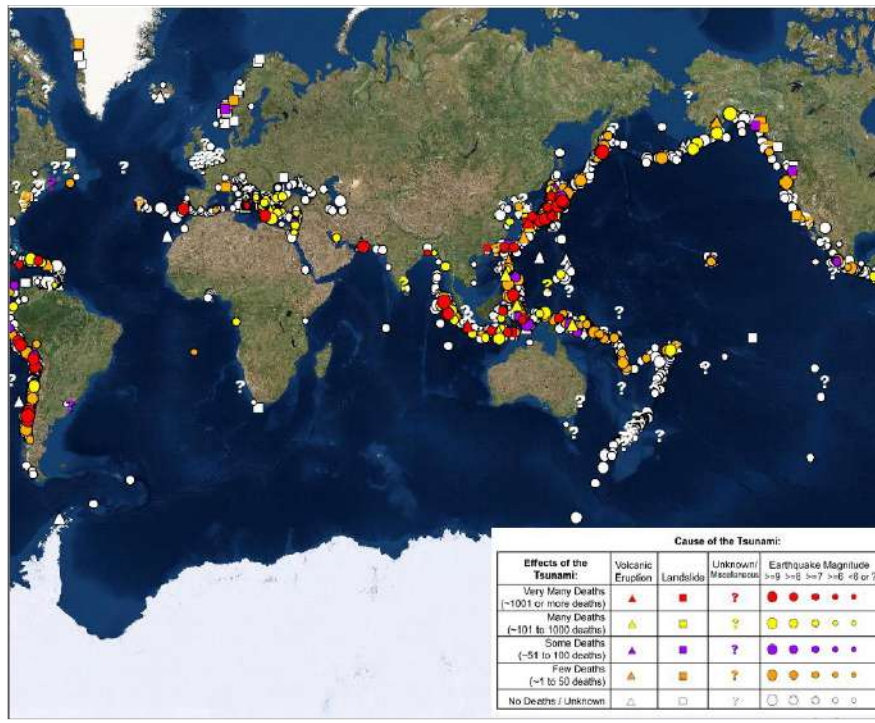


Fig. 12: Tsunami events elaboration with symbols for cause or fatalities (NOAA National Centers for Environmental Information, Natural Hazards Viewer).

information, and it is used to execute its functionalities with different modules. A Geographic Information System is used to manage remote sensing information to separate application data for analysis. Globally, many comparison studies have been conducted using remote sensing techniques, and reports have been issued to inform various government bodies to take immediate action. Operational considerations for tsunami modeling and a number of current operational models are introduced in this study.

## ACKNOWLEDGEMENT

The author would like to thank UPES Dehradun for facilitating the space to carry out the research work. The corresponding author thanks Mr. Saikat Banerjee, CubicX India for the great support in terms of the data processing and analysis. Also, thankful to Dr. Surya Prakash Tiwari, Assistant Professor, King Fahad University of Petroleum & Minerals for the continuous help in the improvement of this paper.

## REFERENCES

Arii, M., Koiwa, M. and Aoki, Y., 2014. Applicability of SAR to marine debris surveillance after the great east Japan earthquake. IEEE JSTARS, 7(5): 729-1744.

Bryant, E. 2001. Tsunami: The Underrated Hazard. Cambridge University Press, New York.

Craig, W. and Sulem, C. 1993. Numerical simulation of gravity waves. J. Comp. Phy., 108: 73-83.

Chatterjee, B., Porwal, M.C. and Hussain, Y.A., 2008. Assessment of tsunami damage to the mangrove in India using remote sensing and GIS. Int. Soc. Photogramm. Remote Sens., 45: 283-288.

Chaturvedi, S.K., Guven, U. and Srivastava, P.K., 2016.Measurement of tsunami wave Eigenfunctions in deep, intermediate, and shallower regions. Curr. Sci., 11(12): 750-756.

Chaturvedi, S.K., Srivastava, P.K. and Guven, U. 2017. A brief review on tsunami early warning detection using the BPR approach and post-analysis by SAR satellite dataset. J. Ocean Eng. Sci., 2(2): 83-89.

Chaturvedi, S.K. 2019. A case study of the tsunami detection system and ocean wave imaging mechanism using radar. J. Ocean Eng. Sci., 4(3): 203-210.

Chaturvedi, S.K., Guven, U. and Srivastava, P.K. 2020. Measurement and validation of tsunami Eigenvalues for the various water wave conditions. J. Ocean Eng. Sci., 05(01), 41-54

Dean, R.G. and Dalrymple, M. 1984. Water waves and mechanics for engineers and scientists, Prentice-Hall, Inc., Englewood Cliffs.

Dean, R.G., 1986. Evaluation and development of water wave theories for engineering applications. Presentation of Research Results. Florida Univ. Gainesville C.

Eze, C.L and Uko, D.E. 2000. Mathematical evaluation of tsunami propagation. J. Appl. Sci., 4: 213-216.

Filloux, J. H. 1970. Bourdon Tube Deep Sea Tide Gauges in Tsunamis in the Pacific Ocean. Honolulu University Press, Hawai, USA, pp. 223–238.

Geist, E.L. 1998. Local tsunamis and earthquake source parameters. Adv. Geophys., 39:117-209.

Helm, A. and Stosius, R., 2007. Status of GNSS reflectometry-related receiver developments and feasibility studies within the German Indonesian tsunami early warning system. Int. Geosci. Remote Sens., 116(54): 5084-5087.

Josheph, A. 2010. Tsunamis: Detection, Monitoring, and Early-warning technologies. Report by National Institute of Oceanography, India.

Kânoglu,U. and Synolakis, C.E. 1998. Longwave run-up on piecewise linear topographies. J. Fluid Mech., 374: 1-28.

Lin, F.C., Sookhanaphibarn, K. and Pararas-Carayannis, G. 2013. REMOTE: Reconnaissance & monitoring of tsunami events. Sci. Tsunami Hazards, 33(2): 86-111.

Liu, P.L., Cho, Y.S. and Briggs, M.J. 1995. Run-up of solitary waves on a circular island. J. Fluid Mech., 302: 259-285.

Madsen, P.A. and Schäffer, H.A., 2010. Analytical solution for tsunami runup on a plane beach: single waves, N-waves and transient waves. J. Fluid Mech., 645: 27-57.

Martino, L., Ulivieri, C., Jahjah, M. and Loret. E., 2009. Remote sensing and GIS techniques for natural disaster monitoring, In Philip, O. (ed), Space Technologies for the Benefit of Human Society and Earth. Springer, New York, pp. 331-382.

Murty, T.S., Rao, A.D. and Nistor, I., 2006. Numerical modeling concepts for tsunami warning systems. Curr. Sci., 90(8): 1073-1081.

Okal, E.A. 1988. Seismic parameters controlling far-field tsunami amplitudes: A review. Natural Hazards, 28: 67-96.

Prins, J.E. 1958. Characteristics of waves generated by local disturbance. AGU, 39: 865-874.

Sirikulchayanon, P., Sun, W. and Oyana, T.J. 2005. Assessing the impact of the 2004 tsunami on mangroves using remote sensing and GIS techniques. Int. J. Remote Sens., 29(12): 3553-3576.

Tadepalli, S. and Synolakis, C.E. 1994.The run-up of N-waves on sloping beaches. Proc. of Royal Soc. London, 445: 99-112.

Tadepalli, S. and Synolakis, C.E. 1996. Model for the leading waves of tsunamis. Phys. Rev. Lett., 77(10): 2141-2144.

Titov, V.V. 2000. Tsunami Forecasting. In Bernard, E.N. and Robinson, A.R. (eds.), The. Sea. Vol. 15. Harvard University Press, Cambridge, pp. 371-400.

Todorovska, M.I. and Trifunac, M.D., 2001.Generation of tsunamis by a slowly spreading uplift of the seafloor. Soil Dyn. Earthquake Eng., 21: 151-167.

Westen, V. and Soeters, R. 2009. Remote sensing and geographic information systems for natural disaster management presented at natural disasters and their mitigation: A Remote Sensing and GIS Perspective. Indian Inst. Remote Sensi., 16: 31-76.

Ward, S.N. 1980. Relationships of tsunami generation and earthquake source. J. Phys. Earth Sci., 28: 441-474.

Zielinski, A. and Saxena,N. 1983. The rationale for measurement of mid-ocean tsunami signature. Marine Geodesy, 6: 331-337.

Nature Environment and Pollution Technology
An International Quarterly Scientific Journal

p-ISSN: 0972-6268
(Print copies up to 2016)
e-ISSN: 2395-3454

Vol. 20 | No. 5 (Suppl) | pp. 2137-2147 | 2021

Original Research Paper

https://doi.org/10.46488/NEPT.2021.v20i05.031

Open Access Journal

# Recognition of Image-Based Plant Leaf Diseases Using Deep Learning Classification Models

**Sakshi Takkar*, Anuj Kakran**, Veerpal Kaur*, Manik Rakhra*†, Manish Sharma***, Pargin Bangotra**** and Neha Verma*****

*School of Computer Science and Engineering, Lovely Professional University, Phagwara, Punjab, India
** Quantum University, Roorkee, Uttrakhand, India
***Department of Physics, School of Basic Sciences, Bahra University, Shimla Hills, Shimla, Himachal Pradesh, India
****Atmospheric Research Laboratory, Department of Physics, SBS&R, Sharda University, Greater Noida, India
*****KRM DAV Nakodar, Punjab, India
†Corresponding author: Manik Rakhra; rakhramanik786@gmail.com

**Nat. Env. & Poll. Tech.**
**Website: www.neptjournal.com**

*Received:* 03-06-2021
*Revised:* 03-07-2021
*Accepted:* 13-07-2021

**Key Words:**
Plant diseases
Convolutional neural network
Support vector machine
Artificial neural network

## ABSTRACT

Plant diseases are spread by a variety of pests, weeds, and pathogens and may have a devastating effect on agriculture, if not handled in a timely manner. Farmers face umpteen challenges from a proper water supply, untimely rain, storage facilities, and several plant diseases. Crops disease is the primary threat and it causes enormous loss to farmers in terms of production and finance. Identifying the disease from several hectares of agricultural land is a very difficult practice even with the presence of modern technology. Accurate and rapid illness prediction for early illness treatment to crops minimizes economical loss to the individual and further proves to be productive for healthy crops. Many studies use modern deep learning approaches to improve the accuracy and performance of object detection and identification systems. The suggested method notifies farmers of different agricultural illnesses, prompting them to take further essential precautions before the disease spreads to the whole agricultural field. The primary objective of this study is to detect the illnesses as soon as they begin to spread on the leaves of the plants. Super-Resolution Convolutional Neural Network (SRCNN) and Bicubic models are employed in the system to identify healthy and diseased leaves with an accuracy of 99.175 % and 99.156 % respectively.

## INTRODUCTION

Agriculture is one of the most important economic activities of the Indian subcontinent and two-third population is directly involved in farming and related occupations. Agriculture has long been considered India's backbone, dating back to the Indus Valley civilization. To earn income, mankind established their residence land according to agricultural facilities and favorable conditions. Agriculture is important in most developing countries because it provides jobs and contributes a significant portion to GDP (Pradhan 2007). Bacterial growth and diseases are a primary threat for the crops and affect the agricultural cycles and patterns too. To overcome this problem, a variety of pesticides, fertilizers, and research-based remedies are used nowadays. Agriculture is getting attention in every five-year plan and preference is given for the development of agriculture in India.

The agricultural field needs more up-gradation due to changes in weather and economic conditions in the country. The crops in the fields should be healthy to get more productive results. Technical and proper research-based methods are required to monitor the crops regularly. Crop disease is one of the reasons for decreasing the quantity and quality of crops in the fields. The use of toxic pathogens, extreme change in climate conditions, and poor disease control are one of the factors of poor food production. Large numbers of pesticides are available to control the diseases of crops in agriculture and to increase the production of crops in the fields. Identifying the current disease of the crops and finding the appropriate pesticide to control the diseases is a task that requires the advice of experts in the field of agriculture that makes this task very consuming and expensive. Accurate and timely identification of diseases of crops is one of the reasons for successful agriculture. It is also very important to spend less time and money to identify the hazardous diseases on crops. These diseases on plants and crops can be pre-identified with some kind of initial tracks and spots developed on leaves and fruits. Many farmers use their knowledge or seek assistance from other professionals to spot crop diseases with their naked eyes. Due to the

similarities in symptoms of crops, this method raised the possibility of human error and faulty illness diagnosis. This type of disease diagnosis mistake leads to the overuse of pesticides and fertilizers that contains heavy metals, which reduces crop yield and even pollutes the environment through deposition in various areas, resulting in radiological and chemical exposures to humans, flora, and fauna (Bangotra et al. 2019, 2021, Pandit et al. 2020, Mehra et al. 2015).

Nowadays, server-based and mobile-based technologies are used to identify the diseases of crops accurately (Sladojevic et al. 2016, Huang et al. 2014). Modern approaches like Machine Learning and Deep Neural networks are used to increase the accuracy of results in finding diseases of crops. There is a need for a Machine Learning Vision system to identify the disease from the image of crop and to suggest the pesticide as a solution to control the disease. Various researchers have conducted studies in this field by using traditional machine learning algorithms like Support Vector Machine (SVM), Artificial Neural Network (ANN), Random Forest algorithm, K-Means method, and Convolutional Neural Network.

## PLANT DISEASES

1. **Apple Scab:** Apple scab is a serious disease of apple that attacks both fruits and leaves. Olive green spots or pale yellow spots appear on the upper surface of the leaves. Dark and velvet spots appear on the lower surface of the leaves. Apple with this scab disease is not fit for eating. This disease reduces the quality and size of fruits. Apple scab can cause total failure of crops without control measures.
2. **Black Rot:** Black rot is a disease that is caused by bacteria that can infect crops. It is very difficult to control this disease by the growers. Generally, the loss of crops happens in hot and humid weather conditions. These diseases are generally found in apples and Grapes. Disease symptoms appear as yellow and dead tissues at the edge of the leaves in older plants. The spot on leaves get larger and infect other plants and fruit bunch very rapidly.
3. **Bacterial Spot:** Bacterial spot is a dangerous disease of plants found in warm and humid weather conditions. Bacterial spot occurs on pepper and tomatoes. Symptoms on the leaves appear as small yellow-green lesions which get deformed and twisted and change into the dark, water-soaked, and greasy lesions. This disease is due to bacteria that attack the vegetation, stems, and fruits of tomatoes and pepper. Once this is present on the plants it is very difficult to control the disease and these spot results in unmarketable fruits and vegetables.
4. **Black Measles:** Black measles occur in grapes and is also known as grapevine measles, esca, or Spanish measles. The term measles refers to artificial spots that appear on the grapes. The symptom on the leaves appear as a 'Tiger Stripe' pattern and it becomes more serious from year to year. During the season, the spot merges over the surface of the grapes and makes the grapes black. Spots on the berries can appear any time after the fruit set and before some days of the harvesting.
5. **Cedar Apple Rust:** Cedar apple rust is a fungal disease that occurs in apples. The infected leaves show yellow to orange round spots on the upper surface. As soon as the infection grows, the spots also appear on the lower surface of the leaves. This disease can affect the stems and fruits. When the disease of the fruits grows, then the lesions on the fruits may crack and appear brown in color.
6. **Citrus Greening:** Citrus greening is one of the dangerous plant diseases in the world. Once a plant is infected due to this disease then there is no cure. This disease is caused by one disease-infected insect- Asian Citrus Psyllid. This disease is mostly found in oranges. This disease shows the symptoms like yellowing of leaves, dieback of twigs, and decline in vigor which leads to death of the entire plant.

**Common Rust:** Common rust is one of the serious fungal diseases which attack the roses, corns, and tomatoes, etc. This disease occurs mostly in mild and moist conditions. Rust is actually spread by spores from infected to healthy plants. The spores are generally transferred by wind or water. This is the reason rust appears often after watering. Yellow or white spots appear as symptoms on the upper part of leaves. This results in leaf distortion and deformation.

7. **Early Bight:** Early blight disease is very common in potatoes and tomatoes which are caused by the fungus name *Alternaria Solani.* Firstly, its symptoms appeared on old leaves as small brown spots with a pattern of Bull's eye. When it spreads than its color changes to yellow. After the stem, fruit, and upper portion of the plant get infected and crops can be devastated. Early blight disease develops at moderate to warm temperatures.
8. **Gray Leaf Spot:** Gray leaf spot is a fungal disease that attacks the corn plants which is also known as maize. First, symptoms of this disease are noticed in the lower leaves. The region on the leaf begins as a small yellow dot spot. As time passes this yellow spot changes to

brown color and then to a gray rectangular shape. This region appears as the shape of a matchstick which slowly results in the killing of leaves. The grayish color on the leaves appears due to the presence of fungal spores.

9. **Late Blight:** Late Blight is a disease that attacks potatoes and tomatoes. This disease is caused by the water mold of Phytophthora infestans. This disease mostly occurs in humid regions where the temperature is ranging between 4-29°C. The infected tomatoes and potatoes may get rot within two weeks. This disease spreads very quickly in fields and results in total crop destruction if they are not controlled.
10. **Leaf Blight:** Leaf Blight is a fungal disease that attacks grapes. This disease is caused by a fungus named *Helminthosporium turcicum* Pass. This disease occurs in humid conditions and it shows symptoms with reddish-purple or tan spots and it gets bigger on the leaves. The symptoms on the leaves first appear on older or lower leave but after then it spreads on the younger or upper leaves. This drastic disease gives a burnt appearance to the leaves.
11. **Leaf Mold:** Leaf mold is a disease that is found in tomatoes. This disease causes loss in tomatoes which are found in high tunnels or greenhouses due to humidity in those environments. This disease is caused by a fungus named *Passalora fulva*. The oldest leaves are infected first due to this disease.
12. **Leaf Scorch:** Leaf Scorch is a disease that attacks strawberries. It is a serious disease that is caused by the bacterium *Xylella fastidiosa*. The first symptom which can be noticed is the browning of leaves in the mid-summer. The symptoms get worse throughout the late summer and after then gets fall. As the disease progresses over the years, branches and trees decline slowly. The symptoms first appear on the lower branches and then on the upper leaves.
13. **Leaf Spot:** Leaf spot is a serious disease that is found in tomatoes. This disease is a fungal disease that is caused by bacteria. Leaf spots show symptoms with brown color but spots can be tan or black depending on the type of fungus. Some Concentric rings or dark margins are also found around the dark spots. Leaf spot diseases actually weaken the shrub or trees by blocking the photosynthesis process.
14. **Mosaic Virus:** Mosaic Virus is a disease that attacks tomatoes. This disease affects the leaves which show symptoms with spots of yellow, white, light, and dark green color. After then leaves may be curled, malformed, and reduced in size. This virus can also infect pepper, pear, cherry, and potatoes. This may reduce the fruit's number and size. This can create yellowish rings on the leaves if leaves ripen in warm weather.
15. **Northern Leaf Blight:** Northern leaf blight is a disease that affects the corn leaves. This disease is caused by the fungus Setosphaeriaturcica. Symptoms generally appear on lower leaves with gray-green color and then turn to pale or tan color. Dark gray spores are produced under moist conditions and it gives regions a dirty gray appearance. Spores are generally transferred by wind or by the splashing of water.
16. **Powdery Mildew:** Powdery Mildew is a fungal disease that affects a variety of plants and it reduces the quality and quantity of fruits and flowers. When the fungus takes over on one of your plants then the spores make a layer of mildew on the top of leaves. The spores are then transferred to other plants by the wind. This disease can slow down the growth of plants and reduces the quality of crops.
17. **Spider Mites:** Spider mite is a disease that eats plants and they look like tiny spiders. Most of the spider mites get active in dry and hot conditions. Because of the feeding of spider mites, white to yellow spots appear on the upper surfaces of leaves. The eggs also stick on the leaves' undersides. As the disease infiltration, the color of leaves appears as bronze and then becomes stiff.
18. **Target Spot:** Target spot is a disease that attacks the tomato leaves. Initially small, dark-brown spots appear on the upper parts of older leaves, and then eventually its size increases and makes concentric rings. This disease is spread by air-borne spores. This is a fungal disease and affects many other crops like pepper, papaya or cucumber, etc.
19. **Yellow Leaf Curl Virus:** Tomato yellow leaf curl disease is caused by the yellow leaf curl virus. The leaves which are infected are curled inward or upwards. The infected plants reduced the flowers and fruits in large numbers. This disease is not seed-borne but is spread by whiteflies. This disease is generally found in tropical and sub-tropical regions which cause economic loss.

## BACKGROUND AND RELATED WORK

Badage (2018) elaborated that disease in plants is caused by insects and various pests. Plant diseases decrease the productivity of crops. Farmers face a lot of problems and losses due to these various crop diseases. The system is proposed by the author who tells about crop diseases and actions to control them. This proposed system is divided into two phases: the first phase includes training of the datasets of crop diseases

and the second phase includes the identification of crop diseases by using Canny's edge detection algorithm (Badage 2018). Maniyath et al. (2018) proposed some techniques on the leaf-based image classification to find out the results and plant diseases. Random Forest algorithm was used to identify healthy and diseased leaves from the leaf-based image dataset. Various steps have been implemented like the collection of the dataset, feature extraction method, and training of dataset and classification approach. The machine learning approach gives a clear picture of training the dataset and classification of images.

Sladojevic et al. (2016) argued that Convolution Neural Network achieved more accurate results in the leaf image classification to identify plant or crop diseases. This new approach of training the dataset is a quick and easy method of implementation. This proposed model could find out thirteen different types of plant diseases by identifying the surroundings or edges of leaves. This proposed method showed the experimental results with an average precision of 96.3% (Sladojevic et al. 2016). Saleem et al. (2019) analyzed that early identification of plants diseases is very prominent for healthy crops and plants. Many machine learning algorithms were used for the detection and identification of plant diseases but the subset of machine learning i.e. deep learning techniques showed more accurate results as compared to other machine learning algorithms. Various deep learning techniques were combined with other visualization techniques to identify the symptoms and diseases of plants. Performance metrics were used to evaluate the deep learning techniques (Saleem et al. 2019).

Sarangdhar & Pawar (2017) analyzed the particular attack of diseases that decrease the production of cotton crops. In this study, a vector machine algorithm was used to identify five different types of cotton leaf diseases. An android app will be used by the farmers where diseases after identification will be informed with their remedies. This android app also identifies the soil type with its moisture and humidity. This system has been made with sensors and raspberry pi that makes the system more effective. The accuracy achieved with this proposed system is 83.26 %.

Huang et al. (2014) proposed new spectral indices that are used to identify the different diseases on wheat crops. Optimized spectral indices were obtained by the combination of a single band and the difference of wavelength between two different bands. RELIEF-F algorithm has been used by an author to identify the wavelengths from the leaf spectral data. This algorithm is more effective as it can deal with multiclass classification problems. This study indicates new spectral indices can easily detect diseases by using hyperspectral data.

Qin et al. (2003) analyzed the stresses of rising diseases for pest management in fields. The research was carried out on a rice field, and correlations between ground data and image data were made. The experiment results show that remote sensing imagery has a very important application and ground data shows an average accuracy of more than 70% for classification (Qin et al. 2003)we first examine the applicability of broadband high-spatial-resolution ADAR (airborne data acquisition and registration. Rothe & Kshirsagar (2015) proposed a pattern recognition system to identify the different cotton plant diseases. This work was done on the images of cotton leaves taken from the fields. The contour model was used for the segmentation of images and training of the adaptive neuro-fuzzy inference method. The accuracy for the classification is approximately 85%. The diseases of cotton leaves were identified by using a back propagation neural network.

Gulhane & Kolekar (2015) used Principal Component Analysis (PCA) and K-Nearest Neighbor (KNN) method to diagnose the diseases of cotton leaves in fields. In a number of cases, human assistance in identifying diseases may be incorrect. Machine learning models have been created to determine the accuracy of disease detection in cotton leaves plants. Implementation of PCA/KNN equipped with multi-variate techniques was used to analyze the statistical data. The PCA/KNN bases classifier showed a classification accuracy of 95% (Gulhane & Kolekar 2015). Revathi et al. (2011) proposed a computing technology to help farmers all over the world to take care of the crops from various diseases. The author had proposed a method to diagnose the diseases of cotton plants by capturing the image using a mobile camera and then categorized the diseases using a neural network. The work is based on the image segmentation technique where RGB color feature image segmentation is used to identify the disease spots on cotton plants (Revathi et al. 2011).

Blessy & Joy Winnie Wise (2018) selected Convolutional Neural Network (CNN) technique to identify the disease spots on the plants. The image of the sample leaf was used as an input where green pixels from the image were marked in green color that represents the healthy part of the image. Further, this green area from the image was removed to calculate the rest of the infected area from the image. Following the extraction of characteristics from the affected areas, the CNN model is used to classify the diseases. After diagnosing the disease, detailed information about diseases was sent to the mobile of farmers with the solutions through GSM device.

Rastogi et al. (2015) studied the automatic detection of crop diseases based on the two phases used in the proposed system. In the first phase, pre-processing of leaf images, feature extraction, and classification using Artificial Neu-

ral Network (ANN) was done to recognize the leaves. In the second phase, K means-based segmentation was done to identify the defected areas, then feature extraction was done to find the defected portion and classification of the disease identified by using ANN. After the identification of diseases, grading was done based on the amount of disease present in the leaf.

Owomugisha et al. (2014) proposed machine learning techniques to identify bacterial diseases in banana plants. The computer vision technique was investigated to make an algorithm that is further divided into four phases. In the first phase, images of banana leaves were captured using a digital camera. In phase two, feature extraction techniques were used to send the data in phase three for classification. In phase three, different classifiers were used to identify the diseases. In the last phase, the performance of all the classifiers was compared based on Area under Curve (AUC) parameter for evaluation. Tian et al. (2012) presented an SVM- based Multiple Classifier System to recognize the patterns of wheat leaf diseases. Encouraging results were obtained by using this proposed methodology to identify the diseases from wheat diseases. Three different types of SVM classifiers were used as color features, shape features, and texture features for training sets.

Shi et al. (2015) proposed an automatic crop disease recognition method that takes the statistical features from leaf images and meteorological data and combines them. The Probabilistic Neural Network (PNN) method was used to identify the classification accuracy. Infected crop leaves images were captured by using a digital camera to extract the statistical features like color, shape, and texture by using the image processing method. PNN classifier accuracy rate was 90% which is more than the accuracy rate of other classifiers.

Ashqar & Abu-Naser (2018) presented a deep learning technique to identify tomato leaves diseases using image-based recognition. Around 9000 images dataset of healthy and diseased tomato leaves were collected under controlled conditions. Training of deep convolutional neural network was done to identify the five diseases. The proposed method showed an accuracy of 99.84% that made this approach more feasible to diagnose the tomato leaves diseases in agriculture (Ashqar & Abu-Naser 2018). Revathi & Hemalatha (2012) analyzed a comparative study of crop diseases using machine learning techniques in the field of agriculture. The algorithms like SVM machine learning algorithm, decision tree algorithm, and artificial neural network were used to represent the work. Data mining technique is one of the innovative techniques and used to predict various crop diseases. This study was based on the applicability of data mining techniques with a comparative analysis to find out the accuracy and other performance parameters for crop disease prediction (Revathi et al. 2011).

Sethy et al. (2018) developed a prototype to identify the diseases of rice crops using computational intelligence and machine learning techniques. Numerous diseases on the rice crops appear as a spot on the leaves and if diagnosis of the diseases has not been done on time, then it can cause great harm to rice crops. The pesticide-based treatment of crops can cause severe environmental pollution. In this proposed methodology, Fuzzy logic was introduced with a K-means algorithm to identify the degree of the sternness of disease on rice crops. This proposed methodology showed an accuracy of 86.35%.

Shruthi et al. (2019) presented a comparative analysis of various machine learning techniques to identify the best technique for crop disease detection. It was observed that Convolution Neural Network provides more accuracy to identify the diseases from crops (Shruthi et al. 2019). Reza et al. (2016) framed a research methodology to detect jute plant diseases using image processing and machine learning techniques. The proposed methodology involves an android application that helps to capture the pictures of jute plant diseases and to send the pictures to the server to identify the jute plant diseases. The features were extracted from the captured image and extracted values were compared with the values stored in the database that helped to identify the leaf diseases. The classification of the diseases was done by using a Multi-SVM classifier. After that, the final result was sent to the farmer within a fraction of seconds with the necessary solutions or control measures through the android application (Reza et al. 2017).

## MATERIALS AND METHODS

In this proposed system, a dataset of 54,343 images of different plant species was taken that involves diseased plants or healthy plants images of various fruits and vegetable crops. The dataset was split into three sets: training set, validation set, and testing set. Training is done by using the pre-trained model Inception V3 by fine-tuning the last layers of the network. Four custom convolutional and max-pooling, layers have been added on the top of transfer learning architectures. At the last, two dense layers have been used with 64 neutrons and 2 neurons respectively. The last layer is used for classification with softmax as an activation function. Training of the model has been done by 20 epochs or iterations by changing the various parameters like batch size, optimizer, pre-trained weights, and learning rate. To reduce the overfitting between the batch normalization and different layers, 30% dropouts were used to reduce the internal covariate shift and this actually helps the model to avoid getting stuck in the local

optimum. The evaluation metric named Multi-Class Log Loss was also used in the model with some data generators for training data and testing data. These generators help to load the required amount of data directly from the source folders with the batch sizes as per need of the detection and help to convert the batches into training data and training models. To do a fair comparison between the results of all experiments, an attempt has been made to normalize hyper-parameters across all the experimentations and research.

**Pre-processing and Training the Model:** Pre-processing is the foremost step that is performed on the images. In this step, the database is pre-processed such as reshaping of an image, resizing of an image, and conversion of an image into an array form (Fig. 1). Pre-processing is also done on the test images in the same way. A database consists of 54,343 images of different plant species and out of all the images any image can be used as a test image. The database is used to train the dataset using the Inception V3 model and it further helps to identify the test image and the disease of the test image. After the training of the model, the software can find the diseases in the plants that were already stored in the database. After the completion of training and pre-processing, the evaluation is done between the test and trained model to predict the disease.

**Collection of Database:** Acquiring valid database collection is the initial step of any image processing-based project. There are many ways to generate the database as either to store all images or to collect the images from different sources and make own database for processing. The Kaggle Plant Village Dataset database was used in the present study. At first, the data was labeled and cleaned for prior image processing. For image processing, images with good resolution and angles were selected to ensure a high accuracy algorithm detection system. After the selection of all the images from the database, in-depth knowledge was gained for different plants and their diseases. Different types of plant diseases with their symptoms were studied in this processing system. After the deep and detailed study, image segregation was done to label the images and the following steps were performed:

1. The input test image was acquired and pre-processing was done accordingly. After pre-processing, the image was converted into an array form for evaluation.
2. Then the dataset was segregated and pre-processing has been done.
3. After pre-processing, training of dataset has been done by using Inception V3 model and further classification has been completed.
4. In the next step, a comparison of the test and trained model was done and the final results have been obtained as per system inputs.
5. In the last step, the software displayed, whether the plant is diseased or healthy.

**Classification Models:** To classify datasets, two models were used: SRCNN (Super-Resolution Convolutional Neural Network) Model and Bicubic Model.

- ***SRCNN (Super-Resolution Convolutional Neural Network) Model:*** In deep learning, generally Convolutional

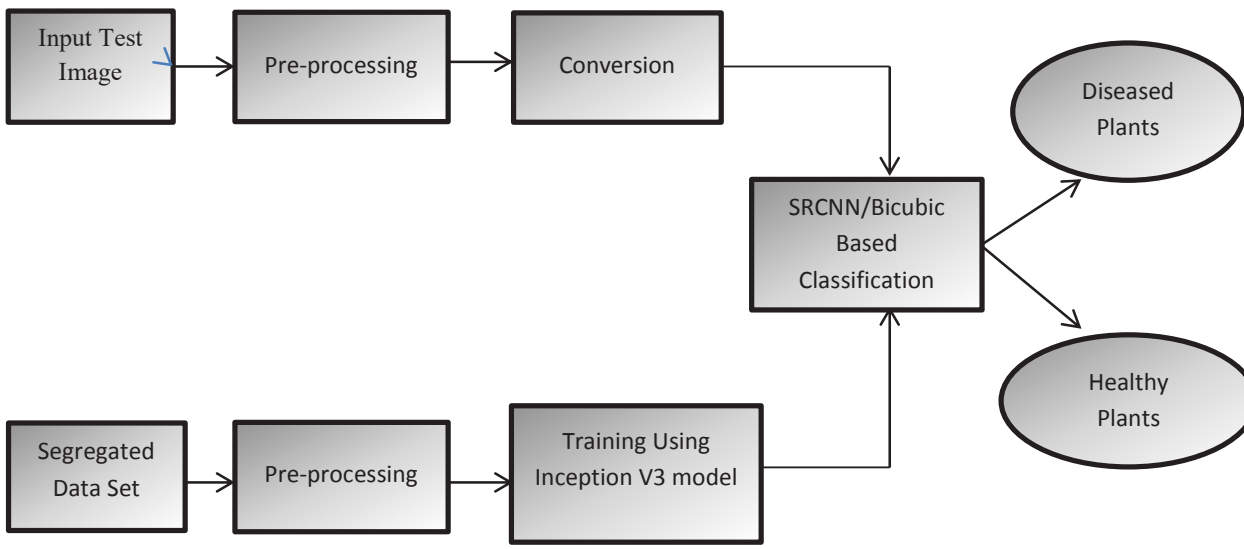


Fig. 1: Flowchart for plant disease detection.

Neural Network (CNN) is used for image classification. The objective of Super-Resolution (SR) is to recuperate high-resolution images from low-resolution images. The SRCNN network involves mainly four operations: pre-processing, feature extraction, non-linear mapping, and reconstruction.

1. *Pre-processing:* This step means upscaling of low-resolution to high-resolution images.
2. *Feature Extraction:* This step extracts the set of feature maps from the upscaled low-resolution image.
3. *Non-Linear Mapping:* Mapping of feature maps that represents low-resolution to high-resolution patches.
5. *Reconstruction:* Produces or reconstructs the high-resolution image from high-resolution patches.

SRCNN is a deep convolutional neural network that is used for end-to-end mapping of low-resolution to high-resolution images (Fig. 2). This model is used to improve the quality of low-resolution images. With this approach of Super Resolution, a better quality of images can be obtained from even a small size of input images. The performance of this network can be evaluated by using different parameters such as Mean Squared Error (MSE), Peak Signal to Noise Ratio (PSNR), and Structural Similarity (SSIM) Index.

- ***Bicubic Interpolation Algorithm*:** Bicubic Interpolation Algorithm is a two-dimensional system that uses a polynomial technique for enlarging or sharpening digital images (Fig. 3). This algorithm (samples dimension: 4x4 and 16 samples at a time) upscale low-resolution images before going to the network. However, the computational cost increases with each pre-up sampling step. This algorithm is mainly used in computer editing software or by editors for reconstructing and resampling the images. During interpolation of an image, the pixels get distorted from one grid to another grid. This is a very slow algorithm as it takes time to process during the resampling of an image. There are two interpolation algorithms: Adaptive Interpolation and Non-Adaptive Interpolation.

  a) *Adaptive Interpolation:* Adaptive interpolation algorithm depends on what the image is introducing. Adaptive algorithms are used in exclusive techniques which are used in various latest photo editing software like Adobe Photoshop and Photozoom Pro.

  b) *Non-Adaptive Interpolation:* Non-adaptive interpolation method treats all the pixels equally. Non-adaptive algorithms involve various other algorithms like the k-nearest neighbor, spline, Bicubic, and bilinear.

## RESULTS AND DISCUSSION

### Dataset Description

In this study, a plant disease village dataset of 54,343 images have been taken which are fine-tuned using a well-known model Inception V3 after pre-processing, and the dataset has been taken from Kaggle Repository. This dataset involves the study of different plants like Apple, Blueberry, Cherry, Corn, Grape, Orange, Peach, Pepper bell, Potato, Raspberry, Soybean, Squash, Strawberry, Tomato, etc. The different sets of healthy and diseased plant images are used. The research

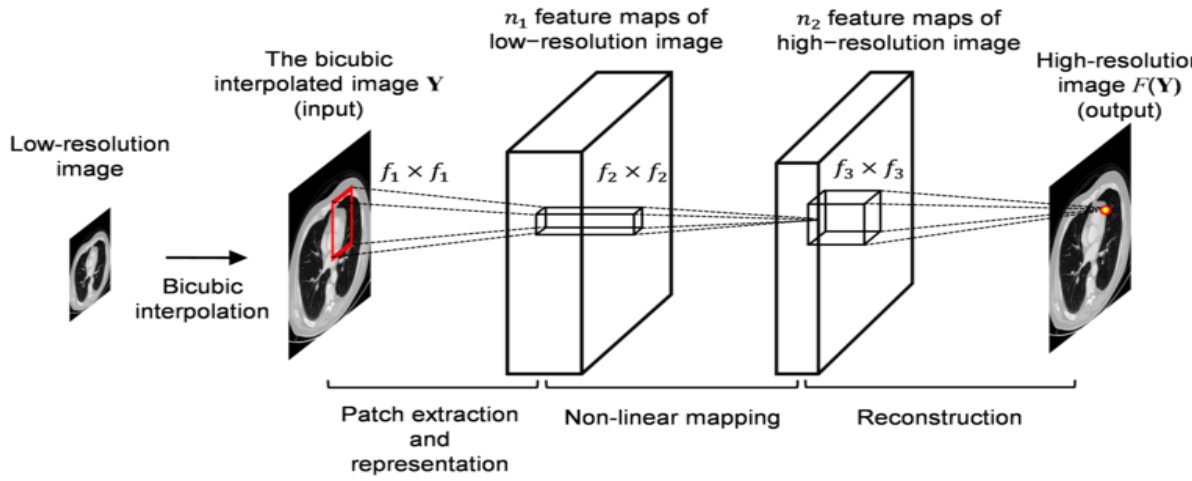


Fig. 2: SRCNN based classification model.

Table 1: Dataset for image classification of leaf disease.

| Sr. No. | Plant Category | Disease/ Healthy | Number of Original Images |
|---|---|---|---|
| 1 | Apple | Apple Scab | 631 |
| 2 | Apple | Black Rot | 622 |
| 3 | Apple | Cedar Apple Rust | 276 |
| 4 | Apple | Healthy | 1646 |
| 5 | Blueberry | Healthy | 1503 |
| 6 | Cherry | Healthy | 855 |
| 7 | Cherry | Powdery Mildew | 1053 |
| 8 | Corn | Common Rust | 1193 |
| 9 | Corn | Gray Leaf Spot | 514 |
| 10 | Corn | Healthy | 1163 |
| 11 | Corn | Northern Leaf Blight | 986 |
| 12 | Grape | Black Measles | 1384 |
| 13 | Grape | Black Rot | 1181 |
| 14 | Grape | Healthy | 424 |
| 15 | Grape | Leaf Blight | 1077 |
| 16 | Orange | Citrus Greening | 5508 |
| 17 | Peach | Bacterial Spot | 2298 |
| 18 | Peach | Healthy | 361 |
| 19 | Pepper Bell | Bacterial Spot | 998 |
| 20 | Pepper bell | Healthy | 1479 |
| 21 | Potato | Early Blight | 1001 |
| 22 | Potato | Healthy | 153 |
| 23 | Potato | Late Blight | 1001 |
| 24 | Raspberry | Healthy | 372 |
| 25 | Soybean | Healthy | 5091 |
| 26 | Squash | Powdery Mildew | 1836 |
| 27 | Strawberry | Healthy | 457 |
| 28 | Strawberry | Leaf Scorch | 1110 |
| 29 | Tomato | Bacterial Spot | 2128 |
| 30 | Tomato | Early Blight | 1001 |
| 31 | Tomato | Healthy | 1592 |
| 32 | Tomato | Late Blight | 1910 |
| 33 | Tomato | Leaf Mold | 953 |
| 34 | Tomato | Leaf Spot | 1772 |
| 35 | Tomato | Mosaic Virus | 374 |
| 36 | Tomato | Spider Mites | 1677 |
| 37 | Tomato | Target Spot | 1405 |
| 38 | Tomato | Yellow Leaf Curl Virus | 5358 |
| | | | 53343 |

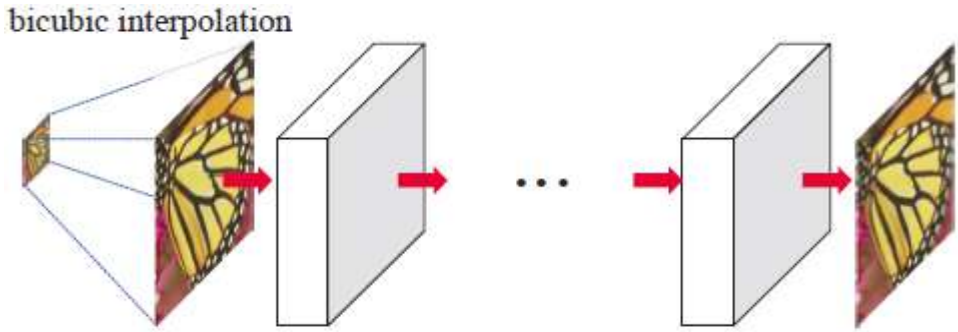


Fig. 3: Bicubic Interpolation based classification model.

has been done on different diseases like apple scab, bacterial spot, black measles, black rot, cedar apple rust, citrus greening, common rust, early blight, gray leaf spot, late blight, leaf blight, leaf mold, leaf scorch, leaf spot, mosaic virus, northern leaf blight, powdery mildew, spider mites, target spot, and yellow leaf curl virus. Table 1 describes the plant category, healthy or diseased image, and the number of images in each category.

### Experimental Results

In each model, data is divided into two sets- training set and testing set. Training has been done by using the Inception V3 model and the dataset has been split into 70-30, 50-50, and 30-70. In the training phase, we train the classifiers and in the testing phase, testing is done to analyze the performance of the classifier. Results are demonstrated using different parameters like accuracy, loss, validation accuracy, validation loss, and learning rate by epochs using two different classifiers SRCNN and Bicubic algorithm as shown in Table 2. Out of these classifiers, the SRCNN classifier shows better accuracy as compare to Bicubic (Table 3). The graphs of training and validation accuracy by epochs for the Bicubic and SRCNN model have been depicted in Fig. 4.

## CONCLUSION

Protection of crops in an agriculture field is a very tedious task and still, there is a need for a qualitative study to know about the crops and their likely weeds, pathogens, and pests. The present methodology identifies diseases in plants to increase the productivity of crops in fields. The system is developed for the benefit of farmers and the agricultural sector. In this system, deep learning models were used for the detection of plant diseases using different leaf images to identify whether the leaf is healthy or diseased. The outcome

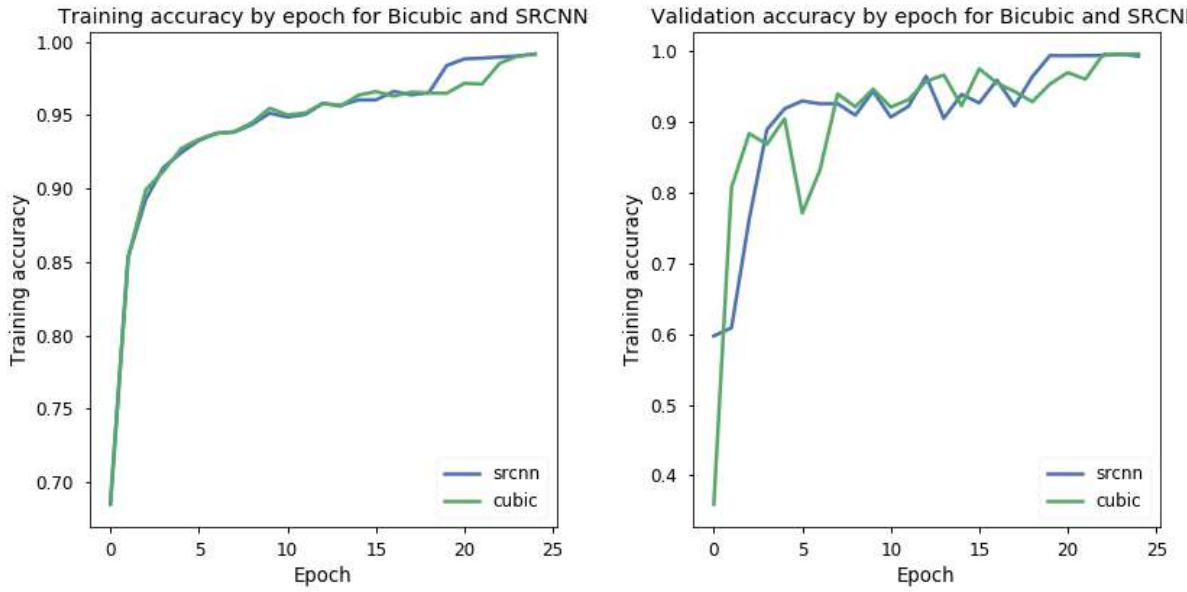


Fig. 4: Graphs representing training and validation accuracy for models.

Table 2: Comparison of bicubicvs SRCNN classifier.

Bicubic Result by Epoch

| Epoch | Acc | loss | lr | val_acc | val_loss |
|---|---|---|---|---|---|
| 0 | 0.68675 | 1.078107 | 0.001 | 0.359188 | 3.793237 |
| 1 | 0.853313 | 0.452098 | 0.001 | 0.807466 | 0.675127 |
| 2 | 0.899355 | 0.314722 | 0.001 | 0.883504 | 0.393525 |
| 3 | 0.911813 | 0.27287 | 0.001 | 0.868497 | 0.433363 |
| 4 | 0.927396 | 0.225642 | 0.001 | 0.904577 | 0.324232 |
| 5 | 0.933563 | 0.206778 | 0.001 | 0.771073 | 0.849628 |
| 6 | 0.937688 | 0.195976 | 0.001 | 0.831978 | 0.864499 |
| 7 | 0.93885 | 0.188665 | 0.001 | 0.93972 | 0.185791 |
| 8 | 0.944938 | 0.166638 | 0.001 | 0.921461 | 0.267373 |
| 9 | 0.954747 | 0.139192 | 0.001 | 0.946598 | 0.169225 |
| 10 | 0.95025 | 0.148785 | 0.001 | 0.92096 | 0.29281 |
| 11 | 0.951493 | 0.149138 | 0.001 | 0.931528 | 0.23313 |
| 12 | 0.958125 | 0.130086 | 0.001 | 0.957604 | 0.129822 |
| 13 | 0.956125 | 0.131764 | 0.001 | 0.966483 | 0.120217 |
| 14 | 0.963573 | 0.11314 | 0.001 | 0.922961 | 0.291764 |
| 15 | 0.966125 | 0.108081 | 0.001 | 0.975175 | 0.074392 |
| 16 | 0.963009 | 0.112118 | 0.001 | 0.955103 | 0.145883 |
| 17 | 0.96575 | 0.10554 | 0.001 | 0.943034 | 0.19108 |
| 18 | 0.965137 | 0.105917 | 0.001 | 0.928589 | 0.264863 |
| 19 | 0.964938 | 0.110921 | 0.001 | 0.953789 | 0.142576 |
| 20 | 0.97175 | 0.089099 | 0.001 | 0.96986 | 0.093184 |
| 21 | 0.971209 | 0.087371 | 0.001 | 0.96048 | 0.147692 |
| 22 | 0.985438 | 0.04471 | 0.0002 | 0.99556 | 0.016243 |
| 23 | 0.990236 | 0.030135 | 0.0002 | 0.995373 | 0.013251 |
| 24 | 0.991563 | 0.024861 | 0.0002 | 0.996248 | 0.013701 |

SRCNN Result by Epoch

| Epoch | acc | loss | lr | val_acc | val_loss |
|---|---|---|---|---|---|
| 0 | 0.685 | 1.076052 | 0.001 | 0.597313 | 1.825342 |
| 1 | 0.853563 | 0.456332 | 0.001 | 0.608867 | 1.734919 |
| 2 | 0.892846 | 0.326332 | 0.001 | 0.762569 | 0.936293 |
| 3 | 0.914438 | 0.266576 | 0.001 | 0.889007 | 0.34634 |
| 4 | 0.924454 | 0.234888 | 0.001 | 0.918772 | 0.274175 |
| 5 | 0.932875 | 0.209391 | 0.001 | 0.929777 | 0.229069 |
| 6 | 0.937688 | 0.196275 | 0.001 | 0.925775 | 0.234507 |
| 7 | 0.938537 | 0.189037 | 0.001 | 0.925775 | 0.282873 |
| 8 | 0.943688 | 0.173809 | 0.001 | 0.909642 | 0.28659 |
| 9 | 0.951368 | 0.151127 | 0.001 | 0.943534 | 0.188381 |
| 10 | 0.94875 | 0.15574 | 0.001 | 0.906891 | 0.306541 |
| 11 | 0.950491 | 0.154059 | 0.001 | 0.922149 | 0.271082 |
| 12 | 0.958 | 0.129596 | 0.001 | 0.96467 | 0.110303 |
| 13 | 0.95675 | 0.131862 | 0.001 | 0.90514 | 0.346343 |
| 14 | 0.960381 | 0.120436 | 0.001 | 0.939032 | 0.210869 |
| 15 | 0.960438 | 0.126139 | 0.001 | 0.926963 | 0.260596 |
| 16 | 0.966201 | 0.103237 | 0.001 | 0.959042 | 0.139745 |
| 17 | 0.963875 | 0.110578 | 0.001 | 0.922836 | 0.268867 |
| 18 | 0.96545 | 0.108457 | 0.001 | 0.964107 | 0.109852 |
| 19 | 0.983813 | 0.046763 | 0.0002 | 0.993997 | 0.018768 |
| 20 | 0.988375 | 0.036806 | 0.0002 | 0.993684 | 0.017171 |
| 21 | 0.988859 | 0.034741 | 0.0002 | 0.993934 | 0.018891 |
| 22 | 0.989688 | 0.031454 | 0.0002 | 0.994122 | 0.019938 |
| 23 | 0.990299 | 0.029428 | 0.0002 | 0.995998 | 0.012489 |
| 24 | 0.99175 | 0.025347 | 0.0002 | 0.993184 | 0.02261 |

Table 3: Shows the comparison report with other models.

| Model Proposed | Classification Accuracy |
|---|---|
| Bicubic | 99.156 |
| SRCNN | 99.175 |

of experimental results and comparison between two models SRCNN and Bicubic demonstrates the accuracy to recognize the correct disease in plants. Out of these two models, SRCNN gives an accuracy rate of 99.175 % in recognizing plant diseases. Diseases are not the specific problem in the agricultural sector but crops growing in good soil and getting nutritious food protect the plant from various pest attacks. The experimental result represents the effectiveness of our proposed system and it can be widely used in the agricultural sector for the help of farmers.

## REFERENCES

Ashqar, B.A.M. and Abu-Naser. S.S. 2018. Image-based tomato leaves diseases detection using deep learning. Int. J. Academic Eng. Res., 2(12): 10-16.

Badage, A. 2018. Crop disease detection using machine learning: Indian agriculture. Int. Res. J. Eng. Technol., 5(9): 866-869.

Bangotra, P., Sharma, M., Mehra, R., Jakhu, R., Singh, A., Gautam, A.S. and Gautam, S. 2021. A systematic study of uranium retention in human organs and quantification of radiological and chemical doses from uranium ingestion. Environ. Technol. Innov., 21: 101360.

Bangotra, P., Mehra, R., Jakhu, R, Pandit, P. and Prasad, M. 2019. Quantification of an alpha flux-based radiological dose from seasonal exposure to 222Rn, 220Rn, and their different EEC species. Sci. Rep., 9: 2515.

Blessy, A. and Joy Winnie Wise, D.C. 2018. Detection of affected parts of plant leaves and classification of diseases using CNN technique. Int. J. Eng. Tech., 4(2): 823-829.

Gulhane, V.A. and Kolekar, M.H. 2015. Diagnosis of diseases on cotton leaves using principal component analysis classifier. 11th IEEE India Conference: Emerging Trends and Innovation in Technology, INDICON, 11-13 December 2014, Pune India. IEEE, India, pp.1-5.

Huang, W., Guan, Q., Luo, J., Zhang, J., Zhao, J., Liang, D. and Zhang, D. 2014. New optimized spectral indices for identifying and monitoring winter wheat diseases. IEEE J. Select. Topics Appl. Earth Observ. Remote Sens., 7(6): 2516-2524.

Maniyath, S.R., Vinod, P.V., Niveditha, M., Pooja, R., Prasad Bhat, N., Shashank, N. and Hebbar, R. 2018. Plant disease detection using machine learning. Proceedings - 2018. International Conference on Design Innovations for 3Cs Compute Communicate Control, ICDI3C, 25-28 April, 2018, Bangalore, India. IEEE, India, pp. 41-45.

Mehra, R., Bangotra, P. and Kaur, K. 2015. $^{222}$Rn and $^{220}$Rn levels of Mansa and Muktsar district of Punjab, India. Front. Environ. Sci., 3:37.

Pradhan, R.P. 2007. Indian agriculture in the globalization era: The performance and determinants. J. Global Econ., 3(1): 3-12.

Owomugisha, G., Quinn, J.A., Mwebaze, E. and Lwasa, J. 2014. Automated vision-based diagnosis of banana bacterial wilt disease and black Sigatoka disease. International Conference on the Use of Mobile ICT in Africa, 9-10th December 2014, Stellenbosch, South Africa. Stellenbosch University, Department of Electrical & Electronic Engineering, South Africa, pp. 1-5.

Qin, Z., Zhang, M., Christensen, T., Li, W. and Tang, H. 2003. Remote sensing analysis of rice disease stresses for farm pest management using wide-band airborne data. Int. Geosci. Remote Sens. Symp. 4(C): 2215-2217.

Pandit, P., Mangala, P., Saini, A, Bangotra, P., Kumar, V., Mehra, R. and Ghosh, D. 2020. Radiological and pollution risk assessments of terrestrial radionuclides and heavy metals in a mineralized zone of the Siwalik region (India), Chemosphere, 254: 126857.

Rastogi, A., Arora, R. and Sharma, S. 2015. Leaf disease detection and grading using computer vision technology & fuzzy logic. 2nd International Conference on Signal Processing and Integrated Networks, 19-20 Feb, 2016, Noida, India. IEEE, India, pp. 500-505.

Revathi, P. and Hemalatha, M. 2012. Advance computing enrichment evaluation of cotton leaf spot disease detection using Image Edge detection. 2012 3rd International Conference on Computing, Communication and Networking Technologies, ICCCNT 2012, (July).

Revathi, P., Revathi, R. and Hemalatha, M. 2011. Comparative study of knowledge in crop diseases using machine learning techniques. Int. J. Comput. Sci. Inf. Technol., 2(5): 2180-2182.

Reza, Z.N., Nuzhat, F., Mahsa, N.A. and Ali, M.H. 2017. Detecting jute plant disease using image processing and machine learning. 2016 3rd International Conference on Electrical Engineering and Information and Communication Technology, (ICEEiCT), 22-24 September, Dhaka, Bangladesh. IEEE, India, pp. 11-26.

Rothe, P.R. and Kshirsagar, R.V. 2015. Cotton leaf disease identification using pattern recognition techniques. 2015 International Conference on Pervasive Computing: Advance Communication Technology and Application for Society, ICPC, 8-10 Jan, 2015, Pune, India. IEEE, India, pp. 1-6.

Saleem, M.H., Potgieter, J. and Arif, K.M. 2019. Plant disease detection and classification by deep learning. Plants, 8(11): 32–34.

Sarangdhar, A.A. and Pawar, V. 2017. Machine learning regression technique for cotton leaf disease detection and controlling using IoT. Proceedings of the International Conference on Electronics, Communication and Aerospace Technology, 20-22 April 2017, Coimbatore, India. Institute of Electrical and Electronics Engineers (IEEE), India, pp. 449-454.

Sethy, P.K., Negi, B., Barpanda, N.K., Behera, S.K. and Rath, A.K. 2018. Measurement of disease severity of rice crop using machine learning and computational intelligence. Proc. Comp Sci., 167(1): 516-530.

Shi, Y., Wang, X.F., Zhang, S.W. and Zhang, C.L. 2015. PNN based crop disease recognition with leaf image features and meteorological data. Int. J. Agric. Biol. Eng., 8(4): 60-68.

Shruthi, U., Nagaveni, V. and Raghavendra, B. K. 2019. A review on machine learning classification techniques for plant disease detection. 2019 5th International Conference on Advanced Computing and Communication Systems, ICACCS 2019,15-16 March 2019, Coimbatore, India, Institute of Electrical and Electronics Engineers, India, pp. 281–284.

Sladojevic, S., Arsenovic, M., Anderla, A., Culibrk, D. and Stefanovic, D. 2016. Deep neural networks-based recognition of plant diseases by leaf image classification. Comput. Intell. Neurosci., 2016: 54-79.

Tian, Y., Zhao, C., Lu, S. and Guo, X. 2012. SVM-based multiple classifier systems for recognition of wheat leaf diseases. World Autom. Congr. Proc., 5(1): 2-6.

Nature Environment and Pollution Technology
An International Quarterly Scientific Journal

p-ISSN: 0972-6268
(Print copies up to 2016)
e-ISSN: 2395-3454

Vol. 20 | No. 5 (Suppl) | pp. 2149-2156 | 2021

Original Research Paper

https://doi.org/10.46488/NEPT.2021.v20i05.032

Open Access Journal

# Statistical Modelling of a Comparative Phytotoxicity Study of Treated Yellow 10Gw Dye Solution With Copper and Aluminum in Electrocoagulation Process

**Kalivel Parameswari*, M. Vijila**† and P. Jegathambal*****
*Department of Chemistry, Karunya Institute of Technology and Sciences, Coimbatore-641114, Tamil Nadu, India
**Department of Mathematics, Karunya Institute of Technology and Sciences, Coimbatore-641114, Tamil Nadu, India
***Department of Water Institute, Karunya Institute of Technology and Sciences, Coimbatore-641114, Tamil Nadu, India
†Corresponding author: M. Vijila; vijilamoses@karunya.edu

**Nat. Env. & Poll. Tech.**
**Website: www.neptjournal.com**

*Received:* 15-06-2021
*Revised:* 25-07-2021
*Accepted:* 29-07-2021

**Key Words:**
Electrocoagulation
Yellow 10GW dye
Analysis of variance
Linear trend

## ABSTRACT

This work was carried to compare the efficiency of Cu and Al electrodes in the elimination of Yellow 10 gw dye solution with the optimization of operative factors such as pH, NaCl, contact time, and current density in the electrocoagulation method. Analysis of variance (ANOVA) was used to assess the impact of these variables, with significance set at $P<0.05$. The data was statistically examined with Origin2021 and SPSS software, and significant differences between mean values were determined using analysis of variance (ANOVA). For each experiment, duplicates were kept, and the efficiency of Yellow 10 gw dye solution for those parameters was derived using analysis at a 5% level of significance. The utility of treated dye solutions using both the electrodes was tested on *V.radiata* in terms of germination percentage, root, and shoot length with distilled water as control. For all of the qualities examined, significant disparities were found among entries. The dye solution used with Al resulted in much higher germination (100%), root length (9.72 cm), and shoot length (24.5 cm).

## INTRODUCTION

Textile industry processes use a lot of water, particularly for wet processes like dying, and as a result, the wastewater generated contains synthetic dyestuffs. It has also been documented that nearly 10% of the dye is lost during the dyeing process due to a lack of fabric adherence (Garg & Kaushik 2018). These synthetic dyes in water pollute and affect all water sources, including groundwater and surface water. They can have a negative impact on marine life, agricultural practices, and human health. Furthermore, the majority of the synthetic dyes used in these units have not been tested for their environmental and health effects. Chemical oxygen demand (COD), color, and salt levels in effluent from various units in a textile hub are all high, and the volume of water produced and discharged as waste by these sectors is rapidly expanding, and it contains a variety of contaminants (Rasalingam et al. 2014).

To treat the wastewater produced by the textile industries, methods like chemical, physical, biological, electrochemical are employed. Among which chemical treatments include coagulation, ozonation, advanced photochemical oxidation, (Glaze & Chapin 1987, Marcucci et al. 2002, Molkenthin et al. 2013), filtration techniques such as reverse osmosis, nanofiltration (Merayo et al. 2013), ultrafiltration, and microfiltration using suitable membranes (Chakraborty et al. 2003, Wang et al. 2016). Each of these approaches has its own advantages, but they are all costly and time-consuming. Physical treatment, on the other hand, necessitates the use of extra chemicals and produces a significant volume of sludge.

Disperse dyes are one of the many forms of synthetic dyes available, and are non-ionic, sparingly soluble in water, and applied to hydrophobic fibers from an aqueous phase (Clark 2011). They are mostly used on polyester, but they have also been used on nylon, cellulose acetate, and acrylic fibers, however, some of the dyes' wet-fastness capabilities on these substrates are not great (Saquib & Muneer 2003, Hassan et al. 2009). Diverse chromophores for instance azo, anthraquinone, and triphenylmethane, contribute to the structural diversity of synthetic disperse dyes. Azo dyes are the most common disperse type, accounting for more than half of all disperse dyes (Qiu et al. 2020). Due to their resistive character and non-biodegradable activity, these dyes are classified as persistent (Jamil et al. 2020, Shamey 2009). Anthraquinone dyes are the second most often used dyes after azo dyes because of their inexpensive cost, quick accessibility, and high dyeing effectiveness. Anthraquinone dyes are more harmful to microorganisms and human cells because they have a more complicated and stable structure than azo dyes (Novotnyet al. 2006). In contrast to azo dyes,

the carbonyl group in the anthraquinone structure acts as an electron acceptor, requiring an electron donor to react and serve the structure; however, research reveals that anthraquinone dyes are difficult to degrade when compared to azo dyes (Mishra & Maiti 2018). The combined effects of resonance in the anthracene structure make it more difficult to decolorize AQ colors than azo dyes (Lizama et al. 2001, Sekuljica et al. 2016), raising questions about the possibility of a successful decolorization operation (Khataee et al. 2016).

Photocatalytic oxidation (Samanta et al. 2018), Fenton oxidation (Lovato et al. 2017), ultrasonic catalytic oxidation (Santos et al. 2005) are some of the treatment methods for anthraquinone dye degradation. AOP is notable for its extremely fewer reaction times, typically a few minutes, high efficacy, and dye sedimentation on decolorization of AQ dyes, but it is also notable for its high cost, which makes scaling up difficult (Castro et al. 2014, Khataee & Kasiri 2010).

Recent research has looked at biological strategies for AQ dye degradation in aerobic and anaerobic cultures (Cesaro & Belgiorno 2013, Padmanaban et al. 2013). The challenge is to develop reliable, cost-effective, and environmentally sustainable bioremediation methods that overcome the limitations of traditional methods (Husain & Ulber 2011, Li et al. 2019). There are also no data on the toxic, mutagenic, or carcinogenic intermediate products produced during the degradation of certain AQ colors, making it difficult to choose the correct type of treatment procedure.

Amongst the electrochemical methods, electrocoagulation does not involve any additional chemicals and is a relatively simple procedure that creates a small amount of sludge (Zhou et al. 2019) and it has become the focus of wastewater treatment research in recent years since it is easy to operate and produces less sludge. In this sense, electrocoagulation appears to be a viable alternative to physical and chemical methods since the procedure is simple to implement. EC appears to be a promising option for removing dissolved solids and colloidal particles from textile dyeing wastewater in the tertiary treatment stage. The efficacy in the dye abatement depends on the anodization, hydroxides production, size, and the colloidal properties of the particles. Reactive Blue 19 (Khoshhesab & Ahmadi 2016) and basic Yellow 28 dye effluent were successfully eliminated using the EC technique (Gaber et al. 2013, Sangeetha et al. 2009), Red disperse, Blue reactive, and mixed dyes (Phalakornkule et al. 2010, Polgumhang et al. 201). Abatement of Yellow 10gw dye (a type of anthraquinone disperse dye) aqueous solution was studied in this work focusing on optim1ze the operative parameters such as pH, electrolyte, current density, and contact time for maximum abatement of the dye using two different electrodes, one with Al electrodes and the other with Cu electrodes and the findings were compared to the efficacy of the electrodes used.

An analytical technique like X-ray Photoelectron Spectroscopy (XPS) analysis was employed to investigate the efficiency of the EC process in the sludge separated. To examine the possibility of reusing the treated dye solution, phytotoxicity tests with *V.radiata* seeds were performed, and the results were compared to the control (distilled water) in terms of percent-age of germination, length of root, and shoot. We previously analyzed the performance of $Zn/TiO_2$ electrodes prepared by spray pyrolysis in treating Coralene Red 3G dye for color removal in electrocoagulation technique with optimization of operating parameters. The efficiency of color removal for parameters such as pH, dye concentration, electrolyte, applied current, and time was estimated using design experts software and an ANOVA design model (Nayak & Pal 2020, Praveen et al. 2011).

In another study, we had discussed and compared the efficiency of Al-Al and Cu-Cu electrodes in the elimination of Blue SI dye aqueous solution in the electrocoagulation process with the optimization of operational parameters such as pH, the concentration of electrolyte, current density, and electrolysis time using design experts' software and the experimental data were analyzed by variance analysis (ANOVA) (Kalivel et al. 2019).

## MATERIALS AND METHODS

Two sets of experiments were conducted with Cu and Al electrodes for optimization of operative factors such as contact time, pH, current density, and electrolyte concentration for the abatement of Yellow 10 gw dye solution.

For each process, 250 mL of the Yellow 10 gw dye (150 mg,) solution as test solution was taken in a 500 mL beaker with DC connection and stirrer. In the first set, we used Al as anode and cathode, in the next set of experiments Cu was used as anode and cathode, and the results were compared for each operational parameter used. The experiments were conducted at 25°C. The consequence of initial pH (5, 6, 7, 8, 9), contact time (5, 10, 15, 20, 25 mins), current density (20, 40, 60, 80, and 100 $Am^{-2}$) and electrolyte concentration (NaCl: 1 to 5 $gm.L^{-1}$) were studied on the dye abatement. The dye absorbance was determined before and after the process with the Jasco V-670 spectrophotometer, and the dye concentration was assessed with the absorbance at 542 nm.

Dye abatement efficiency (DAE %) was calculated using the following

$$DAE\% = 100 * (A_a - A_b)/A_a \quad \ldots(1)$$

Where $A_a$ and $A_b$ were the absorbance of dye solution before electrocoagulation and at time t, respectively.

**Phytotoxicity Investigation**

Dye components can influence the entire photosynthesis process and eventually inhibit plant growth, even at very low concentrations in water, and dye degradation releases a range of intermediate products that must be non-toxic to the environment. To determine the likelihood of the treated water being reused, a phytotoxicity study was conducted on the growth of V.radiata seeds using a 150mg.$L^{-1}$ Yellow 10gw dye solution, a treated dye solution with Al and Cu, and tap water as a control. Twenty sterilized seeds were placed in a 250 mL beaker with 150 g autoclaved soil and exposed to sunlight after being soaked in 0.1 percent (w/v) mercuric chloride and then splashed three times with distilled water to remove any traces of mercury.

With an equal volume of treated, untreated Yellow 10gw aqueous solution and tap water, the seed germination and plant growth were studied. Germination percentage, root, and shoot length were calculated after 10 days, and the results were compared to the control

$$\% \text{ of Germination} = \frac{\text{number of seeds germinated}}{\text{Total number of seeds sown}} * 100 \quad \ldots(2)$$

## RESULTS AND DISCUSSION

The effects of various parameters on the percentage of color removal of the Yellow 10gw dye aqueous solution were determined using analysis of variance (ANOVA). The p-value associated with the F statistics is used to assess if they are high enough to establish statistical significance (Kalivel et al. 2020). The regression model equation fitted by the curve is a second-order polynomial equation for the percentage color removal of Yellow 10gw dye aqueous solution as a function of pH(X1), NaCl (X2), current density (X3), and contact time (X4) (Kunasekarn et al. 2017).

A phytotoxic investigation of treated Yellow 10gw dye solution with Al and Cu was carried out at room temperature for 10 days in a seed germinator, with statistical modeling used to determine the significance level of dye removal efficiency. Yellow 10gw dye solution removal efficiency was taken as the second-order polynomial equation.

$$Yi = b_0 + \sum b_i x_i + \sum b_{ii} x_{ij}^2 + \sum \sum b_{ij} x_i x_j \quad \ldots(3)$$

Where $Y_i$ is the amount of efficiency of removing the dye

$b_0$ = Constant coefficient

$b_i$ = Regression coefficients for linear effects

$b_{ii}$ = Quadratic coefficients

$b_{ij}$ = Interaction coefficients and $x_i$, $x_j$ are the parameters.

| | | | |
|---|---|---|---|
| Std. Dev. | 0.0004 | $R^2$ | 0.312 |
| Mean | 0.0101 | Adjusted $R^2$ | 0.429 |
| C.V. % | 4.18 | Predicted $R^2$ | -0.3459 |
| | | Adeq Precision | 4.5474 |

When comparing pH to time, the $r^2$ value was 0.312, which was significant at $P < 0.05$. In the current study, this method was used to measure the effectiveness of adsorption of the Yellow 10Gw dye solution under a variety of conditions, including pH, NaCl, current density, and contact time.

From Table 1, we found no statistically significant ($p > 0.05$) differences in pH for Cu electrodes. Therefore, we could not conclude that the model explains variation in the operational behaviors such as pH, NaCl, contact time, and current density.

Fig. 1 reveals that some of the variances in the response are attributable to time, and the graphs are not randomly spread, implying that for Cu electrodes, a non-linear regression method is recommended.

Table 2 shows that there was a statistically significant (p 0.05) difference in pH for Al electrodes depending on the

Table 1: pH with Time in Cu electrodes.

| Source | Sum of Squares | Df | Mean Square | F-value | p-value | |
|---|---|---|---|---|---|---|
| B-Time | 1.016E-07 | 1 | 1.016E-07 | 0.5654 | 0.4613 | |
| $A^2$ | 1.428E-07 | 1 | 1.428E-07 | 0.7951 | 0.3837 | |
| AB | 4.185E-07 | 1 | 4.185E-07 | 2.33 | 0.1434 | |
| A-pH | 4.870E-07 | 1 | 4.870E-07 | 2.71 | 0.1161 | |
| $B^2$ | 7.492E-07 | 1 | 7.492E-07 | 4.17 | 0.0553 | |
| Model | 1.615E-06 | 5 | 3.230E-07 | 1.80 | 0.1615 | not significant |
| Residual | 3.413E-06 | 19 | 1.796E-07 | | | |
| Total | 5.028E-06 | 24 | | | | |

time period. Therefore, there is enough evidence to say that the model explains variation in the operational behaviors such as pH, NaCl, contact time, and current density.

Fig. 2 suggests that some of the variations in the response are due to contact time. As the pattern is quite random, this indicates that a linear regression model is appropriate for Al electrodes.

The F-value of 2.90 indicates that it is statistically significant at the 5% level.

**Phytotoxicity study on *V. radiata***

When comparing Yellow 10gw dye solution with treated dye solution utilizing Al, Cu in this study, the value of r2 was 0.378 (significant at P > 0.05). We discovered that plant's root and shoot length grown in Yellow 10gw dye solution treated with Al electrodes resulted in increased length of both.

According to Fig. 3 and 4, Al electrodes were the best when compared to other electrodes.

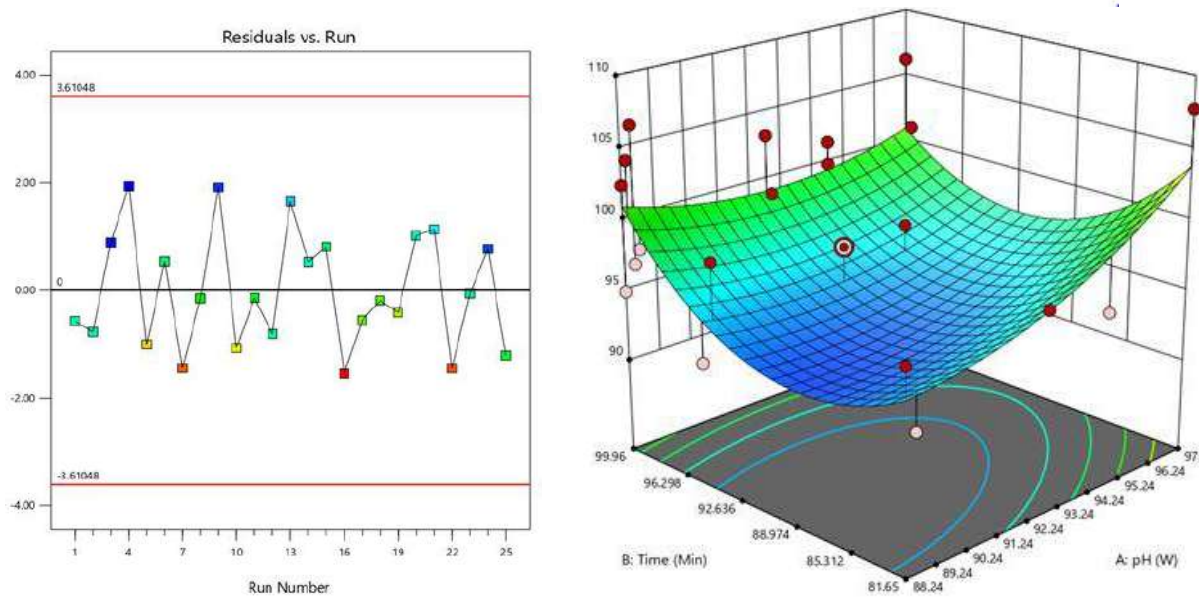


Fig. 1: Residual and surface diagram for pH Vs contact time.

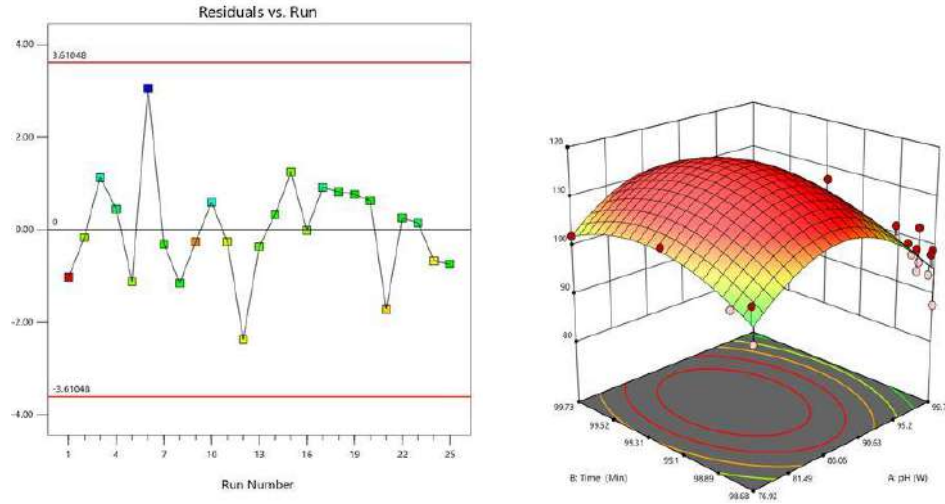


Fig. 2: Residual and surface diagram for pH Vs contact time

Table 2: pH with contact time in Al electrodes.

| Source | Sum of Squares | Df | Mean Square | F-value | p-value | |
|---|---|---|---|---|---|---|
| Model | 2.161E-06 | 5 | 4.322E-07 | 2.90 | 0.0411 | significant |
| A-pH | 4.532E-07 | 1 | 4.532E-07 | 3.04 | 0.0971 | |
| B-Time | 1.974E-07 | 1 | 1.974E-07 | 1.33 | 0.2637 | |
| AB | 1.889E-08 | 1 | 1.889E-08 | 0.1269 | 0.7256 | |
| $A^2$ | 6.453E-07 | 1 | 6.453E-07 | 4.34 | 0.0511 | |
| $B^2$ | 1.064E-06 | 1 | 1.064E-06 | 7.15 | 0.0150 | |
| Residual | 2.828E-06 | 19 | 1.488E-07 | | | |
| Total | 4.989E-06 | 24 | | | | |

## XPS Analysis of Sludge

Al and Cu XPS survey spectra as well as high-resolution core line spectra [(Al, Al2p) and (Cu, $Cu2p^3$)] (a-d) are given in Fig. 5. It has been claimed that the capacity of Al to generate dimeric, trimeric, and polynuclear hydrolysis products can be formed during the anodization process (Saha et al. 2015, Jeurgens et al. 2002, Liu et al. 2016).

However, the development of different forms of M(OH) n is dependent on various factors, including the composition of the anode metal during anodization, hydroxides from the cathode, and so on. This study contributes to a better understanding of the electrochemistry of metal hydroxide

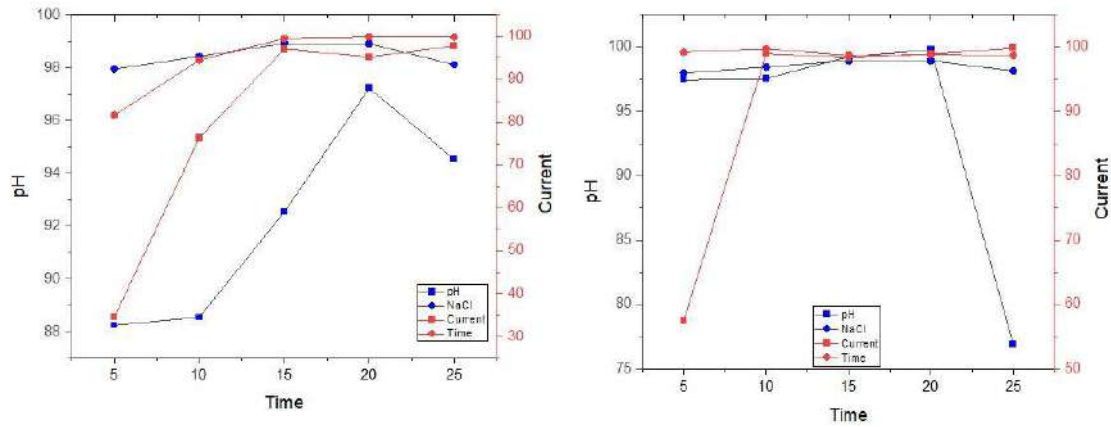


Fig. 3: Linear trend for phytotoxicity of dye solution and the treated dye solution using Al, Cu

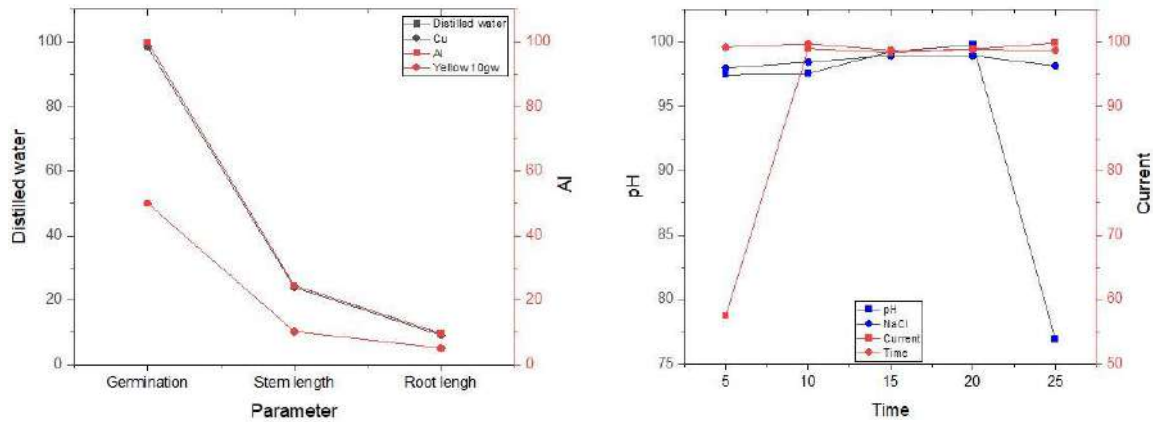


Fig. 4: Linear trend for phytotoxicity of dye solution and the treated dye solution using Al and Cu.

Table 3: Overall statistics and analysis of variance.

Descriptive statistics for phytotoxicity of Yellow 10gw dye solution treated dye solution using Al

| | Sample Size | Mean | Standard Deviation | SE of Mean |
|---|---|---|---|---|
| Germination | 10 | 86.028 | 30.90759 | 9.77384 |
| Stem | 10 | 39.609 | 31.82887 | 10.06517 |

ANOVA for phytotoxicity of Yellow 10gw dye solution Vs treated dye solution using Al

| Source | df | Sum of Squares | Mean Square | F Value | Prob > F |
|---|---|---|---|---|---|
| Model1 | 10 | 773.6178 | 10773.6178 | 10.94682 | 0.00391 |
| Error | 18 | 17715.20085 | 984.17783 | | |
| Total | 19 | 28488.81866 | | | |

Fit statistics

| R-Square | Coeff Var | Root MSE | Data Mean |
|---|---|---|---|
| 0.37817 | 0.4994 | 31.37161 | 62.8185 |

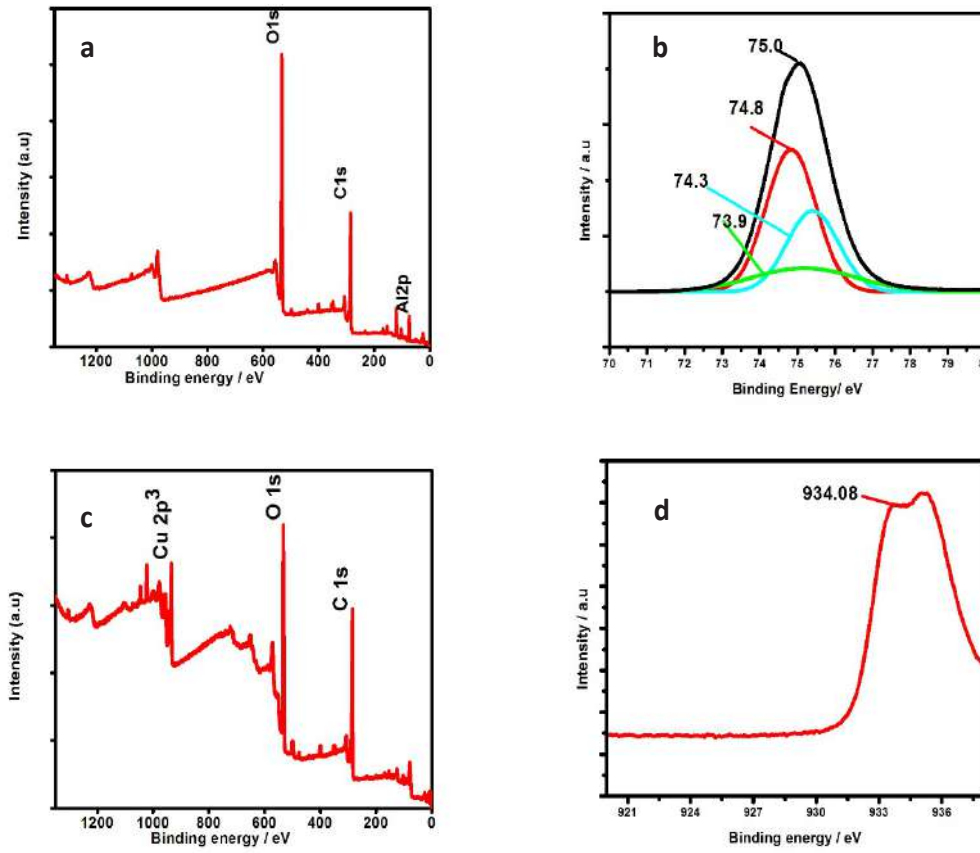


Fig. 5: Al and Cu XPS survey spectra and high-resolution core line spectra [(Al, Al2p) and (Cu, Cu2p3)].

formations, as well as a better understanding of the different types of metal hydroxides that are produced, which aids in the coagulation of dye molecules and the evaluation of the electrodes' efficacy in the removal of dye pollutants. From the high-resolution core spectra of Al2p, the binding energy value of Al as gibbsite 74.4 eV [γ- $Al(OH)_3$], bayerite [$Al(OH)_3$] 75.0 eV [$Al(OH)_3$], boehmite [AlO(OH)] 73.9 eV and pseudoboehmite [AlO(OH)] 74.3 eV were found and it was noteworthy to conclude that there are four types of hydroxides of Al formed, such as [$Al(OH)_3$] gibbsite, [$Al(OH)_3$] bayerite, [AlO(OH)] boehmite and [AlO(OH)] pseudoboehmite.

XPS analysis of copper electrodes revealed a binding energy value of 934.06 eV for copper in its +2 oxidation state, showing that the metal hydroxide as flocs formed in the EC operation with copper was Cu(OH)2, which was supported by published work (Kloprogge et al. 2006). The efficacy of Al metal over Cu was substantiated by XPS studies of the respective sludge in the process.

## CONCLUSION

The percentage of Yellow 10gw dye removed from aqueous solution using Cu and Al electrodes in the EC method exhibits a linear relationship with pH, electrolyte concentration, contact time, and current density, and with a substantial interaction between the amount of adsorbent and dye concentration. The use of Al exhibited better results in the germination, root, and shoot length of *V.radiata* than the dye solution used with Cu electrodes in comparison to the control in the phytotoxicity research of *V.radiata* with treated dye solutions. The improved performance of Al was demonstrated by XPS analysis of the corresponding sludge, which revealed four different types of hydroxides as adsorbents in the Al process versus just one hydroxide from the process used with copper electrodes.

## REFERENCES


Castro, E., Avellaneda, A. and Marco, P. 2014. Combination of advanced oxidation processes and biological treatment for the removal of benzidine-derived dyes. Environ. Prog. Sustain. Energy, 33(3): 873-885.

Cesaro, A.N.V. and Belgiorno. V. 2013. Wastewater treatment by a combination of advanced oxidation processes and conventional biological systems. J. Biorem. Biodegrad., 15: 208.

Chakraborty, S.M.K., Purkait, S., Das Gupta, De, S. and Basu, J.K. 2003. Nanofiltration of textile plant effluent for color removal and reduction in COD. Sep. Purif. Technol., 31: 141-151.

Clark, M. 2011. Fundamental principles of dyeing, Handb. Text. Ind. Dye. Princ. Process.Types Dyes, 1:2-11

Gaber, M., Ghalwa, N.A., Khedr, A.M. and Salem, M. F. 2013. Electrochemical degradation of reactive yellow 160 dye in real wastewater using C/$PbO_2^-$, Pb+Sn/$PbO_2$+$SnO_2^-$, and Pb/$PbO_2$ modified electrodes. Chemosphere, 5(1):1-7.

Garg, V.K. and Kaushik, P. 2018. Influence of textile mill wastewater irrigation on the growth of sorghum cultivars, Appl. Ecol. Environ. Res., 6: 1-12.

Glaze, W., and Chapin, D. 1987, The chemistry of water treatment processes involving ozone, hydrogen peroxide, and ultraviolet radiation. Ozone: Sci. Eng., 9: 335-342.

Hassan, S.S., Awwad, N.S. and Aboterika, A.H. 2009. Removal of synthetic reactive dyes from textile wastewater by Sorel's cement. J. Hazard. Mater. 162(2): 994-999.

Husain, Q., and Ulber, R. 2011. Immobilized peroxidase as a valuable tool in the remediation of aromatic pollutants and xenobiotic compounds: A review. Crit. Rev. Environ. Sci.Technol., 41(8): 770-804.

Jamil, A., Bokhari, T.H., Javed, T., Mustafa, R., Sajid, M., Noreen, S., Zuber, M., Nazir, A., Iqbal, M. and Jilani, M.I. 2020. Photocatalytic degradation of disperse dye Violet-26 using $TiO_2$ and ZnO nanomaterials and process variable optimization. J. Mater. Res. Technol., 9(1): 1119-1128.

Jeurgens, L.P.H., Sloof, W.G., Tichelaar, F.D. and Mittemeijer, E.J. 2002. Composition and chemical state of the ions of aluminium-oxide films formed by thermal oxidation of aluminium. Surf. Sci., 506: 313-332.

Kalivel, P., Palanichamy, J. and Vijila, M. 2019. Efficient removal of coralline red 3G dye in EC process with Zn/$TiO_2$ using a statistical algorithm. Int. J. Recent Technol. Eng., 61: 2277-3878.

Kalivel, P., Vijila, M. and Palanichamy, J. 2020. Optimization of color re- moval of blue si dye with al, Cu electrodes in electrocoagulation process using statistical modeling, optimization of color removal of blue SI dye with Al, Cu electrodes in electrocoagulation process using statistical modeling. EM Int., 39(3): 778-783.

Khataee, A., Gholami, P., Vahid, B. and Joo, S.W. 2016. Heterogeneous sono-Fenton process using pyrite nanorods prepared by-thermal plasma for degradation of an anthraquinone dye. Ultrason. Sonochem., 32: 357-370.

Khataee, A.R. and Kasiri, M.B. 2010. Photocatalytic degradation of organic dyes in the presence of nanostructured titanium dioxide: Influence of the chemical structure of dyes. J. Mol. Catal. A: Chem., 328(1-2): 8-26.

Khoshhesab, Z.M. and Ahmadi, M. 2016. Removal of reactive blue 19 from aqueous solutions using NiO nanoparticles: equilibrium and kinetic studies. Desalin. Water Treat., 57(42): 20037-20048.

Kloprogge, J.T., Loc, Duong, V., Barry, Wood, J. and Frost, R. L. 2006. XPS study of the major minerals in bauxite: Gibbsite, bayerite, and (pseudo) boehmite. J. Coll. Inter. Sci., 296(2): 572-576.

Kunasekarn, R., Kulandaivelu, G. and Arumugam, Y. 2017. Correlation analysis for shoot/root parameters under polyethylene glycol (PEG) induced water stress in sorghum (Sorghum bicolor (L.) Moench) genotypes. Int. J. Chemical Stud., 5(6): 389-399.

Li, H.H., Wang, Y.T., Wang, Y., Wang, H.X., Sun, K.K. and Lu, Z.M. 2019. Bacterial degradation of anthraquinone dyes. J. Zhejiang Univ. Sci., 20(6): 528-540.

Liu, Q., Qin, H., Boscoboinik, J.A. and Zhou, G. 2016. Comparative study of the oxidation of NiAl (100) by molecular oxygen and water vapor using ambient-pressure x-ray photoelectron pectroscopy. Langm, 32: 11414-11421.

Lizama, C., Freer, J., Baeza, J. and Mansilla, H.D. 2001. Optimized photodegradation of reactive blue 19 on $TiO_2$ and ZnO suspensions. Catal. Today, 76(2-4): 235-246.

Lovato, M.E., Fiasconaro, M.L. and Martin, C.A. 2017. Degradation and toxicity depletion of RB19 anthraquinone dye in water by ozone-based technologies. Water Sci. Technol. 75(4) 813-822.

Marcucci, M., Ciardelli, G., Matteucci, A., Ranieri, L. and Russo M. 2002. Experimental campaigns on textile wastewater for reuse by means of different membrane processes. Elsevier Sci., 149: 137-143.

Merayo, N., Hermosilla, D., Blanco, L., Cortijo, L. and Blanco, A. 2013. Assessing the application of advanced oxidation processes, and their combination with biological treatment to effluents from the pulp and paper industry. J. Hazard. Mater., 26: 420-427.

Mishra, S. and Maiti, A. 2018. The efficacy of bacterial species to decolorize reactive azo, anthraquinone, and triphenylmethane dyes from wastewater: A review. Environ. Sci. Pollut. Res., 25(9): 8286-8314.

Molkenthin, M., Olmez-Hanci, T., Jekel, M.R. and Alaton, I.A. 2013. Photo-Fenton-like treatment of BPA: Effect of UV light source and water matrix on toxicity and transformation products. Water Res., 47: 5052-5064.

Nayak, A.K. and Pal, A. 2020. Statistical modeling and performance evaluation of biosorption removal of Nile blue A by lignocellulosic agricultural waste under the application of high-strength dye concentrations. J. Environ. Chem. Eng., 8(2): 116-136.

Novotny, C., Dias, N., Kapanen, A., Malachova, K., Vandrovcova, M., Itavaara, M. and Lima, N. 2006. Comparative use of bacterial, algal, and protozoan tests to study the toxicity of azo- and anthraquinone dyes. Chemosphere, 63(9): 1436-1442.

Padmanaban, V.C., Prakash, S.S., Sherildas, P., Jacob, J.P. and Nelliparambil, K. 2013. Biodegradation of anthraquinone-based compounds: Review. Int. J. Adv. Res. Eng. Technol., 4: 15-39.

Polgumhang, C., Tongdaung, W., Karakat, B. and Nuyut, T. 2010. Electrocoagulation of blue reactive, red disperses and mixed dyes, and application in treating textile effluent, J. Environ. Manage., 91(4): 918-926.

Praveen, K.C., Radha, K.V. and Balasubramanian, N. 2011. Electrochemical treatment of plating effluent: Kinetics and statistical modeling. Arch. Environ. Sci., 5: 17-23

Qiu, J., Tang, B., Ju, B., Zhang, S. and Jin, X. 2020. Clean synthesis of disperses azo dyes based on peculiar stable 2,6- dibromo-4-nitrophenyl diazonium sulfate. Dyes Pigments, 17: 107920.

Rasalingam, S., Peng, R. and Koodali, R. T. 2014. Removal of hazardous pollutants from wastewaters: Applications of $TiO_2$-$SiO_2$ mixed oxide materials. J. Nanomater., 11(3): 42.

Saha, G., Shihabudheen, Maliyekkal, M., Sabumon, P.C. and Pradeep, T. 2015. A low-cost approach to synthesize sand-like AlOOH nanoarchitecture (SANA) and its application in defluoridation of water. J. Environ. Chem. Eng., 3: 1303-1311.

Samanta, M., Mukherjee, M., Ghorai, U.K., Sarkar, S., Bose, C. and Chattopadhyay, K.K. 2018. Ultrasound-assisted catalytic degradation of textile dye under the presence of reduced graphene oxide enveloped copper-phthalocyanine nanotube. Appl. Surf. Sci., 449: 113-121.

Sangeetha, R., Lee, C.W., Chellammal, S., Palanichamy, C.S. and Basha, A. 2009. Evaluation of electrochemical oxidation techniques for degradation of dye effluents: A comparative approach. J. Hazard. Mater., 171(15): 748-754.

Santos, A.B.D., Bisschops, I.A.E., Cervantes, F.J. and van Lier, J.B., 2005. The transformation and toxicity of anthraquinone dyes during thermophilic (55 degrees C) and mesophilic (30 degrees C) anaerobic treatments. J. Biotechnol., 115(4): 345-353.

Saquib, M. and Muneer, M. 2003, TiO 2-mediated photocatalytic degradation of a triphenyl-methane dye (gentian violet), in aqueous suspensions. Dyes Pigments, 56(1): 37-49.

Sekuljica, N.Z., Prlainovic, N.Z., Jovanovic, J.R., Stefanovic, A. B., Djokic, V. R., Mijin, D.Z. and Jugovic, Z.D.K. 2016. Immobilization of horseradish peroxidase onto kaolin. Bioprocess Biosyst. Eng., 39(3): 461-472.

Shamey, R. 2009. 12 - Improving the coloration/dyeability of polyolefin fibers. In Ugbolue, S.C.O (Ed.), Polyolefin Fibres. Woodhead Publishing, Sawston, UK, pp. 363-397.

Wang, Z., Xue, M., Huang, K. and Liu, Z. 2016. Textile dyeing wastewater treatment. Adv. Treat. Text. Effluent, 2(3): 11-21

Zhou, X., Zhou, Y., Liu, J., Song, S., Sun, J., Zhu, G., Gong, H., Wang, L., Wu, C. and Li, M. 2019. Study on the pollution characteristics and emission factors of PCDD/Fs from dispersing dye production in China. Chemosphere, 228: 328-334.

*... Continued from inner front cover*

- The text of the manuscript should run into **Abstract, Introduction, Materials & Methods, Results, Discussion, Acknowledgement** (if any) and **References** or other suitable headings in case of reviews and theoretically oriented papers. However, short communication can be submitted in running with **Abstract and References.** The references should be in full with the title of the paper.
- The figures should preferably be made on a computer with high resolution and should be capable of withstanding a reasonable reduction with the legends provided separately outside the figures. Photographs may be black and white or colour.
- Tables should be typed separately bearing a short title, preferably in vertical form. They should be of a size, which could easily be accommodated in the page of the Journal.
- References in the text should be cited by the authors' surname and year. In case of more than one reference of the same author in the same year, add suffix a,b,c,.... to the year. For example: (Thomas 1969, Mass 1973a, 1973b, Madony et al. 1990, Abasi & Soni 1991).

## List of References

The references cited in the text should be arranged alphabetically by authors' surname in the following manner: (Note: The titles of the papers should be in running 'sentence case', while the titles of the books, reports, theses, journals, etc. should be in 'title case' with all words starting with CAPITAL letter.)

Dutta, A. and Chaudhury, M. 1991. Removal of arsenic from groundwater by lime softening with powdered coal additive. J. Water Supply Res. Techno. Aqua., 40(1) : 25-29.

Hammer, D.A. (ed.) 1989. Constructed Wetlands for Wastewater Treatment-Municipal, Industrial and Agricultural. Lewis Publishers Inc., pp. 831.

Haynes, R. J. 1986. Surface mining and wetland reclamation. In: Harper, J. and Plass, B. (eds.) New Horizons for Mined Land Reclamation. Proceedings of a National Meeting of the American Society for Surface Reclamation, Princeton, W.V.

## Submission of Papers

- The paper can be submitted by e-mail as an attachment in a single WORD file at **contact@neptjournal.com**
- The paper can also be submitted online in a single WORD file through the **online submission portal** of journal's website: **www.neptjournal.com**

## Attention

1. Any change in the authors' affiliation may please be notified at the earliest.
2. Please make all the correspondence by e-mail, and authors should always quote the manuscript number.

**Note:** In order to speed up the publication, authors are requested to send the publication charges as soon as they get the 'initial acceptance' letter, and also correct the galley proof immediately after receipt. The galley proof must be checked with utmost care, as publishers owe no responsibility for mistakes. The papers will be put on priority for publication only after receiving the processing and publication charges.

# Nature Environment and Pollution Technology

## (Abbreviation: Nat. Env. Poll. Tech.)

**(An International Quarterly Scientific Journal)**

Published by

**Technoscience Publications**

A-504, Bliss Avenue, Opp. SKP Campus
Balewadi, Pune-411 045, Maharashtra, India

In association with

**Technoscience Knowledge Communications**

Mira Road, Mumbai, India

For further details of the Journal, please visit the website. All the papers published on a particular subject/topic or by any particular author in the journal can be searched and accessed by typing a keyword or name of the author in the 'Search' option on the Home page of the website. All the papers containing that keyword or author will be shown on the home page from where they can be directly downloaded.

**www.neptjournal.com**



Published for Proprietor, Printer and Publisher: Mrs. T. P. Goel, A-504, Bliss Avenue, Balewadi, Pune, Maharashtra, India; Editors: Dr. P. K. Goel (Chief Editor) and Prof. K. P. Sharma